Blast Noise Management and Prediction

Ph. D Thesis

Gethin Wyn Manuel

A thesis presented for the degree of Doctor of Philosophy

School of Science, Engineering and Environment

University of Salford

United Kingdom

January 2024

Supervisory Team: Prof. David Waddington, Dan Allason, Dr. Antonio J Torija Martinez, Paul Cronin, Dr. Sabine von-Herbing

Abstract

The aim of this work is to manage adverse occupational and environmental impacts from industrial blast noise sources at the DNV Spadeadam Testing & Research Site. Situated in Cumbria, UK, the site carries out crucial major hazards work including improving safety concerns within industry decarbonization sectors and government agencies and performs a variety of explosives and blast testing. This PhD project is concerned with two issues related to blast noise: *occupational* blast noise impacts to personnel in the near field, and *environmental* blast noise impacts on communities at long-range.

Part I of this thesis concerns assessments of hearing protection suitability for the protection of site personnel against two differing blast operations carried out at the DNV Spadeadam site. Field measurements of real-world personnel exposures were found to exist beyond the scope of the current national legislative guidance for the selection of hearing protection against impulsive noise, DEF-STD 27:2015. Analysis of waveforms showed that both personnel exposures contain frequency and temporal characteristics not currently represented by the scope of the legislative guidance.

Part II of this thesis is dedicated to implementing tools for the management of blast noise impacts at long-range on residential communities, for a variety of industrial blast and explosion testing carried out at the site. Currently, the operational decisions regarding large explosion trials rely upon computationally expensive prediction models. A Live Noise Monitoring System (LNMS) was deployed across a number of sensitive residential receptors, to monitor environmental noise levels from the site's activities, and correlate the noise measurements with measured and forecast meteorological data. The monitoring network identified that smaller but more frequent blast operations most adversely impacted long-range communities. The database of measurements has been used to assess the performance of existing heuristic and computational models for the prediction of noise impacts up to a number of days in the future. Furthermore, a data-driven model in the form of a deep neural network has been trained and validated for the prediction of noise impacts from a unique explosive process using surface meteorological data. Further measurements characterising the source terms of the operation are required to improve the model. It is concluded that blast noise impacts are best managed by a combination of live monitoring networks and a mixture of predictive tools.

Acknowledgements

Firstly, I'd like to express my sincerest gratitude to my supervisor Professor David Waddington from the University of Salford for his consistent support given to me throughout the past 4 years. Your guidance has always kept me focused on what really matters, especially when undertaking this project from which there are so many issues that one could be led to pursue instead. I can't thank you enough for investing in me as a researcher, and a student and for mentoring me to be the best version of myself. I look forward to many more years working together. I'd also like to extend the same thanks to my other co-supervisors from the University of Salford, Dr. Antonio Torija Martinez, and Dr. Sabine von-Hunerbein for their invaluable support over the years.

Equally, I'd like to thank DNV, for sponsoring this work and for supporting me through my PhD project. In particular I'd like to thank my supervisory team at DNV, Dan Allason and Paul Cronin for their support over the years, and Dr. Lisa Witty for reading my entire thesis. Your decades of experience and patience has been crucial to this work, and I look forward to working together in the future. A huge thank you to Jez Lawton and Mark Dixon for putting up with me in the Control Room over the last few years. Your kindness, friendship and dare I say professionalism has truly underpinned this project, so I am grateful for that. Also, to everyone at the Spadeadam site who has helped set up instrumentation for the project, helped with software, or lent a hand in anyway.

I'd like to extend my deepest thanks to the project's Expert Advisory Panel, Dr. Rodger Munt and Mike Forrest, and to my Examiners, Prof. Keith Attenborough and Dr Olga Umnova. They have all given up so much of their time in order to help me understand a plethora of complex issues surrounding this research topic, provide feedback on lengthy reports and help get me through the theoretical topics. They are a huge inspiration to me, and I only wish I could be half the experts that they are.

A special note here to 24 Acoustics, especially Dave Coles for being on hand to support the deployment of the noise monitoring equipment.

Finally, I'd like to acknowledge all the residents and people living around the Spadeadam site whom I've engaged within over the last 4 years. You are all truly the backbone of this project and without you the measurements that underpin this project would not have been captured.

Dedication

Given the amount of people that have been involved over the last 4 years, this project is dedicated to anyone who has helped in any small way.

However, this work is truly dedicated to my entire family and those closest to me. To Holl, Mam, Dad, and Gav.

I'm so grateful for your continued belief in me.

Contents

List of Figures

List of Tables

1 Introduction

1.1 DNV Spadeadam Site Introduction

The DNV Spadeadam Research and Testing Centre (DNV Spadeadam), part of the wider DNV Group, is a world-class major hazards testing facility in Cumbria in the North of England. The site is situated within RAF Spadeadam, a large Ministry of Defence area used for electronic warfare training. DNV Spadeadam conduct a plethora of fire, explosion, and blast testing, under the umbrella term of major hazards testing, which serves many industries, including maritime and energy sectors and government agencies. Major hazards testing allows customers to test processes and obtain real-world data on product behaviour and capabilities under extreme conditions. The data gathered can be used to provide consultancy to industry on infrastructure and occupational safety.

Figure 1 - Map of wider Spadeadam area. North-Eastern Cumbria and Western Northumbria.

DNV's strategic aim is to ensure the site is world-leading in all aspects of safety, including occupational and environmental noise impact. Such impacts put the site at risk of litigation

caused by adverse impacts of noise on site personnel and on the residents in the neighbouring regions. Improved far field noise predictions should allow the following:

- Improved scheduling of testing, reducing costs induced by potential delays.
- Larger explosion trials conducted without generating significant noise disruption.
- Extending the trials season by increasing the number of available trial slots.
- Improved productivity and reduced secondary carbon emissions, by decreasing site visits required for clients.

Currently, business operations are relied upon by the Met Office Noise Evaluation Tool (MONET), which provides impulsive noise predictions based on parabolic equation (PE) methods. The method uses hourly-averaged vertical sound speed profiles to predict noise contours and then extrapolates to make estimates of peak unweighted sound pressure level at a number of receivers from 2-20 km away.

Although PE methods can model complex wave propagation over long-distance, the MONET is computationally intensive but still has several uncertainties which are not accounted for. Such uncertainties arise from the range-dependent meteorology and ground impedance found at Spadeadam which are not accurately modelled by MONET, in addition to the temporal fluctuations in the meteorology. The required complex and rapidly varying meteorological data are not effectively available to make useful noise predictions via computationally expensive PE methods. To address this deficiency, a data-driven heuristic model is proposed for the prediction of impulsive noise at several sensitive locations around the DNV Spadeadam site.

In order to make best predictions of noise from the Spadeadam site, it is important to set some relevant context about the surrounding environment.

1.1.1 DNV Spadeadam Testing Activity

DNV Spadeadam has several test ‘pads’ to meet the specific test requirements of their clients. The typical areas and types of explosion testing are labelled in Figure 2. The plethora of test processes demonstrates the varying complexity of impulsive sound sources at the site, some of which deviate significantly from the assumed point source detonations often seen within the scientific literature.

Blast testing up to 1Tn of TNT equivalence is carried out on Pad C. Such high TNT equivalence are required by clients to test impulse loading and fragmentation against, vehicles, building structures, glazing systems and a wide range of components, all of which can be assessed using a range if international standards. Another form of blast testing known as Explosive Depth Hardening carried out at the EDH Zone, forms a major part of DNV's business, serving the UK's railway infrastructure. The process improves safety by increasing the strength of vulnerable steel railway segments, such as crossings, by changing the structure of the steel, induced locally by a shock wave.

DNV has over 20 years experience in researching flammable gas cloud explosions by using custom testing rigs to study the influence of confinement and congestion on deflagrations and detonations. A typical gas explosion test may involve one of the many explosion chamber rigs located along the site, which can be used to provide overpressure pulses with peaks ranging from 60 mbar-4 bar and durations of 50 msec-300 msec. Such explosions form an integral part of Spadeadam's unique Hazard Awareness training courses, which provide customers with real-life demonstrations of the hazards they may face in industry. Course attendees often witness a demonstration of confined and congested flammable gas explosions, a phenomenon that DNV's research has been world leading on.

Similarly, vessel ruptures, commonly known as BLEVE, have been researched at Spadeadam for many years. Such processes arise from a physical explosion from sudden release of pressurised combustible or non-combustible liquid. While past research has focused on the release of combustible liquids such as LNG, current research is dedicated to non-flammable substances and cryogens. The process and storage of liquid hydrogen has particularly complex needs, where trace amounts of air can form unstable mixtures with detonative capabilities similar to solid explosives. Research on hydrogen detonations will form a major part of DNV's future operations on Test Site West, in order to support the energy transition.

Less commonly, Rapid Crack Propagation testing of polyethylene and other non-metallic pipe resistance is also carried out on site, along the FP Area. These trials provide critical information on pipe design within sustained pressure applications.

Figure 2 - Detailed map of testing and firing locations at DNV Spadeadam.

This broad range of explosives testing carried out at the site is by no means the limit of DNV's capabilities in explosion research. However, it shows the range of impulsive noise sources whose near and far-field exposures must be properly understood within the context of occupational and environmental noise legislation. In order to understand the far-field overpressures generated from these operations as the shock waves propagate out to the neighbouring residential areas, it is critical to understand the role of Spadeadam's unique geography has on sound propagation.

1.1.2 Spadeadam Geology and Land Characteristics

The site spans 50 hectares within over 350 hectares of secure MOD land on the Spadeadam plateau. According Cumbria County Council (2011), the key characteristics of the landscape are described by:

- high, rolling or undulating moorland and plateau
- large areas of coniferous planting

The geology of the land is mainly Carboniferous sandstone and gritstone underneath extensive peat, with hills rising from 150-520 m. The landscape is dominated by large areas of coniferous forest plantation, with Sitka Spruce as the most common species by far. Around these plantations are vast areas of blanket bog, rush pasture and purple moor-grass, with some isolated pockets of hay meadow and woodland around the River Irthing.

Figure 3 - An aerial shot looking west along part of the DNV Spadeadam Test Site

1.1.3 Meteorology around Spadeadam

Site situation is of key importance. At an altitude of around 260m, Spadeadam sits along the north-side of an east-west pass bounded to the north by the Cheviot Hills and to the South by the Pennine Hills, with both ranges containing peaks above 550m within 15km of Spadeadam. These mountain ranges have a direct influence on the macro-scale meteorology at Spadeadam, and inflict diverse and unpredictable weather systems. The undulating topography covered by large forest plantations, moorland and fens, vary significantly with distance and azimuth from the test site, which in turn affect the local micrometeorology over Spadeadam.

The relevance to sound propagation is that the vertical profiles of wind and temperature in the lower atmospheric boundary layer are not uniform over such a combined system of varying landscape and meteorology. Such inhomogeneity in the sound propagation medium produce complex sound radiation patterns, of which for nominally the same blast events, can vary by

several orders of magnitude. The significance of which is that such uncertainties directly affect DNV's capability to perform blast testing or not, based on occupational noise hazard and adverse environmental impact.

Sound refraction over large distances is influenced by the meteorology higher up in the Earth's Atmospheric Boundary Layer (ABL), where sound speed varies vertically and horizontally depending on the ABL characteristics.

The following features of the ABL are influential on vertical sound speed structure.:

(a) variation in thermal buoyancy, as a consequence of differing thermal radiation properties attributed to forestry, moorland, etc.,
(b) wind direction changes based on Coriolis effects, depending on terrain roughness, and
(c) meteorological distortions around the undulating terrain, with effects governed by the Froude number

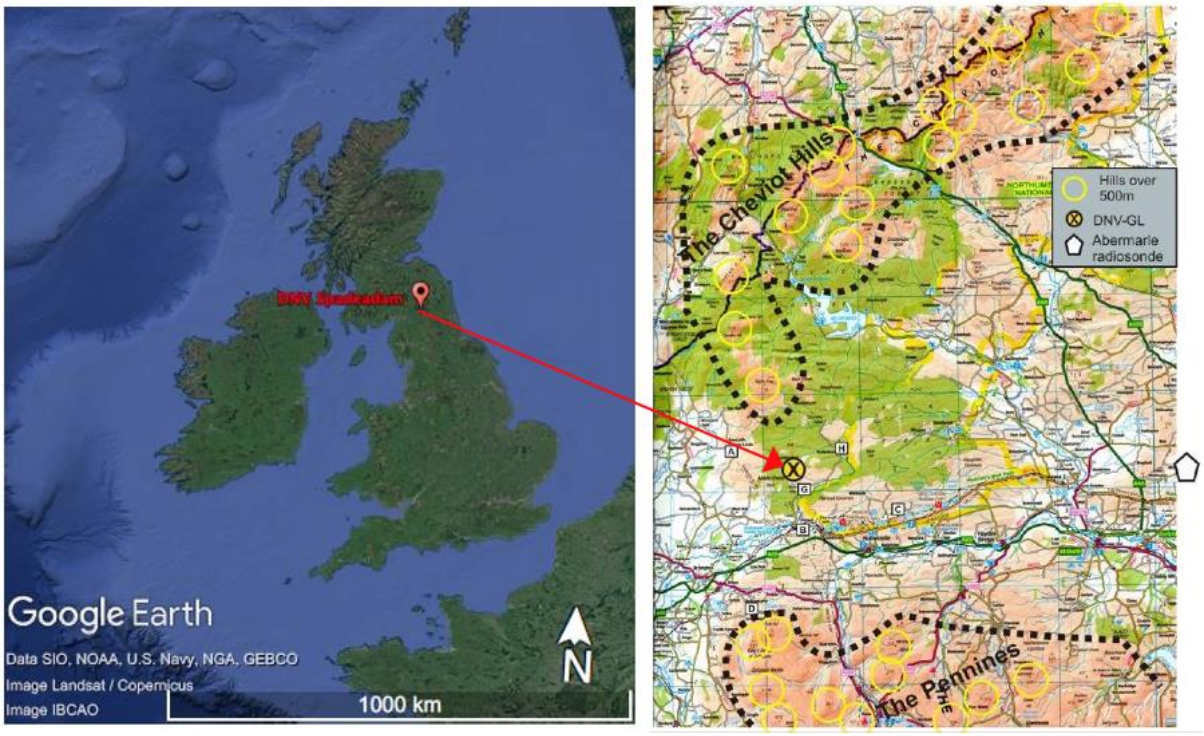

Figure 4 - Site location within the UK (left) and the local topography of the area (right)

1.1.4 Spadeadam Ecology

The unforested uplands of north-east Cumbria and west Northumberland is generally referred to as moorland, peatland, bog or mire, all of which have varying ground properties. Some discrete areas of exceptionally deep peat are known as the Border Mires. Before afforestation

and agricultural settlement, the Border Mires belonged to a matrix of moorland type habitat with pockets of native woodland. Following intense afforestation by the Forestry Commission during the two world wars to provide timber, the landscape is characterised by bog peninsulas within spruce forest, a combination of ombrotrophic (rain-fed) and geogenous (rain and ground-fed) areas.

The extensive coniferous plantation provides nesting sites for birds of prey, including goshawk and buzzards, as well as a reserve for red squirrels. This is significant because of the potential effects of high-amplitude impulsive noise on habitat suitability for sensitive wildlife. Comments from local complainants often show concern for noise effects on wildlife in such a sensitive area and can sometimes be a key motivation to complain about noise for some residents. It is also important to understand how the distribution of land use impacts local populations in the area, whose right to acceptable levels of environmental noise is the ultimate goal of the project.

1.1.5 Land Use and Settlements

Probably the most significant population by proximity to the site and size is the village of Gilsland, situated around 4 miles south-south-east of DNV Spadeadam. The village has a population of around 400, with several settlements and farms set apart from the village centre.

Another reason why Gilsland is important to this research is because of its historical significance, with local features of Hadrian's Wall, such as the Poltross Burn Milecastle attracting many additional visitors to the village. Neighbouring to the south-east is the smaller village of Greenhead which has a similar sized population. Outside Greenhead is the Blenkinsopp Castle retirement park consisting of around 175 people living in static holiday homes. The combination of a high concentration of mainly retired and elderly population with static holiday homes, makes it a highly sensitive area to impulsive noise.

Further to the east and south-east are smaller groups of settlements before the market town of Haltwhistle with a population of 3,811, around 11km from the site. Stone-built houses are common in the area, along with it being attractive to visitors of Hadrian's Wall and being the exact geographic centre of Great Britain.

From the south to the west, land use is mainly farmland with several villages, including Lanercost, Kirkambeck, Hethersgill and Roadhead. The most significant population in this

area is Brampton, with over 4000 people, approximately 15 km south-west of DNV Spadeadam. Noise complaints in these areas are less-frequent but become likely when the winds pass over Spadeadam from the North and East.

Within the immediate vicinity of the site (~5 km), due to the nature of the secure MOD land in all directions, there are only a handful of isolated farms with several of the residents living near the site for many decades. Complaints from these properties are highly unlikely, although exposures are often greater and are greater more frequently. This is due to the mutual relationship between the site and the residents and the relative tolerance of these residents compared to those further away to noise and other disturbances that may be inflicted upon the residents from the RAF operations.

Finally, some other significant areas consist of Kielder Forest Park, ~2 0km North-north-west, and the active MOD Otterburn Artillery Range, about 40 km North-west.

1.1.6 Summary

Clearly there are many factors that impact the source-pathway-receiver propagation medium from Spadeadam, all of which are critical to understand in order to fully address DNV's environmental noise impact. Such factors vary both spatially and temporally and are determined by DNV's activities, the geographical and meteorological influences on propagation, and the residing populations located around the site. This thesis aims to address all of these factors so that they can be included within a heuristic blast noise prediction model.

The next subchapter will discuss the novelty of the research. Once this is established the introduction will conclude with a subchapter on the impact of the research.

1.2 Novelty of Work

The novelty of this work lies in pioneering integration of real-world environmental noise measurement into the management of blast noise from a unique source of impulsive noise, major hazards testing. This is achieved by implementing a live noise monitoring network to gather longitudinal community noise measurements of novel industrial blast processes, coupled with using rapid sound propagation methods for the prediction of long-range blast noise. An evaluation of contrasting propagation models for predicting blast noise from novel

major-hazards testing is offered, by utilising effective and high-quality input data, and making predictions where people are located. This is opposed to the traditional method of noise prediction by using vast quantities of input meteorological data to form noise contours followed by interpolated noise levels at receiver locations.

Furthermore, the utilisation of state-of-the-art, short, medium, and long-term meteorological forecast and real time meteorological measurements for the Spadeadam site, allows rapid short and long-range blast noise predictions. This includes accessible, low quantity but high-quality meteorological data, such as from the on-site automatic weather station, and forecasts. Integration of this meteorological data with an in-house bespoke noise prediction application will give DNV Spadeadam the support to manage operational needs in both the immediate and long-term.

Occupational and Environmental noise from unique but necessary major-hazards testing related to energy sectors and national infrastructure have been evaluated in this thesis. In particular, the Explosive Depth Hardening operations conducted at Spadeadam, with its unique geometrical deployment, temporal and spectral properties compared with other types of explosions, poses problems for managing community response. The distinctive explosion testing at Spadeadam related to the protection of national infrastructure (referred to as ‘Pad C trials’ in this thesis), require weeks of planning and days of preparation, demanding longer-range environmental noise forecasting, evaluated in this work. Finally, the characteristics of noise generated by gas explosions related to net-zero industrial processes have been investigated for their impact on occupational exposure. This variety of major hazards testing carried out at Spadeadam has required the novel developments reported in this Thesis.

These relate to

(a) the exposure of on-site personnel, for which existing assessment methods are shown not to be applicable so ways of improving them are proposed.
(b) the development a new deep learning prediction method capable of utilising effective and high-quality input data, making rapid predictions a number of days ahead of testing.
(c) a pioneering integration of real time predictions with public relations accounting for non-acoustical factors in attitudes and responses.

1.3 Research Impact

The social and economic impacts of this research are far-reaching. Upon successful development and utilisation of heuristic noise management methods, the economic impacts will include better operational management of tests at Spadeadam. Optimised testing opportunities can become more readily available, leading to fewer test delays and thus cutting costs to DNV.

Without a successful noise management strategy, test delays may impact the wider industry. Such impacts affect the national clean energy policy implementation. The ability to test major hazards from hydrogen energy infrastructure is critical to the energy transitions, which DNV are helping to pioneer through its innovative testing capabilities.

On a more logistical note, pre-warning of potential test delays may save valuable time and resources for both DNV and its customers when they are expected to visit site to witness explosion trials. This is more significant than it may seem, with many clients often travelling from abroad, secondary carbon emissions induced by such visits will not be wasted, with every reduction in both DNV and their client's carbon footprints always being beneficial.

The academic impact of this research may be realised through the co-production of knowledge with industry and the management, sharing and transformation of knowledge back to DNV and academia. As a successful blast noise management tool should be based on scientific principles of outdoor sound propagation, such a tool may be generalised to cover industrial sites with similar propagation environments and could therefore be applicable elsewhere. This would be the first of its kind in the world to cover such a range of modern explosive types that differ from standard military application.

The social impact of the project far outweighs the aforementioned impacts, by improving the quality of life of many residents in the area who are frequently exposed to high-level impulsive noise in their homes. The residents, and local communities of the Spadeadam area will be positively impacted through the development of more accurate noise prediction and better management of impulsive noise. With the Spadeadam site being adjacent to the internationally famous Hadrian's Wall, DNV's noise impact can be reduced, so that visitors and tourists can enjoy the natural and historic soundscapes of the area. This was an important consideration for the 1900th Anniversary of the monument in 2022, which likely brought many tourists to the Spadeadam area.

1.4 Research Goals

1.4.1 Project Goals

When the project was conceptualised in the beginning of the latter half of the 2010's, the ultimate goal of the research was to develop a bespoke and validated far-field impulsive noise prediction tool. At the outset of the project in late 2019 where I was based at the University of Salford, away from the work going on at DNV Spadeadam, this was certainly still the overall goal. Following relocation to the DNV Spadeadam site in late 2020 and gaining daily real-world insights into the impacts of major hazard's research on the neighbouring residents, the reality of a what a useful far field impulsive noise prediction tool became clearer.

Whilst addressing the long-range issues of noise from the DNV site, the project attempts to simultaneously investigate the risks of auditory hazard to site personnel from high-level impulsive noise at close range. This separate goal introduced a very important but diverging focal point for the research. Investigations on this topic were agreed to be limited at the project's conception, and was intended as an opportunity for DNV to demonstrate compliance with current health and safety regulations through measurements.

From initial pilot investigations, it became apparent that assessments of hearing protector performance on site personnel at their representative exposure locations were being conducted beyond the scope of the current legislation at the time. This work has been summarised as a chapter in this thesis and suggestions of further work to improve assessment methodologies in this topic have been given.

1.4.2 Project Evolution

What DNV's operational team needed on a day-to-day basis was a rapid approach for the prediction of noise at sensitive receptors around Spadeadam which employs a practical method, not guaranteed to be optimal or perfect, but sufficient for the immediate goals. Such immediate goals might include essential testing related to national infrastructure which have to be carried out rapidly. Heuristic, empirical or otherwise data-driven approaches should therefore be suitable for the following case in question; the prediction of explosive noise impact at sensitive locations, considering propagation through complex meteorological conditions over complex terrain, data for both of which may be unavailable or inaccurate.

From observing DNV's activities at first hand and engaging with the neighbouring communities, the need for both a rapid, near real-time and long-term noise prediction model became apparent. Here, long-term refers to the ability to make predictions of noise impacts on the order of several days to weeks ahead from the current time. Rapid refers to the ability to make these predictions quickly, ahead of essential testing.

1.4.3 Research Questions

In summary, this thesis aims to increase the number of major-hazards test opportunities for DNV Spadeadam by answering the following questions, which are ordered by decreasing importance:

Primary Question

- Can accurate predictions of noise impacts from DNV's unique major-hazards testing be made rapidly at far field receptors using readily accessible real-time meteorological data or long-term forecasts?

Secondary Question

- Are DNV's site personnel adequately protected against the high-amplitude exposures expected from their activity?

Two issues give rise to the primary question. That question is rooted in the propagation physics of sound in the atmosphere and bespoke industrial blast testing unique to the site, the key theme of the project. Ultimately, they aim to shed light on the deep connection between DNV's noise impacts at resident's homes and the encompassing weather at the site. At surface level, this may seem narrowly focused on the research location at hand, but in reality, can be applied to any instance of far field noise impacts on the environment. This also provides guidance on major-hazards testing, and will benefit others involved with complex explosion and blast testing,

The secondary question is exploratory, aimed at extending the scope of this thesis, so that it can serve as a foundation for future research in hearing protection and human response to noise from the diverse and unique activities associated with major hazards research.

1.5 Thesis Structure

This structure is separated into two parts.

1.5.1 Part I

Part I is concerned with the management of occupational blast noise for personnel at the DNV Spadeadam site. This work is contained in a single, large chapter, Chapter 2. The chapter offers an introduction, to scope the issues around selecting hearing protection for some specific blast testing carried out at DNV Spadeadam. An extensive review on the scientific literature and legislative guidance related to this topic is presented in Chapter 2.2. Following this, are two case studies (Chapters 2.3 and 2.4) demonstrating the methodology used to assess hearing protection suitability for industrial blast noise at Spadeadam. Technical discussions are contained in each case study sub-chapter. Part I of the thesis closes with a statement of conclusions and further work required to advance this work.

1.5.2 Part II

Part II of the thesis is solely dedicated to the work on the management and prediction of environmental blast noise impacts from DNV Spadeadam's testing activities. Due to the larger influence of this work on the thesis, this part is larger than Part I and is separated in to separated chapters.

In Chapter 3, an extensive review of the scientific literature related to outdoor sound propagation is offered. The review moves on to address the issues related to community response to blast noise and the legislation required for DNV to operate safely with regards to noise impacts in order to protect people and the environment.

Methodological techniques are presented in Chapter 4, firstly for the management of blast noise impacts at Spadeadam, before presenting those used for the development of heuristic prediction models related to Spadeadam's activity.

The results of measurements gathered from the Live Noise Monitoring System are presented in Chapter 5, where the performance of previously existing, and newly developed data-driven models for the prediction of environmental blast noise impacts are evaluated.

In Chapter 6, a discussion on the performance of existing and extended models for predicting blast noise from major-hazards is offered.

Part I

Managing Occupational Blast Noise

Overview

The aim of this Part of the thesis is to present the work done on managing and predicting environmental blast noise impacts from test activity carried out at DNV Spadeadam. This work contrasts that done in Part I, as it is involves the propagation of blast waves over long-range and concerns two key components:

a) *Management* of the blast noise impacts on the community;
b) *Prediction* of blast noise impacts on the community.

One would argue that component b), the *prediction* of blast noise is a strategy that must be utilised to successfully carry out component a), the *management* of community blast noise impacts. Therefore, the prediction of blast noise is an essential part of managing community blast noise impacts.

This part of the thesis begins with a chapter reviewing the scientific literature on all aspects import to the management and prediction of environmental blast noise.

Following this chapter, methodological techniques used for the management and monitoring of environmental blast noise impacts from Spadeadam on the community, and for the development of heuristic prediction models for blast noise at Spadeadam.

The performance of such models is assessed, before conclusions are stated, followed by setting out the further work required to advance the management of environmental blast noise.

2 Assessment of Hearing Protection Suitability for Blast Noise at DNV Spadeadam

2.1 Introduction

This part of the thesis is dedicated to the investigation of the suitability of hearing protection devices used at DNV Spadeadam for the specific purpose of controlling auditory risk to personnel on site. The applicability of current legislative guidance and measurement standards for the prescription of hearing protection devices is assessed for use against several complex and industrial blast and explosion noise sources.

The University of Salford has previously been involved with the research on hearing protection suitability for high-amplitude impulsive, including gunfire noise for The Police Service of Northern Ireland (G. W. Kerry, 2004a) and for the Ministry of Defence at Eskmeals (G. W. Kerry, 2004b). Following this research, Salford were tasked by DNV Spadeadam to provide advice on hearing protection suitability for a number of their blast and explosion operations for the purpose of protecting personnel. Therefore, this part of the thesis has themes related specifically to the operations carried out at Spadeadam.

Chapter 2 starts by setting out the research motivations for this work. Following this subchapter, a literature review is presented on the current state of the legislative guidance and best practices on measuring and providing consultancy on hearing protection for impulsive noise. Furthermore, several case studies from field measurements at DNV Spadeadam are presented. Part 1 of the thesis closes by forming conclusions from this work and provides the necessary steps required to undertake future work related to the advancement of this field.

2.2 Literature Review

2.2.1 Blast Wave Theory

2.2.1.1 Shock Formation

One of the main elements of uncertainty when predicting outdoor blast propagation comes from the source type. Explosions are events of high energy, exhibiting complex propagation characteristics due to their non-linear nature. The non-linearity of isolated shock pulses arises from a portion of a wave traveling at a different velocity compared to other parts of the wave, when subjected to such dynamic changes in pressure. This effect causes the wave to steepen into a sawtooth wave (Naugolnykh & Ostrovsky).

A detailed analysis of shock formation is presented by Morse (1986), where the total propagation speed of the disturbance is the sum of local sound speed and the fluid velocity, and at this point a crest of a wave will overtake the trough, corresponding to an infinite velocity gradient in the wave. Due to the violent nature of explosions, the number of uncertainties associated with them, and the fact that they tend to exist beyond the realm of normal acoustics waves, they are often categorised as one type of sound source, when in fact, many variations of blasts exist.

2.2.1.2 Rankine-Hugoniot Expressions

The Rankine-Hugoniot relations are discussed widely in literature as a tool to describe the relationship between the state of media on both sides of a shock front. Kinney and Graham (1985) discuss the concept of utilising the shock front as a reference point for pressure, temperature and velocity, and to assume that media moves towards the shock front and passes through it. Additionally, by assuming the shock has a constant velocity combined with the stationary shock perspective, the medium on each side of the shock may be defined. The medium in front of the shock is moving at the shock velocity $dR_s/dt = R_s$, with pressure p_0, density ρ_0 and temperature T_0. The medium behind the shock, i.e. the medium where the shock has already propagated through, has a velocity u_0 with properties p, ρ and T. The equations of motion are then used to relate the medium travelling towards the shock with the medium the shock has already passed through. By combining the equations of mass continuity and momentum, and by rearrangement, the equations express how pressure relates to the density of the medium as a function of the shock speed. This can be improved further

by including the energy equation, expressed in terms of enthalpy, where the shock is assumed to be a constant volume travelling at constant speed. By assuming that the medium is a perfect gas and that enthalpy is a function of temperature alone, the Shock Hugoniot equation is found.

$$\frac{\gamma}{\gamma-1}\left(\frac{p}{\rho}-\frac{p_0}{\rho_0}\right)=\frac{1}{2}(p-p_0)\left(\frac{1}{\rho_0}+\frac{1}{\rho}\right) \qquad \textit{Equation 1}$$

The Shock Hugoniot equation tells us the pressure and density properties, p and ρ respectively, behind the shock as a function of the properties ahead of the shock, p_0 and ρ_0 respectively, with the additional factor of the specific heat ratio of the two gases, γ. Finally, by simplifying the Shock Hugoniot equation further in terms of the pressure and density ratios of the two gases on each side of the shock, the Rankine-Hugoniot Equations for pressure and density are obtained as below.

$$\frac{p}{p_0}=\frac{\frac{\gamma+1}{\gamma-1}\frac{\rho}{\rho_0}-1}{\frac{\gamma+1}{\gamma-1}+\frac{\rho}{\rho_0}} \qquad \textit{Equation 2}$$

$$\frac{\rho}{\rho_0}=\frac{\frac{\gamma+1}{\gamma-1}\frac{p}{p_0}+1}{\frac{\gamma+1}{\gamma-1}-\frac{p}{p_0}} \qquad \textit{Equation 3}$$

The so called Hugoniot equations are used to thermodynamically describe shock fronts travelling through matter, by linking the pressure P_0, internal energy E_0 and density ρ_0 before the shock in the uncompressed medium with the corresponding values in the compressed region which the shock has already passed through (P_0, E_0 and ρ_0). Although the following citation is rather distant from the literature on noise from blasts, Appendix I of Melosh (1989) provides a reasonably easy to follow derivation of the 3 Hugoniot equations. Density is expressed as the specific volume V = 1/ρ. Through expressions of the conservation of mass, momentum and energy across the shock front, the known quantities of the initial pressure, energy and density in the uncompressed region allow derivation of the unknown equivalent quantities behind the shock front (Boslough & Asay, 1993).

$$\rho(U-u_p)=\rho_0 U \qquad \textit{Equation 4}$$

$$P-P_0=\rho_p u_p U \qquad \textit{Equation 5}$$

$$E - E_0 = \frac{1}{2}(P + P_0)(V_0 - V)$$ *Equation 6*

2.2.1.3 Blast Characteristics and Parameters

When analysing blast wave propagation, blast waves are characterised by more specific parameters, rather than the physical parameters of the blast described by the Rankine-Hugoniot equations. These are well-defined in literature, where a Friedlander curve is usually used to represent the blast wave pressure in time.

Firstly, the blast waves are assumed to be *ideal*, where *ideal* means a discontinuous positive pressure rise from ambient conditions to a peak value, Baker (1973). The peak pressure value is often referred to as the *peak side-on pressure*, *peak pressure* or the *overpressure*. Following this peak pressure is a decay in the positive overpressure (usually of an exponential nature) back to ambient pressure, forming the positive phase of the blast. Pressure then falls below ambient pressure before returning to ambient conditions, resulting in the negative phase. Due to this negative phase, the exponential expansion of the initial supersonic blast wave, will decelerate into a subsonic wave. After this point of transition, conventional linear acoustic propagation can assumed (Munt, 2018). Consequently, the energy within the leading blast wave front also decays with distance.

By simply measuring the time between each of these features, the transient character of the blast is captured, resulting in further parameters, namely, the arrival time, rise time, impulse length, suction phase length as described in detail by Gottlieb, Ritzel, and Miskew (1981). Integration of the positive and negative phases on a pressure-time trace, give positive and negative impulses, I^+ and I^- respectively. These are important parameters of the blast wave, often used for assessing shock loads on structures (Kinney & Graham, 1985).

$$I^+ = \int_{t_s}^{t_s+\tau^+} [p(t) - p_0]\, dt$$ Equation 7 (Kinney & Graham, 1985)

$$I^- = \int_{t_s+\tau^+}^{t_s+\tau^+ +\tau^-} [p_0 - p(t)]\, dt$$ Equation 8 (Kinney &

Graham, 1985)

The temporal parameters of a blast are often described differently in different literature and there have been attempts to standardise these metrics. A widely accepted convention is to separate the waveform in time into 4 parts. The NATO report, NATO (2003) summarises how these definitions were first coined, where the A-duration and B-duration were outcomes of the aforementioned CHABA (1968) report on impulse noise damage risk criteria, the C-duration was introduced by Pfander, Bongarts, and Brinkmann (1975) and the D-duration by Smoorenburg (1982).

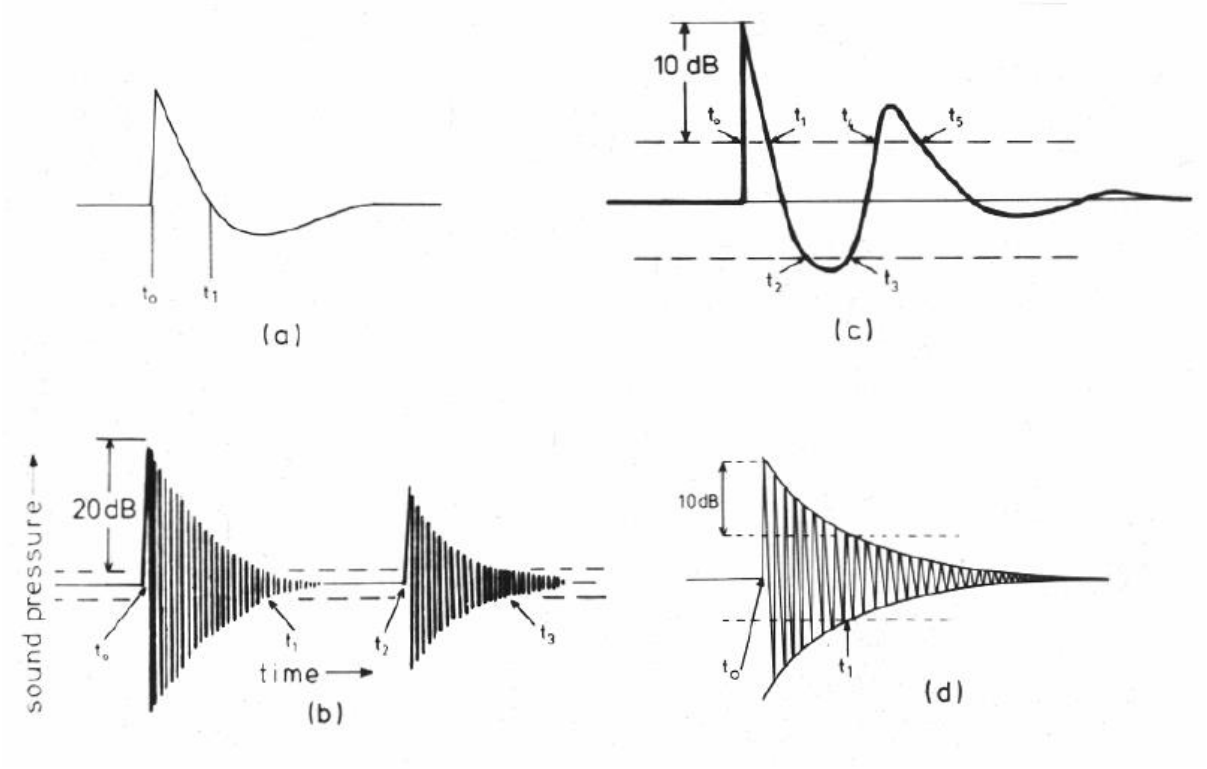

Figure 5 - Definitions of impulses, adapted from NATO (2003).

2.2.1.4 Ideal and Non-ideal blasts

According to Baker (1973), the simplest form for describing ideal shock time-pressure history was presented by Flynn (1950).

$$p(t) = p_0 + P_s^+\left(1 - {}^{t}/_{T^+}\right), \quad 0 < t \leq T^+ \qquad \text{Equation 9 (Baker, 1973)}$$

Where *t* is time measured after arrival time,

In reality, a shock's time-pressure history may differ from this ideal representation, where transient characteristics are effected by many factors, such as, the initial conditions of the source or the effects of the measurement instrumentation. Ethridge and Agency (1965)

proposed a form to better represent the decay of the positive phase, by using time constants, rather than a linear representation, shown below.

$$p(t) = p_0 + P_s^+ e^{-ct}$$ Equation 10 (Ethridge & Agency, 1965)

Further adaptations to this have been made in an attempt to better represent the decay rate of the blast, however, simplification of the time-pressure waveform is usually acceptable for estimating its parameters.

Baker's text also describes the work of Olson, Larson, and Goldstein (1960) whom observed long rise times from ambient to peak overpressure from time-pressure histories of bursting air-filled pressure vessels. These rise times were of the same order of magnitude of the decay times. This work was a critical recognition of how source characteristics will affect the resulting temporal blast parameters.

Baker continues by describing how deviations from ideal blast characteristics are likely observed and are more significant in the near field. Very small variations in the initial source conditions cause blast characteristics to deviate from the ideal case. For example, where solid explosives are encased, the disturbances of ballistic shocks from casing fragments appear as artefacts superimposed on the primary shock pressure-time history. Additionally, variations in the initial sphericity of shock waves may arise from imperfections in source shape. Baker claims that the effects from such conditions become less significant in the far field, due to smoothing effects from atmospheric absorption, resulting in almost ideal conditions.

In most air blast theory, source geometry is simplified by assuming a point source. This means that for a point emitting a spherical wave, the wave has properties as a function of one space dimension, radial distance from source centre. However, some blast sources may consist of a line of detonations, occurring either simultaneously or in series, resulting in a cylindrical source. Shock fronts from these sources expand cylindrically rather than spherically but will remain a function of only one space coordinate if one considers distances that are short compared with the length of the line source.

2.2.1.5 Blast Scaling Laws

Furthermore, the characteristics found either by the Rankine-Hugoniot relations or by observation of a blast time-pressure history, such as the peak pressure, P_s, duration, τ, and impulse, I_+ as a function of distance from the source may all be derived from scaling rules. Generally, for explosives, these parameters scale with the cube root of the charge mass of a TNT equivalent, W, ($W^{1/3}$), known as Hopkinson Scaling formulated by B. Hopkinson in 1915, as described in Kinney and Graham (1985). These parameters are scaled according to the scaled distance, Z, by using a standard set of curves, where R is the distance from the point of detonation.

$$Z = \frac{R}{W^{\frac{1}{3}}} \qquad \text{Equation 11}$$

For cylindrical sources the blast peak over pressure is scaled according to the following law, rather than just by $R/W^{1/3}$, for distances that are short compared to the length of the line source.

$$P_s = f\left(R\left(\frac{W}{L}\right)^{\frac{1}{2}}\right) \qquad \text{Equation 12 (Baker, 1973)}$$

Baker (1973) describes the work of Kennedy (1946), which found that the decay with distance from cylindrical sources is much slower than from spherical sources. This realisation was extended by Lindberg and Firth (1967) who investigated the theoretical variation of overpressure ratios with scaled distance of spherical, cylindrical and infinite plane blast sources, and found that plane sources result in even slower decay rates than cylindrical sources.

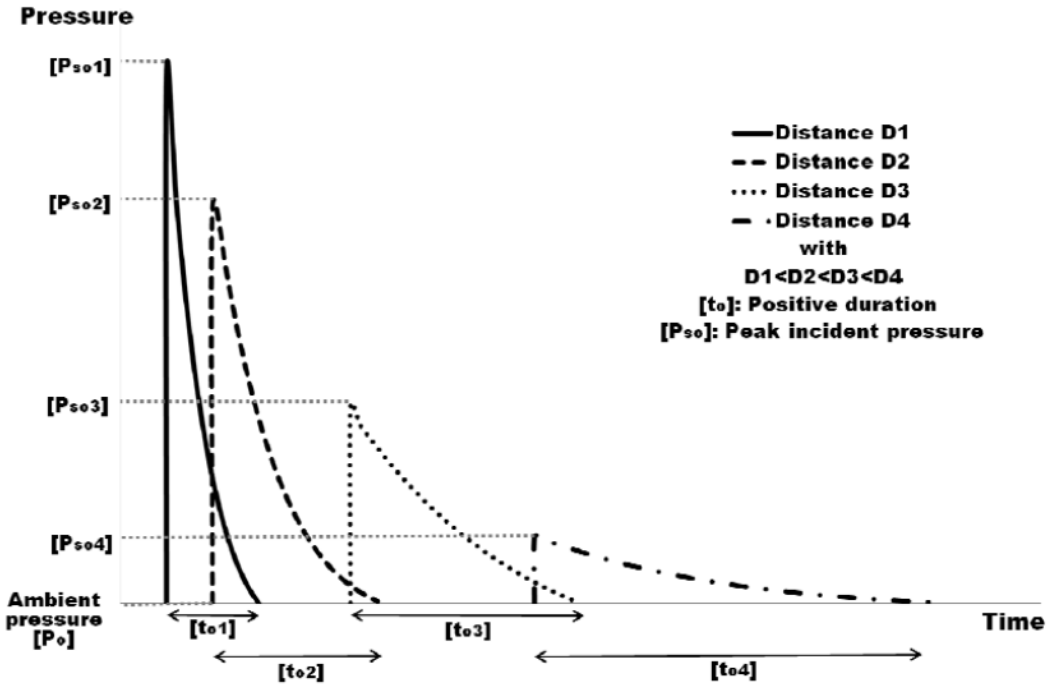

Figure 6 - Influence of distance on the positive phase of a blast. Adapted from Vasileios and George (2013).

Following the initial non-linear decay of a blast wave from any of these sources, there is a point where acoustic propagation can be assumed. A previous study relating to blasts at Spadeadam, by Munt (2018), describes the theory of this transition to acoustic behaviour. The point at which linear acoustic behaviour may be assumed is at the radial distance R>R' and through the extrapolation of scaling laws, the following relationship is found.

$$p_s - p_0 = 1kPa \text{ at the scaled distance } \frac{R'}{W^{\frac{1}{3}}} = 71m.kg^{1/3} \qquad \textit{Equation 13 (Munt, 2018)}$$

It is said by Munt (2018) that from this distance, the peak overpressure would decay linearly according to spherical divergence.

$$p_s - p_0 \propto \frac{1}{R} \text{ as } R \to \infty \qquad \textit{Equation 14 (Munt, 2018)}$$

Of course, this is an assumption, however Munt (2018) discusses how various empirical expressions have been constructed to approximate the realistic energy decay of a blast wave in the far field from when linear acoustic decay can be assumed. Munt continues by pointing out the difficulty in establishing which of the expressions is most accurate due to the small

variations in sound level for a given distance from each of the expressions, which in reality would be sensitive to the myriad of propagation effects present in long range propagation, i.e. from atmospheric absorption or refraction.

Blast parameters are scaled using a chart such as the one in Figure 7, where the derivation of scaled parameters was determined by experimental studies. The most widely used and accepted for the determination of blast parameters is the Kingery-Bulmash approach, however other curves have been developed to scale blast parameters for particular blast conditions, such as nuclear detonations. An example of a scaling chart for one parameter (peak overpressure) and how various scaling rules compare to one another is shown in Figure 7.

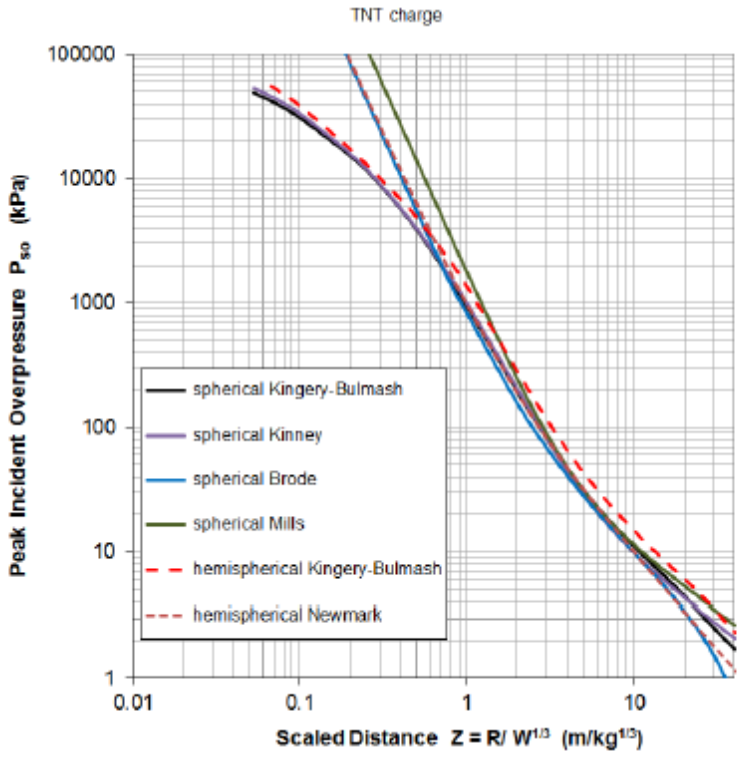

Figure 7 - Comparison of curves for determining the peak incident overpressure as a function of scaled distance for both spherical and hemispherical blasts. Adapted from Vasileios and George (2013).

2.2.1.6 Types of Blast

In the near-field, blast waves propagate non-linearly, meaning that the extrapolation and derivation of source parameters, such as sound intensity and power levels rely heavily on approximations. Due to the many types of blasts, variations in how the resulting blast wave propagates following an ignition occurs. Lautkaski (1998) describes how blast waves can be separated into two types, *shock waves* and *pressure waves*. Figure 8 shows this as a

difference in pressure profile with time. Shock waves (left) exhibit an instantaneous pressure rise, followed by a positive phase, of duration t_p (referred to as τ in this work) where the pressure of the wave decays from peak pressure, P_s to ambient pressure p_o.

Conversely, some explosive sources may produce a blast wave that resembles the schematic on the right-hand side of Figure 8, where the rise time to P_s and decay time to p_0 is much longer. This results in a lower overall maximum pressure, due to the spreading of energy with time. It is important to note this difference in blast wave types, as many different blast sources are present at Spadeadam, which consequently produce different blast waves.

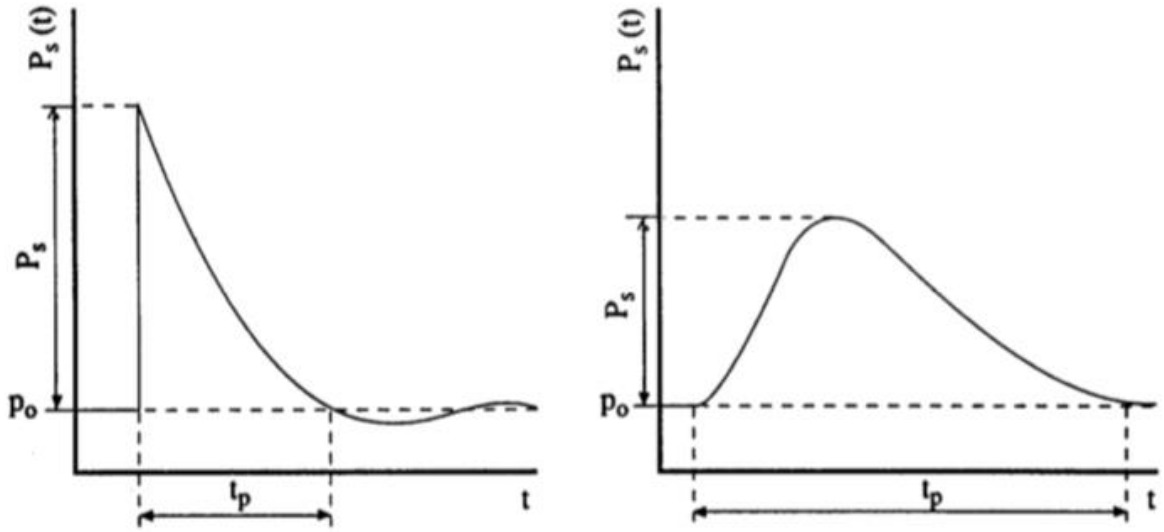

Figure 8 - Transient pressure response of a shock wave (left) and a pressure wave (right) (Lautkaski, 1998)

Gas Explosions: Enclosed and Vapour Cloud Gas Explosions

The research on gas explosions carried out by DNV GL Spadeadam involves 2 main rigs, the explosion chamber and the *vapour cloud test rig*, although some others are used. The latter is often used for observing the two types of waves and is also used for demonstrations in the Hazard Awareness courses. It demonstrates the combustion of a flammable mixture, often referred to as a vapour cloud explosion, in which the deflagration of a confined gas or vapour cloud is shown. During deflagration, the reaction zone, or flame front, is accelerated, resulting in the generation of a *pressure wave* propagating at very high, but subsonic speeds. However, the speed of the pressure wave can be significantly increased when flammable mixtures are confined or are within congested environments, which is often the reality for

many industrial environments. Both the explosion chamber and vapour cloud test rig simulate this effect. Under such conditions, the deflagration of a flammable mixture may transition into detonation, where the flame speed reaches speeds greater than the speed of sound within the unreacted medium. In this instance, the type of blast wave experienced is a *shock wave*. Explosions from detonations are associated with events such as the bursting of a pressure vessel.

Although shock waves travel at speeds above Mach 1, they can be completely absorbed during this transition from *deflagration* to *detonation* (M. A. Liberman et al., 2010), where flame speeds of the fireball following ignition can travel at speeds above Mach 5. Such violent events exhibit increases in flame speeds due to distortion of the flame from turbulent effects. Wall friction, high flow velocities near relief vents and obstacles all create turbulent eddies. Larger eddies contribute to an increased surface area of the flame, leading to a faster burning rate for a flammable vapour. Smaller eddies increase the diffusion of heat and mass. During a deflagration to detonation transition, this principle feature resulting from the flame acceleration is the formation of compressed pockets of unreacted flammable mixtures ahead of the flame reaction zone. Liberman, et al. (2010) describes this as a positive feedback loop mechanism of large amplitude pressure pulses accelerating the flame. The significance of this, is that the pressure exerted by the blast is proportional to the flame speed, essentially increasing the magnitude of the blast and hence the experienced sound pressure level.

Furthermore, flame speeds in vented gas explosions, such as those demonstrated by the explosion chamber at Spadeadam, are described by Lautkaski (1998) to be sensitive to hydrodynamic instabilities between unburned and burned gases. This results in an external explosion, which reverses the flow through the vent.

Such mechanisms create a large deviation in the resulting overpressures experienced from the same blast set-up. Random distributions of a contained flammable mixture can cause a cellular structure within the flame front. The idea of acoustic waves trapped within an enclosure during vented explosions is discussed by (Fakandu, Andrews, & Phylaktou, 2016; Lautkaski, 1998). According to Lautkaski (1998), the acoustic wave is coupled with the oscillating cellular instabilities of the flame front, leading to amplification of the acoustic wave. It is tempting to speculate from this that resonances may cause the deviations in the amplitude of the propagating acoustic wave between tests with the same initial conditions.

Solid Explosives: Explosive Depth Hardening

The facility at DNV GL Spadeadam is world renowned for its extensive testing on both known and unknown explosion mechanisms. Furthermore, the facility is committed to understanding the lesser known explosion mechanisms, such as those used for rail hardening. Such events are known as *explosive depth hardening* (EDH). EDH is a comparably recent method for rail hardening, in where a metal rail is strengthened by the resulting incident shock wave of a detonation contact explosive. According to TheFreeDictionary.com (2020), this has been an independent method of strengthening materials since the 1950's. However, due to the small number of facilities that currently perform this method, noise measurements from it are not well documented in scientific literature, in comparison with other explosive events.

The test is comprised of laying a 2mm sheet of plastic explosives such as Semtex over a segment of rail track, usually parts of the track that are under the highest stresses from carriages, such as crossovers. A single test may include up to 4 or 5 track segments, up to a combined weight of roughly 10kg TNT equivalence. Tests at Spadeadam on Manganese steel tracks have produced hardened zones of up to 15mm deep, considerably larger than the depths produced by other chemical hardening processes along the rail. Detonations are controlled via electronics and are therefore simultaneous. Resulting overpressures from tests at Spadeadam are reported to be around 15mbar, corresponding to peak sound pressure levels in the region of 160dB at the overpressure measurement point.

The process of detonation is considerably more complex than the idealised point source model, where the sheet of explosives is ignited at particular detonation points along the rail. From each detonation point, the energy is transferred in each direction, along the remaining lengths of the track. For rail crossovers, where a segment might have gaps, bridging links are used to transfer the energy from the detonation point to the other parts of the track.

The directionality of this type of explosive is not well understood. Usually, in the far field where the size of the overall test zone is very small compared to the distance to the receiver point, the source directionality may be assumed as spherical. However, in the near field, EDH may have a highly directional wave front, resulting from the use of several detonation points, dotted along a single segment. From the theory set out in Baker (1973) for non-ideal shock sources, those which deviate from perfect sphericity are likely to produce particular propagation characteristics that differ to the normal spherical shock fronts from point sources.

Physical Explosions: Hydrogen Detonations and BLEVEs

One alternative fuel to natural gas is hydrogen. The current development of hydrogen infrastructure for power within urban environments such as in houses, has consequently resulted in a significant amount of research into the safety of storing hydrogen. A study by D. Li, Ma, and Shen (2015) compared explosions from hydrogen/air to methane/air mixtures and found that flame speeds were higher from hydrogen explosions, whereas the methane explosions produced longer impulses. Maximum overpressures and rates of pressure rise resulting from hydrogen were also found to be significantly higher than those from the methane/air mixture, due to different flame and gas activity characteristics.

Other sources, such as from physical explosions are defined as the result of a sudden catastrophic rupture of a pressurised gas or vapour filled vessel by means other than reaction, or the sudden phase change from liquid to vapour of a superheated liquid (Schaschke, 2014). One example of a catastrophic physical explosion is a boiling liquid expanding vapour explosion (BLEVE), where a vessel of liquid is exposed to extreme heat, such as a fire, resulting in the release of vapours from the liquid and subsequently a rise in pressure within the vessel.

DNV GL Spadeadam currently research many variations of physical explosions, however the mechanisms of noise generation can be varied, and turn this in provides motivation for understanding these mechanisms and how they generate noise, and in ultimately how they impact the immediate noise environment.

2.2.2 Measurement of Blast Noise in the Near Field

2.2.2.1 Instrumentation

Transducer Requirements

Blast waves are considered to exist at the boundary of normal acoustic waves, due to their rapid transient nature. Therefore, specialist measurement equipment is necessary to capture these extreme temporal and dynamic characteristics.

The current best-practice guidance in the U.K, DEF-STD 27 mandates the use of a Class 1 rated sound level meter, that is in compliance with the current instrumentation standard BS EN 61672:2013 (BSI, 2013) for measuring blast sources, given their nature.

Dynamic Range

Due to the nature of high intensity sound levels, there is usually a need for a ¼" transducer for measurements, in order to eliminate the effects of overloading the microphone. Smaller diameter microphones are less sensitive and will extend the measurement range of the instrumentation beyond the typical maximum levels experienced within normal environments. The U.S. Military-Standard 1474:E:2015 advises that only measurement microphones with a diameter less than 0.25" are suitable for the measurement of short duration high level sound (Department of Defense, 2015). In the far field, due to atmospheric absorption the high frequency components of a blast are attenuated over long distances more severely than lower frequencies. Due to this attenuation, the influence of the microphone should not be as significant on the sound field and therefore measurements in the far field can be taken with a free field microphone. Brueck (2016) highlights how the atmospheric attenuation is less severe in the near field, and therefore all frequencies of the blast should be considered. At close ranges to the explosion, where sound levels are above ~160dB, a pressure response microphone is more suitable. However, at this proximity where high frequencies are yet to be absorbed by the atmosphere, the orientation of the microphone may influence how the upper frequencies react with the diaphragm.

Legislation	Comment on instrumentation dynamic range
Def-Stan 0027:2015	• Dynamic range should be set to account for peak levels at a minimum of 10dB above the actual source peak level • Dynamic range sufficient to capture the full range of sound pressure levels within the event
MIL-STD 1474E: 2015	• Sensor diameters should not exceed more than 6.4mm (0.25in) • Above 171dBPeak, condenser microphones shall not be use unless otherwise specified by the manufacturer to be capable of measuring such pressure levels.

Table 1 - Guidance on instrumentation sampling rate requirements according to BS EN 458:2016, DEF-STAN 00:27 2015 and US MIL-STD 1474E:2015

Sampling Rate

Extremely high sampling rates are required to capture the nearly instantaneous pressure discontinuity and other extreme temporal characteristics of a blast. This is extremely important for blast measurements, where low sample rates may lead to information loss during recordings. Ultimately, loss of signal information increases the uncertainty when carrying out auditory risk assessments.

US MIL-STD 1474E:2015 advises that measurements should be made with a sound level meter capable of making peak sound pressure level measurements with the total rise time of the instrumentation not exceeding 200 microseconds (μs) (Department of Defense, 2015).

The guidance on sampling rates from the U.K. DEF-STAN 27 is very limited in comparison with the guidance from US MIL-STD 1474E. The guidance does however refer to BS EN 61672:2013 for sound level meter measurement requirements.

2.2.2.2 Measurement Procedures

Measurement Parameters

Measurement methodologies for high-level impulsive sounds depend upon the desired outcome of the measurement, whether that is to estimate personal hearing exposure, frequency content, or for the selection of hearing protection. In the U.K., the determination of all three of these can be made using the HML methodology described in BS EN 458:2016 and the extended version in DEF-STD 0027 MODUK (2015). The methodology and its relevance to selecting hearing protection is discussed in much more detail in chapter 6 of this literature review, where it is compared with other measurement procedures. The measured noise parameters needed to complete the HML method include the A-Weighted and C-Weighted Peak SPLs and the A-Weighted Equivalent SPLs.

The US MIL-STD 1474E takes into consideration many other parameters which should be measured, for selecting hearing protection. The measurement parameters of interest from each document are summarised in the table below.

Standard	Recommended noise parameters to be

	measured
BS EN 458: 2016	• Maximum C-Weighted Peak Sound Pressure Level (L_{Cpeak}) • C-Weighted Sound Pressure Level, (L_{pC}) • A-Weighted Sound Pressure Level, (L_{pA})
Def-Stan 0027:2015	Section 9.3 Required Noise Data • Maximum C-Weighted Peak Sound Pressure Level (L_{Cpeak}) • Maximum C-Weighted Sound Pressure Level with fast time constant, (L_{CFmax}) • Maximum A-Weighted Sound Pressure Level with fast time constant, (L_{AFmax}) • A-Weighted Sound Exposure Level for a known specified number of events (L_{AE})

MIL-STD 1474E:2015	Section 4.9.1 Metrics
	• Overall SPLs:
	  ○ Unweighted SPL
	  ○ A-Weighted SPL
	  ○ C-Weighted SPL
	• Unweighted Peak SPL
	• Octave Band SPLs:
	  ○ Full Octave Band SPL (for areas where HPDs or communication devices are worn)
	  ○ One-third Octave Band SPL (for areas where speech intelligibility is to be determined or if the source has any tonal components)

Table 2 - Measured Noise Parameters according to BS EN 458:2016, DEF-STAN 00:27 2015 and US MIL-STD 1474E:2015

The measurements listed by DEF-STD 27 are recommended by Brueck (2016), in order to assess both instantaneous personal noise exposure and daily personal noise exposures against the criteria set-out in the Control of Noise at Work Regulations. The sound exposure level of a blast event may be relevant for smaller sources at Spadeadam, such as EDH tests, where numerous repetitions of tests may be performed within a single 8-hour day. According to Brueck (2016), there is also a risk associated with the $L_{AEq,8hour}$ and given that this parameter also has both upper and lower daily/weekly action values and limits set out in the Control of Noise at Work Regulations, it is necessary to determine.

According to notes in section 7 of DEF-STD 0027, the measurement procedure should be carried out at a time that reflects the worst-case personnel exposure, but consideration should be taken to account for operating conditions outside of ‘normal’ conditions. Additionally, where personnel locations are known and are stationary, measurements should be taken at these locations in order to be representative of personnel exposure. Further to this, measurements should be taken at heights of 1.6m above the ground and 0.8m above seats respectively for standing and sitting stationary head positions.

Any normal reflective surfaces that would be present during normal operating conditions should not be excluded from the measurement, as the reflections may increase the resulting sound pressure levels at the receiver point and therefore should be accounted for. Notes on the type of ground between the source and receiver should also be documented, for later use during analysis.

Microphone Orientation

Brueck (2016) advises that a free field microphone be oriented so that the transducer is perpendicular to the sound source. Brueck also advises that pressure-response microphones be pointed upwards, so that the sensing surface is parallel to the direction of the incident blast wave.

MIL-STD1474E provides very specific guidance for various transducer types and differing measurement environments. The orientation guidance agrees with the guidance proposed by Brueck, where for blunt, cylinder shaped transducers the US DOD standard advises that transducer surfaces are pointed upwards. The following figure from MIL-STD 1474E illustrates this orientation respective to the direction of an incident blast pressure wave.

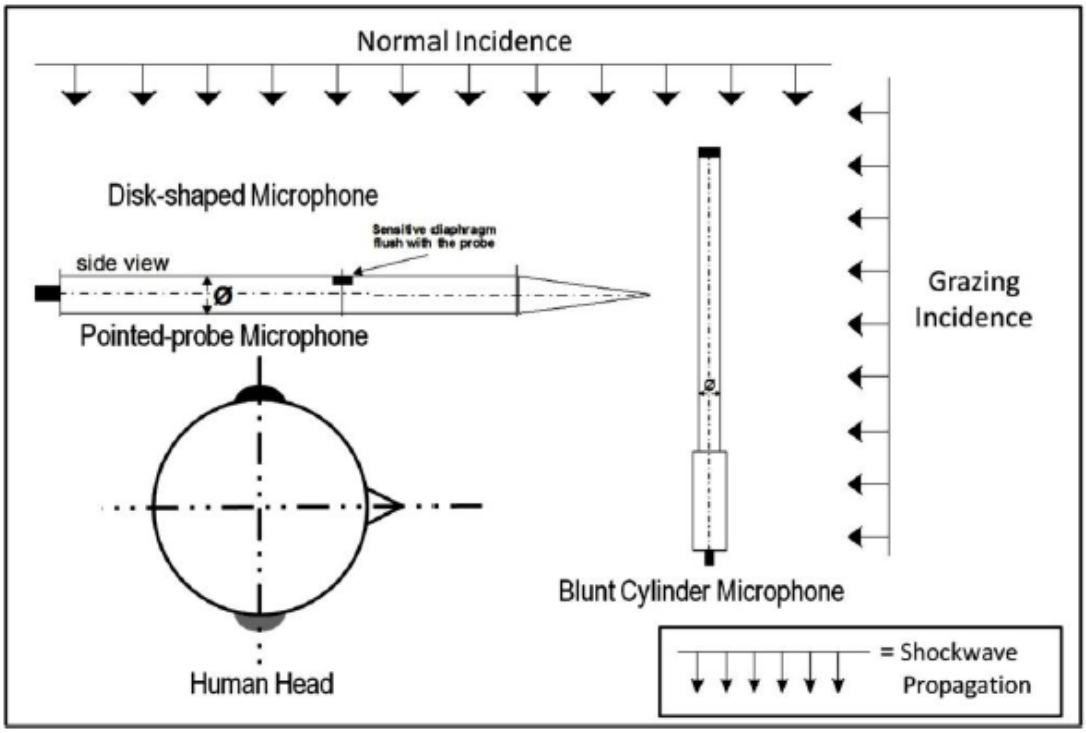

Figure 9 - Blast wave angle of incidence with respect to various sensors. Adapted from US MIL-STD 1474E:2015

MIL-STD 1474E gives additional guidance on the accurate measurement of incident pressure waves using probe microphones where it states that any direct or reflected sound at a non-grazing angle of incidence should be no more than 10° from the true angle of grazing incidence. The figure shows that all microphones types should be oriented to measure at grazing incidence, as normal-incidence should be avoided, where it can lead to an increases in pressure and overestimate peak sound pressure levels, due to reflection off the surface of the diaphragm (Department of Defense, 2015). By pointing a pressure response microphone perpendicular to the source, the effects of diffraction around the microphone due to its influence in the sound field.

Section 4.7.2.3 of the standard also suggests that for the purpose of defining risk, multiple measurements should be taken to account for varying angles of incidence, introduced by effects causing deviations of sound propagation in to the ear, such as head diffraction and reflections (Department of Defense, 2015).

2.2.2.3 Surface Waves

The nature of blast wave additionally introduces vibrational effects on measurement equipment that should be account for in order to ascertain accurate readings. Such affects arise from ground-borne vibration and surface waves associated with the blast event. Although smaller diameter microphone are less-sensitive to sound waves, Brueck (2016) describes them as having a higher response to vibration. This means that the use of vibration isolation with microphone mounts such as tripods, is necessary for environments where structure borne vibration may occur.

The purpose of this section of the literature review was to indicate how measurements of blasts are influenced by their physical characteristics of the instrumentation and the blast itself. It is critical to understand how they to the mechanisms of hearing loss, and how these mechanisms can be attributed to specific physical properties of a blast wave.

2.2.3 Near Field Human Response to Blast Noise

Hearing loss exists in many forms, and there are many causes, such as from noise, aging or infection. A reasonably large amount of research has been conducted on the many types of hearing loss, specifically on noise induced hearing loss, as it is in the best interests of industry to reduce its impact on its employees. However, most of the research originated in the medical industry and by the military. The research has revealed many problems with noticing NIHL but moreover, detecting that hearing loss in one individual resulted from a given exposure. This is because NIHL is cumulative over time, from many exposures. However, the NIHL associated with blasts is not vastly different from general NIHL in terms of hearing loss with frequency. Not only this but for a given population there is a very large individual susceptibility to noise induced hearing loss. Hearing loss from noise is not always obvious due to loud sounds still perceived as loud (‘Recruitment’), whilst quiet sounds are inaudible (Joris, 2009) The same effect occurs with hearing loss from ageing or disease and therefore making it difficult to identify the cause, as discussed in M. C. Liberman (2017).

The vast amount of research has revealed that many mechanisms of hearing loss exist, at many anatomical sites within the ear. In order to understand noise induced hearing loss and where the damage of associated blasts trauma occurs, the general anatomy of the ear is presented, as described in chapters 1 and 2 of Roberts (2002).

2.2.3.1 The Ear

The anatomy of the ear is split into 3 main sections, namely, the outer, middle and inner ear, before reaching the Central Auditory Nervous System (CANS). The role of the outer ear is to direct sound energy into the ear canal towards the tympanic membrane (ear drum). From here, the sound is transferred to the middle ear, which consists of the ossicles, a 3-component interconnected bone structure. The role of this section is to amplify sound energy, before it reaches the inner ear. This is achieved through the movement of the stapes onto the oval window, by concentrating vibrations of the ossicles onto a smaller area, known as the stapes footplate, with the same force. This is an essential mechanism for reducing the impedance discontinuity between an air-filled middle ear and a fluid filled inner ear.

Inner Ear

The last component of the middle ear, the stapes, transfers its energy to the inner ear by pressing on the oval window, which is the first entry in to the cochlear. The cochlear is a spiralling structure of 3 chambers with many components to encode the temporal, dynamic and frequency characteristics of an incoming sound stimulus.

Beyond the other side of the oval window is a fluid filled chamber that loops back around to the basal end of the cochlear to the round window. This chamber is separated into two parts, with the top one connected to the oval window called the Scala Vestibuli, and the bottom half connected to the round window, the Scala Tympani. There is a point which connects both at the apical end of the chamber called the *helicotrema*. The fluid within these chambers is rich in sodium (Na^+) and calcium (Ca^{2+}) ions called *perilymph*, similar in composition to cerebrospinal and extracellular fluids. In between these chambers is another, the scala Media, containing an intracellular fluid known as *endolymph,* rich in potassium (K^+) ions (Kurabi, Keithley, Housley, Ryan, & Wong, 2017; Roberts, 2002).

At the 2 boundaries that reside between each scala vestibula and the scala media is *Reissner's Membrane* and at the boundary between the scala media and the scala tympani is the *basilar membrane*. As a sound wave is transferred from the oval window and motion is set up within the fluid filled chambers, causing the upward and downward vibrations along the basilar membrane.

Situated on the basilar membrane is the *organ of Corti* which runs the along the length of the cochlear. This element contains the sensory and non-sensory cells responsible for encoding a sound wave and providing feedback from the brain to the auditory system, the *inner* (IHC)

and *outer hair cells* (OHC). These cells have rows of *stereocilia*, whose deflection is the first process of electromechanical transduction of sound. These hair cells are deflected due to contact with another membrane at the top of the organ of Corti, called the *tectorial membrane*. This membrane slides horizontally over the tips of the stereocilia depending on the corresponding movement of the basilar membrane.

The basilar membrane has many physical properties that conserve the frequency characteristics of an incoming sound wave. To put it crudely, high frequencies result in a peak membrane displacement near the basal end, and low frequencies correspond to peaks at the apical end of the membrane. Therefore, a particular frequency exhibits a greater membrane displacement at a given point along the membrane, resulting in the upward motion of the corresponding hair cell (or number of hair cells), situated above that part of the membrane.

This motion results in hair cell contact with the Tectorial Membrane, situated above the hair cells, however, this membrane moves laterally, deflecting the stereocilia horizontally around their pivot point where they fuse at the top of the hair cell body. This is the active mechanism for sending information to the brain. For a given frequency, results in the movement of a particular region of the basilar membrane, leading to the movement of a particular area of hair cells and therefore their corresponding bundles of stereocilia. As these are deflected by the tectorial membrane above, the bundles deflect together as they are interconnected by extracellular strands called *tip links*. This tissue is paramount, as the stereocilia are sequentially organised along a hair cell progressively increasing in height, and therefore only the tallest hair cell contacts the tectorial membrane. The connecting tip links between each cilium means that they are all deflected according to the direction of the tallest tip link.

The relevance of this anatomical set up is in how the various parts of the hair cell are bathed in the different fluids, where the body of the hair cell is surrounded by perilymph and the stereocilia are surrounded by endolymph. During the displacement of stereocilia by connection with the tectorial membrane, the opening of mechanosensitive channels allows the flow of calcium ions from the endolymph down to the hair cell body, due to the difference in electrical potential and ionic composition between the two fluids. This in turn results in synaptic transmission of auditory information to the Central Auditory Nervous System through the liberation of neurotransmitters. Roberts (2002) offers two explanations as to how these mechanosensitive channels open, given the rapid temporal characteristics they would

need to possess at such high frequencies. The first hypothesis is that deformation of the stereocilia causes mechanical linkages to open. Another hypothesis is that the tension upon the interconnecting tip links causes these channels to open or close according to the direction of the hair cell motion. The literature suggests that the latter hypothesis is favoured, as this explains why hair bundles are sequentially ranked according to height, where deflection towards the tallest stereocilia will open the channel and close the channel when deflection is in the opposite direction.

Finally, the electrical potential between the two cochlear fluids is paramount for the response of the hair cell, where it controls the release of a chemical transmitter onto a connecting afferent nerve (Roberts, 2002). Through the modulation of the receptor potential at the bottom of the hair cell, the auditory stimulus is represented by the increase and decrease of action potential firing rate controlled by hair cell depolarisation and hyperpolarisation respectively. Moreover, for this work, it is the appreciation of the cochlear fluids and their influence within the stereocilia's mechanosensitive channels that is fundamental for understanding the mechanisms of inner ear hearing loss.

2.2.3.2 Mechanisms of Hearing Damage and Noise Induced Hearing Loss

The mechanisms of *noise induced hearing loss* (NIHL) have been pursued extensively by the scientific community. Given the complexity of the auditory systems anatomical structure, NIHL is an extremely complicated and variable phenomenon that can manifest from varying combinations of noise related trauma. For example, mechanisms of damage can accumulate from many years of high noise levels, or it can result from a single event of acoustic over-stimulation. Moreover, it can result from a combination of both. Therefore, for a given individuals hearing loss to be understood, an understanding of where various mechanisms of NIHL occur within the pathway of the auditory system is essential.

Roberts (2002) categorises types of NIHL as *conductive* and *sensorineural*, depending on where the mechanism of loss occurs within the auditory system, where the former refers to the outer and middle ear sections and the latter refers to the inner ear and central auditory nervous system. A number of blast injury studies claim that overall the auditory system is the most vulnerable to injury and is therefore the most frequently observed injury following blast exposure (Mizutari, 2019). Otologists face many varying cases of blast induced auditory injury, and in the last decade, many studies have taken place to determine the mechanism of injury based on their anatomical site. In many cases, conductive hearing loss is treatable, or

may recover spontaneously and therefore temporary, whereas sensorineural hearing dysfunction is permanent (Mizutari, 2019). Cochlear hair cells do not regenerate, and when destroyed by high intensity sound, permanent deafness is caused.

Outer-Ear and Middle-Ear Mechanisms

Tympanic Membrane Injuries

According to Mizutari (2019), the tympanic membrane (TM) is the tissue that is most vulnerable to blast exposure in the human body. This work describes the high number of cases of tympanic membrane perforation (TMP) for victims of various bombings. Mizutari (2019) continues to explain the high number of spontaneous healing rates of TMs following perforation, usually found within military situations, compared to unusually low rates found in civilian related blast events, with the latter caused by a build-up of shrapnel or debris within the outer ear after blast exposure.

Thorough research on TMPs is documented in a review of auditory blast injury's by Garth (1994), where a study in the early 20th Century was carried out to determine the lowest static overpressure of TMPs (Zalewski, 1906). Garth goes on to explain how the work of Stinson (1985), found that the levels of stress during blast exposure far exceed the normal stress limits of the TM, causing changes in its mechanical properties, such as stretching its radial fibres, leading to greater compliance. The contribution to TMP from the transience of the blast wave has been debated. During the positive phase of the blast, the TM obtains a degree of cushioning support from the ossicles, where the pressure increases inside the middle ear due to the decrease in volume. Garth (1994) offers evidence to suggest that TMs were more likely to be perforated under *static* negative pressures, where the TM gains no support from the ossicles. A counter argument presented by Garth is that, TM injuries are more a consequence of the positive impulse pressure, due to the associated risk of cholesteatoma development (a build-up of TM fragments resulting in infection) within the middle ear.

Ossicular Injuries

Choi (2012) lists the sheer amount of potential injuries to the ossicles, such as disarticulations, fractures and dislocations of the ossicular chain components, where the most commonly observed injury was joint disruption between the malleus and incus (incudo-malleolar joint disruption).

Inner-Ear Mechanisms

Temporary sensorineural effects within the inner ear, such as temporary threshold shift and tinnitus, following blast wave exposure can occur. Though, these effects can subside gradually, or in some cases be permanent. The mechanisms of damage within the cochlear extend from the idea of stereocilium fatigue to cellular processes resulting from chemical changes within the hair cells.

Morphological Changes from Mechanical Damage

Within the review of blast induced auditory injuries by Choi (2012), the idea of mechanical damage on the inner-ear components is discussed. This is where large amplitudes exerted on the BM can rupture both IHCs and OHCs from the organ of Corti. Further to this, the integrity of the organ of Corti membrane is compromised, leading to changes in its permeability or holes, where cochlear fluids can mix (discussed below). Choi explains that OHCs were most likely to succumb to morphological changes, such as disarrangement, swelling or dis-attachment, and that these effects were more likely to occur on HCs located near the basal end of the cochlear. From this, one can speculate that damage from this mechanism is more likely to result in hearing loss of higher frequencies.

A review of 3 separate studies by Roberto, Hamernik, and Turrentine (1989) of blast exposure performed on animals found that the most profound damage in the cochlear was the dislocation of the organ of Corti from the basilar membrane and associated fractures of the surrounding tissue.

Mixing of Cochlear Fluids

A study by Kurabi et al. (2017) suggests that intense sounds can compromise the structure of the sensory epithelium, or the hair cells main body (Choi, 2012), which forms the barrier between the endolymph and perilymph fluids. Kurabi et al. (2017) states that hair cell death can occur from their exposure to high potassium levels in perilymph. A similar idea is discussed in an earlier study by Talaska and Schacht (2007), where chemical influx into the hair cells cause imbalances in redox homeostasis, leading to the activation of cell death pathways. Grant postulates that the mixing of perilymph and endolymph fluids within the cochlear is also a cause for temporary sensorineural effects, within the inner ear, such as temporary threshold shift and tinnitus. Within Grant's review, permanent damage is said to conversely be associated with the effects such the detachment of the organ of Corti and actual

stereocilia defects, including permanent bending and breakage, found in blast exposures on Chinchillas by Hamernik, Turrentine, Roberto, Salvi, and Henderson (1984).

Cochlear Synaptopathy

On the other hand, a review of preclinical studies by Kobel, Le Prell, Liu, Hawks, and Bao (2017) suggests that it is the synaptic connections between inner-hair cells and its connecting spiral ganglion neuron that is most susceptible to damage from noise. Other studies (Cho et al., 2013; Mizutari, 2019) and current research (Kujawa, 2019) have also supported this idea that the most vulnerable component of the inner ear is the synaptic connection between a hair cell and the sensory neurons. This is called cochlear synaptopathy, and is a concern to researchers of this field, where the condition can be found in ears with intact hair cells and normal audiograms. This has led to the conclusion that a phenomenon known as 'hidden hearing loss' must exist. This may therefore shed some light on individual cases where a permanent threshold shift following many exposures is not detected.

2.2.4 Hearing Protection for High Intensity Impulsive Noise

2.2.4.1 Hearing Protection

The concept that noise exposure should be reduced as much as is reasonably practicable is one that is acknowledged by most national regulations, especially in the UK. This statement aims to apply practices that use hearing protection as a last resort. In industry, employers and equipment manufacturers aim to reduce the personnel exposures at the source of the noise, for example, through the use of acoustical isolation via enclosures, or through vibrational isolation if the sources produces secondary noise from the radiation of partitions in contact with the source. Where personnel exposures are still unacceptable, the noise source may be attenuated during the propagation pathway, for example, through the use of acoustical barriers. Only when an attempt to reduce exposures at the source or during propagation, or if these options are not possible, should attenuation at the receiver be considered, for example, by means of hearing protection.

2.2.4.2 Types of Hearing Protection

In the United Kingdom the main guidance on hearing protection is found in BS EN 458:2016 Institution (2016) wherein, various hearing protection devices are described. Hearing protection devices (HPD's) in the form of *earmuffs* generally consist of cups placed and sealed over each ear and are usually are lined with sound absorbing material. These can also

be helmet mounted for use with head protection. This type of hearing protection differs to *earplugs*, which can be *readily shaped*, *user-formed* or *custom moulded* protection that is inserted into the ear canal. Both earmuffs and earplugs can offer level dependent protection, which according to (Institution, 2016) may be better suited for intermittent or impulsive high level noise.

Various HPD's for impulsive noise provide differing levels of sound attenuation across their respective frequency bands and therefore, care should be taken when prescribing protection for individuals who experience numerous types of impulse noise under normal operational conditions. As stated in Defence Standard 0027, the choice of hearing protection within these environments is unlikely to be influenced by the HPD's attenuation alone, and therefore factors not related to sound attenuation should also be considered (MODUK, 2015). Such factors consist of situational awareness and communication abilities, which may be compromised by the introduction of HPD's. Hence, providing the maximum amount of attenuation is not usually a desirable attribute, given that this is likely to cause overprotection. Commonly, in many occupational environments where high level impulsive or explosive noise may occur, such as on offshore/onshore oil and gas platforms, factories, or military training environments, special operational conditions and emergencies in the interest of safety take priority over the preservation of hearing.

Other non-acoustical factors such as how ergonomic factors are arguably of equal consideration to acoustical factors. The ergonomic factors of hearing protectors include factors such as comfort, robustness and compatibility with other equipment. Other factors may include improper fitting of hearing protection. A 2009 study carried out by Liz Brueck at the Health and Safety Laboratory for the Health and Safety Executive Executive (2009) found that 3 of twelve groups observed under normal conditions and 1 in 4 groups within outdoor environments had problems with ensuring correct use of hearing protection. Furthermore, 1 in 7 individuals did not use hearing protection properly.

2.2.4.3 Issues with Hearing Protector Attenuation

In reality, hearing protector attenuation is best viewed in terms of Insertion Loss (IL), defined as the difference in sound pressure level at the outer ear canal with and without the hearing protector. This is because the actual hearing protector attenuation is limited by transmission factors via various pathways, such as leakage around the hearing protector, noise produced

within the ear canal by vibration of the hearing protector, sound transmission through the protector and bone conduction through other parts of the head.

Transmission through Personal Protective Equipment

According to studies by R. Davis and Clavier (2016) , Chordekar, Adelman, Sohmer, and Kishon-Rabin (2016) and Clavier, Dietz, Wilbur, Zechmann, and Murphy (2012) the transmission of sound to the inner ear from impulsive sources is possible via conduction of the temporal bone. The main defensive mechanism of hearing protection against continuous sound is to reduce the amplitude of vibrations of the temporal bone. In the study by Clavier et al. (2012), where the influence of head protection on impulsive noise is investigated, the peak level was shown to decrease by 8-12dB. Conversely, head protection, was shown to increase the duration of the impulsive wave inside the head. The physiological effect of this is currently unknown, however, as head protection is often mandatory within environments where an individual might encounter impulsive noise, this should be a consideration when prescribing specific hearing protection in combination with head protection. Conversely, a study by Chordekar et al. (2016) on the effect of flanking through the head found that non-osseous pathways such as soft-tissue were more likely contributors to the transmission of impulses to the inside of the head.

One other aspect of hearing protection design arises from the amplitude response of the hearing protection to a particular wave amplitude, that is, whether the device reacts linearly or non-linearly. The study conducted by Clavier et al. (2012) showed that the amplitudes within the head were linear with the peak input amplitude. According to R. Davis and Clavier (2016), the National Institute for Occupational Safety and Health (NIOSH) found that hearing protectors react non-linearly with blast waves, providing more attenuation. The combination of sound that is transmitted through hearing defender and through bone conduction must be accounted for when assessing risks to hearing.

2.2.5 Legislation and Guidance for the Selection of Hearing Protection for Blast Noise

2.2.5.1 UK Occupational Noise Legislation and Guidance

The Control of Noise at Work Regulations 2005

In the United Kingdom, the current regulations regarding noise in the workplace are enforced by the Control of Noise at Work Regulations (2005). This legislation applies to all employers,

with the exception of the special circumstances such as the MOD under special operational conditions, i.e. emergencies, during conflict. The details of this legislation are deeply rooted in industrial noise policy, where the first piece of legislation was The Noise at Work Regulations 1989. This work contained only one limit regarding *peak sound pressure levels,* covered under a daily personal noise exposure of an employee of 200 Pascals (140dB).

The current regulations in the UK were introduced following the updated European Physical Agents Directive 2003/10/EC – Noise in 2003. The objective of this was to introduce mitigation measures for employers to protect workers according to a newly defined set of risk predictors based on physical parameters, namely, a *daily* and a *weekly noise exposure level* and a *peak noise exposure level*. Consequently, legislation in the U.K. became The Control of Noise at Work Regulations 2005, which introduced a reduction in the risk predictors, along with requirements regarding personal protective equipment such as personal hearing protection devices, where mitigation through noise control measures at the source or during propagation were not possible.

The current version of the guidance defines lower and upper action values along with an exposure limit value which must never be exceeded, defined in the table below.

Risk Predictor	**Average Daily or Weekly Sound Pressure Level (dBA)**	**Peak Sound Pressure Level (dBC)**
Lower Action Level	80	135
Upper Action Level	85	137
Exposure Limit	87	140

Table 3 - Exposure Limit Value and Action Values adapted from The Control of Noise at Work Regulations 2005 "The Control of Noise at Work Regulations" 2005)

Usually, the daily or weekly sound pressure levels are the most common parameters that form limiting factors for industrial noise. However, noise from sites concerned with blast noise will depart from industrial applications due to the large variations in sound pressure levels from day to day. This leaves the exposure limit value for peak sound pressure levels of 140dB as the first limit which at ear noise levels must be reduced to through means of noise control. The regulations state that where employees are exposed to noise levels at the ear between the upper action and exposure limit levels, then the employer must provide hearing protection and ensure that they are used by the employee (section 84b). The employer must

also provide guidance on how the hearing protection devices should be worn and cared for. Where noise levels lie between the lower and upper action limits, then hearing protection should be provided where an employee asks for it, but it is not a requirement to make their use compulsory, according to the regulations (section 84a).

Furthermore, the regulations state that, following the outcome of an occupational noise risk assessment where hearing protection is provided, the employer must ensure the hearing protection devices provide suitable sound attenuation characteristics for the noise source of interest. This means that the frequency distribution and temporal character of the noise source should be considered, along with the adequacy of the device for operational use and or use with any necessary personal protective equipment, such as head protection.

In order to undertake an auditory risk assessment against high intensity impulsive noise according to the guidelines within the Control of Noise at Work Regulations 2005, the best practice guidance in the U.K. is set out in the hearing protection standard (BS EN 4582016). This standard currently specifies 4 methods for assessing hearing protection attenuation against a given sound type and the recommended methodology for impulsive noise is the HML method. The standard has predominantly concerned blasts from smaller explosive sources, or impulsive sound from industrial origin. The MOD standard Defence Standard 0027:2015 (MODUK, 2015) has an extended version of the HML method, based on a previous revision of BS EN 458. However, the sources at Spadeadam are also beyond the scope of this standard. This standard however, is the best guidance in the UK and therefore, an assessment of occupational impulsive noise risk should be made by following either one of the procedures set out in the above standards, and then by referring back to the action levels set out in The Control of Noise at Work Regulations 2005. The limitations of these standards are discussed in detail in this section of the literature review chapter.

2.2.6 Methods for the Selection of Hearing Protection for High Level Impulsive Sound

2.2.6.1 UK Guidance

BS EN 458:2016

Four assessment methods are presented within BS EN 458:2016 for the determination of hearing protection attenuation, namely the;

- Octave-band method;
- HML method;
- HML check method;
- SNR method

From these methodologies, only the HML method is suggested for use with impulsive noise, and its procedure is described in Appendix B of the standard. Although, some high-level impulsive sources are included, most of the noise sources in Appendix B are atypical of the explosive sources at DNV GL Spadeadam, as they are limited to those of an industrial character. Furthermore, the method is restricted to explosives with equivalent TNT charge masses of up to 8kg.

The *HML* method, for a given hearing protector, uses the high (H), medium (M) and low (L) attenuation values provided by the manufacturer, obtained in accordance with BS EN ISO 4869-2:1995. This shortened method characterises the source's frequency components and predicts the *effective C-Weighted Peak SPL* (L'_{pk}) and the *effective Equivalent A-Weighted SPL* ($L'_{A,eq}$) at the ear. An assessment is made by comparing these values with the relative national regulations, where a value between 5dB and 10dB below the national regulations is acceptable. These metrics are calculated as follows.

$$L'_{Cpk} = L_{Cpk} - d_m\ [dBC]$$

$$L'_{Aeq} = L_{Aeq} - d_m\ [dBA]$$

Where, d_m is the modified sound attenuation value of the hearing protector, found according to the following table.

Noise Type	**Modified Sound Attenuation Value, d_m (dB)**
1	L-5
2	M-5
3	H

Table 4 - Modified Sound Attenuation Values according to Appendix B of BS EN 458:2016 Institution (2016)

Where noise sources are categorised based on their frequency distribution, impulses with most of their acoustic energy distributed in the lower, middle or high frequency ranges are classified as Type 1, 2 or 3 respectively. Given that explosions are low frequency dominated, noise type 1 would be of most interest to this work but as previously mentioned, BS EN

458:2016 excludes explosions of charge weights above 8kg and therefore, excludes most explosive sources at Spadeadam.

MODUK DEF-STAN 0027:2015

For noise sources exceeding the limitations of BS EN 458:2016, the current best practice in the United Kingdom is to refer to DEF-STD 0027:2015 MODUK (2015). DEF-STD 0027:2015 is specifically concerned with the measurement of impulse noise from military weapons, explosives and pyrotechnics (MWEP's), and consequently, the selection of hearing protection against this type of noise. This document is an extension of the 1994 version of BS EN 458 Institution (1994), where the HML method includes further modified hearing protection sound attenuation values, which are also based on source frequency characteristics. At the time of the 2015 DEF-STD 0027 review, the latest version of BS EN 458:2004 provided limitations in the form of even more generic noise categories, such as 'rifles'. This provided motivation for the MOD to extend the scope of this method to include larger and more low frequency dominated sources from the likes of MWEP's (MODUK, 2015). The outcome of the latest DEF-STD 0027 review was a table with extended noise type categories, shown in Table 5 below.

LCFmax – LAFmax (∂)	**Modified Sound Attenuation Value**
≤ 0	H
> 0 to 1	M
> 1 to 3	M-5
> 3 to 5	L or M–5 if a lower value
> 5 to 10	L-5
> 10	Conditional use of L–5. See 12.7

Table 5 - Modified Sound Attenuation Values for different impulse sounds according to DEF-STD 0027:2015 MODUK (2015)

Converse to the 2016 version of BS EN 458, sound source frequency distributions are determined according to the *difference in C-Weighted and A-Weighted Maximum SPL's (∂),* leading to 6 noise type categories. Each category consists of a corresponding modified sound attenuation value. Most of the sources of interest to at DNV GL are categorised by having a ∂ in excess of 10dB. DEF-STD 0027:2015 states that there is a "conditional use" of L-5 for ∂ values in excess of 10dB, where in this category, approval should be sought by the Ministry

of Defence before carrying out assessments with this method, stated in section 12.7 of the standard MODUK (2015). Brueck (2016) states that even using this extended method to estimate HPD attenuation is unreliable for low frequency sounds with ∂ values in excess of 10dB.

The defence standard is reviewed every 5 years as a requirement, and this method is said to be under review in order to extend the HML method to include noise sources beyond the scope of BS EN 458:2016 and the current DEF-STD 0027 method.

The purpose of the defence standard is to perform the HML method using these extended frequency categories and the corresponding modified attenuation value to obtain an effective peak sound pressure level L_{Aeq} at the ear as follows.

The effective at ear sound pressure levels are then presumed to be compared with the regulations set out in the Control of Noise at Work Regulations 2005, as in BS EN 458:2016.

The advice given in DEF-STD 0027:2015 is not applicable to level-dependent hearing protectors.

2.2.6.2 Other Standards and Guidance

ANSI/ASA 12.42 – 2010

The ANSI standard is of relevance to Spadeadam in that it provides a calculation method specifically for assessing the insertion loss (IL) of hearing protectors against impulsive noise. Through the use of the method based on transfer functions, the standard provides guidance on the instrumentation requirements, in addition to data reduction techniques. Annex H outlines the MATLAB code needed for calculating the insertion loss from an impulsive source and the uncertainties for this are accounted for within Annex G of the document. Additionally, the standard discusses bone conduction limits for hearing protection devices with in para 9.6.3 of the document, according to Department of Defense (2015).

Three free-field peak impulses with ranges of levels between 166 and 170dB, 148 and 152dB and 130 and 134dB are needed to perform the method for assessing insertion loss from impulsive noise in ANSI 12.48, according to Williams (2012). These impulses must also contain A-durations between 0.5s and 2ms. Through these parameter definitions, the non-linear behaviour of hearing protection devices within impulsive environments is captured (Department of Defense, 2015). Following some signal processing such as truncating, filtering and frequency analysis (both FFT and IFFT) with specifications defined within the

body of the standard, an average frequency dependent transfer function from the measurement device representing a level after hearing protection to an unprotected ear is derived. The impulsive peak insertion loss (IPIL) is then calculated as the peak sound pressure level of the unprotected ear signal minus the peak sound level of the measured protected ear (Williams, 2012).

ANSI/ASA 12.68 – 2007

The ANSI/ASA 12.68:2007 document provides 3 calculation methodologies for the determination of the A-Weighted SPLs when a hearing protector is worn, with use of the hearing protector's attenuation data. Although an American standard, it's relevance to Spadeadam is that it extends the HML method to include sources with lower frequency distribution than those included in DEF-STD27 and BS EN 458. The extension is within the NRS graphical method (NRS(G)), which extends the difference in C and A Weighted SPLs to around 16dB, compared to 10dB in DEF-STD 27. The NRS method is an assessment methodology, used to obtain a parameter known as the Noise Reduction Statistic.

US ARL MIL-STD 1474E:2015

The aforementioned US MIL-STD 1474-E: 2015 is a document that describes the measurement procedures and conditions for establishing noise limits to promote personnel safety, speech intelligibility and security from acoustic detection within the context of US army operations. The state-art-methodology exists within the physical modelling section of the impulse noise assessment in MIL-STD-1474-E:2015. Appendix B of the standard, establishes impulsive noise level limits, where impulsive noise levels exceed 140dB at personnel occupied areas. Impulsive noise limits should be established by either of the following metrics:

- Auditory Risk Units (ARU); or the
- A-Weighted Equivalent Continuous Impulse Sound Pressure Level ($L_{IAeq100ms}$)

ARUs are discussed in detail within the physical modelling section of this literature review chapter.

$L_{IAeq,100ms}$

This parameter stems from the equal energy model, which characterises the A-Weighted equivalent total energy of the impulse of 100ms (Department of Defense, 2015). Within blast noise literature, this is typical of most impulsive noise definitions, however, impulses particularly from gas explosions, can have significantly longer durations. 100ms is likely to

be too short to account for most of the impulse durations of explosions typical at Spadeadam, the parameter may be modified to assess the equivalent sound energy over longer durations. It works in a similar way as a sound exposure metric, which aims to assess the impulsive noise dose for a single impulse and then extrapolate to obtain the equal equivalent energy over an 8-hour working day, $L_{Aeq,\,8hrs}$. The only difference is that is characterises the exposure over 100ms (or its extended time interval) rather than 1s as in a sound exposure level measurement.

For A-durations less than 2.5ms:

$$L_{IAeq,8hr} = L_{IAeq,100ms} - 54.6 - 1.5 * 10\log_{10}\left(\frac{A-duration}{0.2\ ms}\right)$$

(Department of Defense, 2015)

For A-durations greater than 2.5ms:

$$L_{IAeq,8hr} = L_{IAeq,100ms} - 71.0$$

(Department of Defense, 2015)

Considering the simplicity of this metric, the nonlinear behaviour of hearing protection under high level impulsive conditions is still captured (Department of Defense, 2015). The additional benefit of using this metric is the lack of computing power needed to perform such simple calculations. Furthermore, the metric is based on the well-studied $L_{Aeq,\,8hr}$ metric which is familiar in the context of European and British legislation and guidance. However, this version adapted specifically for impulse noise has not been systematically evaluated or peer-reviewed, according to Department of Defense (2015).

2.2.6.3 State of the Art Methods and Metrics for Assessing Auditory Damage

Physical Modelling – Auditory Hazard Assessment Algorithm for Humans

Thorough studies on the physiological effects of blast noise have been carried out in the United States and are incorporated into a hazard assessment algorithm within MIL-STD 1474-E:2015.

The most reviewed and successful physical model is the Auditory Hazard Assessment Algorithm for Humans (AHAAH), referred to in MIL-STD 1474E, developed by G. R. Price and Kalb (1991). This algorithm is a physical model of the ear, based on electroacoustic principles to determine damage to hearing of personnel within a military environment. This is a mathematical model which emulates the transfer function from free field to stapes motion in

the middle ear. The middle ear motion is then traced to determine basilar membrane displacement, and ultimately calculate a hazard function for intense impulses. The model requires a time-pressure history as its input, and may be used to assess, various protected, unprotected, warned or unwarned ears, in any combination Department of Defense (2015). By using a physical model, the non-linearities associated with the middle and inner ear can be accounted for.

Auditory Risk Units

Sound pressure levels above 130dB cause non-linear stapes movements, due to the increasing stiffness of its connecting elements (G. Richard Price & Kalb, 1986). According to G. Richard Price and Kalb (1986), this increase in stiffness results in a protection mechanism (for warned ears); a reduced efficiency in energy transfer to the cochlear for high sound pressure levels. This study by Price and Kalb was the preliminary research on this effect vital for formulating the AHAAH model. This work determined the significance of stapes stiffness over other non-linearities associated with the movement of the ossicles. Following tracing of energy to the basilar membrane, MIL-STD 1474E describes how displacement calculations are discretised into 23 segments in order to roughly represent 1/3rd octave band, so that frequency encoding across the length of the membrane is maintained. From the squared sum of these peak displacements at each location along the membrane, the hazard is represented by Auditory Risk Units (ARU), as below.

$$ARU = \sum D^2$$

Equation 15 (Department of Defense, 2015)

Where D is the peak upward basilar membrane displacement in microns.

Not only does the model provide ARU's to represent the overall displacements of the basilar membrane to a given waveform, but additionally reveals the envelope of these displacements along the basilar membrane in order to assess the effect of frequency on the displacements. This allows an insight into which components of the waveform are responsible for the highest displacements, such as high frequency components associated with the dynamic pressure change upon arrival into the ears, or the overall impulse length of the blast.

MIL-STD-1474-E refers to this model as one of 2 means for an occupational impulse noise assessment and for prescribing hearing protection against impulsive noise, as it has been

systematically evaluated against a range of datasets and has been peer-reviewed. The ARU metric has also been used as a tool to evaluate auditory risk of hearing loss from airbag deployment in the automotive industry. It is used by at least one other nation and was also supported by the American Institute of Biological Sciences (AIBS) as a means for assessing auditory risk. However, the AIBS proposed that critical assumptions regarding nonlinear stapes movements used within the physical model require further research (Department of Defense, 2015).

Statistical Parameters

Of recent, the advancements in acoustical analysis software with machine learning has resulted in the ability for enhanced signal feature extraction. Further to this, the statistical parameters of a signal are also used to objectively describe waveforms, as a way of classifying signals. The research of this field has led the ability to observe correlations between the statistical parameters of a signal with the risk of auditory impact from the signal. It is recognised that equal energy metrics, such as the $L_{eq,}$ do not account for the temporal variations of a signal. Therefore, by using an equal energy metric alone, there would be no observable difference between the predicted noise induced hearing following two temporally varying signals with overall equivalent exposure levels (R. I. Davis et al., 2012), as the equal energy hypothesis states that NIHL is a function of the total exposure energy alone (Zhao et al., 2010). These two studies investigated how a sample of workers subject to complex non-Gaussian (non-G) noises (those which contained high level transients, such as impacts, impulses, intermittent or other complex characteristics), experienced increased levels of noise induced permanent threshold shifts (NIPTS) compared to a worker sample subjected to Gaussian (G) noises (such as broadband, steady signals). Before these studies, other epidemiological studies showed that workers exposed to other non-G noises (specifically impact noise transients) showed an increased incidence of hearing loss. Further to this animal studies such as those mentioned within Part 4 of this chapter and those by Hamernik et al. (1984), showed high level transient noise exposures resulted in increased levels of hearing loss when compared with equivalent energy G-noise.

The study by R. I. Davis et al. (2012) claims that for noise exposure of equal energies but differing temporal characteristics, kurtosis may differentiate the associated risk of hearing and sensory cell loss between them. *Kurtosis* is a statistical metric that is sensitive to a signal's temporal characteristics, where it is defined as the ratio of the fourth-order central moment to the squared second-order moment of a signal's amplitude distribution.

Clearly, there are several metrics used by within various guidance to assess auditory risk and hearing protection suitability for blast exposures. The state-of-the-art methods differ to those within the U.K. standards and guidance in that they take into account the temporal characteristics of a signal. Furthermore, the output metric of the AHAAH physical model is the only metric that directly addresses a hearing damage metric, as it is an accumulation of upward deflections along the basilar membrane, taking account of which temporal and frequency dependent components on a waveform result in the highest displacements and hence accumulate the most hazard, and consequently the site of the hazard along the basilar membrane.

2.3 Case Study 1 – Confined Vented Explosion Chamber Demonstration

2.3.1 Background

A common type of impulsive noise exposure at Spadeadam results from a demonstration on site known as a Confined Vented Explosion Chamber demo, and is referred to throughout this thesis as CVE. This demonstration is a vital part of the research carried out by DNV on gas explosions. It is mostly used for demonstrations in DNV's Hazard Awareness courses, which they provide as training for industry. The chamber demonstrates the combustion of a confined flammable mixture followed by a sudden external explosion.

As part of this thesis, the purpose of this case study was to investigate whether DNV were providing adequate hearing protection to the personnel viewing the demonstration.

Results from 3 separate field trials are presented in this case study. The DEF-STD 27 assessment methodology presented in Section 2.2 is carried out on each set of results and its suitability for the prescription of hearing protection against this blast demonstration is reviewed.

2.3.2 Theory

During deflagration of a hydrocarbon gas, the reaction zone, or flame front, is accelerated, resulting in the generation of a pressure wave propagating at very high, but subsonic speeds. However, the speed of the pressure wave can be significantly increased when flammable mixtures are confined or are within congested environments, which is often the reality for many industrial environments. Under such conditions, the deflagration of a flammable mixture may transition into detonation, where the flame speed reaches speeds greater than the speed of sound within the unreacted medium. In this instance, the type of blast wave experienced is a shock wave. Explosions from detonations are associated with events such as the bursting of a pressure vessel.

Although shock waves travel at speeds above 1 Mach, they can be completely absorbed during this transition from deflagration to detonation (M. A. Liberman et al., 2010), where flame speeds of the fireball following ignition can travel at speeds above Mach 5. Such violent events exhibit increases in flame speeds due to distortion of the flame from turbulent

effects. Wall friction, high flow velocities near relief vents and obstacles all create turbulent eddies. Larger eddies contribute to an increased surface area of the flame, leading to a faster burning rate for a flammable vapour. Smaller eddies increase the diffusion of heat and mass. During a deflagration to detonation transition, this principle feature resulting from the flame acceleration is the formation of compressed pockets of unreacted flammable mixtures ahead of the flame reaction zone. (M. A. Liberman et al., 2010) describes this as a positive feedback loop mechanism of large amplitude pressure pulses accelerating the flame. The significance of this, is that the pressure exerted by the blast is proportional to the flame speed, essentially increasing the magnitude of the blast and hence the experienced sound pressure level.

Furthermore, flame speeds in vented gas explosions, such as those demonstrated by the explosion chamber at Spadeadam, are described by Lautkaski (1998) to be sensitive to hydrodynamic instabilities between unburned and burned gases. This results in an external explosion, which reverses the flow through the vent.

Such mechanisms create a large deviation in the resulting overpressures experienced from the same blast set-up. Random distributions of a contained flammable mixture can cause a cellular structure within the flame front. The idea of acoustic waves trapped within an enclosure during vented explosions is documented (Fakandu et al., 2016; Lautkaski, 1998) . According to Lautkaski (1998), the acoustic wave is coupled with the oscillating cellular instabilities of the flame front, leading to amplification of the acoustic wave. It is tempting to speculate from this that resonances may cause the deviations in the amplitude of the propagating acoustic wave between tests with the same initial conditions.

2.3.3 Hearing Protection and Assessment Methodology

For the purpose of assessing personnel noise exposures, two contrasting hearing protection devices commonly used on site were assessed for their suitability in attenuating noise from the CVE demonstration. The hearing protection devices were:

- 3M EAR 1100 Plugs
- 3M Peltor Optime III Muffs

The attenuation data from the hearing protection devices taken from the respective manufacturers' datasheets (3M, 2019a) and (3M, 2019b) are plotted in Figure 10.

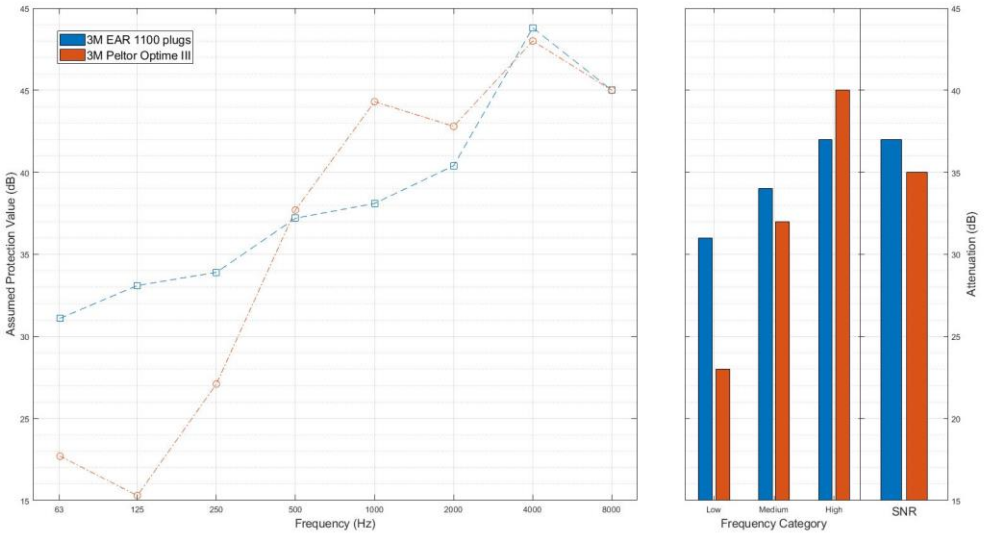

Figure 10 - Attenuation data for hearing protection devices used in the CVE trials.

At the time of the January 2020 field trials, the personnel viewing the CVE demonstrations were given the 3M EAR 1100 plugs. The purpose of these trials is to assess the suitability of this device, and a contrasting earmuff device is used to make comparisons.

The methodology used to carry out this assessment was the DEF-STD 27 methodology, which is detailed within the literature review of this chapter.

2.3.4 Field Trials

CVE field trials carried out under this research program were carried out in January and August 2020. Additionally, historic measurements carried out by DNV from 2016 have been analysed and are presented here.

Table 6 describes the proceedings of the field trials from which measurements of occupational blast noise from a CVE were carried out . During each Explosion Chamber test, the weight of the propane within the chamber was 7 kg, a standard weight representative of the usual hazard awareness demonstrations. Hydrocarbon flammability mixtures are listed for the January 2020 trial, however, this mixture is estimated to be within the range of 4.75%-4.90% in all cases.

Table 6 - Trial plan of tests carried out during the field trial.

Field Trial	Number of Tests	Flammability Mixture (%)	Congestion
2016	1	n/a	No
January 2020	3	4.78-4.86	Yes
August 2020	1	n/a	Yes

2.3.4.1 Demonstration Conditions

The enclosure was filled with 7 kg of propane and was allowed sufficient time to mix with the air within the enclosure. During the January 2020 and August 2020 trials, a scaffolding structure was placed within the enclosure during each test, used on the hazard awareness courses to demonstrate the effect of adding congestion within a confined area during an explosion. The size of the scaffolding structure was 0.1% of the total enclosure volume. Each test run had nominally the same set-up and negligible differences in the mixture were assumed. No congestion was included during the 2016 DNV trials.

2.3.4.2 January 2020

During the January 2020 trials, noise measurements were made at 2 separate locations, using the following instrumentation.

- Brüel &Kjær 2250 Sound Level Meter (Outdoor and Indoor positions)
- Brüel & Kjær Type 4136 1/4" Free Field Microphone Cartridge (Indoor)
- GRAS High Pressure Field Microphone Type 40BH (Outdoor)

All Transducers were situated at a height of 1.5m. The sound level meter used for the outdoor, near-field measurement was hand-held in order to reduce the influence of ground-borne vibration. The indoor sound level meter was mounted on a tripod and positioned in the middle of the hall where site visitors gather. It was placed in the centre of the room to minimise the influence of reflections from nearby indoor surfaces.

Outdoor instrumentation (positions 1) was situated in the centre of the 'viewing area', where personnel are situated during the situation. Indoor instrumentation (positions 2) was situated inside DNV's Lord Cullen Test Centre (LCTC) building, which is the site's main visitor centre, and is the next most sensitive receptor position for this demonstration. The layout of the demonstration area is indicated within Figure 11.

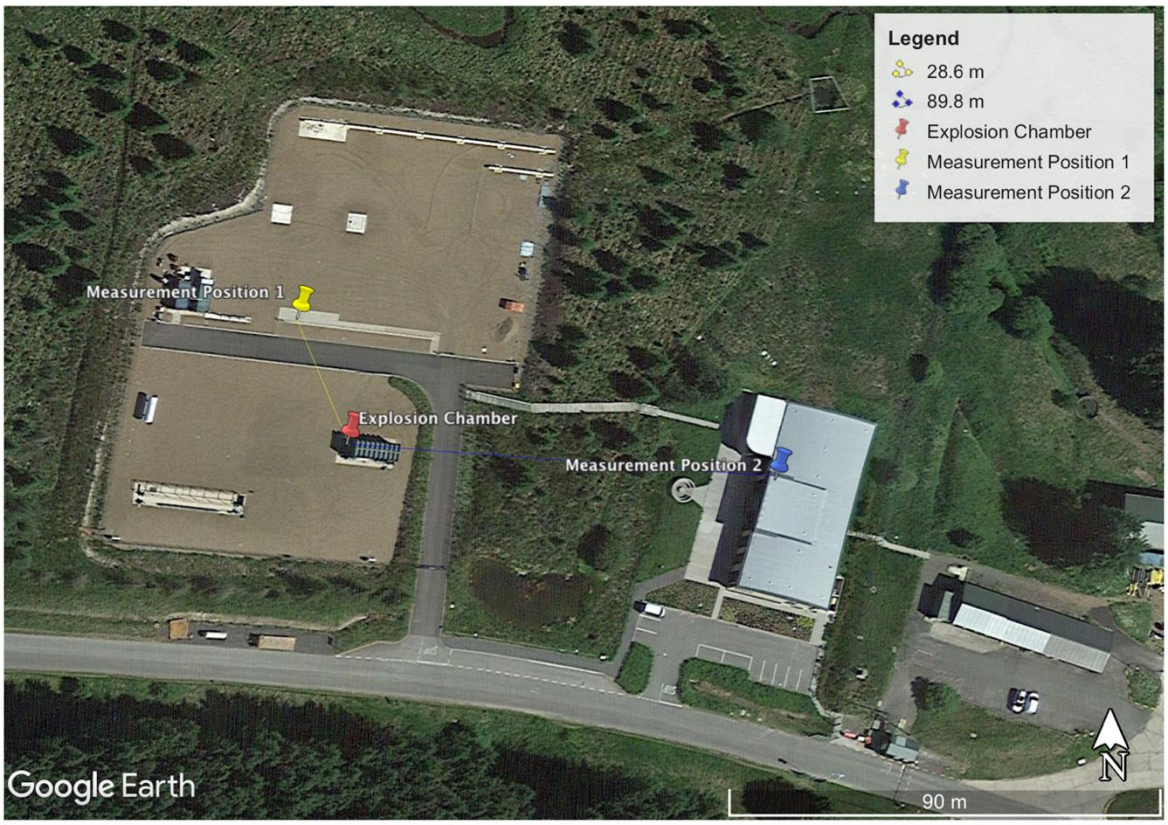

Figure 11 - Measurement Positions during January 2020 field trial.

The purpose of the trial was to determine the magnitude of noise exposures experienced during explosion chamber observations and then assessing the hearing protection provided to these personnel, by using the methodologies described in BS EN 458:2016 or DEF-STD 0027:2015.

Three nominally identical tests involving the explosion chamber were performed, and measurements were carried out under the same atmospheric conditions. Throughout the field trial temperatures remained between 8.7-8.8 °C, wind speeds below 0.5 ms^{-1} and no detectable wind direction.

Table 7 - C-Weighted peak sound pressure levels measured at the observers position during the January 2020 field trial.

Test Number	Measurement Position	LCPeak (dB)	δ (dB)
1	Outdoors	166.6	16.1
	Indoors	130.8	22.3
2	Outdoors	163.8	22.2
	Indoors	127.6	27.1
3	Outdoors	162.2	21.2
	Indoors	129.8	25.3

One notable observation from Table 7 is that sound pressure levels at the outdoor position varied significantly, irrespective of the constant environmental and test conditions. Furthermore a ∂ value of above the 10 dB limit found within in DEF-STAN 0027 was recorded during all tests. From the outdoor positions, this indicates that the blasts from the explosion chamber are more low frequency dominated.

The indoor positions showed LCpeak values below the lower action level of 135 dB within the national regulations, indicating that no further noise control is necessary at the indoor position. The δ value at the indoor positions is larger than outdoor, due to the attenuation of high frequencies by the building façade.

However, the results of this field trial were significant in showing that overpressures measured during explosion chamber demonstrations are beyond the scope of DEF-STAN 0027. This led to another field trial being planned to measure pressure-time histories of the blasts so that they could be investigated more thoroughly.

A worst-case DEF-STD 27 assessment of hearing protection attenuation for the January field trials is shown in Table 7, for the greatest LCPeak value of 166.6 dBC.

Table 8 - Modified Attenuation Values of hearing protection devices (m) according to DEF-STD 27.

Hearing Protection Device	**Modified Attenuation (m) according to DEF-STD 27 (dB)**
3M EAR 1100	26
3M Peltor Optime III	18

Table 9 - DEF-STD 27 Assessment of hearing protection for January 2020 CVE trials.

Measurement	**Hearing Protection Device**	**Modified Attenuation (m) according to DEF-STD 27 (dB)**
1	3M EAR 1100	140.6
	3M Peltor Optime III	148.0
2	3M EAR 1100	137.8
	3M Peltor Optime III	145.8
3	3M EAR 1100	136.2
	3M Peltor Optime III	144.2

2.3.4.3 August 2020 Field Trials

In August 2020 another measurements of the explosion chamber was made, this time using two pressure gauges to make observations specifically within the viewing area.

The following instrumentation was used during the tests.

- PCB Model 137B Quartz ICP Blast Pressure Pencil Probe
- PCB Model 482C16 ICP Signal Conditioner

All Transducers were situated at a height of 1.5m. The positions of these transducers is shown in figure August measurement locations.

Calibration of the PCB Blast Probes is undertaken on-site. ‘Push Tests’ were carried out before each field trial to ensure that the expected signal was present from each probe. Field Calibration of the sound level meters was undertaken using an appropriate calibrator with a 1/4" adapter.

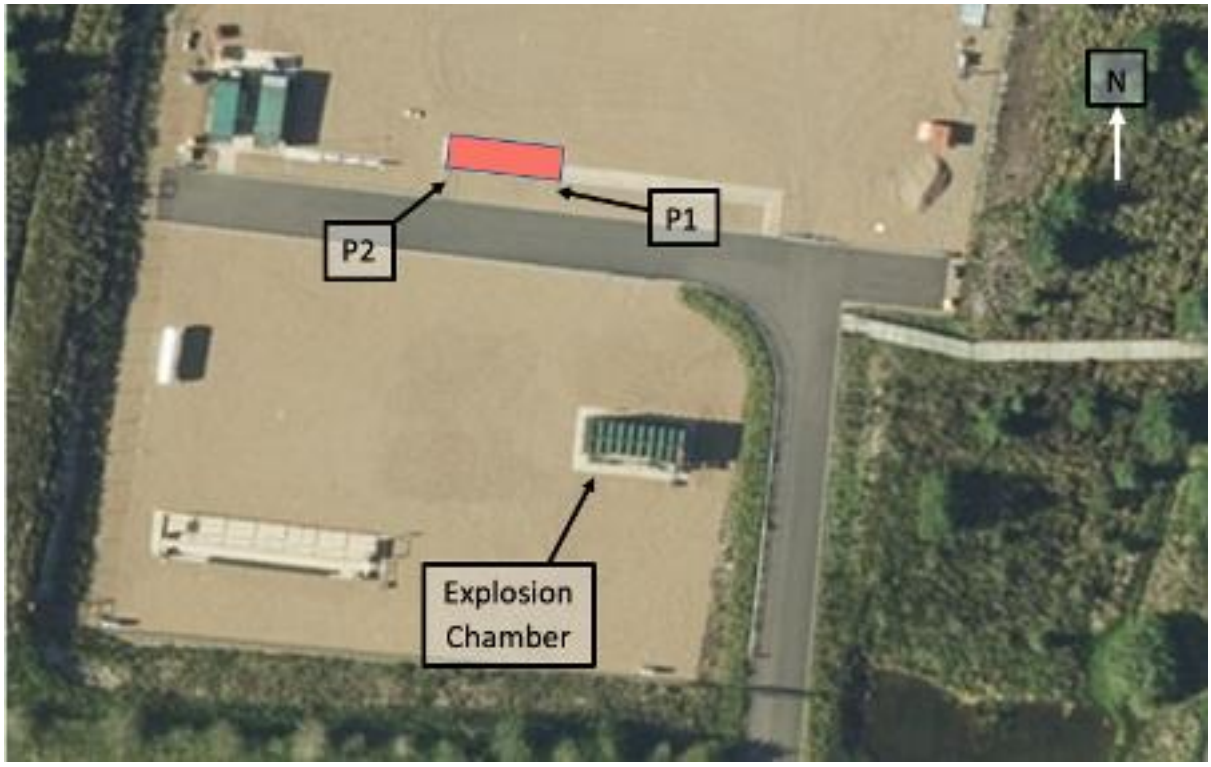

Figure 12 - Measurement locations during the August 2020 trials. P1 and P2 (location of pressure gauge) are representative of the worst-case personnel positions. The red coloured area represents the area that personnel will be present during hazard awareness demonstrations.

2.3.4.4 August 2020 Field Trial Results

Figure 13 shows the recorded overpressure traces from the extremities of the visitor observation positions. Overpressures are measured to be 168 dB Lin (~42mBar) across the two extremities and are assumed to be consistent across the whole viewing area. The consistency in waveform shapes in the pressure traces also provide some reassurance to the measurements.

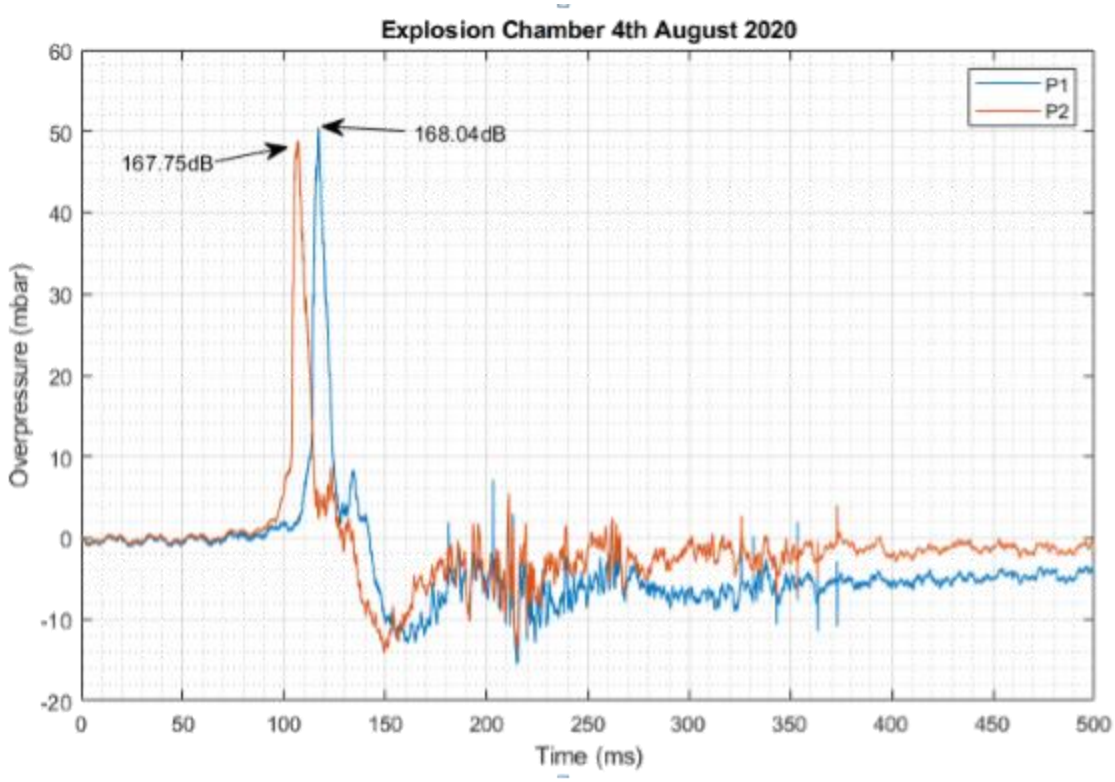

Figure 13 - Recorded overpressures from Explosion Chamber test during August 2020 field trials.

Table 10 - Recorded levels at the observer position during the August 2020 explosion chamber field trial.

Measurement Position	LZPeak (dB)	LCPeak (dB)	δ (dB)
Position 1	168.0	162.5	15.2
Position 2	167.7	163.4	15.2

Following the methodology set out in DEF-STAN 0027, the frequency categorisation of the blast based on the δ greater than 10 dB indicated a modified sound attenuation value of 5 dB at both positions. Given that overpressures were almost identical, a worst-case assessment is carried out, based on the exposure at position 2 which had a greater LCPeak. This was chosen over the measurement with the greater LZpeak on the basis that it is LCPeak that is specified in the assessment criteria of DEF-STAN 0027.

Table 11 - Worst-case at-ear C-Weighted Peak SPLs using DEF-STAN 0027 methodology.

Hearing Protection Device	DEF-STD 00-27:2015 LCPeak (dB)	US MIL-STD 1474E:2015 AHU

3M EAR 1100 Plugs	136.5	0.72
3M Peltor Optime III Muffs	144.6	0.34
No Protection	168.0	88.85

Additionally, the AHAAH model within MIL-STD 1474E was used to calculate AHU this worst case exposure.

Results from the AHAAH model indicate that the over-ear protection device (3M Peltor Optime III) performed better for the august 2020 explosion chamber demonstration. However, AHU's were very low in both cases of hearing protection and were acceptable according to the US MIL-STD 1474E assessment.

Assessments using the UK DEF-STAN 0027 indicated that only the in-ear protection device (3M 1100 In-Ear plugs) provide acceptable attenuation against the explosion chamber test, with the C-weitghted Lpeak below the between the upper action level and action limit within the national regulations. According to the same assessment, the over-ear protection did not provide adequate protection against the explosion chamber demonstration.

2.3.4.5 2016 Explosion Chamber Tests

Finally, data from earlier field trials is analysed to measure overpressures from the same explosion chamber. Although the same mass of flammable gas (7kg) and similar concentrations were used, the test differed due to the absence of congestion within the chamber. The main effect of this is a smaller overpressure being generated by the explosion, and consequently lower noise levels at the observer position.

Only one measurement position was utilised, and was situated within the centre of the same observation area used in both 2020 field trials. Measurements were carried out using the same pressure gauge as in the August 2020 trial, with sampling rates of 200 kHz.

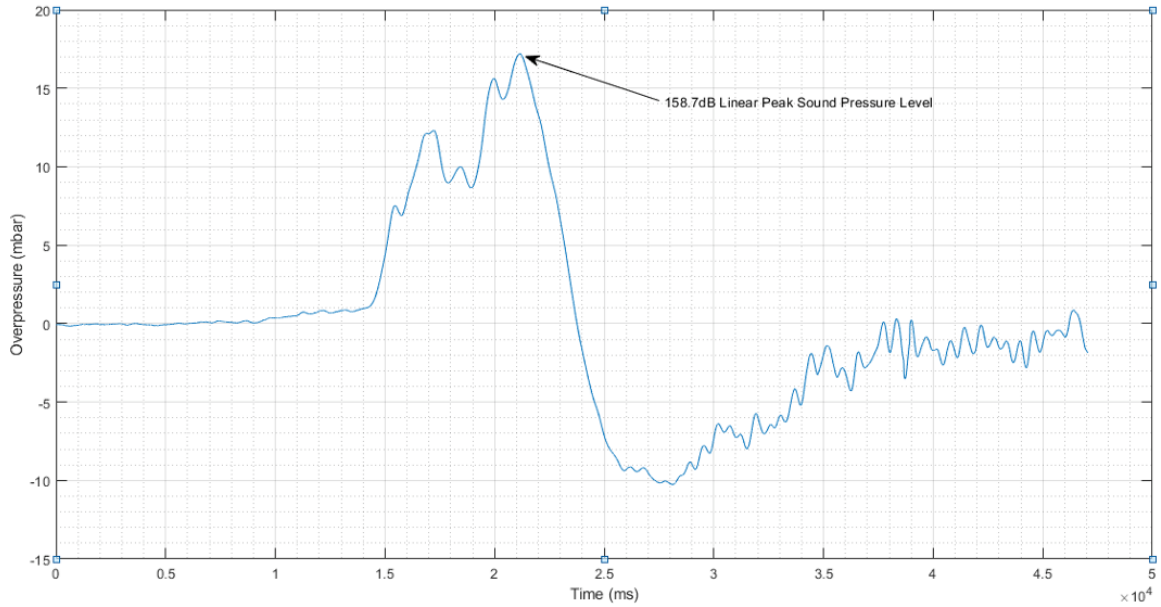

Figure 14 - Overpressures in millibars recorded at external transducer during 2016 DNV GL Explosion Chamber test.

Table 12 - Overpressures converted into peak and maximum sound pressure levels measured at the external position.

L_{ZPeak} (dB)	L_{CPeak} (dB)	δ (dB)
158.7	148.8	19.9

By observation of Table 12, the LCPeak pressure level is less than that measured at same position in both the 2020 field trials. With the absence of congestion within the enclosure during this trial, one should expect a lower overpressure. This is in agreement with the mechanism of pressure increase during the initial stages of an explosion imposed on a flammable source by congestion and confinement.

Further to this, the δ value is within the range experienced at the same position during the 2020 trials. However, the value exceeds that expected within the scope of DEF-STAN 0027, with values greater than 10 dB described by Brueck (2016) to result in unreliable results when using the HML extension method.

Table 13 compares the metrics of two hearing protectors used to describe auditory risk from DEF-STD 0027:2015 and MIL-STD 1474E:2015 for the signal measured during the explosion chamber test.

Hearing Protection Device	Assessment Metrics for Auditory Risk Assessment from the external measurement	
	DEF-STD 0027:2015	US MIL-STD 1474E:2015
	L'_{CPeak} (dBC)	AHU (Warned)
3M 1100 In-Ear Plugs	122.8	0.0083
3M Peltor Optime III	130.8	0.0497

Table 13 - Metrics used for assessment of auditory risk from DEF-STD 27 and US MIL-STD 1474E, during the 2016 DNV trials.

2.3.5 Discussion of results

From the field trials presented above, it has been shown that measured exposures from the CVE are greater when congestion is used within the Explosion Chamber. Each outdoor measurement showed differences in C and A-Weighted LMax,F levels beyond the 10 dB scope of DEF-STD 27. This shows that impulsive noise exposure from this demonstration is low frequency dominated, a common feature of gas explosions. Normally, differences of less than 10dB are expected when assessing hearing protection against blasts, according to DEF-STD 27 however, differences greater than 20dB were observed at the outdoor worst-case position. Note, the delta values for the indoor positions are affected by the building façade. The delta values measured at the outdoor positions would result in unreliable results when using the HML extension method within DEF-STD 27, as described by (Brueck, 2016).

During the January 2020 trials, the measurements show that at the indoor position, exposures were below the lower action level within the national regulations, and therefore no further noise control needs to be implemented. The outdoor measurements show considerable variation in measured overpressure within the viewing area from the demonstration, for nominally the same test conditions and negligible changes in atmospheric conditions. The mechanism for this variation is currently unknown. It is speculated that the random process associated within the initial ignition of the contained flammable mixture leads to instabilities in the noise generating source.

The HML method in DEF-STD 0027:2015 found that at-ear C-Weighted Peak sound pressure levels were just acceptable in 2 out of 3 tests with the foam ear plugs, but were unacceptable during all tests when using the earmuff device. However, without analysis of the waveforms associated with each test, no comparison could be made with the AHAAH model. This may have provided acceptable results, given that the explosion chamber is mainly low frequency dominated and these frequencies do not accumulate auditory risk in the same way according to the principles of the AHAAH.

Moreover, the HML method was invalid in this case, given that the difference in C and A-Weighted maximum levels for each test far exceed the 10 dB limit set out in DEF-STD 0027:2015.

Finally, the August 2020 trial showed that variation in noise exposure across the viewing area is negligible and analysis of the worst-case scenario showed the ear plugs and ear muffs would provide an at-ear LCPeak of 137.4 dBC and 145.4 dBC respectively.

2.3.6 Conclusions from the trials

It is concluded from all the trials involving the explosion chamber demonstrations that personnel exposures from this noise source exist beyond the scope of those specified by the frequency categorisation used in the DEF-STD27 methodology. The significance of this is that the current standard may not be adequate for assessing hearing protection suitability from this kind of demonstration.

Furthermore, the January trials found that there can be considerable variability in personnel exposure for nominally the same demonstration under constant environmental conditions. This is important for the accurate assessment of hearing protection suitability, where variability in LCPeak during the trials was up to 4.4dB, and could be higher. Such variability is at the same magnitude as the difference between action levels within the national regulations.

Extensive measurements should be carried out to address both of these findings, and also to characterise any directivity associated with the demonstration, for use in making accurate long-range blast noise predictions.

2.4 Case Study 2 – Explosive Depth Hardening

2.4.1 Background

Another common explosion test carried out at the DNV site is the Explosive Depth Hardening (EDH) operation. This is an essential industrial process used for strengthening national railway infrastructure.

As part of this thesis, the purpose of this case study was to investigate whether DNV were providing adequate hearing protection to the personnel undertaking the EDH process. This case study is based directly on the findings presented in Manuel and Waddington (2023b) and much of the writing in this subchapter is taken from that paper and is expanded upon for the purpose of this thesis.

As in the previous case study, the results from field trials are presented in here and the DEF-STD 27 assessment methodology is carried out on each set of results and its suitability for the prescription of hearing protection against this operation is reviewed.

2.4.2 Explosive Depth Hardening Operation

This case study is concerned with the impulsive noise generated during the process known as Explosive Depth Hardening (EDH) carried out at DNV Spadeadam. The process is well-established for strengthening materials and is a major part of DNV's operations that supports national transport infrastructure in the UK. EDH is a relatively complex process and has acoustic source characteristics that deviate substantially from the idealized hemispherical explosive often assumed within best-practice guidance and within the technical literature, such as in Baker (1973).

The technology increases the lifetime of railway crossings through changing the steel's microstructure (Zhang et al., 2010). During EDH operations, explosives are laid onto the test fixture (rail crossing) and are detonated, applying the resultant forces directly into the fixture via the shock wave. An example schematic of the test process is shown in Figure 15. Given that multiple points along a test fixture may need treatment, multiple detonators are used to generate the required shock forces locally at the precise areas along the test fixture. This condition was satisfied with 3 separate explosive charges during these assessments.

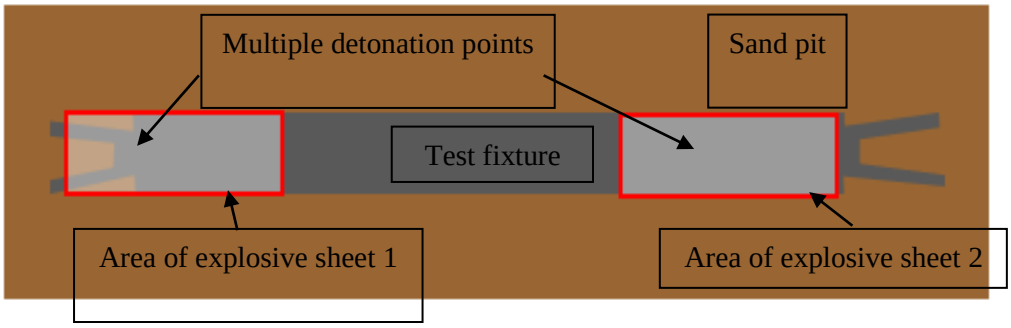

Figure 15. Bird's eye view of EDH test set up.

Testing windows are repeated 2-3 times per week on average, with around 4 individual explosions carried out within a testing window. The testing rig is placed on the top of a sand pit. Testing is conducted in open-air, as no barriers or enclosures are present. An operator conducts the tests remotely from a distance of 130 m. The position of the test operator with respect to the EDH zone is depicted in Figure 16 by the location of a pressure gauge (labelled P1).

Figure 16. EDH test layout and measurement positions. P1 marks the position of a pressure gauge at the location of the test operator. P2 was a supplementary pressure gauge used during the November trials (see Table 15).

The hearing protection device (HPD) used by the test operator during all field trials were the 3M Peltor LEP-200 Earplugs which are an electronic level limiting device. According to DEF-STD 27, active HPD's should be assessed using the HML method as if they are passive

devices, based on the assumption that only the passive attenuation characteristics apply during high level noise.

Table 14 - Test operator's HPD: 3M Peltor LEP-200 Earplugs octave band, High-Medium-Low and Single Noise Rating attenuation characteristics.

Hearing Protection Device		Attenuation (dB)							
		Frequency (Hz)							
		63	125	250	500	1000	2000	4000	8000
3M Peltor LEP-200 Earplugs	Mean Attenuation	-	34.5	31.5	36.2	33.4	34.8	34.9	38.8
	Standard Deviation	-	6.0	5.4	5.6	4.3	3.8	5.0	4.0
	Assumed Protection Value	-	28.5	26.1	30.6	29.1	31.0	29.9	34.8
	HML	H	M	L					
		31	30	29					
	SNR	32							

2.4.3 Material and Methods

The paper presented by the author and supervisor of this Thesis to the Journal of Applied Acoustics on this topic contains an extension to the literature review in Section 2.2, with particular focus on criticism of the aforementioned AHAAH model, relevant to the USA and other regions. As the guidance relevant in the UK, which include the Control of Noise at Work Regulations (2005) and the methodologies of DEF-STD 00:27 have been presented in subchapter 2.2 and 2.3 of this Thesis, they are not included in this subchapter. However, the reader may wish to refer to those subchapters for reference.

2.4.3.1 Other Methods

The aforementioned US MIL-STD 1474-E: 2015 (Department of Defense, 2015) describes measurement and assessment procedures for determining noise limits to promote personnel safety within the context of US Army operations. A brief review of the standard along with extended literature is discussed here.

Appendix B of the standard provides impulsive noise level limits where levels exceed 140 dB at personnel occupied areas. Impulsive noise limits should be established by either of the following metrics:

- A-weighted Equivalent Continuous Impulse Sound Pressure Level ($L_{IAeq100ms}$)
- Auditory Risk Units (ARU)

$L_{IAeq,100ms}$ stems from the equal energy model, which characterizes the A-weighted equivalent total energy of an impulse of 100 ms (Department of Defense, 2015). Within blast noise literature, this is typical of impulsive noise definitions, however, impulses particularly from gas explosions can have significantly longer durations. 100 ms is likely to be too short for some impulse durations of explosions typical at DNV Spadeadam, though the metric can be modified to assess the equivalent sound energy over longer durations, based on A-duration length. $L_{IAeq,100ms}$ has similarities to the sound exposure metric, by characterizing exposure over 100 ms (or its extended time interval) rather than 1s as in a sound exposure level measurement.

The benefit of this metric is the low computational effort needed to perform such simple calculations in addition to the nonlinear behaviour of hearing protection under high level impulsive conditions is still captured (Department of Defense, 2015).

The Auditory Hazard Assessment Algorithm for Humans (AHAAH), referred to in MIL-STD 1474E, developed by G. R. Price and Kalb (1991) is a physical model of the ear, based on electroacoustic principles to determine damage to hearing of personnel within a military environment. The model emulates the transfer function from free field to stapes motion in the middle ear. The middle ear motion is then traced to determine basilar membrane displacement, and ultimately calculate a hazard function for intense impulses. The model requires a time-pressure history as its input, and may be used to assess, various protected, unprotected, warned or unwarned ears, in any combination,

According to the original work on AHAAH (G. Richard Price & Kalb, 1986), sound pressure levels above 130 dB cause non-linear stapes movements, due to the increasing stiffness of its connecting elements, resulting in a protection mechanism (for warned ears) due to a reduced efficiency in energy transfer to the cochlear. This study by Price and Kalb was the preliminary work on middle ear muscle contraction (MEMC) effect, and following transfer through the middle ear, energy is traced through the basilar membrane (BM). MIL-STD 1474E describes how BM displacement calculations are discretised into 23 segments in order

to roughly represent 1/3rd octave bands, so that frequency encoding across the length of the membrane is maintained. From the squared sum of these peak displacements at each location along the membrane, the hazard is represented by Auditory Risk Units (ARU).

However assumptions that the MEMC are valid in the AHAAH model have been investigated thoroughly through a series of studies on the reflex and disproved it as being 100% prevalent in the general population (Flamme, Deiters, Tasko, & Ahroon, 2015; Flamme, Deiters, Tasko, Jones, & Ahroon, 2019). Such findings suggest that although MEMC can be performed, they should not be assumed to be present when carrying out assessments of auditory injury from blast noise and should not be included within impulsive noise damage risk criteria.

MIL-STD-1474-E refers to this model as one of two means for an occupational impulse noise assessment and for prescribing hearing protection against impulsive noise, as it has been systematically evaluated against a range of datasets and has been peer-reviewed. The American Institute of Biological Sciences (AIMS) propose in their 2010 peer review of AHAAH that the LAeq8 model be used as an interim method until the AHAAH model is further validated in critical areas (Department of Defense, 2015), such as in its influence under various conditions and a more quantitative understanding of MEMC at high levels. A subsequent review by the Blast Injury Research Coordinating Office on a biomechanically based auditory standard is expected this year. Following updated literature in the field, improvements to the performance of the model have been achieved by modifying the AHAAH to create the Integrated Cochlear Energy (ICE) model, removing the inverted dose-response relationship shown by the AHAAH model alone (Zagadou, Chan, Ho, & Shelley, 2016).

ANSI/ASA S12.42-2010 (R2016) (American National Standards Institute, 2010) is of relevance to industrial blast noise in that it provides a calculation method specifically for assessing the impulse peak insertion loss (IPIL) of hearing protectors against impulsive noise. Through the use of the method based on transfer functions, the standard provides guidance on the instrumentation requirements and data reduction techniques. Annex H of that guidance outlines the MATLAB code needed for calculating the insertion loss from an impulsive source and the uncertainties for this are accounted for within Annex G of the document. Additionally, the standard discusses bone conduction limits for hearing protection devices within para 9.6.3 of the document, according to Department of Defense (2015).

Three free-field peak impulses with ranges of levels between 166 and 170 dB, 148 and 152 dB and 130 and 134 dB are needed to perform the method for assessing insertion loss from impulsive noise in ANSI 12.42. These impulses must also contain A-durations between 0.5 ms and 2.0 ms, and are used to evaluate the performance of hearing protection devices for various dynamic and temporal features of impulses. Following some signal processing, such as truncating, filtering and frequency analysis (both FFT and IFFT) with specifications defined within the body of the standard, an average frequency dependent transfer function from the measurement device representing a level after hearing protection to an unprotected ear is derived. The impulsive peak insertion loss (IPIL) is then calculated as the peak sound pressure level of the estimated unprotected level in the fixture minus the peak sound level of the measured protected ear (American National Standards Institute, 2010) .

The ANSI/ASA 12.68:2007 (R2020) (American National Standards Institute, 2007) standard provides three calculation methodologies for the determination of the A-weighted SPLs when a hearing protector is worn, with use of the hearing protector's attenuation data. Although an American standard, it's relevance to Spadeadam is that it extends the HML method to include sources with lower frequency distribution than those included in DEF-STD27 and BS EN 458. The NRS graphical method (NRS(G)) extends the difference in C- and A-weighted SPLs to around 16 dB, compared to 10 dB in DEF-STD 27. The NRS method is an assessment methodology, used to obtain a parameter known as the Noise Reduction Statistic.

Recent advancements in acoustical analysis software with machine learning has resulted in the ability for enhanced signal feature extraction. Statistical parameters of signals are also used to objectively describe waveforms to classify signals. By using an equal energy metric alone, there would be no observable difference between the predicted noise induced hearing loss (NIHL) following two temporally varying signals with overall equivalent exposure levels (R. I. Davis et al., 2012), as the equal energy hypothesis states that NIHL is a function of the total exposure energy alone (Zhao et al., 2010). These two studies investigate how a sample of workers subject to complex non-Gaussian (non-G) noises (those which contained high level transients, such as impacts, impulses, intermittent or other complex characteristics), experienced increased levels of noise induced permanent threshold shifts (NIPTS) compared to a worker sample subjected to Gaussian (G) noises (such as broadband, steady signals). Earlier epidemiological studies show that workers exposed to other non-G noises (specifically impact noise transients) show an increased incidence of hearing loss. Further, animal studies such as by Hamernik et al. (1984), showed high level transient noise exposures

resulted in increased levels of hearing loss when compared with equivalent energy G-noise, although the exposures from this study are not as relevant to blast noise, as they considered complex exposures involving both continuous and impulsive noise.

The 2012 study by Davis et al., claims that for noise exposure of equal energies but differing temporal characteristics, kurtosis may differentiate the associated risk of hearing and sensory cell loss between them. Kurtosis is a statistical metric that is sensitive to a signal's temporal characteristics, where it is defined as the ratio of the fourth-order central moment to the squared second-order moment of a signal's amplitude distribution.

Clearly, there are several metrics used within various guidance to assess auditory risk and hearing protection suitability for blast exposures. The state-of-the-art methods differ to those within the U.K. standards and guidance in that they take into account the temporal characteristics of a signal. The output metric of the AHAAH physical model is directly correlated to noise induced temporary threshold shift, and accounts for temporal and frequency dependent components of a waveform.

2.4.4 Field Trial Results

2.4.4.1 Testing Window

Measurements from 4 separate EDH testing windows have been analysed in this study. Table 15 outlines the test details. The values of Δ (column 5) represent the difference in C and A-Weighted Maximum Sound Pressure Levels (L_{CMax}-L_{AMax}) as per the guidance, while final column, L'_{CPeak}, represents the adjusted C-Weighted Peak level as per the DEF-STD 27 guidance.

Table 15. EDH testing details.

Date	TNT Equivalence (kg)	L_{CPeak} (dB)	Lz_{Peak} (dB)	Δ (dB)	L'_{CPeak} (dB)
03/08/2020	6	148.6	150.0	15.6	124.6
03/08/2020	6	146.2	146.2	17.8	122.2
03/08/2020	8	151.2	153.4	11.3	127.2
03/08/2020	8	152.1	155.4	11.6	128.1
05/08/2020	10	150.4	154.4	17.3	126.4
05/08/2020	10	151.5	155.5	16.9	127.5
06/11/2020	10	158.6	159.8	10.2	134.6
06/11/2020	10	157.0	158.1	9.3	133.0

06/11/2020	10	152.7	156.0	12.4	128.7
06/11/2020	10	153.8	156.2	12.1	129.8
10/11/2020	7	152.2	154.4	12.5	128.2
10/11/2020	7	151.6	153.5	11.9	127.6
10/11/2020	7	151.7	153.8	12.1	127.7

2.4.4.2 Instrumentation

The following instrumentation was used during the tests.

- PCB Model 137B Quartz ICP Blast Pressure Pencil Probe (Pressure Gauge)
- PCB Model 482C16 ICP Signal Conditioner

During the 6th of November field trial, pressure gauge 1 failed during the first two tests. Upon comparing the remaining pressure gauge 1 data with pressure gauge 2 through the 5 remaining tests during the November trials, LCpk measurements at P2 were no greater than 1.5 dB in 4 out of 5 tests, and no more than 2.3 dB overall compared to P1. Consequently, data from pressure gauge 2 was assumed as representative of the operator's location and is also a more conservative approach. The use of this data is further justified by the SPL variation at an individual pressure gauge being within and sometimes greater than this range. All Transducers were situated at a height of 1.5 m.

Field calibration of the PCB Blast Probes are undertaken on site via 'push tests' which were carried out before each field trial to ensure that the expected signal was present from each probe. Field Calibration of the sound level meters was undertaken using an appropriate calibrator with a ¼ " adapter.

2.4.4.3 Pressure Gauge Measurements

Pressure gauge measurements from the entire testing period are shown in Figure 17. Some correlation between the peak SPL data and TNT equivalence was measured, though considerable variation is shown in the 10 kg tests, especially during the November trials. it is unclear whether this is caused by differences in test fixture configurations. One explanation could be due to meteorological effects, as the testing window lasted longer than in August. However, no significant change in meteorological parameters was found.

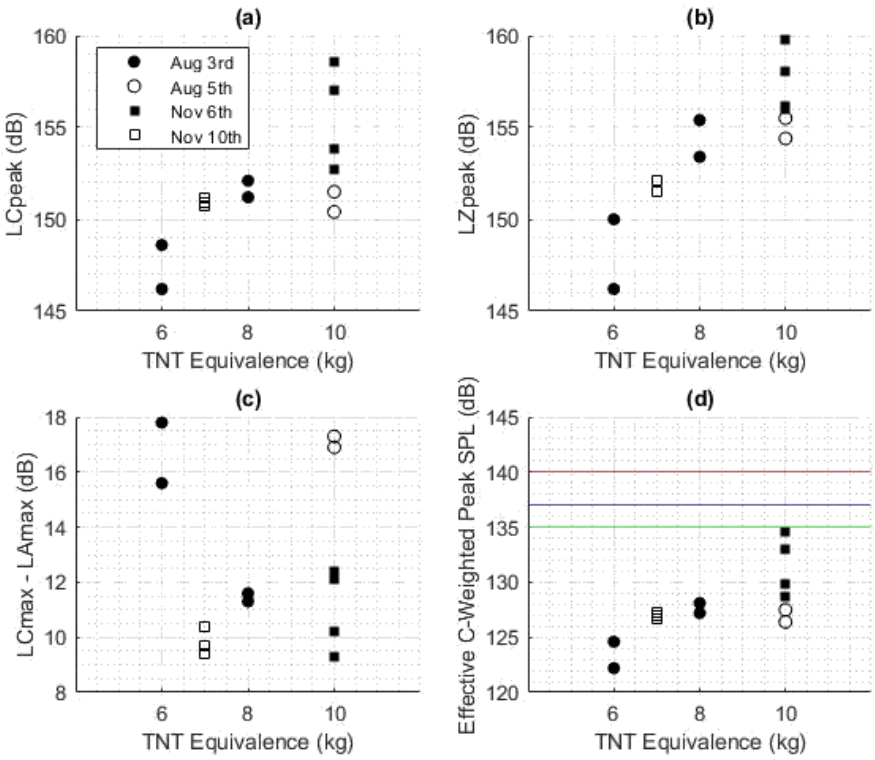

Figure 17. Pressure gauge measurements of all EDH tests across all field trials. (a) C-weighted peak SPL, (b) Z-weighted peak SPL, (c) Δ values and (d) Operator's effective at-ear C-weighted peak SPL using 3M Peltor LEP-200 Earplugs following the DEF-STD 27 method. The red, blue and green lines on (d) represent the limit, upper and lower actions specified in the Control of Noise at Work Regulations.

Moreover, according to the DEF-STD method, the test operator's earplugs provided sufficient attenuation such that the effective at-ear C-weighted peak SPLs (L'_{CPeak}) during all tests were below the lower action level specified in the CoNWR, However, the Δ (L_{CMax}-L_{AMax}) values, were greater than 10 dB in 11 of 13 tests, with several results above 15 dB, well beyond the scope of the guidance, as per note 12.7 in DEF-STD 27. Further investigations into the spectral components were made by observation of the recorded pressure-time histories.

2.4.5 Discussion

In several cases, recorded waveforms showed impulse shapes which significantly deviated from the assumed ideal impulses that may be expected from a Friedlander curve. Some waveforms had multiple pressure peaks superimposed upon the overall signal, as well as significant noise artefacts, as shown in Figure 18. Some examples of the recorded pressure time histories for various EDH configurations across all field trials are included in Figure 19.

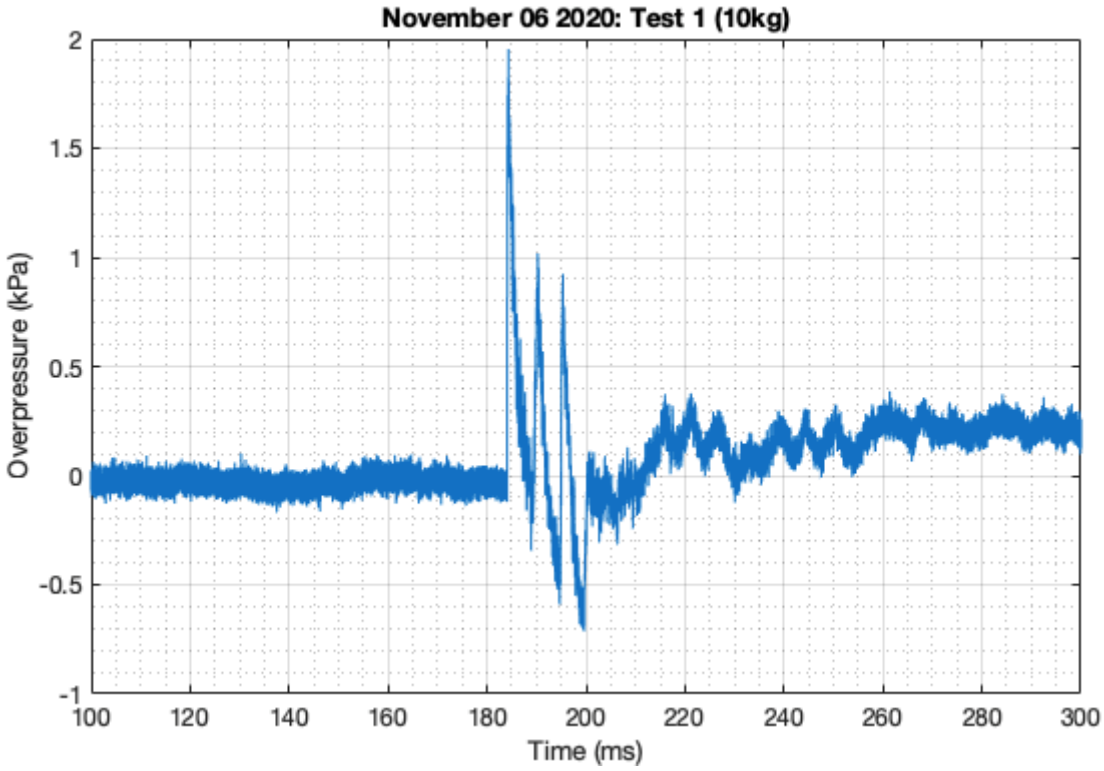

Figure 18. Example of multiple pressure peaks observed within an EDH exposure waveform.

Although the nature of these pressure peaks has not been determined, they are a significant part of the waveform's character and subsequently of personnel exposure. Three pressure peaks reflect the geometry of the detonators that were set up on the test fixture. It is speculated that each pressure peak could be related to the detonation of the three individual charges that were laid linearly one behind the other along the test fixture with respect to the observer.

Similar waveform characteristics were recorded within the repeated 10 kg test carried out shortly after on the 6th November, which had the same source geometry. Additional pressure peaks are superimposed on the waveforms recorded during the 11th November trials, although these are less defined.

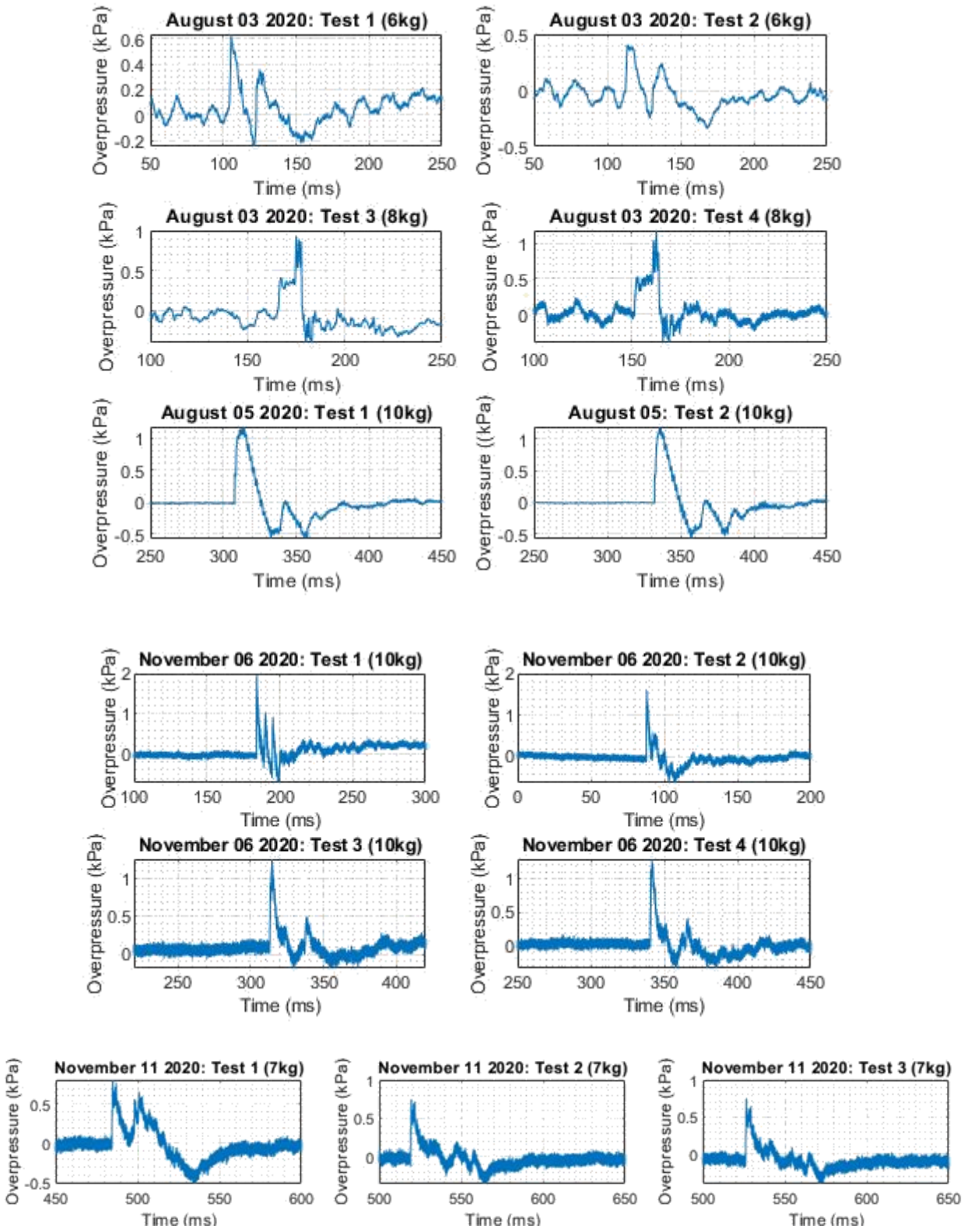

Figure 19. All EDH waveforms at the location of the test operator, 130m from the detonation.

As shown in Figure 19, pressure time histories from August EDH operations are similar between repeated tests of the same TNT equivalence. This phenomenon is also observed during the November trials. However, for the supposedly same TNT equivalence, the

waveforms are not consistent between the August and November field trials, or between different TNT equivalences within the same field trials.

For example, the August 6th 8 kg tests, have significantly different waveform characteristics, where the 8 kg tests show a plateauing in overpressure, followed by 3 pressure peaks. These measurements suggest an artefact induced along the measurement chain, through excessive vibration on the transducer and consequently motivated the need to repeat the trials again in November. The 10 kg August trial data show a more typical blast wave pressure-time history.

As discussed above, the first November 6th 10 kg tests differ significantly in shape to the August 10 kg tests, whereas the later tests on November 11th are more similar in character, with the one single pressure peak, followed by an assumed ground reflection.

Electrical noise is prevalent on the signals captured during the November field trial due to the transducer cables running a long distance over damp ground. However, the peak levels recorded during these trials are consistent with those from the August trials, and therefore it is assumed that the November measurements are still adequate for assessing exposures.

Due to the additional signal features observed within the waveforms, the MIL-STD methods could be used to better inform the assessment outcome in future, though the use of any methods other than the DEF-STD 27 guidance is non compulsory in the UK. Considerable uncertainties would be introduced through the use of the AHAAH assessment, firstly by the assumption that the middle ear muscle contraction (MEMC) is fully activated throughout all impulses (Department of Defense, 2015) . Furthermore, it should not be assumed that the individual test operator has the potential to perform MEMC at all, let alone in all cases (Flamme et al., 2015) . For this reason, unwarned results should be used, representing no activation of the MEMC.

Moreover, the 3M Peltor LEP-200 HPD used in the assessment is not listed within the AHAAH model and therefore would be applied in the assessment by adapting the attenuation characteristics of the most similar HPD, such as triple flanged earplugs available within the model to fit the specific requirements of the HPD in the assessment.

2.4.6 Case Study Conclusion

This study concludes that according to the UK best practice guidance, noise exposures from EDH operations carried out at DNV Spadeadam are acceptable with the use of the test

operator's specific hearing protection. However, field trials measurements revealed that this operation generates impulsive noise with characteristics beyond the scope of DEF-STD 27, due to excessive low-frequency noise. Such exposures have uncertainties which need to be quantified to best address the assessment outcome.

Analysis of the waveforms showed additional signal features, such as multiple pressure peaks, superimposed on the pressure-time histories. The origin of these signal features is currently unknown, and hence it is unclear whether these form an intrinsic part of the noise exposure. Furthermore, electrical noise and artefacts added additional uncertainties which should be further investigated.

Finally, the correlation between LC_{peak} and TNT equivalence should be further investigated, as it is speculated that the orientation of the test fixtures, along with the number and arrangement of detonators can significantly affect the exposure of the test operator. A series of field trials should be designed to investigate this effect. Such measurements may produce derivations of acoustic source characteristics which can be used for long-range propagation modelling. The significance of this would be in allowing DNV to better predict the near-field exposures, in addition to the long-range noise from EDH operations to mitigate their impact on the surrounding communities.

2.5 Conclusions on Part I

This subchapter summaries the findings from this chapter of the research on the suitability of current assessment methodologies for the selection of hearing protection for the case studies presented above.

2.5.1 Literature Review

- Guidance documents from other nations and governing bodies have been reviewed, and a number of contrasting methodologies for the assessing the suitability of hearing protection against blast noise have been presented.
- A review of the legislation found that the most current standard to satisfy national regulators for the selection of hearing protection devices against blast noise sources at Spadeadam, is MOD DEF-STD 27:2015.
- Measurement techniques and instrumentation requirements have been outlined, and field trials were designed for the assessment of hearing protection suitability against two common blast test operations at Spadeadam.

2.5.2 Case Study 1 – Explosion Chamber Demonstration

- The maximum C-weighted peak level measured across the personnel zone was 166.6dBC (January 2020 with a Class 1 Sound Level Meter and high pressure microphone).
- Pressure gauge measurements recorded similar peaks of 163dBC across the viewing area.
- For this test only the in-ear style hearing protection (both active and passive) provided enough attenuation to be below the CoNaWR action limit (140dBCpk).
- Measurements across the viewing area showed that exposures can vary for nominally the same test and environmental conditions.
- Exposures from this demonstration are have frequency characteristics beyond the scope of the UK legislative guidance for the selection of hearing protection.

2.5.3 Case Study 2 – Explosive Depth Hardening

- The maximum C-weighted peak level measured across all trials was 158.6dBC.
- According to the HML assessment method, against this exposure, all in-ear plug type protection devices provide sufficient attenuation so that exposure is below the CoNaWR 140dBC limit.
- The test operative's active ear plug protection 3M LEP-200 is assumed to provide attenuation in the same way as passive hearing protection does under such high-level exposures.
- Significant signal artefacts were present on the field trial recordings and the nature of these recording need to be investigated.

2.5.4 Uncertainties Associated with the AHAAH Model

The uncertainties with all AHAAH assessments within this research are large. One reason is due to the lack of accurate electro-acoustic models for input into the AHAAH, that represent the exact foam and ear muff protection devices used which have been assessed. An assumption has been made that the performance of these hearing protection devices could be simulated by the performance of a similar devices, already modelled by the AHAAH.

The hazard calculation also assumed a warned response, believed to be likely of that experienced at Spadeadam, where individuals can hear a countdown to the blast, in addition to being able to observe the flash of the blast, which arrives at the receiver before the blast wave, leading to the assumption that individuals experience some form of warning. However, as discussed in section 2.4, not all individuals can perform the middle-ear muscle contraction required for the warned response. However, given that MIL-STD methodology is not required under UK legislation, this part of the assessment has no legal basis in the UK.

2.6 Further Work

The further work required in this specific research area of occupational blast noise relevant to Spadeadam is summarised here.

Firstly, extensive field trials must be carried out on the other blast testing demonstrations and operations carried out at Spadeadam. For example, exposures from the relatively recent addition of the 'hydrogen detonation' to the Hazard Awareness training course must be investigated. However, it is likely that the frequency characteristics of these exposures will again exist beyond the scope of the current legislation.

In which case, an investigation into quantifying the uncertainties associated with the current standards must be carried out. Such uncertainties include the effects of impulse sounds dominated by low-frequency and those which contain additional time-pressure characteristics, such as multiple pressure peaks.

The aforementioned noise sources must also be investigated further with additional field trials, in order to quantify the source characteristics of each operation. Such measurements could a) supplement a long-range prediction model for the accurate determination of long-range impacts, and b) quantify any directionality that may relevant in the near-field e.g. for personnel at other parts of the site.

2.6.1 Implications for the Revision of DEF-STD 0027

The guidance in DEF-STD 0027:2015 is currently being updated at the time of writing. The findings of this part of the thesis involving blast testing at Spadeadam has been presented to the Health & Safety Executive (HSE), and Ministry of Defence (Qinetiq) who are overseeing the latest revision (see Appendix A). This thesis found that personnel exposures at Spadeadam exist well beyond the scope of the existing defence standard. This is a consequence of the standard being primarily aimed at assessing high-level exposures from gunfire noise and military weapons. These exposures differ to those at Spadeadam, which involve longer duration impulses, with significantly more energy at low frequencies, and for impulses containing more complex temporal characteristics.

There is significance to the exposures at Spadeadam being beyond the scope of the types specified in the defence, because it is unclear how the effectiveness of a given hearing

protection device is, as the dominant frequency of the blast decreases, or in other words, for large scale blasts involved in major hazards testing.

It is therefore appropriate that a series of field trials and further analysis be undertaken to address the limitations imposed by the current standard on assessing hearing protection performance against the exposures generated by the processes at Spadeadam.

Firstly, it is proposed that the trials are repeated with the pressure gauges used previously, but set to a lower sensitivity to avoid the signal artifacts present in the current measured recordings, particularly in those from EDH where peak exposures were slightly lower. While real-world measurements where personnel are situated is always a priority, it is desirable also to quantify the source directivity of each noise hazard at Spadeadam. Source term information will accompany both nearfield and farfield prediction models, so that exposures can be simulated for personnel at other areas of the site, as well as predicting blast noise impacts at long-range.

Simultaneously, analysis using other methodologies for assessing hearing protection suitability should be carried out, so as to inform decisions on prescribing hearing protection according to the techniques used in other countries. Recently, a paper by TNO in the Netherlands (van der Eerden, van Pruissen, & Salomons, 2023), compared a simple energy-based method (ASEL), with the AHAAH model, which is also used by the MOD in the Netherlands, and the Pfander criterium, used by the German MOD, for a variety of impulses. Van der Eerden et al investigated whether these models correlated with one another when impulses increased in duration, i.e. for larger weapons, which is relevant to the exposures at DNV Spadeadam.

A similar approach could be used here, also including comparison with the original damage range criteria proposed by CHABA as a reference and the adapted versions of AHAAH based on cochlear energy (ICE) proposed by Zagadou et al. (2016). This ensemble approach may be useful to see how the models correlate with one another for large impulses and for those that contain additional signal characteristics such as those at Spadeadam.

Part II

Managing and Predicting Environmental Blast Noise Impacts

Overview

The aim of this Part of the thesis is to present the work done on managing and predicting environmental blast noise impacts from test activity carried out at DNV Spadeadam. This work contrasts that done in Part I, as it is involves the propagation of blast waves over long-range and concerns two key components:

c) *Management* of the blast noise impacts on the community;
d) *Prediction* of blast noise impacts on the community.

One would argue that component b), the *prediction* of blast noise is a strategy that must be utilised to successfully carry out component a), the *management* of community blast noise impacts. Therefore, the prediction of blast noise is an essential part of managing community blast noise impacts.

This part of the thesis begins with a chapter reviewing the scientific literature on all aspects import to the management and prediction of environmental blast noise.

Following this chapter, methodological techniques used for the management and monitoring of environmental blast noise impacts from Spadeadam on the community, and for the development of heuristic prediction models for blast noise at Spadeadam.

The performance of such models is assessed, before conclusions are stated, followed by setting out the further work required to advance the management of environmental blast noise.

3 Literature Review

Summary

The aim of this chapter is to review the scientific literature on the propagation of impulsive sound outdoors. The literature concludes that the meteorological feature that dominates receiver blast noise levels is the vertical gradient of the vector winds in the lower atmosphere, followed by temperature gradients. Later in this chapter, the literature on community response to blast noise is reviewed. The chapter closes with an assessment on the suitability of available meteorological data sources for best implementation in a heuristic noise prediction model. This chapter sets the knowledge foundation required to develop the proposed heuristic noise prediction modelled presented in the remaining chapters of this thesis.

3.1 Background

Over the decades, the University of Salford's field measurement personnel and capability has been recognised internationally by outdoor sound propagation researchers. Beginning in 1977 with work for ICI, impulse noise research continues to this day. Salford pioneered a range of field trials between 1987 and 1996, with the primary aim of investigating the propagation physics of impulsive sound. More specifically, there was a focus on gathering data on the effects of meteorology, topography, and ground terrain on the propagation of blast noise over both short and long range. This work led to the development of explosive noise management tools to be used at military and testing ranges, based on explosive scaling laws and extensive meteorological measurements. Two phases of trials were carried out, with the first conducted at various sites in the UK (Porton Down, Shoeburyness and RAF Binbrook). The second series of trials related to measurements of impulsive noise over forested, hilly terrain in Norway, in collaboration with the Norwegian Government and numerous international bodies (Hole, 1999; G. W. Kerry, 1996).

In combination, these trials have established Salford's authority and credibility as a major research institution in the field of blast noise propagation. A list of the field trials carried out by Salford is included in Appendix B.

Based on work carried out by Salford at another test facility in Cumbria (Qinetiq Eskmeals), this research stems from an enquiry by DNV to help manage complaints from local residents. Upon reviewing Salford's previous work in collaboration with Qinetiq on computational outdoor sound prediction models, it was concluded that the current state-of-the-art models (GTPE etc.,) would not satisfy DNV's operational requirements. Hence, the decision was made to develop a heuristic model specific to the Spadeadam site, under work known as DABENIM (Development of A Bespoke Environmental Noise Impact Method).

Preliminary field trials were conducted at Spadeadam by the University of Salford in 2017 as part of DABENIM, where a heuristic noise prediction model was shown to perform at least as well as the currently used noise prediction model, MONET. The heuristic model was developed through the following key stages.

1) Evaluation and assessment of noise prediction models
2) Field trial of Smart Noise Monitoring (SNM) system
3) Heuristic method for explosive noise impact prediction

The first stage concerned the modelling requirements and input meteorological and terrain data for the prediction of long-range blast propagation through the atmosphere, including the effects of refraction. A broader review has been conducted for this report, where many prediction models and the quality and suitability of available meteorological data has been reviewed.

Secondly, a field study of blast noise measurements at Spadeadam using a multi component SNM system was trialled as a potential replacement for the current noise forecasting predictions. The main principle of this system is to use pilot explosions to generate comparatively low-level noise that is measured in real-time at locations of interest, with results fed back almost instantly to the test site range controllers.

The data gathered from this trial were further exploited to develop a heuristic noise prediction method. By correlating the data captured during the trial with meteorological data, 'rules-of-thumb' were derived for the prediction of noise at sensitive receptors based on the best available current meteorological data. From this, it was shown that with more measurements, a heuristic model could be constructed for this complex site at reduced computational cost to the current system, without significant reduction in prediction accuracy. Following

DABENIM, DNV enquired about on-site hearing protection advice, and hence, this I-Case was conceptualised to include on-site noise management with the expansive further work on a heuristic model.

This research aims to expand on the 3 aforementioned developmental stages, by presenting a review of the associated long-range sound propagation theory needed to understand the modelling requirements of the current state-of-the-art noise prediction models. Following this is a review of the best available meteorological data sources for the Spadeadam site, including both forecast and measured data for use in sound prediction modelling.

Furthermore, the human response to blast noise has been explored through a review of appropriate measurement techniques and a suitable acoustic metric. This is important for the purpose of predicting annoyance from blast noise, where both acoustical and non-acoustical factors may contribute to the overall annoyance of an individual's noise exposure. Additionally, the annoyance of an individual is not necessarily representative of community annoyance, given that both noise levels and attitudes towards noise will inevitably differ within the surrounding community. A thorough understanding of the human perception of blast noise is critical for the correct choice of acoustic metric used for the Live Noise Monitoring system, in order to best predict annoyance and hence complaints.

3.2 Principles of Atmospheric Acoustics

Outdoor sound prediction requires a thorough understanding of the fundamental properties of the propagation medium, namely the atmosphere. Additionally, an understanding of the interaction effects of sound with the ground is paramount. This chapter provides supplementary information on the mechanisms which dominate propagation variability so abundantly in outdoor sound propagation. The aim of the chapter is to set the theoretical context which has driven the historical development of sound prediction models used at DNV Spadeadam and alike.

In outdoor sound propagation, schemes have been developed to classify atmospheric boundary layers (ABL) to represent their effects on sound propagation. Meteorologically neutral atmospheres do not represent acoustically neutral conditions, see 3.2.2.3. The Pasquill classes have been adopted for sound propagation analysis in the CONCAWE scheme (Marsh, 1982), represented as 6 categories. These are based on the combination of temperature and vector wind speed information.

Zouboff, Brunet, Bérengier, and Sechet (1994) used this information to form a table of qualitative descriptions on receiver sound levels, as shown in Table 16. With T1-T5 roughly corresponding to Pasquill classes A-G respectively, where T1 is strong radiation, and T5 being night-time. The categories for wind conditions, W1-W5 are represented in the same way (W1 being strong wind, ~3.5ms^{-1}).

Furthermore, Attenborough, Li, and Horoshenkov (2006) go on to discuss how the classes are asymmetrical around the *zero meteorological influence* class, because there are typically more conditions that would result in sound attenuation than enhancement. Moreover**,** the magnitudes of the attenuations are generally greater than those of the enhancements. This was observed experimentally in Waddington and Lam (2002). This introduces difficulties in estimating the uncertainty of noise levels around an average level in monitoring schemes, i.e., 100dB ±10dB. In reality, fluctuations are more likely to take the form of, -10dB in upwind conditions, compared to +7dB in downwind conditions, for example. This kind of asymmetry was shown in earlier measurements by Zouboff et al. (1994).

Table 16 - Qualitative descriptions of meteorological effects on noise levels based on the meteorological classes in Zouboff et al. (1994) and with qualitative descriptions by Attenborough et al. (2006).

Temperature Gradients	**Wind Conditions**				
	W1	W2	W3	W4	W5
T1	-	Large attenuation	Small attenuation	Small attenuation	-
T2	Large attenuation	Small attenuation	Small attenuation	Zero meteorological influence	Small enhancement
T3	Small attenuation	Small attenuation	Zero meteorological influence	Small enhancement	Small enhancement
T4	Small attenuation	Zero meteorological influence	Small enhancement	Small enhancement	Large enhancement
T5	-	Small enhancement	Large enhancement	Small enhancement	-

3.2.1 The Atmospheric Boundary Layer

The Earth's atmosphere is widely recognised as a fluid flowing over a solid surface. The phenomenon of fluid flow over any surface results in the generation of a boundary layer, and hence, the atmosphere's flow over the Earth's surface results in the Atmospheric Boundary Layer (ABL). Stull defines the ABL as:

> *"...that part of the troposphere that is directly influenced by the presence of the earth's surface, and responds to surface forcings with a timescale of about an hour or less" (Stull, 1988)*

The *troposphere* is the lowest atmospheric layer, of which there are many. Atmospheric layers are separate entities to the atmospheric boundary layer and are used to describe specific conditions at altitudes above the surface. What is meant by Stull's quote is that the ABL is the physical layer that results from the Earth's response to a diurnal variation in temperature, resulting from its exposure to the Sun's radiation, and from the ABL's flow over the Earth's surface (land and sea), which directly influence the vertical structure of the ABL.

ABL processes over flat, homogenous terrain are well established and are characterised into 3 types:

- Unstable Boundary Layer
- Stable Boundary Layer; and
- Neutral Boundary Layer

The first two types are dominated by thermal properties of the ground surface, which form important considerations for vertical sound speed profiles in outdoor sound propagation. *Unstable* boundary layers are often called convective or mixed boundary layers, characteristic of daytime heating from the sun and low wind. Heating of the ground results in a positive temperature lapse with altitude.

Stable boundary layers result from radiative cooling of the Earth, resulting in a negative temperature lapse rate. These layers are characteristic of (but not limited to) night-time conditions and winter mornings.

Neutral boundary layers are qualitatively far from neutral and are dominated by high wind speeds and widespread cloud cover. The word *neutral*, is used in reference to the lack of a strong temperature gradient and hence this type is often referred to as a *dynamical* boundary

layer. D. K. Wilson (1996) expands on this in his guide on atmospheric boundary layers for acousticians. A temperature gradient will still exist in a neutral boundary layer, in the form of the dry adiabatic rate which results from the expansion (and therefore cooling) of air with altitude caused by a decrease in atmospheric pressure. This is different to an acoustically neutral atmosphere, which would have no wind or temperature gradients, should it exist.

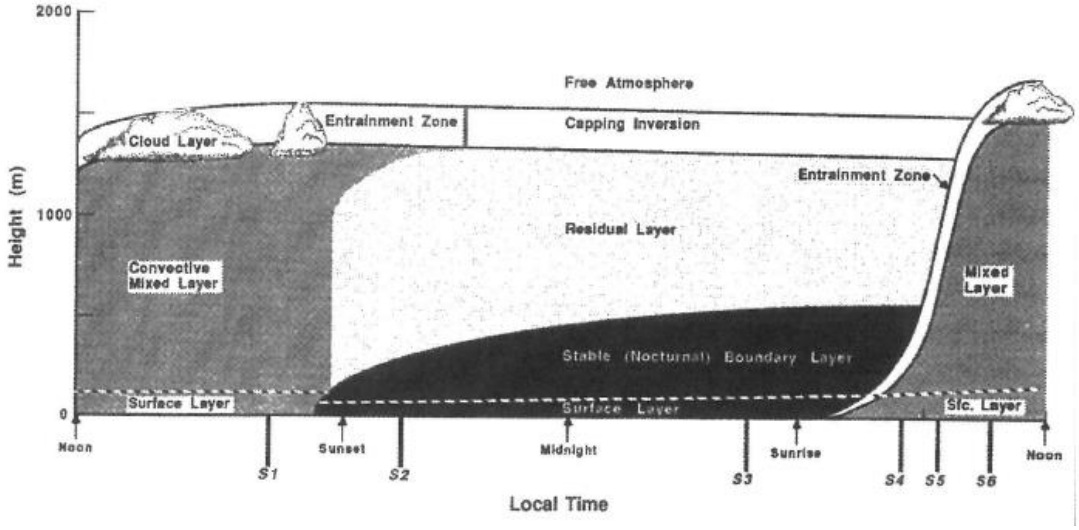

Figure 20 - Diurnal variation in ABL development as defined in Stull (1988).

Figure 20 illustrates the temporal development of the ABL as it transitions between unstable (convective) and stable (often nocturnal) conditions.

These processes are well-defined for flat homogenous terrain with uniform surface roughness, where boundary layer flow tends to equilibrium with the surface properties. When the ABL flow encounters a surface discontinuity, which could be varying ground conditions, a resulting discontinuity in the flow is observed. This is an adapted flow dependent upon the new surface properties, and can be categorised as an *internal* boundary layer, which develops within the encompassing ABL. Such structures are important for outdoor sound propagation, although they are often neglected by the assumptions of spatial and temporal meteorological homogeneity in general weather observations. They are important because they may impose immediate disruption upon the assumed features of the dominant ABL which may encompass them. Such internal layers may be marked by the sudden discontinuity in wind speed and/or direction, air temperature and other parameters which may indicate a change in refractive index of the medium (see 3.2.2).

3.2.1.1 Ekman Layer

Some changes in wind direction with height can be explained by Ekman motion theory, first explained by the meteorologist and oceanographer, Vagn Walfrid Ekman. In the northern hemisphere, the Coriolis effect deflects objects in motion to the right of their direction by apparent force (Society, 2021). The result is a layer known as the Ekman layer which is a structure of winds near a horizontal boundary which has its flow rotated with increasing height from the boundary.

3.2.1.2 Geostrophic wind

The pressure gradient force is responsible for the flow of winds between high- and low-pressure areas. Friction is strong near the surface and therefore this flow is slowed. With increasing altitude, surface friction is decreased and therefore wind speed is stronger. Because the Coriolis effect is proportional to wind speed, wind deflection increases with altitude. At some height, the deflection will be such that it flows perpendicular to the pressure gradient force, where the Coriolis force and pressure gradient force are in balance. The wind at this height is called the geostrophic wind and typically occurs at an altitude where air pressure is approximately 500mbar. This wind may signify the top of the ABL where there is no surface influence on the flow.

3.2.2 Refraction

Refraction is the effect of a change of wave direction or wave bending, resulting from sound speed changes along the propagation medium. Sound speed changes are a function of the refractive index of the medium. A simple model of atmospheric refraction is based on sound speed function *c* with height *z*, such that:

$$c(z) = \begin{cases} c_1 \, for \, \leq z_1 \\ c_2 \, for \, > z_1 \end{cases} \qquad \textit{Equation 1}$$

Where c_1 and c_2 are the sound speeds at heights *z.* This function is more widely known as the *vertical sound speed profile.*

Vertical sound speed profiles are a function of the adiabatic sound speed in the propagation medium, which is a function of the temperature at height *z* (see C.3.1). Therefore, the atmosphere may be seemingly perceived as still by an observer unaware of the diurnal vertical temperature gradients which form from;

- the daytime heating of the sun (upward refraction); and

- the night-time longwave radiative cooling (downward refraction).

The vertical sound speed profile can be combined with the effective horizontal sound speed to describe a moving atmosphere, using the horizontal wind component in the direction of propagation *u*. The resulting effective sound speed c_{eff}, is described below. Over flat homogenous terrain, the effective sound speed is assumed to be a function of the vertical temperature and wind gradients and thus a function of *z*.

$$c_{eff}(z) = c(z) + u(z) \qquad \textit{Equation 2}$$

Because these gradients show more variation in the lower parts of the atmosphere just above the ground, the vertical profiles are better represented logarithmically.

$$c_{eff}(z) = c_0 + b \ln\left(\frac{z}{z_0} + 1\right) \qquad \text{Equation 3 (Attenborough et al., 2006)}$$

Where, c_o is the sound speed at ground level, and z_0 is roughness length of the ground surface. Finally, *b* is a constant used to describe either downward refraction (typical values are 1 m/s) or upward refraction (-1 m/s). Figure 21is a logarithmic sound speed profile for c_0 = 340ms^{-1}, z_0 = 0.1m and *b* = 1 ms^{-1}.

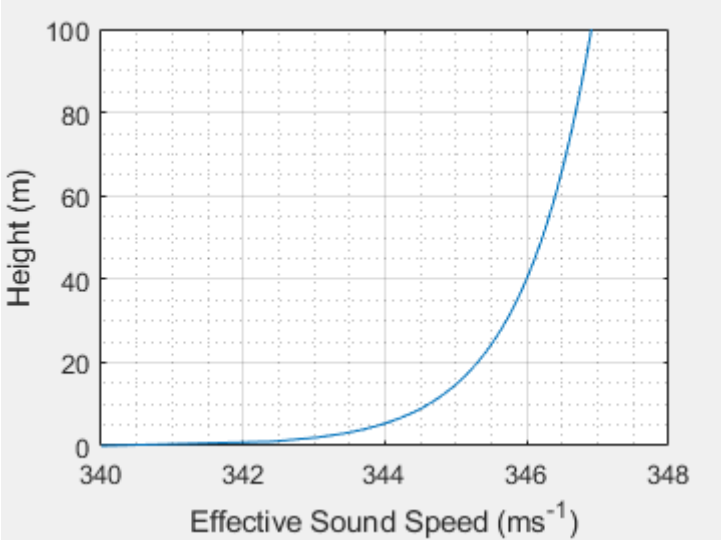

Figure 21 - Logarithmic effective sound speed profile, adopted from Salomons (2001).

The isolated effects of refraction on a travelling wave can be more easily visualised by modelling sound waves as rays that take straight paths from the source and are curved from their paths to a receiver via refraction. The next two sub sections will study the influence of refraction from temperature and wind in isolation.

3.2.2.1 Temperature Gradients

In an atmosphere with no wind, temperature is the major influence on the speed of sound, as shown in Equation 4.

$$c = \sqrt{\frac{\gamma RT}{M}} \qquad \textit{Equation 4}$$

Where c is the speed of sound, γ is the adiabatic index (ratio of heat capacities at constant pressure to constant volume), R is the gas constant $R = 8.31J/mol\ K$, M is the molecular mass and T is the absolute temperature in degrees Kelvin.

Where temperature varies, sound speed varies, leading to sound rays following curved paths as opposed to straight lines. Curve radius at any arbitrary point is inversely proportional to the velocity gradient at that point (Ingård, 1953), where a linear temperature gradient would produce circular ray paths. In reality, temperature gradients are non-linear and hence in isolation, produce cycloidal ray paths (distorted arcs).

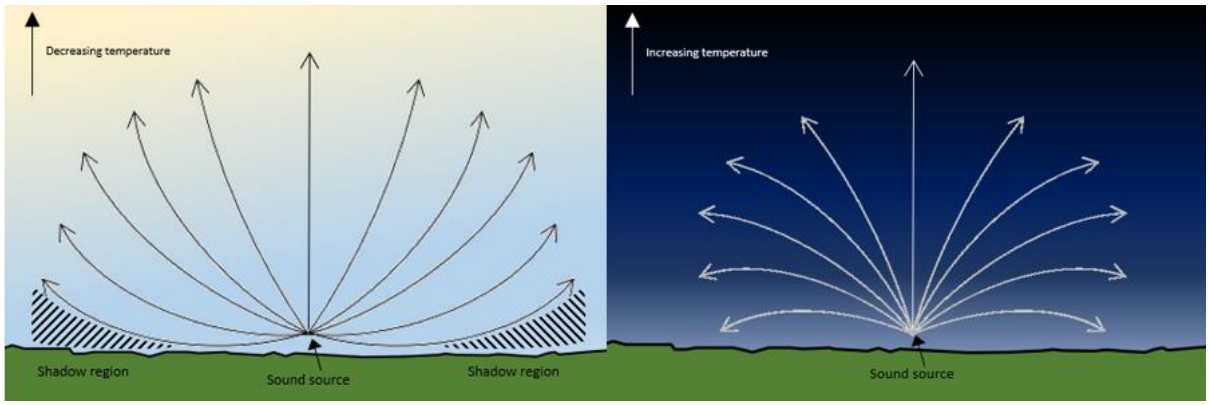

Figure 22 - Visualisation of upward refraction (left) and downward refraction (right) of sound rays, adapted from Brüel and Kjær Sound and Vibration Measurement (2001).

During convective boundary layers, (usually daytime), where thermal heating of the ground causes the usual temperature lapse rate of decreasing temperature with height above ground, sound rays are refracted upwards, (see left of Figure 22). The result is the formation of a shadow region at some distance from the source depending on the strength of the temperature gradient. Ingård (1953) gives an example of a temperature profile of 1°C/100m, where the radius curvature will be about 56km and the distance to the shadow zone of 1.2km.

During stable boundary layers, (usually nocturnal), no shadow region is formed, because sound rays are refracted downwards towards the ground (see right side of Figure 22). This is the result of an inverted temperature lapse, where temperatures at the ground may be

significantly cooler than above. Much of the literature on atmospheric sound propagation limits this phenomenon to night-time, however, weak stable boundary layers may be present during early morning hours, inhibited from transitioning to a convective boundary layer by the presence of a capping inversion, especially during winter months where sunrise is delayed, and thermal heating may be less. This is of major relevance to blast testing at Spadeadam, where early morning tests are common.

3.2.2.2 Wind Gradients

Sound refraction occurs from the presence of wind speed and direction gradients in the atmosphere, in an analogous way to temperature gradients. However, refraction is no longer symmetric around the noise source, and the direction of refraction is dependent upon the wind direction. Where wind speed increases with height, sound waves propagating downwind will bend downward, and upwards during upwind propagation. As before, the magnitude of ray curvature is inversely proportional to the wind speed gradient (Ingård, 1953).

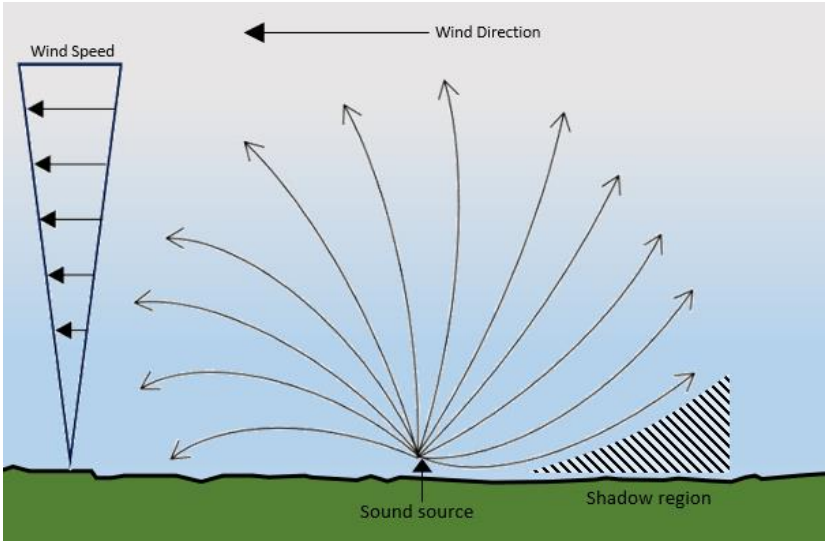

Figure 4 – Sound ray refraction due to wind speed gradient, adapted from Brüel and Kjær Sound and Vibration Measurement (2001)

Ingård (1953) also states that rays that propagate at 90° to the wind (crosswind conditions) are unaffected by the direction of the wind. During combined fields of wind and temperature gradients, wind gradients will dominate the effects of temperature and can cancel the effects of temperature. The formation of shadow zones may not occur during downwind propagation. Upwind from the sound source, the refraction effects of temperature and wind couple to allow strong shadow formation (during the daytime).

3.2.2.3 A Note on Homogeneity

The term, *homogeneity* is used widely in outdoor sound propagation by acousticians to describe atmospheric conditions where sound speed is independent of spatial position in the atmosphere. Usually, conditions are such that sound speed has an inhomogeneous distribution throughout the atmosphere, what atmospheric scientists would call a turbulent atmosphere (where a non-turbulent atmosphere is representative of an acoustically homogenous atmosphere). On the other hand, in turbulence theory, homogeneity refers to the statistical character of the propagation medium, or rather, that "*turbulent fluctuation statistics do not vary with position" (D. K. Wilson, 1996).* Almost paradoxically, in this sense it is not the sound speed but the variation in sound speed that would be assumed constant with position. Although both definitions can be valid dependent on the context, it is critical to understand the difference in definition within the surrounding context.

3.2.2.4 Monin-Obukhov Similarity Theory (MOST)

Monin-Obukhov similarity theory is a widely used approach for deriving vertical sound speed profiles in the atmosphere. The theory is based on the assumption that the turbulence in the atmosphere is driven by buoyancy and shear forces, and that these forces are proportional to the gradients of temperature and wind velocity, respectively. By applying this theory, it is possible to derive the vertical profiles of temperature and wind velocity, which can be used to calculate the speed of sound at different altitudes.

The Monin-Obukhov similarity relations are expressed as dimensionless functions that depend on the Monin-Obukhov length scale and other dimensionless variables. These functions can be used to parameterize the behaviour of the atmosphere in the surface layer, and to model the transfer of heat, moisture, and other variables between the surface and the atmosphere.

The theory is used within the NORD2000 road traffic prediction model for the classification of sound propagation regimes based on measured meteorological data. The profiles are approximated by using the following parameters and a detailed explanation of the theory can be found in (Salomons, 2001).

- Friction velocity, u_*
- Monin-Obukhov Length, L
- Temperature scale, T_*

Attenborough et al. (2006) provide a detailed explanation of Monin-Obukhov similarity theory in their book Predicting Outdoor Sound in the context relevant for such applications. As mentioned above, the minimum requirements for describing the variation of sound speed with altitude through the lower atmosphere is to have known values of wind speed component *u(z)* and temperature *T(z)* as a function of height above ground *(z)*. Similarity theory allows calculation of the those two parameters as follows:

$$u(z) = \frac{u_*}{k}\left[\ln\left\{\frac{z + z_M}{z_M}\right\} + \psi_M\left(\frac{z}{L}\right)\right] \qquad \text{Equation 5}$$

$$T(z) = T_0 + \frac{T_*}{k}\left[\ln\left\{\frac{z + z_H}{z_H}\right\} + \psi_H\left(\frac{z}{L}\right)\right] + \Gamma_z \qquad \text{Equation 6}$$

Several new but necessary terms of the similarity theory are required for definition in the above equations. Attenborough et al. (2006) provide a detailed description of each term in the following format.

u_*	Friction velocity (ms^{-1})	Depends on the surface roughness
z_M	Momentum roughness length	Depends on the surface roughness
z_H	Heat roughness length	Depends on the surface roughness
T_*	Scaling temperature (°K)	283 °K
k	Von Karman constant	0.41
T_0	Temperature (°C) at zero height	283 °K
Γ	Adiabatic correction factor	-0.01 $°Cm^{-1}$ for dry air. Small effect with moisture
L	Obukhov length (m) $> 0 \rightarrow$ stable, $< 0 \rightarrow$ unstable	$= \pm u^2/kgT_*\ (T_{av} + 273.15)$
T_{av}	Average temperature ° C	Given as 10 °C in (Attenborough et al., 2006)

ψ_M	Diabatic momentum profile correction (mixing function)	See eq Z.1
ψ_H	Diabatic heat profile correction (mixing) function	See eq Z.2
χ_M	Inverse diabatic influence or function for momentum	$[1\text{-}16z/L]^{0.25}$
χ_H	Inverse diabatic influence or function for heat	$[1\text{-}16z/L]^{0.5}$

Where if L < 0, i.e unstable conditions;

$$\psi_M = -2\ln\left(\frac{(1+\chi_M)}{2}\right) - \ln\left(\frac{(1+\chi_M^2)}{2}\right) + \arctan(\chi_M) - \frac{\pi}{2} \quad \text{Equation 7}$$

$$\psi_H = -2\ln\left(\frac{(1+\chi_H)}{2}\right) \quad \text{Equation 8}$$

Else if L > 0, i.e. stable conditions:

$$\psi_M = 5\left(\frac{z}{L}\right) \quad \text{Equation 9}$$

$$\psi_H = 5\left(\frac{z}{L}\right) \quad \text{Equation 10}$$

Eq is also applicable if $z \leq 0.5\,L$.

The resulting profiles, known as the Businger-Dyer profiles are derived from Equation 6 and have been shown to give good agreement to measured data up to 100m. Although, a small portion of the atmosphere, this height is relevant to propagation of sound up to 10km.

$$C = A\ln\left(1+\frac{z}{z_0}\right) + Bz + C(0) \quad \text{Equation 11}$$

Note the similarity of Equation 11 to Equation 3, only now there is the A and B terms have different meanings. In the Nord2000 propagation model, from which Equation 6 is found, the

A term represents the logarithmic term, and B represents the linear term of the sound speed profile. C(0) is the reference adiabatic sound speed.

Salomons (2001) gives an equally detailed presentation of these profiles in Appendix N of his book "Computational Atmospheric Acoustics", however, with more emphasis on the meteorological terms pertinent to the derivation of these sound speed profiles, and provides the absolute temperature T, in terms of the potential temperature θ. It is important to understand the difference between the absolute, and potential temperature as they both have key properties of variation with height in the ABL.

As the pressure in the ABL decreases with height due to gravity, for an adiabatic ideal gas, with T as the temperature, p as the pressure and γ the specific-heat ratio of air (=1.4), the following relations for a constant known as the adiabatic lapse rate can be found.

$$\frac{T}{p^{(\gamma-1)/\gamma}} = constant \qquad \text{Equation 12}$$

The adiabatic approximation is that temperature must decrease with increasing height according to the following.

$$a_0 = \frac{dT}{dz} = -\frac{\gamma - 1}{\gamma}\frac{\rho T}{p}g \qquad \text{Equation 13}$$

With ρ as the density, and g the gravitational acceleration ~9.8 ms^{-2}. The dry adiabatic lapse rate, a_0 is typically taken as 0.01 Km^{-1} For example, at Spadeadam, a more typical temperature, pressure and air density than that quoted in the literature may be T = 283.15 K, p = 990 hPa and ρ = 1.26 kgm^{-3}, a dry adiabatic lapse rate of 0.01 is found.

Regarding the Obukhov length, *L*, it is also common in the literature to see these profiles expressed with the reciprocal of *L* (L^{-1}). In which case, $L^{-1} < 0$ represents an unstable atmosphere, $L^{-1} = 0$ neutral, while L^{-1} represents a stable atmosphere.

The Harmonoise and Nord2000 (Eurasto, 2006) sound propagation models use a simplified method of deriving the atmospheric profiles of temperature and wind using similarity theory. It is done by using the aforementioned key parameters; friction velocity (u_*), temperature scale (T_*) and Obukhov length (L), (referred to as the "Monin-Obukhov length") in (Eurasto, 2006). The following look-up tables (Table 17 to Table 21) are used to choose meteorological

wind and stability classes based on wind speed (vector, i.e. in the direction of propagation), time of day and cloud cover (measured in oktas), and finally derive the Monin-Obukhov similarity parameters.

Table 17 - Wind Speed Classes based on 10m vector wind, from Eurasto (2006).

Wind speed at 10 m above ground, u_{10} (m/s)	**Wind Speed Class**
0-1	W1
1-3	W2
3-6	W3
6-10	W4
>10	W5

Table 18 - Atmospheric stability classes based on time of day and cloud cover, from Eurasto (2006).

Time of Day	**Cloud Cover (oktas)**	**Stability Class**
Day	0/8 – 2/8	S1
Day	3/8 – 5/8	S2
Day	6/8 – 8/8	S3
Night	5/8 – 8/8	S4
Night	0/8 – 4/8	S5

The first parameter of the stability theory, the friction velocity u^* is derived from Table 19, based on wind class.

Table 19 - Friction velocity, u based on wind class, from Eurasto (2006).*

Wind Class	**Friction velocity, u_* in m/s**
W1	0.00
W2	0.13
W3	0.30
W4	0.53
W5	0.87

Thus, the temperature scale T_* in ° Kelvin is determined from the following matrix of wind and stability class.

Table 20 - Temperature scale, T based on atmospheric stability class and wind class, from Eurasto (2006).*

Temperature Scale in ° K	**S1**	**S2**	**S3**	**S4**	**S5**
W1	-0.40	-0.20	0.00	+0.20	+0.40
W2	-0.20	-0.10	0.00	+0.10	+0.20
W3	-0.10	-0.05	0.00	+0.05	+0.10
W4	-0.05	0.00	0.00	0.00	+0.05
W5	0.00	0.00	0.00	0.00	0.00

Finally, the inverse of the "Monin-Obukhov length", *1/L* is determined from the matrix of wind and stability classes.

Table 21 - Inverse of Monin-Obukhov length, L based on stability and wind classes, from Eurasto (2006).

	S1	**S2**	**S3**	**S4**	**S5**
W1	-0.08	-0.05	0.00	+0.04	+0.06
W2	-0.05	-0.02	0.00	+0.02	+0.04
W3	-0.02	-0.01	0.00	+0.01	+0.02
W4	-0.01	0.00	0.00	0.00	+0.01
W5	0.00	0.00	0.00	0.00	0.00

Finally, the constants A and B of Equation 6 are determined based on stability classes and time of day.

During the day

$$B = \frac{u_* \cos(\alpha)}{kL} + \left(\frac{1}{2}\frac{c_0}{T_{ref}}\right)\left(0.74\frac{T_*}{kL} - \frac{g}{c_p}\right) \qquad \text{Equation 14}$$

During the night

$$B = 4.7\,\frac{u_* \cos(\alpha)}{kL} + \left(\frac{1}{2}\frac{c_0}{T_{ref}}\right)\left(4.7\frac{T_*}{kL} - \frac{g}{c_p}\right)$$ Equation 15

$$A = \frac{u_* \cos(\alpha)}{kL} + \left(\frac{1}{2}\frac{c_0}{T_{ref}}\right)\left(0.74\frac{T_*}{kL}\right)$$ Equation 16

There are several new terms here which need defining, such as c_p which is the specific heat capacity of air at constant pressure (=1005 J/kg K) and α, which is the angle between the wind direction (from which blowing) and the direction from source to receiver. The von Karman constant is also referenced as c_{vk} in the Harmonoise and Nord2000 literature.

Upon calculating A and B, a specific propagation situation can be assigned based on aggregated values of A and B. This quantises the effectively infinite propagation scenarios (where A and B vary continuously), to 25 meteorological classes, defined by particular intervals of A and B.

Table 22 - Meteorological class intervals for linear (B) profile parameters

	B1	B2	B3	B4	B5
Interval	$-\infty < B \leq -0.08$	$-0.08 < B \leq -0.02$	$-0.02 < B \leq 0.02$	$-0.02 < B \leq 0.08$	$-\infty < B < \infty$
Given Value	-0.12	-0.04	0	0.04	0.12

Table 23 - Meteorological class intervals for logarithmic (A) profile parameters.

	A1	A2	A3	A4	A5
Interval	$-\infty < A \leq -0.7$	$-0.7 < A \leq -0.2$	$-0.2 < A \leq 0.2$	$0.2 < A \leq 0.7$	$0.7 < A < \infty$
Given Value	-1.0	-0.4	0	0.4	1.0

3.2.3 Influence of Ground on Propagation

3.2.3.1 Ground Impedance and Interference Effects

Ground effects for an elevated source and receiver arise from the interference of direct and reflected sound waves as they travel between the source and receiver. Either an attenuation or enhancement can occur, but it is usually an amalgamation of both for sounds containing many frequency components. On an acoustically hard ground (concrete, asphalt), sound pressure is doubled over a wide audible frequency range and the frequencies of the destructive interferences can be calculated from the following.

$$f_n = (2n+1)\frac{c}{2(r_2 - r_1)}, n = 0,1,2 \dots n \qquad \textit{Equation 17}$$

Where r_2 and r_1 are the path lengths of the ground-reflected and direct rays from source to receiver respectively.

Ground effects on outdoor sound propagation have been the subject to many detailed experimental and theoretical studies found within the literature of the last century. There can be many types of waves within the ground surface, resulting from incident airborne sound waves. However, simplified models which describe the ground as a *locally reacting surface* where the single type of compressional wave within the ground is considered to travel mainly in the pores and normal to the surface, are generally preferred. Piercy, Embleton, and Sutherland (1977) point to a lack of evidence that propagation over ground is not adequately predicted by this simplified model in comparison with a more complex one.

A locally refracting ground assumes that the speed of sound in the ground (c_1) is much smaller than the speed of sound in the air (c), $c_1 \ll c$. In turn, this allows a refractive index (n_1) $\gg 1$, where $n_1 = c/c_1$ and incident rays are refracted towards the normal of the ground-air surface, and air ground interactions are independent of angle of incidence of the incident sound rays (Attenborough, 2014).

A locally reacting ground can be characterised acoustically by the relative normal-incidence surface impedance (Z) and its inverse, the relative admittance (B), where a perfectly hard ground would have infinite impedance and zero admittance. In terms of how much sound energy is reflected back to the air, the locally reacting surface may be represented by the

amplitude reflection coefficient, R_p for a *plane wave* incident at some angle upon aground, shown in Equation 6.

$$R_p = \frac{\sin\phi - Z_1/Z_2}{\sin\phi + Z_1/Z_2}$$ *Equation 18 (Piercy et al., 1977)*

Where ϕ is the incident angle of the plane wave. Z_1 is the *characteristic impedance* of the air = ρc, and Z_2 is the acoustic impedance of the surface. Both R and Z_2 are represented in complex notation, where the imaginary term of the Z_2, accounts for the reactance of the surface, X, as shown in *Equation 7*.

$$Z = R + iX$$ *Equation 19*

Plane Wave Assumptions

For propagation over a perfectly reflecting hard surface (Z is infinite), where the reflection coefficient R_p is 1, the phase change upon that reflection is zero (Piercy et al., 1977). In reality, surfaces are never perfectly reflecting but Z may be very large as opposed to infinite, and for normal incidence, sin(ϕ) = 1, R_p will be almost 1.

For very long-distance propagation of a plane wave over this hard but finite surface, ϕ is very small and hence the term sin(ϕ) is very small compared to the impedance ratio. In this case, R_p is effectively -1, signifying a 180° change in phase upon reflection. Ultimately, this means cancellation by destructive interference of the incident and reflected waves, which is essentially a shadow zone with acoustical depth dependent upon the value of the ground impedance (Piercy et al., 1977). This is an attenuation in dB in excess of that already caused by geometrical spreading and atmospheric absorption.

$$A_e = 20\log_{10}[2\sin\phi\ Z_2/Z_1]$$ *Equation 20 - (Piercy et al., 1977)*

Ground surfaces are often characterised generally as either acoustically hard or soft, where in ISO 9613-2, all surfaces concerning trees and vegetation are considered to be acoustically soft (Attenborough et al., 2006). However, Attenborough, Bashir, and Taherzadeh (2011) state that variation in the influence of ground impedance from different types of "grassland" can be significant. Such effects are recognised in recent prediction schemes (Nord 2000 and

Harmonoise) and by standard methods for deducing ground impedance from short-range propagation measurements. Porous ground surfaces are generally elastic, and such an elastic response may be significant for blast noise which concerns such low frequency noise (Attenborough et al., 2011).

Spherical Waves

By considering a point source at location S, producing a sound pressure p, at receiver R, the acoustic pressure of a spherical wave over a plane boundary with acoustic impedance Z_2 may be calculated by the Weyl-Van de Pol solution.

$$\frac{p}{p_0} = \left(\frac{1}{r_1}\right)\exp(-ikr_1) + \left(\frac{R_p}{r_2}\right)\exp(-ikr_2) + \left[\left(1 - R_p\right)\left(\frac{F}{r_2}\right)\exp(-ikr_2)\right] \qquad \textit{Equation 21}$$

Where p_0 is the pressure resulting from the source at receiver R without the influence of the ground surface (i.e. a direct ray) and k is the wavenumber, $2\pi/\lambda$. The direct and reflected ray paths are represented by distances r_1 and r_2 respectively. The reflected distance arises from the reflection but may be visualised as appearing from an image source, as depicted in Figure 23.

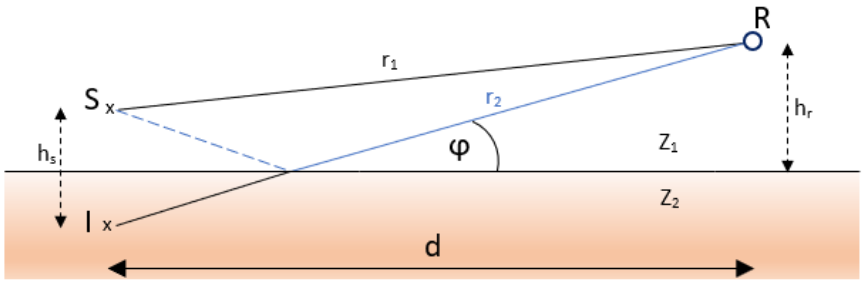

Figure 23 Propagation and reflection of sound from a point source S, over a ground with impedance Z2. Adapted from Piercy et al. (1977) and Attenborough (2014).

Finally, the term F arises from a need to capture the influence of the wavefront curvature, with distance along the boundary, and is a mathematical function of the numerical distance, *w*.

$$w = \left(\frac{1}{2}ikr_1\right)\left(\sin\phi + \frac{Z_1}{Z_2}\right)^2 \qquad \textit{Equation 22}$$

This numerical distance is essentially scaling the distance with respect to sound frequency, f and the grazing angle ϕ.

The analytical solutions for a spherical wave above the ground are presented by (Attenborough, 2014), are in terms of the pressure, rather than a ratio of reflected and direct pressure (p/p_0), with representation of the inverse square term in $p = \frac{e^{-ikR_1}}{4\pi R_1}$. Of course, within Attenborough's descriptions, the solutions still include the parameter F, where F(w) referred to as the boundary loss factor given by Equation 22, where *erfc* refers to an associated error function.

$$F(w) = 1 - i\sqrt{\pi}w \exp(-w^2)erfc(iw) \qquad \textit{Equation 23}$$

This term still represents the interaction of the spherical wavefront with the ground surface. Attenborough states that the term within the square brackets of Equation 20 may be interpreted as a spherical wave reflection coefficient, Q, as in Equation 23.

$$Q = R_p + \left(1 - R_p\right) F(w) \qquad \textit{Equation 24}$$

Regardless, there is a correction to the plane wave solution using this spherical term, and the contribution of that wave curvature to the total sound field is carried forward in a term called the *ground wave*, from the original development of the analytical solutions which originally concerned the propagation of electromagnetic waves over hard surfaces.

For application to blast noise travelling over large distance, ($R_2 \rightarrow \infty$) then $|w| \rightarrow \infty$, and hence, the spherical wave correction term tends to zero ($F \rightarrow 0$), and with these conditions, plane wave propagation over a rigid boundary can be assumed.

Non reacting ground surface

In cases where the ground cannot be assumed as an impedance plane (n1 not much larger than 1), refraction of sound into the medium depends on the angle of incidence (Attenborough, 2014). Meaning that the impedance no longer depends only on the properties of the medium, but also the angle of incidence into that medium, with an effective impedance. The cases involving these ground types are referred to by (Attenborough et al., 2006) as layered extended-reaction grounds. In summary, this is dealt with by using an

effective impedance, which is expressed in Attenborough's works as it's inverse, the effective admittance, B_e, of which there are solutions for computation.

Ultimately, the relevance of these situations is that some surfaces, such as forest floors (which surround Spadeadam), have a highly porous layer of forest litter built up upon a hard sublayer, requiring the need to be modelled with this effective admittance.

Delaney and Bazley Model

The well-known single-parameter model (Delany & Bazley, 1970) for acoustic impedance is widely recognised in the field of outdoor sound propagation, which uses *effective flow resistivity* σ_e as the sole parameter to characterise the ground. The propagation constant *k* and normalised characteristic impedance are given by

$$\frac{k}{k_1} = \left[1 + 0.0978\left(\frac{f}{\sigma_e}\right)^{-0.7} - i0.189\left(\frac{f}{\sigma_e}\right)^{-0.595}\right] \qquad \textit{Equation 25}$$

$$Z = \frac{\rho_1 c_1}{\rho c} = 1 + 0.0571(f/\sigma_e)^{-0.754} - i0.087(f/\sigma_e)^{-0.732} \qquad \textit{Equation 26}$$

Where *f* is the sound frequency.

Flow resistivity

Within the ground impedance literature, surfaces may be more commonly known by their range of effective flow resistivities, σ_e. This may be deduced from measurements of a frequency spectrum of a sound field. Alternatively, σ_e may be used to compute the sound pressure level spectrum for a given surface with known σ_e, through Equation 26. The effects of a surface with high flow resistivity (hard ground) are apparent in a frequency spectrum with sharp interference minima. On the other hand, soft grounds with low flow resistivity

have ever increasing phase change on reflection with increasing frequency.

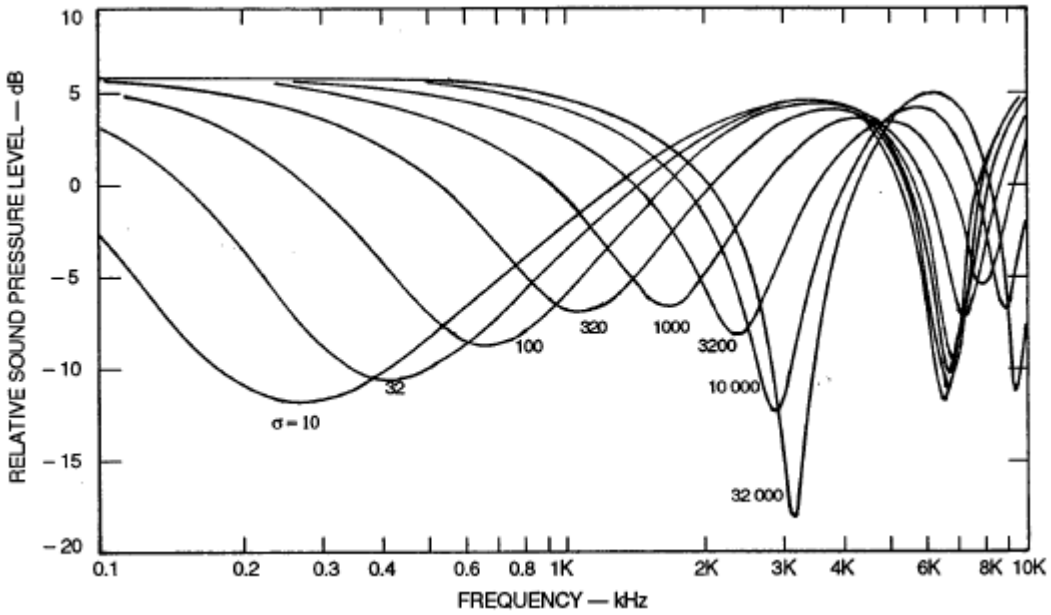

Figure 24 - Excess attenuation spectra using variable flow resistivity (Tony F. W. Embleton, 1996) originally from T. F. W. Embleton, Piercy, and Daigle (1983).

Figure 24shows that for hard ground, with very high σ_e, the interference minima occur at a frequency coinciding with the path length differences between direct and reflected rays and are at 1/2 and 3/2 of the wavelength for that particular geometrical configuration. Very soft ground on the other hand, for example a very low σ_e of 10 kPa m/s^2 has a minimum occurring firstly between 200-300Hz for the particular geometrical set-up. It's worth noting that the minima become more refined to a particular set of frequencies as σ_e increases.

A two-parameter model, proposed by Attenborough can be used for the determination of ground impedance, by using flow resistivity and a parameter relating to porosity.

$$Z = 0.436(1 - i)\sqrt{\frac{\sigma_e}{f}} - 19.74i\frac{\alpha_e}{f} \qquad \textit{Equation 27}$$

Where α_e is the *effective rate of porosity change with depth*, with units m^{-1}. Equation 26 is presented in a simple form, where the constants, 0.436 and 19.74 are functions of the constants π, γ, c and ρ_0, and may be presented using these terms in other literature. This model is also known in the literature as the variable depth model and is often used in conjunction with experimental free-field methods of deriving ground impedance of ground surfaces, such as in ANSI S1.18-2010.

Attenborough (2014) claims that considerable evidence suggests that this single-parameter model overestimates the attenuation of high flow resistivity (hard) ground. This model was used for fitting impedance relationships to measured data in Nicolas, Berry, and Daigle (1985), where unsatisfactory fits occurred at low-frequency.

Table 24 - Characterisation of ground surface by effective flow resistivity, obtained through measurement by (T. F. W. Embleton et al., 1983)

Surface Type	**Effective flow resistivity, σ_e (kPa s/m^2)**
0.1m new fallen snow, over older snow	10-30
sugar snow	25-50
floor of evergreen forest	20-80
airport grass or old pasture	150-300
roadside dirt, ill-defined, small rocks up to 0.01-m mesh	300-800
sandy silt, hard packed by vehicles	800-2500
thick layer of clean limestone chips, 0.01- to 0.025-m mesh	1500-4000
old dirt roadway, small stones with interstices filled by dust	2000-4000
earth, exposed and rain-packed	4000-8000
very fine quarry dust, hard packed by vehicles	5000-20000
asphalt, sealed by dust and use	~30000
upper limit, set by thermal conduction and viscosity	$2x10^5 – 1x10^6$

The list of enhanced theoretical models is significant, with models including more physical parameters for characterising the ground and porous materials. Such models include porosity and tortuosity of the pores of the material, for example Attenborough's four-parameter model. However, the uncertainties reduced by using more detailed physical models may be swept up by the other sources of uncertainty relevant to outdoor sound propagation which are of significance, such as from turbulence. Although it is beneficial for this research to have an awareness of the other more detailed ground impedance models, the Delaney & Bazley and variable porosity models, are adequate for the needs of modelling blasts at Spadeadam.

ANSI S.12.17-1996

ANSI standard 12.17-1996 provides simple calculations for the propagation of impulsive sound from explosives over 3 ground surface types. Annex B of the standard contains calculations for the C-Weighted Sound Exposure Level, (LCE). The details of each calculation are outlined in Table 25.

Firstly, the ANSI 12.17-1996 method only provides corrections for 3 types of land, with only one of which (through dense forest) being relevant to the Spadeadam landscape. Furthermore, this method, however convenient, does not provide enough detail to make analytical solutions of the combined meteorological and ground effects on sound propagation, such as the influence of refraction, and is limited by assumptions of an acoustically neutral atmosphere.

Parameter based models such as those discussed in the following are more useful for the understanding of blast propagation over various ground at Spadeadam.

Table 25 - ANSI S.12.17-1996 Annex B adjustments to C-Weighted Sound Exposure Level of impulsive noise for 3 differing ground types.

Ground Surface	**Calculation**
Over water	$LCE = 111.1 - 22.4\log_{10}(d/1) + C$
Dry-arid land	$LCE = 106.1 - 32.6\log_{10}(d/1) + C$
Through dense forest	$LCE = 95.9 - 32.3\log_{10}(d/1) + C$

The term C in Table 25 is the explosive adjustment term, which factors in the TNT equivalence of the explosive, with mass *m* in kilograms.

$$C = 8.2\log_{10}(m/1) \qquad \textit{Equation 28}$$

The source-receiver distance is d.

Interaction with Snow

An important consideration for this thesis is the interaction of blast waves with snow. Spadeadam's latitude means that snow is common throughout winter months and widespread from source to receiver. The interaction of blast waves with snow covered ground is consequently of significance to this thesis, and knowledge of how snow effects low-frequency impulsive sound is presented here.

General research on sound propagation above snow (5-50 cm thick) was carried out by Nicolas et al. (1985), but for very short propagation distances (up to 15 m). That research also

concerned the effects of snow on frequencies between 200-500 Hz, greater than the peak frequency of blasts relevant to Spadeadam's testing. The authors however came to a conclusion that comparison of a model simulating snow with measurements suggested that at lower frequencies, snow covered ground behaves as a semi-infinite porous ground.

D. G. Albert and Hole (2001) took these findings and applied it to snow cover effects on blast impulses generated by 1 kg C4 explosions, using a porous medium model. The model (rigid-ice-frame model) was a version of Attenborough's rigid-frame porous impedance model (Attenborough, 1985), which has shown to give good agreements to measurements, especially at low frequencies relevant to blasts. The blasts recorded in Albert and Hole's 2001 paper were carried out in 1995 on open field pastureland by a number of research groups from all over the world, including the Acoustics Research Centre of the University of Salford as part of a series of blast noise field trials in Norway (Kerry, 1996). Recorded pulses of the C4 detonations had a broad frequency content between 10-100 Hz, peaking at 30 Hz. A linear source-measurement array was used to detonate C4 explosives at 2 m above ground, and record impulses at 0.6-2000 Hz sampling frequency at 100, 200, 400, 750, 1100, 1300, 1400 and 1500 m upwind and downwind, 0, 2, 4 and 8 m above ground. The thickness of the snow in general ranged from 11.0-20.5 cm thick, with most values between 14-16 cm, a range typical of Spadeadam.

Albert and Hole carried out an inversion technique in their paper to derive the conditions of the snow for their rigid-porous model in a homogenous atmosphere, a method of iteratively tuning the parameters of the model until good agreement with measurement is found. They achieved a good agreement between measured and simulated waveforms (see Figure 25), showing that simulations of impulse propagation over snow using a rigid-porous ground surface in homogeneous atmospheres could match the pulse broadening effects observed in the physical measurements. Effective flow resistivities were derived by the inversion technique for each source-receiver geometry and were more consistent downwind (16-31 kPa sm^{-2}) and were higher and fluctuated more randomly with distance upwind (34-74 kPa s m^{-2}).

A key conclusion reached by Albert and Hole is that blast waves propagating over snow exhibit pulse broadening effects. Pulse broadening refers to the increase in the duration of the waveforms with increasing propagation distance above snow. Albert and Hole used a Fast Field Program (FFP) (see section 3.3 on propagation models), to calculate the waveforms of the C4 explosions at the measurement distances of the field trials. The mechanism

responsible for this broadening effect is claimed by Albert and Hole to be the combined interaction of the snow and the wind. They explain this by comparing the effects on downwind to upwind waveforms, where the downwind waveforms are expected to have increased amplitude relative to a homogeneous atmosphere, as more energy is refracted towards the microphone. The interaction with the snow in the downwind direction however, decreased the waveform amplitude and increased its duration.

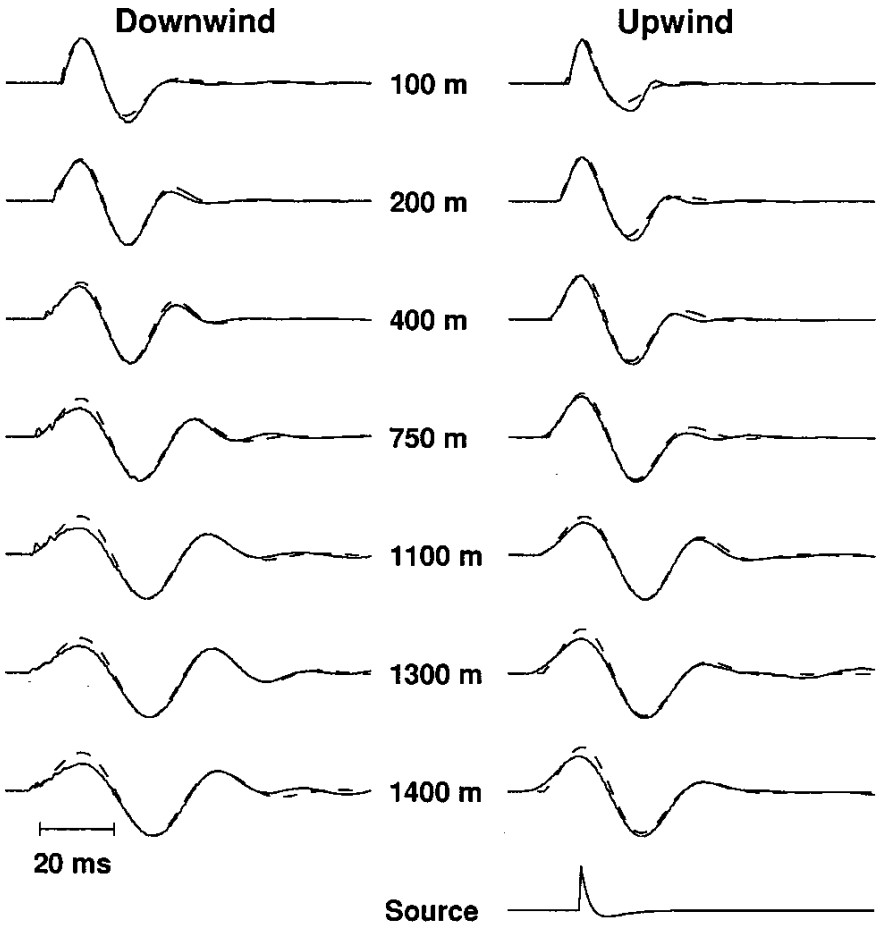

Figure 25 - Normalised pressure-time histories recorded 2m agl upwind and downwind of 1kg C4 explosions (solid line), superimposed with predicted waveforms using the rigid-porous medium model (dashed), taken directly from D. G. Albert and Hole (2001).

Air-ground coupling of low-frequency sound and vibration

Under certain propagation conditions, a coupling effect between an atmospheric sound wave (a sound wave in air), and the surface wave (a wave travelling along or within a surface of the ground). This mechanism is described by Press and Ewing (1951) who give a detailed theoretical explanation of what they refer to as "ground roll", claiming that effective coupling is achieved when the phase velocity of the surface wave is equal to the speed of sound in air. The same mechanism is described much more recently by D. G. Albert, Taherzadeh,

Attenborough, Boulanger, and Decato (2013) as air-to-seismic coupling and the resulting effect as an air-coupled seismic wave. The resultant seismic wave in the ground is a Rayleigh wave.

As the speed of Rayleigh waves in layered ground varies with frequency, (Press and Ewing state this variation with respect to wave period), the ratio of the Rayleigh wave speed essentially comes into and out of phase with the atmospheric sound speed (periodically exceeding and falling short of the speed of sound in air), giving rise to a surface wave pattern in the ground. Much of the earlier research in the early 1950's in this area was focused on the strong coupling effects of matched Rayleigh wave and atmospheric sound speed, for example Ewing, Jardetzky, Press, and Beiser (1957), and the aforementioned 1951 paper by Press & Ewing.

Application of Air-ground interaction to blast noise

Christian Madshus et al. (2005) apply their focus directly on air-ground coupling to low-frequency sound and vibration propagating over long distances from blasting. The experimental data analysed in that work came from the so called "Norwegian Trials" mentioned throughout this thesis carried out between 1994-1996 at 2 sites in Norway.

During the Norwegian trials, monitoring stations were set up to capture above and below ground measurements of hundreds of spherical C4 charges weighing 1, 8 and 64 kg, detonated 2 m above ground. Significant expertise was required to obtain such an extensive measurement database, consisting of different instrumentation teams from different research groups. Along with extensive meteorological instrumentation, the acoustic measurement instrumentation itself consisted of (slightly) buried seismometers, a microphone directly above the surface and the seismometer, and another microphone above the former at 1m above ground. During winter months, ground sensing equipment was placed both on top of the frozen ground, and within the top of the snow cover. Madshus et al's paper analysed the air and ground instrumentation from a particular station at the Finnskogen site ("Long range site") during the summer months.

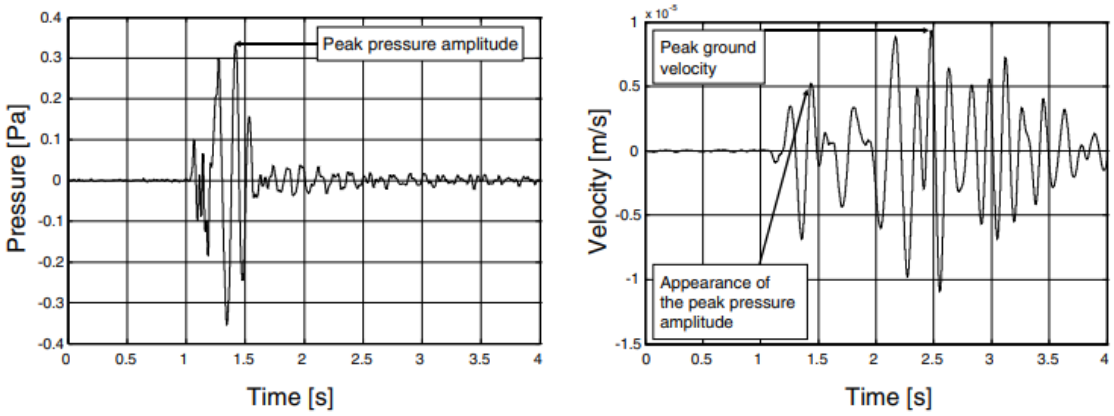

Figure 26 - Comparison of air overpressure and seismic velocity waveforms from Christian Madshus et al. (2005) for an 8 kg C4 charge at 16 km.

Madshus et al presented a typical set of air and ground pressure time histories for a blast that claims to show the fundamental nature of low-frequency air-ground interactions from blasting. The waveforms show the air overpressure (sound wave on the right of Figure 26) as a comparatively short transient compared to the air induced ground response, which exhibits additional signal features, such as the tail of oscillations that follows after the peak of the pressure pulse arrives.

Ground vibration at some receiver point from blasting can arrive by a seismic or an acoustic pathway. The seismic mechanism is perhaps unsurprisingly via strong vibrations excited in the ground immediately around the explosive, especially in the case of buried charges. Madshus et al explain how that at relatively short-range, observations of the individual seismic waves (compressional, shear and Rayleigh waves) may be made, related to the source-receiver geometry and the respective seismic speed of each wave type in the ground. On the other hand, the acoustically transmitted vibration is a consequence of the ground's response to acoustic excitation via air overpressure propagating immediately above the ground surface, and is controlled by the sound speed in air. Figure 27 shows the response at 200 m of the microphone against a seismometer for a partly-buried 50 kg charge, quoted by Christian Madshus et al. (2005) from earlier study carried out by C. Madshus and Nilsen (2000).

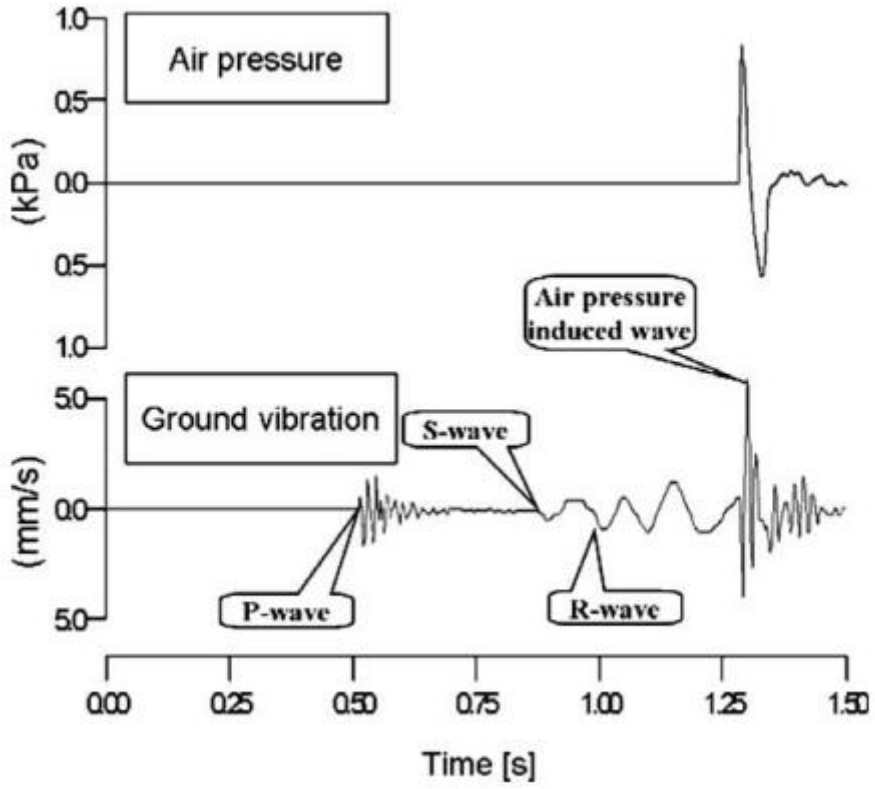

Figure 27 - Air overpressure vs ground response from a partially buried 50 kg charge originally from C. Madshus and Nilsen (2000), taken directly from Christian Madshus et al. (2005). The compressional (P-wave), shear (S-wave) and Rayleigh waves (R-wave) are all visible on the seismometer trace.

Another comparison is made of the decay rate for seismically and acoustically transmitted waves, the former being much faster than the latter for above ground, on the ground and slightly buried charges.

A detailed explanation of the theory of air-ground coupling is given by Madshus et al. who state that the "tail" of the ground response vibrations results from the continuous interaction of the air-propagating wave as it interacts with the ground from source to receiver, instantaneously exciting vibrations through interactions with the surface which propagate as seismic waves along and through the ground. Whether these vibrations arrive before or after the air propagated wave depends on the ratio of the seismic speed of the ground compared to the speed of sound in air, and in the case presented in Figure 27, the sound speed is greater than the seismic speed, as the dominant vibrations arrive after excitation of the airborne wave. Interestingly, the length of the "tail" relates to the ratio of seismic to atmospheric sound speed, as well as the source-receiver geometry and ground layering, and is said by Madshus et al. (2005) to represent "a memory" of the ground.

Effect of air-ground coupling on ground impedance

Christian Madshus et al. (2005) came to an interesting conclusion about the effects of air-ground coupling on ground impedance with relevance to low-frequency long-range sound propagation. By following the theme of comparing peak overpressure ($\hat{p}$) of the measured blasts to the corresponding peak ground velocity ($\hat{v}$) as a ratio, a rough metric of air-ground interaction is formed which they term the pseudo acoustic-seismic Impedance, $\widetilde{Z_{ag}} = \frac{\hat{p}}{\hat{v}}$. In Figure 28, they plotted the measured results against the expected value of the specific Rayleigh wave impedance, $\bar{z}$ of the ground at the site and found $\widetilde{Z_{ag}}$ to be consistently less than $\bar{z}$, leading the authors to conclude that the ground effectively has a different response from blast to blast depending on $\widetilde{Z_{ag}}$, despite no material changes to the ground otherwise.

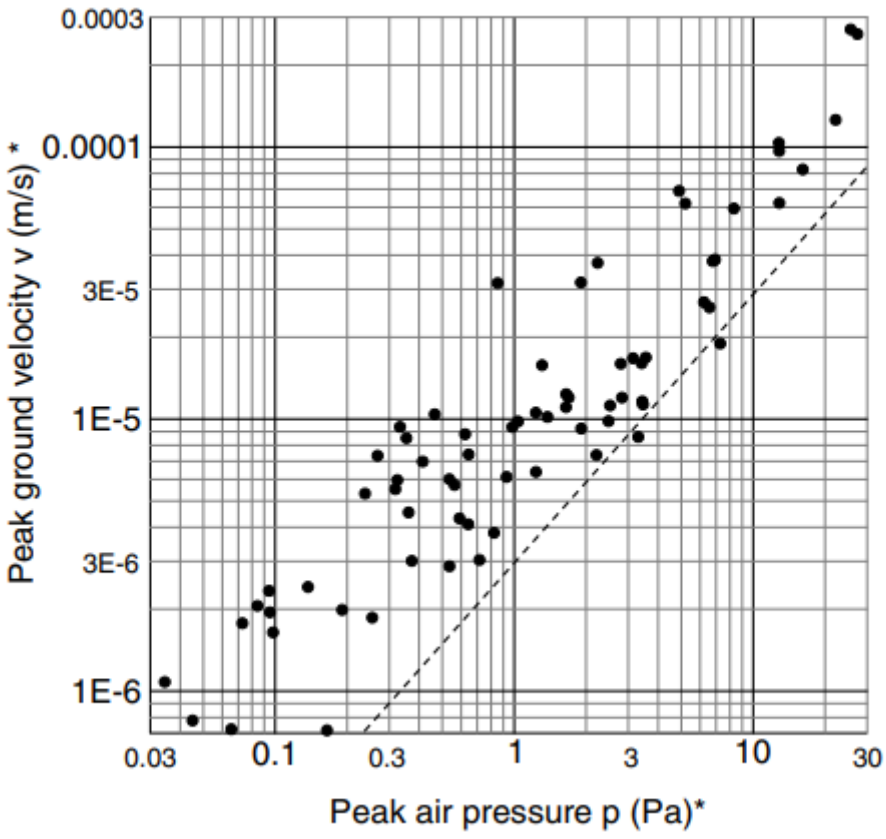

Figure 28 - Peak ground velocity against peak air pressure (pseudo acousto-seismic impedance) for each blast (filled circles). Specific ground impedance is represented by the dashed line (Christian Madshus et al., 2005).

Further theoretical development in their paper pioneered by simulations using a theoretical impedance model investigated the effects varying ground permeability and impedance, and subsequently the authors were able to determine whether the behaviour of the ground was

driven by viscoelastic to porous dependency as a function of frequency. This gave the authors the confidence to conclude that the interaction between the air pressure waves and the Rayleigh waves in the ground effects the ground impedance.

D. G. Albert (1993) had earlier applied this focus by comparing geophone measurements with predictions of ground motions induced by airborne acoustic impulses using a viscoelastic model of the ground, but more importantly, at the same site during the summer and winter (comparing soil and snow cover). Albert found that soil ground motions were modelled successfully, whereas with snow, the decay rates were always underpredicted by the simulations. Under certain conditions snow was found to increase the amplitude of air-surface waves, the mechanism for which is claimed to be an impedance matching effect of thin layers of snow.

Implications of using the D-B model in the time domain

The previously discussed Delany-Bazley model is widely used for predicting the effects of porous materials on sound reflection, and in the context of outdoor propagation may be used for simulating the reflection of a sound wave along the ground. A primary reason for the widespread use of the Delaney-Bazley model in noise mapping is attributed to its simplicity and reasonable agreement with measurements, given that is only has one parameter, that being the flow resistivity, commonly accepted as the most important physical parameters (Taraldsen & Jonasson, 2011).

An important aspect of modelling acoustic propagation in the time-domain however, concerns avoiding the violation of causality. Taraldsen criticises the use of the Delaney-Bazley model in certain cases (Taraldsen, 2005), such as at low-frequency, as it violates the laws of causality. The concept of causality is a fundamental physical principle, which governs that the effect of a cause cannot occur before the cause itself and in an acoustical context refers to a sound pressure at a given point in space cannot depend upon sound pressure at a later time.

At low frequencies, when using the D-B model negative values for the real part of the flow resistivities are encountered, a non-physical consequence of the model. The work of Dragna, Attenborough and Blanc-Benon addressed the implications of using single-parameter ground impedance model at low-frequencies (Dragna, Attenborough, & Blanc-Benon, 2015), and express how the real parts of complex density become less than zero. Dragna et al used predictions to demonstrate that frequency-domain solutions with physically admissible

models rather than single parameter semi-empirical models yielded greater prediction accuracy.

Kirby expands on this in his paper on modifications to the Delaney-Bazley model (Kirby, 2014) where he suggests low-frequency corrections are required for surface impedance or absorption coefficients in porous material, such as the ground. Miki (Miki, 1990) had originally proposed a correction for this issue, but Kirby concluded that an alternative method based on physical properties should be used.

3.2.3.2 Ground Impedance Measurement

The standard utilises measurements of the interference between direct and reflected sound (known as level differences) to deduce the *normalised specific acoustic impedance* and impedance model parameters (σ_e and α_e) determined by best fits to templates of calculated level differences. Ultimately it is possible to deduce the real and imaginary parts of the normalised specific acoustic impedance ratio ($Z/\rho_0 c$) of outdoor ground surfaces.

The newest revision of the standard utilises 2 geometries (A and B), where A covers a greater frequency range, and B generally emphasises ground effect at frequencies greater than 1kHz and may be better suited for hard grounds. Both geometries make use of upper and lower microphone measurements, from which complex sound pressure ratio *T* is formed. Within ANSI S1.18-2010, equations 1-2 and 3-4 of the standard represent the real and imaginary parts of normalised specific acoustic impedance from the 1-parameter and 2-parameter models respectively. Measurements of the level differences are compared to the template level differences shown in Figure 29through to Figure 32.

A series of steps are followed to compare the computed level difference $LD_c(f)$, with the average level measured difference $LD_{av}(f)$ found from the measured the complex pressure ratio, T. Finally, the parameters for which this difference is minimum is found.

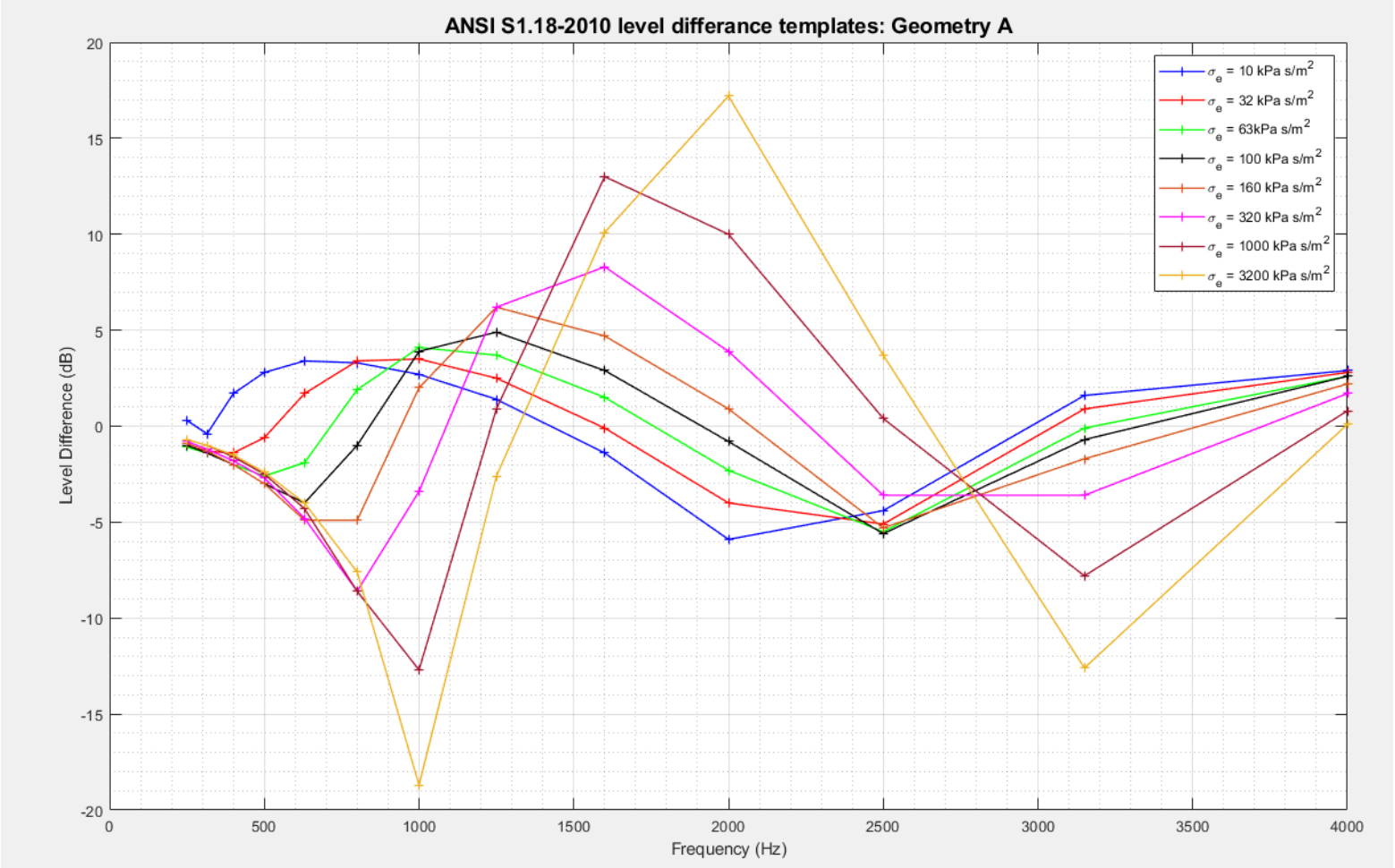

Figure 29 - ANSI S1.18-2010 level difference template curves for geometry A using 1-Parameter model, with a range of σe.

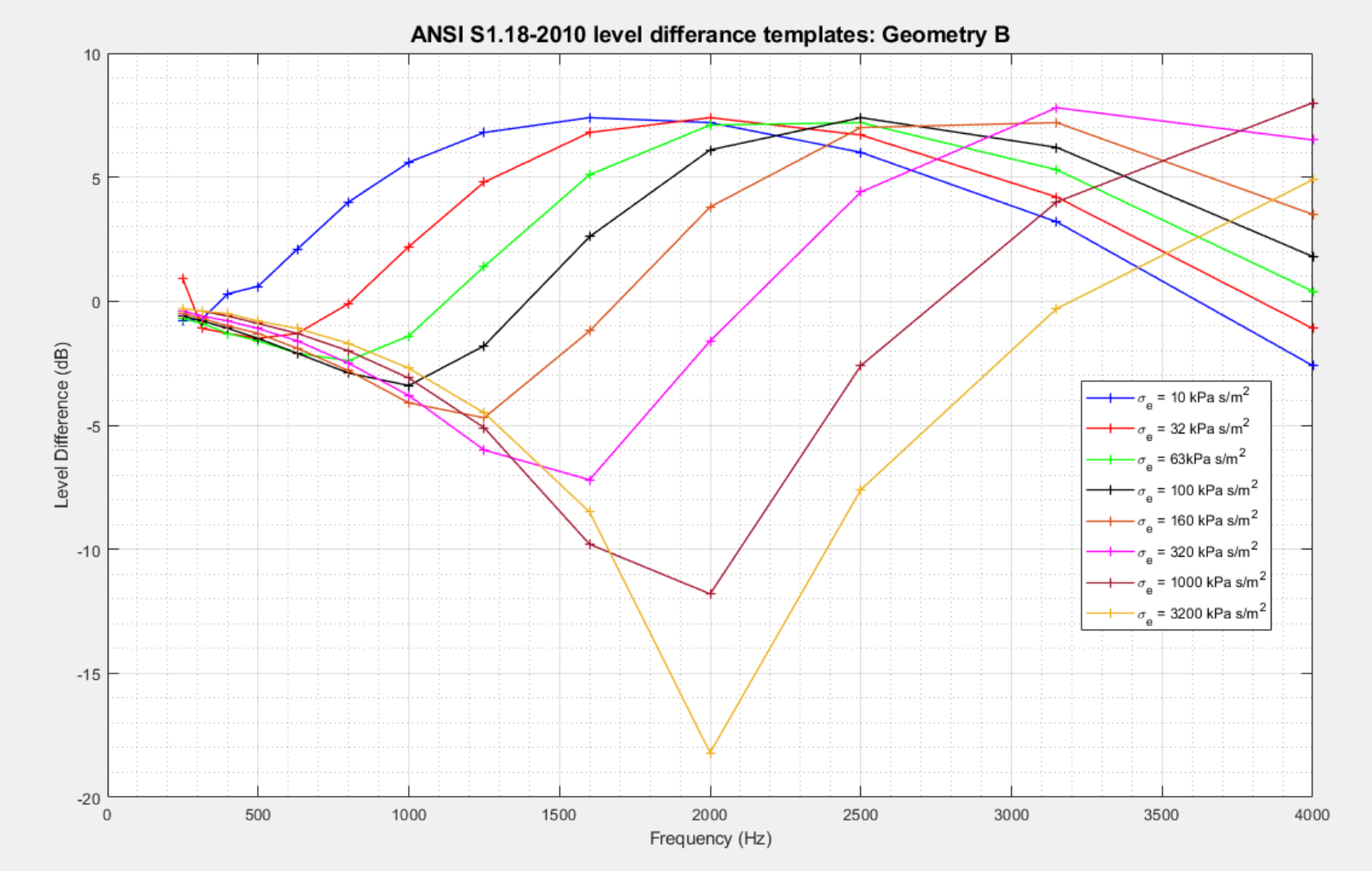

Figure 30 - ANSI S1.18-2010 level difference template curves for geometry B using 1-Parameter model, with a range of σe

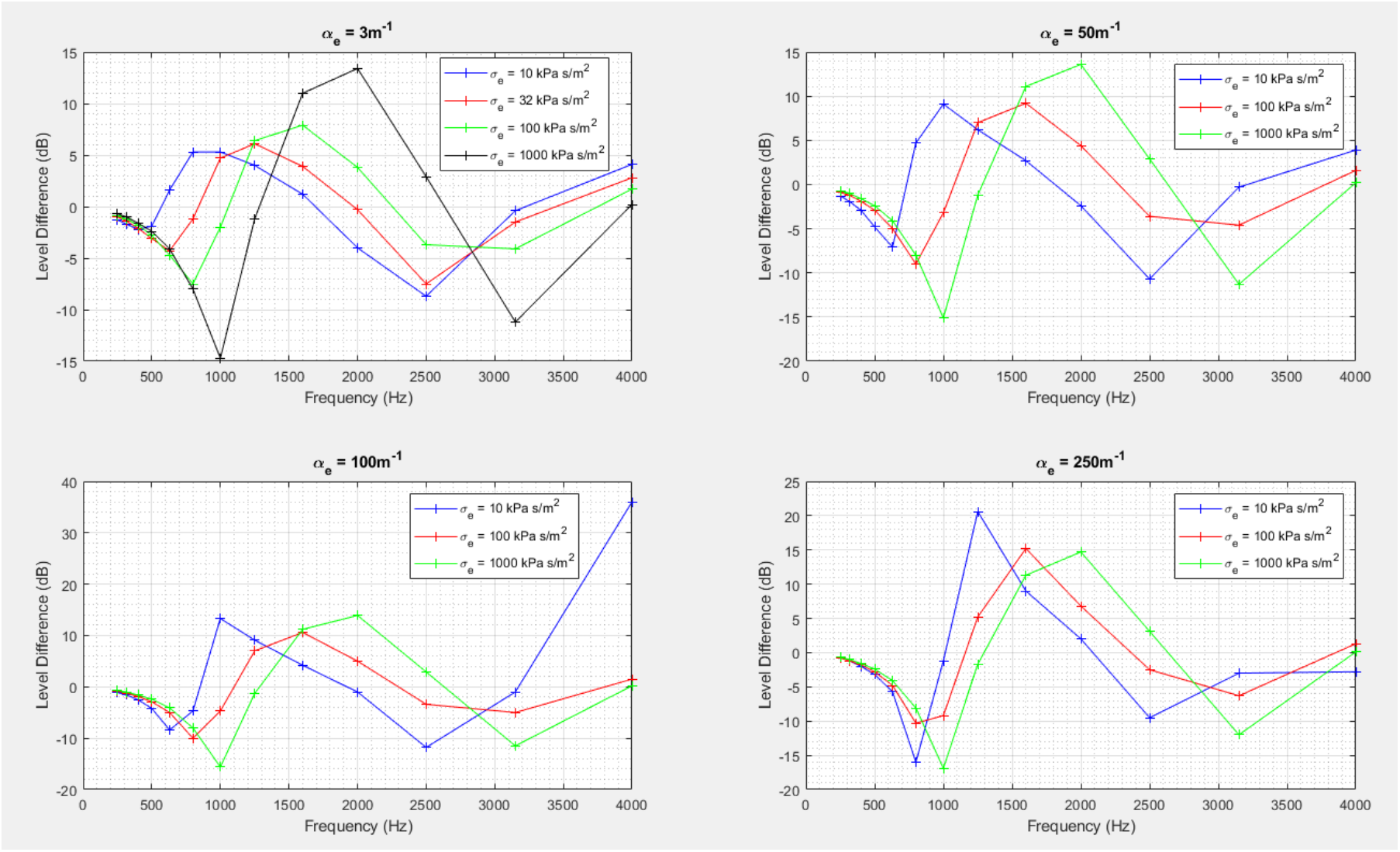

Figure 31 - ANSI S1.18-2010 level difference template curves for geometry A using 2-Parameter model, with αe from 3m-1, 50m-1, 100m-1 and 250m-1 and a range of σe

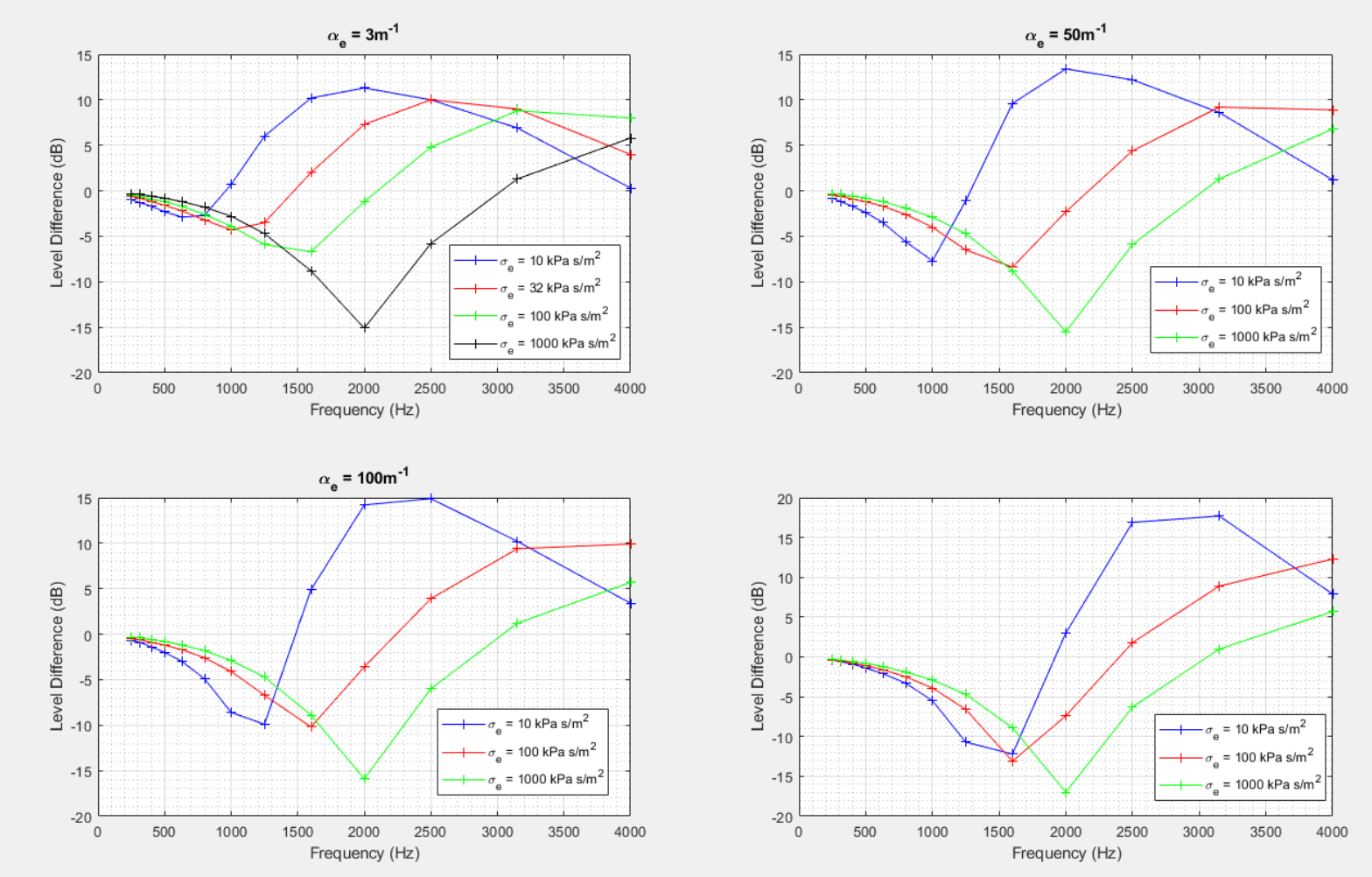

Figure 32 - ANSI S1.18-2010 level difference template curves for geometry B using 2-Parameter model with αe from 3m-1, 50m-1, 100m-1 and 250m-1 and a range of σe.

Tony F. W. Embleton (1996) summarises the literature on the experimental determination of ground impedance by measurement throughout the late decades of the 20th Century. To capture this kind of ground characterisation with sufficient accuracy is an important problem in outdoor acoustics. Measurements are complicated by the effects of turbulence and other outdoor factors which may contaminate. In-situ measurement techniques for the determination of acoustic impedance of ground surfaces have evolved over many decades, in response to the need to overcome a limitation of existing methods (Tony F. W. Embleton, 1996). Acoustic impedances are computed by using measurements of the sound field above a surface in conjunction with the appropriate theory. This type of method differs from more thorough investigations of the impedance of acoustic materials, which are based on the well-established impedance tube methodologies. The limitations of this method in outdoor propagation is that they are invasive, hence the reliance on free-field methods.

Measurements at Spadeadam

Free-field ground impedance measurements were conducted for two testing ranges by the University of Salford. Firstly, at Spadeadam in 2002, and secondly at Larkhill in 2003. The ground impedance of many different terrain types surrounding Spadeadam were characterised by the University of Salford as part of a program for the purpose of determining the propagation of noise from military helicopter training exercises in collaboration with QinetiQ Farnborough.

At Spadeadam, the Delaney & Bazley 1-Paramenter and 2-Parameter (variable porosity) models were used to derive ground impedances, through the measurement of excess attenuation spectra from a point source. These measurements were in accordance with the experimental set-up detailed in ANSI S1.18-1999, now ANSI S1.18-2010 (ANSI, 2010), with 3 experimental geometries over 3 positions, for 5 different locations around the test site, totalling 45 measurements.

The ground impedance measurements at Spadeadam characterised most of the site as having an effective flow resistivity varying between 80-140 kPa m/s^2 (kRayls) (R. M. Munt et al., 2003; Waddington, 2002). However, one area had a very high but narrow range of σ_e (410-430 kPa s/m^2), that being a small area of close-cropped grass and firm hard ground. On the other hand, the effective flow resistivities within the pine forests had a mean of 38 kPa s/m^2, with that area described as “within deep pine wood with wet pine needles”.

Figure 33 - ANSI S1.18-1999 excess attenuation spectra measurements at 2 of the locations during Spadeadam 2002 field trials (Waddington, 2002).

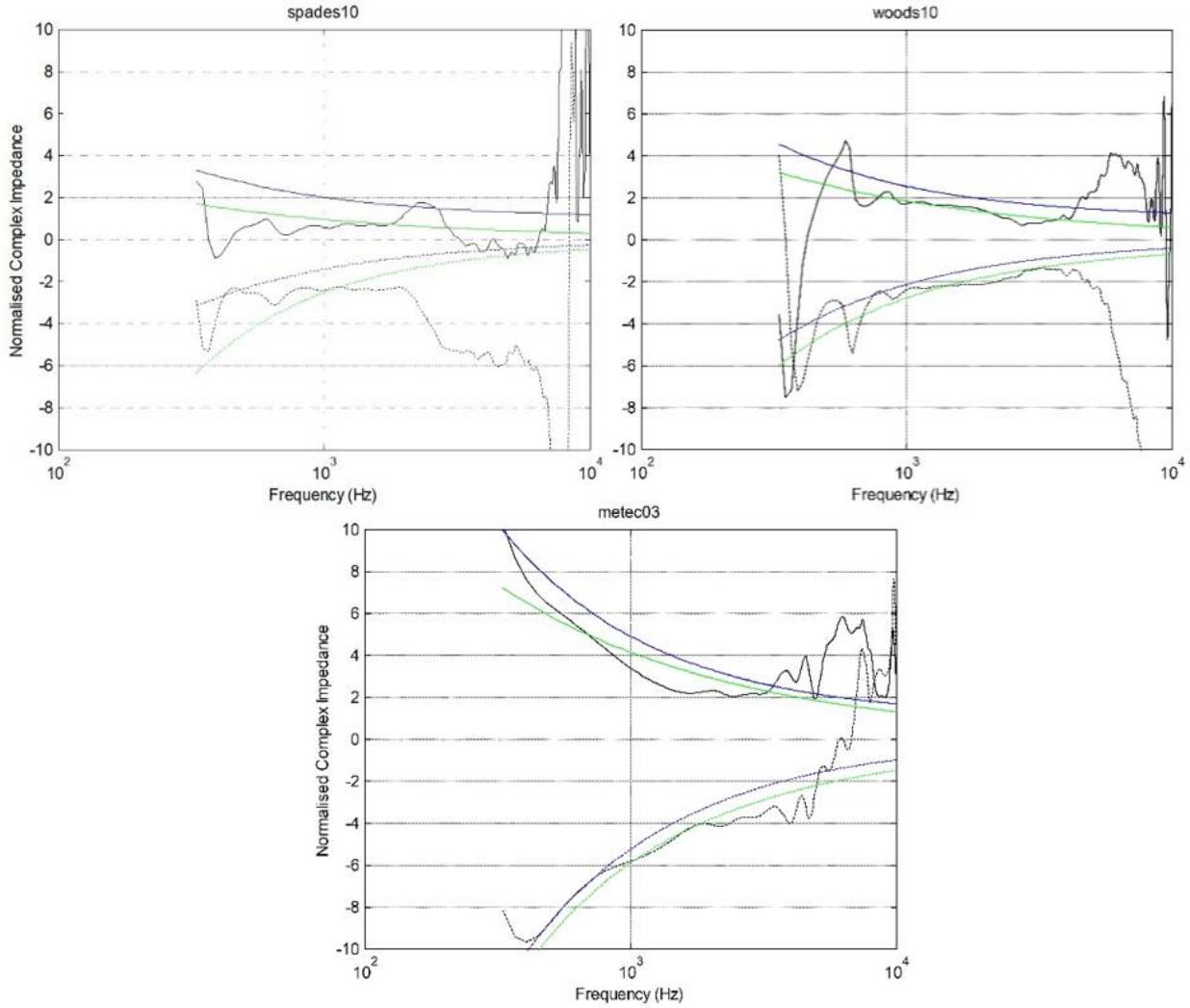

Figure 34 - Normalised complex impedance of grounds around Spadeadam. Long grass close to QiniteQ compound (top left), flat 25cm grass and reeds near woods (top right) and near Metec RASS close cropped grass and firm hard ground (bottom centre) (Waddington, 2002)

A table of minimum, maximum and mean effective flow resistivities for each surface was generated by this work.

Table 26 - Range of effective flow resistivity for 5 ground types around Spadeadam, derived from fitted data.

Ground Description	**Min σ_e (kPa s/m^2)**	**Max σ_e (kPa s/m^2)**	**Mean σ_e (kPa s/m^2)**
Long grass close to QinetiQ compound	120	150	130
Near woods, flat 25cm grass and reeds	120	140	125
Near woods, 15cm cut grass and moss	140	180	154
Deep in woods, deep, wet pine needles	30	60	38
Near METEC RASS. Close-cropped grass and firm hard ground	410	430	420

The findings of these field trials were that the 1-Parameter Delaney & Basley model produced fits with good agreement to the measured data. However, the 2 Parameter (variable depth) model provided a better least square fit to the data.

Figure 35 presents the measured excess attenuation from the field trials for 2 different ground types.

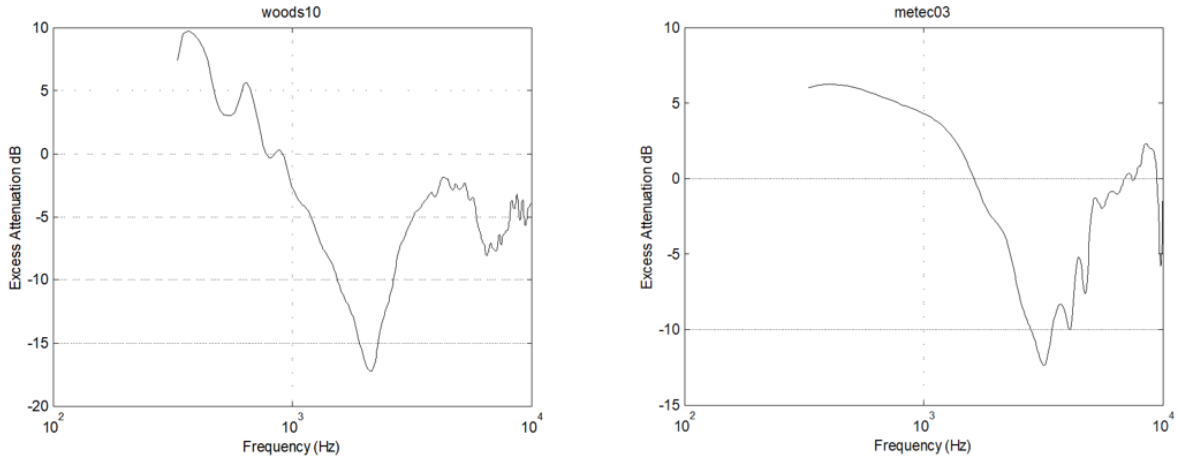

Figure 35 - Measured excess attenuation spectra for ground near woods (left) and long grass near compound (right).

3.2.3.3 Summary of Ground Impedance

The measurements of ground impedance conducted at Spadeadam in 2002 are essential for the creation of a heuristic blast noise model for Spadeadam, as the interaction of blast waves with the ground will vary under different refraction conditions. Therefore, it is essential to know the extent to which sound will be reflected, absorbed and altered when incident upon each surface type around the Spadeadam site.

These measurements may well be supplemented by further ground impedance measurements, given the change to the Spadeadam landscape since the beginning of this research project and undoubtedly throughout the last 2 decades. Such changes include vast felling of pine forests to the immediate southern boundary of the test site, which will influence the average ground impedance of the area. Moreover, the potential loss of ground with low σ_e, so near to the detonation areas may now provide chance for blast waves to initially propagate with less attenuation than previous, before being subject to refraction further away.

It would also be of benefit to estimate through measurement, the range of σ_e across much of the pastureland, and moorland which encompass the site further away. From this, and by using the theoretical framework discussed, an appreciation of the ground interaction effects under various propagation conditions to various receivers may be understood qualitatively, and these effects must not be ignored and must be corrected for within the successful implementation of a heuristic model.

3.2.4 Sound Transmission Through Vegetation

The dense forests around the Spadeadam site are an important consideration for noise propagation. Transmission loss mechanisms such as absorption and scattering may occur from the incidence of a sound wave onto vegetation, foliage, or trees, and this is a widely researched topic in the scientific literature. A topic of debate is the precise location of where these mechanisms manifest within the vegetation. M. Swearingen and White (2005) noted that research before this study had not established whether forests could attenuate noise from military blasting (30 – 80Hz), due to a lack of data at low frequencies, though the research had been attempted by (D. Albert, 2004; D. Albert, G. , Kerry, & Madshus, 2004).

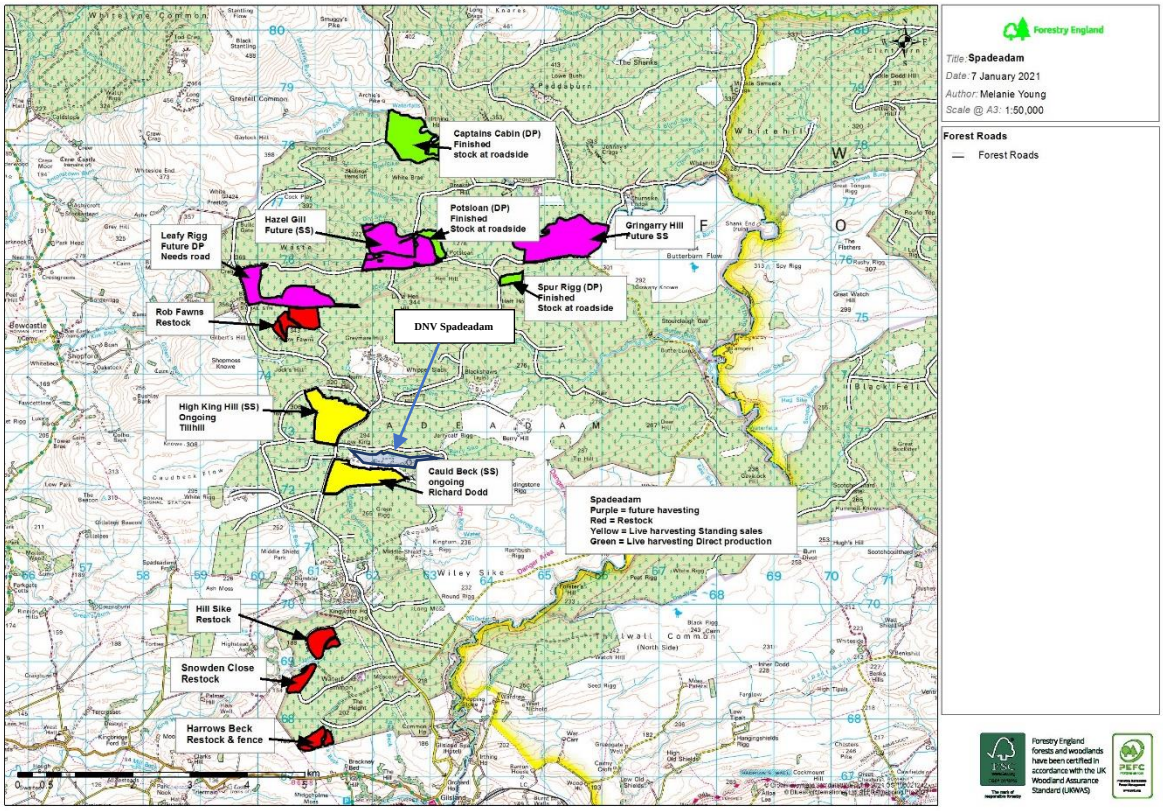

Figure 36 - Map of terrain and current ground type in the Spadeadam area, with Forestry England map of future forest management overlaid.

Sound waves can be attenuated by the canopy of the forest when incident upon tree trunks and their associated branches. There are two mechanisms of absorption here: *reverberant scattering*, where sound reflects from the larger trunks, and *thermal/viscous losses* attributed to friction against leaves.

The general concept of forests as noise barriers has evolved from research involving forest attenuation on road traffic noise, which has frequencies in the region of several hundred to several thousand Hz, beyond the region of frequencies resulting from blasts, which are likely to be in the order of a few Hz to several tens of Hz. Given that the characteristic wavelength of a blast wave, say one dominated by a 50Hz peak frequency, will be around 6.7m, the dimensions of a pine forest will be smaller relative to this characteristic wavelength. Hence, very little interaction with the actual foliage and branches would take place.

In forests, layered matter from the tree canopy can develop over many decades. This forest litter contributes to the increased surface roughness, porosity, and tortuosity of the ground layer, depending on its specific properties increasing the overall ground impedance significantly. The layering of the forest litter on the ground is likely a more significant mechanism of attenuation for blasts than the actual trees. Anecdotally, field observations from within the dense coniferous forests at Spadeadam have said to be akin to anechoic conditions. The contribution of forest litter to ground impedance will be discussed in detail in section 2.1.4.

3.2.4.1 Scattering from Forrest Edges

Whilst the influence of forests on sound propagation with respect to the trees and ground litter have been discussed before, a separate effect related to forest boundaries is focused upon here.

M. E. Swearingen, White, Guertin, Albert, and Tunick (2013) investigated the effects of forest as well as boundaries in isolation on impulsive sound compared to measurements in an open field. They found when impulsive signals propagated through a forest edge that they yielded complex pressure time histories for receivers inside and outside the forest, and attempted to separate the numerous physical mechanisms and their respective influence.

Swearingen et al. used acoustic and meteorological measurement arrays to measure the difference in attenuation of sound generated from a propane canon which provided repeatable impulses centred at 125 Hz every 30 s. The site which these measurements were taken at is of relevance to Spadeadam, where the influence of a distinct stand of Norway pine trees next to a military installation, with mixed land types, including open grassland, is a common scene around the DNV site. The forest edge was straight and had an abrupt change to open grassland, again similar to Spadeadam. Forest litter consisting of dead pine needles with an average depth of 28 mm, ranging from 13-41 mm topped the ground layer within the forest.

Swearingen et al. performed estimates of the ground impedance in the forest and open field were performed from measurements using a blank round from a pistol. The authors performed the inversion process (mentioned in 3.2.3.1 subsection on the effects of snow of this thesis), to derive a flow resistivity and layer depth respectively of 119 kPa s m^{-2} and 3.1 cm (open field), and 43 kPa s m^{-2} and 5.4 cm (forest). A comparison of the study site in M. E. Swearingen et al. (2013) is shown in Figure 37, compared to pictures of similar environments around Spadeadam.

Figure 37 -Top: M. E. Swearingen et al. (2013) test site, comprising of open field and forest edge (top left), and test site within the forest (top right). Bottom: Typical stands of forests around DNV Spadeadam (bottom left) and typical forest litter and ground c conditions within forests surrounding Spadeadam (bottom right).

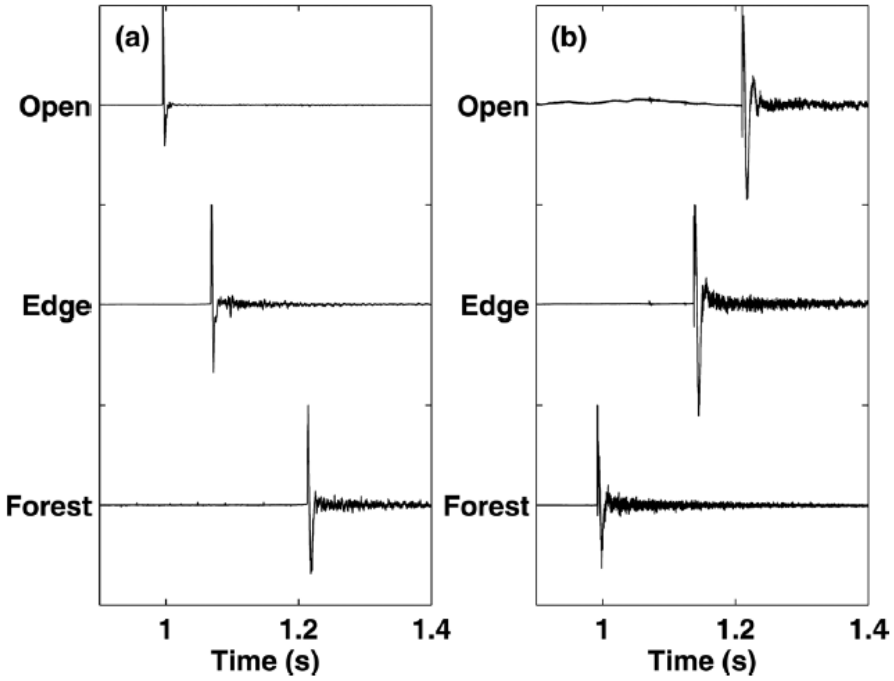

Figure 38 - Recorded pressure time histories of propane cannon impulses propagating into and outside of a forest, from (M. E. Swearingen et al., 2013).

Figure 38 shows normalised pressure time histories collected by M. E. Swearingen et al. (2013) from the propane cannon impulses propagating into the forest (a) and outside of the forest (b). The authors note that when the source is located int forest, greater reverberation is evident on the waveforms.

With respect to attenuation, peak levels of the propane cannon decayed at a rate of 43dB per decade of distance (dB/dd) when propagating into the forest from the open field. When the cannon was operated inside the forest, the decay rate was just 36 dB/dd.

Current impulsive noise propagation models, such as the sonARMS model (see subchapter 3.3 on propagation models) can simulate the effects of reflections from forest edges by an extension of a solution provided by J. M. Wunderli and Salomons (2009). By extending the calculation which models trees as cylinders, the tree top canopy is additionally included as surface of scattering spheres (J. Wunderli, 2012). The addition of scattering spheres to represent the canopy came from comparisons of measurements to the ‘cylinder-only’ models

which found that predictions were not accurate for short propagation distances, and that the vertical directivity was not representative of realistic forest edge reflections.

While improving on the simplicities in the scattering effects of trees is important, reasonable simplifications have to be made to account for the hundreds if not thousands of individual trees which need accounting for within sound mapping and noise prediction. Consequently, the contributions of representative cylinder (trees) are calculated for various forest edge segments and am empirical correction was derived to account for the reflection effects and how they vary with frequency and forest depth, (J. Wunderli, Pieren, & Heutschi, 2012).

3.2.4.2 Effect of terrain type on sound speed gradients

Meteorologically, large areas of forest are meso/micro scale surface discontinuities, which will impact the horizontal and vertical processes of the ABL (Tunick, 2003). Dense woodland contributes to drag forces against the wind, whereas shadowing on the forest floor inhibits the development of thermal plumes and buoyant air parcels, compared to the same area of open-field. White and Swearingen (2004) were the first to attempt to account for the problem of forest-dependent sound speed gradients *in combination* with the additional ground impedance and absorption losses from forests. They note that in addition to the absence of ground heating, ground cooling from radiative losses is also absent within forest environments. Strong wind shears have been associated above the forest canopies. The implications of these findings for Spadeadam are that meteorological profiles can be significantly more complex and varied than those measured at other sites. The effects that the forests have must be understood, especially in the context of felling and restocking large, forested areas, as proposed in Figure 36.

3.2.5 Ground Terrain and Barriers Effects

In addition to distorting the meteorological profile in the first 100m of the atmosphere, hills affect sound propagation as a barrier does. The extent of the barrier effect is governed by the wavelength of the blast wave in comparison with the hill height and may be quantified by the Fresnel Number (Maekawa, 1968). Accurately modelling the shape of the hill is an important consideration when concerned with the determination of ray diffraction into a shadow zone behind a hill. At short range behind the hill, the extent of the attenuation is dependent on the meteorology distortion and additional turbulent effects caused by the hill’s presence.

By solving the Euler or Navier Stokes gas-dynamic equations in time, with an adapted terrain grid to account for terrain, the effect of terrain barriers in the path of a strong blast waves may be studied. Such computationally intense work was prevalent in the 1970/80's when interest was in the study of shock distortion from gun blast and the nearfield interactions with complex structures such as helicopter blades. Such computational methods are also ideal for solving local shock disruptions over an isolated hill, which may be one of few hills of interest to a firing range. However, for DNV Spadeadam, the numerous hills and possible combinations of interactions coupled with the number of receptors does not justify the use of such computationally expensive methods.

When blasts degenerate to weak solitary waves at large distances, a scenario can be represented analytically by the linear Euler equations of homentropic flow. In such cases, the focus is shifted from large shock disruption, to diffraction around a barrier or hill. Under these conditions it is beneficial to transform the weak shock waveform to its Fourier series components in order to apply the acoustic methods for describing effects such as refraction, diffraction and ground impedance. By applying a transfer function for each frequency component along the propagation path, the combination of such effects can be observed, followed by a reforming of the waveform through a reverse Fourier Transform.

However, given the number of highly variable propagation combinations, a qualitative understanding of the impact of the combined effects of hill refraction on blast waves is more appropriate, to this research project. By using a simplified model of a hill, such as that suggested by(Hadden & Pierce, 1981), one could calculate the diffraction at the blast wave's dominant frequencies and hence deduce the effect of diffraction on the sound pressure level at a receptor, for a range of meteorological profiles, in qualitative terms.

3.2.5.1 Meteorological Compression over hills

At long distances from the blast source, where blast waves will have degenerated to linear acoustic waves, the compression of the meteorological profiles above a hill crest along the propagation line becomes relevant. Wind profiles are distorted around a hill, becoming most compressed at the crest as shown in Figure 39. Additionally, there is a potential for wind shear through horizontal flow distortions around the sides of the hills. The combination of vertical and horizontal disruption results in turbulent features on the lee side of the hill. The extent of these effects is dependent upon the wind speed, and the wavelength of the blast relative to the hill size. Additionally, the Richardson Number is utilised relating to

atmospheric stability and vorticity. The Froude number also governs the extent of the effects concerning buoyant and inertial forces and in combination, will strongly vary the influence of the meteorology around Spadeadam.

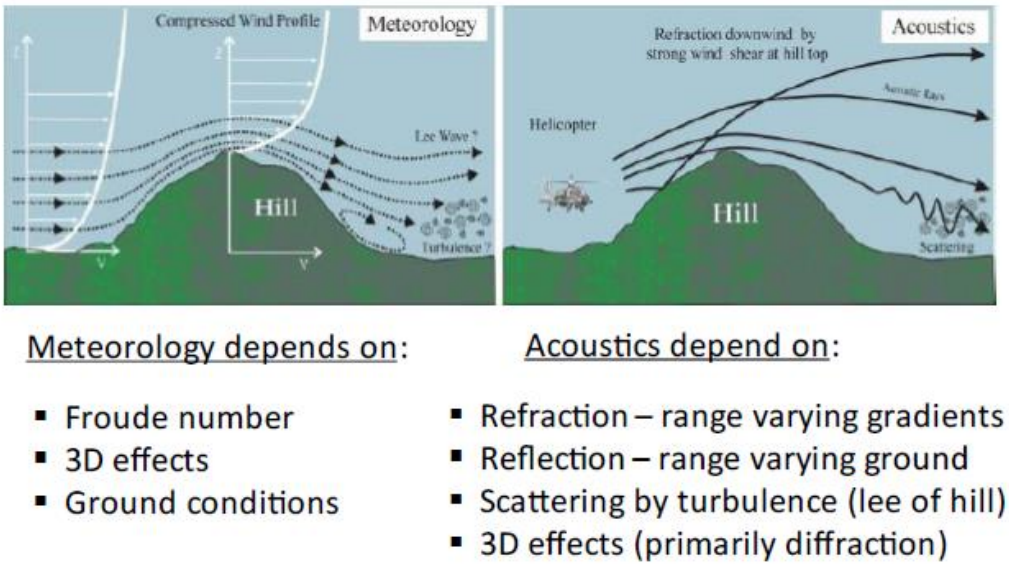

Figure 39 - A visualisation of meteorological compression over hills and the corresponding acoustic ray behaviour from flow distortion by hills (R. Munt, 2021).

Isolated small hills in the landscape around Spadeadam may affect the meteorology in the bottom 100m of the ABL above a hill, with the flow distortion features, influencing local sound propagation, extending into the lee of the hill. Compression of the meteorological profile may refract rays into the lee of the hill and turbulence may also enhance scattering into a shadow region.

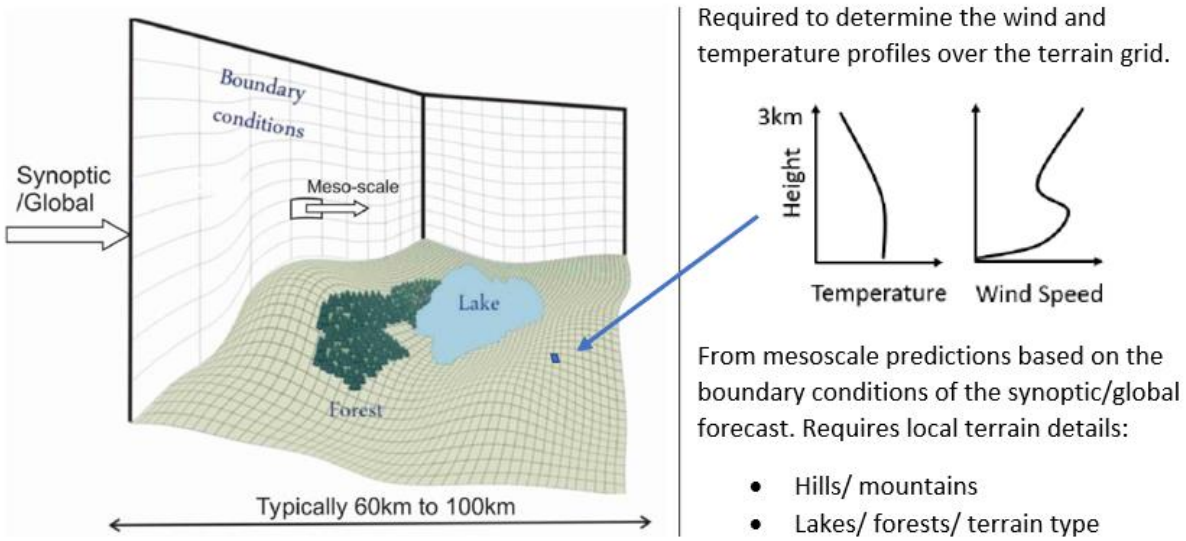

Figure 40- Combined synoptic/global and mesoscale meteorological resolution of meteorological profiles relevant to sound propagation over ground with varying terrain and type, from (R. Munt, 2021).

3.2.5.2 Flow in Mountainous Terrain

Although the Spadeadam plateau is not directly comparable to alpine mountain valleys, the topographical features of the surrounding mountain ranges (North Pennines, Cheviot Hills), have peaks that affect the mesoscale meteorological flow over the test facility. Some features of mechanical flow characteristic of mountain boundary layers are, speed up of flow over hills, Foehn winds and flow through gaps (Emeis, 2011).

3.2.6 Atmospheric Absorption

As a sound wave propagates through the air, the transferred energy is dissipated by various absorption mechanisms. In the atmosphere, the respective influence of these mechanisms varies with altitude. Furthermore, given the energy involved in blast waves, they can propagate well beyond the aforementioned ABL and even beyond the remaining troposphere, which has its upper bounds at around 11km above ground level (agl) on average. The components of very energetic blasts deflected directly upwards are said to propagate beyond the stratosphere and into the thermosphere up to an altitude of 160km (Sutherland & Bass, 1996), both of which layers have significantly different temperature and wind gradients compared to the troposphere and ABL and can be refracted back down to receivers on the Earth's surface. Sutherland and Bass (1996) state that there are two forms of atmospheric

absorption; *classical* and *relaxational*, of which the latter has two sub-forms; vibrational and translational.

At higher altitudes classical absorption transfers energy from the sound wave to the surrounding air molecules to equivalent heat energy or random kinetic energy. Salomons (2001) describes classical absorption as a mechanism arising from the temperature gradients associated with the sound wave itself, which are partly reduced by heat flow and depends on the viscosity of the air. The accompanying velocity gradients of a sound wave are analogously reduced by momentum transfer which again depends on viscosity. Both gradients are proportional to sound frequency and hence the attenuation is greater at higher frequency.

Relaxational losses are initiated through the redistribution of translational or internal energy of the air molecules. The passing of the sound wave through the air medium causes periodic compression and expansion of the air, where under compression, the diatomic oxygen and nitrogen molecules are brought into excited states of vibrational and rotational states (Salomons, 2001). During expansion, molecules relax to their original positions. Water molecules act as an important catalyst in allowing these molecular processes and hence, this type of atmospheric attenuation depends on air humidity. ISO 9613-1 (International Organisation for Standardisation, 1993) states how wide variations in water vapour are present near the ground, and by over two orders of magnitude from sea level to an altitude of 10km.

At lower altitudes, vibrational relaxational mechanisms are said to dominate attenuation compared to classical and translational relaxational absorption at higher altitudes.

Atmospheric absorption is generally assumed to be a combination of each mechanism forming a lumped parameter, α, dependent on atmospheric temperature and humidity and on the frequency components of the sound wave (Attenborough et al., 2006; Salomons, 2001). Both Attenborough et al. (2006) and Salomons (2001) give a detailed description of the calculation of this absorption for various humidity, temperature, and atmospheric pressure limitations in the following steps, which are originally presented in ISO 9613-1. (International Organisation for Standardisation, 1993).

Equation 29

$$\alpha = f^2 \left[\left(\frac{1.84 \times 10^{-11}}{\left({}^{T_0}/_{T}\right)^{-0.5} {}^{p_s}/_{p_0}} \right) + \left(\frac{T_0}{T}\right)^{2.5} \left(\frac{0.10680 e^{{}^{-3352}/_{T}} f_{r,N}}{f^2 + {f_{r,N}}^2} + \frac{0.01278 e^{-2239.1/T} f_{r,O}}{f^2 + {f_{r,O}}^2} \right) \frac{nepers}{m \cdot atm} \right]$$

Where $f_{r,N}$ and $f_{r,O}$ are the relaxational frequencies of nitrogen and oxygen respectively.

$$f_{r,N} = \frac{p_s}{p_{s0}} \left(\frac{T_0}{T}\right)^{1/2} \left(9 + 280H \cdot e^{-4.17\left[\left(\frac{T_0}{T}^{1/3} - 1\right)\right]} \right) \qquad \textit{Equation 30}$$

,

$$f_{r,O} = \frac{p_s}{p_{s0}} \left(24.0 + 4.04 \times 10^4 H \frac{0.02 + H}{0.391 + H} \right) \qquad \textit{Equation 31}$$

Where f is the frequency of the wave, T is the absolute temperature of the atmosphere in degrees Kelvin, $T_{01} = 293.13\ K$, H is the molar concentration of water vapour = $\rho_{sat} r_h p_0 / p_s$, r_h is the relative humidity, p_s is the atmospheric pressure. $\rho_{sat} = 10^{C_{sat}}$, where $c_{sat} = -6.8346(T_{01}/T)^{1.261} + 4.6151$. Salomons (2001) provides the same steps for calculating absorption in dBm^{-1}.

A detailed explanation of the significance of absorption at each stage is presented by Salomons (2001), where 3 distinct regions are shown to exist for air. These regions are separated by the aforementioned relaxational frequencies of the gasses.

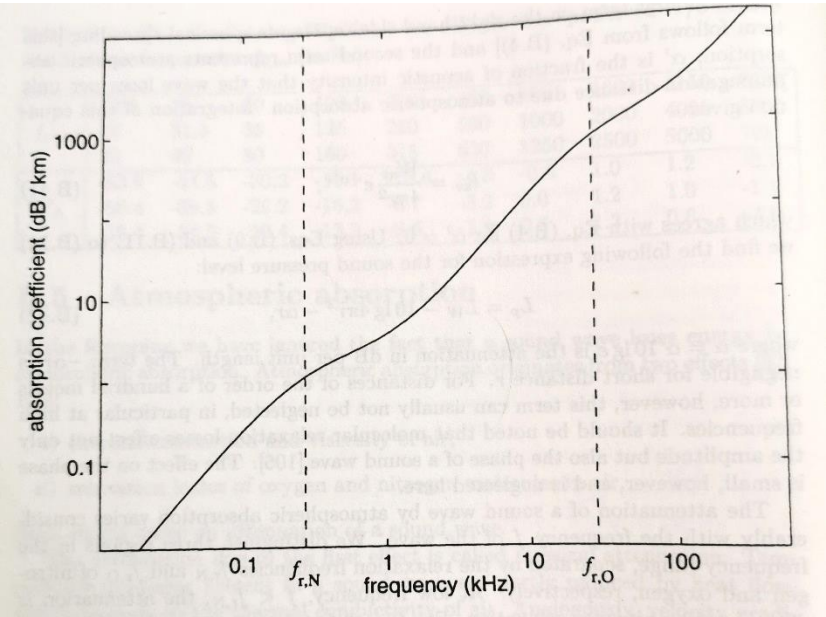

Figure 41 - Atmospheric absorption coefficient α, (dBm-1) as a function of frequency at T = 20C, RH = 80% and pa = 1atm calculated using formulae in ISO 9613 (International Organisation for Standardisation, 1993) taken from Salomons (2001).

Equation 30 to Equation 31are for the determination of attenuation with frequency for pure tones and the resulting response is shown in Figure 41. Nitrogen relaxation is the dominant mechanism in the low frequency range, $f < f_{r,N}$, followed by oxygen relaxation in the range $f_{r,N} < f < f_{r,O}$. Above the resonant frequency of oxygen relaxation, sound is attenuated by classical absorption.

Salomons (2001) however, presents the concept of atmospheric absorption as an exponential amplitude decay with distance, which may be represented by a small imaginary term, $(-k_i r)$ added to the wavenumber in an adapted version of the point source sound pressure equation, as such.

$$p_c(r) = S\frac{e^{(ikr)}}{r}e^{(-k_i r)} \qquad \textit{Equation 32}$$

Salomons concludes by describing the effects of phase changes induced by atmospheric absorption on sound waves, which also varies with frequency.

In reality, phase changes are negligible and hence, atmospheric absorption is only significantly affecting the amplitude of a sound wave. BS5727 presents formulae to account for the effects of atmospheric absorption at a range of temperatures and humidities, although originally intended for aircraft noise.

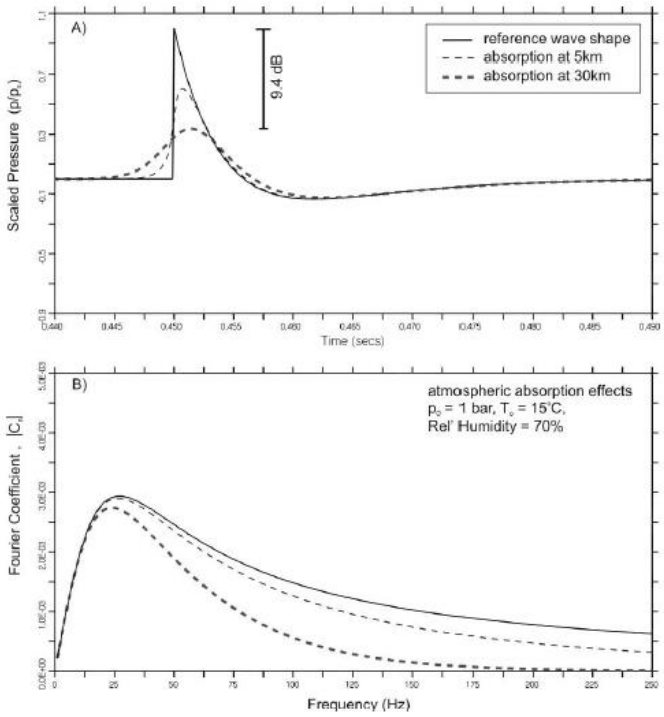

Figure 42 - Example of the effect of atmospheric absorption with distance on waveform shape and corresponding frequency response (R. M. Munt, 2018; D. K. Wilson, 1996).

It may be observed that higher frequencies are significantly attenuated by atmospheric absorption, due to these frequencies being closer to the resonant frequency of the oxygen molecules in air. On the other hand, low frequencies do not couple effectively with this resonant frequency and hence are not attenuated as significantly. Of significance is the change to the waveform shape from atmospheric absorption at large distances, where the missing high frequency components, needed for defining a sharp shock front and consequently small impulse length τ, are attenuated. The resulting waveform has a longer impulse length with increasing distance, due to the smearing of the shock front and emphasis on the lower frequencies to the waveform shape.

3.2.7 Turbulent Scattering

Previous examination on the effects of wind gradients on sound propagation have assumed highly idealised laminar scenarios of constant wind flow, when in reality, wind is gusty and such gustiness increases with wind speed. For a continuous sound source, the resulting sound pressure level at a receiver would fluctuate in response to these sudden perturbations of wind.

The complete character of the atmosphere is independent of time, where fluctuations in its spatial profile may display large changes on the order of hours, or small-scale local

perturbations on the order of minutes and seconds (Salomons, 2001), with the former and latter representing general weather movements, and atmospheric turbulence respectively.

Turbulence is the disruption of fluid flow from its general direction of travel, antithetical to laminar flow where, fluid particles flow parallel to one another. A fluid medium, such as the ABL has flow particles that move irregularly from their straight-line paths. This produces swirls known as eddies, which have deviations in the main flow speed. The term is used to describe the region of turbulent flow, which is locally limited to and may be visualised as a 'frozen fluctuation' within the surrounding flow. The height above ground (among other variables) generally controls the potential size that an eddy can be, and therefore there is a spectrum of possible eddy sizes, which represent the characteristic periods of where local medium fluctuations can exist, with large eddies representing slow but energetic changes in atmospheric profile, and small eddies representing transient but local fluctuations.

A turbulent atmosphere changes the effective sound speed, c_{eff}, which Salomons (2001) represents as an equivalent quantity known as n, the refractive index, which has fluctuations μ more or less equally about a mean value $\bar{n}$, in a turbulent atmosphere.

$$n = \bar{n} + \mu \qquad \textit{Equation 33}$$

The fluctuation μ is dependent upon the turbulent temperature fluctuation T_t and the turbulent wind velocity fluctuation u_t in the following.

$$\mu = \frac{-T_t}{2T_0} - \frac{u_t}{c_0} \qquad \textit{Equation 34}$$

Where, c_0 is the sound speed at temperature T_0.

For most outdoor propagation applications, the turbulent field is represented by random realisations of the refractive index, where the medium is considered as 'frozen' to the perspective of a sound wave which evolves through the medium at a much higher speed with respect to the evolution of the surrounding turbulent eddies. However, long distance propagation of blast waves from Spadeadam may take up to 45 seconds to reach the furthers complainants at around 14km. It is therefore uncertain whether the frozen turbulence hypothesis is valid under such long ranges.

3.2.7.1 Kolmogorov Energy Cascade

Turbulence spectra are used to encapsulate the range of possible turbulent eddy sizes within a fluid in a statistical sense, which as mentioned, range from scales comparable to the height

above ground to millimetres. Kolmogorov (1941) developed a universal statistical scaling of a central region of the turbulent energy spectrum, known as the inertial subrange, which generally covers the range of most audible sound frequencies relevant to sound propagation prediction for the purpose of noise control. The problem is elucidated with lower frequencies and infrasound (Chessell, 1976), such as those present in blast waves, which have corresponding wavelength comparable to eddy sizes at the outer limit of the inertial subrange, approaching another range, the energy subrange. This range is not modelled accurately by a universal statistical characterisation, as it is dependent on many physical conditions.

Energy is transferred from larger eddies to smaller eddies in a process known as the energy cascade. There is a continuous transfer to successively smaller sizes which continues until all kinetic energy is converted to heat through dissipation by molecular viscosity processes. At this end of the spectrum is the dissipation length scale, where turbulence is considered as isotropic, according to Kolmogorov's 1st theory of turbulence (Kolmogorov, 1941). The eddy sizes within the dissipation subrange are on the order of millimetres and are generally of no concern to outdoor sound propagation, as the sizes of the eddies are incomparable to the wavelengths of audible sound waves.

Between the energy and dissipation subranges is the inertial subrange.

Gaussian and Van-Karman spectra

Several statistical models are proposed for the description of eddy size distribution.

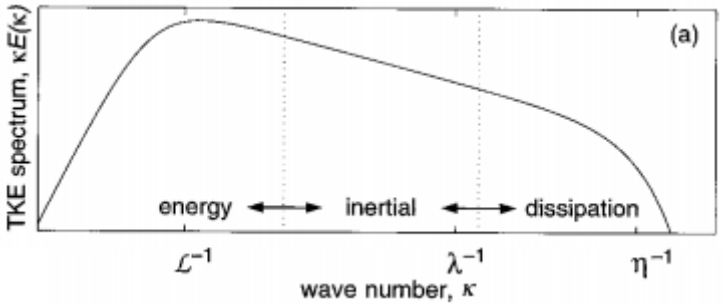

Figure 43 - Spectral view of the 3 turbulence subranges from D. Keith Wilson, Brasseur, and Gilbert (1999).

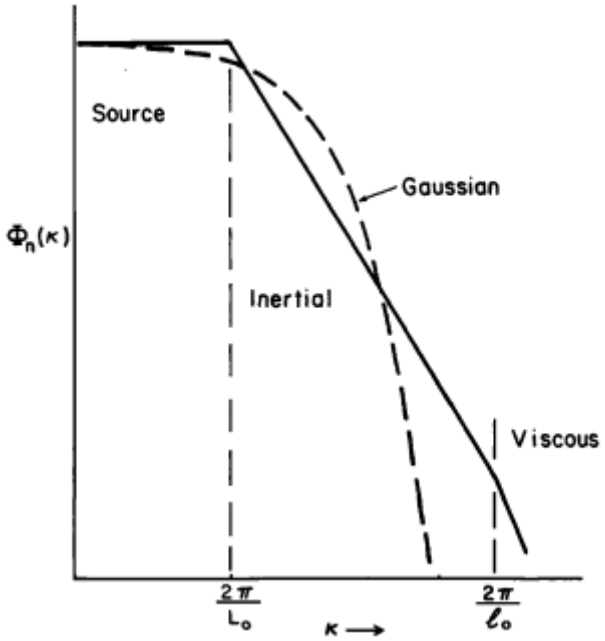

Figure 44 - Spectral density of refractive index fluctuations (Φn(K)) as a function of the spatial Fourier turbulence component (K). From Daigle, Embleton, and Piercy (1986).

In Figure 44, *K* is inversely proportional to the turbulent eddy size. The quantities L_0 and ℓ_0 represent the outer and inner subranges, labelled here as Source (energy containing) and Viscous (dissipative) respectively, with the Inertial subrange in between. The dotted curve represents the fluctuation density within the energy containing subrange simulated by a Gaussian function.

The respective effects of the inertial and energy subranges on sound propagation are summarised by D. Keith Wilson et al. (1999), where it is stated that larger scale turbulence dominates the acoustic phase fluctuations on a propagating sound wave. On the other hand, the smaller motions are said to influence the overall amplitude of the sound wave, though in reality it is often an amalgamation of these effects which complicates this idealised theory, based on the fact that usually most sound propagation problems do not involve pure tones.

Gaussian Model

The commonly used Gaussian model of turbulence simulates the refraction index energy spectrum, $\Phi_n(K)$ in Equation 3 below (Attenborough et al., 2006).

$$\Phi_n(K) = \langle \mu^2 \rangle \frac{L^2}{4\pi} e^{(-\frac{K^2L^2}{4})} \qquad \textit{Equation 35}$$

With *L* as a single scale length proportional to the correlation length, ℓ_G, as

$$L = \ell_G \frac{\sqrt{\pi}}{2}$$ *Equation 36*

It is generally accepted that the Gaussian spectrum provides a poor overall description of the turbulent spectrum, however, it is often used throughout the scientific literature and within prediction models due to its ease of implementation. This simplified model of turbulence provides results in an analytical form (Attenborough et al., 2006).

The Gaussian model is widely recognised within the outdoor sound propagation literature as being favourable for its accuracy at representing turbulent spectra over a narrow frequency range, which may be applied adaptively to a specific noise source spectrum. It is not intended for the Gaussian model to perfectly represent the entire energy cascade, or even a wide wavenumber range, merely to approximate the relevant range of turbulent eddies that are likely to affect the specific acoustic propagation.

Empirical values for a Gaussian length scale, K, were proposed originally by (Daigle, Piercy, & Embleton, 1978, 1983) and are found later in other work (Chevret, Ph, Blanc-Benon, & Juvé, 1996; Daigle et al., 1986; Gilbert, Raspet, & Di, 1990; Juvé, Blanc-Benon, & Chevret, 1994) as around 1-1.2m near the ground. Empirical values within the literature for the turbulent fluctuation μ_0^2 range from 10^{-6} and 10^{-5} , with Table I in Daigle et al. (1978) proposing a list of derived values for μ_0 and the characteristic length scales of turbulence from wind L_v and temperature L_T, for different weather conditions.

von Kármán model

Shown in Figure 45 is the accuracy of the von Kármán model (thin solid line) as compared with an actual turbulent spectrum (bold solid line), where there is little deviation over a broad range of wavenumbers. This is due to the von Kármán model satisfying the conditions of the Kolmogorov spectral density within the inertial subrange (λ). With relevance to sound propagation, it is within the energy subrange (L, shown within Figure 45 as $\mathcal{L}$).

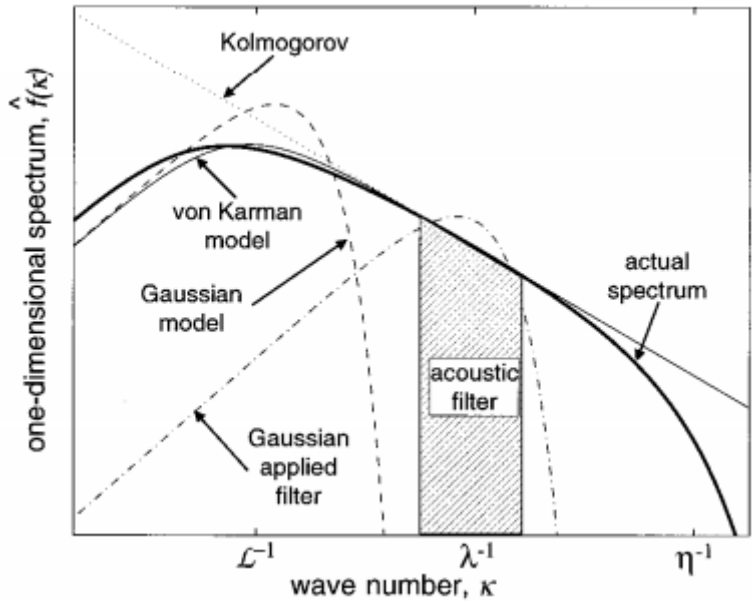

Figure 45 - A comparison of an actual turbulent spectrum with modelled spectra, from D. Keith Wilson et al. (1999).

3.2.7.2 Discussion on Turbulence

Both the Von Karman and Gaussian models provide a good qualitative description of the effects of the energy-containing subrange on sound scattering and may give reasonable approximations under specific conditions when the correct parameter values are selected. However, the limitations of the models arise from the assumption that the turbulence within the energy subrange is isotropic and homogenous, which in reality, is not the case. This may be visualised by the incoherence in correlation length in the direction of the wind vector, which is much larger than the correlation length parallel to the wind vector (Salomons, 2001).

Additionally, as is now recognised within the scientific literature, specific parameter values for modelling the turbulence subranges of interest using Gaussian functions may not necessarily be appropriate (D. Keith Wilson et al., 1999), as the values have been found empirically based on field trials at a specific site. Each specific location is likely to have its own turbulent characteristics based on the interaction of its local climate with the surrounding terrain type and topography among many other variables (Daigle et al., 1986). This is probably the most important consideration for the representation of turbulence in a future heuristic model for the Spadeadam area.

3.2.8 Specific Meteorological Phenomena

Due to the specific terrain around Spadeadam and its geographic location relative to the North Pennines and Cheviot mountain ranges, the interaction of different air masses may be complex. As a result, specific weather phenomena other than normal wind and temperature gradients may occur which have their own effects on sound propagation. The appearances of such meteorological phenomena can be treated as particular events or episodes. Such atmospheric events specific to Spadeadam which may affect sound propagation include:

- The passing of warm/low fronts
- Occluded fronts
- Heavy fog and low stratus cloud
- Föhn winds
- Low Level Jets

3.2.8.1 Weather Fronts

Fronts represent the boundary between colliding air masses (Dunlop, 2004; "Weather Fronts," 2021). With the respective name representing the dominant air mass, i.e. warm fronts represent a transition zone where cold air is replaced by warm air. A front may be identified by clouds and precipitation which precede and follow the front for hundreds of miles. There may be distinct visual features which an observer can use to identify frontal movements, but there are also relevant features to sound propagation.

The slope of the front refers to the vertical height of the front over a horizontal distance.

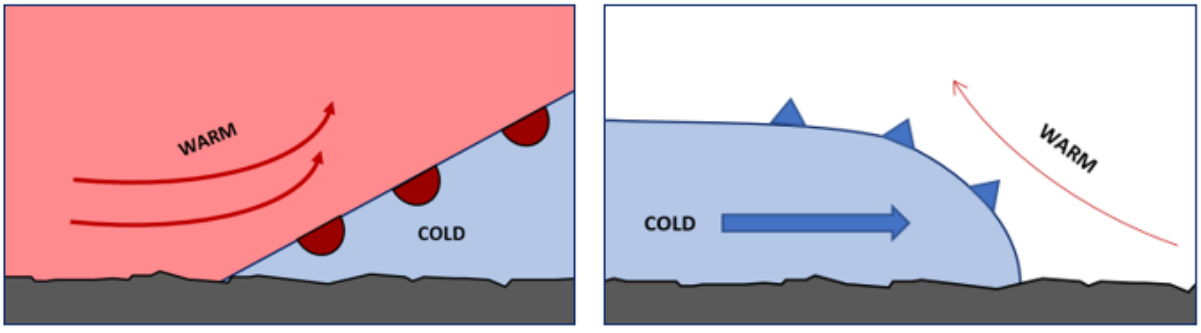

Figure 46 - Warm (left) and cold (right) frontal formation.

Warm fronts

Warm fronts are the advancement of warm air rising over cold air where warm air is less dense (lighter) than cold air. The arrival of a warm front may be identified by the structure of specific cloud layers. In general, the successive arrival of the characteristic cloud types in Table 28 indicates an approaching warm front.

A warm front slope has a distance scaling of 1:100 – 1:150 and with the characteristic cloud development, the warm front is approximately 600-900km (12 hours) away when the first cirrus is overhead (Met Office, 2012).

Cold fronts

A cold front signifies the presence of a cold air advancing and pushing underneath warmer air, because it is denser, thus replacing warm air at the surface (Met Office, 2012). At the approach of a cold front, the arrival features in Table 27 may be common. The transition zone of a cold front is narrower than that of warm front, with a slope of 1:50-1:75. The layering cloud sequence which signifies a warm front may appear in reverse order ahead of a cold front. Cold fronts are generally less stable the warm fronts, with more turbulent features a common occurrence. As the cold front arrives significant changes to sound propagation may come from sudden changes to wind, temperature, and pressure.

Finally, as the cold front passes the wind may change direction slightly and become gustier.

Table 27 - General features relevant to atmospheric sound propagation of warm and cold front at the respective approach, arrival, and departure stages (Dunlop, 2004; Met Office, 2012).

Front Stage	Front Features	
	Warm Front	Cold Front
Ahead of front	Characteristic Cloud Development: • Cirrus • Cirrostratus • Altostratus • Nimbostratus Features: • Wind increases and backs towards the south (n. hemisphere)	• Wind backs slightly and increases in strength • Pressure falls very close to the front • Cloud thickening from stratocumulus to nimbocumulus • Bands of precipitation parallel to the direction of the front

	• Signs of crossed wind • Pressure drop increases with time • Cloud cover increases • Temperature decreases • Precipitation 200-400km ahead of surface	
Arrival of front	Features: • Winds veer (n. hemisphere) • Temperature may rise dependent upon precipitation	Features: • Sudden veering of winds • Conditions becoming blustery • Abrupt rise in pressure • Abrupt drop in temperature
Behind front	Features: • Winds increasingly veer from surface to high-altitude wind	• Winds may back slightly then steady • Winds become more gusty and therefore stronger • Scattered, broken cloud depending on front speed

Occluded fronts

Occluded fronts occur as a result of cold fronts over-taking warm fronts, as cold air masses move faster. Their name alludes to a hidden warm front with the arrival of cold, dense air from behind results in the lifting of warm air from the surface. Either a warm or cold occlusion may form, depending on where the coldest air is situated with respect to the incoming cold front.

Where the air ahead of the front is colder than the air behind, the occluded front is a warm occlusion, typical of wintertime in the British Isles. Alternatively, a cold occlusion is when the air ahead of the front is warmer than the air behind and is typical of occlusions during

summertime in the British Isles. Their significance is that they may arrive suddenly (especially cold occlusions) and cause abrupt weather changes. The formation of both types occluded fronts is depicted in Figure 47.

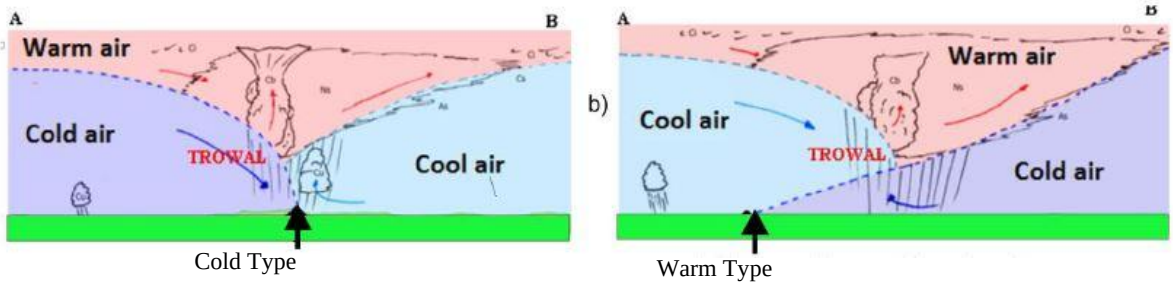

Figure 47- Frontal features of cold occlusion (left) and warm occlusion (right) (R. M. Munt, 2020)

The significance of weather fronts, especially occlusions, is that they display typical meteorological characteristics, such as sudden changes to wind. The advantage of recognising fronts is that they can be identified on large-scale synoptic weather charts such as surface pressure maps. This skill will aid the long-term prediction of blast noise, allowing an operator to make predictions on the order of days to weeks ahead, to estimate the likely magnitude of noise and thus, noise complaints.

3.2.8.2 Heavy fog and low stratus cloud

The influential work of Cole and Dobbins (1970) summarised sound propagation through atmospheric fog and claims that it can be described as a system of suspended liquid droplets within a mixture of their vapour and inert gases. Excitation of this system by a sound field results in mass, heat, and momentum exchange between the surrounding mixture, finally resulting in general sound attenuation. However, attenuation is said to be dependent on the droplet conditions, as stated in early research by Knudsen (1946), where the effects of water fog on sound attenuation within a reverberation room were measured. Knudsen showed that, larger droplet sizes were responsible for less attenuation as compared with smaller droplets, and states that the magnitude of attenuation can be deduced from the measured visibility or density and particle size of the fog. This is based on the fact that attenuation measurements were (to a first approximation) in agreements with theoretical values of attenuation and independent observations.

Cole and Dobbins expanded upon this theory in their later work 1971 to find that deviations of up to 35% between theoretical and observed attenuation. Consequently, further corrections were made by Davidson, to improve agreements with experimental data. The corrections to

the effects of mass transfer between vapour and droplets produced lower attenuation shown under realistic observations.

Comparatively recent research in the field of propagation through simulated fogs by Mahanta, Vajpayee, and Sadek (1986) experimented with the use of a temporary fields of suspended water droplets as a means of noise reduction. Their experimental results showed that the size of the droplets had the most significant effect on the absorption of sound in the medium, where attenuation was inversely proportional to droplet size. However, the study also observed the isolated effects of, atomisation pressure, mass flow and mass ratio on droplet size and consequent sound attenuation with frequency and distance from the sound source. Mahanta et al. (1986) concluded that for their specific experimental set-up, attenuation peaks at a mid-frequency range, and is followed by a slight decrease with increasing frequency, but nonetheless found small attenuation at low frequency, for a range of droplet conditions.

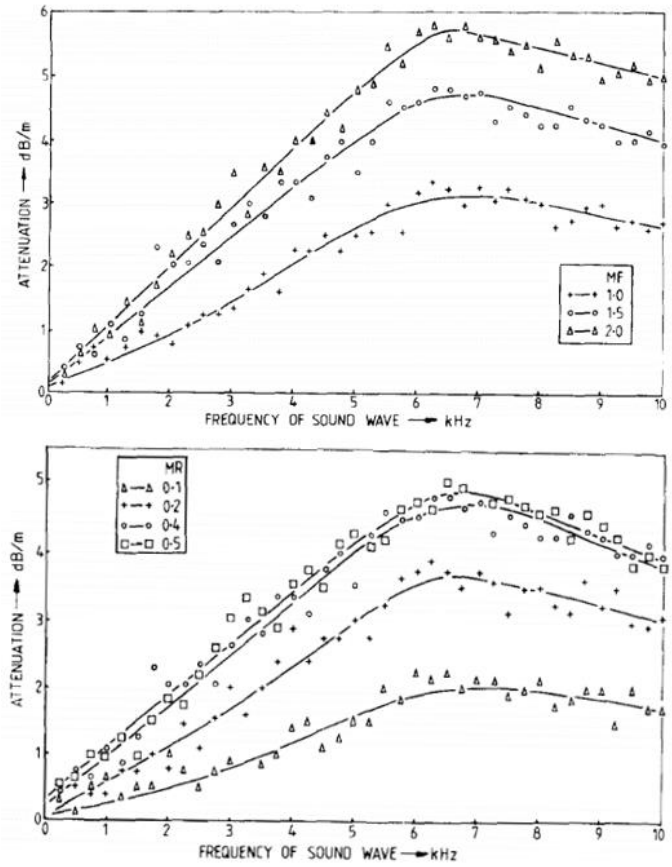

Figure 48 - Acoustic attenuation per meter (dB/m) vs frequency for varying fog mass flow, MF (top) and mass fraction (bottom). Adapted from Mahanta et al. (1986).

Nevertheless, it is important to consider that Mahanta et al. (1986) simulated the fog effects under highly idealised conditions using a controlled experimental set-up and their work did not feature atmospheric fogs. Under some outdoor propagation scenarios concerning normal continuous acoustic sources and comparatively small distances, these effects can be important dependent on the context. For Spadeadam, such effects cannot be said to have dominance over the experienced sound pressure level at a receiver due to the number of other atmospheric effects, such as refraction, which are of higher importance during long range propagation. This concept was the conclusion of experimental work by Wiener (1961) on propagation through ocean fogs who stated that the effects of wind and temperature gradients predominated over the attenuation effects of fogs and low cloud.

Cole and Dobbins concluded that at low frequency, the velocity, temperature, and mass of the suspended droplets can remain in mechanical and thermodynamic equilibrium with the surrounding field. Their experimental findings on atmospheric fog show almost constant attenuation with frequency in the low frequency range of 10^2 - 10^3 Hz with droplet size of 2.5μm, (with a lower and narrower frequency range for small droplet size), before a transitional zone at mid frequency and subsequent constant attenuation at high frequency. Initial data by Wei (1950) for low frequencies indicated this trend in attenuation due to mass transfer, but agreements were limited to orders of magnitude.

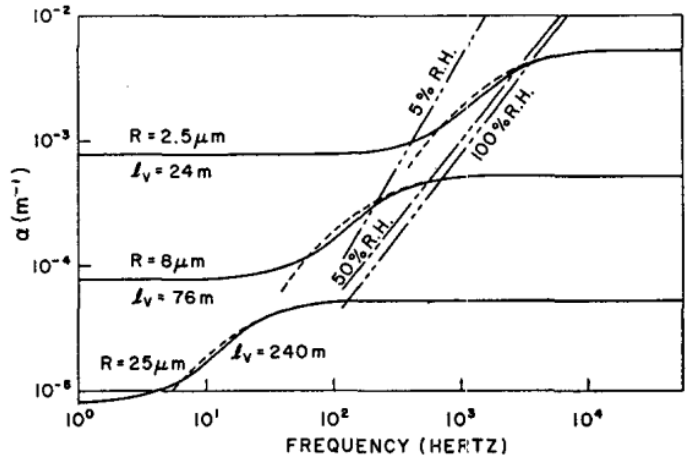

Figure 49- Acoustic attenuation per meter (dB/m) vs frequency for varying droplet size from the experimental data of Cole and Dobbins (1970).

3.2.8.3 Low Level Jets

The effects of a stable boundary layer on wind is of interest for studying atmospheric sound propagation, in that the formation of low-level jets can act as atmospheric waveguides (Waxler, Gilbert, & Talmadge, 2008). Low level jets are zones of high wind speed at

relatively low altitude (Makarewicz, 2016) that may have super-geostrophic speeds, forming during stable boundary layer development (Stull, 1988). They are a result of diurnal variation in ABL stability within underlying large-scale horizontal pressure gradients, according to Emeis (2011), within which is a thorough description of their formation and appearance in the remote-sensing literature.

Recent research on the effect of low-level jets on sound propagation in the last decade have mostly concerned noise from wind turbines, and the downward refraction of sound rays from the wind turbine hub down to the ground, due a to a maximum in wind speed around the turbine hub (Conrady, Bolin, Sjöblom, & Rutgersson, 2020). Although, focusing on wind farm noise, Marcillo, Arrowsmith, Blom, and Jones (2015) summarise other investigations of long-distance propagation during SBL conditions from other sound sources, for example, Waxler et al. (2008) studied how the waveform of impulsive signals evolves during ducted propagation. The term *ducted* in that respective work, specifically refers to downward refraction occurring nocturnally from a strong geostrophic wind and well-defined temperature inversion, rather than the downward refraction from low-level jets, which concern wind speed maxima at lower altitudes than the geostrophic wind height. Nonetheless, similarities can be drawn, along with some considerations from the work of Herrin, Kim, and Stump (2006), also relevant to the propagation of blasts at Spadeadam.

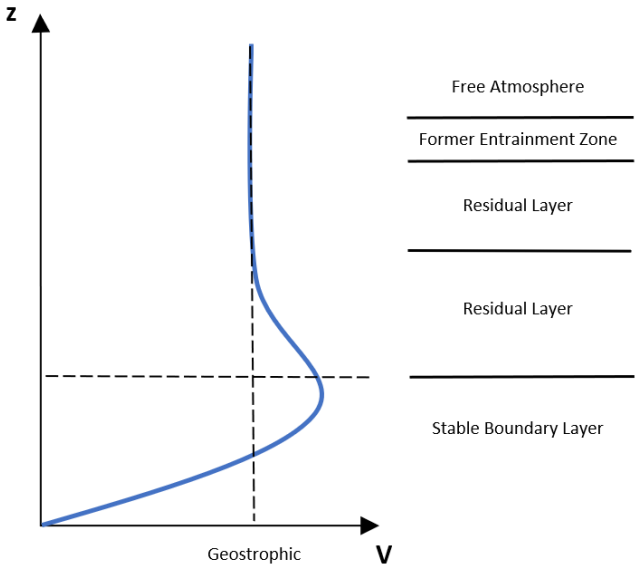

Figure 50 - Idealised wind speed profile of a stable boundary layer in a high pressure zone, adapted from Stull (1988).

In fact, early studies of impulse propagation under such conditions (I. Chunchuzov, Kulichkov, Otrezov, & Perepelkin, 2005; I. P. Chunchuzov, 2004; I. P. Chunchuzov, Bush, &

Kulichkov, 1990) , concerned stable boundary layers and their features which cause fluctuations in acoustic signal propagation over long distances. Chunchuzov's later studies being primarily focused on the turbulence statistics, characteristic of stably stratified atmospheres, all concern the idea of a tropospheric waveguide, and it's influence on sound levels at long distance.

Going forward, the considerations from the wind farm studies (Conrady et al., 2020; Makarewicz, 2016) should be utilised for the Spadeadam project, in addition to the detailed theories of pulse propagation under effects of low-level jets, trapping propagation near the ground.

It would be of further interest to explore the significance of low-level jet phenomena on enhanced sound levels at receivers around Spadeadam. Currently, the frequency of occurrence of this atmospheric phenomenon in the area is not known and its impact on sound levels should be further investigated through measurements.

3.2.9 Summary of Propagation Physics

The mechanisms that drive sound propagation relevant to Spadeadam have been reviewed. Additionally, their relevance to blast waves and appearance in the academic literature has been presented.

A comprehensive study on the propagation effects is offered by Ingård (1953) who states that the attenuation caused from precipitation (fog, rain and snow) are of secondary order to the audio frequency range. The more significant propagation factors include temperature and mostly wind gradients, which can form shadow zones at near range to the source, depending on the strength of the gradients. Overall, the presence of wind can easily eliminate the formation of temperature gradient induced shadow zones, in a sector of the downwind direction (60-180°), and hence dominates propagation.

Ground attenuation is also a dominant factor when both source and receiver are near the ground. An understanding of the varying ground impedance around Spadeadam is critical, where different ground types not only affect sound wave propagation through absorption and phase changes, but also through thermal and flow distortions to the meteorological profiles above the ground. A chapter will be dedicated to the availability of ground impedance and ground terrain data and their influence on the results produced by blast noise prediction models.

Moreover, ground impedance should not significantly alter with time, at least not on the scale that meteorology evolves. The dominant propagation features will be governed by how the effects of particular ground impedances and terrain couple with some clearly defined wind-induced refraction events. This will include the effects of propagation through vegetation as a lumped ground impedance parameter. Over time, a qualitative understanding of sound pressure levels can be obtained for each source-receiver path with specific lumped ground impedances for individual cases of refraction.

By characterising the statistical characteristic of the turbulence under such conditions, one could aim to provide mean sound pressure level predictions with a range of expected deviations from the mean.

Of secondary importance, (i.e. in the absence of wind gradients) are temperature gradients, which may dominate propagation during calm conditions (early mornings). Following this, lower order effects, such as fog may only then become relevant.

The measurement of blasts noise at multiple receiver points surrounding Spadeadam is the only way to correlate sound pressure levels with such propagation effects.

3.3 Long-Range Prediction Models

3.3.1 Introduction

Noise prediction models in their simplest forms evaluate noise levels at a receiver from a source either analytically, or by using mathematical approximations. For long-term predictions, continuous noise sources allow propagation conditions to be averaged in time. Moreover, propagation conditions vary much less over short-distances and hence, assumptions about these conditions in time and space will often suffice.

Alternatively, models which evaluate noise levels over greater distances suffer from a trade-off between accuracy and computational expense. Usually, these predictions require finer details about the propagation medium, which has a greater influence on the sound propagation over long distances compared to short distances. Therefore, approximations about the physical conditions of the propagation medium, namely the atmosphere and the ground conditions, should be as limited as possible, especially in areas of complex meteorology and terrain such as at DNV Spadeadam. On the other hand, large quantities of data result in long calculation times (L'Espérance, Nicolas, Herzog, & Daigle, 1992). Secondly, sound sources such as blasts occupy such a fractional timeframe, consequently influenced by the fluctuating atmosphere induced by turbulence, as time evolves.

Questions are raised by the trade-off between model accuracy and computational expense, such as whether heuristic models can be used to predict the typical noise levels within an area under specific propagation conditions using ‘rules of thumb’. Early heuristic models have been conceptualised for Spadeadam (Lacy, 2017), and used for estimating blast noise at other sites (Kerry, Saunders, & Sills, 1987) and for other noise sources (L'Espérance et al., 1992).

3.3.2 Ray Tracing

Ray Tracing models rely on the geometric acoustic theory of acoustic ray propagation. Ray acoustics is based on the *Huygens Principle* for optic rays. High frequency acoustic waves are assumed to propagate as rays, analogous to light rays. Such approximations greatly simplify the calculation requirements but impose strict limitations on the frequencies that can be used in accurate predictions (Kuttruff, 2019; Savioja & Svensson, 2015) .

Ray tracing has its place fundamentally in room acoustics, where it is particularly useful for estimating reverberation characteristics and other objective acoustic parameters to a high degree of accuracy. This accuracy can be attributed largely to the lack of both spatial and temporal refractive inhomogeneities in indoor environments, meaning that reasonably accurate predictions need only account for geometric reflections from the surfaces within the room.

Conversely, long-distance outdoor sound propagation has ample opportunity for wave effects to take place as a result of refractive index changes throughout the propagation medium. Of course, these effects are well understood, as phenomena such as refraction are well defined in optics and are thus transferrable to high frequency acoustic waves.

3.3.2.1 Advantages

The main advantage to ray-tracing prediction tools is their comparable computational speed across a wide-frequency range and range-dependent conditions. The interaction of progressing wave traces can also be modelled through simple rules. Ray interactions with solid boundaries are conveniently modelled using the geometrical laws of specular reflection, and the redirection of rays due to sound speed inhomogeneities is modelled by Snell's law of refraction.

3.3.2.2 Disadvantages

The main disadvantage of the ray tracing approach arises from the fact that acoustic propagation is not entirely geometric (Acoustics Research Centre, 2006b), especially at low frequencies, due to wave effects. Further interpretations of the ray-based results are necessary, for example, the determination of ray amplitude. A simple and highly standardised approach is to calculate the amplitude using the square root of the area between adjacent rays. Other methods are possible, though they will not be discussed here. Due to the curving of rays from both wave effects and inhomogeneous media, the inevitable crossing of rays (known as 'caustic' rays) gives rise to an area of zero and consequently infinite amplitude.

Solutions to the infinite amplitude induced by caustic rays include simple heuristic approaches, such as attenuation by the inverse square law, which trades the accurate modelling of ray dilution for simplicity (Acoustics Research Centre, 2006b).

Furthermore, refraction effects cause sharp cut-off zones in ray-tracing models, such as sharp boundaries to shadow-zones during upwind propagation. In realty, turbulent effects cause sound to be scattered into shadow zones from the shadow boundary.

3.3.2.3 Larkhill Ray Invariant (LARRI) Model

LARRI Main Model

The LARRI model is a hybrid prediction method that has been used by various UK Ministry of Defence ranges for many years. It uses a blended ray-tube and numerical approach to improve predications compared to a previous model, Larkhill Mark II, which imposed a significant frequency limitation, due to the assumption of sound rays at high frequencies.

A benefit of the simple ray tube method is that it is computationally inexpensive, meaning that general trends in propagation can be visualised quickly (Walkden & West, 1988). First-order approximations can therefore be made before tests, according to the expected propagation conditions during testing. Peak pressure predictions from the model have large uncertainties according to G. Kerry, Saunders, and Sills (1987).

The second part of the LARRI model utilises the Fast Field Program (FFP) (see C.6.4.1). The implementation of the FFP by Y.-L. Li, White, and Franke (1994) provided the prediction tool with the ability to include wind gradients. The model is well described and referred to as the Acoustic Prediction Package (APP) by M. West, Turton, and Kerry (1996), who although appreciated its limitations, acknowledged it as a progressor in the field of long-range sound propagation.

Larkhill Simplified Model (LSM)

The LSM is an empirical method based on the vertical sound speed profile derived from the 10m and geostrophic winds. It is discussed in detail in two parts (Turton, Bennetts, & Nazer, 1988a, 1988b). The relationship between winds at the upper and lower bounds of the troposphere above flat ground is well understood and is dominated by three apparent forces; (1) the pressure-gradient force, (2) the Coriolis effect and the (3) friction against the Earth's surface. These effects do not only determine the vertical profile of wind speed, but the first two effects also affect the direction of the wind speed. However, the LSM only accounts for the speed change with height to form a profile.

The model predicts the distances at which a 130dB and 120dB peak SPL will occur at. The empirical equations were designed for a 5lbs (2.23 kg) solid charge weight.

$$d_{130} = 3.240 - 2.536e^{\{-0.050(v_g - v_{10})\}}$$ Equation 16 (Turton et al., 1988a)

$$d_{120} = 4.860 - 3.075e^{\{-0.078(v_g - v_{10})\}}$$ Equation 17 (Turton et al., 1988a)

For any other charge weight of weight *W* in lbs, a correction to the 130dB and 120dB distances was also provided by Turton et al. (1988a). The correction is in the form of a multiplication factor, *F* as below.

$$\log_{10} F = 1.1 \log_{10}\left(\frac{W}{5}\right) \log_{10}\left(\frac{d_{120}}{d_{130}}\right)$$ Equation 18 (Turton et al., 1988a)

3.3.3 Parabolic Equation Models

Parabolic Equation (PE) Models are significantly more sophisticated prediction methods which are not limited by layered atmospheres and homogenous ground conditions (E. Salomons, 2001). Additionally, PE models allow for the wave effects occurring during propagation to be accounted for. The interactions of waves as they propagate through the atmosphere are thus modelled, a feature that ray tracing models are incapable of. In addition to wave interactions in the air, the subsequent ground interactions can also be modelled.

K. Gilbert and White (1989) presented a PE method for atmospheric acoustics known as the Crank-Nicholson PE (CNPE). The initial CNPE method was a 2-D axisymmetric approximation of the 3-D Helmholtz wavefield which traced the wavenumber of the field at the reference refractive index along a 2D propagating field, *rz*, with $k_{eff} = \omega/c_{eff}$ where c_{eff} is the effective sound speed. The quantity $q_c(r,z)$ is also traced and is related to the complex pressure amplitude $p_c(r,z)$ associated with the axisymmetric approximation of a 3D Helmholtz equation for a sound field within a moving medium, to a 2D one, where variation in the sound field with azimuthal angle is assumed to be negligible.

Further developments to the solution in 1993 by (K. E. Gilbert & Di) gave rise to what is known as the Green's Function Parabolic Equation (GFPE), a significantly faster model, which does not suffer from the same errors as CNPE. The GFPE model was enhanced from 2D to 3D again by Di and Gilbert (1998).

A summary of the trade-offs between the CNPE and GFPE is outlined in Table 28.

PE Version	Accuracy	Speed
CNPE	• Accurate up to elevation angles of 35° • Generally, more accurate than GFPE for situations with wide-angles and large sound speed gradients	• Slower than GFPE
GFPE	• Accurate enough in most applications	• More efficient than CNPE

Table 28 - Summary of the qualitative accuracy and speed CNPE and GFPE according to E. Salomons (2001)

Frequency domain PE schemes have shown to be effective at predicting long-range (up to 40km), low frequency (<100 Hz) propagation over range-dependent environments. Appearing within the scientific literature firstly through the contributions of Lentovich and Fock (1946) for applications involving the modelling of electromagnetic wave propagation. Simplified 2D models assumed that for noise propagation, horizontal meteorological gradients were second to vertical gradients. Alternatively, it was acknowledged that 3D propagation should be considered in complex hilly terrain, where horizontal gradients have significant effects on propagation.

The first example of a 3D PE method in Cartesian coordinates was developed by Vladimir Ostashev, Blanc-Benon, and Juvé (1997), following Ostashev's book on a wave-equation for use in moving media with arbitrary inhomogeneities, the first of its kind. The book, (VE Ostashev, 1997), served as a guide to outdoor acoustic propagation work, encompassing the effects of arbitrary discontinuities in sound speed and air density, for applications in noise control to atmospheric sensing. This work served as a foundation for others to include more complex meteorological profiles and the modelling of spherical waves which are not easily represented on Cartesian coordinates, such as the cylindrical coordinate system by Cheng, Morris, and Brentner (2009).

The importance of horizontal gradients was demonstrated following comparison between 3D and 2D methods, where the 2D model displayed maximum errors up to 20dB at long-distance during downwind propagation following verification with analytical methods. However, such comparisons were only made above flat terrain.

3.3.3.1 Multi-Azimuth Parabolic Equation (MAPE) Model

The classical 'small angle' PE methods such as those by Lentovich and Fock (1946) had been used across a plethora of physical applications for solving the propagation of waves in media. Narrow-angle PE methods assume the idea that waves propagate along one preferred direction, at least up until the 1970's where wide-angle PE methods were developed to represent the more realistic conical propagation of waves in the atmosphere and oceans. Wide-angle parabolic equations better represent the effects of turbulence induced, horizontally scattered sound into shadow-zones, which occurs over long-distances. According to a summary of the research by Vladimir Ostashev et al. (1997), the initial work of (V. E. Ostashev & Tatarskii, 1978) progressed the field of atmospheric acoustic simulation through derivation of an equation used to describe how all waves scatter forwards, which was analogous to the wide-angle PE. The wide-angle parabolic equation model was used for long range propagation firstly by K. Gilbert and White (1989) followed by developments at the University of Salford by Martin West (1992) for a hypothetical non-moving atmosphere, and by (Juvé, Blanc-Benon, & Chevret, 1994; Juvé, Blanc-Benon, & P. Chevret, 1992). In parallel to this research, further work on the use of the wide-angle PE in turbulent media was done by V. E. Ostashev and Tatarskii (1995), to tackle sound scattering. Finally, the knowledge was then combined and summarised by Vladimir Ostashev et al. (1997) with the derivation of a new wide-angle PE model for use in turbulent media.

3.3.3.2 Generalised Terrain Parabolic Equation (GTPE) Model

The original developments of the GTPE model by the University of Salford (Sack & West, 1995; M West & Sack, 1994) were motivated by the need to model acoustic propagation over hills. However, range dependent meteorology was derived from single layer measurements of vertical profiles which can account for speedup/compression of the profile over hills, but does not accurately capture the nuances of more complex effects related to hills such as Fohn effects, hydraulic jump, and anabatic and katabatic wind flows. Additionally, canyoning and turbulence from lee wave rotors is also not accounted for. Further modifications to the model made in 2003, provided the user with the ability to input range-dependent meteorology for a generally more accurate depiction of the ABL above the whole terrain. However, the requirements for this are a fine-grid meso or even microscale meteorological prediction in the range of 100m – 4km. Such fine resolutions will increase computational time.

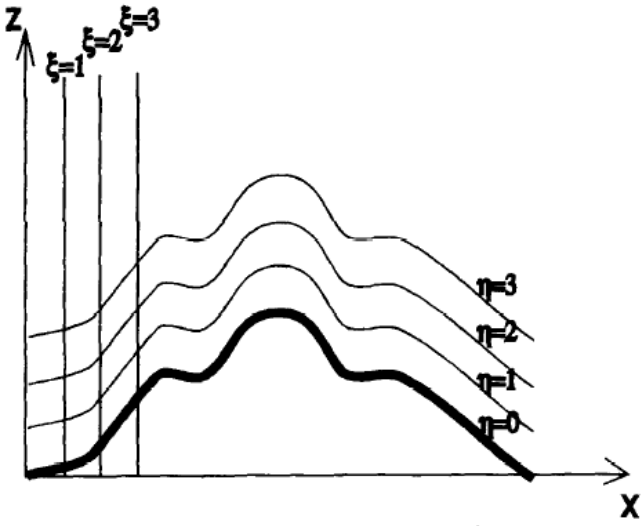

Figure 51 - Terrain mapping following transformation as shown in Sack and West (1995).

This method of 2D transformation differs from those previously offered within PE models, which depend on circular conformal sectioning of the atmosphere above the terrain however, interpolation errors are prevalent. Other non-circular transform methods avoid these interpolation errors but demand unrealistic sampling of the meteorological profile above ground.

The terrain is modelled through the transformation of terrain from Cartesian coordinates into a terrain-following coordinate system, known as the sigma transform, as shown in Figure 51. This concatenates the terrain profiles into equally stepped height bins. It is recognised that there is a limitation in the maximum slope of the undulating ground, <30° (E. Salomons, 2001). This is a result of unstable solutions arising from a 2nd derivative of the ground profile within the transform for large changes in terrain profile (Acoustics Research Centre, 2006b; M West & Sack, 1994). Within the initial testing of the model, comparisons were made for propagation over a simple Gaussian shaped hill against the well-known Maekawa model (Maekawa, 1968). The study found that the predicted attenuation agreed with the Maekawa model at distances beyond 700m from the hilltop. Conversely, the GTPE predicted attenuation was significantly excessive within the immediate shadow zone of the hill.

However, the GTPE method still provides improvements over the MAPE for complicated but smooth terrain profiles. It is noted in (Sack & West, 1995) that the GTPE method offers computational speeds that (nearly) match the original CNPE method, with the addition of a more complex PE method.

3.3.3.3 A Hybrid Ray-based/ PE model: GridTracePE

The current version of GridTrace is currently a hybrid PE/ray-based prediction model (Acoustics Research Centre, 2006a). GridTrace was initially developed in 2003 as a 2D propagation model over flat ground with range dependent ground impedance. A secondary development phase produced a model that could account for 2D mountainous terrain, range-dependent meteorology, and turbulence effects on sound propagation. Further developments combined the ray-tracing based GridTrace model (optimising speed and capability for predictions at high-frequency) with PE theory, providing reassurance in accuracy in low-frequency predictions. According to the program documentation, which was released in 2006, ongoing improvements to the model were in place to derive turbulence induced attenuation statistics. The aim was to address the variation in acoustic attenuation from real turbulence, providing mean and standard deviation in attenuation.

The model is based on Fortran code and is delivered as a stand-alone program, although it has additional modules for compatibility in other Fortran programs.

GridTrace Ray method Component

Acoustics Research Centre (2006b) contains a highly detailed analysis of the improvements to the GridTrace ray tracing component of the model. Improvements up to GriTracePE V4.08 will not be discussed in detail within this text. Instead, a summary of the improvements to the inclusion of turbulent scattering effect is as follows:

- Introduction of random realisations of turbulence induced amplitude and phase fluctuations in the ray tracing process to calculate the standard deviation of the attenuation at receivers where rays are detected (non-shadow zone)
- Incorporation of turbulence induced ray scattering model into the virtual barrier model to calculate the mean standard deviation of the attenuation within the shadow zone.

Turbulence

As previously discussed turbulence is best represented by a by the von Karman statistical function, as it is related to the Kolmogorov theory of the turbulent energy cascade. Turbulence is accounted for within GridTracePE by means of random realisations of the sound speed vertical profile according to a Gaussian model of turbulence. This means a

decorrelation of the ray phases at a receiver following their transmission through turbulent eddies.

Quoted values for the setup of Gaussian modelled turbulence within the GridTracePE model are quoted to be $\mathscr{L} = 1.1$m and $\mu_0^2 = 3^{-5}$, which are well in agreement with the range of value proposed within the scientific literature review, as discussed in section **Error! Reference source not found.**.

PE component of the model

The PE module of the GridTracePE model utilises a wide-angle version Crank-Nicholson PE. The model allows range-dependent meteorological and terrain input, which are implemented along each step of the PE routine. Validation of this initial set-up has been demonstrated with a comparison of measurements and a boundary element model (BEM), against results of the GridTracePE. Good agreement was found between all, following analysis of data gathered during a previous field trial (Sennybridge).

Validation of prediction components

Within (Acoustics Research Centre, 2006c), each component of the model has been validated independently against a series of benchmark cases. The LamPE model showed very good agreement with measurements of the benchmark cases. The ray based model of GridTrace showed generally good agreement, but with notable errors in the 10Hz test case, where geometrical acoustic assumptions break down. However, the speed of the ray tracing component in combination with the LamPE module provides the user with flexibility in speed and accuracy required during predictions. Discussions on the performance of the combined model against other specific test cases, such as turbulence, propagation over a hilltop and other are also offered.

3.3.3.4 Met Office Noise Evaluation Tool (MONET)

Until spring 2023, the Met Office Noise Evaluation Tool (MONET) was the prediction model used by DNV Spadeadam for the large scale blast testing. MONET is a parabolic equation model and was developed in 2000 by the Department of Applied Mathematics and Theoretical Physics (DAMTP) at Cambridge University and the Meteorological Office use as a prediction tool at MOD firing ranges (Hume, 2000).

Motivation

Motivation behind the MONET came from the recognition of a previous models' limitations, the Acoustic Prediction Package (M. West et al., 1996). The APP provided partial coverage as only predictions at the locations where sound rays where incident on the ground were made. Additionally, the breaking down of the ray theory when rays cross imposes further limitations in the prediction.

Source Conditions

The prediction starts with the equivalent charge weight for an explosive or ammunition source, followed by the 'atmospheric input'. This can come from 3 sources of data: Met. Office mesoscale meteorological data, data from a local radiosonde ascent and finally, the choice of ICAP atmospheric profiles. Currently, the standard method uses data sourced from the Met Office Numerical Weather Prediction available with hourly resolution. This data is then cross-checked with measured conditions from nearby automatic weather stations (the nearest being at RAF Spadeadam). The issuing meteorologist may adjust the input data near the surface to reflect the more realistic surface conditions which may not be represented by the numerical prediction data.

The key parameters of the input data are composed of vertical wind speed and direction profiles along with virtual temperature, which are of course critical to noise propagation.

The dominant frequency of the blast is believed to be characterised by a 40Hz pure tone, as this is the frequency which causes damage to windows and buildings (Hume, 2000). This alone may introduce significant uncertainties in the modelling of the blast wave from the source, where the dominant frequency is inversely proportional to the positive impulse length, which may vary significantly not only with charge size but also with source type. Gas explosions are said to have significantly longer impulse lengths and therefore have significant low frequency energy compared to solid explosions.

Unweighted peak sound pressure level in dB is the calculated parameter which has a 130dB contour chosen as the limit for receivers.

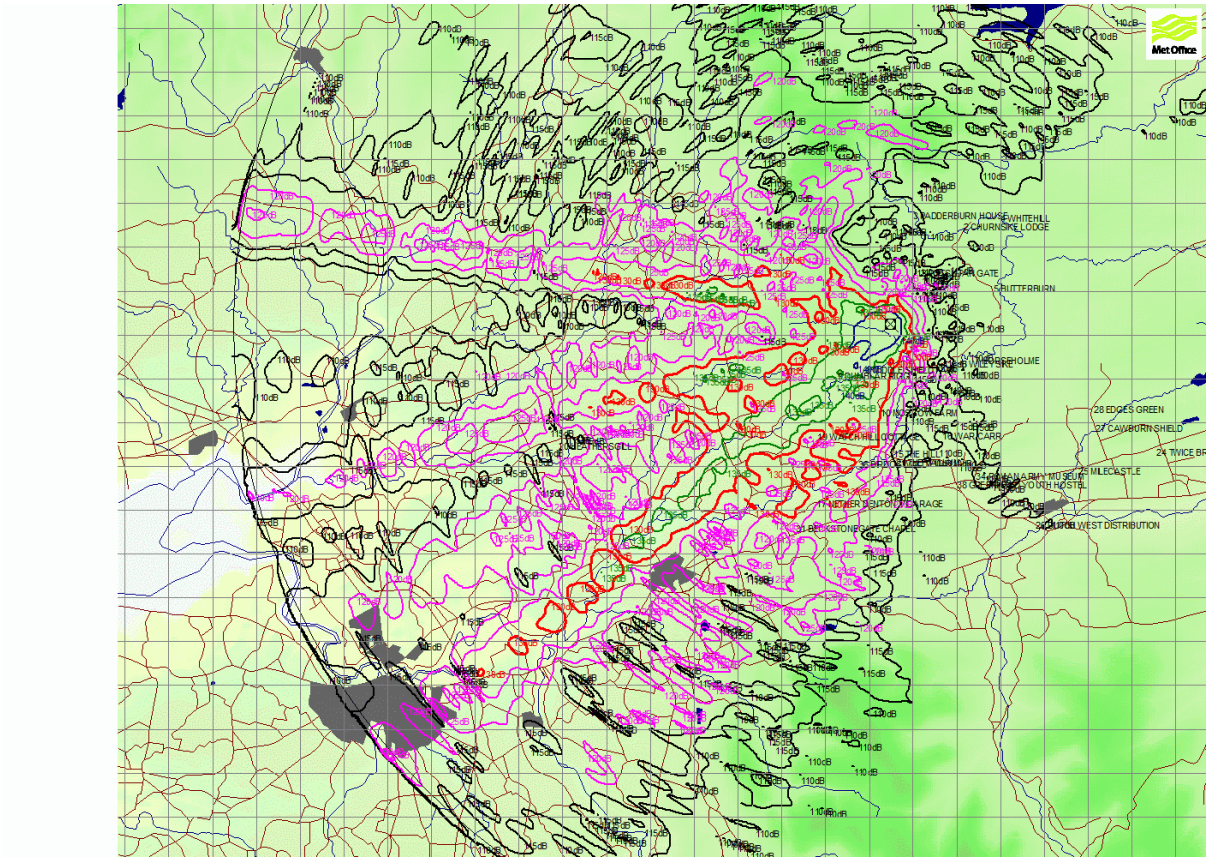

Figure 52 - Example of a MONET noise footprint used by DNV GL Spadeadam range controllers to determine the commencement of blasting. Noise contours are overlaid onto an area map.

Range Limitation

Predictions are limited to a radius of 30km in each direction from the blast origin, at which contours tend to 0dB. This boundary condition may lead to inaccuracies in predictions at long-distances around 20km. The long-distance blast noise levels are an important consideration for Spadeadam, given that complaints may come from distances on the order of 15km and therefore may be inaccurately represented within predictions as a result of this boundary smoothing. Under extreme meteorological circumstances, propagation out to beyond 30km may be possible.

Ground Impedance and Terrain

Further uncertainties are introduced into the MONET by the assumption that all ground terrain is simulated as either hard or soft, meaning that variations in terrain roughness and absorption may not be captured. This is a significant problem especially for the Spadeadam area which has many types of ground surface, that also vary with range. The MONET accounts for non-flat terrain by placing imaginary sources on a planar surface to emulate the same effects from uneven terrain, a commonly accepted boundary condition (Hume, 2000).

Furthermore, given that the MONET is a PE model, airborne interactions between sound waves are account for.

2D to 3D Interpolation

Within many MONET plots for various tests at Spadeadam over the years, patterns within the contour lines have been noted to show possible repeated errors occurring along the radial lines matching the radial angles at which propagation is simulated. It seems that there is an error within the smoothing algorithm which interpolates the contour values between the radial calculations (every 15°) so that the full circumference contours may be continuous. The resulting effect is ridges within the noise contours which are not seemingly related to any topographical or meteorological features.

Uncertainty

Currently, the expected uncertainty within the model predictions are said to be very difficult to gauge based on a lack of measurement data. From the Met. Office's own investigations, the RMS error is stated to be around 6dB. Several sources of uncertainty have been considered, including from atmospheric turbulence which is not represented within the model and errors related to the magnitude of the noise source.

Validation

Finally, a validation of the model has not been published, other than a minimal validation by Hume (2000). The model has not been peer reviewed within any academic journals, and there are concerns with the accuracy and associated uncertainties within the prediction.

3.3.3.5 Met Office Sound Wave

In spring 2023, MONET was superseded by a new version known as Sound Wave. Information on the Sound Wave model is presented directly from the Sound Wave information sheets contained in Figure 53 and Figure 54.

The model validation is not included in this thesis due to the lack of large scale tests using predictions from this services before this research was submitted. However, there is an aim to validate the model performance and how different the predictions are to MONET against real-world measurements, as part of further work.

Met Office

Key features of the output of the Met Office's noise forecasting tool "Soundwave"

This document provides essential background information to the user to aid the interpretation of the Soundwave forecasts issued by the Met Office.

1) Soundwave is designed to advise on noise nuisance risks associated with artillery fire on and around training ranges. It provides an estimate of noise levels in dBC, that is, weighted to the human ear response and this advice is provided as either maps or point values.

2) Soundwave replaces the previous Met Office Noise Evaluation Tool (MONET) system; MONET will be decommissioned in Spring 2023, after which time it will be no longer available.

3) The amount of noise perceived at a given location from either the gun fire or the shell detonation depends on many factors including the location of the noise source, the weather conditions, the type of explosive or gun, the charge weight and height of detonation, surrounding vegetation, and the topography.

4) Soundwave will use all these factors in its prediction of a noise level, but uncertainties exist in all elements of the Soundwave prediction system, just as they do in any other prediction system.

5) Sound propagates more effectively downwind than upwind, and propagates further when the lowest layers of the atmosphere are cooler than those above, as often occurs in the early morning.

6) Soundwave will be more effective than MONET in predicting the favoured directions in which the noise propagates.

7) There will be considerable uncertainty, sometimes over 10dB, in a point-specific prediction of a noise level. Averaging over a wider spatial area will provide a more robust estimate.

8) We should not consider the positioning of small spatial scale variations in a noise contour produced by Soundwave to be precise; the system will produce only a general indication of noise levels.

Figure 53 - Met Office Soundwave model information sheet: Part 1.

9) Microphone observations of noise may be used alongside Soundwave output to understand noise nuisance risks, but we should be aware that a microphone is only a single point measurement of a single explosion and may also record noise from other sources, such as vehicles passing nearby.

10) Lying snow will absorb noise and reduce the nuisance impact of noise. This is not represented within Soundwave (nor was it represented in MONET).

11) The sea surface is considered a flat, reflective surface in Soundwave, without representation of waves or of tides (nor did MONET represent waves or tides).

12) Soundwave can only qualitatively represent the effect of terrain when it is steeper than about 30%. The system does not represent echoes from near vertical slopes, such as sea cliffs or quarry faces.

13) Soundwave will often produce patterns of noise propagation that are more directional in nature than those from the previous MONET system. It will also likely estimate larger values for noise at large distances from the source in the downwind direction. We have confidence that Soundwave provides a better characterization of the propagation pattern than MONET based on tests with analytical solutions to the noise propagation.

14) Soundwave will often produce estimates of noise in the upwind direction from the source (the direction from the source that is the quietest) that are lower than those in MONET. The estimates from Soundwave are also often lower than those observed in this situation.

15) The changes between Soundwave and MONET predictions are largely a result of numerical, rather than physical, differences in the way in which the different systems solve the sound propagation problem.

Figure 54 - Met Office Soundwave model information sheet: Part 2.

The model information sheets provide some high-level guidance on the contents of the new model, but provide no detail on the mechanics model. However, there is an emphasis on the fact that Soundwave will focus more on downwind propagation, or favourable directions as they are referred to in the information sheets (point 6). Point 13 explains how the new model

is likely to produce more directional patterns of sound than MONET, and that long-range enhancements are better represented in the new model. Upwind predictions are said to be lower than those produced in the same direction by MONET (point 14). Point 14 also states that upwind predictions are likely to be less than observed levels in reality, which is not a desirable effect. Upwind predictions are important, because in reality, atmospheric turbulence scatters sound into upwind shadow zones, thus increasing levels for predictions compared to those not accounting for atmospheric turbulence. It is therefore unclear if Soundwave is including turbulence in its modelling and why its predictions give less emphasis to upwind receptors.

3.3.3.6 Backscatter limitations of PE Models

In reality, as sound propagates through the atmosphere, some energy makes its way back towards the source by a mechanism called *backscatter,* from a myriad of physical objects, (barriers, forest edges *etc.).* Moreover, when applied to the structures of the lower atmosphere, the rather desirable effects of backscattered sound from changes in refractive index caused by atmospheric structures makes acoustic remote sensing possible via devices such as SODARs (Emeis, 2011, 2021).

Although the PE method can be used to make predictions in two directions with respect to the source (i.e upwind and downwind), it is still a one-way approach, meaning that the propagation of sound through a medium back towards the source is neglected. Therefore, the effect of backscatter from the atmosphere or barriers is not possible with the standard one-way PE method. This has particular relevance to modelling the influence of barriers on propagation with PE models. K. Attenborough, Li, and Horoshenkov (2006) write about this effect in their book when describing an initial attempt to model absorbing barriers with the PE method in refracting atmospheres (E. M. Salomons, 1994), who modified the pressure at the representative grid points of the barrier locations to be zero, and thus the normal velocity onto the barrier also being zero, representing a rigid boundary. However, as the PE method can only model propagation in one way, the reflection of sound from the barrier back towards the source was neglected. E. Salomons (2001) notes this in the appendices of his book with respect to backscatter neglection from the one-way properties of PE models.

This undesirable effect is a limitation of the Parabolic Equation method for accurately modelling the scattering and reflection effects from forest edges and terrain which have been discussed in section 3.2 of this thesis. K. Gilbert and White (1989) wrote about the difference

between a one- and two-way PE method in their original paper on its application to outdoor sound propagation, when presenting the operator solutions to the wave equation. They firstly introduce the two-way Helmholtz equation for the acoustic pressure *P* for an azimuthally symmetric environment, with wavenumber *k*, given by *ω/c(r,z)*, where ω is the circular frequency and c is the sound speed at range *r* and height *z*.

$$\left(\frac{\partial^2}{\partial r^2}+\frac{1}{r}\frac{\partial}{\partial r}+\frac{\partial^2}{\partial z^2}+k^2\right)P=0 \qquad \text{Equation 19}$$

The two-way propagation of sound becomes apparent with their farfield equation of the variable $u = \sqrt{r}P$, which is

$$\left(\frac{\partial^2}{\partial r^2}+Q\right)u=0 \qquad \text{Equation 20}$$

With Q defined as $\frac{\partial^2}{\partial z^2}+k^2$, and because of the second derivative of r in Equation 20, both forward and backward propagation of sound is permitted. Gilbert and White simplified the method to a one-way approach by making k independent of range, and writing it as a product of two operators. The result is the one-way version with the partial derivative in terms of the variable u, which explicitly excludes two-way propagation, but allows two directional propagation (with respect to a centred source) depending on the sign in Equation 21 being positive or negative. West, Sack (and together with Gilbert) refer to *u* as the velocity potential in their papers (Sack & West, 1995; M. West, Gilbert, & Sack, 1992), and symbolise it as Ψ, but nonetheless describe the same solutions.

$$\frac{\partial u}{\partial r}=\pm i\sqrt{Q}\,u \qquad \text{Equation 21}$$

Despite Salamons' attempt to model outdoor diffraction of sound over a barrier in 1994, the two-way parabolic equation approach with relation to backscattering had already been applied to underwater acoustics (Collins & Evans, 1992). M. West et al. (1992) had already described the solutions for a two-way PE method in their paper, and Sack and West expand on it in later their work in 1995 with respect to a simulating propagation over a smooth terrain profile, laying the foundation for what became the Generalised Terrain Parabolic Equation (GT-PE).

3.3.4 Heuristic, Empirical and Other Models

Whilst sophisticated PE models aim to predict noise accurately and everywhere, the purpose of a heuristic noise prediction model is much simpler. Heuristic models do not intend to predict sound levels with perfect accuracy at many receiver points but to provide the realistic outcome of blasting. For example, whether blasting should occur or not, based on the current propagation conditions. Indeed, many nuances of the propagation footprint will be discounted due to the lack of input data, though the advantage of minimal input data means less dependence on computational power and time. Therefore, predictions are much more rapid, even for long-term noise forecasts in the future (i.e., weeks away)

Heuristic methods have been developed from general engineering purposes, which are based on other prediction models, for example the work of L'Espérance, Nicolas, Herzog, and Daigle (1992) created a ray-theory-based heuristic model which accounts for the main effects of absorption, geometrical spreading and ground effect. Their model accounted for refraction with linear sound speed profiles in order to make analytical solutions of propagation and includes atmospheric turbulences and diffraction into shadow zones.

3.3.4.1 European Models

A considerable amount of theoretical and field work from various facilities in mainland Europe has significantly progressed the community's understanding of blast noise over recent decades. In 1996 the international 'Ad Hoc Working Group of Low Frequency Impulsive Noise' established a test plan (E, 1996) for gathering source measurements of various explosive and military weapons. Other trials included long range trials of large explosions (up to 64kg C4), many of these trials were carried out in Norway, and an overview of those trials is presented by Kerry in (G. Kerry, 1996). This section of the literature review details the important work done across Europe on blast noise management.

Germany

Karl Hirsch's work which has spanned decades has been significant at successfully managing noise impacts from weapons and shooting ranges across Germany. In 2003, Hirsch presented a paper on an engineering-based model for predicting long-range propagation considering terrain features (Karl-Wilhelm Hirsch, 2003). The work aimed at addressing noise from large weapons over several kilometres, accounting for shielding effects of hilly terrain under

refractive conditions not considered in the current standards at the time for long range sound prediction, which was mainly ISO 9613 and considered straight paths only.

For context, Hirsch's work dates back several years earlier, and aimed to build on the current methods used at the time in Germany, which were the Technical Instructions for Protection against Gun Noise. That guidance included a model based on an empirical formula to describe the 'noise load' of a single impulsive event.

$$L_i = S_i + R_i - 20\log\left(\frac{r}{r_0}\right) + A_i\log\left(\frac{r}{r_0}\right) + B_i\left(\frac{r}{r_o}\right) + C_i \ldots \quad \textit{Equation 22}$$

With L_i, the single event level, S_i and R_i the source level and directivity (both at 250m) respectively, and A, B C are additional propagation corrections. The propagation equation is described in more detail by Trimpop & Bütikoffer (Trimpop & Bütikofer, 2012) in equation 2, with 4 propagation corrections, D_{dis}, D_{abs}, D_{sit} and D_{met}.

$$L_{CE}(d,\alpha) = L_{CE,250m} + D_{dir}(\alpha) - [D_{dis}(d) + D_{abs}(d) + D_{sit}(d) + D_{met}(d)] \quad \textit{Equation 23}$$

Where $L_{CE,250m}$ is the C weighted sound emission level (previously referred to as the source level) at 250m, calculated according to (E, 1996). D_{dir} (α) is the directivity pattern of the emission level as a function of radiation angle α. The propagation corrections are; D_{dis} (geometric spreading correction), D_{abs} (air absorption correction), D_{sit} (sound reduction due to other effects, such as ground) and finally D_{met} (meteorological correction).

$$d_{dis}(d) = 20\log\left(\frac{d}{250m}\right) \quad \textit{Equation 24)}$$

$$d_{abs}(d) = \beta_0(d - 250m)\left(\frac{d}{1m}\right)^{\beta_1} \quad \textit{Equation 25}$$

$$d_{sit}(d) = -K_{lin}(d - 250m) - K_{log}\log(d/250m) \quad \textit{Equation 26}$$

$$d_{dis}(d) = -\left(0.0012 + \frac{0.042v_{wind}}{v_0}\right)K_{met}\log\left(d/250m\right) \quad \textit{Equation 27}$$

This method accounts for temperature inversions by increasing wind speed with a constant value of 2.37m/s, resulting in an increased result for the L_{CE}.

Such a model was developed for the purpose of making rapid predictions of military activities for large areas surrounding shooting ranges, with source descriptors of weapons based on source CSEL and directivity measurements at 250m taken in Germany, the UK and the US.

Weber Method for Estimating source spectra

Within Hirsch's work, the recognition that without accurate representation of an impulsive source characteristics, then accurate predictions of noise would not be possible. The Weber Spectrum (Weber, 1939) was a widely used method at the time that utilises the initial blast radius R as a descriptor for the complex spectrum of sound generated by an explosion. The original method has been extended and is now included in the current version of ISO 17201-2:2006 (International Standards Organisation, 2006). The title of Weber's original work in 1939 roughly translates to "the sound spectrum of bangs from sparks gaps and guns with a contribution to application possibilities in electroacoustic measurement technology". The method is generally based on the ideal image of an explosion, where a hot gas bubble is generated at the moment of firing, initially expanding supersonically ($v_{gas} \gg c$), until its speed decreases to the speed of sound, at which point sound can be emitted. The model is said to be useful for correlating the size of explosives with the total sound energy that is emitted. The method is described in detail by Hirsch in much of his early work (Karl-Wilhelm Hirsch & Trimpop, 2000) and in more detail by Wunderlii (J. Wunderli, 2004), to apply the model for in-air explosions, where the Weber-Radius, a parameter known as R_w describes the size of the exploding source when it radiates the blast.

$$R_w = \sqrt[3]{\frac{Q_m}{q_w}} = \sqrt[3]{\frac{Q_c \cdot \sigma_{ac} \cdot \sigma_{cg}}{q_w}} = \sqrt[3]{\frac{m_c \cdot \sigma_{cb} \cdot \sigma_{ac} \cdot \sigma_{cg}}{q_w}} \qquad \textit{Equation 28}$$

Where R_w is related to the TNT equivalent mass of the explosive and the following parameters as described in (International Standards Organisation, 2006; J. Wunderli, 2004) and much of Hirsch's work.

Q_m: Total acoustical energy emitted by the explosion [kJ]

Q_w: Energy density in the gas sphere when reaching the speed of sound = 2.25kJ/m3

Qc: Total chemical energy of the explosive [kJ]

σ_{cg}: Proportion of the chemical energy that is transformed into kinetic gas energy (default value = 45%)

σ_{ac}: Proportion of the kinetic gas energy that is transformed into acoustical energy (default value = 4%)

m_c: Mass of explosive [g]

σ_{cb}: Conversion factor giving the amount of released energy per unit explosive [kJ/g] (TNT: 4.31 kJ/g)

A source spectrum S(ω) is given by applying a Fourier transformation to the source sound pressure signal as in eq (3).

$$S(\omega) = \frac{P_0}{\pi}\left[\frac{a}{a^2 + \omega^2} + j\frac{\omega}{a^2 + \omega^2}\right] \qquad \textit{Equation 29}$$

Here, $a = \frac{3c}{R_0}\sqrt{1 + \left(\frac{c}{\omega R_0}\right)^2}$ and $P_0 = 14.4kPa$, a constant originally chosen by Weber. In equation (2) ω is the frequency, c the speed of sound and R_0 the Weber-radius. From here, the 1/3 Octave band spectrum is derived and calculate the Radius R_0 for a given CSEL in a certain propagation direction around the source.

In much of his work throughout the later 1990's and early 2000's, Hirsch used this method and argued that it was important engineering means for estimating the characteristics content of source spectra. The Weber model was described in detail in by Buchta and Hirsch in their paper on the applicability of C-weighting as an acoustical descriptor for blast and shooting noise (Buchta & Hirsch, 1996). Hirsch later used the method in his paper (Karl-Wilhelm Hirsch, 1998), as a method to compare predictions with measurements with a focus on investigating the influence of local ground reflections. Around the same time, Hirsch validated the Weber model experimentally for charge sizes ranging between 0.5 and 20kg in (K-W Hirsch, 1998).

The model now forms the basis for the calculation of source spectra from small arms weapons and gun-blast in the international standard ISO 17201-2:2006, which is due to be reviewed soon at the time of writing.

WinLarm

Much of the work done in Germany by Hirsch was later developed into a desktop software environment, for running predictions of noise at shooting ranges. WinLarm® is a DOS-based

noise prediction software suite, with several programs and is maintained by Cervus Consult GmbH and the Institut fur Larmshutz GmbH on behalf of the German Ministry of Defence.

Hirsch proposed an approach for managing noise from military training areas that would align with Germany introducing a new daily shooting rating scheme. Hirsch's model was also focused on being an operational tool used by range managers to make an ensemble of rapid predictions, available within minutes. Use of sophisticated computational models was dissuaded in favour of a ray tracing process to describe the propagation effects of the atmosphere with reasonable technical accuracy.

Noise management in Germany

A review of shooting noise management in Germany is given in (Schreckenberg & Großarth, 2021), which refers to how shooting noise is not given the same treatment as other forms of noise (transportation, industrial noise etc.) within German regulation. This was commented on in (Lenart, Bauerschmidt, & Hirsch, 2011). The German armed forces self-impose noise management in the form of the following restrictions, from (Schreckenberg & Großarth, 2021).

- Daily average noise levels of 70 dBC L_{den} in mixed zones and 65 dBC L_{den} in residential areas including all shots from large guns is not to be exceeded more than 5% of the days in a year
- The maximum level of 100 dBC L_{den} in mixed zones and 95% dBC L_{den} in residential areas for a single noise event is not to be exceeded more than 5% of the days in a year
- Both goals must e fulfilled for every inhabited grid cell with dimensions 250 x 250m.

Switzerland: sonARMS

The work of Wunderli in Switzerland has contributed greatly to the currently operational Swiss Shooting sound calculation model, sonARMS (J. Wunderli, Pieren, & Heutschi, 2012). It was developed by Empa, Merz Technik and the Swiss Federal Office for the Environment FOEN and is applicable to both civil and military activity. Its propagation model is the sonX model, also developed at Empa, which includes the following features.

- Range dependent ground properties, based on analytical solutions for spherical waves
- A ray tracing algorithm for meteorological effects
- Models for the description of reflections from rigid surfaces, including coherent reflections, and scattering
- Diffuse scattering by forest edges and cliffs

sonARMS can make predictions of muzzle blast, sonic booms and detonations. The acoustic metrics calculated and used for assessment are the sound exposure levels, LE and the fast-weighted A-weighted maximum sound pressure levels LAMax.

The models implementation followed military shooting noise limits introduced in Switzerland in 2010. A weapons database with source strength information feeds the first stage of the model, which makes calculations including ground reflections for a homogeneous atmosphere, before being passed to a second stage which accounts for meteorological effects. The second stage is modelled with ray tracing.

For the source description, 1/3 Octave Band spectra are formulated from 25Hz to 5KHz, and by taking an energetic sum of detonation (D), muzzle blast (M) and projectile (P) sound, a total spectral sound exposure level $L_{FE,\,tot}$ is calculated as below.

$$L_{fE,tot} = L_{fE,D} \oplus L_{fE,M} \oplus L_{fE,P} \qquad \textit{Equation 30}$$

Further, the contributions of direct (dir), reflected (ref), forest scattered (for), and cliff reflected (cliff) sound is added to the three partial sources (i = D, M, P), to form the following.

$$L_{fE,tot} = L_{fE,D} \oplus L_{fE,M} \oplus L_{fE,P} \qquad \text{Equation 31}$$

For direct sound, a frequency-dependent sound source level $L_{f,q}$ for each partial source *i*, is combined with a frequency and angle-dependent (α) directivity correction $D_{f,(\alpha)}$, along with corrections for corrections for geometrical divergence, air absorption, ground and shielding effects, foliage attenuation, lateral sound paths, meteorological effects, and non-linear effects, which all vary with each partial source and are frequency dependent.

Representation of the source in sonARMS

Explosive source terms in the sonARMS model are similarly represented by a combination of either measurements of theoretical derivation. Wunderli acknowledges the non-linear conditions at close range to the source (peak pressures approximately above 1kPa), with respect to the sonX propagation scheme which operates in the linear acoustic regime. Where measurements near the source are not feasible, the aforementioned Weber model is

performed, on the basis of charge weight for detonations, in 1/3 octave bands from 25Hz to 5kHz. Wunderli refers to the ISO standards, ISO 17201 (parts 1 and 2 for measurement and calculation respectively) (International Standards Organisation, 2005, 2006) and ISO 13474 (International Standards Organisation, 2009).

Meteorological representation

Meteorological effects included in sonARMS combine, air absorption, with shielding effects and the contributions or lack of shadow zones into a single meteorological correction which is applied to the direct sound calculation. Vertical atmospheric profiles are generated separately by and meteorological pre-processor which uses wind, temperature and humidity information from the European COSMO-2 Weather Prediction Model.

Wunderli and Rotach's Implementation of the COSMO-2 Weather Prediction Model

Originally implemented for another Swiss sound prediction package, sonRAIL, the ray tracing approach of all the Swiss propagation models can follow arbitrary and range dependent sound speed profiles. Wunderli and Rotach developed a profile calculator (J. M. Wunderli & Rotach, 2011) which uses simple surface level input data to compare generated profiles with the fine COSMO-2 model, which has a fine grid resolution of 2.2km x 2.2km.

As input into the profile generator, the following information is required on a horizontal grid of 190x130 points.

- Long-wave and short-wave radiation balance,
- Global and long-wave incoming radiation
- Temperature at 2m above ground
- Temperature, relative humidity, wind speed and direction at 10m
- Temperature, wind speed and direction at heights of approximately 33m, 65m, 108m and 160m
- Geographical location
- Distribution of land and water
- Surface roughness, z_0

Using Monin-Obukhov similarity theory (MOST), the profiler generates vertical profiles from the following stages.

Calculation of surface radiation balance

$$Q_h = \left[\frac{(1-\alpha)+S}{1+S}\right] \cdot Q_* \cdot (1-a) - \alpha\beta' \qquad \text{Equation 32}$$

Where α is a factor describing moisture availability on the ground, S a linear approximation according to equation (Z), a for describing the energy flux into the ground, Q_* a net radiation balance and β^1 an advection correction = $5Wm^{-2}$.

$$S = \frac{c_p}{L_e \cdot \left(\frac{dq_s}{dT}\right)} \approx 0.21 + \frac{1.8}{40\ (35 - T[°C])}, \qquad \text{Equation 33}$$

Where C_p is the specific heat of dry air at constant pressure, L_e the evaporation energy of water, and (dq_s/dT) a gradient of the saturation of humidity in air.

Calculation of friction velocity u_*

During the daytime ($Q_h > 0$), the characteristic parameter of a wind profile in the surface layer, the friction velocity u_*, is determined below.

$$u_* = \frac{k \cdot v_m}{\ln\left[\frac{z_m - 0.5h_r}{z_o}\right]}[1 + d_1 \ln(1 + d_2 \cdot d_3)] \qquad \text{Equation 34}$$

As seen in other sections on MOST in this thesis, k is the von-Karman constant of roughly 0.4, v_m the horizontal component of the wind speed at height z_m in ms^{-1}, h_r the height of the roughness elements in metres, z_0 the roughness length in metres, and finally, d_1, d_2, and d_3 are parameters dependent upon the roughness length, explained in (J. M. Wunderli & Rotach, 2011).

At night (when $Q_h < 0$), u_* is calculated according to Equation 35. Where g is the gravity constant 9.81 ms^{-1}. An important parameter here is Θ_* , the turbulent temperature scale determined according to **Error! Reference source not found.**.

$$u_* = \frac{k \cdot v_m}{2\ln\left[\frac{z_m - 0.5h_r}{z_0}\right]} \cdot \left[1 + \sqrt{1 - 4\left(\frac{4.7 \cdot g \cdot z_m \Theta_* \ln[(z_m - 0.5h_r/z_0)]}{k \cdot T_m \cdot v_{m^2}}\right)}\right] \qquad \text{Equation 35}$$

Where g is the gravity constant 9.81 ms-1. An important parameter here is Θ*, the turbulent temperature scale determined according to

Where g is the gravity constant 9.81 ms-1. An important parameter here is Θ*, the turbulent temperature scale determined according to

$$\Theta_* = \min\left[0.09\left(1 - 0.6 \cdot N^2, \frac{k \cdot T\_m \cdot v_m^2}{18.8 \cdot z_m \cdot \ln\left[\frac{z_m - 0.5h_r}{z_o}\right]}\right)\right]$$ *Equation 36*

Where N is the percentage of cloud cover.

Wunderli and Rotach go on to describe the procedure for deriving the Linear and Logarithmic parameters of the vertical atmospheric profiles under a variety of scenarios. Additional techniques are outlined for the extrapolation of Lin-Log profiles, such as with a roughness sub-layer, extrapolation for greater heights, modification for small wind speeds and adaptation to varying surface properties.

sonARMS Accuracy

Where N is the percentage of cloud cover.

Wunderli and Rotach go on to describe the procedure for deriving the Linear and Logarithmic parameters of the vertical atmospheric profiles under a variety of scenarios. Additional techniques are outlined for the extrapolation of Lin-Log profiles, such as with a roughness sub-layer, extrapolation for greater heights, modification for small wind speeds and adaptation to varying surface properties.

sonARMS Accuracy

An analysis of the accuracy to which sonARMs can make predictions has been included in Wunderli et als paper. Uncertainties are separated into those derived from the source and propagation parts of the model. As the propagation part belongs to the now sonX (then sonRAIL) model, the validation of the propagation scheme had been carried out previously for sonRAIL, under distinct propagation scenarios. The high-quality standards applied in ammunition and weapon production yield very reproducible sound source levels and thus the variation in source levels is thought to be low (for military weapons). The uncertainties of the model here lie in the source terms derived through measurements which have been undertaken in the linear acoustic region (i.e at distances on the order of 100m for

overpressures below 1kPa), and has overall been estimated to be around 2dBA. The combined uncertainty has been estimated to be 3.5dBA.

Netherlands

A review of the literature on shooting noise in other countries in mainland Europe did not find any definitive guidance on the prediction, measurement or assessment of shooting, blast or impulsive noise. One webpage ("Noise from Shooting Ranges,") contained information on shooting noise for the Netherlands and stated that there is no standard fixed for military shooting noise in the Netherlands, however, gave information on noise limits for civilian shooting ranges. According to the webpage, a rating level is calculated, combining information on overall levels and the number of shots.

$$L_r = L_{shot} + 10\log N - 33 \qquad \text{Equation 37}$$

Where L_r is the rating level, L_{shot} is the shot level measured in impulse and N is the number of shots per hour. It is not conclusive whether there is any frequency or time weighting applied to this metric.

A table is given for civilian shooting range noise limits.

Table 29 - Limits for noise from shooting ranges in the Netherlands

Types of surroundings	**Rating level, L_r**		**Shot level L_{shot}**	
	Day	Evening	Day	Evening
Residential	50	45	75	73
Rural	45	40	73	70
Quiet Zone	40	30	65	65

The webpage then goes on to describe a calculation of noise from military shooting ranges in a similar method, with the calculation of the rating level, L_r.

$$L_r = L_{shot} + 10\log N - C_m - 66.2 \qquad \text{Equation 38}$$

Where in this case, the parameter N is the number of shots per year, and C_m is a meteorological correction. The calculation goes on to describe how for heavy weapons, if the difference between $L_{i,linear}$ and $L_{i,A}$ is 35dB and if $105 < L_{i,linear} < 125$ then

$$L_r = L_{shot} + 10 \log N + C - C_m - 66.1 \qquad \text{Equation 39}$$

Where $C = (L_i - 105)/2.2$. Alternatively, if $L_i > 125$, $Lr = L_{shot} + 10 \log N - C_m - 57.2$. It therefore seems that there are penalties involved for frequency and level variations, however, the source of this information was not determined.

NIELS

Following a meeting with Frits van der Eerden at TNO in the Netherlands, who co-authored many of the papers mentioned on nonlinear models (see next section), as well as on blast noise control, the author was made aware of another model used in the Netherlands known as NIELS. Impulsive Noise Emission Measurement Analysis (NIELS) is a software designed to process acoustical measurements of impulsive noise to obtain descriptions of noise source energy to be used in further predictions (van der Eerden, 2023). It has 3 components:

- Direct
- Short range indirect
- Long range indirect

The theory of the 3 modules are described by van der Eerden and van den Berg (2010) and are discussed in the section on Nonlinear Models in this thesis. In general, however, the direct method is the simplest and most appropriate method for characterising sound source terms for impulsive noise generated by small arms, as measurements can be made at close range and the ground effects of the muzzle blast can be corrected in the time domain. The short range indirect method uses a spectral component to include the effects of an absorbing ground. The Long-range indirect method, as the name suggests, includes a source characterisation derived from measurements taken further away, and hence is more suitable for large blasts, such as demolitions, akin to those carried out at Spadeadam. Consequently, the effects of meteorology which are more relevant at longer ranges can be accounted for in this method.

In general though, the software has a graphical user interface for visualising source measurements at various angles around the source perhaps collected simultaneously by many

microphones on different channels, displaying the pressure-time histories and 1/3 Octave band spectrum of each channel.

3.3.4.2 Nonlinear Models

Much of the chapter on prediction modelling for blast noise has revolved around making predictions with linear acoustic approximations, for example, by using parabolic equation models to describe acoustic propagation from sound sources with an artificially derived sound power level, thus ignoring the non-linear effects at short range. This subchapter details the work done on nonlinear models to describe the near field propagation of a blast wave and its subsequent use in predictions of long-range noise impacts from explosives and military activity.

In particular, the work of the Dutch MOD and TNO throughout the 2000's progressed the application of nonlinear models for the prediction of blast waves. In 2005 (van der Eerden & Vedy, 2005), Van der Eerden and Vedy developed a 3-stage approach to model the propagation of high amplitude waves produced by large military weapons and blasts. The method firstly involved a process to deal with the highly non-linear effects of a strong shock near the source with an unsteady Euler method, using a Flux-Corrected Transport (FCT) technique. As the shock travels, the degeneracy of the wave into a weak shock is modelled by a Nonlinear Progressive-wave Equation (NPE) method and subsequently the linear acoustic propagation is finally modelled by a Parabolic Equation (PE) method. Earlier work by Vedy in 2002 (Vedy, 2002b) had investigated the FCT technique for solving flows in porous materials. This work has application for including ground impedance effects within the nonlinear models.

Much of this modelling work had been inspired by the need to accurately describe the impulse propagation and interaction with porous materials, which was investigated intensively in the work of Umnova, Attenborough and Cummings (Umnova, Attenborough, & Cummings, 2002) around the same time as Vedy's 2002 work. As described in the section on blast noise control, this work at the University of Hull in the early 2000's informed the joint work of the US ERDC, Dutch MOD and University of Hull on absorbing surfaces for blast sound (Keith Attenborough, Cummings, Dutta, Schomer, & Salomons, 2004).

TNO's implementation of non-linear models

Returning to the Dutch implementation of non-linear models, van der Eerden and Vedy (van der Eerden & Vedy, 2005) presented a paper in 2005 which integrated two non-linear models

(FCT method and NPE method), with the traditional parabolic equation PE model to simulate the propagation of a blast wave from source to receiver. A later paper by Frits van der Eerden and Frank van den Berg in 2010 (van der Eerden & van den Berg, 2010) describes in detail the methodology used to achieve a simulation of a blast wave following near field measurements but rather in the context of quantifying the explosive source strength.

Firstly, the integration of the 3 computational methods (FCT, NPE and PE) will be presented here, before the so-far undescribed methods (FCT and NPE) will be detailed.

Integration of FCT/NPE/PE

Van der Eerden and Vedy's 2005 paper details the coupling of each model with respect to one another, in order to model the propagation of a high-amplitude non-linear shock wave from a blast, as it progressively slows to a linear acoustic wave at long range.

FCT and NPE Coupling

A 3-dimensional version of the FCT implementation is used to compute the 3-dimensional unsteady Euler equations on an axisymmetric rectangular grid, discretely tracking the total air pressure, velocity and density of the shock wave as it progresses at close range to the source. The total air pressure includes the instantaneous sound pressure superimposed on the static pressure. This is done in the time domain.

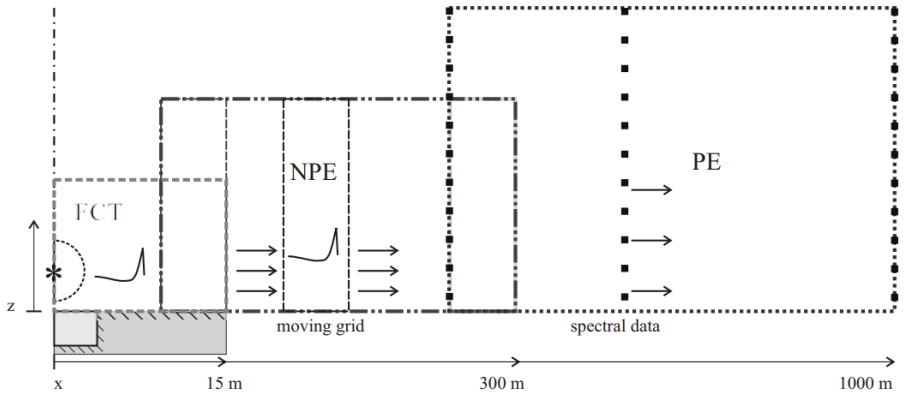

Figure 55 - Calculation schematic of a shock wave from source to receiver showing the coupling between the Flux-Corrected Transport (FCT) method and the Non-linear Progressive-wave Equation (NPE), followed by coupling of the NPE with the Parabolic Equation (PE) method, taken directly from van der Eerden and Vedy's 2005 paper .

A similar rectangular grid is used for the NPE part of the solution, with an overlap from the FCT solution providing a starting position. A wider and coarser grid represents this part of the calculation, which typically takes the propagation out to several hundreds of metres from the source. Van der Eerden and Vedy describe the NPE as a method based on pressure

perturbations around the static pressure of weak shock waves (peak pressures < 10 kPa, or less than 174 dB), with a small angle approximation of < 10° relative to the horizontal plane.

NPE and PE Coupling

The coupling between the NPE and PE part of the simulation provides a smooth transition in propagation modelling between a region where the disturbance is a weakly non-linear shock wave (< 10 kPa / 174 dB but greater than 1 kPa/ 154 dB) and a high amplitude but linear acoustic wave (< 1 kPa / 154 dB). The key part of this transition is to transform the simulation from the time domain (NPE) to the frequency domain, as the PE model is based on the spectral representation of the wave equation. As van der Eerden and Vedy showed in their paper, and as illustrated in Figure 56, the transformation to the PE model is made at grid points at higher range above ground than the NPE method, much like the NPE method does when transition from the FCT method.

FCT Method

Following a section in their paper on source strength determination based on measurements in the linear acoustic range (i.e. 100's of meters from the source, peak pressures < 1 kPa), the so-called FCT method is introduced as a numerical technique.

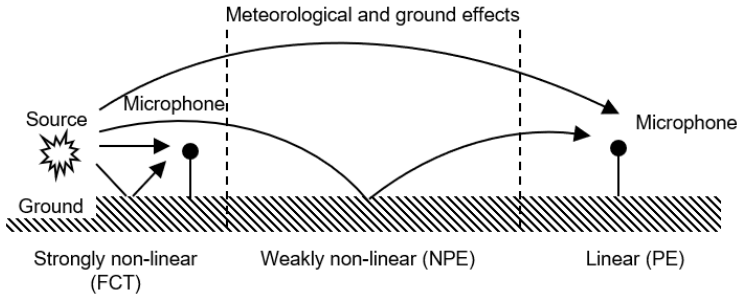

Figure 56 - Modelling techniques used at each of the propagation regions, adapted directly from .

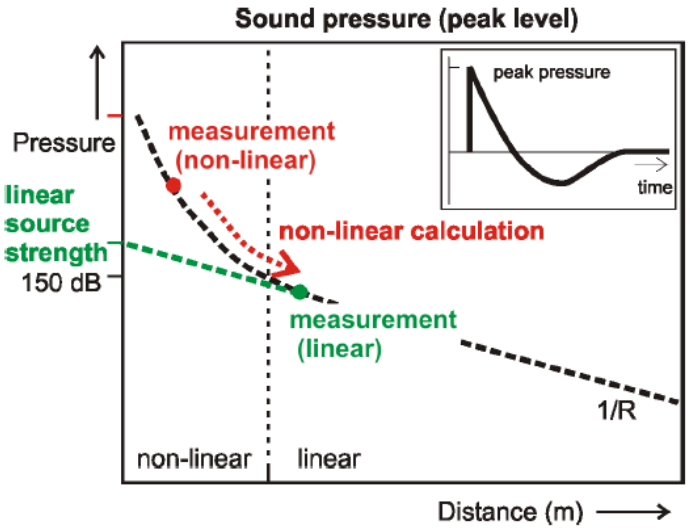

Figure 57 - Representation of linear and non-linear source strength of a blast wave, taken directly from (van der Eerden & van den Berg, 2010).

The Flux Corrected Transport (FCT) numerical technique is an algorithm originally developed by Boris and Book (Boris & Book, 1971) and is a solution to the three-dimensional unsteady Euler equation:

$$\delta_t \boldsymbol{Q} + \delta_x \boldsymbol{F} + \delta_y \boldsymbol{G} + \delta_z \boldsymbol{H} = 0 \qquad (1)$$

Where $\boldsymbol{Q} = (\rho, \rho u, \rho v, \rho w, E)^T$ contains the density and momentum components, along with total energy density $E = \frac{p}{\gamma - 1} + 0.5\,\rho(u^2 + v^2 + w^2)$, as a vector, and $\boldsymbol{F}$, $\boldsymbol{G}$ and $\boldsymbol{H}$ are flux vectors as described in Vedy's earlier work (Vedy, 2002a).

Using the FCT algorithm, accurate reproductions of strong flow discontinuities, i.e. shocks, are achieved without oscillations and overdamping artefacts introduced with classical discretization. The computation is started with a Gaussian pulse at time t=0 s, with a starting pressure, and is propagated using the FCT code to distances of up to a few tens of metres, according to (van der Eerden & van den Berg, 2010). The peak amplitudes are then tuned to match near field measurements of the source (e.g. at 3, 25, 50 and 100 m as shown by van der Eerden and van den Berg), to find the starting conditions for the pressure, velocity, density and energy of the shock at the source. The simulations produced in (van der Eerden & Vedy, 2005) are extended up to 5m height above ground.

Van der Eerden and van den Berg compared the simulation produced by a 1-D FCT algorithm against real-world measurements, within which the ground effect is not included. A

typical waveform for a blast is shown by the simulation, whereas the measurements shown the initial peak overpressure, followed by another peak cause by the ground reflection. By performing an axisymmetric 2-D FCT simulation, the effect of the ground reflection is captured in the simulation and matches the general shape of the measured pressure time history. The authors then go onto describe the propagation as the wave evolves from a strong shock to a weak shock, to a linear acoustic wave.

An important application of the FCT method is described in the last part of van der Eerden and van den Berg's 2010 paper, on the design of mitigation with absorptive barriers, close to the source of the shock. The author's state that the absorbing properties of a barrier can be defined in the FCT method by the porosity, flow resistivity and Forchheimer's nonlinearity coefficient. Simulations of barrier interaction with the shock wave produced by small arms are given, including the effects of gravel filled gabions. As mentioned before, much of this work is founded upon that done by Umnova, Attenborough and colleagues at the University of Hull at the time.

NPE Method

Some description of the NPE method is given in (van der Eerden & Vedy, 2005) and has already been discussed in the previous pages. However, a more detailed description with similar application is given by McDonald, Caine and West in (B. E. McDonald, Caine, & West, 1994). McDonald et al provide a tutorial for the detailed derivation of the NPE solutions with application to time-domain modelling of weakly non-linear propagation of high-intensity pulse wave forms in air. Some years later, McDonald extended the NPE with a high-angle formulation (B. Edward McDonald, 2000), within which he describes the base NPE model as follows.

$$\frac{\delta^2 \rho}{\delta t^2} = \nabla^2 p + \delta_i \delta_j (\rho v_i v_j) \tag{2}$$

With ρ, p and v being density, pressure and velocity respectively, a horizontally moving, wave-tracking frame is progressed in the time domain along direction r at speed c_0, which is the speed of sound in the propagation medium in equation 3, the derivation of which is given in (B. Edward McDonald, 2000).

$$\frac{DR}{Dt} \approx -\frac{\delta}{\delta r}\left(c_1 R + c_0 \frac{\beta}{2} R^2\right) - \frac{c_0}{2} - \frac{R}{r} - \frac{c_0}{2} \int_{r_f}^{r} \frac{\delta^2}{\delta z^2} dr \tag{3}$$

In van der Eerden and Vedy's work, the NPE calculations start by taking the instantaneous pressure obtained from the FCT prediction by the time it has reached around 10 m from the source and a similar calculation grid is used to simulate the evolution of the wave in the time domain. Van der Eerden and Vedy achieved distance increments of 102 mm using a grid with horizontal (dx), vertical (dz), and time (dt) spacings of 0.25 m, 0.125 m and 0.3 ms respectively, with sound speed 340 m/s.

Inclusion of ground absorption in NPE method

Van der Eerden and Vedy included the reflection from an absorbing ground in their NPE calculation by using a linear flow resistivity at the boundary conditions for pressure and velocity at the ground-air interface. They refer to an earlier work done by Ambrosiano et al who first used this for modelling nonlinear wave propagation underwater, for a boundary separating water and water saturated sand (Ambrosiano, Plante, McDonald, & Kuperman, 1990).

Summary of Nonlinear models

Nonlinear models have successfully been used in combination with traditional linear approaches in the context of simulating the propagation of high-energy blast waves from source to receiver, and for deriving the source levels of explosive sources. For unconventional explosion sources such as gas explosions, the measurement derived source-term approach used by van der Eerden and van den Berg is an attractive method for simulating propagation over long-range.

3.3.4.3 Salford Surface Wind (SSW) Prediction Model

This prediction model was briefly discussed in the literature review. The SSW is an empirical model developed for the purpose of supporting the Meteorological Office with noise predictions for MOD test and training ranges (G. Kerry et al., 1987). Following a regression analysis of a large dataset of blasts and measured meteorological conditions formed by 1,639 blast levels over 6 months, the Salford Surface Wind empirical model was developed. The following formula was offered to estimate peak sound pressure level, *L*, for a given charge weight *W* at a distance *d*.

$$L = K_1 + K_2 \log_{10}(W) - (K_3 + K_4) \log_{10}(d) + F_v \qquad \textit{Equation 40}$$

Where, K1 and K2 are 204.6 dB and 11.9 dB respectively describe the source level at 1m AGL from the blast origin. K3 and K4 are coefficients set to 20dB and 9dB, to describe attenuation from spherical spreading and ground interactions respectively. Finally, F_v represents atmospheric refraction effects.

$$F_v = 0.18V_{10}\cos(\theta)\log_{10} d \qquad \textit{Equation 41}$$

From wind speed V_{10} in ms^{-1} at 10m AGL and the angle θ which represents the angle between the wind vector and the direction from the source to receiver.

The model consequently has very low demands for input data, with distance between source and receiver being essentially constant for each receiver, 10m wind speed and direction are the only real variables. These correspond to what is known as the vector wind speed for simplicity, which feeds into the refraction term *F* which describes the magnitude of refraction effects.

A major criticism of this model is that it was developed to be used at another test site, which has very different terrain type and topography to Spadeadam. As noted in the literature review, not only does the terrain affect sound propagation but also the formation of meteorological profiles and boundary layer flow over the area, which affects propagation in its own way. However, early investigations using this model show that prediction errors are relatively low, see Chapter 5. Lacy (2017) also proved that this model could regularly achieve lower prediction errors than a number of other prediction models including MONET against measurements of different blasts under varying propagation conditions at Spadeadam. It is believed that these small prediction errors may just be for certain locations around Spadeadam, where the specific terrain and ground impedance closely match what was at the SSW development location, where ground impedance and terrain is factored into the model through *K3* and *K4*. Prediction errors have been shown to be at least >23dB in Lacy's field trials and it is hoped that the cause of this will be investigated within the scope of this project's planned future work.

3.3.4.4 Heuristic Method from DABENIM Work

The purpose of the heuristic model is to provide likely sound levels at off-site locations for different sized blasts using a single model, based on basic meteorological phenomena and measurements. However, the major drawback of such a model is in its simplicity, that it is basic and may not account for nuances in weather which may cause particular noise

enhancement that may not be predicted. Such cases might occur during the passing of warm fronts, when temperature profiles are more complex.

On the other hand, the model will be significantly more effective for more regular conditions, where no significant weather fronts are nearby. There is also the advantage of only needing basic weather data (wind speed and direction) as a requirement. Given that the wind direction has the greatest effect on overall noise levels, computational expense is minimal, given that there are no propagation calculations, as the model is measurement based. Only correction terms are used to account for specific wind vectors, and changes in charge weights.

It was recognised that it is important to note that many other factors influence the noise propagation including the speed of the wind. Higher wind-speeds cause increased turbulence in the air, which results in greater acoustic scattering up- and down-wind. With higher wind-speeds however, the likelihood of deviations from lapse in the temperature profile of the lower atmosphere decreases.

The heuristic prediction method proposed in Lacy's research work is purely measurement based and is derived from measurements at the control building on the Spadeadam test site of a 100 kg blast at a short distance of around 400 m. This level was slightly reduced due to trees between the measurement position and the blast site. These trees made the data recorded effectively useless for the primary purpose of analysis in terms of noise propagation but were perfect for a first-order heuristic model. The trees are effectively providing "ground attenuation" between the source and receiver which is difficult to calculate in most circumstances. This allowed simple scaling rules to be used to give an approximate level based on relative distance from the source for each location in the zero-wind condition.

For the interaction with the wind, a logarithmic approach was adopted to represent the enhancements and attenuations based on approximately 12 dB enhancement downwind and 12 dB attenuation upwind. These values came from an experiment into the effects of wind attenuation at various speeds over distances of 100 m upwind and downwind of the controlled noise source.

The model is shown roughly to have zero attenuation or enhancement when during cross-wind conditions, and up to 12 dB enhancement directly downwind and up to 12 dB attenuation directly upwind.

For large distances, the attenuation upwind can be significantly greater than 12 dB but this has been accounted for in the model by setting an artificial noise floor which effectively

ignores the blast noise when below 100 dB peak based on distance attenuation as well as the wind attenuation.

The measurement of the 100 kg blast taken at the DNV control building was 147.6 dBLin, at a distance of 382 m away from the blasts source. The expected level was slightly reduced to what would be expected in the free-field, however, along this propagation path was a small but dense section of pine conifers, effectively providing ground attenuation. This allowed the use of simple scaling rules for approximate level based on relative distance from the source to each receiver for the zero-wind condition. Table 31 allows scaling corrections to be applied for different blast sizes.

Table 30 - Heuristic Model look-up table based on 100kg blast for some off-site locations.

		Peak Sound Pressure Level (dB)								
		No Wind	Wind Direction							
Location (dir. With respect to site)	Distance (km)	0	N	NW	W	SW	S	SE	E	NE
DNV G Wiley Sike (SE)	2.45	124	129	132	130	122	112	112	114	120
DNV H Butterburn (NE)	5.04	108	<100	100	110	118	110	102	<100	<100
DNV B Gilsland (S)	6.31	112	124	122	112	106	100	102	112	119
DNV A Bewcastle (NW)	8.73	108	<100	<100	<100	<100	102	<100	<100	<100
DNV C Cawburn (SE)	10.29	104	104	113	116	110	102	<100	<100	<100

DNV D Hallbankgate (SW)	13.73	<100	108	105	<100	<100	<100	<100	<100	104

Blast Weight	20kg	10kg	2kg	1kg
Level Reduction (re. 100kg)	-5dB	-7dB	-12dB	-14dB

Table 31 - Scaling corrections to aid the heuristic model.

A criticism of the model is that the zero-wind condition is not specific enough, i.e. whether wind has to be absolutely zero, or whether small wind speeds such as 1-2 m/s should be included within this category. The issues introduced by this vagueness is highlighted in Chapter 5 during the preliminary investigations.

3.3.4.5 United States Bureau of Mines Model

An empirical method proposed in Report 8485 by Siskind, Stachura, Stagg, and Kopp (1980) for the United States Bureau of Mines (USBM) model takes account of the surface wind components between source and receiver in the following key equation, for peak sound pressure level in dB.

$$L = K_1 + K_2 \log(w) - 25.6 \log(d) - 1.18V \cos(\theta) \log(\frac{d}{100}) \qquad \textit{Equation 42}$$

The values set for constants K_1 and K_2 are governed by the type of explosive involved, where w is the charge weight in kg. Distance from source to receiver is represented in d and the angle between the surface wind direction and the azimuth between source and receiver is θ.

3.3.4.6 ANSI S2.20 Model

A peak sound pressure level equation is also offered by the ANSI S2.20 (ANSI, 1983) model, which includes some guidance on atmospheric propagation effects. The following steps outline the methodology of the standard, starting with Equation 43 for yield.

$$Y = \frac{W_1}{W_0^{1/3}} \qquad \textit{Equation 43 (ANSI, 1983)}$$

Where $W_0 = 2.1 \times 10^5$ kg TNT or 4.2×10^5 kg for a surface blast or a free-air blast respectively and W_1 is the weight of the explosive.

$$R = \frac{Actual\ Distance}{Y}$$ *Equation 44 (ANSI, 1983)*

$$\Delta P = \frac{A_1}{R_3} + \frac{A_2}{R_2} + \frac{A_3}{R\left(\ln\left\{\left[R/R_0\right] + 3e^{\left[-\frac{\left(R/R_0\right)^{0.5}}{3}\right]}\right\}\right)^{0.5}}$$ *Equation 45 (ANSI, 1983)*

Where $A_1 = 3.18x10^{11}$, $A_2 = 1x10^9$, $A_3 = 9x10^6$ and $R_0 = 445.5(m)$.

Finally,

$$L = 20\log\frac{\Delta P}{2 \times 10^{-5}}$$ *Equation 46 (ANSI, 1983)*

3.3.4.7 Larkhill Prediction Model and Refinement from G. Kerry et al. (1987)

In G. Kerry et al. (1987) are modifications to the equations used in the Larkhill prediction model based on further analysis of original measurements of blasts. The original equations from the Larkhill model, Equation 47, Equation 48 and Equation 49 for the predicted peak sound pressure level from a gelignite explosion is given as:

$$L = K_1 + K_2\log(W) - 25\log(d) + A_1 + A_2$$ *Equation 47 (G. Kerry et al., 1987)*

Where K_1 and K_2 are explosive type dependent constants, with values of 195.4 and 11 respectively for a gelignite explosive. A_1 and A_2 are meteorologically dependent and are found by the following equations:

$$A_1 = 0.5N\log(0.0062d)$$ *Equation 48 (G. Kerry et al., 1987)*

Where N is the weighted ray return density, a term used when sound rays are predicted to return to the surface as a result of a downward refracting atmosphere (enhancement conditions).

$$A_2 = 700G\log(0.0062d)$$ *Equation 49 (G. Kerry et al., 1987)*

Whereas, the equation for A_2 introduces the term G to represent the speed of sound gradient in the lowest 150m of the atmosphere when rays are predicted to be refracted upwards (shadow conditions).

Finally, the refined equations are presented as follows.

$$L = K_1 + K_2 \log(W) - 20 \log(d) - \frac{1.5d}{1000} + A_1 + A_2$$

Equation 50 (G. Kerry et al., 1987)

With *K1* and *K2* refined a K1 = 185.4 and K2 = 10.2, and *A1* and *A2* revised below.

$$A_1 = 0.5N \log(d)$$

Equation 51 (G. Kerry et al., 1987)

With *N* during enhancement conditions now defined as the number of rays returning to the surface with the area defined as d±1000m. For shadow conditions, A_2 to is used as above.

$$A_2 = 20G\sqrt{d}$$

Equation 52 (G. Kerry et al., 1987)

As before, *L,W, d* and *G* are defined in the same way as in the original interpretations.

The modified equations showed favourable results compared to measurements, making it tempting to speculate that the refinement of prediction models based on long-term measurement studies can improve predictions.

3.3.4.8 ISO 9613 and CONCAWE

ISO 9613 parts one (Calculation of the Absorption of Sound by the Atmosphere) and two (General Method of Calculation) are centred primarily on the attenuation of noise as it propagates through the atmosphere. ISO9613-1 and -2 exist as internationally agreed, standardised models. Essentially, the models were prepared for general sound propagation from steady sources (not blast noise), however, it is important to mention as it provides a comprehensive guide to the mechanism of sound absorption and attenuation in the atmosphere. It is technically a heuristic method and works in most locations under the majority of atmospheric and meteorological conditions.

The total sound attenuation A_{total} is defined in Equation 53

$$A_{total} = A_{div} + A_{atm} + A_{gr} + A_{bar} + A_{misc}$$

Equation 53

Where A_{div} is the attenuation due to geometrical divergence (spreading), A_{atm} is the attenuation due to atmospheric absorption, A_{gr} is the attenuation due to ground effects, A_{bar} is the attenuation by a barrier and finally A_{misc} is the attenuation due to any other miscellaneous effects. Before substitution into Equation 53 each of the above are calculated separately based on the techniques used within the standard, and give varying degrees quantitative accuracy at the expense of computational time.

A similar scheme which will not be discussed in length due to its similarity in design and application to the ISO 9613 model is the CONCAWE prediction tool. CONCAWE is essentially empirical but has its roots in sound prediction for the petrochemical industry. It has a somewhat more complex way of accounting for highly variable meteorological conditions and interactions with the ground and other obstacles. It is referred to later in this chapter, where comparisons of it results against benchmark models is discussed within the academic literature.

3.3.5 Other Models

3.3.5.1 Fast Field Program (FFP)

E. Salomons (2001) describes the FFP as a numerical method based on a *layered* atmosphere, where the vertical sound speed profile is discretised into horizontally homogenous layers of equal effective sound speed. Following this, the sound field is computed in the horizontal *wavenumber* domain and finally back in the spatial domain from an inverse Fourier Transfer, thus it is commonly referred to as the Wavenumber Integration method.

Two dimensional, axisymmetric versions were adapted for atmospheric acoustics by (Lee, Bong, Richards, & Raspet, 1986; R. Raspet et al., 1985) which accounted for wind using the effective sound speed. Later developments by (Nijs & Wapenaar, 1990; D. K. Wilson, 1993) allowed 3-D calculations to be possible. However, significant errors within Nijs & Wapenaar's method were highlighted by Richard Raspet, Yao, Franke, and White (1992), who stated that the one-dimensional transform used in Nijs & Wapenaar's method is not justified under certain conditions. Moreover, vertical variations in atmospheric density are not accounted for in the model, although Nijs & Wapenaar acknowledged at the time that the density neglections were the same order of magnitude as the typical adiabatic lapse rates of the temperature. Richard Raspet et al. (1992) offered solutions for a propagation matrix which accounts for pressure and density gradients.

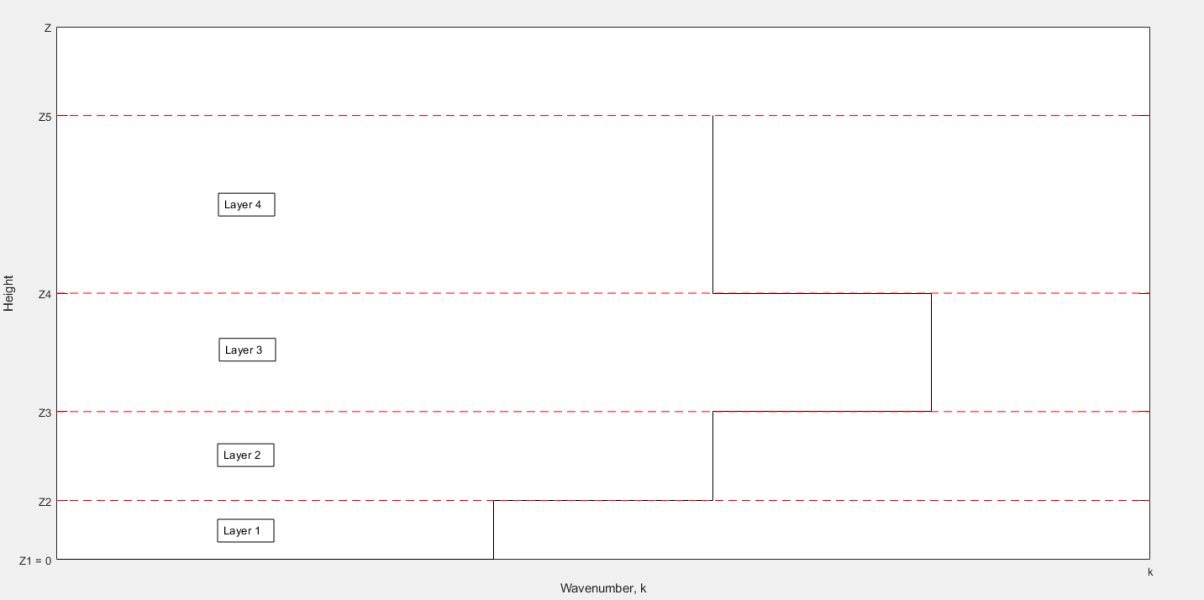

Figure 58 - Visual representation of the discretised atmospheric layers FFP, adapted from (E. Salomons, 2001)

3.3.5.2 Waagan Model

The Waagan model (Waagan, 2014) simulates blast propagation within the MATLAB environment based on sparse linear algebra and an absorption layer of 50 wavelengths. It is an implementation of a PE method, used extensively in studies of blast propagation from test sites in Norway. The layer is truncated above 1500m above the ground and uses a 1/10 wavelength resolution, (Crank, Nicolson, & Hartree, 1947). Varying degrees of complexity have been compared for angle spacings and frequency resolutions: 10°, 5° and 1° and 1/1 octave, 1/3 octave and 1/12 octave band respectively. Additionally, varying heights and ranges have been considered. Though, the accuracy of the model as compared with measurements has been difficult to ascertain, the relative computational speed of the model has objectively been shown to be 20 times faster using a 5° at 1/3 octaves compared to a 1° 1/12 octave band configuration. Also, worth noting is the overall calculation uncertainties are greater than those introduced between the model configurations.

3.3.5.3 HOWARD Model

The Heterogeneous One-Way Approximation for Resolution of Diffraction (HOWARD) model is a prediction method using a one way approximation to solve the homogenous frequency-domain equation (Dagrau, Rénier, Marchiano, & Coulouvrat, 2011). It has been modified to include atmospheric flow, although it remains as a 1-dimensional model. 3-D developments have since been made, which produced promising realisations of non-linear

acoustic propagation (such as that from gunfire) (Luquet, Marchiano, & Coulouvrat, 2014), followed by further developments by Luquet (2016).

3.3.6 Machine Learning Models

Within the last decade, the appearance of statistical learning models has become much more prevalent within the academic literature. Learning models seek to approximate simulated or surrogate data, or experimental observations through the use of training datasets (Hart, Reznicek, Wilson, Pettit, & Nykaza, 2016). These models have solid foundations in geo-physical mapping and appear numerously in the worldwide noise mapping academic community (Baume et al., 2009). Having said that, their application to blast and impulse noise prediction is exiguous. Secondly, the rapid advancement of easily implementable machine learning techniques in conjunction with the growth in data-driven computing, has facilitated the use of neural networks in long-range outdoor sound propagation prediction (Mungiole & Wilson, 2006).

3.3.6.1 Nykaza Geo-statistical Model

With a shift in community noise mitigation research towards a monitoring-based approach, data driven techniques have been developed for interpolating noise levels over large areas (on the order of km). The work of Nykaza's PhD thesis proposes a hybrid geo-statistical based spatial interpolation model, (a geo-acoustic model) for the estimation of single-event noise levels. E. Nykaza (2013) expresses that a shift in noise management methods to more 'data-driven' models is motivated by more readily available and deployable monitoring equipment. Such methods do not suffer from the large input data needed for accurate prediction methods, such as those discussed within the previous chapters.

A geo-statistical model is a type of spatial interpolation model which assumes data is generated by some underlying random process, as opposed to deterministic interpolation methods. The main advantage of geostatistical models is that they provide estimates of the variance of a variable of interest (VOI), such as the sound pressure level (SPL), whereas deterministic models only provide information on the VOI.

Nykaza's model estimates the SPL and variance from CNPE simulated datasets of blast noise over grassland, evaluated for a series of meteorological conditions and atmospheric

stabilities, with a range of wind directions. The dependence of the model accuracy on and sensor densities, is explored, for realistic noise monitor densities, from 3-49 monitors over a 64km^2 grid. This is achieved by sampling the CNPE model output with many combinations of monitor densities and geometries over the whole range of interest (ROI).

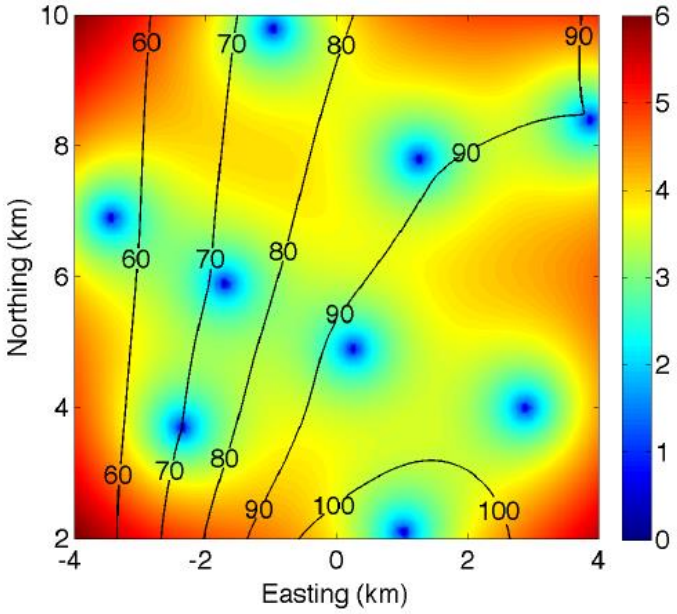

Figure 59 - An example of a geo-acoustic interpolation map, from (E. Nykaza, 2013). A SPL uncertainty (2σ) map overlaid with SPL contours for a 9-monitor sampling configuration located across the ROI.

Spatial interpolation methods have been used for steady sound propagation predictions, though they are few, and only some have provided estimates of the accuracy in sound pressure level which occur from the mechanisms described in the previous review chapters, also with a much smaller ROI (~0.1km^2) (Baume et al., 2009). The performance of Nykaza's geo-acoustical model is evaluated against other spatial interpolation models, in terms of root mean square error (RMSE), mean bias error, and a metric which combines both the SPL and variance.

The worst-case RMSE in SPL from the model was 3dB for the case of 5 monitoring locations in what was considered the worst meteorological conditions (weakly stable, crosswind), for a given type of model (5 Parameter model). A thorough description of the model configurations is given in (E. Nykaza, 2013).

3.3.6.2 Artificial Neural Networks

In the last decade, increasing attention has been given towards artificial neural networks (ANN) for their ability to solve complex classification and prediction problems in acoustics.

In particular, is the number of studies published on the application of deep neural network (DNN) models, a type of ANN, and other similar machine learning models, for the prediction of adverse environmental effects from mine blasting.

Review of Neural Networks for Blast Impact Prediction

A paper by Ozer, Karadogan, Ozyurt, Sertabipoglu, and Sahinoglu (2020) provides a comprehensive summary of the history of neural network (NN) use for blast effect prediction, as well as a significant contribution by an extended NN model which will be discussed later. Firstly however, Ozer et al. (2020) refer to early methods of predicting overpressure from explosives using the Support Vector Machine (SVM) approach (Khandelwal & Kankar, 2011), and with non-linear codes (Hasanipanah, Jahed Armaghani, Khamesi, Bakhshandeh Amnieh, & Ghoraba, 2016; Keshtegar, Hasanipanah, Bakhshayeshi, & Esfandi Sarafraz, 2019). Genetic algorithms (GA) have been used on datasets of airblast overpressure for prediction (Amiri, Bakhshandeh Amnieh, Hasanipanah, & Mohammad Khanli, 2016; Jahed Armaghani, Hajihassani, Marto, Shirani Faradonbeh, & Mohamad, 2015). Gaopale, Rodrigo Jr, and Itumeleng (2019) developed ANN prediction models for the prediction of air overpressure.

Other work with NN models has equally focused on ground vibration from blasting, in particular from mining which generates significantly more ground vibration due to it nature, compared to the blasts involved in most major hazards testing and military application. Kuzu, Fisne, and Ercelebi (2009) developed ANN prediction models of ground vibration from blasting, and more recently, Nguyen et al. (2021), developed nature inspired optimisation algorithms for the prediction of blast induced ground vibration. Combined air overpressure and ground vibration prediction has been attempted with neuro-fuzzy techniques (Jahed Armaghani, Hajihassani, Sohaei, et al., 2015).

While there are a significant number of different neural network techniques as described in the previous paragraphs, at the core of ANN models in their application towards predicting the effects of blasting are large datasets from particular study sites. When coupled with a NN model, patterns in the data can be found and correlations between propagation parameters with the desired prediction metric (i.e air overpressure, ground vibration) can be made. Where most of the published work relates to mine blasting, many of the model input variables are related to the source term of the explosive, and moreover are controllable variables. Explosive charge weight, hole depth, maximum charge delay are just a few of these variables

but there are many more. The uncontrollable variables are intrinsically related to the propagation component of the source-path-receiver model, such as meteorological properties, though simpler physical parameters are used in the NN models such as wind direction and air temperature, as opposed to more comprehensive descriptions of the ABL, as discussed in Section 3.2.

Structure and Types of Artificial Neural Networks

The structure of an ANN is shown in Figure 60 which is taken directly from Nguyen and Bui (2018), listing the input variables used in the model. To the right of the input layer, is the hidden layer, which there were more than one of in each of their models, and finally the output layer which gives the output variable prediction, in this case air overpressure (AOp).

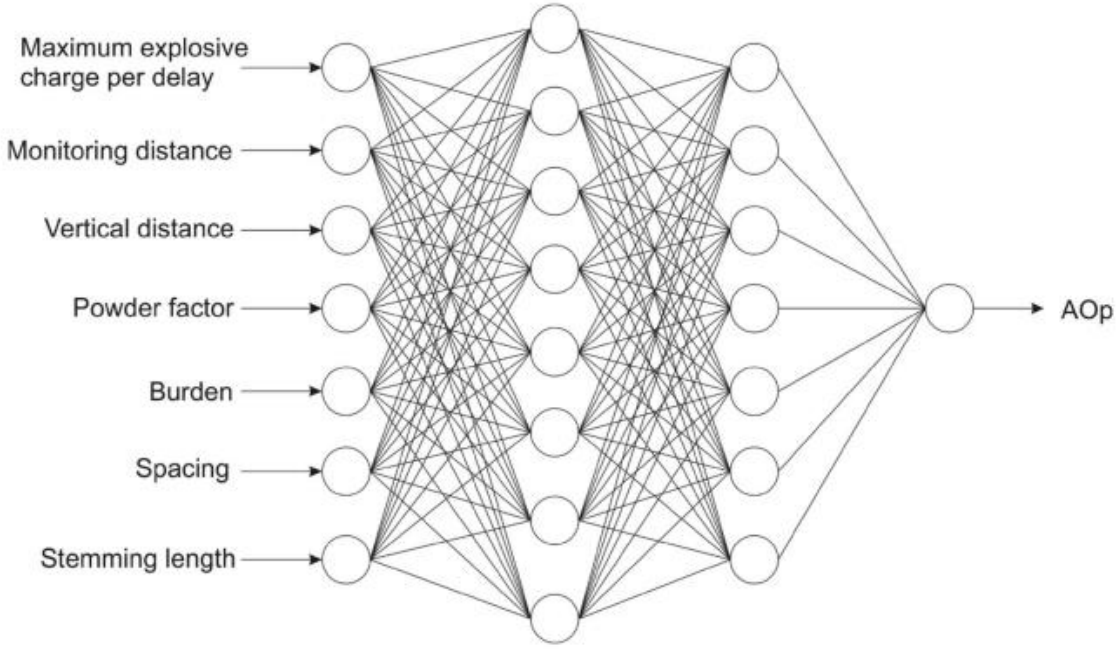

Figure 60 - Structure of ANN, taken directly Nguyen and Bui (2018) from paper, with the input variables listed on the left representing the input layer.

Common in machine learning is the technique of splitting a dataset into two parts; the training and testing sets, which usually comprise of 80% and 20% of the data respectively. Nguyen and Bui (2018) used this split and selected the samples at random. The results of each model in terms of their predictive power are shown in Table 32. The numbers in the title of the ANN models represent its structure according to the number of neurons in each layer, with the first representing the input layer (number of variables into the model, which was 7 in this case), followed by 3 numbers representing the number of neurons in each hidden layer, and the final layer being just 1 neuron, as there was just 1 output (air overpressure).

The number of layers and neurons in each layer required for a specific problem is difficult to determine exactly in advance. Generally, the greater the number of hidden layers and neurons in the hidden layers, the greater the training time, and problems such as overfitting can arise. In machine learning, overfitting refers to the problem of the model learning patterns in the training data too well, where noise and random fluctuations in the training data are modelled accurately by the model. On the other hand, underfitting can arise from not enough neurons or hidden layers, and a NN cannot model the training data, nor generalise when presented with new data.

Methodology for ANN prediction of Blast Effects

In general, across the scientific literature of this field, a particular "blast-effect generating" study area is chosen, usually a mine, and monitoring stations are deployed to gather measurements of air overpressure or ground vibration. In the case of Ozer et al. (2020), 74 monitoring stations positioned in all directions around an excavation site in Istanbul captured 158 blasting shots under a variety of atmospheric conditions. The source-receiver distances in their study were much less (up to 150m), than those considered in the typical predictions of blast noise (several km). Nguyen and Bui (2018) made just 117 observations of blasting, with over 100 monitoring stations though at longer distances (hundreds of metres), with much larger explosive yields.

Although the exact number and details of measurements vary across each study, the general principal is to surround a blast source with hundreds of monitors at close range and gather data to build and train the ANN. Usually, some metric relating to the charge weight is recorded, along with many other variables intrinsic to the source if they are mine blasts. The atmospheric effects (typically wind direction, velocity and temperature etc.) are recorded, along with the source-receiver distances. A significant proportion of this usually randomised dataset (80-90%) is given to an ANN for training, whereas the remaining data is used for testing.

Assessment of DNN models

While the number of ANNs and associated machine learning models for the prediction of environmental effects from blasting is large, and the applications are wide-ranging, Nguyen and Bui (2020) offer a comprehensive analysis of the performance of different ML techniques. While their conclusions are limited to their analysis, because it is not inclusive of the performance of models developed by other research groups at other sites, it is a

significant contribution to the literature in this field, where a number of different techniques have been trained on a large dataset of blast induced overpressure. Nguyen and Bui (2020) compared the performance of models that learned correlations between measured air overpressure and wind speed, direction and relative humidity, The following performance metrics were used to evaluate the prediction capability of various ML models.

- Root Mean Square Error (RMSE)
- Determination Coefficient (R^2)

The RMS error is defined is a common metric for describing the performance of prediction models and is defined below.

$$RMSE = \sqrt{\frac{1}{n}\sum_{i=1}^{n}(y_i - \hat{y}_i)^2} \qquad \text{Equation 54}$$

Where Y_i and $\hat{y}$ are the predicted and measured outputs respectively, over the total number of data n. The RMSE is a valuable metric as it is a metric which describes the distribution of prediction errors and has been used for comparing the performance of heuristic prediction models in Section 3.3.4. The determination coefficient, R^2 (sometimes written as r^2), is numbered between 0 and 1 and provides an idea of how well a particular model fits the data that is presented to it (with 1 being a perfect fit), defined below, with $\bar{y}$ being the mean of the y_i values.

$$R^2 = 1 - \frac{\sum_i \left(y_{,i} - \hat{y}\right)^2}{\sum_i (y - \bar{y})^2} \qquad \text{Equation 55}$$

Other metrics are sometimes used in particular studies such as the Mean Absolute Error (MAE) which measures the average size of the errors between measured and predicted data.

Performance of ANN models

Nguyen and Bui (2020) found that a Boosted Smoothing Spline combined with a Genetic Algorithm (GA-BSTM) yielded the highest prediction accuracy. In an earlier study, Nguyen and Bui (2018) compared many prediction models for the prediction of air overpressure from mine blasting against the USBM empirical model for 113 recorded blast events from mining operations at the Nui Beo open-pit coal mine in Vietnam. The models included in their analysis are listed in Table 32, but essentially contain 5 variants of ANN with different

compositions and numbers of hidden layers, the empirical version of USBM adjusted for their specific site, a random forest (RF) model, and a hybrid ANN-RF model. Interestingly, no meteorological variables were considered in the formation of their ANNs and only, the monitoring distance and vertical distance are considered true variables of the propagation path, whereas all others listed are factors affecting the source.

Table 32 - individual performance of models during on testing data.

Model	RMSE	R2
Empirical	5.704	0.429
ANN 7-4-5-16-1	1.469	0.942
ANN 7-3-11-20-1	1.405	0.945
ANN 7-18-9-20-1	1.184	0.960
ANN 7-19-6-20-1	1.094	0.966
ANN 7-16-8-19-1	1.339	0.953
RF	1.550	0.939
ANN-RF	0.847	0.985

Figure 61 - Individual performance of empirical and ANN models during testing for the dataset collected by Nguyen and Bui (2018).

Nguyen and Bui concluded that ANNs are superior for their predictive power than empirical models in this particular case of air overpressure from blasting, with the best ANN achieving and R^2 of 0.967, but conclude that determining the correct number of layers and specific structure is difficult. By combination with a RF model (ANN-RF Hybrid), a R^2 of 0.985 is achieved in terms of predictive power when faced with testing data, with the testing data being just 80% of a total of 113 measured observations. The details of each model including the random forest model can be found in their paper.

The study of optimised deep neural networks of Nguyen et al. (2021) for the prediction of ground vibration found that a DNN coupled with nature inspired optimisation techniques outperformed standard DNNs. In particular, their Harris-Hawk optimisation algorithm coupled to a DNN achieved an RMSE of 1.537 and R2 of 0.93 when trained on a dataset of 183 ground vibration measurements with at 200-300m with around 100 measurement positions.

While many of these ANNs achieve significantly lower prediction errors than those considered typically in blast noise impact assessment, they are limited to particular study sites

which monitored blasts at much closer range. The propagation uncertainties at the shorter distances are significantly lower than those considered in classical long-range outdoor sound propagation, and therefore it is yet unclear how a similar model would perform for the monitoring distances considered at Spadeadam.

Nonetheless, ANNs can determine complex relationships between multiple input variables and some output variables, despite only capturing a small dataset, making them an attractive alternative model for predicting environmental impacts from blasts.

3.3.6.3 Summary of Learning Models

On the whole, research concerning the use of statistical learning models in outdoor blast noise prediction is promising. In spite of Nykaza's geo-acoustic model, and the NN models discussed by Hart et al. (2016) showing very low errors compared with the numerical CNPE predictions for such large quantities of propagation realisations, propagation conditions were still limited to flat-terrain. Furthermore, range-dependent impedance was not present in Nykaza's simulated dataset, due to the sheer scale of the ROI. Nykaza's work also only accounted for the sound pressure level of simulated noise events, where no frequency information was present. The improvement of surrogate and training datasets is acknowledged in both of the aforementioned studies as further work.

Deep neural networks developed from mining data are popular and can achieve significantly lower prediction errors and high coefficients of determination, they are limited to particular study sites and to relatively short distances.

3.3.7 Prediction Models Summary

Common to all numerical prediction models is the need for vast quantities of input data. The scale of such quantities of data soon expands exponentially with distance from a detonation point, as the time-varying meteorological, ground and topographical parameters which effect sound propagation becomes so variable. Furthermore, the transience of a blast event requires such detail of the propagation medium, so innately stochastic, such that the uncertainties presented by even the state-of-the-art measurement and prediction tools result in wildly varying noise impacts for seemingly identical atmospheric states by an observer.

The requirements for the mere calculation of atmospheric refraction place a model significantly beyond the allowable time frame of a prediction.

E. Salomons, Van Maercke, Defrance, and de Roo (2011) summarise the capabilities and limitations of many of the propagation models discussed, as a guide to determining the most appropriate method for the prediction of blast noise over the range of interest relevant to Spadeadam.

The method of refining prediction models by measurement (heuristic methods) such as those developed by Kerry et al. are shown to be preferrable. RMS prediction errors for the aforementioned heuristic methods and the original Larkhill model have been compared by G. Kerry et al. (1987) and are shown in Table 33.

	Source-Receiver Distance (km)						
	0-2	2 - 4	4 - 6	6 - 8	8 - 10	10 - 12	>12
No. of Measurements	138	105	61	58	30	17	6
Prediction Method	**RMS Error (dB)**						
Original Larkhill	5.8	5.4	9.1	10.1	10.6	14.6	9.0
Modified Larkhill	4.8	5.6	5.8	5.7	5.6	13.3	8.8
SSW	4.6	5.0	5.3	5.9	2.7	3.1	3.9
USBM	3.7	8.9	13.9	15.1	9.3	9.0	16.6
ANSI S2.20	5.6	10.7	10.2	11.4	11.6	14.8	8.6

Table 33 - Summary of G. Kerry et al. (1987) RMS prediction errors for different source-receiver distances at Larkhill for the data collected on day 4 of their experimental trial.

Characteristic	Engineering Models		Hybrid Models						
			Approximate semi-analytical	Numerical					
	ISO 9613	SSW	Ray Tracing	FFP	CNPE	GFPE	MAPE	GTPE	MONET
Computing time	Fast	Fast	Fast	Slow	Slow	Medium	Slow	Slow	Slow
Accuracy	Poor	Variable	Medium	Exact	Very good	Good	Good	Good	Medium
Ideal frequency range	63-8000Hz	Low	High	Low	Low	Low and mid	Low and mid	Low and mid	40Hz
Range-dependent conditions	No	Yes	No	No	Yes	Yes	Yes	Yes	No
Shadows and caustics	No	N/A	No	Yes	N/A	N/A	N/A	N/A	Yes
Elevated sources	No	N/A	Yes	Yes	~	~	~	Yes	N/A

Table 34 - Summary of prediction model capabilities and limitations, adapted from (E. Salomons et al., 2011).

A ‘look-up’ table for Spadeadam has been generated by a University of Salford MSc research dissertation (Lacy, 2017), for the aim of calibrating atmospheric conditions using a small explosive (1kg) before scaling up in charge weight to the desired test charge weight TNT equivalence. Table 35 gives peak sound pressure level increase with charge weight, based on known relationships originally established by (Baker, 1973). These are the minimum differences in suggested relative increases in peak level and should hold assuming that meteorological conditions do not change significantly.

Charge Weight	Peak Level (re. 100dB)	Level increase (re. 1kg)
1kg	100dB	N/A
2kg	102dB	2dB
10kg	107dB	7dB
20kg	109dB	9dB
100kg	114dB	14dB

Table 35 - Blast weight approximate relationships

The hypothesis of blast scaling via atmospheric calibration was further investigated by comparing predictions of blasts using the known relationships of Table 35 in conjunction with downwind enhancements and upwind attenuation, logarithmically corrected symmetrically around a reference measurement. Table 36 gives approximate peak sound pressure levels for various locations around Spadeadam under a range of wind directions.

		Peak Sound Pressure Level (dB)								
		No Wind	Wind Direction							
Location (respect to site)	Distance (km)	0	N	NW	W	SW	S	SE	E	NE
Wiley Sike (SE)	2.45	124	129	132	130	122	112	112	114	120
Butterburn (NE)	5.04	108	<100	100	110	118	110	102	<100	<100
Gilsland (S)	6.31	112	124	122	112	106	100	102	112	119
Bewcastle	8.73	108	<100	<100	<100	<100	102	<100	<100	<100

(NW)										
Cawburn (SE)	10.29	104	104	113	116	110	102	<100	<100	<100
Hallbankgate (SW)	13.73	<100	108	105	<100	<100	<100	<100	<100	104

Table 36 - 100kg Blast Level Heuristic Look-up Table for raw wind direction (not vector) (Lacy, 2017).

Lacy went on to compare predictions using the tools from this heuristic model against predictions made by a range of prediction models, against measurements of other blasts at Spadeadam under a range of meteorological conditions. For that limited range of conditions and blasts, the heuristic model performed at least as well as MONET, with errors of 8.4dB between predicted and measured Peak SPL for the heuristic model. ISO 9613 and Larkhill Simplified Model (LSM) performed particularly badly against the heuristic model, with errors of up to around 33dB and 21dB respectively. Finally, the SSW heuristic model was highly accurate in some cases, but also had errors greater than 23dB against measurements.

Prediction Model	**Minimum Error (dB)**	**Maximum Error (dB)**
Heuristic Model (with wind)	-1.5	8.4
SSW	-0.7	>23.0
MONET	3.7	21.0
LSM[1]	7.9	20.8
ISO 9613	17.5	32.5

Table 37 - Range of deviations in predicted Peak SPL against measured SPL from various prediction models for a range of blast and propagation conditions at Spadeadam (Lacy, 2017).

[1] The LSM model has approximate errors, due the fact that this model gives predictions of 130dB and 120dB distances from the sources, meaning that there is a slight mismatch between these distances and the respective measurement points at which the errors are evaluated

3.4 Legislative Guidance and Best-Practice on the Management of Community Noise Impacts

Overview The purpose of this chapter is to present the relevant legislation on environmental noise and vibration limits relevant to the operations carried out at DNV Spadeadam, in addition to the guidance on the measurement of impulsive sound at sensitive receptors. The chapter concludes with a review of the literature on human response to environmental impulse noise. The chapter draws from literature on a number of fields related to environmental noise, such as weapons noise and sonic booms.

3.4.1 Legislation and Guidance on Environmental Blast Noise and Vibration

3.4.1.1 Background

This chapter presents the legislation and guidance on environmental blast noise impacts relevant to the testing carried out at DNV Spadeadam.

Much of the legislation around impulsive noise is naturally related to the context of military training, testing and firing. However, military policy is still relevant to the activity carried out at DNV Spadeadam, which is situated within the large MOD range, RAF Spadeadam, but it not operated or related to the MOD. However, some work carried out at DNV Spadeadam has military context. A series of reports carried out by Southdowns Environmental Consultants (2016) on behalf of Qinetiq LTD on the assessment of potential building damage effects from range activities at both MOD Shoeburyness and Pendine. These reports contain an extensive literature review of current policy, legislation and guidance related to the impacts of environmental impulsive noise, upon which this literature review is built upon.

In the UK, the MOD has a duty of care to protect members of the public from the impacts of noise and vibration generated from their training activities, whilst maintaining the required standard of testing, evaluation and training support in the interests of national security. MOD policy is contained within the MOD Corporate Environmental Protection Manual (*Leaflet 4.1 Environmental Noise*, 2010) on the legal obligations and mitigations required for managing environmental noise. In (*Leaflet 4.1 Environmental Noise*, 2010) it is stated that the effects of environmental noise are to be mitigated as far as is reasonably practicable, whilst achieving

operational imperatives. It also mentions, the reduction of disturbance to local communities including residential areas. Further, the MOD 'considers itself bound by the noise provision of the *Environmental Protection Act Part III* 1990) (EPA) regarding its application to everyday activities.

EPA 1990 Part III contains a class of statutory nuisances that local authorities can demand remedial action upon over waste management and the control of emissions into the environment. However, the MOD has exemption from such statutory nuisance when they concern activities directly related to national security. With relevance to DNV Spadeadam, some blast testing work is directly related to MOD operations and is considered essential in the interests of national security and for the protection of national infrastructure.

Under such circumstances, this does not allow DNV Spadeadam to operate without a duty of care to its local residents and should follow MOD policy under such circumstances which is, 'to reduce and where possible avoid, or minimise at best, the causes and effects of statutory nuisance and to comply with all relevant UK environmental legislation' ("Leaflet 4 Statutory Nuisance," 2010).

Regarding the research on the physical effects of blast on residential properties, much of the work has been done throughout the 20th century by the United States Bureau of Mines (USBM). The USBM conducted scientific research relating to blasts carried out under the context of mining and mineral extraction.

Detailed research carried out in the 1970's into structure response and damage from the air overpressure and vibration effects of blasting. 'Safe' damage criteria thresholds were developed through extensive scientific research, combined with reviews of the then current literature on sonic boom effects from overland supersonic flight.

The USBM empirical methods for the estimation of air overpressure from blasting have been reviewed in section 3.3 of this chapter.

3.4.1.2 HSE CBI EIG Guidance for the Safe Disposal of Explosives

The HSE/CBI EIG Guidance for the Safe Management of the Disposal of Explosives (CBI, Group, & Executive, 2020) quotes a distance of 215 $W^{1/3}$, where W is the charge weight, to an impulsive noise level of 140 dB (unweighted) which is the exposure limit which must not be exceeded according to the Control of Noise at Work Regulations 2005 (CoNAWR) ("The Control of Noise at Work Regulations," 2005), though the level quoted in that legislation is

C-weighted. As an example, for a 1000 kg charge on Pad C, gives $215W^{1/3}$ gives a distance of 2150 m which covers a large part of the DNV Spadeadam site but also some RAF installations and roads. The RAF Installations include Berry Hill (~1800 m), Grey Mare (~1200 m), and R7 (~1600 m) with all distances quoted from Pad C. Under such a circumstance, liaison with RAF would be made to ensure that personnel are excluded from within the 2150 m radius or should be undercover in a suitable building when the test is carried out. If personnel have to be outside the 2150 m radius, they should still be provided with suitable hearing protection.

It is also recommended that traffic on the RAF roads within the 2150 m radius should be stopped while the test is fired to avoid the risk of drivers having accidents because they are distracted by sudden noise. The 2150 m radius is based on neutral weather conditions and can be reduced or increased by local weather conditions. For this reason, the area including the primary RAF buildings at the entrance to the site which lies outside the 140 dB zone, should be included as though within, requiring personnel in the area to be indoors for the duration of such a large test.

Figure 62 - 140dB overpressure radius from a 1000kg test on Pad C, a radius of ~2150m during neutral propagation conditions.

Another important consideration is Middle Shield Farm, the closest non-DNV or RAF residential building, which is technically outside of the RAF site boundary but sits within the 140 dB radius for a 1000 kg explosion trial under neutral propagation conditions. This is a residential building and steps should be taken here to notify the residents that they should be located inside the building during a trial.

3.4.1.3 BS 5228-1:2009 Code of Practice for noise and vibration control on construction and open sites – Part 1 Noise

Although not directly covering blast noise, BS 5228-1 (Institution, 2009) provides guidance on noise related to industrial activities, particularly for impulsive noise associated with piling which has some relevance to this study.

Clause 8.6.9 of the standard provides some guidance on blasting. A good relationship between the operator and the community is suggested, and local residents should be given notice of the test program with specific blasting times, along with updates should there be any deviation from the program. BS5228 points to other policy on blast noise, including, MPG 9 on noise, blasting and vibration limits, and the National Planning Policy Framework (NPPF) on noise limits for general minerals extraction and production.

An important note is that this standard still acknowledges the research by Siskind (Siskind et al., 1980), which showed that structural damage would not be expected at levels below 180 dB (lin), most windows cracking at around 170 dB (lin) and prestressed and poorly mounted windows cracking at 150dB (lin).

BS 5228-1 acknowledges that there is no accepted practice to set limits for air overpressure due to the large uncertainties in meteorological conditions which influence propagation and thus local air overpressure and that measures should be taken to mitigate noise generation at the source.

Other BSi guidance, such as BS6472-2: 2008 (Institution, 2008), Guide to evaluation of human exposure to vibration in buildings , references the USBM research in the context of damage criteria for structures. Also applicable to DNV Spadeadam are BS ISO 4866 (2010) (Standardization, 2010) and BS 7385 Part 2 (Institution, 1993).

3.4.1.4 Summary of Physical Effects and Quantities from the Legislation and Guidance

The physical effects from blasting have been summarised within Southdowns Environmental Consultant's extensive review of the scientific literature (Southdowns Environmental Consultants, 2016) and are included in Where *v* is the peak vibration in mms-1, *Q* the charge mass in kg, and *D* the distance in m and *k* and *e* are constant and exponents associated with the site. The absence of measured site constants for ground-borne vibration propagation at Spadeadam means the estimates can only be made using empirical relationships derived at other locations such as those in (R. Kumar, 2016). Given the large variability of the local geology around Spadeadam, considerable uncertainties are expected when using these basic laws.

With regards to ground-bourne vibration, all charges carried out at the Spadeadam site considered within this thesis are raised above ground level or resting on the ground. As they are not buried, the connection between the blast wave and the ground is weak so there is little potential for significant vibration. In 2003 measurements of ground shock were carried out at about 3.5 km from the Spadeadam Site for a 100 kg TNT equivalent charge. The recorded ground shock gave a peak velocity of 0.25 mms-1 (Advantica, 2003). This is significantly lower than the threshold for cosmetic damage to residential buildings 15 mms-1 according to BS7385 (Institution, 1993) or the acceptable magnitude for the exposure of people of 6 mms-1.

Potential noise levels are predicted using the Met Office's MONET model and the data generated is used to schedule noise generating tests. The criteria used to assess noise impact prior to testing is that residents outside of the boundary of the RAF Spadeadam Site should not be exposed to impulsive noise levels in excess of 125 dB (linear) but this is not always achievable. The HSE/CBI EIG The Use of Structural Justification to Underpin an HSE/ONR Explosives Licence (EIG, 2017) states:

- Explosive Test Facilities
    - Explosive test facilities where intentional firings are conducted must provide higher protection (than that at Class D distance) to people from fragments and debris and not subject them to peak sound pressure (noise) in excess of 135 dB(C) (equivalent to 0.112 kPa) without hearing protection (with an absolute limit of 140 dB(C)).

Note, that the guidance here refers to a C-Weighted peak sound pressure level which accounts for human response to loud impulsive sounds, and is consistent with the national occupational noise guidelines, the CoNAWR ("The Control of Noise at Work Regulations," 2005). This differs to the linear weighting (Z-Weighting) used within most prediction schemes including MONET.

Table 38 and Table 39.

Vibration effects such as those shown in Table 39 are currently not considered within DNV Spadeadam's acoustic assessment for blast testing or within this thesis. Some basic laws can be used based on scaled distance laws to predict ground-bourne vibration from blasting, such as the Langefors Formula or the more commonly used square root scaled distance formula, found within (Siskind et al., 1980)

$$v = k\left(\frac{D}{\sqrt{Q}}\right)^{-e}$$

Where v is the peak vibration in mms^{-1}, Q the charge mass in kg, and D the distance in m and k and e are constant and exponents associated with the site. The absence of measured site constants for ground-borne vibration propagation at Spadeadam means the estimates can only be made using empirical relationships derived at other locations such as those in (R. Kumar, 2016). Given the large variability of the local geology around Spadeadam, considerable uncertainties are expected when using these basic laws.

With regards to ground-bourne vibration, all charges carried out at the Spadeadam site considered within this thesis are raised above ground level or resting on the ground. As they are not buried, the connection between the blast wave and the ground is weak so there is little potential for significant vibration. In 2003 measurements of ground shock were carried out at about 3.5 km from the Spadeadam Site for a 100 kg TNT equivalent charge. The recorded ground shock gave a peak velocity of 0.25 mms^{-1} (Advantica, 2003). This is significantly lower than the threshold for cosmetic damage to residential buildings 15 mms^{-1} according to BS7385 (Institution, 1993) or the acceptable magnitude for the exposure of people of 6 mms^{-1}.

Potential noise levels are predicted using the Met Office's MONET model and the data generated is used to schedule noise generating tests. The criteria used to assess noise impact prior to testing is that residents outside of the boundary of the RAF Spadeadam Site should

not be exposed to impulsive noise levels in excess of 125 dB (linear) but this is not always achievable. The HSE/CBI EIG The Use of Structural Justification to Underpin an HSE/ONR Explosives Licence (EIG, 2017) states:

- Explosive Test Facilities
    - Explosive test facilities where intentional firings are conducted must provide higher protection (than that at Class D distance) to people from fragments and debris and not subject them to peak sound pressure (noise) in excess of 135 dB(C) (equivalent to 0.112 kPa) without hearing protection (with an absolute limit of 140 dB(C)).

Note, that the guidance here refers to a C-Weighted peak sound pressure level which accounts for human response to loud impulsive sounds, and is consistent with the national occupational noise guidelines, the CoNAWR ("The Control of Noise at Work Regulations," 2005). This differs to the linear weighting (Z-Weighting) used within most prediction schemes including MONET.

Table 38 – Air overpressure effects, adapted from (Southdowns Environmental Consultants, 2016).

Level (dB lin)	**Effect**	**Source**
180	Onset of structural damage	BS 6472, BS 5228
171	General window breakage	USBM
170	Most windows crack	BS 6472, BS 5228
160	Cracking of pre-stressed or poorly mounted windows	BS 6472, BS 5228
152	Some window breakage	BS 6472, BS 5228
150	Pre-Stressed or poorly mounted windows may crack	USBM
140	Reasonable threshold to prevent glass and plaster damage	USBM
134	USBM ‘Safe’ Maximum (0.1 Hz high pass)	USBM

133	USBM Maximum Recommended Level (2.0 Hz high pass)	USBM
129	USBM Maximum Recommended Level (5.0 or 6.0 Hz high pass)	USBM
120	Secondary vibration effects including rattling windows and objects	BS 6472, BS 5228, USBM
<120	No material effects	-
105 dB (C, Slow)	USBM Maximum Recommended Level	USBM

Table 39 - Vibration effects, adapted from (Southdowns Environmental Consultants, 2016)

Level	**Effect**	**Source**
50 mms^{-1}	Produce structural damage to residential type structures	USBM
50 mms^{-1} at 40 Hz	Guide value to prevent cosmetic damage to property	BS 7385
15-20 mms^{-1} at 4 Hz and 15 Hz	Guide value to prevent cosmetic damage to property	BS 7385
12.7 mms^{-1}	Outset of cosmetic damage (USBM recommended for such relatively unusual vibration)	USBM

The HSE/CBI EIG Guidance for the Safe Management of the Disposal of Explosives in Table F6.3 of the document gives recommended distances to persons in the open or in buildings and this is reproduced as Table 40 and Table 41.

Based on Table 40, the distances in column 2, for persons in the open, are based on $215W^{1/3}$, i.e. a noise level of 140 dB. Whereas the distances in column 6 for off-site buildings are based on $312W^{1/3}$, which equates to a noise level of about 136 dB (Douglas, 1987). Applying $312W^{1/3}$ to a 1000 kg charge would give a minimum recommended distance of 3120 m.

The calculated distances to $215W^{1/3}$ (140 dB) and 312 $W^{1/3}$ (136 dB) for the range of explosive tests that have been conducted on the DNV Spadeadam site and the proposed 1000 kg test are given in Table 42. Again, it should be noted that these distances are based on neutral weather conditions and can be increased or reduced by the local weather conditions.

Although the off-site blast loadings are very low there is always a finite probability of structural damage occurring due to poorly constructed buildings, badly made glazing systems etc. Siskind et al. (1980) suggest that there is a low probability of structural damage at pressure levels less than 140 dB (0.2 kPa). Glazing is the most likely structural component to fail and figure 40 in Siskind et al. (1980) suggests that for normal glazing the probability of a window breaking at 140 dB is less than 10^{-5}. It should be noted that the data that this is based on is from the 1960s and modern glazing systems are likely to be significantly more robust.

Table 40 - Distances for people from Table F6.3 From Guidance for the Safe Disposal of Explosives (CBI et al., 2020)

	Persons in open either on or off site		
Weight of Explosive (kg TNT)	Persons in open where blast effect is expected (m)	Persons in open where blast effect is possible but not expected(m)	Persons in open where blast effect is possible but unlikely (m)
0.1	-	-	-
0.5	-	-	-
1	215	48	31
2	271	62	38
5	368	84	52
10	463	108	65
20	584	134	82
50	792	183	111
100	998	230	140

Table 41 - Distances for buildings from Table F6.3 From Guidance for the Safe Disposal of Explosives (CBI et al., 2020)

	Buildings On-Site	Buildings Off-Site		
Weight of Explosive (kg TNT)	Buildings in the occupation of person	Buildings not in the occupation of person	Buildings not in the occupation of person	Buildings not in the occupation of person

	conducting the disposal operations (m)	conducting the disposal operations where blast effect is expected (m)	conducting the disposal operations where blast effect is possible but not expected (m)	conducting the disposal operations where blast effect is possible but unlikely (m)
0.1	-	143	61	53
0.5	-	245	105	91
1	24	310	132	114
2	34	390	167	143
5	58	530	227	194
10	91	670	285	245
20	138	850	360	309
50	225	1150	486	419
100	300	1450	615	528

Table 42 - Calculated distances to $215W^{1/3}$ (140 dB) and $312W^{1/3}$ (136 dB)

Charge Weight (kg TNT)	$215W^{1/3}$ (m) [140 dB]	$312W^{1/3}$ (m) [136 dB]
100	998	1450
500	1706	2476
640	1853	2689
1000	2150	3120

3.4.1.5 Other Guidance

According to the US Defence Technical Information Center's (DTIC) central resource for DoD and government-funded scientific, technical and engineering research, the Strategic Environmental Research Development Program (SERDP) and the Environmental Security Technology Certification Program (ESTCP) are developing the next generation of tools and technologies for blast noise management. Such tools aim to predict, monitor, assess impacts and reduce the level and impact of military noise. Furthermore, the Office of Explosives and

Blasting (OEB) sets guidance and enforces law of surface mine blasting which is designed to protect the public and their property.

3.4.2 Quantification of Community Response to Impulsive Noise

The ultimate purpose of this research project was to provide DNV Spadeadam with a new robust and cost-effective noise management strategy. By extending the work completed previously at Spadeadam, the deployment of the Live Monitoring Network (LMN) was to aid in providing the control room at DNV with effective real-time feedback noise levels for a given blast. From the real-time noise level, the expected exposure at a receiver when scaling up a test can be derived from heuristic rules related to the site. Thus, the combined system aims to estimate receiver noise level more accurately for real-time propagation conditions compared to estimations made by the current noise prediction tool, MONET.

The success of the system is completely dependent upon the reporting of objective sound levels which correlate with the risk of noise complaints from distant receivers. Many acoustic metrics may be used to describe the temporal variations of noise at a receiver, hence the need to determine which metric is the most likely indicator of complaints. This is due to the nature of how people respond differently to different noise events. The following discussion aims to critically analyse the use of noise metrics related to blasts within the scientific literature and to extract the noise metric most likely to correlate with complaints.

3.4.2.1 Objective Assessment of Environmental Noise Impact

Historically, the impact of anthropogenic noise has been determined by objective assessment methods (Birgitta Berglund, Lindvall, Schwela, World Health Organization, & Environmental Health, 1999). Many objective acoustic metrics exist to encapsulate the plethora of both man-made and natural sound sources, so that they may be categorised and evaluated based on the physical measurements of their respective sound energy. The noise impact of a sound source on a receiver is universally rated by the degree to which it exceeds predefined acceptable quantities of specific objective acoustic metrics. For example, a given level of noise at a receiver from a sound source may exceed what is thought to be an acceptable threshold, and the extent to which a threshold is exceeded indicates the magnitude of the impact of the noise sources on the receiver. Generally, when thresholds are exceeded, noise impacts are negative. Many factors influence the acceptable criteria, such as the type of noise event and the background noise.

3.4.2.2 Objective Environmental Noise Metrics

Metrics are a concise numerical description of a physical phenomenon or process. With regards to noise, various metrics describe many of the subjective components of a noise event in an objective way. For example, peak and maximum sound pressure levels generally describe the magnitude of a noise event, whereas equivalent continuous sound pressure levels generally aim to describe the time varying energy of a noise event as a single value for a specified time period of the noise signal.

The historical evolution of noise metrics used to correlate community annoyance with objective measurements of blast has been summarised in detail by Valente, Nykaza, and Swift (2013). Valente et al. state that despite over 50 years of research, the community response to blast noise remains an issue to the US DoD. This is due to the subjective nature of noise annoyance, where non-acoustic factors may influence correlation with well researched objective metrics.

3.4.2.3 Discrete Noise Event Methodology

Peak Sound Pressure Level (L_{Pk})

On the surface level, the Peak Sound Pressure Level seems to be the most appropriate objective metric for the determination of a given level of annoyance for blast noise. This is because a peak level at a receiver can be easily attributed to a particular blast event. The peak sound pressure is a very relevant metric for describing a blast noise event, as it is defined by being the greatest absolute value of instantaneous sound pressure, which occurs within a specified time interval (Takinami, 1999). This is often confused with the maximum sound pressure of an event, which is measured using time weightings.

The metric may be further specified through the application of a C-Weighting filter to the metric, LCPk. C-Weighting is representative of how humans respond to sound above 100 dB. C-Weighting is also an indicator of low-frequency content, abundant in noise from blasts. This is due to the relatively small amount of low-frequency filtering from C-Weighted values, compared with the more commonly used A-Weighting curve. Although, the linear (Z-Weighted) peak sound pressure levels are not weighted at any frequency, unweighted levels do not represent the behaviour of how human ears respond to sound, especially at high sound pressure levels above 100dB, typical of blast noise exposures. Moreover, the audible rattle mentioned earlier, is said to be better represented through the use of C-Weighting, because

the specific low-frequencies that are responsible for producing rattle are filtered out by other weightings (Larry Pater et al., 2007).

Following the research throughout the 1970's, the previously mentioned equal energy metrics, (DNL and SEL) were the most commonly used in blast-response studies. However, the suitability of equal energy metrics was beginning to be questioned in the early 1980's, through other lines of research, which aimed to investigate variations of peak and sound exposure metrics. Bullen and Hede aimed to encapsulate the effect of non-acoustical variances in the General Reaction (GR) response metric, using various weighted mean, peak and exposure levels, accumulated peak level (APL) and the number of audible events among other metrics (Bullen & Hede, 1982). They deduced that peak metrics were unsuitable for relating to community reaction because peak levels were not generalisable to other impulsive sources. Peak metrics were used in other areas, namely by Fidell, Horonjeff, Schultz, and Teffeteller who suggested taking peak levels and peak vibration levels correlated well with the percentage of those highly annoyed (Fidell, Horonjeff, Schultz, & Teffeteller, 1983). From this work, they suggested that the annoyance increases at a greater rate compared to those that the energy models suggest. Murray and Avery showed a strong correlation between peak noise levels and the percentage highly annoyed from a dataset of mine blasts (Murray & Avery, 1984).

In the early 1990's a turning point in blast noise management was initiated by Luz, Lewis, and Russell who first described the problematic nature of correlating the average annoyance reported by residents from blasts with the yearly average exposure (George A. Luz, Lewis, & Russell, 1994). This study investigated the annoyance of individual weapon blasts. When judgements of 4 homeowners were compared to outdoor measured linear Peak SPLs, "moderate annoyance" was found above 115 dB (George A. Luz et al., 1994). Luz says this is consistent with the work of Pater's 1976 work, where a low probability of complaints was found below 115 dB from weapons blast.

Furthermore, it was found in the 1994 study that correlations with flat weighted peak levels exceeded 0.9 at each monitoring site. This was, however, a pilot study, which failed to obtain participant ratings of cumulative annoyance at the end of each day of exposure. The identified drawbacks were readdressed by Larry Pater et al. (2007). Parallels are drawn here to other work carried out by Salford on human response to railway noise and vibration, which research the best quantities for representing annoyance.

Sound Exposure Level (SEL, L_E)

Individual events can often be assessed using the sound exposure level metric. This is particularly useful for determining the dose of an individual resulting from a number of individual noise events. By adding up the SEL of individual events, one can determine the LAEq,T over a standard period for example, an 8-hour working day. It is important to note that the sound exposure level represents the complete energy of the event normalised to 1 second. According to Birgitta Berglund et al. (1999) the A-Weighted SEL (ASEL) alone has been shown to be inadequate for representing how humans respond to loudness from complex industrial noise. It was shown that this metric was inadequate for large and small weapons (B Berglund, Berglund, & Lindberg, 1986). However, a C-Weighted version of the SEL (CSEL) might be more appropriate given that the C-weighting represents how humans respond to loud sounds. CSEL has been shown to be useful in rating impulsive sound from firing ranges (Buchta & Vos, 1998; J. Vos, 1995).

The work of Vos throughout the late 20th Century on the correlation of CSEL and ASEL with community response further developed the field. Vos conducted many studies on the response of individuals to impulsive noise from small firearms. In 2001 a study compared the annoyance of 16 subjects related to 14 different impulse noises from firearms under 2 conditions: outdoors, and indoors with closed windows (Joos Vos, 2001). It was shown later by Vos that annoyance as rated indoors with windows closed, could be adequately predicted from the outdoor A-weighted and C-weighted sound exposure levels of the impulse sounds (J. Vos, 2003). The explained variance in the mean ratings by outdoor ASEL was increased by adding a second variable (CSEL-ASEL)(ASEL), where higher values of explained variance indicate a stronger strength of association. Vos deduced that the addition of the term (CSEL-ASEL)(ASEL) implies that annoyance increases with the increase in low-frequency energy of the sound, what is called the " heaviness" of the sound.

In 2003, Vos described the benefit for both A and C-Weighted rms level integrated over 125ms or expressed as SELS (integrated over 1s) which was originally shown by P. D. Schomer and Sias (1998) for explaining differences in the annoyance cause by sonic booms and blast sounds and by Buchta and Vos for explaining differences in annoyance caused by rifle impulses (Buchta & Vos, 1998).

The significance of Vos' research on SELs throughout the early 2000's is explained by Valente et al. (2013), where the combined metric of ASEL and CSEL could be used as an

indoor annoyance predictor with an outdoor metric. Moreover, it was shown by Vos that the variance in response metrics can be predicted from this combination of the "heaviness" metric and the ASEL (ASEL*(CSEL-ASEL)).

Vos' work wasn't without criticism however. Brink and Wunderli (2010) suggested that although combination metrics performed well in laboratory conditions, the CSEL-ASEL metric did not offer a significant increase in predictability under field observations when used as a secondary explanatory variable, due to differences in how subjects respond to noise in laboratory settings compared to within their homes.

Maximum Sound Pressure Level (L_{max})

A common parameter for assessing individual noise events is the A-Weighted Maximum Sound Pressure Level, LAmax. This is measured using a fast response time of 125 ms, which is usually a small enough sampling period to cover the noise event. Such noise events might be vehicle or aeroplane pass-bys and the metric is used to determine the impact of night-time noise events. However, this parameter does not fully represent the maximum value of the sound pressure level during an event, as it is integrated over a time period, which may be inadequate for such short duration blasts. Maximum noise levels are usually weighted over time periods fast or slow.

The choice of the LAmax metric within the WHO guidelines is related to its applicability to predicting sleep disturbance from transport noise at night. The acceptable permitted value of LAmax is based on the frequency distribution of LAmax levels.

On a more practical note, early pilot testing of the Intelligent Noise Monitor (INM) system (See the methodology in Chapter 4 of this thesis) was completed at DNV Spadeadam during May 2019. The aim of the test was to demonstrate the ability of the INM to report a noise level directly to the control room, shortly after a test. The metric chosen at the time was a Fast time weighted Maximum A-weighted SPL ($L_{Amax,\,F}$). The justification for the choice of this metric stemmed from the guidelines stated in WHO Guidelines for community noise (Birgitta Berglund et al., 1999) and from BS 8233 where a recommendation of below 45dBA was a suitable target for outdoor amenities.

3.4.2.4 Long-Term Average Noise Methodology

The management of long-term average noise levels has its roots in the field of transportation noise, such as aircraft and road traffic. The methodology uses long-term averaged sound

exposures as a stimulus metric to relate to a percentage of the population that is highly annoyed as a response metric. Typical assessment periods are 1 year. This is a historical approach which was originally adopted by the U.S. Army using the CDNL metric as described below. It is stated that despite their poor correlation, energy-based stimulus metrics such as the CDNL have been adopted by the blast noise research community (Valente et al., 2013).

Day-Night Level (DNL)

The current US Military Blast Noise Assessment Procedure given in AR 200-1 (200-1, 2007) mandate that the C-Weighted Day-Night Level (DNL) be used for managing noise sensitive areas. This metric averages the sound energy over and entire day and is common for long-term averaging noise levels of many noise source types. One major problem with the DNL and other noise metrics that average over time is the assumption of the equal energy hypothesis. Valente et al. explain how 100 events of 142 dB peak SPL can bring an annualised CDNL of 62 dB which is suitable for all land uses (Valente et al., 2013). However, a peak level of say, 142 dB, is certain to cause a negative adverse impact and is even above the allowable limit of impulse noise stated in the Control of Noise at Work Regulations 2005. Furthermore, the time period over which noise is averaged has a profound effect on the resulting apparent noise impact. Limitations of the DNL metric are excellently explained (Larry Pater et al., 2007), with the inclusion of Figure 63 as a visualisation of the DNL paradigm. The DNL method will provide no difference in 10,000 blasts over a year compared to 10,000 over a day. The equal energy assumes that the total sound exposure is averaged over the assessment period regardless of the magnitude of the noise level. Meaning that 1,000 noise events of a given sound exposure level is the same as one event with a magnitude 1,000 times as much energy, given by the equal energy hypothesis.

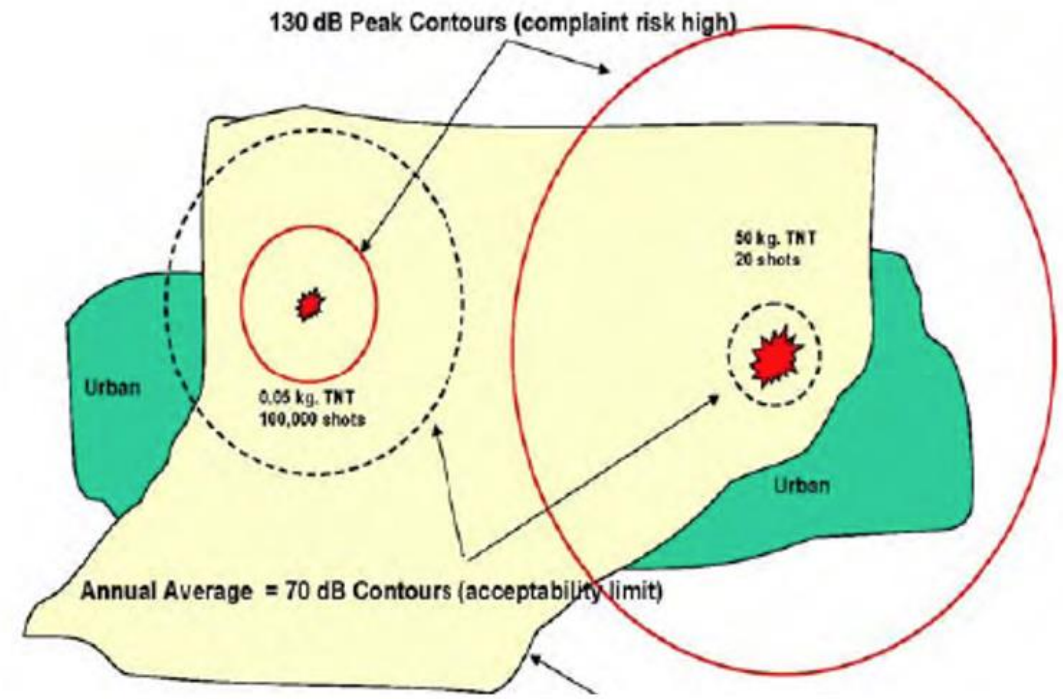

Figure 63 - Long-term average noise level paradigm from (Larry Pater et al., 2007).

This is paramount to members of the community exposed both infrequently and frequently to blasts because humans are unlikely to react to the average noise level of an area in the same way as the perceived loudness of an individual noise event, such as a blast. As a result of this realisation, C-Weighted sound exposure levels have been used to capture both the individual event response and then convert noise events into long-term averaged noise levels.

3.4.2.5 Annoyance

A review of the annoyance caused by blast noise (Edward T. Nykaza, Hodgdon, Gaugler, Krecker, & Luz, 2013) highlighted how noise complaints are often used to indicate adverse impacts on noise environments. Additionally, an important consideration is that an absence of complaints does not indicate a low community annoyance. However, the relationship between individual complaints and wide-spread community annoyance is not established and therefore implementing testing restrictions based on individual complaints is not fully appropriate as a means of reducing community annoyance.

Noise annoyance is notoriously a subjective psychological phenomenon based on an individual's perception of noise (Guski, Felscher-Suhr, & Schuemer, 1999; Palca & Lichtman, 2011). Given that it is a subjective metric, it cannot be measured directly by a sound level meter and is typically assessed via surveys on 5 or 11-point scales. Survey results categorise members of the community into various percentages of highly annoyed people,

based on how they rate annoyance to a particular noise event on the point scales. The points are then correlated with an objective metric to correlate noise level with annoyance.

Section 5 of the WHO Guidelines for Community Noise discusses the assessment of the impact of environmental noise and states that the uncertainty involved in the calculation of exposure-response relationships should be considered. Such uncertainties can arise from:

- Social factors: the population structure (such as age and health status);
- Physical factors: (climate and local meteorology, geography)

The variation in annoyance with the type of noise source has been investigated thoroughly. The variation of community response was quantified for audible rattle caused by different vibration sources (Woodcock et al., 2016). This research also thoroughly reviewed the significant contribution of audible rattle to the annoyance from vibration. This is of significant importance to blast research, where secondary causes of annoyance such as audible rattle are likely to occur from large overpressures passing through occupied structures.

Additionally, the preconception of property damage from the rattling associated with blasts is widespread among communities exposed to high levels of blasts. This is related to a long list of non-acoustical factors that are associated with complaints, identified as early as the mid-20th Century (Nixon & Borsky, 1966). Such factors include source familiarity, necessity and importance of the source, the ability of reducing it, neighbourhood attitude and finally a general readiness to complain. Pater also listed non-acoustical factors such as startle effects, habituation, building vibration, fear of damage to property, a belief that one should complain, a belief that more can be done to reduce the noise impact and finally, the interference of the noise event with various activities (LL Pater, 1976).

Valente et al. 2013 described how the number, timing and level of blast events are all important considerations for complaints .

By far the most influential and relevant piece of scientific literature to managing complaints at DNV Spadeadam is the work of Luz, who summarised the U.S. Army's detailed approach to the management of community response to explosion noise (G. A. Luz, 2011). The management strategy is a systematic approach, formed by half a century of research on noise from military activities and 3 historical phases. The final phase was the noise complaint management approach, which for the first time had a set of noise complaint guidelines

developed from the work of Pater. Table 43 states the guidelines, which relates a risk of complaint to a single event unweighted peak sound pressure level.

Table 43 - Noise Complaint Guidelines developed by LL Pater (1976).

Risk of Noise Complaint	**Single Event Linear Peak SPL (dB)**
Low	< 115
Moderate	115-130
High	>130
Risk of physiological damage to unprotected ears and structural damage claims	>130

Furthermore, the management strategy sets out the basic elements of a noise complaint management program. The relevant elements of the plan have been adapted for DNV GL Spadeadam and are detailed in Table 44.

Table 44 - Element Noise Complaint Management plan for DNV Spadeadam adapted from LL Pater (1976)

Element	**Nature**
1. Prediction of sound levels of individual acoustic events at a receiver	Acoustical
2. A semi-real-time multi-component noise monitoring system spread across multiple receivers	
3. An understanding of typical reactions to sounds of interest	Psychoacoustic
4. Administrative procedures to ensure complainants know how to register noise complaints	Psychosocial
5. A sensitive procedure for engaging with complainants and for collecting noise complaint data	

Interestingly, the nature of the complaint management elements is acoustical in only the first two. Of course, the main element of relevance to this literature review is element 2. Luz goes on to discuss the sound monitoring scheme implemented around the vicinity of Aberdeen Proving Ground, which reported peak blast levels as a real time indicator of receiver exposures back to the range control. Interestingly, the peak levels originally correlating with

only 64 % of community complaints were improved to 90 % following modifications to the system (E. T. Nykaza, Luz, & Pater, 2008). Finally, Luz explains how attempts to improve such a monitoring system by the final 10 % have been attempted using pattern matching techniques, such as automatically comparing measured waveforms to known blast profiles. Other attempts have used cross-correlation techniques to disregard high peak noise levels caused by wind gusts using two microphones, with considerable success.

3.4.3 Non-Acoustic Factors

The work of Guski, Schreckenberg, and Schuemer (2017) analysed results from noise surveys that revealed for the annoyance response to environmental sound, only about 1/3 of the variance is caused by the purely acoustic factors. In other words, the cumulative noise level itself (e.g. Leq, LDN, LDEN etc.) could only attribute to around 1/3 of the variance in human response to environmental sound. The remaining 2/3 are attributed to other factors, referred to in the literature as ‘non-acoustic’ factors. Therefore, there is a wide range of annoyance response for the same environmental sound stimulus in terms of objective levels, as a result of external factors. Figure 64 shows this phenomenon.

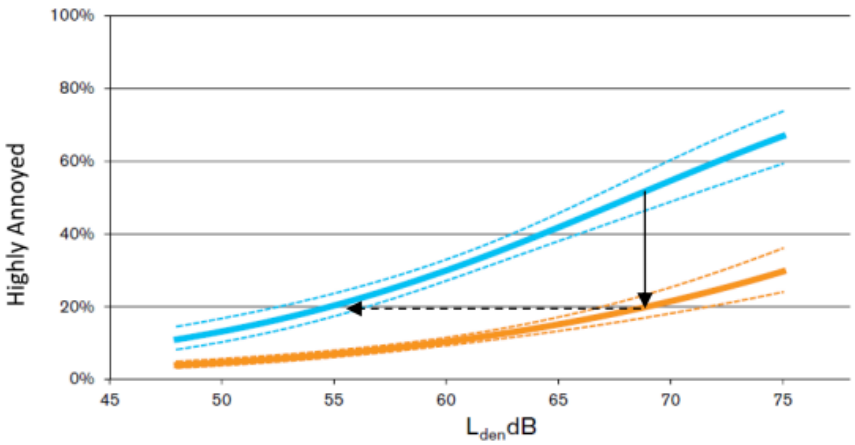

Figure 64 - Difference in the percentage of people being highly annoyed for situations excluding (blue) and including (orange) moderators. Taken directly from FAMOS Guidebook (Eggers et al., 2022a)

The FAMOS project (Eggers et al., 2022b) focused on this topic with application to improving the human response to road traffic noise through modification of these external factors. These non-acoustic factors are referred to as ‘moderators’ in the FAMOS work, and

the study investigated several moderators known to influence the noise annoyance of people exposed to road traffic noise.

3.4.3.1 Relevant Non-acoustic Factors to Community Response to Blast

Although the FAMOS project focused on road-traffic noise, the study reveals the important effects of so-called "moderators" or non-acoustic factors on human-response which are often independent of the sound source or nature of the sound. The list of moderators included in the study are shown in table 1 and are primarily factors which the road owners or administrations can influence to some degree. For example, the factors of "Attitudes towards authorities and road owners" and "Expectations / public relations" have immediate relevance to blast noise from the DNV Spadeadam site, as they are essentially attitudinal factors attributed to people's perceptions of the owner of the noise source. Both are intricately linked to the term "Trust" which is referenced in the FAMOS report as being the degree to which members of the neighbourhood trust the noise producing entity, and reference is made to the NORAH study of exposure-response relationships for aircraft noise on different degrees of trust. In the individual analysis of this factor's influence on noise annoyance alone in the FAMOS study, it is quoted that the difference in reported annoyance for situations characterised by good relations versus bad relations with the noise producing entity is by far larger than the effect of most abatement measures, and therefore the effect is strong. This has significant relevance to DNV Spadeadam's situation, where the benefit of investing in good public relationships with the surrounding neighbours has had a positive impact, reported anecdotally by the researcher through carrying out the research.

Table 45 - Moderators used in the FAMOS study with their respective definitions and effective influence on noise annoyance expressed as shift in noise level (Eggers et al., 2022a; Eggers et al., 2022b).

FAMOS Moderator	Definition	Effect Size
Attitudes towards authorities and road owners	Relationship between sound source owners and the neighbourhood	± 10 dB (Based on "Trust / Acceptance")
Expectations / public relations	Matters relating to abrupt change to or abnormal operations by the sound source owner in the context of increased / decreased noise producing operations	5 to 10 dB

Traffic volume	Number of passing vehicles	~1.5 dB per doubling
Safety expectation	People's perception of safety of the noise producing roads	5 to 8 dB
Vegetation and greenery influencing the visual appearance of the surroundings	Non-acoustic effects of greenery used on noise barriers	6 to 10 dB
Noise barriers (expectations and visual appearance)	Whether the design of the noise barrier meets the expectations of the neighbourhood and whether they were involved in the design	2 dB
Locations and orientation of residences / access to a quiet side	Use of property layout and orientation with respect to noise producing roads	8 to 12 dB
Neighbourhood soundscape	Existing soundscape of the local neighbourhood surrounding noise producing road	Up to 10 dB
Non-controllable personal and demographic variables	Factors such as age, gender, dependency on road transportation, house ownership, social status, income, education, etc.	Not quantified in FAMOS study

Another relevant factor also included in the FAMOS study which could be attributable to community response to impulsive sound at Spadeadam is, "safety expectation". Within the FAMOS study, this moderator in the context of road traffic noise, involved people's perception of the safety of the roads which emitted the noise they were exposed to. For example, the use of reduced speed zones, bumps, bike lanes and many other factors, which had the same combined effect on noise annoyance a 5 dB shift in objective noise level. Safety is a highly relevant aspect of the work carried out at Spadeadam, given that the purpose of the facility is to be a dedicated space for testing major hazards and accidents. The local community's perception of the how safe the work done at Spadeadam is, is bound to have a

significant effect on annoyance perceived by the objective sound produced by the testing, though it is not the goal of this thesis to quantify that effect.

Other effects of significance included in the FAMOS study were “vegetation and greenery influencing visual appearance of the surroundings”, “Locations and orientation of residences / access to a quiet side”, “noise barriers (expectations and visual appearance)” and “Neighbourhood soundscape”. Although not directly controllable by DNV Spadeadam in the context of this research, the effects of greenery (either acoustically or non-acoustically, i.e. visually) are of relevance from the large areas of forest plantation surrounding the site. Moreover, the accessibility of “green areas” and nature reserves is an important factor in influencing annoyance. The author speculates that this moderator could behave polarly, as does the “Trust” moderator in the FAMOS studies, i.e. can increase or decrease annoyance around an average level based on the context. In FAMOS, the non-acoustical effects of greenery is reported to be up to a 10 dB reduction in the noise level. That study refers to a variety of other studies on the non-acoustical impact of greenery on noise annoyance, (Fricke, 1983; Langdon, 1976; Lercher, 1996; Van Renterghem & Botteldooren, 2016) where those studies found effective reductions of at least 10 dB, 15 dB , 5 dB, and up to 10 dB respectively.

Alternatively, the author speculates there may be polarity to this effect, after receiving noise complaints from activity at Spadeadam, where the complainant expressed concern for wildlife living around the test site, clearly increasing the severity of the response. The increased annoyance response may also be linked to the expectation that nature reserves, and tranquil areas should have their natural soundscape preserved, and the influence of industrial impulsive sound may conflict with a receptor’s expectations of their local soundscape.

The acoustic effects of greenery are not discussed in this subchapter and are found within the subchapter on real acoustic effects of forestry and vegetation. The context differs slightly here to that of FAMOS, which concerned greenery in the context of shrubs and trees in the local area or installed on noise barriers. The context for greenery at Spadeadam on the other hand refers to the real effects of acoustic scattering by large forests (including edge scattering), the influence of forest litter on the ground characteristics, or the influence of forests on the micrometeorology.

Conclusions on the influence of non-acoustic factors on annoyance

Evidence of a wide range of effects that non-acoustic factors have on noise annoyance has been found from the real-world studies of the FAMOS project. When ordered by magnitude in that study, the Trust/attitude towards noise producing entity factor was the most influential with an ability to moderate perceived annoyance by ±10 dB.

3.4.4 Conclusions on Community Response to Blast Noise

Although great resistance has been shown towards it, for long-term noise management the scientific literature favours equal energy metrics, such as the CDNL. The SEL metric is used for predicting adverse community reactions to individual impulsive noise and for the derivation of long-term average levels. The CDNL metric however is highly unsuitable for the monitoring system around Spadeadam, as the metric uses time periods on the scale of a year to integrate noise levels over. Clearly, there is a justification for using a more instantaneous descriptor of the noise, otherwise there would be no point in the development of a monitoring system which solely relies on real-time reporting of noise levels.

Therefore, a single event descriptor such as a peak or SEL metric should be used as the display metric on the SNM server, for site control operatives to decide on testing. The peak level should be favoured on the basis that it may be easily scaled with charge weight and TNT equivalence. Though, it is acknowledged that time varying characteristics of the signal such as the impulse length, which also scales with charge weight, is not accounted for by the peak metric. However, a peak metric would be easily comparable to other prediction programs both previous and current at Spadeadam, such as the MONET noise contouring tool which is currently used. This would aid with the ease of interpretation of monitor results for operators at the control room.

Furthermore, a C-Weighted metric is necessary in order to better represent the low frequency components of the signal which often cause secondary annoyance effects, such as audible rattle. Moreover, the C-weighting filter better represents how human ears respond to high level sounds.

Relevant non-acoustic factors have been reviewed for their applicability to community response of blasts from Spadeadam. It is concluded that factors such as “Trust” are likely to have a significant effect on community response, as shown in the FAMOS work, and factors

such as these should be considered when making noise predictions at Spadeadam, as variables affecting uncertainty in noise prediction.

3.5 Blast Noise Control

A management strategy not addressed in this thesis is the concept of blast noise control, meaning the mitigation of noise at the source. Due to the nature of blast noise, generated by high-energy shock waves from explosives, physical barriers must therefore be suitably robust. Additionally, the frequency content involved in blast waves, particularly the frequencies which are not significantly attenuated in long-range propagation are low, i.e. 15 - 125Hz (Keith Attenborough et al., 2004). The consequence of this is that control infrastructure, such as conventional barriers must be large to account for the wavelengths involved, on the order of 50m for attenuation at 15Hz, which is noted in (Keith Attenborough et al., 2004).

To address this limitation, novel techniques to control noise at the source have been extensively researched by various institutions throughout the last few decades. This subchapter of the literature review, presents this work, from early experimental attempts to the modern state-of-the-art in blast noise control.

3.5.1 Large scale surfaces and locally absorbing ground

With respect to controlling noise levels from explosives and artillery fire, much work was done in the 2000's, sparked by a joint project of the ERDC, University of Hull and the Netherlands Ministry of Defense and TNO on absorbing blast sound local to its generation (Keith Attenborough et al., 2004). This multi-phase project produced a series of papers and a joint project report, summarising the group's efforts on analytical and experimental studies. This work spanned both the design and construction of high-energy blast sound-absorbing surfaces, through a number of papers detailing the theory and experimental trials carried out at the US Army's Fort Drum facility (Keith Attenborough et al., 2004; P. Schomer & Attenborough, 2005). This specific work led to TNO developing propagation tools for modelling long range blast with barrier interaction, accounting for nonlinear effects, which is discussed in the section on nonlinear propagation in this thesis.

According to the joint ERDC and Netherlands MOD project report, no theory existed prior on the design of absorbing surfaces at low frequencies in a highly nonlinear environment. An important contribution of this work is the development of a theory to describe the nonlinear

response of rigid porous materials to high amplitude continuous and pulsed sound, allowing for a linear variation of flow resistivity with flow velocity (Forchheimer's non-linearity). As a result of this development, predictions of the acoustic reflection coefficient at the surface of a hard backed rigid porous layer as a function of incident sound pressure and frequency could be predicted.

3.5.1.1 Forchheimer's non-linearity

The joint report mentions several papers which expanded the framework for describing the effects of rigid-porous material on high-amplitude sound through Forhheimer's non-linearity (Umnova et al., 2002; Umnova, Attenborough, Standley, & Cummings, 2003). The theoretical work of Umnova et al on Forchheimer's non-linearity in the early 2000's explored the effects of duration and amplitude for finite amplitude pulses, and experimental results were observed in shock tube tests. This work provided theoretical foundation for the full-scale experimental trials on modifying the conditions of the ground for the absorption of blast noise(Keith Attenborough et al., 2003; P. Schomer & Attenborough, 2005). Forchheimer's non-linearity and its effects on sound absorption for high-amplitude sound has been later investigated (Turo & Umnova, 2010, 2013).

3.5.1.2 Outcomes of ERDC Joint project

The theoretical and numerical advances in predicting non-linear high amplitude sound propagation produced by this work, led to experimental field trials being carried out. In particular, the trials at Fort Drum (P. Schomer & Attenborough, 2005) involved two phases of full-scale tests with C4 detonations. Test one involved detonations surrounded by gravel pits of varying configurations and properties and found that each particular configuration absorbed sound at a certain farfield position. The second test involved ploughing an extended region of ground extending to further distances from the blast site and observed sound absorption for the frequencies of interest up to 100m away. Overall, this work proved that real reduction in blast sound can be achieved by local sound-absorbing surfaces.

The team from TNO who were involved in this joint project later went on to experiment with blast absorbers. Short and long-range measurements above and below a 1.5m high 15m x 15m wide gravel barrier were taken, to determine both its absorptive and shielding properties against roughly 0.64kg TNT equivalent blasts (0.57kg C4) (van der Eerden, Van den Berg, Hof, & Arkel, 2006). Much focus was also on the comparison of results with those produced

by a hybrid model, which combined non-linear near field blast propagation with a long-range model, discussed in the subchapter on nonlinear models in chapter 3.2.4 of this thesis.

Later, TNO conducted full-scale trials with another technique not yet discussed, aqueous foams (Eerden & Carton, 2012). However, the use of aqueous foams dates back much earlier and is covered in the next section.

3.5.2 Foam Mitigation

Aqueous foam for the mitigation of high amplitude sound had been attempted as early as the 1970's, and a summary of this era of work is presented in (R. Raspet, 1981). Experimental reduction using foams had been performed by 3 active groups (2 in Canada – J.S. de Krasinski of the University of Calgary (de Krasinski & Khosla, 1972, 1974; Ramesh & de Krasinski, 1976a, 1976b), F. H. Winfield and D. A. Hill of the Defense Research Establishment in Alberta (Klautt & Hill, 1977; Winfield & Hill, 1977); and in the UK by D. A. Dadley, E. A. Robinson and R. C. Picket at the Royal Armament Research and Development Establishment (Dadley, Robinson, & Pickett, 1976)).

The University of Calgary work rather simply involved the widely available Palmolive Ready Shave foam to achieve overpressure reductions by a factor of 4 at 0.06m for very small explosives (10g of PETN) (W & de Krasinski, 1976). More complex test rigs by Winfield and Hill were built for experimenting with different foam solutions on 0.9kg of RDX and found interesting characteristics of attenuation dependent on foam depth in relation to the fireball diameter (Winfield & Hill, 1977). Both peak overpressure and positive impulse were compared. Temperature measurements were utilised in later work by Klautt and Hill to try and deduce the possible mechanisms of attenuations, one of which was thought to be by cooling the fireball (Klautt & Hill, 1977).

Larger explosives (2.27kg RDX) were detonated surrounded by foams in the UK and achieved a maximum reduction of 17dB in peak overpressure at a distance of 2 scaled metres, followed by a rapid decrease in reduction. Dadley et al. also argued that the foam efficiency was affected by the standoff distance between the source and explosive. Further work went on to investigate the use of foams on explosives in enclosures and on gun blast noise, as was done elsewhere (L. L. Pater & Shea, 1981) around the same time.

Raspet improved this knowledge by investigating both foam depths and charge size and their effects on a variety of acoustic indices, including CSEL (see section 3.4 of this thesis), FSEL

(Fast Sound Exposure Level) and peak level (R. Raspet, 1981). His data was used to develop scaling laws for attenuation. A number of experimental trials investigated the influence of detonations in pits and enclosures on 0.57-2.27 kg of C4. As well as noting the reductions in pressure based metrics (FSEL, CSEL and Peak level), temporal characteristics such as positive phase duration were plotted against scaled foam depth and displayed a tendency to decrease as a function of increased foam distance, indicating the presence of 2 mechanisms; (a) direct reduction to the energy or time of explosive material burn, or (b) a mechanism which disperses energy over a longer time as the wave passes through the foam.

From the experimental trials that CERL conducted, it was concluded then that foams could achieve blast noise attenuation of up to 14 dB for unconfined explosives. Raspet went on to compare both high and low expansion foams, 250:1 and 30:1 respectively and compared their effectiveness as a function of scaled depth as in Figure 65, where scaled foam depth is the foam depth divided by the cube-root of the TNT equivalent charge mass. The relationship of scaled foam depth and noise level (or consequent attenuation on noise level) is reported in later work (Panczak, Krier, & Butler, 1987).

$$Scaled\ foam\ depth = \frac{d_f}{\sqrt[3]{M_{TNT}}} \quad (1)$$

Where d_f is the foam depth in metres, and M_{TNT} is the TNT equivalent mass of the explosive in kg.

Much further research was presented in Raspet's 1981 work to investigate foams in particular geometries, for use with demolition, in plastic bags for increased foam density and on artillery fire. In general, the conclusions from this extensive work are that both low and high expansion ratio foams can provide attenuations on the order of 10 dB with a maximum of 14 dB achieved for confined explosives.

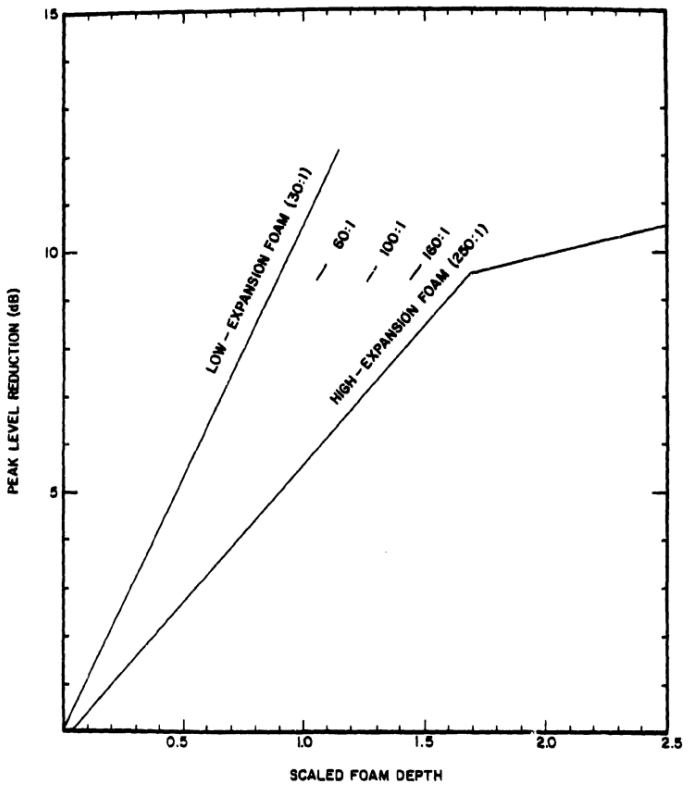

Figure 65 - Reduction in Peak SPL as a function of Scaled Foam Depth, taken directly from (R. Raspet, 1981).

3.5.2.1 Modern Full-scale Experimental Trials of Foam Mitigation

A comparatively inactive period of research on full-scale trials after the late 1980's is apparent in the literature and is restarted following the aforementioned joint study by the ERDC and the Netherlands Ministry of Defence in the mid 2000's. Following the extensive numerical and simulation work carried out in the Netherlands during the early 2000's, in particular by Frits van der Eerden, Frank Van den Berg and Eric Vedy, full-scale experimental trials of mitigation techniques were conducted. In 2007, a paper (Van den Berg & Eerden, 2007) summarised the work done up to then which had initially concerned numerical prediction of blast effects at long range and including barrier mitigation in the near field. Thus, a nonlinear model had to be developed to accurately model the interaction of strong shock waves propagating non-linearly, in turn, slowing and propagating linearly to a distant receiver at many 10s of kilometres away. That work is described in the section on non-linear models in this thesis.

In 2011 Van den Berg and Van der Eerden researched the use of shock wave mitigation via barrier interaction and use of absorbing materials close to the source (Van den Berg & Eerden, 2011). It was in 2012 that the use of foams at full-scale began to be investigated (van der Eerden & Carton, 2012). That study investigated the blast effects and their reduction using two methodologies, (1) a porous barrier at relatively close range (gravel) and (2) water-based foam applied directly onto the explosives. Mitigation at 300 m from the sources was predicted using a model accounting for non-linear interaction with a barrier and porous material. Measurements for validation were also carried out and observed 20-50 % reductions in peak level depending on the mitigation configurations. Later work in 2012 investigated barrier attenuation on muzzle blast from firearms (van der Eerden & Van den Berg, 2012).

Later in 2018**,** Carton investigated the effects of water foams on open air detonations for explosive charges of 20-50 kg of different explosives (RDX, ANFO and a cladding explosive (similar to EDH) (Carton, 2018).

Pressure gauges were set at various distances to capture the blast effects between 5-200m. Foam coverage resulted in average reductions in peak pressure and impulse of 31-36% and 13-17% respectively. Maximum reductions up to 41 % were seen with RDX. However, the study acknowledged that the results were indicative only, and no attempt to optimise the foam properties, shape or dimensions had been made.

3.5.2.2 Laboratory Work

Alternatively, shock wave mitigation has been researched extensively in the laboratory and with small scale experiments for the purpose of investigating the fundamental mechanisms of mitigation. Much of the recent work has been carried out by Ben-Gurion University of the Negev, Israel, which has a Shock Tube Laboratory. Hadjadj and Sadot (2013) summarise this work in their paper, where they refer to other reviews on the topic (Britan, Liverts, Shapiro, & Ben-Dor, 2013; Britan, Shapiro, et al., 2013) and by Del Prete, Chinnayya, Domergue, Hadjadj, and Haas (2013), who have described the essential features of aqueous foam barriers against blast waves in shock waves and full-scale tests.

The highly active group at Ben-Gurion University in particular has produced a broad knowledge base on blast mitigation. Recent research on blast wave mitigation is undertaken by Berger built upon that of Ben-Dor and Sadot, have produced numerous numerical and experimental studies on shock wave attenuation using a variety of novel methods, including

foam and particle suppressions, fluid-structure interaction (FSI) and rigid and dynamic barrier arrays.

The use of foams by this research group has primarily focused on reducing blast effects in general, for the protection of assets from overpressure rather than with regards to environmental noise. However, some research has been focused on sound propagation (Britan, Liverts, & Ben-Dor, 2009).

Another recently active group working on this topic is the Mavlyutov Institute of Mechanics in Russia, particularly Bolotnova and Gainullina who have produced recent papers on the simulation of shock wave interactions with foams (Bolotnova & Gainullina, 2019, 2021). The same research group has performed research on acoustic propagation of sound waves in the presence of bubbles (Agisheva & Galimzyanov, 2020), which although may not seem directly applicable to Spadeadam, shows the knowledge built up by multi-disciplinary research groups.

An investigation into the use of dynamic barriers (Berger, Ben-Dor, & Sadot, 2015) proved the concept of a reactive mitigation process aimed at reducing shock induced pressure jump downstream of a barrier. This has particular use in the cases of intentional hazards inside corridor type structures, such as in tunnels, and aeroplanes. Berger et al argue that the barrier opening ratio is dominant in influencing the attenuation of a shock wave, and that the barriers inclined towards oncoming shockwaves were more effective in providing attenuation. This type of mitigation does not have much relevance to the open-air full-scale field trials at Spadeadam but is nonetheless important knowledge.

3.5.3 Mitigation using water and sprays

Water is universally used in fire suppression as an extinguisher but has also been used for mitigation of a variety of large explosions, in the form of bulk water (Buzukov, 2000; Forsen, Calberg, & Eriksson, 1996; Pitiot, CHabin, & Desailly, 2000). Buzukov experimentally investigated the effects of a water drop curtain on blast parameters, including noise.

Willauer et al investigated the effects of water mists on the overpressures produced by TNT and Destex up to 50 lb (Willauer, Ananth, Farley, & Williams, 2009). Blast parameters were measured with and without mists, and by using a droplet analyser, the mist was characterised. Reductions as much as 40% for TNT and 43 % for Destex were observed for particular mist

concentrations of 70 g/m^3 and droplet Sauter Mean Diameter (SMD) 54 μm , with 60 s spray prior to the detonation. Other free field trials (Tosello et al., 2012) placed pressure gauges within and behind a SMD 100 μm, 50 g/m^3 mist to measure blast parameters from 4.5 kg of Plastrite. A 44 % decrease in overpressure was measured inside the mist but no difference was measured between the gauges located behind the mist and in an equivalent symmetric position.

Recently, the French-German Research Institute of Saint-Louis has been highly active at conducting experimental trials on the use of water mist in shock tubes and open air tunnels (T. Schunck, Bastide, Eckenfels, & Legendre, 2020), and also water films in combination with perforated plates (Thérèse Schunck & Eckenfels, 2021; Thérèse Schunck, Eckenfels, & Rigoulet, 2023) This work expands on previous research with water curtains (Chen, Zhang, Fang, & Mao, 2015; Gebbeken, Warnstedt, & Rüdiger, 2018). Schunk et al's work in 2023 involved measuring blast overpressures and impulse in the free field from spherical 1 kg Composition B (44 g with C4 booster) with and without various configurations of perforated plates. Two types of plates were compared; a firm metal grid and a sheet of chain mail. Numerical simulations were carried out and compared to the experimental results. Schunk et al's field trials found that both overpressure and impulse were reduced by using grids with small holes and that mitigation increased when an water curtain was added. The greatest reduction in overpressure (60, 60 and 62 % for 3 identical tests) were observed for the rigid perforated plate with a water curtain.

3.5.4 Conclusions on Blast Noise Control

From a review of the literature, much work has been done over the last 5 decades on the mitigation of explosions by various techniques. The majority of this work has been focused on reducing overpressure and other blast parameters with respect to building damage and personnel safety. This in turn has been shown to reduce peak noise levels at close range to the explosions, effectively decreasing the sound power level of an explosive source. Although, most work involved laboratory testing in shock tubes, some large scale field trials not too dissimilar to the likes of testing carried out at DNV Spadeadam have been performed with aqueous foams as mitigation.

3.6 Modelling of Environmental Effects

The environmental effects on long-range noise propagation discussed throughout this chapter are evaluated and their relative importance for Spadeadam operations are investigated using a parabolic equation model. These simulations are intended to provide a high-level summary of the effects and their respective influences on blast noise propagating over long range.

By focusing the modelling to sound propagation from typical blasts carried out at Spadeadam, the influence of the main environmental effects, such as atmospheric profiles and ground, can be evaluated for their relevance to blast noise. One source strength is considered, a 10 kg TNT blast, typical of the most common activity carried out at the site, Explosive Depth Hardening.

3.6.1 Description of the source

In order to model the propagation of noise relevant to Explosive Depth Hardening (EDH), the modelling is carried out at the dominant frequency of interest according to the size of a typical 10 kg TNT detonation. The methodology of ISO 17201-2: 2022 (International Standards Organisation, 2006)is used to derive the source terms of a 10 kg detonation.

The chemical energy, Qc for a 10 kg TNT detonation is calculated as $4.45 \times 10^7 J$ from the mass of the explosive, mc and the conversion factor for the amount of energy released per unit explosive for TNT, $\hat{u}$.

$$Q_c = \hat{u} m_c$$

$$Q_c = 10 \times 4.45 \times 10^6 = 4.45 \times 10^7 J$$

To calculate the acoustic energy, Q_m, the proportion of energy transferred from chemical energy to acoustic energy, σ_m is assumed to be 4% (ISO 17201-2:2015). Proportion corrections related to kinetic energy of projectiles are not needed here to represent a spherically symmetrical explosion.

$$Q_m = \sigma Q_c$$

$$Q_m = 0.04 \times 4.45 \times 10^7 J = 1.78\ MJ$$

From this quantity the Weber-radius of the explosion can be found, which represents the size of the sphere around the detonating explosive at which expanding initially supersonic gas

cloud has slowed to equal the local speed of sound, at which point sound is emitted from the explosive. The Weber-radius is found by taking the cube root of the acoustic energy divided by the energy density of the gas sphere at the Weber-radius.

$$R_w = \sqrt[3]{\frac{Q_m}{q_w}}$$

$$R_w = \sqrt[3]{\frac{1.78 \times 10^6}{2.25 \times 10^3}} = \mathbf{9.2\ m}$$

This radius seems comparable with measurements of a 16.5kg TNT demolition which found a Weber radius of approximately 10 m (K-W Hirsch, 1999). For an explosive source with Weber-radius of 9.2 m, the approximate dominant 1/3 octave band frequency is 20 Hz. Simulations in this analysis will therefore be carried out at this frequency.

Since the majority of standard explosion tests at DNV Spadeadam are carried out close to the ground, a nominal height above ground of 0.5 m is chosen for the simulations.

3.6.2 Parabolic Equation Modelling

To model the effects of the atmosphere and ground in isolation on sound propagation, the MATLAB tool, “Outdoor Sound Propagation Calculator” (V. E. Ostashev & Wilson, 2015), is used to make predictions. The tool offers a narrow and wide-angle implementation of a Crank-Nicholson Parabolic Equation (CNPE) model. The wide-angle version is used in this evaluation. A ray tracing model is also available in the program, and has been overlaid on the simulations presented in this section to illustrate the effects of atmospheric refraction and ground reflection on sound rays.

The tool is split into 4 sections, Calculation Parameters, Calculation Type, Ground Properties and Atmospheric Properties.

Calculation parameters allow the user to select the frequency of interest, source height, maximum and minimum receiver range. The frequency that is modelled is dependent on the dominant frequency of the blast which is fundamentally related to the mass of the explosive. The source height is kept to 0.5 m above ground. The size of the domain is set to a positive range of 10 km and a height of 1 km.

The general approach used by Keith Attenborough et al. (1995) is used in this analysis to distinguish between the results of specific propagation scenarios while still generalising to the many propagation conditions possible in reality. Attenborough et al used 4 simple propagation cases to model sound propagation in a domain of 10 km distance and 1 km in height, and compared the results of various prediction models, including PE, against FFP and ray tracing.

3.6.2.1 Atmospheric Conditions

The atmospheric conditions modelled in this analysis are chosen to give contrasting results in order to show the magnitude of variability between possible propagation scenarios, whilst remaining general so that they can be used to give overall insights into noise impacts from blasting under various atmospheric conditions.

Table 46 summarises the propagation conditions modelled here, and the parameters that govern them with their associated values. It is often useful to compare directly conflicting scenarios, such as low and high wind conditions, represented here by the friction velocity parameter. This modifies the vertical sound speed profile by varying the wind profile. The temperature structure of the atmosphere is modified by the specific and latent heat flux parameters, approximately representing Cloudy, Sunny and Nighttime vertical temperature structures. These conditions can be appropriately considered representative neutral, unstable and stable atmospheric boundary layers, thus providing high contrast between atmospheric stability classes.

Table 46 - Atmospheric properties of this analysis and their associated physical properties.

Atmospheric Conditions	**Homogeneous**	**Neutrally Stratified**	**Neutral**		**Unstable**		**Stable**	
			Low Wind	High Wind	Low Wind	High Wind	Low Wind	High Wind
Friction velocity (m/s)	N/A	0.00	0.1	0.6	0.1	0.6	0.1	0.6
Specific heat flux (W/m^2)	N/A	0.0	0	0.0	200.0	200.0	-4.0	-20.0
Latent heat flux (W/m^2)	N/A	0.0	0	0.0	50.0	50.0	-1.0	-5.0

3.6.2.2 Ground Conditions

Similarly, two extremes in boundary conditions representing the ground within the PE model are used indicate the extent of ground effects on sound propagation. While a range of ground types can be selected within the MATLAB tool, direct comparison between an acoustically hard ground (Painted Concrete), and soft (Snow) is made in this analysis. Table 47 summarises the properties of the ground types selected.

Table 47 - Ground types used in this analysis and their associated physical parameters.

Property	Concrete	Snow
Static flow resistivity (kPa s/m^2)	200000	29
Volume porosity	0.400	0.660
Normalised impedance	1088.21 + 1088.20i	10.29 + 10.12i
Normalised wavenumber	609.40 + 609.39i	9.49 + 9.37i

The PE prediction model is using Wilson's model for ground impedance, (D Keith Wilson, 1997). Wilson's model is referred to as a relaxational model and is stated to mimic the Delaney-Bazley while extending its applicability to a wider range of frequencies. In particular, the relaxational model uses the static flow resistivity as does the Delaney-Bazley mode, but includes relaxational times in the model, solved in terms of the normalised impedance and normalised wavenumber. The term "relaxational" in Wilson's model refers to viscous and thermal diffusion processes, then modelling the subsequent return to equilibrium when a ground or porous material is perturbed by sound.

3.6.3 Simulations

3.6.3.1 Baseline Propagation Scenarios

Firstly, comparisons of a homogenous atmosphere above the two contrasting ground surfaces are shown in Figure 66 (top and bottom left). Of course, a homogeneous atmosphere is not realistic, since it assumes constant sound speed with height in the atmosphere. This assumes that both wind speed is zero at all heights above ground and that temperature is constant with height. The key property is that these meteorological profiles do not vary with height, and the particular value of the temperature will only effect the amount of atmospheric absorption (which is very small at the frequency of interest), and has no effect on refraction as it is

constant, However, this does provide opportunity to observe the effects of the interaction of sound with the ground without refraction effects.

Alternatively, a neutrally stratified atmosphere enables the visualisation for the theoretical case of a linearly decreasing sound speed profile modified by the temperature profile alone. Wind effects are not included in a neutrally stratified atmosphere, and hence in the PE model, the wind profile is assumed to be zero at all heights above ground. The wind profile as well as the temperature, humidity and sound speed profile for this case is shown in Figure 67. The most important feature of the meteorological profiles is the sound speed profile, which has both the actual (adiabatic) and effective (including wind) overlaid.

The effect of temperature stratification is shown clearly in Figure 66, with the inclusion of ray paths overlaid on the PE output, by the upward refracting ray paths, representing a shadow zone, as compared to a homogeneous atmosphere. Temperature stratification in the form of a temperature lapse (decrease with altitude) as is normally the case during the daytime, when considered alone has the effect of reducing noise at distance and is independent of source-receptor angle.

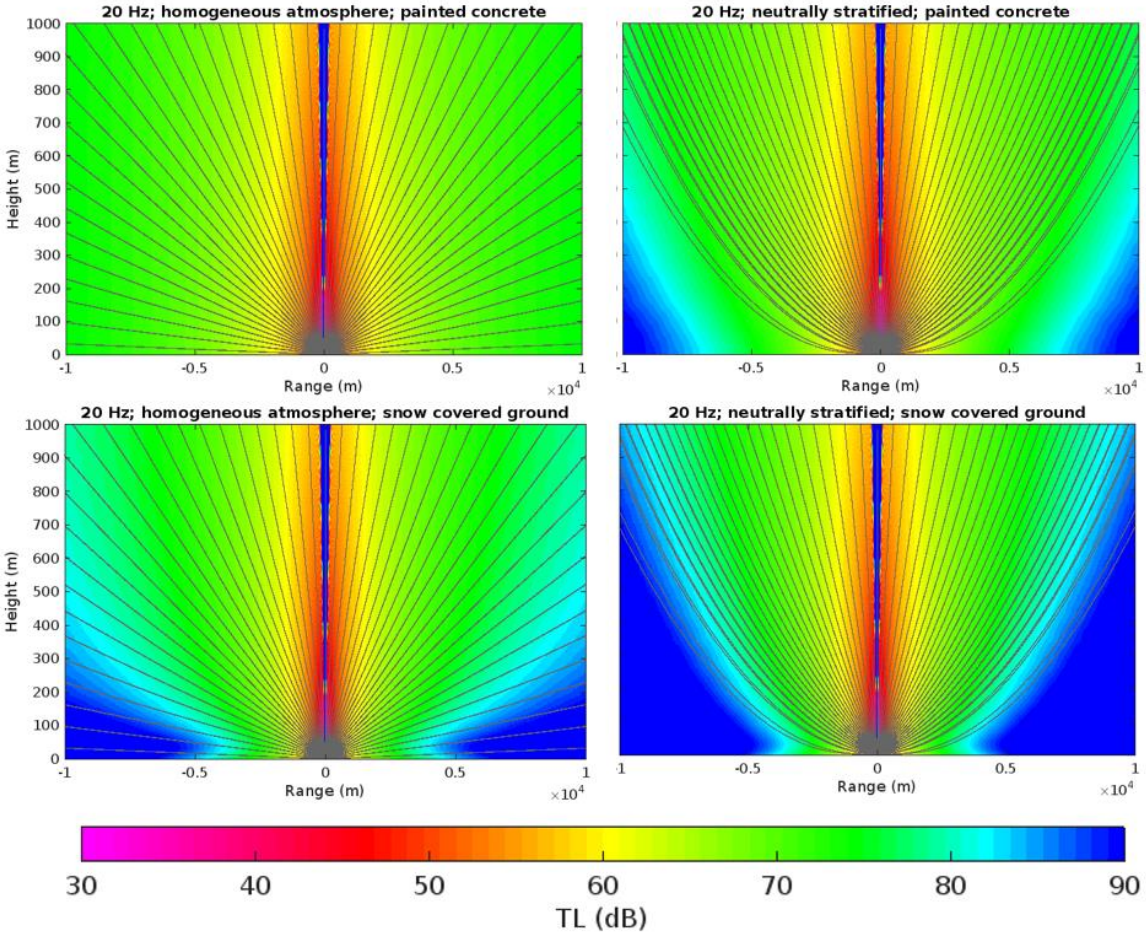

Figure 66 - PE simulations of baseline propagation scenarios, including homogeneous (left panels) and neutrally stratified (right panels), over two contrasting ground surfaces; concrete (top panels) and snow (bottom panels).

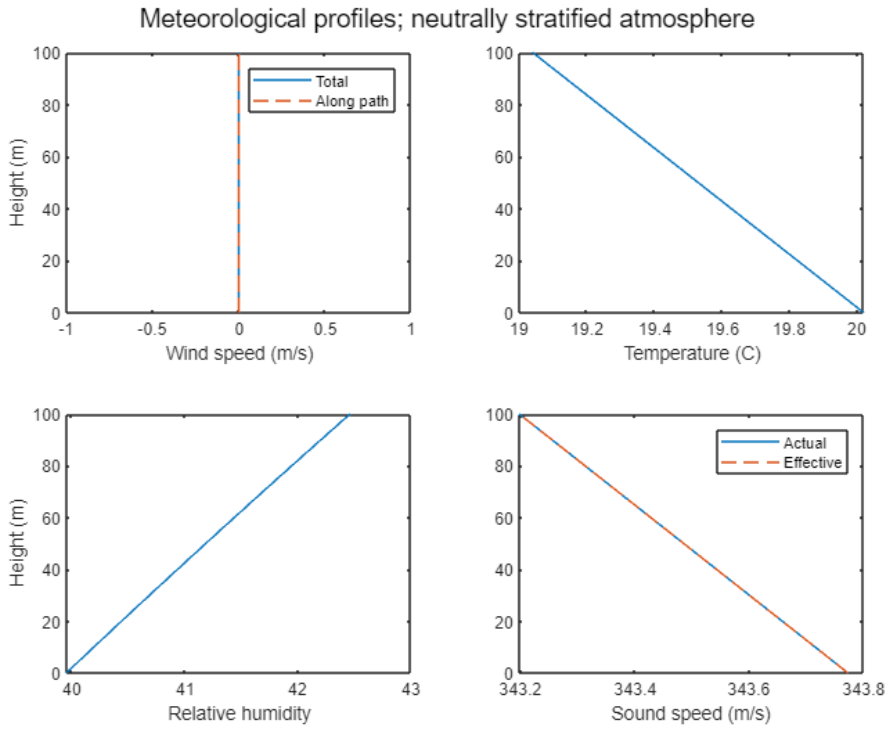

Figure 67- Atmospheric profiles for neutrally stratified atmosphere.

3.6.3.2 Neutral Boundary Layer

For the remaining meteorological classes both low and high wind scenarios are presented. In the case of a neutral boundary layer, the comparison can be made between up and downwind propagation, represented by the positive and negative range on Figure 67 respectively, and in the remaining PE figures in this analysis. The magnitude of the wind effect can be shown by comparing the low and high wind cases. The atmospheric profiles for the low and high wind cases of a neutral boundary layer are similar in that the only physical parameter that differs is the wind speed, as shown in **Error! Reference source not found.**. Overall, the effect is a small shift of the speed of sound at ground level near the source, and a change to its vertical structure. Of course, ignoring that bidirectional simulations have been made for now, in the positive x directions in this case there is wind blowing in the direction towards a receiver. Therefore, the effective sound speed increases gradually in both neutral cases. However, in the case of the low wind, the temperature profile, which is the same as neutral stratification with a constant decrease with altitude according to the dry adiabatic lapse rate (0.98 °C/100 m), dominates the effect on sound speed at higher altitudes when the wind speed starts to

increase linearly rather than logarithmically. The effect is a slight decrease in sound speed (of a few tenths of metres per second) from around 50m above ground. Whereas for the high wind speed case, the magnitude of the wind speed and its profile shape is enough to overcome the decreasing effect on sound speed from the temperature profile, and hence the sound speed continues increasing, though linearly from around 50m above ground.

These differences are translated to the differences in sound propagation seen in both cases from the PE model. In the upwind direction (negative range), the shadow zone is moved closer to the source for the high wind case. Downwind, the transmission loss decreases less rapidly compared to the neutrally stratified atmosphere, due to downward refraction, and the effect is more prominent for propagation over an acoustically hard boundary, as is the case for concrete compared to snow. Transmission loss on the order of approximately 30 dB and 90 dB respectively for concrete and snow is found 4 km and onwards from the source.

Also downwind during the low wind case, much of the energy propagating from the source at relatively high angle is refracted upwards. When high winds are present, the effect on the ray trace is a long-distance enhancement at approximately 5 km.

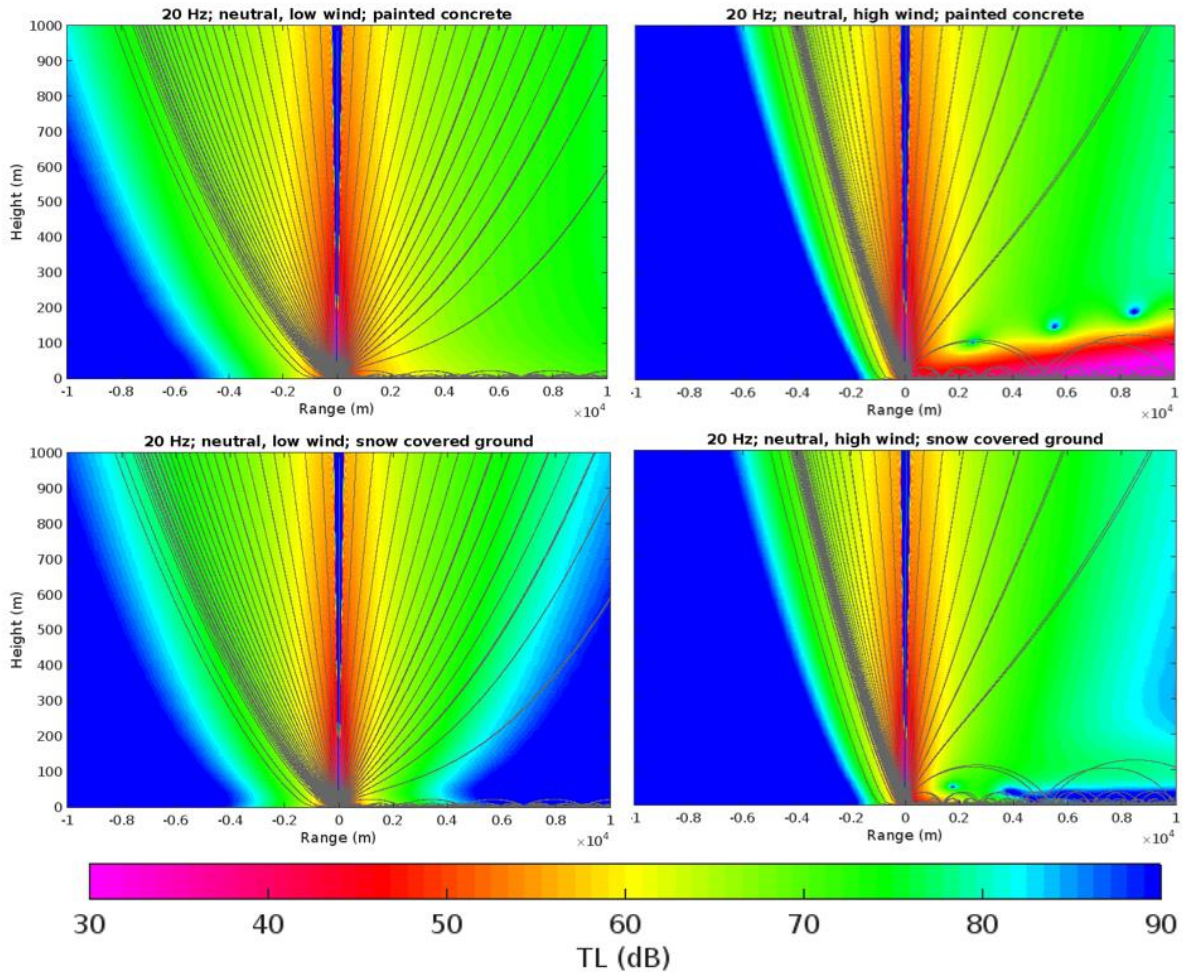

Figure 68 - PE simulations of neutral propagation scenarios, including low wind (left panels) and high wind (right panels), over two contrasting ground surfaces; concrete (top panels) and snow (bottom panels).

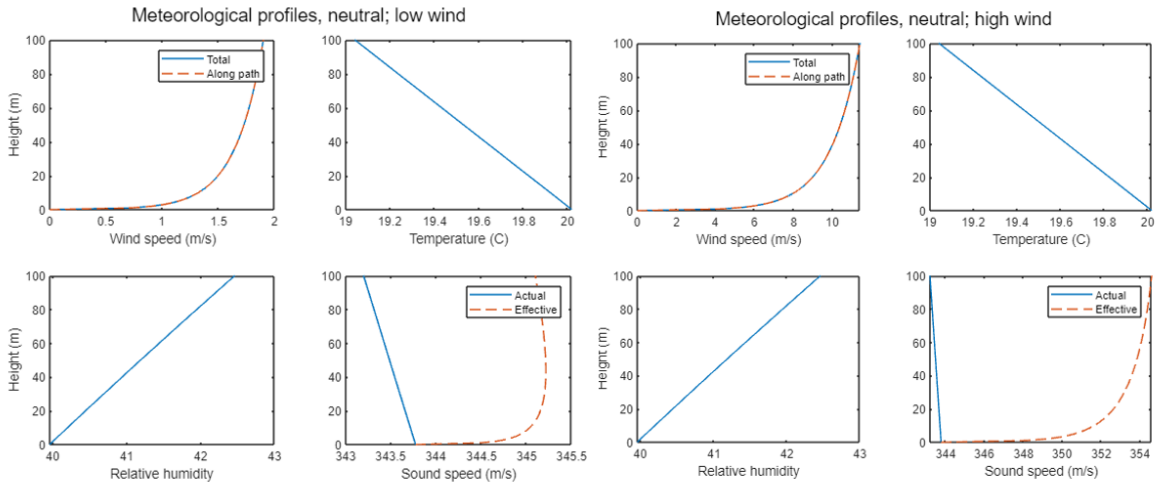

Figure 69 - Meteorological profiles for the neutral propagation conditions.

3.6.3.3 Unstable Boundary Layer

Atmospheric instability increases transmission loss significantly at long range, especially in the case of low wind. This is portrayed in Figure 70. The low wind unstable case is similar to that of the neutrally stratified atmosphere, since temperature is the dominant factor in refraction. The mechanism for this is seen clearly in the temperature, wind and sound speed profiles for the low wind unstable boundary layer case, where the sound speed profile approximately traces the shape of the temperature profile. This is to be expected, where strong thermal heating of the ground is typical of an unstable boundary layer and the adiabatic lapse rate is no longer the case near the ground. The profile decreases rapidly at low altitude before changing to decrease linearly from around 20 m above ground as per the adiabatic lapse rate. Again the temperature dominates the sound speed profile, and even in the high wind case, the sound profile is essentially shifted in magnitude slightly, but still is dominated by the temperature profile higher up.

The dominant effect on sound propagation is upward refraction, particularly for the low wind condition, which yields an equal transmission loss in both directions, with the negative x direction being marginally larger. This scenario is therefore a relatively desirable case for managing noise impacts, when considering that there is increased transmission loss both up and downwind. With no downward refracted energy (according to the ray model) for the low wind case.

For the high wind case, this bidirectional effect is weakened by downward refraction (in the positive x direction), significantly reducing transmission loss at long range. Transmission loss is significantly lower over concrete than snow, though less so for the propagation over concrete in a neutral boundary layer, though this is due to some of the source energy that is propagated at relatively low angle being refracted upwards from the strong thermal effects.

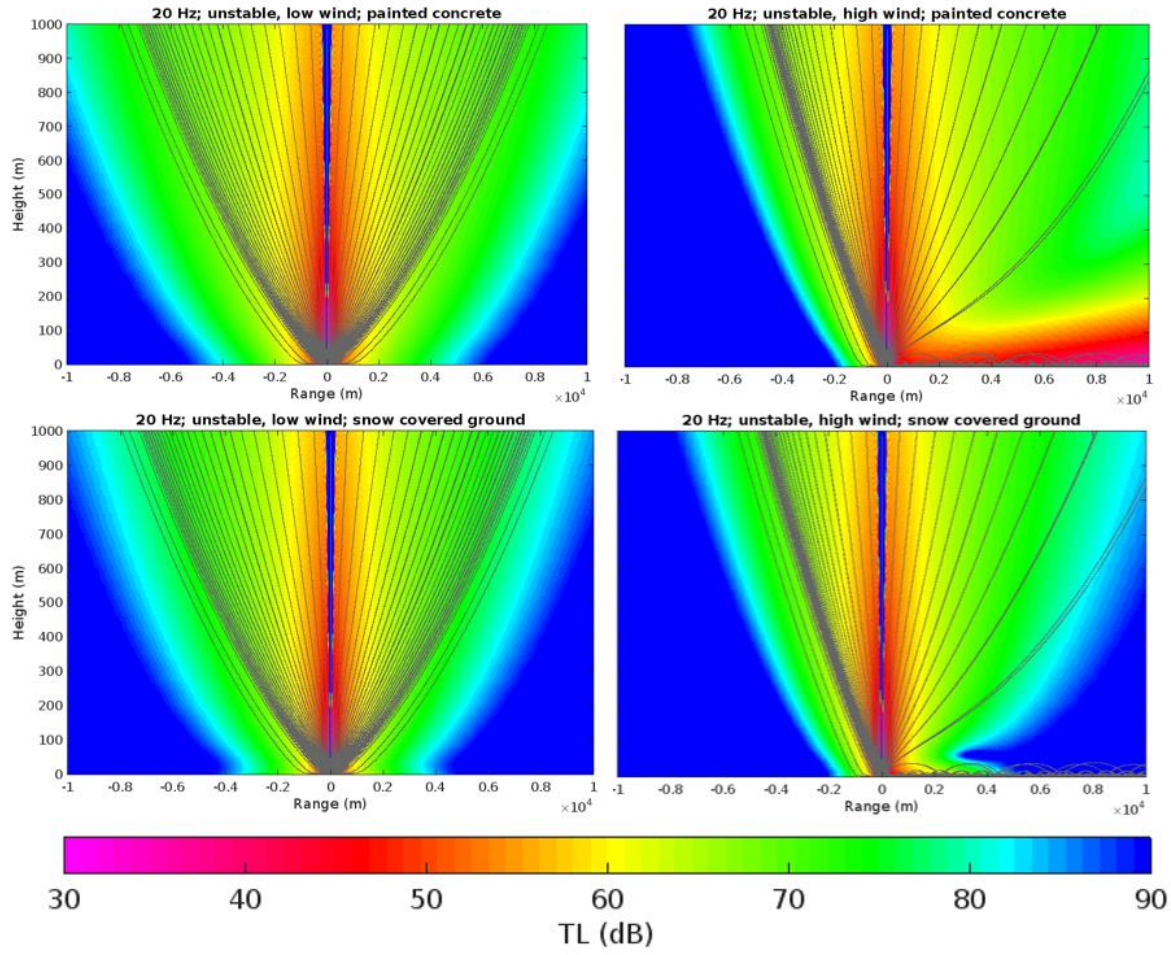

Figure 70 - PE simulations of unstable propagation scenarios, including low wind (left panels) and high wind (right panels), over two contrasting ground surfaces; concrete (top panels) and snow (bottom panels).

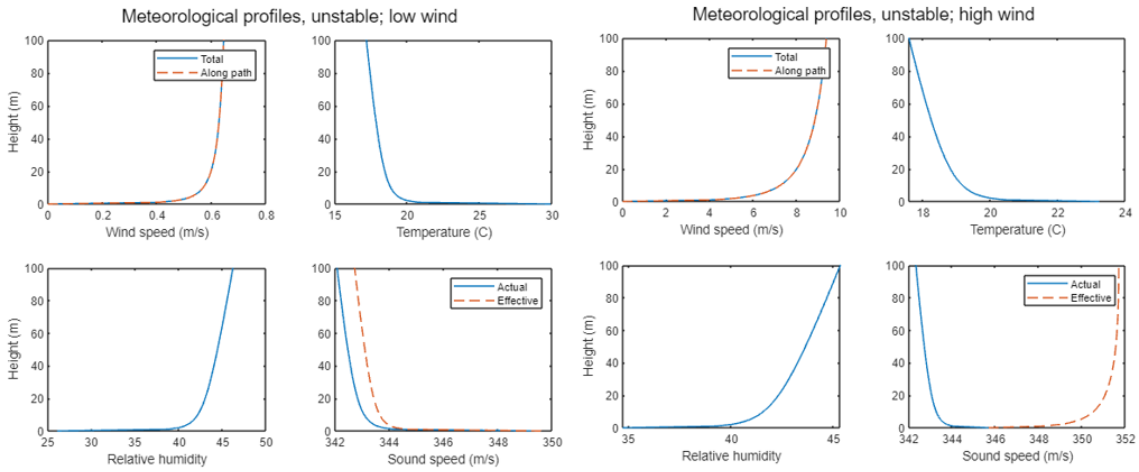

Figure 71 - Atmospheric profiles for the unstable propagation conditions.

3.6.3.4 Stable Boundary Layer

The stable boundary layer produces the most visually interesting effects in the PE plots in Figure 72. The meteorological profiles are the cause of these effects, since the stable case differs from the neutral and unstable scenarios, particularly in respect of the temperature profile, which increases with rapidly with altitude for the first few metres above ground, a typical characteristic of a highly stable atmosphere. The low wind case has a decrease in the positive gradient of the temperature profile, but nonetheless continues to increase linearly with altitude. On the other hand, the high wind cases illustrate a key characteristic of stable boundary layers in the form of a temperature inversion, where the temperature profile initially increases and then decreases with altitude. The effects of this are clearest on the 'actual' (adiabatic) sound speed of Figure 73, which does not include the effects of the wind. In the high wind case, the adiabatic sound speed decays slightly with altitude after reaching some maximum in the first few metres.

In both low and high wind cases however, the combination of the temperature and wind profiles cause the sound speed to increase with altitude, with a rapid increase in the first 10 m in the high wind case, before the positive gradient decreases to a linear relationship from around 40 m.

While the effects on propagation for the low wind case include some long-distance enhancements, the dominant feature is a complex interference pattern, particularly for the case above concrete where the ground reflection is greater. In the case of high wind, there is significantly lower transmission loss in the positive x direction, as compared to the low wind case, with also with long-distance enhancements. A similar meteorological scenario is modelled by Keith Attenborough et al. (1995), who simplified the case of a temperature inversion by assuming linear segments of increasing and decreasing arbitrary sound speed. They also note this effect at low frequency (10 Hz), though their analysis also compared the effect for 100 Hz and 1000 Hz.

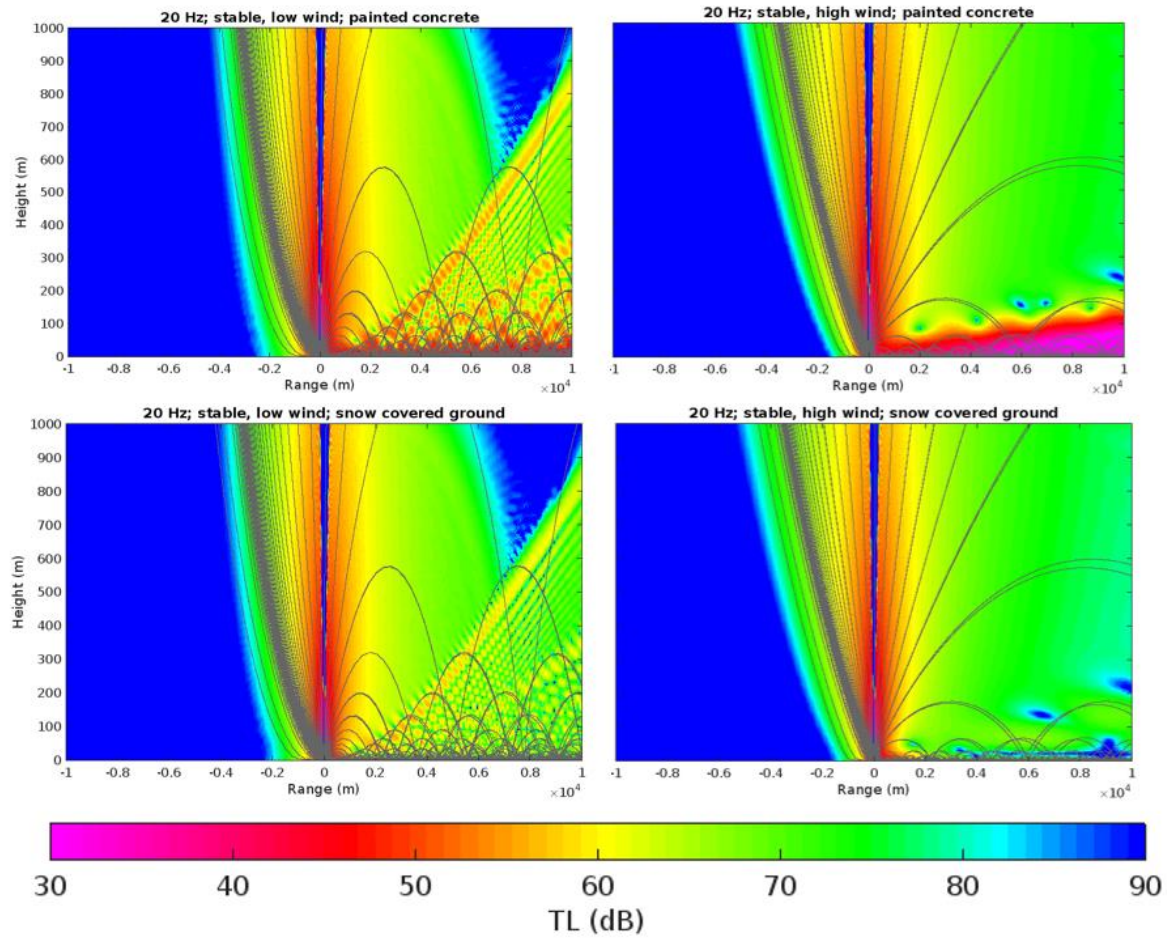

Figure 72 - PE simulations of stable scenarios, including low wind (left panels) and high wind (right panels), over two contrasting ground surfaces; concrete (top panels) and snow (bottom panels).

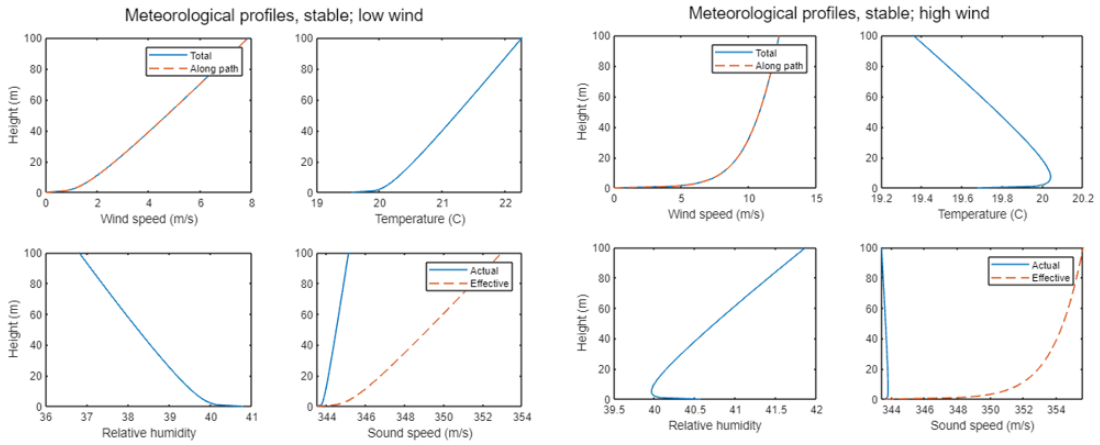

Figure 73 - Atmospheric profiles for the stable propagation conditions.

3.6.4 Conclusions from PE modelling

In this section, the effects of different propagation scenarios on long-range sound propagation relevant to blast noise have been presented using computer simulation. The parabolic equation model combined with a ray tracer is a useful tool for illustrating the general behaviour of atmospheric effects on sound propagation for the dominant frequencies relevant to typical blasts at Spadeadam.

Although using simple representations of propagation schemes by generalising across boundary layer types, as well as not included range-dependent meteorology or ground impedance, the PE models have successfully demonstrated that transmission loss can vary significantly at long-range. In particular, transmission loss at long-distance receptors over hard ground, is significantly less than for a soft ground such as snow.

The determining factor on transmission loss, and thus noise impact is the propagation scenario, which is governed by the sound speed profile in the lower atmosphere, which in turn is controlled and modified by the wind and temperature profiles. Unstable boundary layers, particularly low wind varieties yield particularly high transmission loss at long range, due to the effects of the strong temperature lapse and decreasing sound speed with altitude. Conversely, the stable atmospheres presented here show low transmission loss for the high wind speed case, and this effect is amplified over a hard boundary.

This is applicable to real-world blast noise management, particular for DNV Spadeadam, where the 3 latter propagation scenarios are relevant, as well as the ground types included in this analysis.

3.7 Summary of Literature Review on Long-Range Blast Noise

To summarise these chapters, a review of the physical mechanisms that dominate sound propagation relevant to blast waves at Spadeadam has been carried out. Although, an appreciation of all effects is of importance, where each effect in isolation can influence sound pressure levels at a receiver, some phenomena dominate. Most notably, wind (see Section 3.2). Wind direction is by far the most influential on the magnitude of peak sound pressure level at a receiver point around Spadeadam. Following this is the wind speed, which governs the depth of a shadow zone upwind of the sound source and the magnitude of the downward refraction to receivers downwind, ultimately determining the locations where focusing and enhancements will be. Temperature gradients are important to consider but will be dominated by wind. Therefore, focus on temperature gradients should be noted when they act in isolation (negligible wind), for example, during early morning test periods, when the ABL is more stably stratified, compared to the ABL at other times of the day when tests could occur.

A review of the prediction models and their relevance to blasts at Spadeadam has been carried out. This section concluded that although PE models are the most accurate, the data needed to make predictions is vast. Although, improvements to computation speed have been made, the fact that blasts occupy such a temporal fraction of a rapidly fluctuating propagation medium, mean that the nuances of the meteorology and range of possible peak levels are swept up in the time averaged data, which is what happens with the MONET. Heuristic methods for Spadeadam have been shown to be at least as accurate as MONET in a previous study, and much more accurate than ray-tracing models (LSM) developed at other sites. Even against the well-established SSW heuristic model (based on refinement from over 1000 measurements), the Spadeadam heuristic model performs well.

To improve this review, one could obtain a qualitative understanding of how a blast interacts with the hills and range of ground impedances around Spadeadam under a number of meteorological (refraction) cases. Such an understanding can be obtained using analytical solutions like ray-tracing but should also be aided by the deployment of a multi-component noise monitoring system, so that the range of expected SPLs at receiver positions can be established over a wide-range of conditions.

The literature review has been extended to include the relevant legislative guidance on environmental noise related to blasts, as well as the non-acoustic factors associated with

community response. The latest research on blast noise control has been presented and simulations of propagation and terrain effects have been carried out to inform this literature review on the important propagation factors for predicting blast noise.

4 Methodology

4.1 Introduction

The purpose of this chapter is to present the methodological techniques necessary to analyse and make meaningful conclusions about the environmental impacts of blast noise from DNV Spadeadam.

Firstly, strategies for the management of noise impacts at DNV are presented in 4.2. These include procedures used to manage and record complaints, current prediction strategies and community engagement. This section is concerned with the management aspect of blast noise impacts from DNV Spadeadam.

In 4.3, the system at the core of the project, the Live Noise Monitoring System, is introduced. This tool has two integral parts, the Intelligent Noise Monitors (INMs) used to collect acoustic data, and the Live Knowledge Database (LKD) used to organise and collect metadata associated with each noise producing test event. Some results from an the initial phase of these monitors is presented, along with a brief pilot study prior to the main monitoring window.

Subchapter 4.4 presents the technical methods used to collate the noise, meteorological and associated test meta data.

This chapter closes with the techniques used to analyse the acoustic data collected by the INMs and stored in the LKD, and presents the statistical analyses carried out for the development of heuristic blast noise models.

4.2 Blast Noise Management Procedures

The management of blast noise impacts on sensitive communities is as important if not more important than the accurate prediction of noise levels at specific locations. This is because of the complex non-acoustic factors related to the human response to impulsive noise which currently cannot be adequately represented in any prediction methods.

Management of blast noise is concerned with the technical and procedural techniques used to minimise adverse impacts on the community from blast testing as much as possible. This is achieved through a combination of procedures for managing community expectations and

complaints, ensuring prediction is carried out as best as possible, and investigating the feasibility of unique and large explosion trials.

4.2.1 Complaints Procedure

At the beginning of this PhD project, a dedicated and centralised procedure for the recording and management of community complaints related to blast noise was not present at DNV Spadeadam. A centralised and transparent complaints recording system has been developed as part of this PhD. The complaints system allows cross-referencing of some measured acoustical data, meteorological data and complainant comments, for receptors where noise measurements were taken at the time of complaints.

Additionally, the complaints procedure promotes community engagement, through communication between the site and members of the public.

An example of a complaint questionnaire is shown in Figure 74.

Blast Noise Complaint Template

DNV Spadeadam: Blast Noise Prediction and Management

In the event of a complaint, the following information should be logged.

Complainant Information

1. **Name of complainant:** _____
2. **Address:** _____
3. **Telephone number:** _____
4. **Email address:** _____
5. **Preferred communication method:** phone/email
6. **Date complaint received:** _____
7. **Time complaint received:** _____
8. **At the time of the incident, were they: outside or inside the property?** __ _____
9. **If inside, whereabouts in the house?** _____
10. **How many floors does the house have? (Ground floor is 0):** _____
11. **Did they feel the blast?** _____
12. **Did they hear the blast?** _____
13. **Did the house make sounds?** _____
14. **Time of the noise event to the minute if possible:** _____
15. **A short description of the event, including perceived feelings and sound descriptions:**__ _____ _____ _____
16. **Any other remarks**:

Test Information

1. **Date of test:** _____
2. **Time of test:** _____
3. **Type of test (EDH/Explosion Chamber, etc.):** _____
4. **Location of test:** _____
5. **Project/test operative (if necessary):** _____
6. **Any other information:** _____

Figure 74 - Community noise complaint template.

4.2.2 Predictions for Small Tests

For the majority of small explosion tests (with TNT equivalences of <25kg TNT), predictions are currently made using a number of heuristic methods, such as the EDH NIP decision tree method described later in this subchapter.

Generally, small gas explosions commonly associated with hazard awareness courses on-site do not require particular attention to their prediction, though these have been recorded using the monitoring scheme, and heuristic models for their prediction has been evaluated.

Other than EDH operations (which are referred to by the site as small tests), DNV are mostly concerned with accurately predicting long-range impacts from large explosions.

4.2.3 Predictions Large Tests

As mentioned throughout this PhD, DNV receives long-range noise predictions of large explosions from the Met Office's MONET package. The MONET package has been technically reviewed within the literature review of this part of the thesis. Furthermore, DNV now receives predictions using the new updated versions of MONET - SoundWave.

4.2.4 Feasibility Studies

In January 2023, a feasibility study for a 1000kg TNT equivalent explosion was completed. The study was necessary, although DNV are licensed to carry out explosive trials up to 1000kg at Spadeadam, such a trial has never been completed, with 500kg TNT being the largest carried out since the beginning of this PhD project.

The feasibility study concerned the management of both occupational noise impacts and environmental noise impacts.

The legislation and guidance detailed in section Chapter 3.5 was used to inform on the impacts such a trial would have on occupational noise for DNV site and RAF personnel.

In order to attempt to quantify the noise impacts at long-range and on sensitive communities for a 1000kg TNT trial, a small climatological study was performed in collaboration with the Met Office, using MONET.

The following propagation scenarios were used in the study in order to replicate best and worst-case conditions.

Table 48 - Propagation cases used in the 1000kg TNT Feasibility Study

Propagation Case	**Description**
Case 1: Standard Atmosphere	Standard atmosphere forecast for you to get a flavour as to the noise propagation of 1000 KG when there is no wind shear or

	temperature inversions
Case 2: Light and unstable	Light winds with no inversion/slightly unstable
Case 3: Stable surface inversion-typical of early morning with light N winds	Light winds from the north with a surface inversion (typical of diurnal cooling overnight and therefore an early morning/late PM profile)
Case 4: Stable surface inversion-typical of early morning with light S winds	Light winds from the south with a surface inversion (typical of diurnal cooling overnight and therefore an early morning/late PM profile)
Case 5: Strongly Unstable with winds from North	S/SSW winds as high wind shear, N propagating example
Case 6: Strongly Unstable with winds from South	Inverted S/SSW winds as high wind shear, S propagating example

Analysis of the distribution of noise impacts across a large number of receptor positions up to MONET's 30km limit was carried out. The analysis showed that the most favourable propagation scenarios were:

- Case 1: Standard Atmosphere
- Case 2: Light and unstable
- Case 4: Stable surface inversion, typical of early morning with light S winds (<7kts or 3.6ms-1)
- Case 6: Strongly Unstable with winds from South (20kts or 10.3 ms-1)

Met Office meteorologists were consulted for the quantitative definitions of these cases. In reality, case 1 is an unrealistic propagation scenario, and was used in the analysis as a baseline. Case 2 involved light winds with no clear direction and an unstable atmospheric boundary layer, often associated with warm, sunny days. Case 4 is likely to occur during the early morning, with colder air trapped near the surface by warmer air above, with light winds

blowing from the south. Case 6 involves strong winds from the south with a strong temperature lapse.

These cases were favourable for their northerly propagation due to the comparative lack of residential receptors to the north of the Spadeadam site, compared to the south. The noise footprint for case 6 is shown in Figure 75.

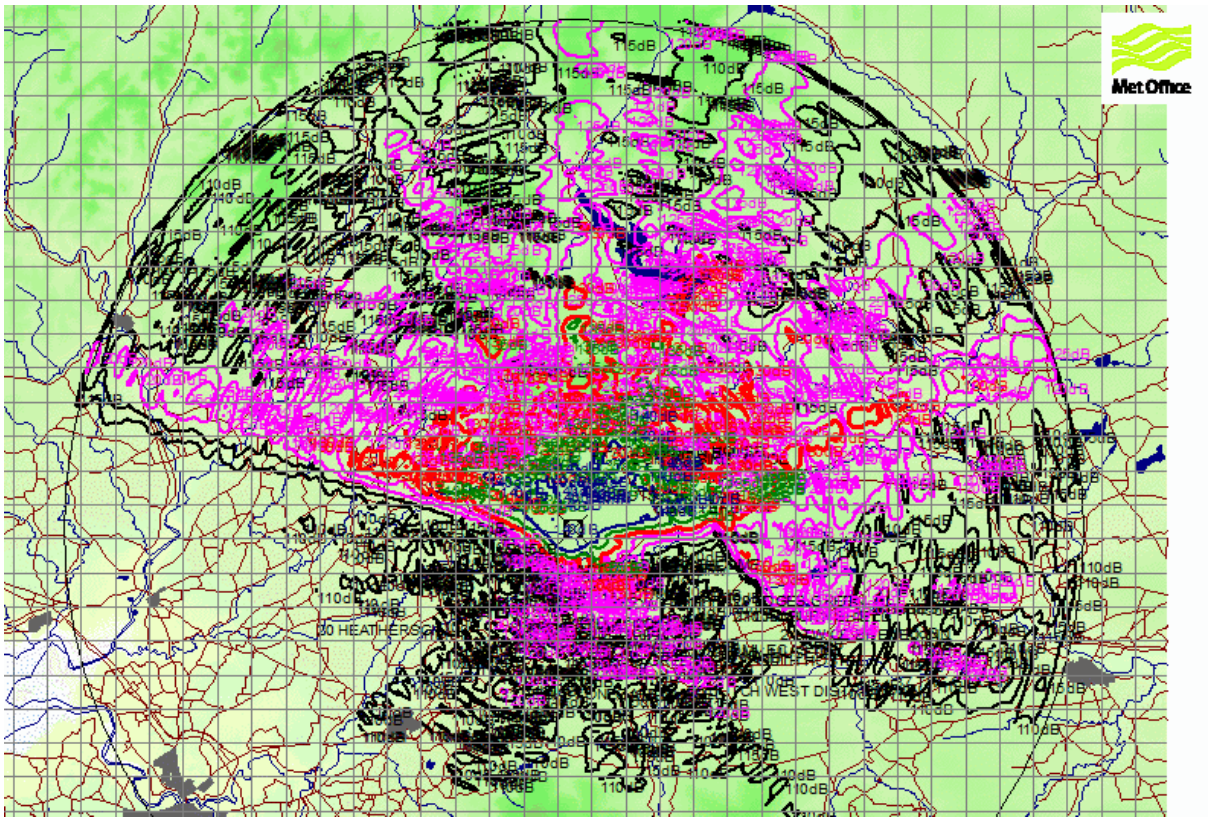

Figure 75 - MONET noise footprint showing propagation case 6: Strongly unstable with winds from the South.

The worst-case scenarios were expected during the following conditions:

- Case 3: Stable surface inversion, typical of early morning, light N
- Case 5: Strong Unstable N

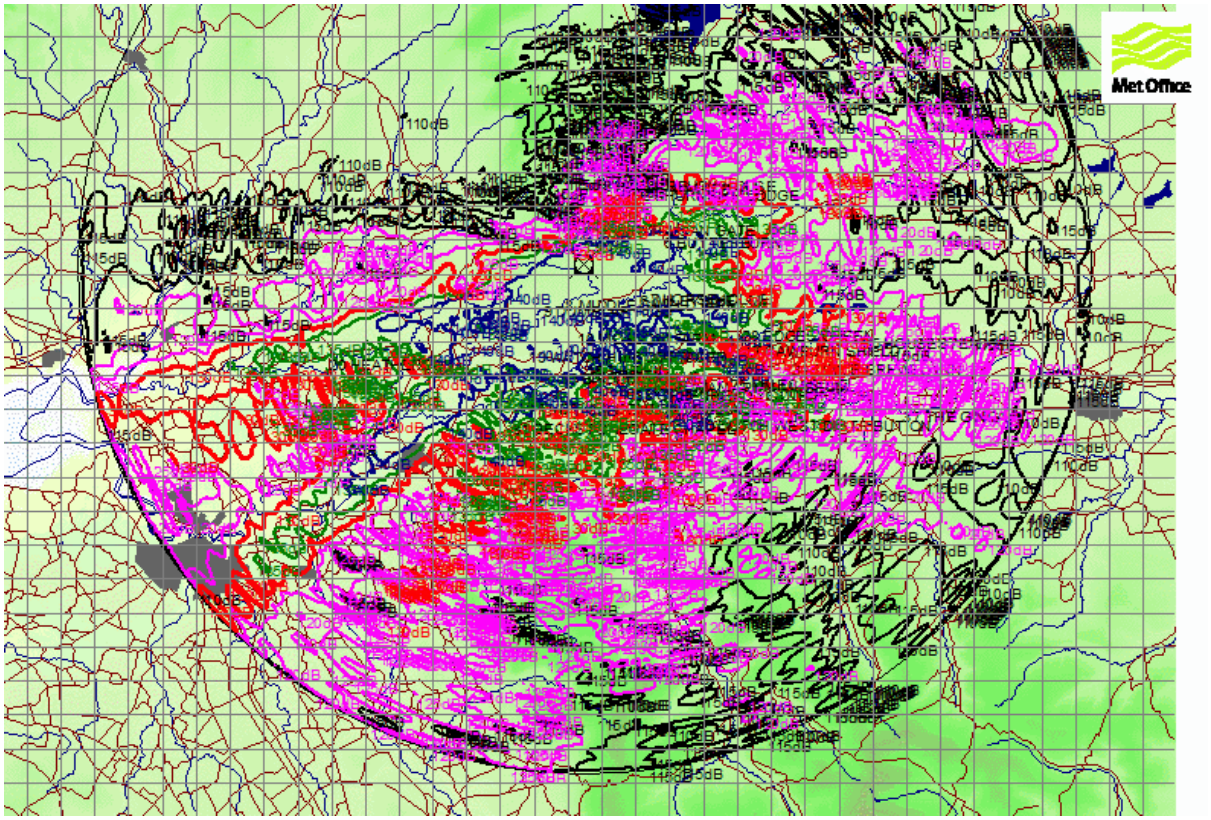

Figure 76 - MONET noise footprint showing propagation case 3: Stable surface inversion – typical of early morning with light winds from the North.

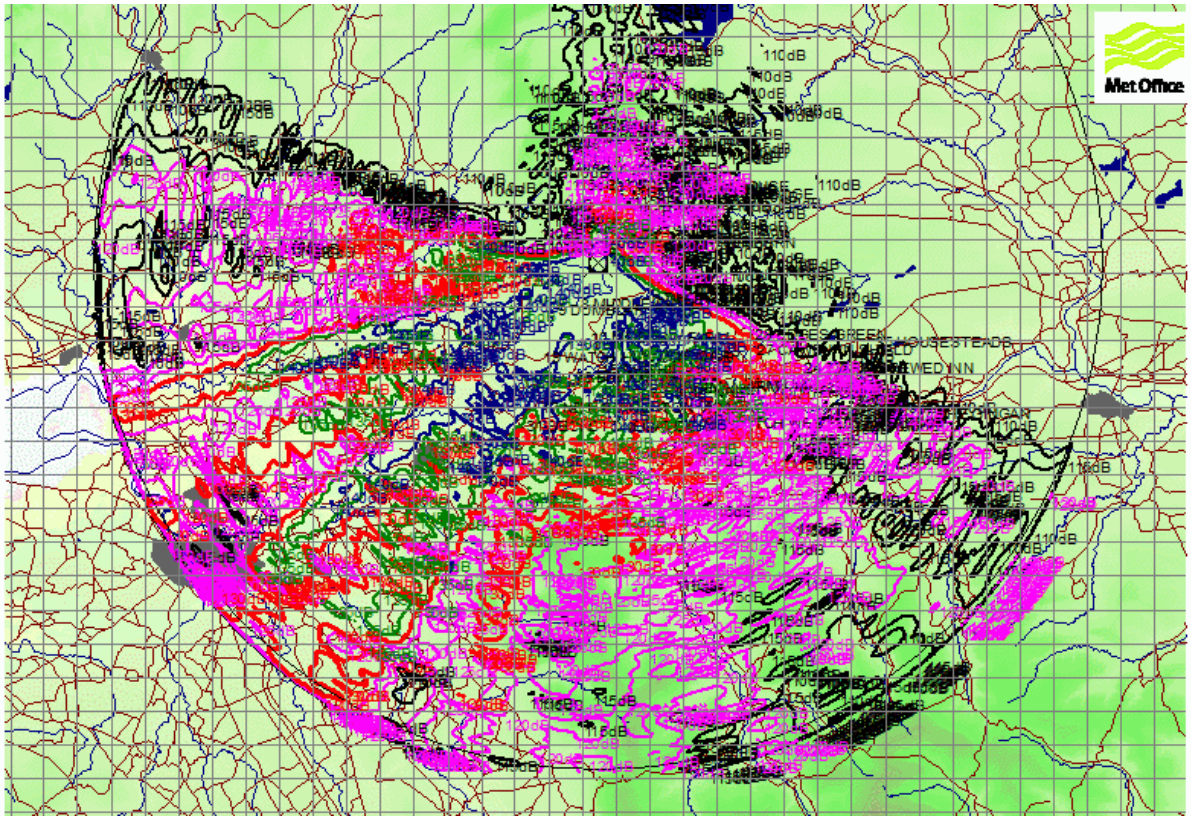

Figure 77 - MONET noise footprint showing propagation case 5: Strongly unstable with winds from the North.

An analysis of average weather conditions at Spadeadam using measured data across 10 years was carried out. This was required to investigate whether particular propagation scenarios could be attributed to seasonality and to deduce the likelihood of the most favourable propagation scenario. This analysis is described in more detail in Chapter 5.1.

The feasibility study concluded that the trial may only be feasible under specific meteorological conditions. Such conditions were restricted by wind direction, which was warm days where strong winds blow from the south.

4.2.5 Other Procedures

Another example of a new management procedure introduced at Spadeadam throughout this PhD project is the procedure related to managing impacts from Explosive Depth Hardening (EDH) operations. This procedure is called the EDH Noise Impact Procedure (NIP).

Following the implementation of the complaint procedure, a number of complaints recorded were attributed to EDH test events. Given that the majority of complaints related to

disturbances from this test in particular, EDH was identified as a potentially problematic activity.

Through the recording infrastructure put in place by the Live Noise Monitoring System (discussed in chapter 4.3, EDH was indeed identified as a problematic test activity. The combined effects of the number of noise events within a given test window, and considerable peak SPL measurements recorded at long-distance monitoring distance are a likely influence on the number of complaints attributed to this source.

As a consequence, the *EDH Management Procedure*, proposes the following:

1. Improved communication between DNV and the client specifically on the number of tests expected to be carried out per week
2. Dedicated prediction of EDH operations as early as possible, up to a few hours before testing
3. Dedicated communication of test activity to sensitive members of the public that are likely to be at risk of adverse noise impacts from EDH operations

Item 1 is an essential part of the procedure in that it allows DNV to plan test windows and de-conflict activity with other on-site activity and also RAF activity. Improved communication aids 2 also, in that DNV can estimate the size of the charges set on the EDH test fixtures in advance, which is essential for adequately predicting the propagation of sound over long-range for this source.

The prediction of EDH began as soon as a number of complaints relating to the activity began before any permanent recording infrastructure was put in place. Some manual recordings were made at complainant locations under a number of conditions, and it was determined that impacts from EDH should be predicted in advance in order to avoid adverse reactions from the community and exceedance of site noise limits at nearby publicly accessible locations beyond the site boundary.

Until a database of measurements could be collated on EDH exposures, a simple heuristic method was used to make operational decisions on test activity and to communicate test activity with residents in specific geographic areas. This method is detailed in Figure 78.

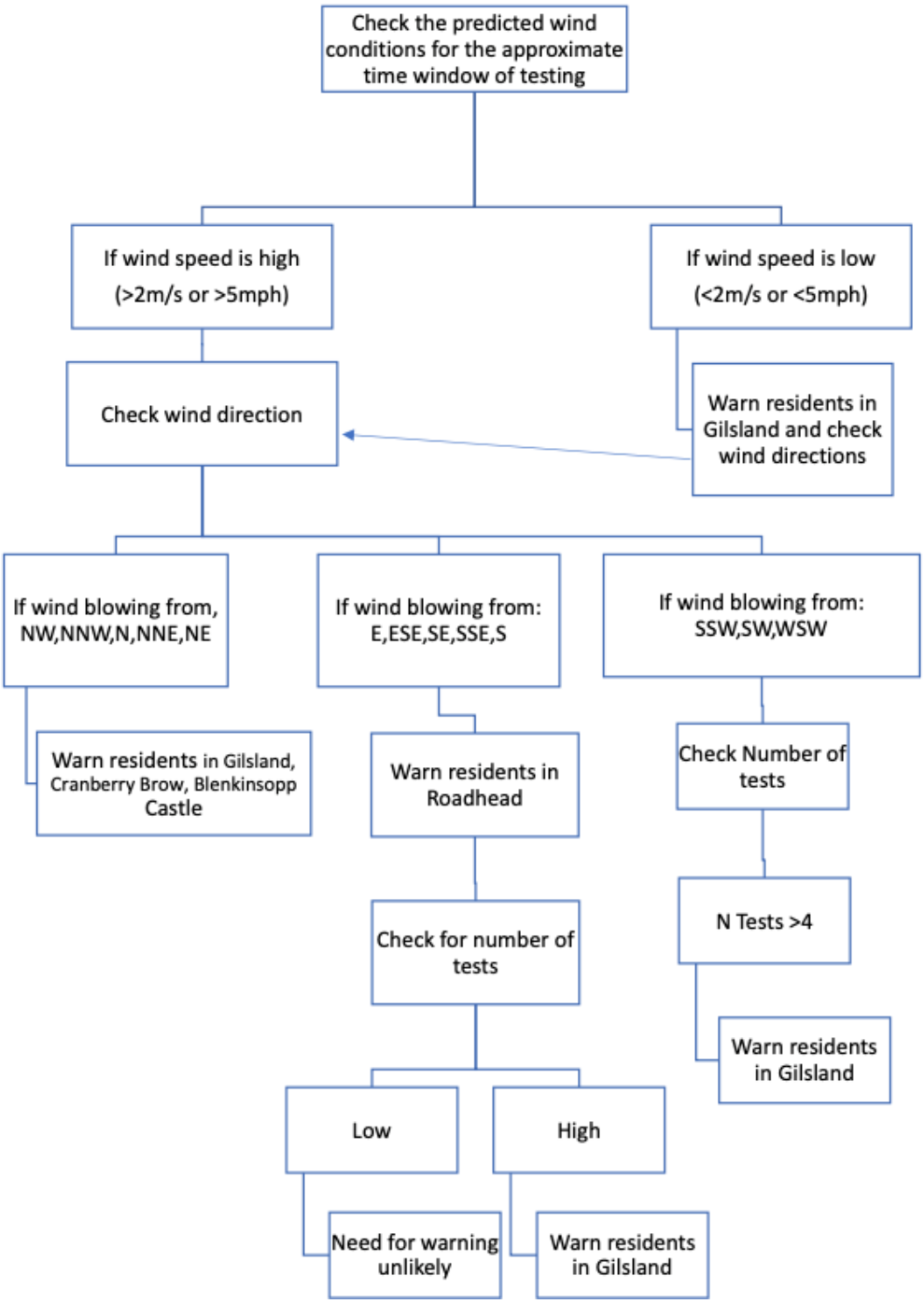

Figure 78 - Decision tree for the management of environmental noise impacts from EDH operations.

Finally, the EDH NIP requires that contingency days are used where noise impacts are expected to exceed the site boundary limits or cause adverse impacts to a number of receptors. This results in test cancellation and postponement to another day and the following criteria are used to determine this.

- excessive peak noise levels (>120dB) are expected at a significant number of off-site properties;
- and/or potentially harmful peak noise levels (>125dB) are expected at any off-site property

Until a dedicated prediction model was developed for the EDH operations (discussed later in this thesis), the EDH decision tree was used to make operational decisions.

4.2.6 Community Engagement

An extremely important factor in the successful management of environmental blast noise impacts is community engagement. Clause 8.6.9 of BS 5228-1:2009 advises that for impulsive noise related to industrial activities, a good relationship between the operator and the community is necessary. This British standard also local residents should be given notice of the test program with specific blasting times, and given updates should there be any deviation from the program.

Since the beginning of this research program, a dedicated community engagement program between DNV has been put in place, which includes an automated notice system and meetings with the local parish councils.

4.2.6.1 Automated Notification System

This PhD project is responsible for the implementation of an automated communication channel between DNV and members of the public. The system communicates information on test activity and the likelihood and severity of adverse noise impacts throughout the day, with specific timings if possible.

The system uses a third-party system, Alert Cascade, to send email, voice, or text messages to users according to their preferences. Such a system, although simple, is extremely important as a foundation of blast noise management infrastructure. This is because it requires a control operative at the DNV Spadeadam site to collate information on testing

activity throughout the day and the week ahead. This streamlines test information into a centralised place which enables the future automation of noise predictions for all test types.

Another important detail of the automated notification system is that it provides security to members of the public for personal information, such as addresses, contact details, etc. The system is also in line with communication infrastructure used at other UK testing ranges, for example at MOD Shoeburyness.

4.2.6.2 Meetings with Local Parish Councils

Finally, it is important to mention that since the beginning of this PhD project, meetings have taken place between the research, key staff at DNV, and members of the local parish council, namely the Gilsland Parish Council.

Such meetings are important for the exchange of information between both relevant to environmental noise impacts. Such a meeting was held on-site on 11th January.

The meeting provided allowed communication from DNV to the parish council on a number of things relevant to this research that the public should be aware of:

- The deployment of the alert notification system.
- New residential and commercial developments in the local area.
- Developments to public spaces immediately surrounding or in the vicinity of the site boundary, including new footpaths and tracks as part of new cycling route initiatives.
- Opportunities for parish councillors to tour the site and understand the operational procedures carried out on site to mitigate and manage noise impacts.

The meeting produced actions including:

- Quarterly follow-up meetings.
- Specific components of the research submitted to the local newsletter and possible non-technical presentations given at local community centres.

4.3 Live Noise Monitoring System

4.3.1 Intelligent Noise Monitors (INM)

A key part of the Live Noise Monitoring System at implemented for DNV Spadeadam is the Intelligent Noise Monitors, produced by 24 Acoustics. INMs are Class 1 Sound Level Meters, conforming to the performance specification of BS EN 61627:2023. Each device is designed to work as an internet connect sound level meter, with its main function to measure noise levels remotely and transmit data back to a dedicated cloud page for display on a website.

4.3.1.1 Hardware

24 Acoustics' INMs are based on a Raspberry-Pi system and are contained within weatherproof cases as shown in Figure 79. The devices are powered by a supplied mains power cable and are designed to run optimally with mains power. However, they do contain a backup battery that can power a monitor for a few additional hours. Microphones are mounted on poles or tripods depending on the specific receptor.

Figure 79 - An example photo of an INM unit.

4.3.1.2 Microphone System

The noise monitors use a PCB Piezotronics 278B02 microphone system, consisting of a 377B02 1/3” microphone capsule and a 426E01 preamplifier.

Calibration is carried out with a B&K Type 4231 with 1/2" adapter installed, using a reference sound pressure level of 94 dB re 1 μPa at 1 kHz.

A windshield is attached to each microphone system to attenuate the effects of wind noise on the recordings.

4.3.1.3 Web Page

The dedicated webpage for the monitoring of live and archive measurements was developed by 24 Acoustics as part of the INM deployment. An example of the live and archived monitoring page is shown in Figure 80.

The key feature of the webpage is to display live peak sound pressure levels (Zpeak) at each monitoring location. These data are sent over a 4G network, where a live view of the latest Zpeak can be viewed, as well as a chart for the last few hours.

Additionally, archived data is stored for each monitor on the webpage, and more importantly, audio recordings associated with each measurements can be listened to. Furthermore, the audio recordings can be downloaded through webpage for analysis of the pressure-time history associated with each 1-minute logging period. Alternatively, these waveforms can be accessed through the USB storage on the device. Figure 81 shows this feature.

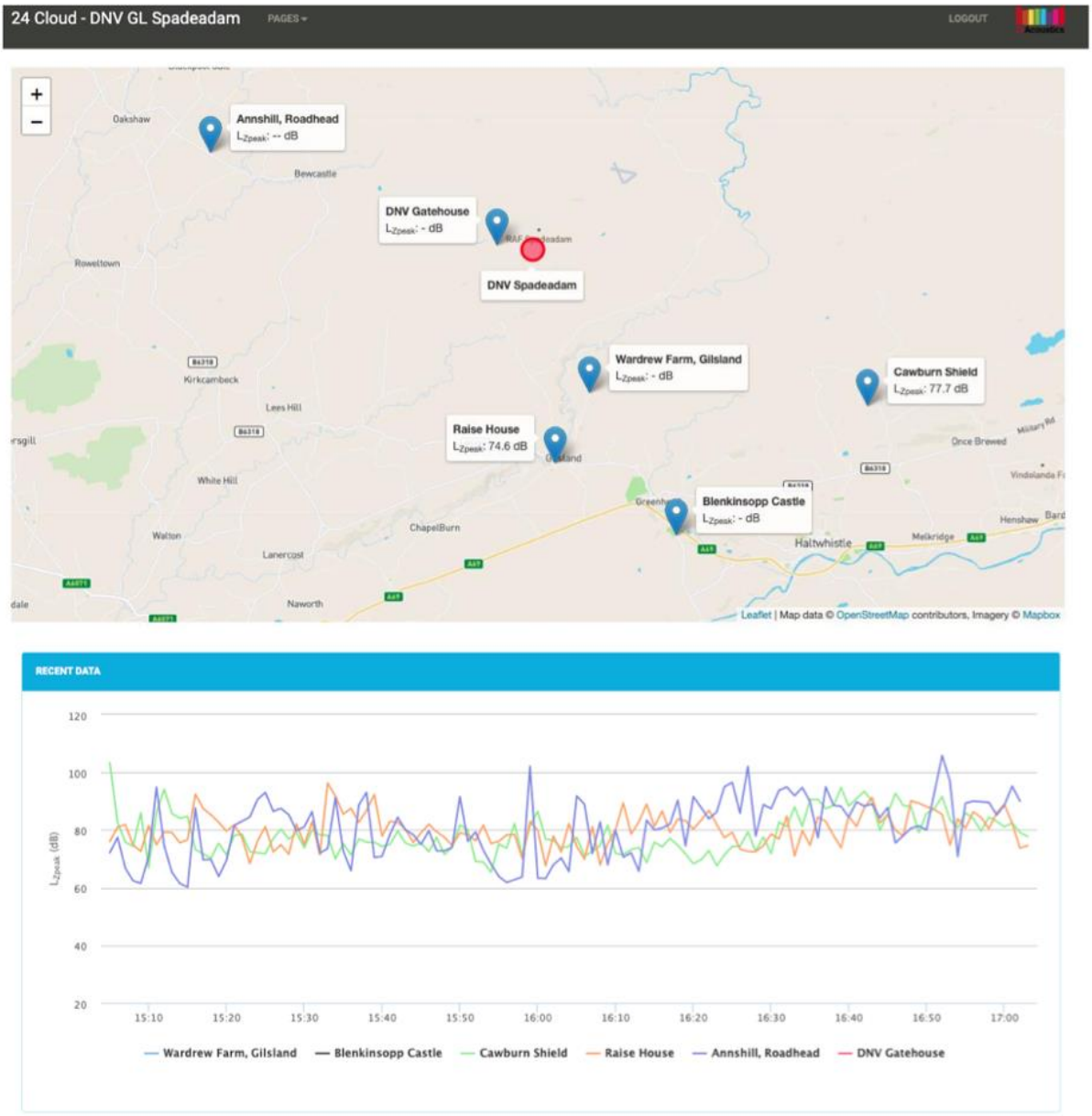

Figure 80 - 24 Cloud web page: Live view.

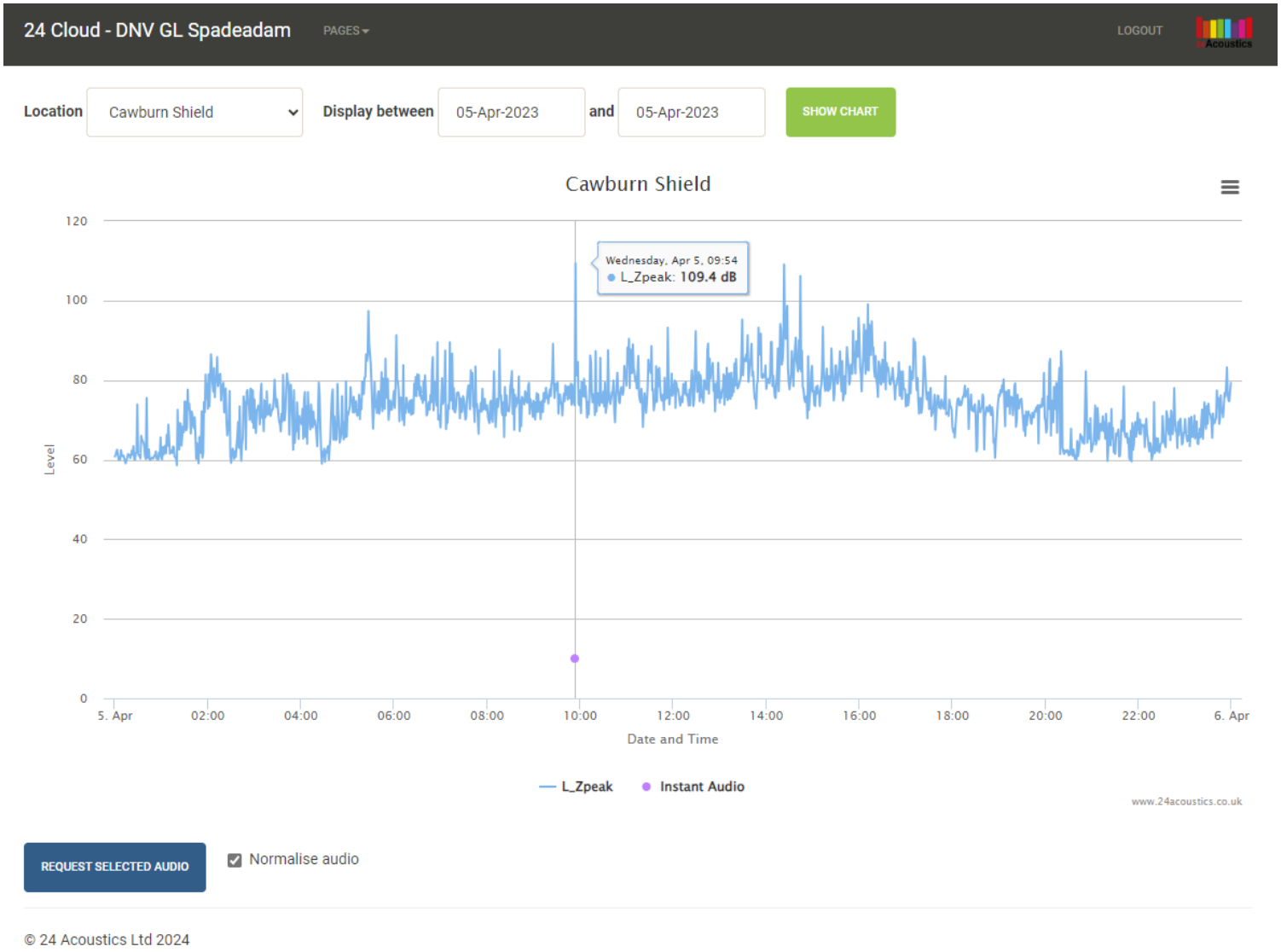

Figure 81 - 24 Cloud web page: Archive view

4.3.1.4 USB Storage

External USB storage is mounted in each system for the archiving of other acoustic indices and of audio files.

4.3.1.5 Justification for the selection of equipment

The University of Salford started working with DNV in January 2017 on a separate MSc project. As part of that stage of that project, the monitoring equipment used was provided by Acoustic1, suppliers of traditional advanced acoustic monitoring equipment. An outcome of that stage of the project was a formal proposal from Acoustic1 to DNV for the provision of the advanced acoustic monitoring equipment required to deliver the requirements of this PhD project. However, for four units, traditional advanced acoustic monitoring equipment was prohibitively expensive.

It was then clear that if this PhD iCASE funded by DNV was to proceed, alternative and more cost effective equipment would need to be developed and produced. Previous research by the University of Salford revealed two possibilities based on Raspberry Pi-type systems. Of just two options, 24 Acoustics had already developed and were regularly deploying and operating their system on a commercial basis and had the track record to guarantee long term delivery and support of such an innovative noise monitoring system. After a number of meetings between November 2018 and May 2020, it became clear that some modifications of their existing system would be required for this specific research at DNV. In summary, at the time of the project's conception, 24 Acoustics were the sole supplier that could provide the equipment needed to complete this PhD iCASE at the Spadeadam site within the budget that DNV are willing to invest.

4.3.1.6 Additional Instrumentation

On occasion, particularly before the procurement and deployment of the INMs, some receptors have measurements taken by other sound level meters. In particular, a Class 1 B&K 2250 Sound Level Meter was used. This instrumentation had was able to make measurements of greater peak sound pressures and was often favoured for receptors expected to be subject to the greatest noise impacts.

4.3.1.7 Monitoring Positions

The locations at which INMs were to be permanently deployed at was dependent upon several factors. They are listed below, in descending priority. The first four factors were

likely to affect the general area of monitoring on a wider scale, such as a particular location. Whereas the latter four were more likely to affect the specific monitoring position at a certain location, such as where the monitor was to be placed in relation to the property at a certain location.

a) Locations of frequent complainants
b) Known hotspots of potential high noise impacts
c) Availability of power options
d) Availability of mobile data signal
e) Suitability for measurements
f) Community engagement benefits

a) Firstly, there was a priority to monitor where the most frequent complainants were located. This was DNV Spadeadam's main priority, where several complainants had complained that their property was being damaged by DNV's activities.

b) Secondly, there was a need to monitor at known hotspots of high noise impacts, either based on the frequency and number of complaints from the area, known propagation influences (such as being downwind from prevailing weather) and experience of range controllers from previous measurements.

c) The availability of power was an important factor in the deployment of a permanent monitor. As most location required outdoor mains sockets to be installed to power the monitors, it was critical that electrical contractors could have access to power and that the operation of a mains socket was safe. As the outdoor socket at INM 143 Cranberry Brow, was not safe for use, an INM was not permanently sited at this locations. This is reflected in the much lower number of measurements at this location, which all had to be carried out either by manned survey methods with the B&K 2250, or by leaving an INM measure (unmanned) on the back-up batteries and collecting the equipment after testing.

d) Similarly, mobile data coverage was critical to the installation of a long-term monitor at a specific location. Given that the entire area consists of sparsely populated, rural Cumbria and Northumberland, mobile data was more often poor than not. At some locations, additional tests had to be made to assess the location suitability, which were critical to the successful implementation of a live noise monitoring network reliant upon connecting and uploading measurements and audio recordings to the dedicated 24 Cloud webpage in real-time.

e) The suitability of the location was important from the point of measurement quality. This factor is specific is relevant to the placement of the monitor and more importantly the microphone, around dwellings and other reflecting surfaces.

f) Finally, an important factor was the occupant at the property where monitoring was carried out. One obvious aspect is that the occupant had to be willing to host a monitor on their property for a long-term basis. This was difficult to achieve given that all permanent monitoring locations had negative perceptions or had previous negative experiences relating to noise impacts from DNV's activities. Each resident had unique willingness to host permanent monitors, for example, some may have been willing to host in order to obtain the measurements required to determine their specific claims. On the other hand, some residents understandably did not want to be inconvenienced by having to host recording equipment on their property, for which they could see no purpose.

Navigating each resident's specific needs involved developing a specific relationship between the researcher and resident on behalf of DNV as neighbours. Residents were always properly reimbursed for the cost of the electricity supplied to their monitor on a yearly basis. Furthermore, the monitor needed to be accessible by the researcher, for calibration and for downloading the data backed-up on the USB storage. Finally, one INM location (145 Raise House) situated on the outskirts of Gilsland was favoured over other more central locations in Gilsland because the occupant was the head of the local parish council. This was an important factor, meaning that the research could be communicated to a wider audience of concerned residents through this unique relationship between DNV and the parish council.

4.3.1.8 Distribution

INM monitoring positions are shown in Figure 82. Note there is a concentration of these positions to the east of the site. More specifically, the permanent monitoring positions (except INM 144) are concentrated in the East-South quadrant, INM 140 Wardrew Farm, INM 141 Blenkinsopp Castle, INM 142 High Close A Burn, INM 143 Cranberry Brow, INM 145 Raise House. These are supplemented by occasional monitoring positions Middleshields, Wyliesike, Butterburn and Churnsike. This distribution generally reflects the prevailing meteorological conditions at DNV Spadeadam, which is dominated by weather from the West.

INM 144 Annshill is the only permanent monitor located to the west of the site, against the prevailing conditions. This location was chosen specifically for the monitoring of noise levels following a several serious complaints to the site relating to noise impacts from DNV's activities, specifically relating to the management of horses at the property.

Figure 82 - Long-term Monitoring positions (generally INMs) shown with red pins, and supplementary occasional monitoring positions (usually manned surveys) shown by blue pins.

4.3.2 Live Knowledge Database (LKD)

The integrity of this research was dependent upon a robust record system in order to account for the number of variables associated with DNV's testing activities. A record system named as the 'Live Knowledge Database' (LKD), was developed at the beginning of the project as a centralised database of DNV's activities which have a potential noise impact at off-site receptors.

Microsoft Excel was used to share the LKD between the researcher at the University of Salford and range controllers at DNV Spadeadam. Records of testing are arranged as described in the following tables.

The LKD consists of a series of sheets used to capture information on the test activity at DNV Spadeadam. Within the LKD, a sheet known as 'INM_Log' records test information at the permanent INM locations, see Figure 82 with all associated data assigned to specific categories. These categories are shown in Table 50 - Test reference metadata.

Table 49 - Live Knowledge Base data collection categories.

Reference Metadata	Test Type Data	Measurement Data	Meteorological Data

The first category in Table 50 - Test reference metadata., the reference metadata, consists of the basic but critical information on each test event. Data collected in this category consists of a unique test identification reference code, and the date and time which the test was carried out on.

Table 50 - Test reference metadata.

Reference Metadata		
Test ID Number	Date	Time

The second category of the LKD consists of the Test Type Metadata, collecting information on the type of test carried out, its associated size, location on the site, and a brief description for collecting any additional information, e.g specific geometrical configurations at the source, client references etc.

Table 51 - Test type metadata.

Test Type Data			
Test Type (see Table 53 - Common impulsive noise generating test types carried out at DNV and their descriptions.)	TNT Equivalence (kg)	Test Location	Test Description

The acoustic data is captured in the Measurement Data Category, consisting of the Peak Sound Pressure Level (LPeakZ) associated with the test and also a signal condition. The

signal condition uses a code system to distinguish between valid and contaminated measurements, and some other information, specified in Table 58 - Measurement error handling and description codes.. Finally, this category record whether a member of the public has commented or complained for a given test, as specified in Table 59.

Within the INM_log worksheet, measurement data are captured for each of the active INMs that are deployed at the time of testing. A separate sheet is used to log the same information either for alternative locations such as temporary monitoring stations, or for complaints from members of the public at alternative locations to the INM locations. For some large tests (usually >30 kg TNT equivalence) a record of a MONET prediction is logged along with the measurement data.

Table 52 - Measurement data.

Measurement Data			
SPL Peak (dBZ)	Signal Condition (see Table 53 - Common impulsive noise generating test types carried out at DNV and their descriptions.	Record of Complaint (Table 59 - Complaint codes assigned to each test event.	MONET Prediction

Finally, the meteorological data and conditions associated with each test are recorded in the Meteorological Data category, with details on this category specified in Table 54.

Test Number	Test Date	Test Time	Test Type	TNT Equivalence (kg TNT)	Test Location	Test Description	LZpk at INM Location	Meteorological Conditions	Record of complaints
805	23/11/2022	10:46	Table 53	6	EDH Zone	EDH 6kg Rail Shot	116.1	Table 54	Table 59

Table 53 - Common impulsive noise generating test types carried out at DNV and their descriptions.

Test Type	**Full Name**	**Description**
EDH	Explosive Depth Hardening	Small-medium explosive process involving the

		strengthening of railway crossings using plastic explosives
Pad C	Pad C	Various processes involving small-large explosion and blast testing on Pad C
CVE	Confined Vented Explosion Chamber (HAC)	Confined Vented Explosion Chamber associated with the Hazard Awareness Training courses (HAC) at Spadeadam, involving the detonation of 7kg of propane-air mixture within a semi confined chamber
VCD	Vapour Cloud Deflagration (HAC)	Flammable vapour cloud deflagration associated with the Hazard Awareness Training courses (HAC) at Spadeadam, involving the deflagration of a fuel-air mixture within a semi-confined rectangular rig.
HYD	Hydrogen Detonation	Detonation of confined hydrogen associated with the Hazard Awareness Training courses (HAC) at Spadeadam
EC	Large Explosion Chamber	Explosions related using the Large Explosion Chamber relating to non-HAC work
BLEVE	Boiling Liquid Expanding Vapour Explosion	Vessel BLEVE

Other	Any other test type	A specific, non-standard or unusual test type not defined by an abbreviation

The meteorological parameters available from each meteorological data source is specified in Section 4.3. Table 54 specifies the origin of each meteorological data source.

Table 54 - Meteorological data sources.

Origin of Data	**Description of source**
DNV	Recorded on the AWS at DNV Spadeadam
RAF	Recorded on the AWS at Berry Hill, operated by RAF Spadeadam
MODH1	1-hourly averaged forecast data, available 0-48 hours before from Met Office DataHub service
MODH3	3-hourly averaged forecast data, available 51-117 hours before from Met Office DataHub service
MR3	3-hourly averaged forecast data, available 0-144 hours before from ECMWF Medium Range Atmospheric Model
MR6	6-hourly averaged forecast data, available 144-240 hours before from ECMWF Medium Range Atmospheric Model
ERA5	1-hourly average archived reanalysis data from ERA-5 Archive dataset

describes how measurement validity is assigned to each record. A number of codes were used to describe the quality of the measurement under various conditions. The following flow diagram explains the process of how these codes are assigned to each measurement.

The LKD also contains other record keeping sheets for the management of other information. For example, the ‘INM_locs’ worksheet contains distance and azimuth angle matrices for

each INM location and common DNV testing locations. Information from this sheet is used in to improve the accuracy of wind vector components calculations.

Table 55 - Location details contained within 'INM_locs' worksheet.

Description	Grid Reference	Easting	Northing	Latitude	Longitude
Pad C	NY 62980 72470	362980	572470	55.04535	-2.5809
EDH Zone	NY 62893 72333	362893	572333	55.04411	-2.58224
Explosion Chamber	NY 62778 72550	362778	572550	55.04605	-2.58407
HAC Area	NY 61479 72591	361479	572591	55.04632	-2.6044
Trench Area	NY 62215 72477	362215	572477	55.04535	-2.59287
JIP Rig	NY 61852 72417	361852	572417	55.04478	-2.59854
Test Site West	NY 60622 72630	360622	572630	55.04661	-2.61783
INM 140 Wardrew Farm	NY 64177 68319	364177	568319	55.00813	-2.56164
INM 141 Blenkinsopp Castle	NY 66437 64525	366437	564525	54.9742	-2.52586
INM 142 High Close A Burn	NY 72006 67912	372006	567912	55.00498	-2.4392
INM 143 Cranberry Brow	NY 74905 65658	374905	565658	54.98488	-2.39367
INM 144 Annshill	NY 53534 75216	353534	575216	55.06923	-2.72916
INM 145 Raise House	NY 63176 66362	363176	566362	54.99048	-2.57704

Table 56 - Distance matrix from 'INM_locs' worksheet.

Distance Matrix (m)	DNV Spadeadam Testing Location					
INM Location	Pad C	EDH Zone	Explosion Chamber	HAC Area	Trench Area	JIP Rig
INM 140	4316	4211	4452	5045	4592	4702
INM 141	8654	8565	8809	& 9454	8992	9111
INM 142	10085	10103	10301	11489	10775	11072
INM 143	13700	13708	13914	15071	14370	14655
INM 144	9809	9765	9594	8345	9077	8759
INM 145	6106	5973	6195	6449	6185	6191

Table 57 - Azimuth Angle (Source-Receiver) matrix from 'INM_locs' worksheet.

Azimuth Matrix (° re North)	DNV Spadeadam Testing Location					
INM Location	Pad C	EDH Zone	Explosion Chamber	HAC Area	Trench Area	JIP Rig
INM 140	163.9	162.3	161.7	147.7	154.7	150.6
INM 141	156.5	155.6	155.5	148.4	152.0	149.8
INM 142	116.8	115.9	116.7	114.0	115.0	113.9
INM 143	119.7	119.1	119.6	117.3	118.3	117.3
INM 144	286.2	287.1	286.1	288.3	287.5	288.6
INM 145	178.2	177.3	176.3	164.8	171.1	167.4

A ‘Special Events’ sheet is used to log information on unusual events, such as uncommon or one-off test types. Alternatively, interesting information on noise from other sources outside from DNV Spadeadam may be captured here, such as noise expected from the Otterburn MoD artillery range, or from RAF Spadeadam training activity. However, it should be noted that the acoustic indices best suited to describing these other noise sources are not included in the worksheet.

Table 58 - Measurement error handling and description codes.

Error Code	**Description of Error Code**
999	No measurement
998	Test event not audible in audio recording
997	Measurement contaminated
Signal Condition	**Description of signal condition code**
1	Overloaded measurement (Zpeak)
2	Contaminated with extraneous noise (Zpeak)
3	Contaminated with wind noise (Zpeak)
4	No measurement (Zpeak)
5	Valid Measurement (Zpeak)
6	Overloaded measurement (Cpeak)
7	Contaminated with extraneous noise (Cpeak)
8	Contaminated with wind noise (Cpeak)
9	No measurement (Cpeak)
10	alid Measurement (Cpeak)

Finally, complaint codes are assigned according to Table 59 - Complaint codes assigned to each test event.. These codes are used to distinguish between the severity of complaints from the public and as part of a management process specifically for logging complaints.

Table 59 - Complaint codes assigned to each test event.

Complaint Code	**Description of complaint code**
0	No comment or complaint from receptor
1	Comment: A receptor or member of the public provided a comment regarding the test event. This type of comment is usually not as sever as complaint code 2 and is can be observational in nature. Such comments might arise when already in contact with receptors and might be said in passing. Alternatively, a complaint code 1 may be assigned to a test event if a member of the public writes comments on the sites social media posts about test activity.
2	Complaint: Complaint code 2 is usually assigned when a member of the public contacted the site specifically to complain about a particular test

	event or number of test events. These types of complaints are usually more severe in nature.

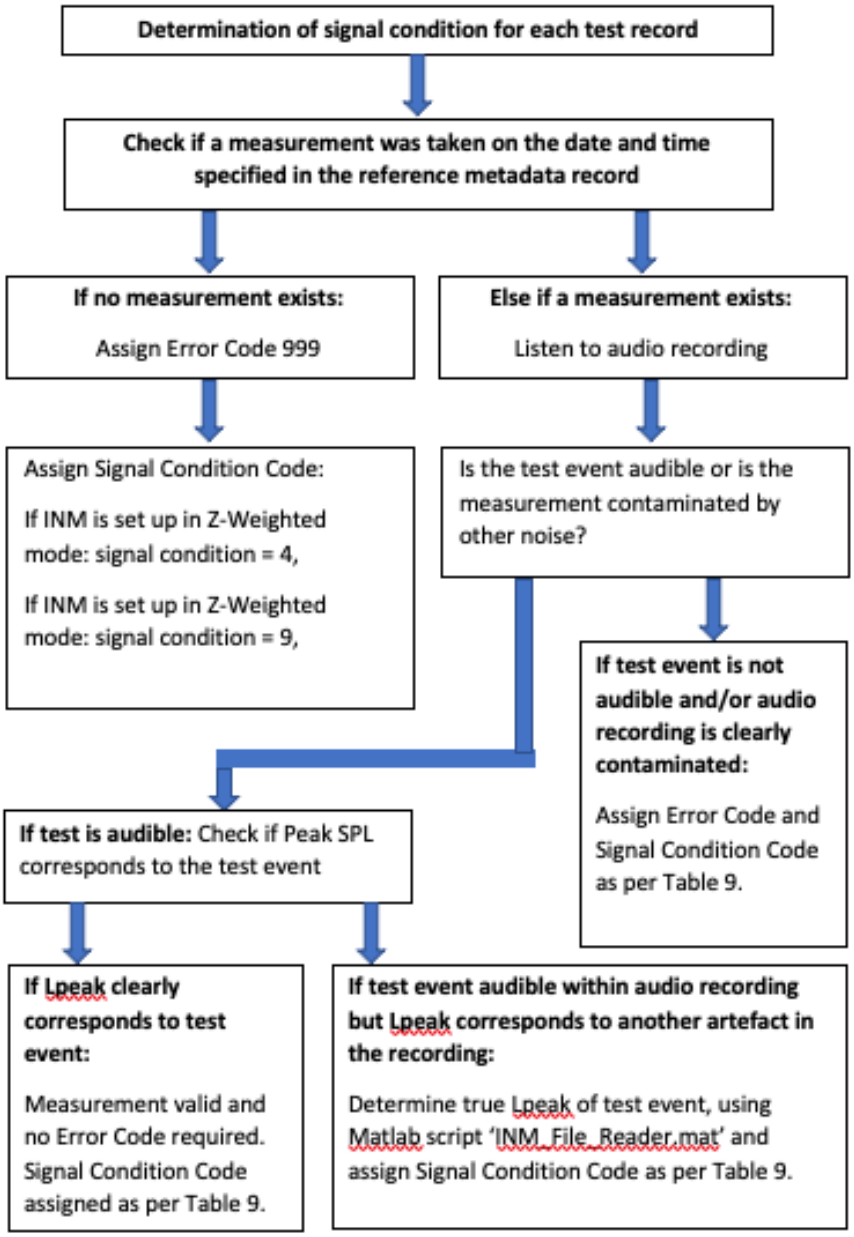

Figure 83 - Flowchart for the assignment of Signal Condition codes and associated error handling codes.

4.4 Data Collation and Pre-processing

Prior to the inception of this project, the management of environmental noise impacts at Spadeadam was solely reliant upon MONET for large explosion trials above 25 kg TNT. The goal of this research was to develop bespoke noise impact management strategies for the Spadeadam site for all of their testing activity, in the form of rapid, short and long-range noise prediction models. The models have been developed upon large quantities of overpressure data gathered at sensitive receivers using the Live Noise Monitoring System. This sub-chapter reports the specific ways that these were collated and processed.

4.4.1 Measured Noise Data

The adverse impacts of Spadeadam's activities from blasting results in impulsive noise at residential receivers. The prediction scheme used throughout the majority of this project (MONET) outputs LZpeak. Note, the new Met Office's new prediction application (SoundWave) has LCpeak as the model output. Previous heuristic models used LZpeak and although other metrics have been reviewed in Chapter 3.4, the focus of this research is on one response variable, LZpeak for consistency with other prediction programs.

The LZpeak data was captured by the Live Monitoring Network as discussed in Chapter 4.3. The techniques used to tag each measurement with specific metadata related to testing and signal quality has already been discussed. However, given that a range of exposures can occur across all the monitoring positions, and for each test type, the measurements have also been separated into 3 noise impact categories, *high*, *moderate* and *low* impact. These have been developed to allow DNV site management to navigate through operational needs, and are developed upon specific criteria to the operations at Spadeadam, and the unique community surrounding the site. Such categories are needed to aid operational decisions, and accounts for the size of the adversely impacted population, the particular sensitivity of the resident and the number of events.

- High Noise Impact
    - An individual receiver is predicted to receive a Peak SPL of >125 dB
    - Peak SPLs above 115 dB are predicted for a large population; or
    - Multiple Peak SPLs between 110-115 dB are predicted for moderate population

- Moderate Noise Impact
    - An individual receiver is predicted to receive a Peak SPL between 115-120 dB
    - Peak SPLs above 110 dB are predicted for a large population; or
    - Multiple Peak SPLs between 105-110 dB are predicted for moderate population
- Low Noise Impact
    - Peak SPLs are expected to be 110 dB at their greatest across all known receivers

4.4.2 Measured Meteorological Data

4.4.2.1 R5BC Weather Station

Measured meteorological data was collected from a David Vantage Pro automatic weather station operated from the DNV Spadeadam R5BC Control Building. This weather station is situated on the roof of the building at a height of 10 m agl. A data logger was used to transfer data directly from the weather station to the Davis WeatherLink software.

Figure 84 - Automatic Weather station situated at DNV Spadeadam R5BC Control Building.

The software was set up so that the data could be viewed remotely through the Davis WeatherLink webpage. However, a Matlab program with a graphical user interface (GUI), Figure 85, was developed to collect specific measurement records of the data remotely through the WeatherLink API service. The program allowed the export of weather records, containing any relevant meteorological parameters to .csv format.

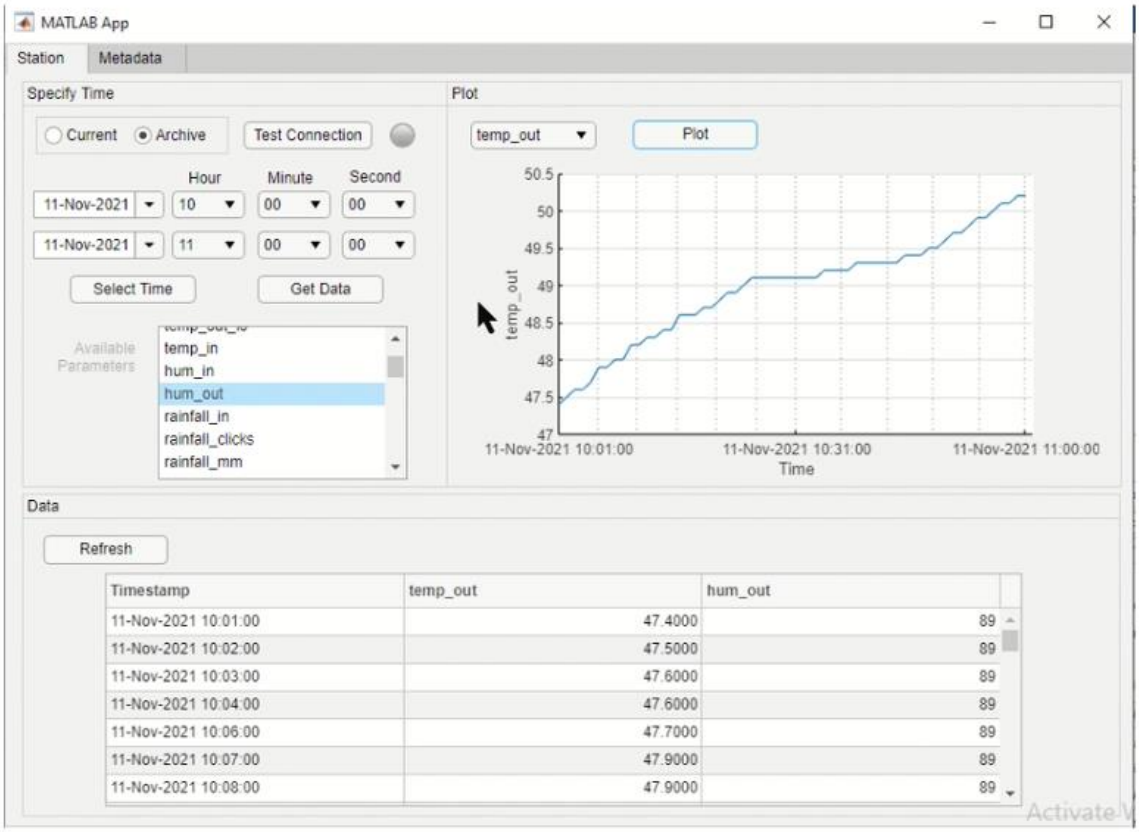

Figure 85 - Custom Matlab application for extracting R5BC Weather Station records.

Data could be input directly and in the correct format to the LKD, where test records were kept, as described in section 4.2. This was done on a case by case basis throughout the main monitoring window. Figure 85 shows the application displaying 1-minute archived weather data captured from the station between 1000 and 1100 on 11 November 2021, with data tabulated showing temperature and humidity. Additionally, temperature is plotted for a visual reference. An important note is that some unit conversion was necessary, for example, the temperature is in units of °F, and additional steps were taken to convert meteorological parameters to SI units upon output.

4.4.3 RAF (Berry Hill) Weather Station

Data from the Berry Hill automatic weather station was collected in bulk from the Iowa Envionmental Mesonet (IEM), developed by the Iowa State University. The IEM maintains an extensive archive record of recorded meteorological data from automatic weather stations

all over the world. Data is available from any station listed for free. The station situated at RAF Spadeadam's Berry Hill building, around 2km from DNV's R5BC building has data available from 1992 to the present.

Data is downloaded in bulk an output in .csv format. However, this contained hourly averaged, and sometimes 30-min data for all hours and as this was not done while at the same time as the noise data was collected into the LKD, custom python code was written to batch collect the relevant meteorological data from the weather station data to match the times specified for each explosive test in the LKD.

The following flow diagram explains the process of how this was achieved programmatically.

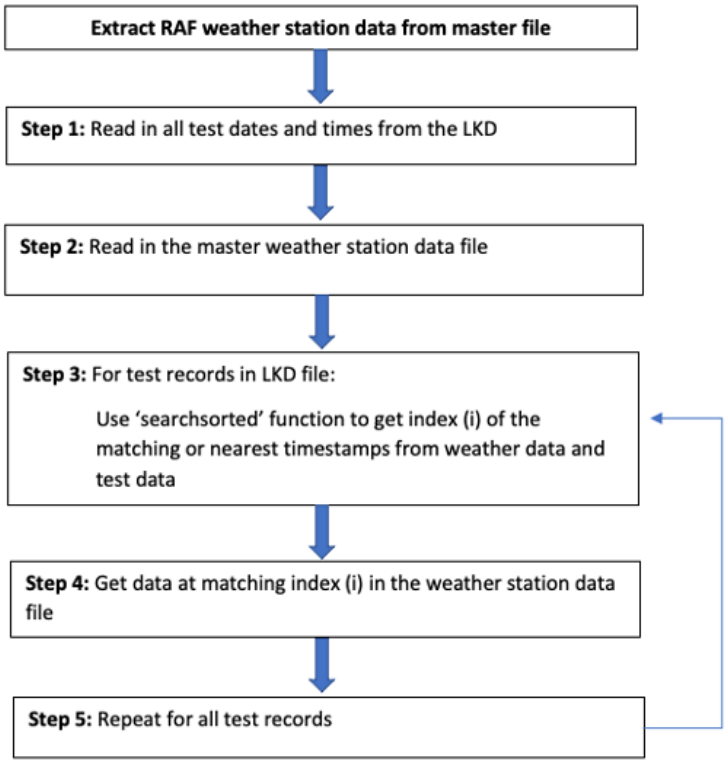

Figure 86 - Flowdiagram of data extraction from Berry Hill weather station master file.

4.4.4 Forecast Data

The forecast data used to evaluate model performance was taken from the Met Office's DataHub Atmospheric Model. In particular, the 2km^2 Lat-Lon Model was used. The model is accessed by calling the API framework, requesting particular meteorological parameters at various heights and at different time steps for a number of hours ahead of the test time.

4.4.4.1 Data Acquisition and Processing

Due to the vast nature of the atmospheric forecast files, an effort was made to ensure treatment of data was done systematically and programmatically. This ensured consistency across each forecast and increased reliability and trust in the data.

Python 2.7 was used to acquire and process the data from the forecast model. A series of scripts were written to 'batch call' the API framework, using the Python http and requests libraries. Data was downloaded daily from the framework, after 0600 hours, so that the 0600 forecast was complete. The basic algorithm is shown below.

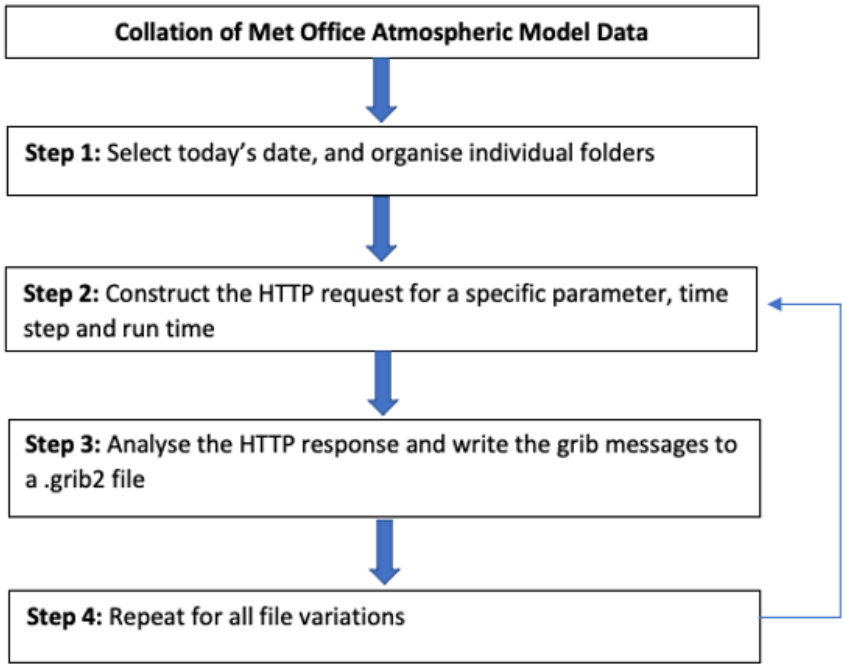

Figure 87 - General flowchart explaining how the Met Office DataHub atmospheric data is collated.

The following code in Figure 88 expands on the algorithm used to obtain the DataHub atmospheric data.

```
url_base = 'https://api-metoffice.apiconnect.ibmcloud.com/metoffice/production/1.0.0'

grib_headers_lower = {
          "Accept":"application/x-grib",
          "X-IBM-Client-Id":{clientID},
          "X-IBM-Client-Secret":{clientSecret}}
for specificParameter in parameters:
    os.makedirs(os.path.join(path, specificParameter, timeSteps))
    os.chdir(os.path.join(path, specificParameter, timeSteps))
    for heightLevel in heightLevels:
        uri = url_base+'/orders/'+orderId+'/latest/'+specificParameter+'_'+heightLevel+'_'+RunTime+'/data'
        print(uri)

        outputFileName = date+'_'+specificParameter+'_'+heightLevel+'_'+runTime+timeSteps+'.grib2'
        response = requests.get(uri,headers=grib_headers)
        print(ressponse)
        gribData = str(response.content)

        with open(outputFileName,"wb") as f:
            for chunk in response.iter_content(chunk_size=8192):
                f.write(chunk)
```

Figure 88 - An example of Python code used to obtain atmospheric profiles from Met Office DataHub service.

A number of HTTP requests are made to the API framework for a specific meteorological parameter field (specificParameter), e.g. wind speed, temperature etc., and at a number of height levels (heightLevel) and for specific run times. The code above outlines the automated process in which data is stored in folders with labels associated to their forecast date, parameter and time steps.

An example response from the code printed to the command line is shown in Figure 89.

```
url1 = https://api-metoffice.apiconnect.ibmcloud.com/metoffice/production,
                /1.0.0/orders/{orderID}/latest/agl_wind-speed_5_+06/data
response1 = <Response [200]>

url2 = https://api-metoffice.apiconnect.ibmcloud.com/metoffice/production,
                /1.0.0/orders/{orderID}/latest/agl_wind-speed_10_+06/data
response2 = <Response [200]>

url3 = https://api-metoffice.apiconnect.ibmcloud.com/metoffice/production,
                /1.0.0/orders/{orderID}/latest/agl_wind-speed_20_+06/data
response3 = <Response [200]>
```

Figure 89 - Example http responses ('response1..3') for http requests ('url1...3)'.

4.4.4.2 Confidence

Some special cases, returned a non 200 HTTP response from the API framework. To mitigate these circumstances, each file was processed on the day, by opening the grib file and reading the data to a *.csv file to check it was compatible.

In certain cases, where the forecasts were requested too early in the morning, it was possible that the day's requests included the results from the previous day's model run. In order to check the validity of the forecasts, all files had their expected forecast cross-referenced against the actual forecast date. This was carried out in programmatically in Python, where

each file was opened, and the first grib message read to determine the actual forecast date. Where a discrepancy between model expected forecast date and actual forecast date was non-zero, these files were recorded in a python dataframe, and written to a .csv file for record. These files could then be renamed programmatically and re-organised into their correct folders.

4.5 Quantification of Atmospheric Vertical Profiles

Finally, the representation of the structure vertical atmospheric profiles within the various meteorological data associated with each test event was extremely important. Their representation was recorded differently depending on the origin of the data.

For forecast meteorological data from the Met Office DataHub atmospheric model, temperature and wind profiles were already attainable and consequently, the direct calculation of vertical sound speed profiles could be achieved through the following.

The profiles were computed at the nearest point to the firing location and accounted for the source-receiver azimuth.

Adiabatic sound speed, c, was computed first to account for the influence of the temperature profile on sound speed.

$$c_a = \sqrt{\frac{\gamma RT}{M}}$$

The effect of wind on sound speed was included by using the vector wind from the atmospheric data. This factor is computed via the following.

$$v_{vect} = (\alpha)\, v$$

Where *v* is the wind speed in m/s and α is the angle difference in radians between the source-receiver azimuth and the wind direction,

$$alpha = \theta - \phi$$

Note here that ϕ is defined in the meteorological sense, as the direction from which the wind is blowing. To ensure that the vector angle between the source-receiver azimuth and the wind direction.

Finally, the vector wind contribution to the sound speed is added to the adiabatic sound speed as per the following, to form the effective sound speed. This is the sound speed in the direction toward the receiver.

$$c_{eff} = c_a + V_{vect}$$

An example of the program outputs is attached below for a receiver located at 130° re North. With winds at the surface forecast to blow from the E/SE, this results in upwind propagation, as reflected by the shape of the sound speed profile.

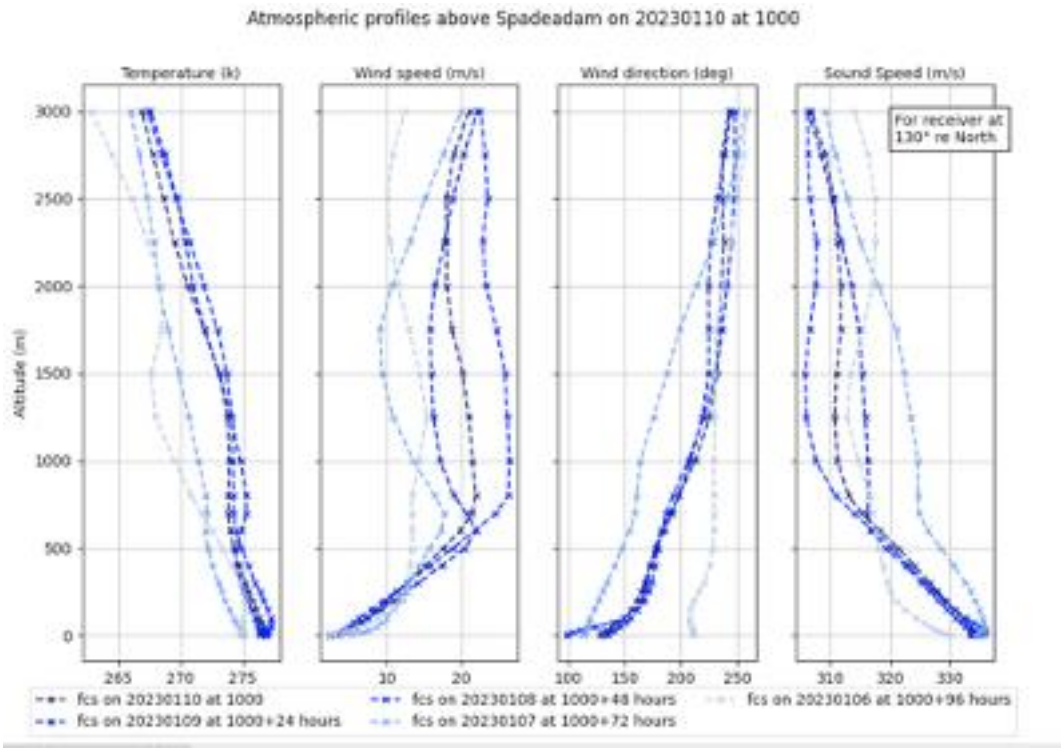

Figure 90 - Sound speed profiles forecasts in direction of receiver 130° re north, derived from Met Office DataHub 2km^2 atmospheric forecast model for 1000Z 10 Jan 2023.

Another example of the propagation scenario for a receiver located approximately to the WNW 290° re north. An example location could be Annshill, Roadhead, ~10 km from Pad C at Spadeadam. Under such conditions, propagation is downwind.

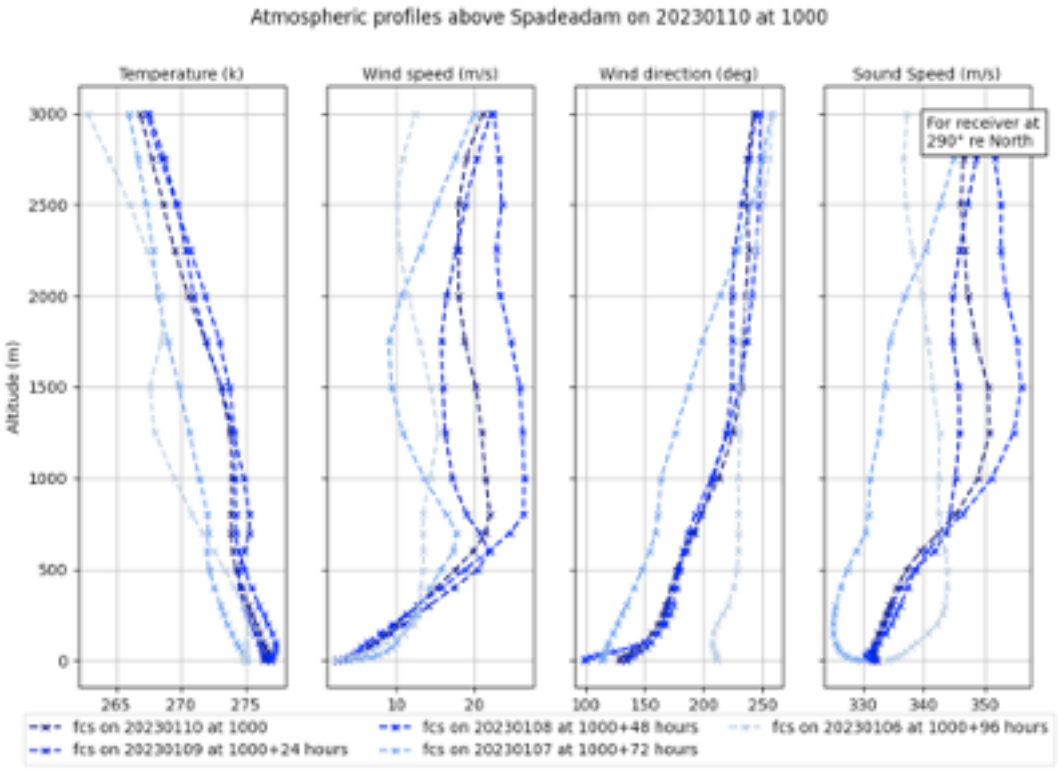

Figure 91 - Sound speed profiles forecasts in direction of receiver 290° re north, derived from Met Office DataHub 2km^2 atmospheric forecast model for 1000Z 10 Jan 2023.

4.6 Analysis of Blast Noise Impact Models

4.6.1 Existing Heuristic Prediction Models

The Live Monitoring Network was used to measure LZPeak levels for all test activity at Spadeadam. Along with each measurement, the measured data from the site weather station, and forecast meteorological data from the Met Office DataHub model were used to make Salford Surface Wind (SSW) predictions of all blast testing.

A Matlab app was also developed to produce graphical and tabulated outputs of SSW predictions for each location, including other locations in the area, shown in Figure 92.

Figure 92 - Custom Matlab application developed to make, visualise and tabulate SSW predictions for a variety of meteorological input data, used in the Initial Monitoring Phase.

For each blast test type, SSW predictions were compared to the measured noise data using the following variable input meteorological data. The meteorological parameters necessary to carry out a SSW prediction is the 10m wind speed and direction.

- R5BC (onsite weather station) Measured Data:
  - 1-minute averaged R5BC Weather Station
- Forecast Meteorological Data (10m wind from Met Office DataHub Service)
  - 00-1 day ahead hourly forecast
  - 1-2 days ahead hourly forecast
  - 2-3 days ahead hourly forecast
  - 3-5 days ahead 3-hourly forecast

4.6.2 Comparison of Empirical Model to MONET

An important part of this thesis is dedicated to the evaluation of the sole long-range noise prediction model used at DNV Spadeadam at the time of writing, the Met Office Noise Evaluation Tool (MONET), described in Chapter 3.3. In Chapter 5, the performance of MONET will be evaluated against a contrasting type of noise prediction model, an empirical

model. The empirical model under comparison will be the existing Salford Surface Wind (SSW) model. As previously explained, this model is a regression model based on measurements of explosives ranging from 1-17 kg and uses relatively few environmental factors to model the propagation towards a receiver (distance, charge weight and 10 m vector windspeed).

Alternatively, the MONET model and its predictive performance will be compared to the SSW model. As MONET is owned by the Met Office, it is operated independently by them on behalf of DNV for large explosion tests, typically for those with explosive charge of 40 kg TNT or greater, though there are some MONET runs available for charges as small as 25 kg TNT. This means that comparisons between MONET and SSW and between MONET and measurements, are limited to the Pad C testing (see Chapter 5.1.2 for an overview of the noise data and associated explosion testing).

The method for comparison comprises of comparing the prediction error of both models against the respective measurements at each monitoring location. The metric of assessment chosen for comparison is the Root Mean Square error (RMSE, or RMS Error), which was described in Chapter 3.3, and is used as a metric to evaluate the performance of the original SSW model, as well as being common in machine learning model as an indicator of prediction capability.

In addition to comparing predictions of both models against measurements at each location, the predictions will also be evaluated in the context of other parameters. In particular, predictions will be compared against the vector wind speed, as a physical descriptor of the propagation conditions, to evaluate MONET's performance in certain propagation conditions.

This part of the thesis serves in quantifying the success of contrasting prediction models for managing blast noise impacts from major-hazards blast testing.

4.6.3 Development of Extended Models

As will be shown in Chapter 5, the majority of measurements made by the Live Monitoring Network were from EDH operations described in earlier chapters. For this reason, the development of an extended versions of the SSW model are limited to measurements from this operation only, and consequently, predictions from the model are limited to this operation. The sample size needed to derive regression models for other blast operations such

as those analysed in the Live Monitoring Phase requires further measurements under more varying meteorological conditions.

4.6.3.1 Features of extended models

The techniques involved in Monin-Obukhov Similarity Theory (MOST) for the description of the lower atmosphere have been used as the basis for an extended prediction model. MOST has been presented in detail in the literature review chapter of this thesis (Chapter 3.2) and this section describes its involvement in improving the accuracy of predictions for EDH noise at long-range. Monin-Obukhov parameters have been derived from the experimental meteorological data in this research to use as model variables for predicting sound propagation of blasts at Spadeadam.

Routine meteorological data (wind and temperature) were collected from the aforementioned measurement or forecast sources, along with cloud cover observations to derive the above MOST parameters. The RAF automatic weather station collected all parameters needed to derive these parameters.

The methodology presented in NORD2000 to make categorical descriptions of the lower atmosphere was used on the RAF weather station data to produce u_*, T_* and L for each record. The result is the derivation of two parameters used to represent the vertical sound speed structure in the surface layer, a logarithmic term (A_{Log}) and a linear term (A_{Lin}).

These two terms were tabulated for each test record according to the measured meteorological data gathered at the time of each test, along with the charge weight (kg), source-receiver distance (m), and vector wind (m/s).

A deep-learning approach is used to build a neural network with the new terms introduced from MOST, along with the original inputs of the SSW model is formed, and its prediction accuracy is assessed.

Deep Neural Network

As an alternative extension of a model for the prediction of noise from major-hazards testing, a number of deep neural networks (DNNs) have been trained on the EDH data set. The method used to develop DNNs is explained here.

The neural networks are developed in the Python programming language using the Keras open-source neural network library on top of the TensorFlow software library,. A number of

other packages are used for managing the data for preparation into a DNN (Numpy, Pandas), and subsequent visualisation and plotting (Seaborn).

Firstly, the data is read into Python from a Comma-Separated Values file (.csv) containing information on the explosion test, propagation conditions and noise monitoring results. This data has already been partially pre-processed in Microsoft Excel, with the any test entries containing invalid data according to the error codes described in Section 4.3.2 of this Chapter. A copy of the data is made to form a new Pandas DataFrame, and check to count and drop any rows containing invalid data.

The data is the split into its training and testing datasets, with 80 % of the data assigned to training and 20 % to testing (also known as validation). The purpose of splitting data is to evaluate the performance of a neural network on data that it has not seen before. The independent variables are usually referred to as 'features' in a machine learning model, and in the case of the training and testing data, are labelled training and testing features. Similarly, the dependent or output variable (in this case LZPeak) is referred to as a 'label', and the features and labels from the training and testing datasets are separated again.

```
# Split the data into training and test sets
train_dataset = dataset.sample(frac=0.8, random_state=0)
test_dataset = dataset.drop(train_dataset.index)

train_features = train_dataset.copy()
test_features = test_dataset.copy()

train_labels = train_features.pop('SPL_dBZ')
test_labels = test_features.pop('SPL_dBZ')
```

The next step is an important step in machine learning, known as normalisation. The purpose of normalisation is to scale the model features (input variables), as some variables may vary significantly more than others, and hence without appropriate scaling, particular variables may seem to be responsible for more variation than others in the output of the model. There are two common methods of normalisation, min-max and z-score, and the latter was used in the formation of DNNs in this thesis. This method refers to the normalisation process that sets the mean of the values in the training features to 0 and the standard deviation to 1.

$$Z = \frac{X - \mu}{\sigma}$$

Where Z is the new normalised value, X is the original value in of the training feature, μ is the mean of the data and σ is the standard deviation of the data. This method of normalisation has and reduces the effect of large outliers. Keras has built in normalisation functionality know as normalisation layers and uses the z-score method.

```
# Normalisation
train_dataset.describe().transpose()[['mean', 'std']]
normalizer = tf.keras.layers.Normalization(axis=-1)
normalizer.adapt(np.array(train_features))
```

The training data is then ready to be given to the neural network for learning, along with the testing data for validation, but firstly, the neural network needs to be built.

The core learning mechanism of what is known as a Multilayer Perceptron (MLP), of which DNNs are just a version of, is the concept of forward and backpropagation through a number of layers connected by connected artificial neurons. In supervised machine learning, the neural network is given both the input and output data as pairs, as if guided by a teacher, and generates outputs based on the model inputs. By comparing the model output to the known output, an error signal is generated, and the network adjusts its parameters until an acceptable level of accuracy or learning is achieved.

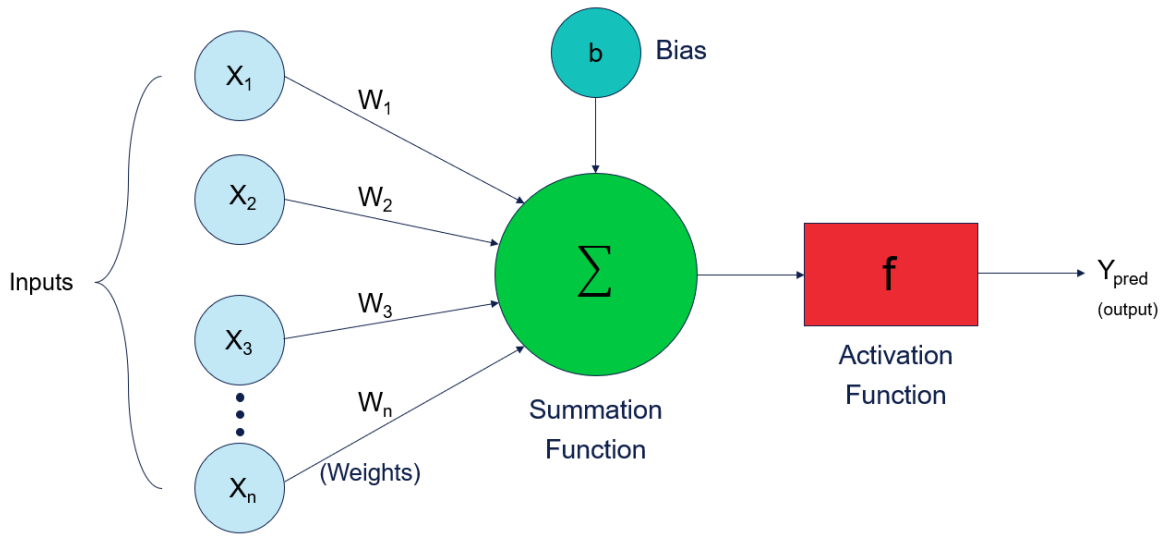

Figure 93 - General schematic of single neuron in a neural network with inputs, weights, biases, summation and activation function, and output.

The weights essentially determine the strength of the connections between neurons and capture the relationship between input features and the desired output variable and can be adjusted. These weights are summed and added to a bias which acts as a threshold for the activation function. The activation function determines the response of a neuron, i.e. whether to activate or remain dormant.

The structure of a deep neural network was defined using the Keras Sequential class which essentially stacks layers of neurons on top of each other, with an input, hidden and output layer. The structure of the layers are defined by the ‘layer.Dense’ property.

The optimizer is specified in the model, which represents a key component of any neural network. The optimizer is an algorithm that adjusts the weights and biases in a model iteratively until they converge to a minimum loss value, and common algorithms are Stochastic Gradient Descent (SGD) and Adam.

It is intended to train various types of neural networks on a proportion of data gathered from the Live Knowledge Database, and validate it by assessing its predictions for input data that it has not been trained on. Using metrics such as the RMS and maximum prediction error, the predictive ability of a deep neural network for blast noise can be will to the Salford Surface Wind model.

5 Results

Overview

In this chapter, the results gathered throughout Part II of this research program are presented. Firstly, an overview of the noise monitoring data and meteorological data is presented, in order to observe general trends in propagation schemes at Spadeadam, and the magnitude of noise impacts from the variety of test activity carried out at the site.

Secondly, results from the initial monitoring phase are presented and the performance of existing heuristic models for blast noise impacts is quantified.

Finally, the performance of new heuristic models for the prediction of noise impacts at sensitive receptors for specific test activity at Spadeadam is evaluated.

5.1 Overview of Measurement Data

5.1.1 Prevailing Wind Conditions

In order to understand noise impacts from Spadeadam's test activity, it is important to evaluate general trends in propagation scenarios within the area.

Over 10 years of data (2010-2022) measured from the RAF/Berry Hill Automatic Weather Station was analysed and the results from that analysis are presented here.

The weather data was split down into months and then only readings taken during normal working hours considered 0800 – 1600 hours. Based on this, wind rose data was generated for each month of the year. This was used to assess the likelihood of particular weather conditions occurring during each month. The analysis was initially carried out as part of the 1000kg TNT feasibility study described in Section 4.2 and is therefore concerned with quantifying the likelihood of favourable wind directions.

Winds were expressed in 16 directions (22.5 ° segments) relative to North (0 °) following the standard cardinal convention, and are defined as the direction from which blowing, as opposed to the direction towards which blowing.

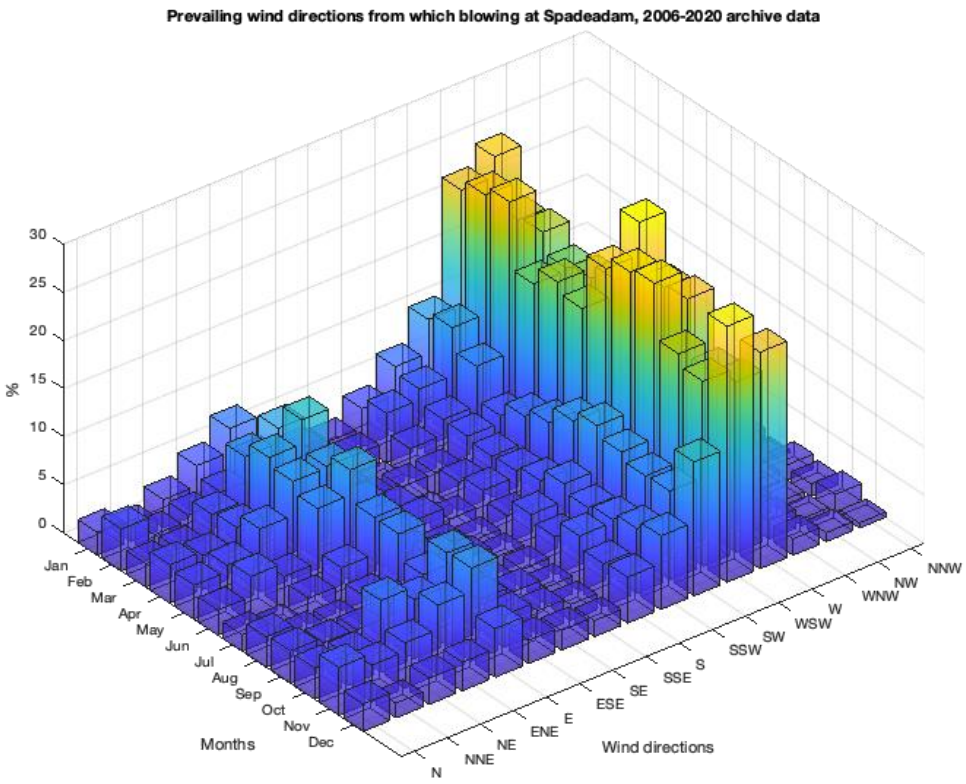

Figure 94 - Prevailing wind directions over DNV Spadeadam measured from 6 Apr 2011 to 31 Dec 2022.

Prevailing winds are from the west, 270° (21.3 % of the time), followed by the west-south-west, 247.5° (21.1 %) and then the south-west, 225° (9.0%). For the most favourable winds with regards to low noise impacts, winds from the south, the analysis concluded that southerly winds (wind blowing from 168.75-191.25°) occurred just 3.9% of the time over the whole analysis period. An analysis of the monthly data showed that southerly winds were most likely (5.7 % of the time) during October, and least likely during April (2.3 % of the time). However, this is a small and negligible difference and the likelihood of southerly winds occurring does not change significantly with the time of year.

Furthermore, the percentage of southerly winds above 5 m/s (~10 kts) was 1.9%, and at least 10 m/s (qualifying for propagation case 6) across all months was just 0.2 %.

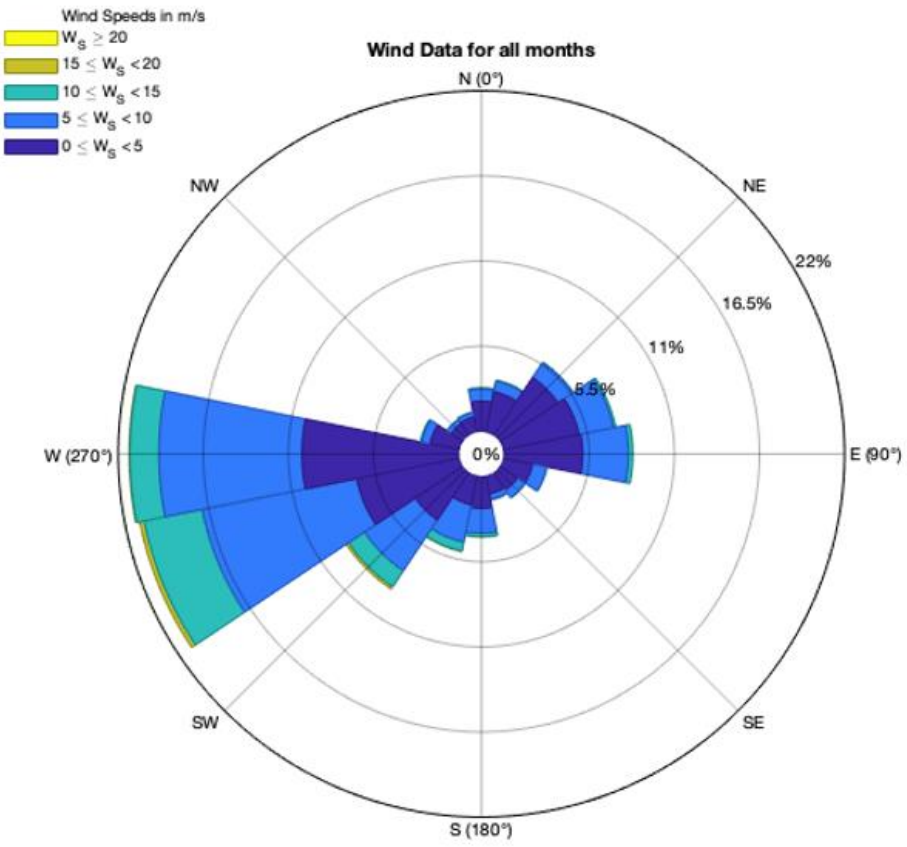

Figure 95 - Wind rose for DNV Spadeadam from 6 Apr 2011 to 31 Dec 2022

It is possible that other combinations of southerly winds would yield noise impacts of the same magnitude as propagation case 6 and these are considered below. The favourable variations on southerlies include, winds blowing from the SE, SSE, and SSW and are considered in combination with S winds in Table 60 . Note that the SW direction is not considered in the favourable variations to form a 90° quadrant around 180°, due to the risk of long-range enhancements to the SE (where many receptors are located) associated with elevated wind shear above SW surface winds. An SSW surface wind may introduce this risk if the vertical wind profile is characterised by a large clockwise wind shear but is included within the table for reference.

Table 60 - Analysis of favourable southerly wind variations from historical data

Directions (°) re. North (0°)	**Average Direction (°)**	**% 0-5m/s**	**% 5-10m/s**	**% 10-15m/s**	**% 15-20m/s**	**% > 20 m/s**	**Total %**
123.75-146.25	135 (SE)	1.3	0.6	0.0	0.0	0.0	2.0
146.25-168.75	157.5 (SSE)	1.2	0.4	0.0	0.0	0.0	1.6
168.75-191.25	180 (S)	2.0	1.6	0.2	0.0	0.0	3.9
191.25-213.75	202.5 (SSW)	1.9	2.5	0.6	0.1	0.0	5.0

Table 61 - Analysis of combined favourable southerly winds

Average Direction (°)	**% 0-5m/s**	**% 5-10m/s**	**% 10-15m/s**	**% 15-20m/s**	**% > 20 m/s**	**Total %**
135-202.5 (SSE-SSW)	6.4	5.0	0.9	0.1	0.0	12.4
	<5 m/s	> 5.0 m/s	>10 m/s	> 15 m/s	> 20 m/s	
	6.4	6.0	1.0	0.1	0.0	

Table 60 and Table 61show that favourable southerly wind variations occur around 12 % of the time, with speeds qualifying for propagation case 6 (described in the feasibility study in section 4.2 arising a combined 1.1 % of the time. By considering surface winds 5 m/s, similar noise impacts to propagation case 6 may also be achievable, this gives the likelihood of favourable conditions for a 1000 kg TNT explosive trial as 6.0 %.

5.1.2 Noise Data

This subsection provides an overview of the noise monitoring data gathered by the Live Monitoring System over the entire monitoring window. This is done first, to observe general

trends in noise impacts at each receptor for various test types. The results of heuristic models for the prediction of such impacts is presented in a later section of this chapter.

A review of the measured INM data is presented here. A first-glance view is used to present general statistics on Lpeaks collected at each sensitive receptor. The ranges of Lpeaks and their standard deviations are presented below, along with the peak SPLs for each test type as a function of charge weight.

Table 62 - Number of measurements for common test types at each INM locations

Test Type	INM 140	INM 141	INM 142	INM 143	INM 144	INM 145	Total
EDH	195	199	193	39	166	81	875
Pad C	19	28	24	10	18	16	115
CVE	15	10	11	0	13	4	53
HYD	9	4	4	0	7	3	27

In order to develop empirical models of noise impacts from specific test activity at Spadeadam, measurements from each test type should be separated, so that the effects of charge weight variation (if applicable) and meteorological effects can be accounted for. Note that the Hazard Awareness demonstrations (CVE and HYD) do not vary in TNT equivalence between tests, and both have an estimated weight of 7 kg TNT. Alternatively, EDH tests vary between 1-10 kg TNT, and CPAD measurements between 2-100 kg TNT.

5.1.2.1 EDH Measurements

From the 6 main INM locations, 875 valid measurements of EDH Z-Weighted peak sound pressure level. The vast majority of these measurements were taken during the main monitoring window of December 2021 to December 2022. Some early measurements (from October 2020-November 2021) were taken at some locations, which were used to determine the need to install INMs in the first place and have been included in the analysis.

Where EDH measurements varied in size, from 2-14 kg over the whole monitoring period, the Seaborn package was used to plot how these data varied across all monitoring positions. Rather than plotting a box and whisker for each variation in charge weight, data was split into 3 categories of similar TNT equivalence, 2-4 kg, 5-9 kg, and 10-14 kg, and is plotted in Figure.

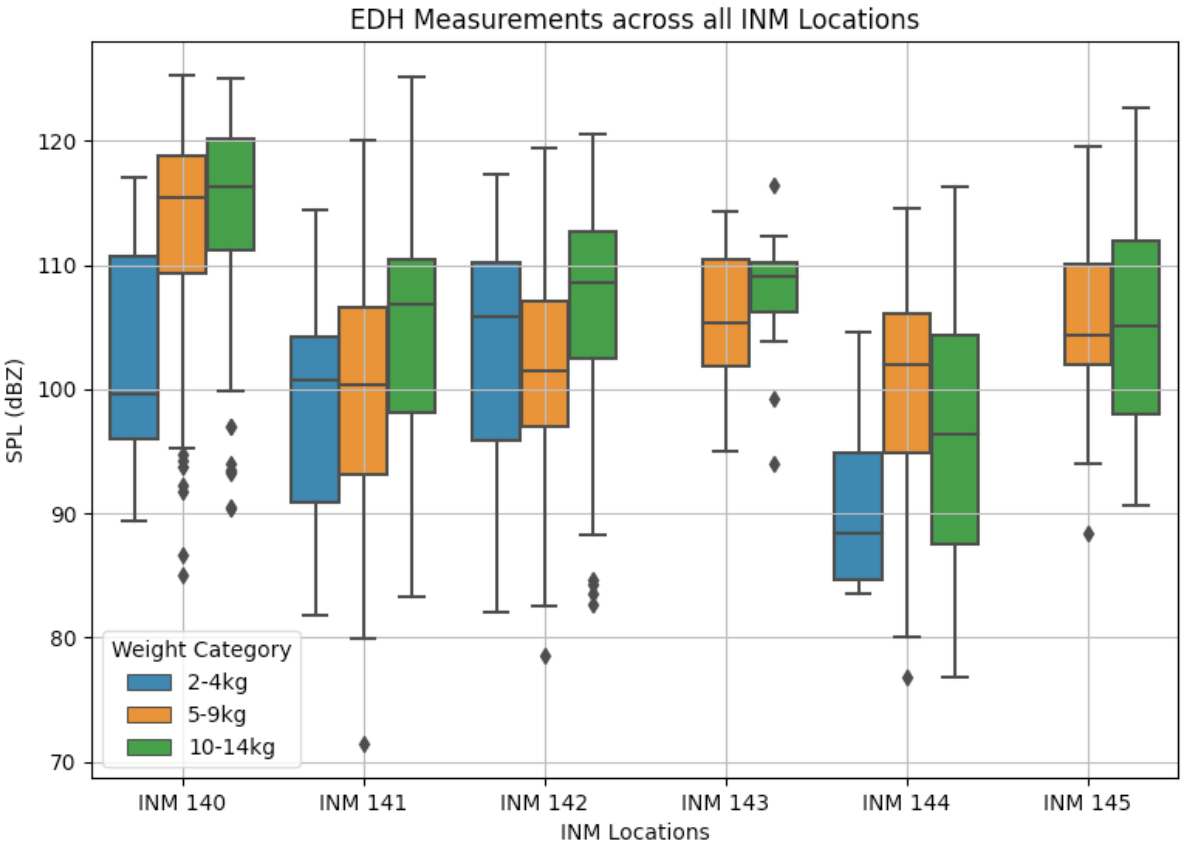

Figure 96 - Box and whisker plots of all EDH Measurements recorded across all monitoring positions throughout the entire monitoring scheme.

5.1.2.2 Pad C Measurements

Similarly, measurements of noise from Pad C varied by TNT equivalence, however the variation was much greater than those from EDH Measurements. Equivalently, categorisation of the data by charge weight was undertaken and plotted as in Figure 96. These categories are named as ‘Small (0.04-8 kg)’, ‘Medium (15-25 kg)’ and ‘Large (50-100 kg)’.

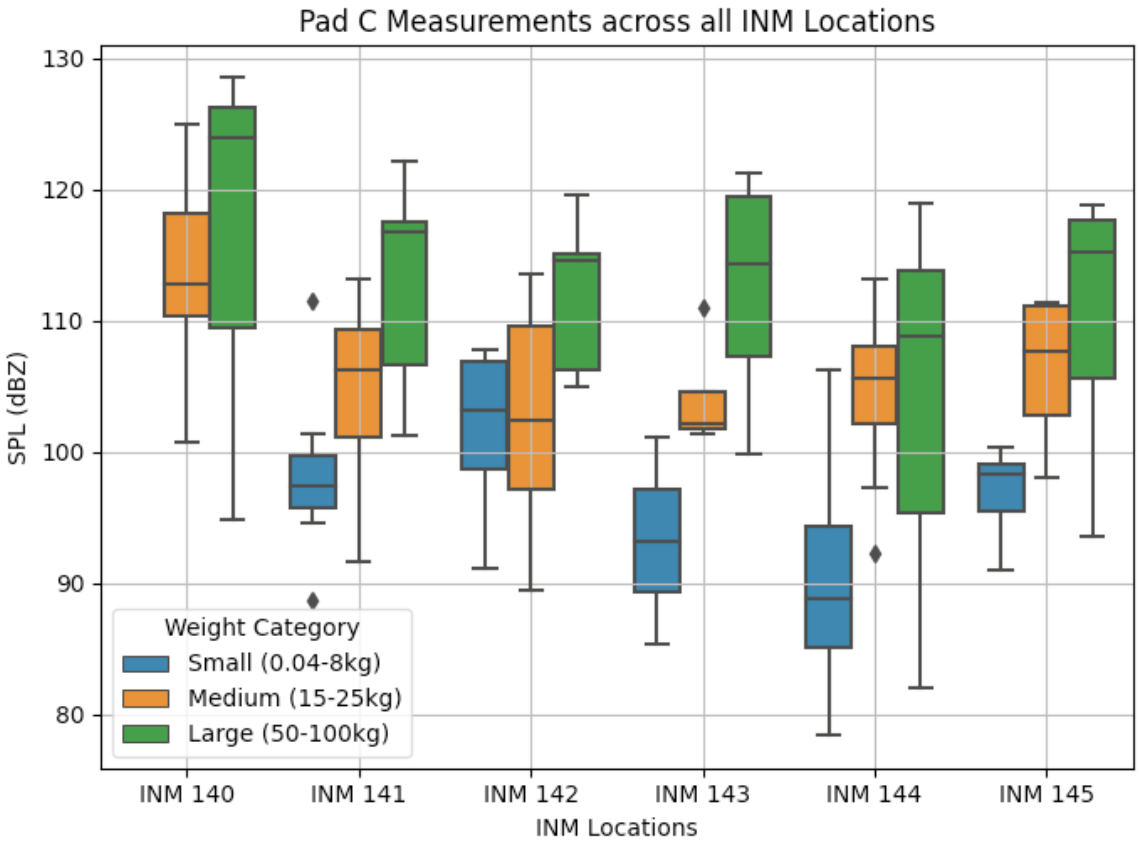

Figure 97 - Box and whisker plots of all Pad C Measurements recorded across all monitoring positions throughout the entire monitoring scheme.

5.1.2.3 CVE Measurements

Measurements across all monitoring locations from CVE (Combined Vented Explosion chamber demonstrations) related to the hazard awareness courses are presented here and are shown in Figure 98. These tests did not vary with explosion size or equivalent charge weight, as volume of flammable gas in the chamber was always kept to 7kg and flammability mixtures were consistent across all tests.

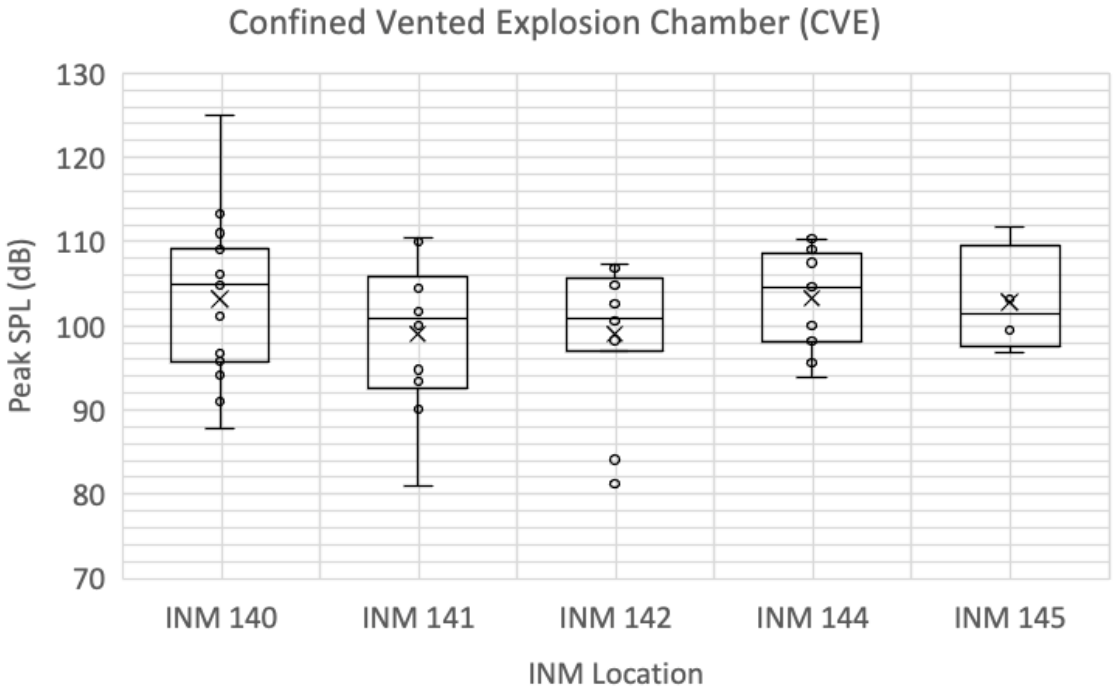

Figure 98 - Box and whisker plots of all CVE Measurements recorded across all monitoring positions throughout the entire monitoring scheme.

5.1.2.4 HYD Measurements

Equivalently, LZpeak measurements from the hydrogen detonations (HYD) are presented in the analysis. Hydrogen detonations were also part of the hazard awareness courses, and all had consistent TNT equivalences of 7 kg TNT.

5.2 Initial Assessment of Heuristic Model Performance

5.2.1 Initial Monitoring Phase

This section presents the results gathered from the Initial Monitoring Stage. The results were initially presented in a conference paper which is included in section C of the Appendices. The purpose of this stage was to determine the performance of existing heuristic models for the prediction of a variety of blast noise impacts at sensitive receptors.

These preliminary data consist of all valid measurements of blast testing carried out by DNV Spadeadam during the initial monitoring phase. Blast testing mainly consisted of Explosion Depth Hardening (EDH) operations. EDH tests are carried out at the SE side of the site, and generally consist of solid explosives with TNT equivalence up to 10 kg. Less frequently, some confined vented gas explosions and deflagrations were performed at the western edge of the site, with less well-defined explosive yields, reported by DNV to range between 7 and 40 kg TNT equivalence. Occasionally, some solid explosives testing with larger explosive yield was carried out in a similar location to the EDH work, but with TNT equivalences of 15 kg. Finally, one measurement of a ‘hydrogen detonation’ is included, which has an estimated explosive yield of 7 kg.

A total of 148 individual explosion and blast events are included in the dataset, spanning from January to April 2022. The number of measurements at each location difference due to several factors included, signal audibility and contamination with extraneous noise at the respective monitors. The following number of measurements were made by each monitor. A combined total of 716 measurements were available across all monitoring positions.

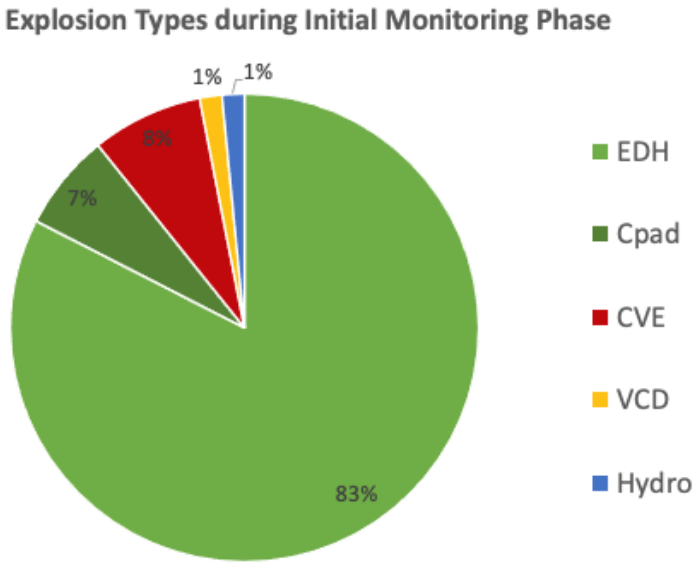

Figure 99 - Proportions of test activity recorded by the INM network during the Initial Monitoring Phase across all INM positions.

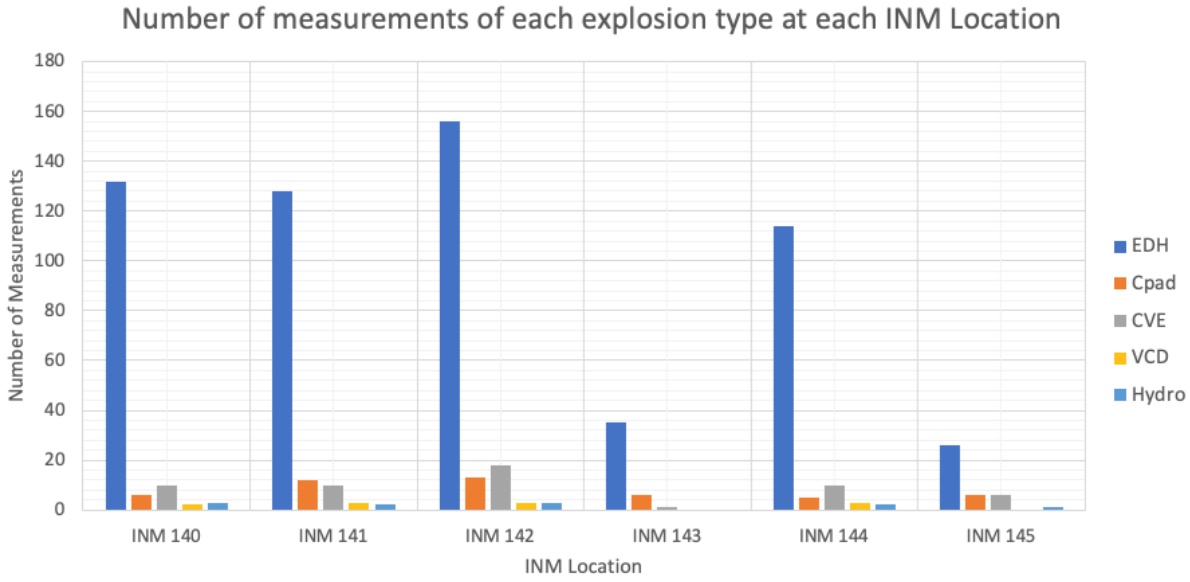

Figure 100 - Number of measurements of each test type made at each individual monitoring location during the Initial Monitoring Phase

The meteorological data captured simultaneously is described in the methodology section of Section 4.3 Initial Monitoring Phase and consisted of measured and forecast data specific to the Spadeadam area.

5.2.2 Performance of SSW model during the Initial Monitoring Phase

For each measurement made at each INM receptor, comparisons between the measured and predicted LZpeak were made. The model used to make predictions was the Salford Surface Wind (SSW) model. Predictions accuracy is assessed according to a number of factors:

- For each forecast time,
- across each measurement station;
- and for each blast type

5.2.2.1 Prediction Accuracy Across All Locations

An analysis of all the SSW predictions over at all the monitoring locations, it is shown that at all forecast times between 0-24 hours to 117 hours ahead of a test time, approximately 15 % of predictions are 5 dB underpredictions, between 20-2 5% are within 5 dB, and finally, approximately 25 % are 5 dB over predictions. There's a low combined percentage of underpredictions of 10 dB or more, and a slightly higher combined percentage of 10 dB or more overpredictions. On two occasions, prediction errors were beyond this range, with a 25.2 dB overprediction at one of the locations in both the 25-48 and 51-69 hour range.

Note, this analysis is the combined results from all monitoring locations, across all forecast timesteps, for all test types and TNT equivalences.

This analysis shows a negligible difference in prediction error across all test types and locations for each forecast time step.

A slight increase in predictions of 15dB greater than measured levels is shown in Figure 101, attributed to the greater proportion of 15dB overpredictions for the VPD test type which is further discussed below.

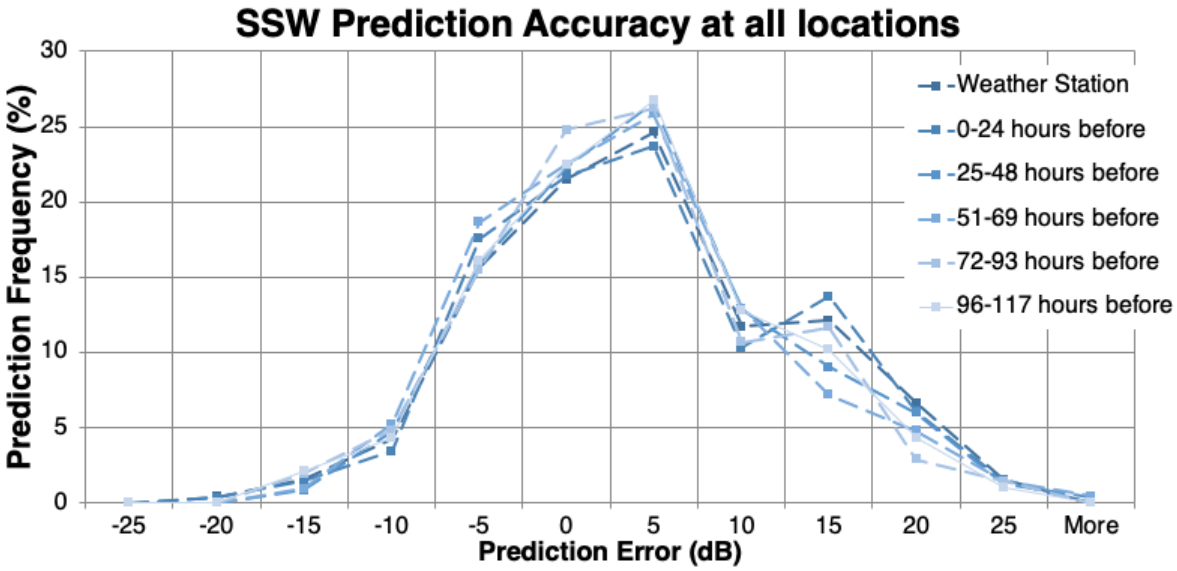

Figure 101 - Histogram of prediction errors as a function of forecast date, from the initial monitoring phase, including data from all monitoring locations, and for all test types.

5.2.2.2 Prediction Accuracy for Each Explosion Type

The analysis of the initial monitoring phase data was extended to observe the prediction accuracy of the SSW model as a function of test type. As shown in Figure 102, the performance of the SSW for the prediction of individual test types can observed.

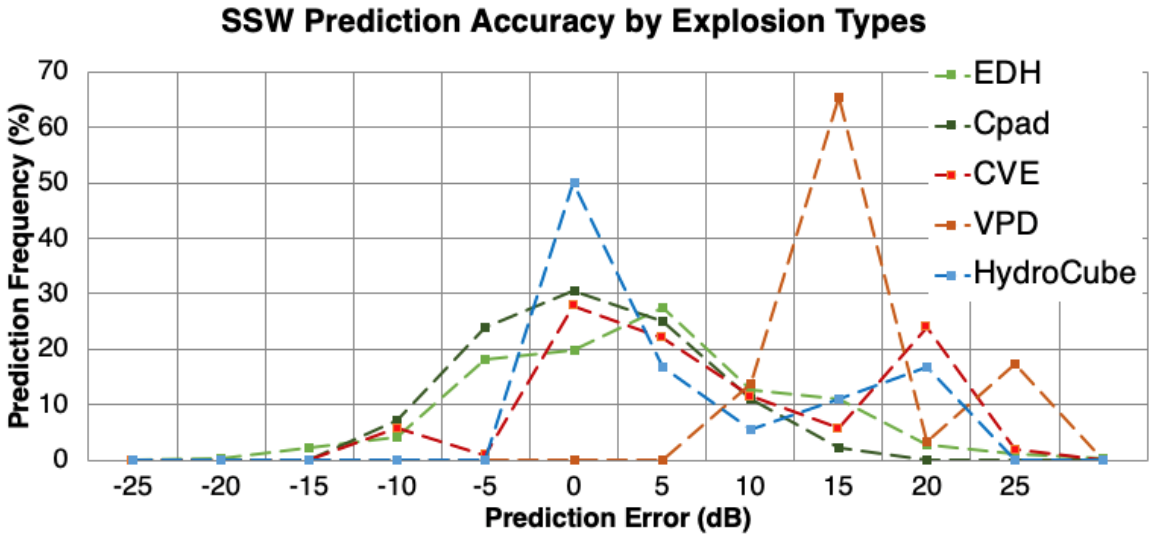

Figure 102 - Histogram of prediction errors as a function of forecast date and test type, from the initial monitoring phase, including data from all monitoring locations.

SSW Performance Against Gas Explosions: CVE and VCD

Figure 102 firstly shows that gas explosions, (those coloured in red hues) are skewed to the right of the x-axis. This means that in general, for the CVE and VPD tests carried out on site,

that predictions were mostly overpredictions when compared directly to measurements of the exposures from these operations.

More specifically, a high proportion of predictions (approximately 65 %) made for the VPD operation, using the SSW model, resulted in prediction errors of 15 dB. For this specific operation, SSW predictions only overpredicted the actual LZPeak.

Predictions for the CVE operations were also more often over predictions, although approximately 30 % of SSW predictions were within 5dB of the actual measured LZPeak for this specific operation.

SSW Performance Against Hydrogen Detonations

For the hydrogen detonations (similarly carried out as part of the hazard awareness courses), prediction errors were within 5 dB across all locations approximately 50 % of the time. In parallel to the CVE and VPD tests, SSW predictions generally resulted in overpredictions.

Performance Against Solid Explosives: EDH and Pad C

Finally, SSW performance against EDH and Pad C measurements are generally more variable than for the gas explosions and hydrogen detonation. As EDH made up a significant proportion of the measurements collected, more meteorological conditions are expected to cause this.

5.3 Assessment of Heuristic Model Performance

This section of the chapter presents the results gathered from the entire Live Noise Monitoring Network over the entire monitoring window, spanning October 2020 to December 2022. Comparisons of measurements are made with the predictions generated using the Salford Surface Wind model for a variety of input meteorological data. Predictions have been performed retrospectively, by using the following meteorological data sources, with the 10m wind speed and direction as the input parameters to the model.

- Measured 1-minute averaged data from R5BC Weather Station
- Measured 1-hourly averaged data from RAF Weather Station
- Simulated 1-hourly averaged data from ERA5 Surface Reanalysis Dataset

Additionally, comparisons are made with SSW predictions using the Met Office DataHub forecast dataset as input meteorological data.

- 1-hourly averaged data forecast 00-24 hours before test time
- 1-hourly averaged data forecast 25-48 hours before test time
- 3-hourly averaged data forecast 51-69 hours before test time
- 3-hourly averaged data forecast 72-93 hours before test time
- 3-hourly averaged data forecast 96-117 hours before test time

The number of possible prediction comparison for each test type and data source are tabulated below. The sum total of possible prediction comparison from all test types across all monitoring locations including each data source, amounts to 11742.

Table 63 - Number of possible comparisons against measured data for each test type and input meteorological data across all monitoring positions.

No. of Comparisons Available	Total	R5BC	RAF	SSW	DH On Day	DH 25-48h	DH 51-69h	DH 72-93h	DH 96-117h
EDH	4659	771	837	836	615	453	384	390	373
Pad C	689	103	113	99	94	69	81	69	61
CVE	350	51	49	55	49	41	33	39	33
HYD	173	23	20	27	23	23	17	21	19
Total	5871	948	1019	1017	781	586	515	519	486

In this analysis, the performance of the model is quantified by the Root Mean Squared (RMSE) Error metric, in dB. The greatest over predictions and underpredictions are useful for assessing model performance and are included in this analysis. The raw data is also tabulated in the appendices.

5.3.1 Short-Medium Range Forecast Performance

In this section, the predictions made with measured and reanalysis datasets as input meteorological data into the SSW model are presented. The model has made predictions for the following test types:

- EDH
- PadC
- CVE
- HYD

5.3.1.1 SSW Predictions of Explosive Depth Hardening

In the following charts, for each input data source for the SSW model, the RMS error is plotted (blue markers), with the minimum over and underprediction errors indicated by the magnitude of the error bars. Note that the RMS error is a scalar, in that is represents the root square mean errors of the both over and underprediction errors, and being positively valued does not indicate that it is more likely to overpredict, but that is that is essentially the uncertainty found from the predictions.

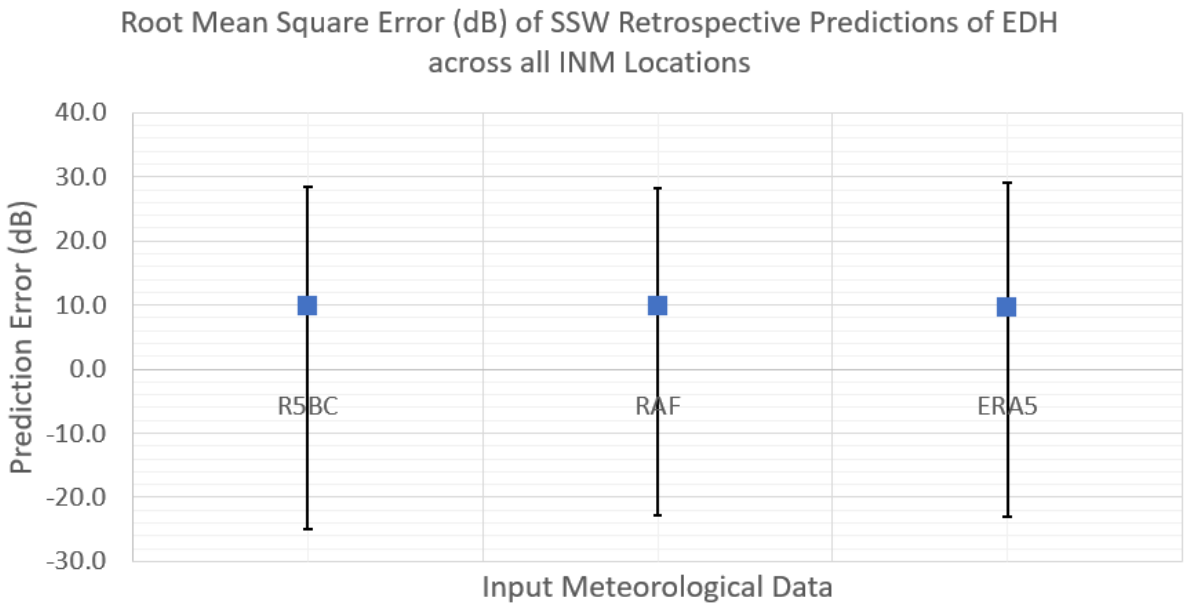

Figure 103 - RMS error of Salford Surface Wind Model for EDH operations, using measured data (1-minute average at R5BC station), (1-hourly averaged at RAF station), (1-hourly averaged ERA5 reanalysis data).

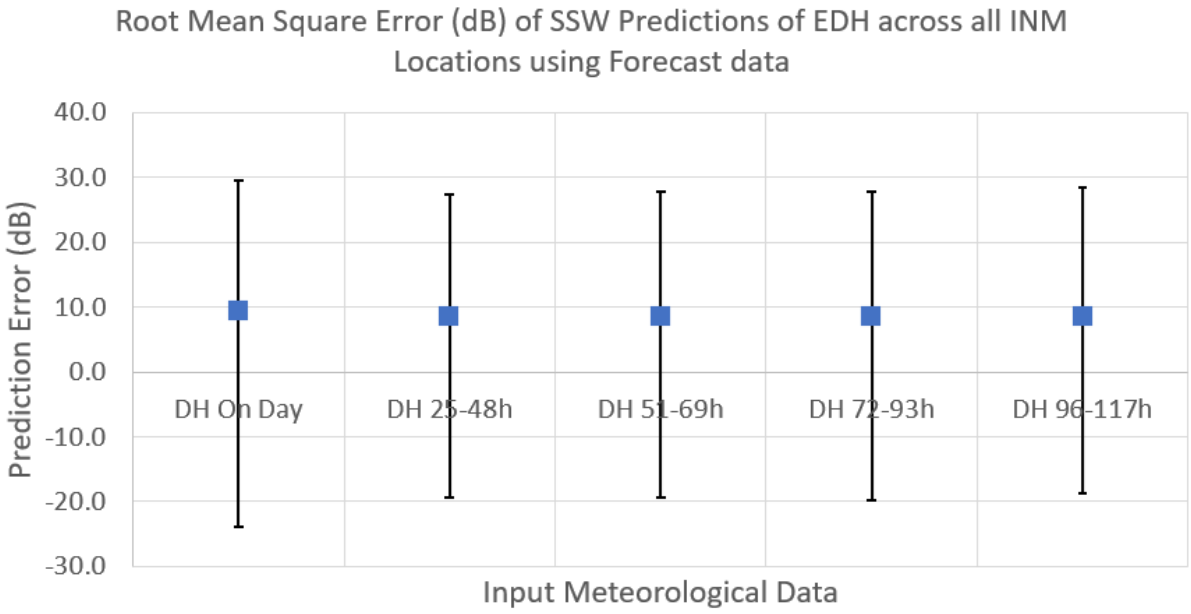

Figure 104 - RMS error of Salford Surface Wind Model for EDH operations, using forecast data.

The results have been further plotted to observe RMS error at each INM location, and both retrospective and forecast predictions are plotted together in the same figures.

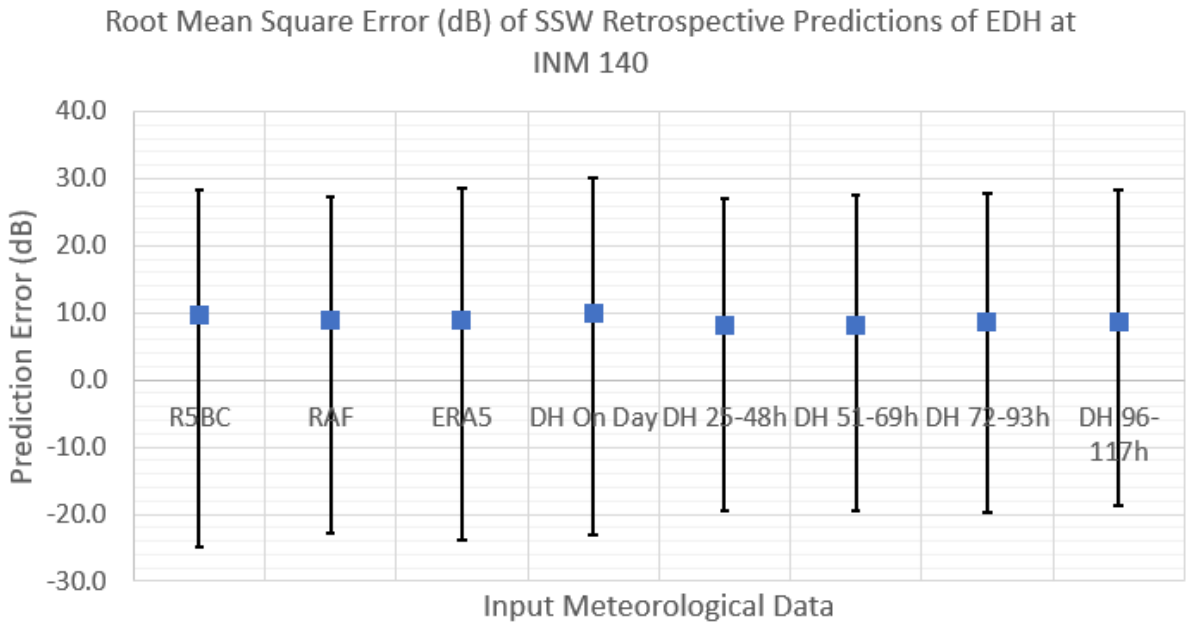

Figure 105 - RMS errors of Salford Surface Wind Model for EDH operations at INM 140, using all input meteorological data.

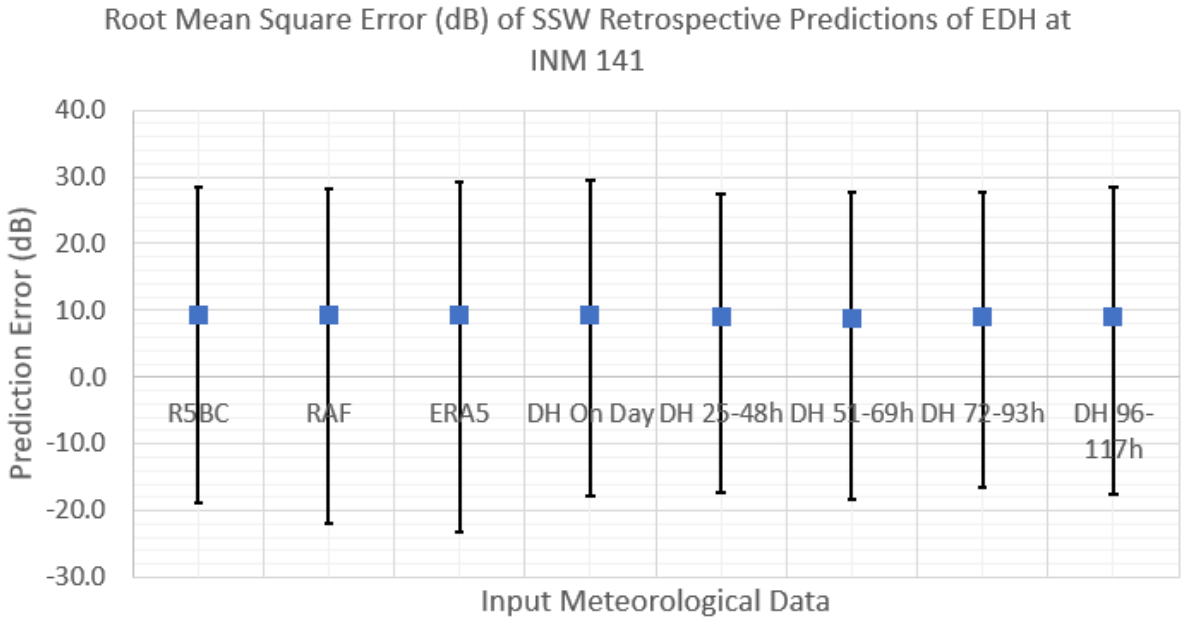

Figure 106 - RMS errors of Salford Surface Wind Model for EDH operations at INM 141, using all input meteorological data.

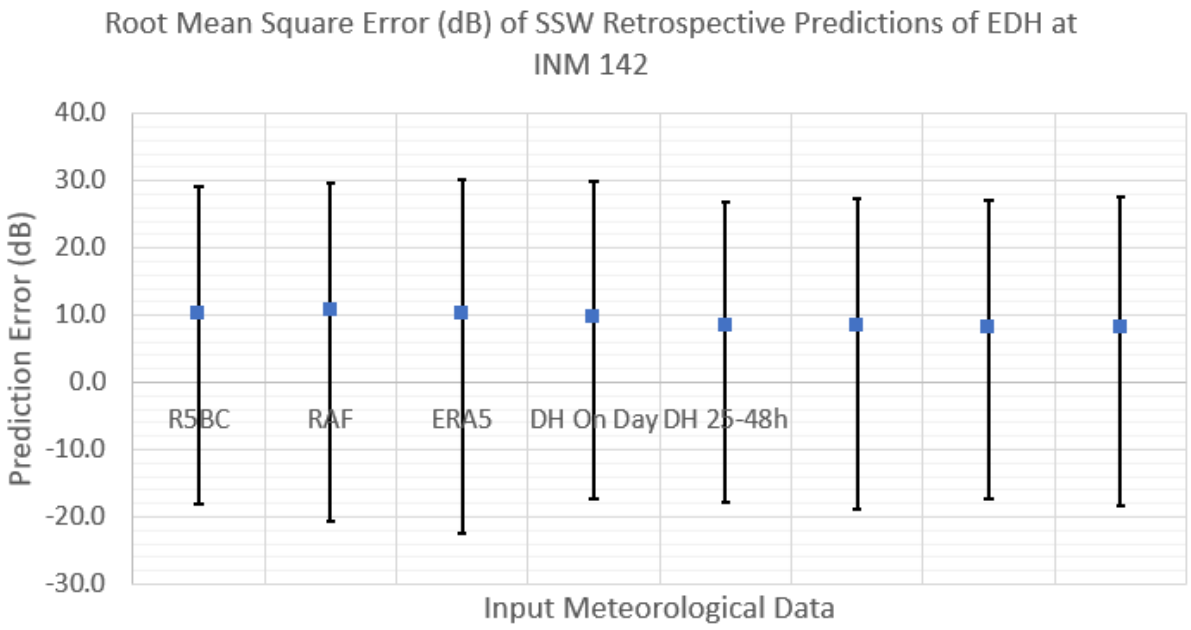

Figure 107 - RMS errors of Salford Surface Wind Model for EDH operations at INM 142, using all input meteorological data.

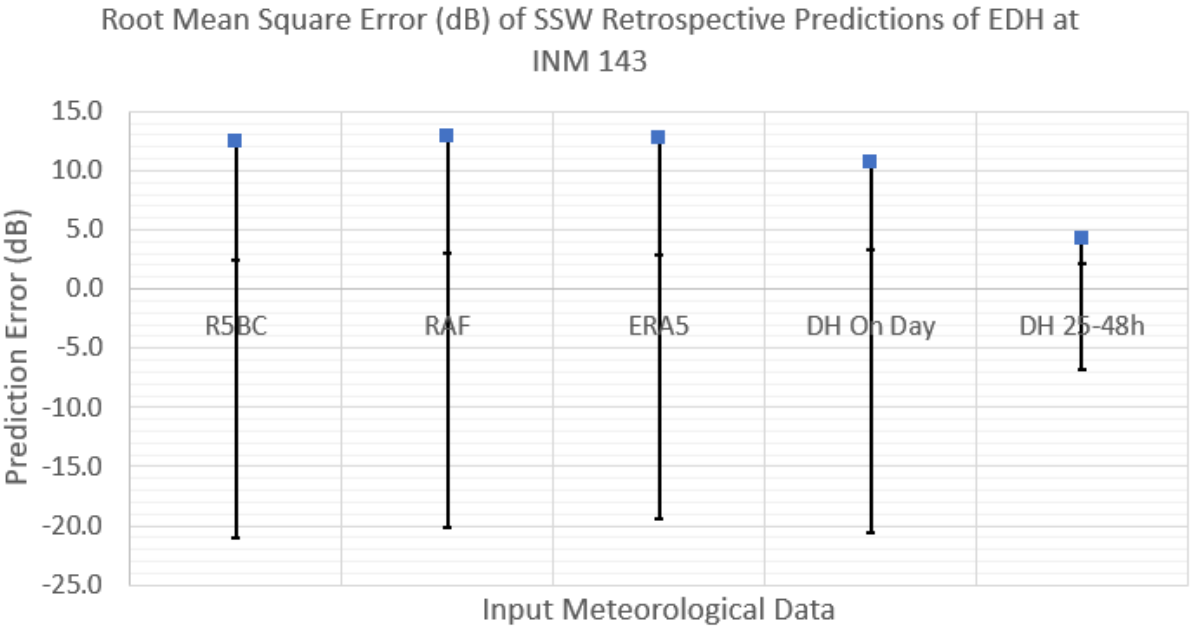

Figure 108 - RMS errors of Salford Surface Wind Model for EDH operations at INM 143, using all input meteorological data.

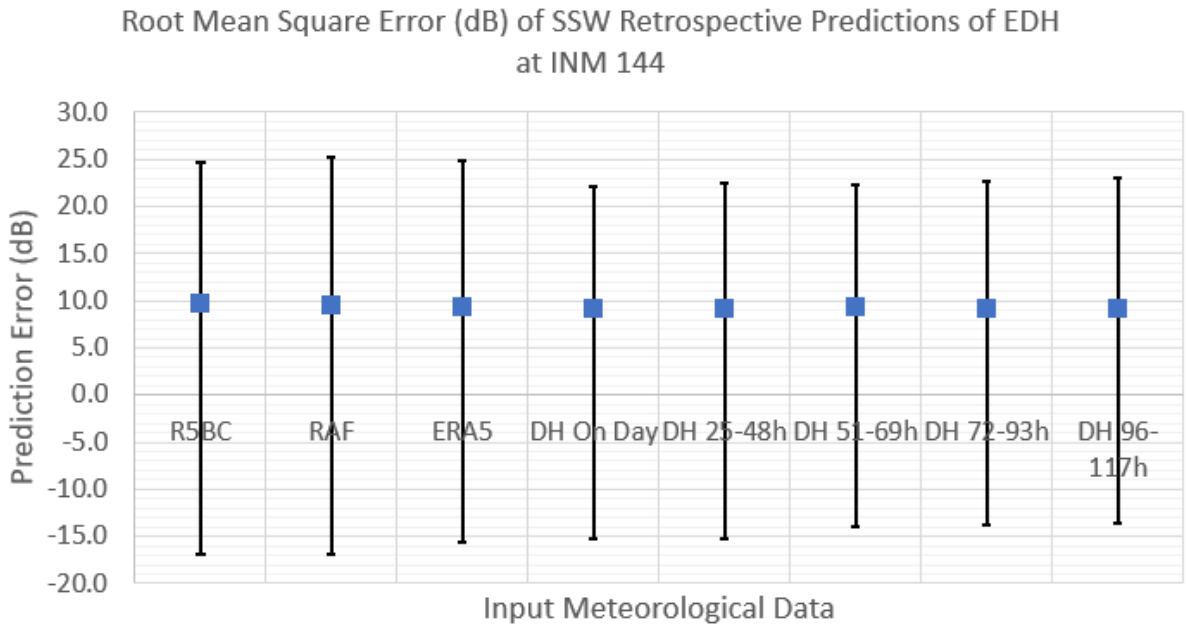

Figure 109 - RMS errors of Salford Surface Wind Model for EDH operations at INM 144, using all input meteorological data.

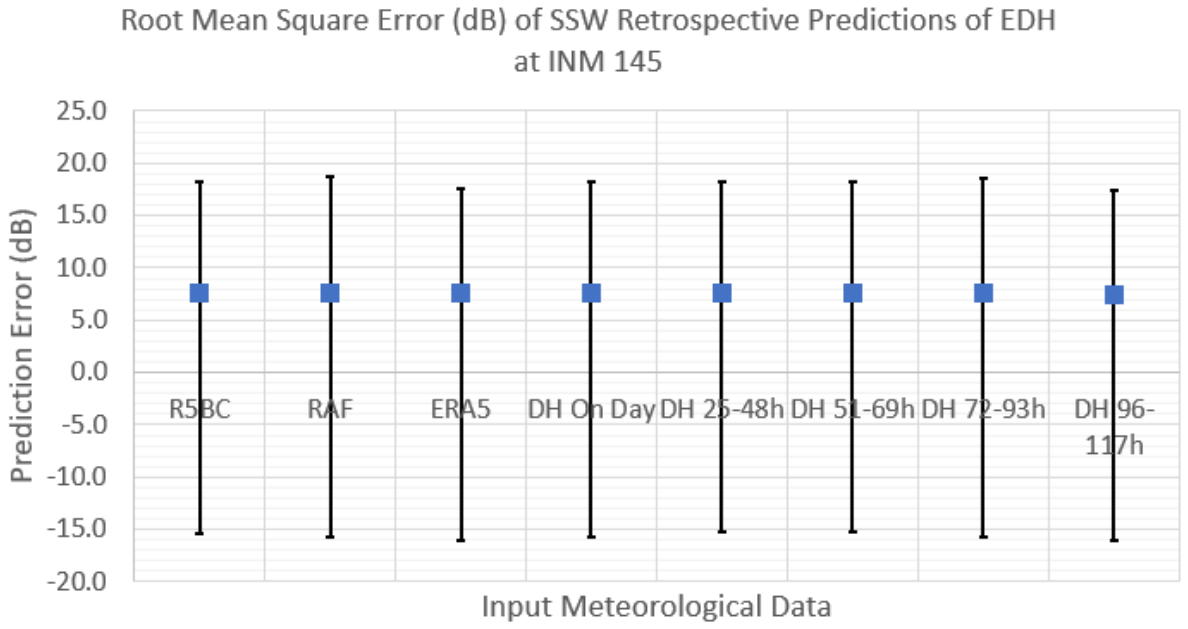

Figure 110 - RMS errors of Salford Surface Wind Model for EDH operations at INM 145, using all input meteorological data.

SSW Predictions of Pad C Explosions

The same analysis has been performed on the data measured from explosions on Pad C. Plots of RMS error contain both retrospective and forecast predictions from here on.

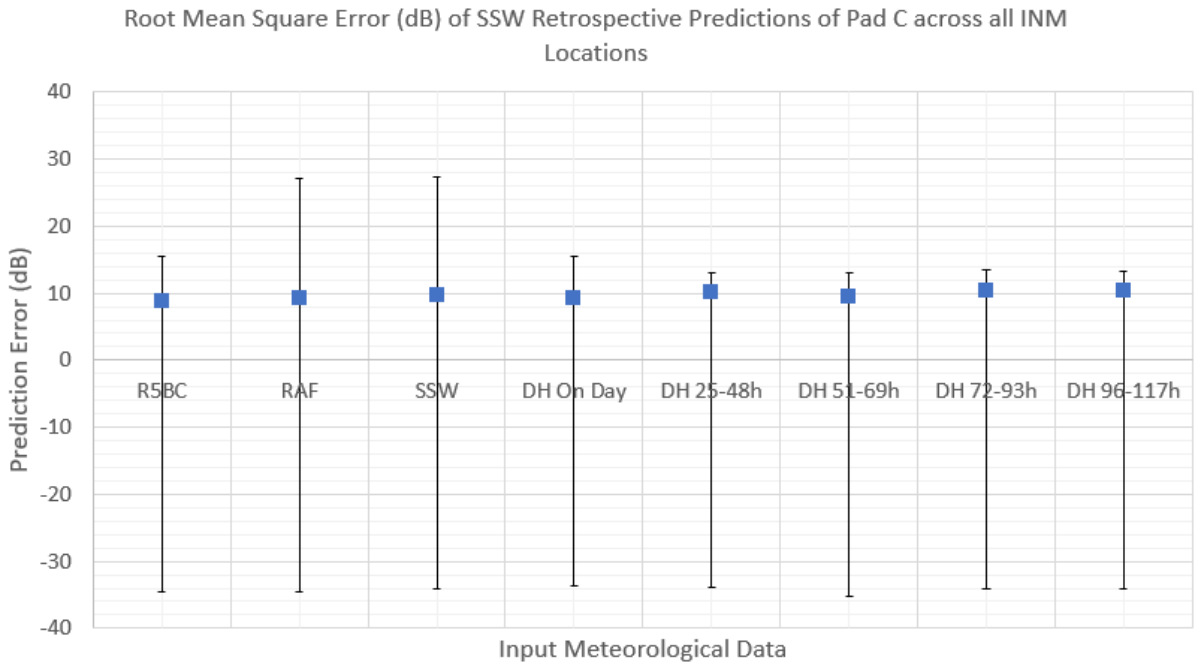

Figure 111 - RMS errors of Salford Surface Wind Model for Pad C operations at all locations, using all input meteorological data.

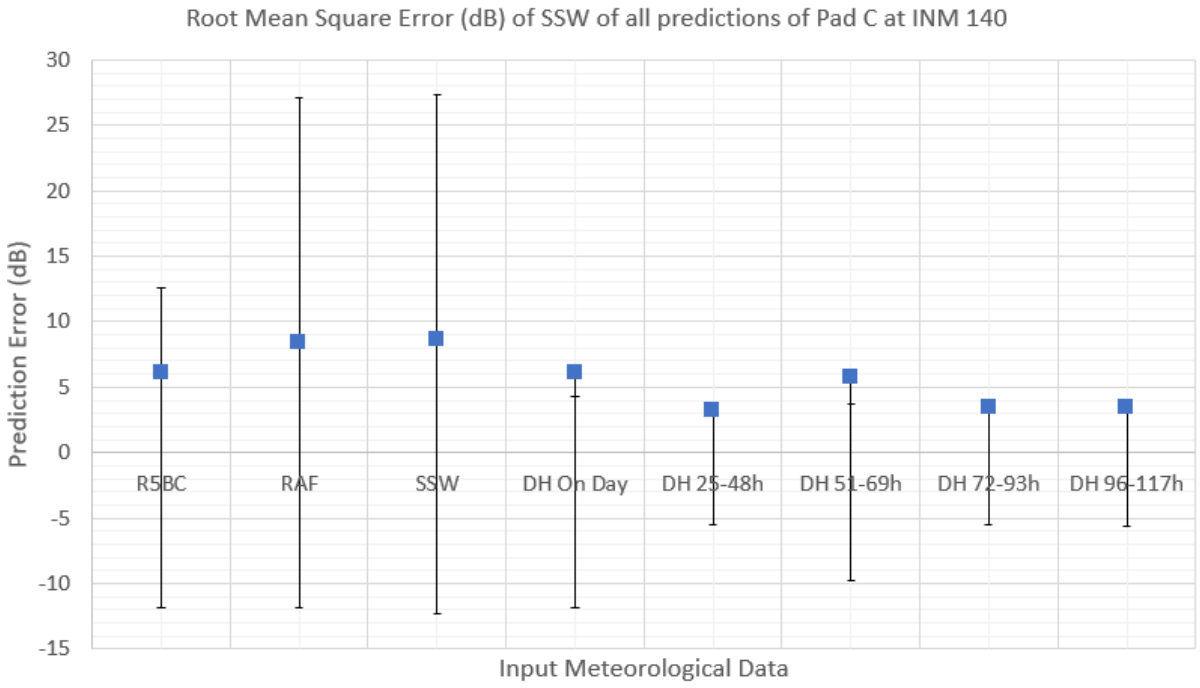

Figure 112 -RMS errors of Salford Surface Wind Model for Pad C operations at INM 140, using all input meteorological data.

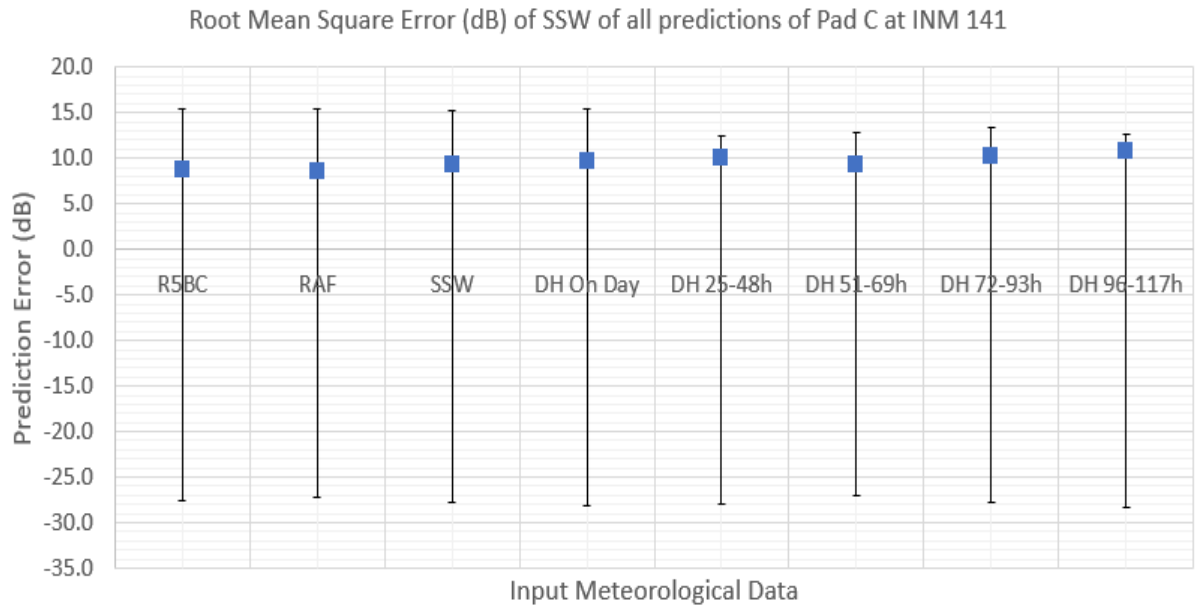

Figure 113 - RMS errors of Salford Surface Wind Model for Pad C operations at INM 141, using all input meteorological data.

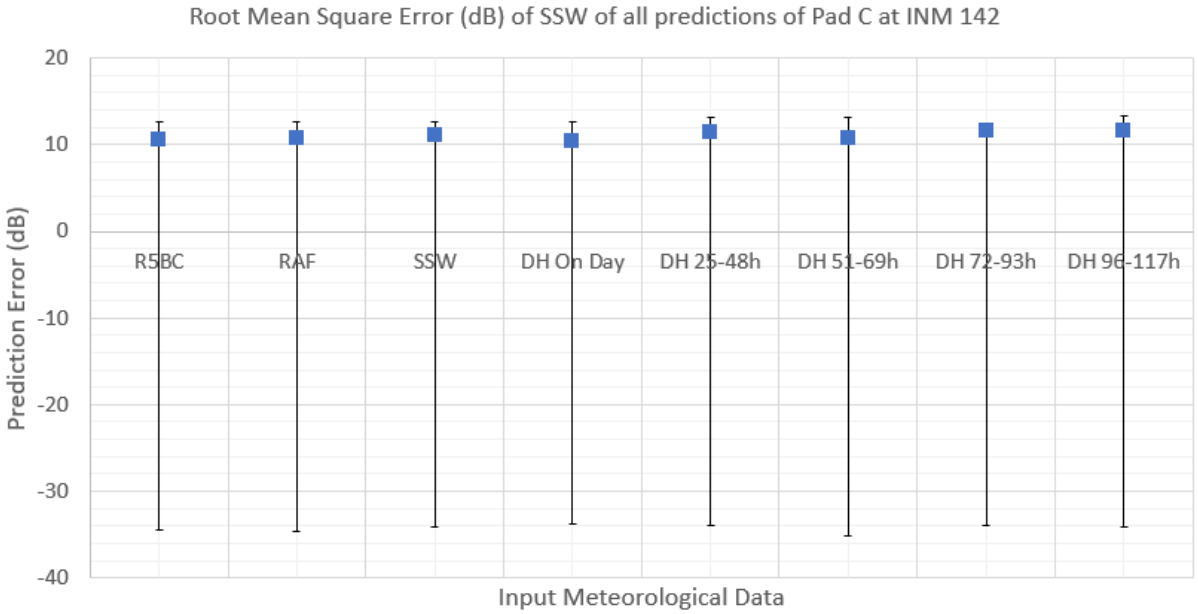

Figure 114 - RMS errors of Salford Surface Wind Model for Pad C operations at INM 142, using all input meteorological data.

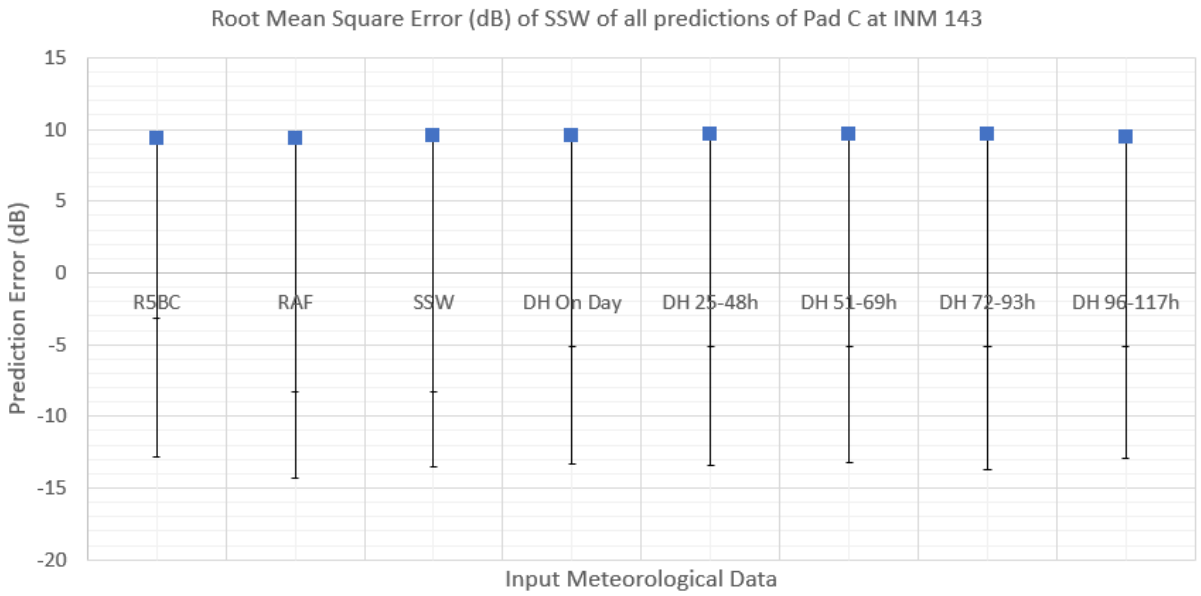

Figure 115 - RMS errors of Salford Surface Wind Model for Pad C operations at INM 143, using all input meteorological data.

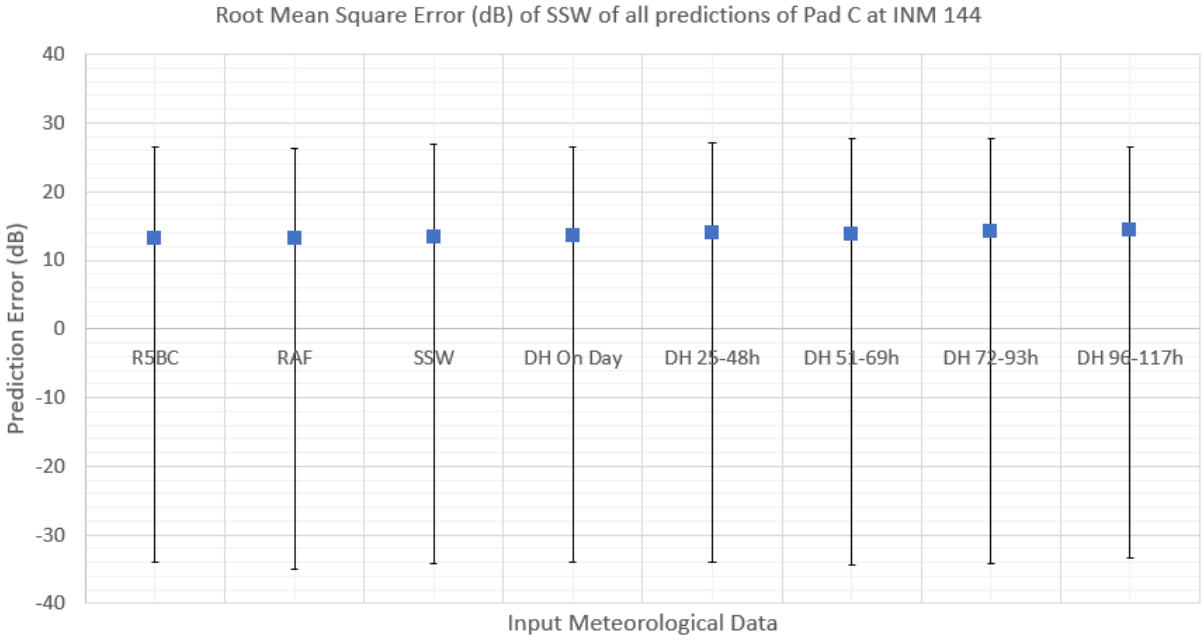

Figure 116 - RMS errors of Salford Surface Wind Model for Pad C operations at INM 144, using all input meteorological data.

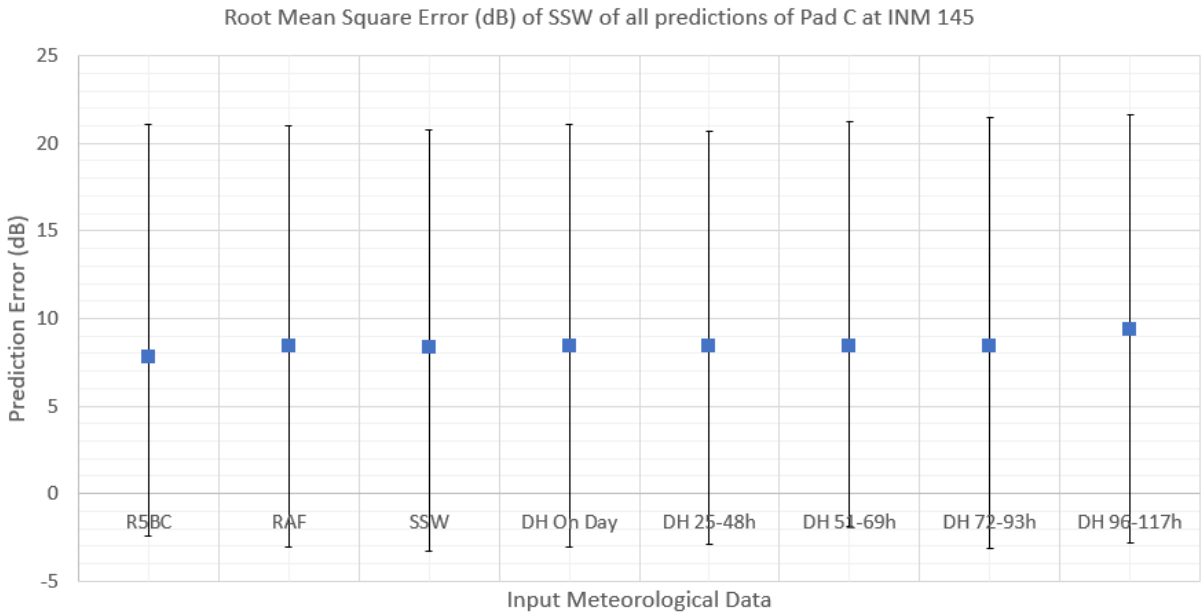

Figure 117 - RMS errors of Salford Surface Wind Model for Pad C operations at INM 145, using all input meteorological data.

5.3.1.2 SSW Predictions of Confined Vented Explosion Chamber

The RMS prediction errors of the SSW for predictions of the CVE operation are shown here with the maximum over and underpredictions. Given that the dataset for the CVE tests was limited in sample size, this section provides only a broad overview of the SSW performance for predicting CVE.

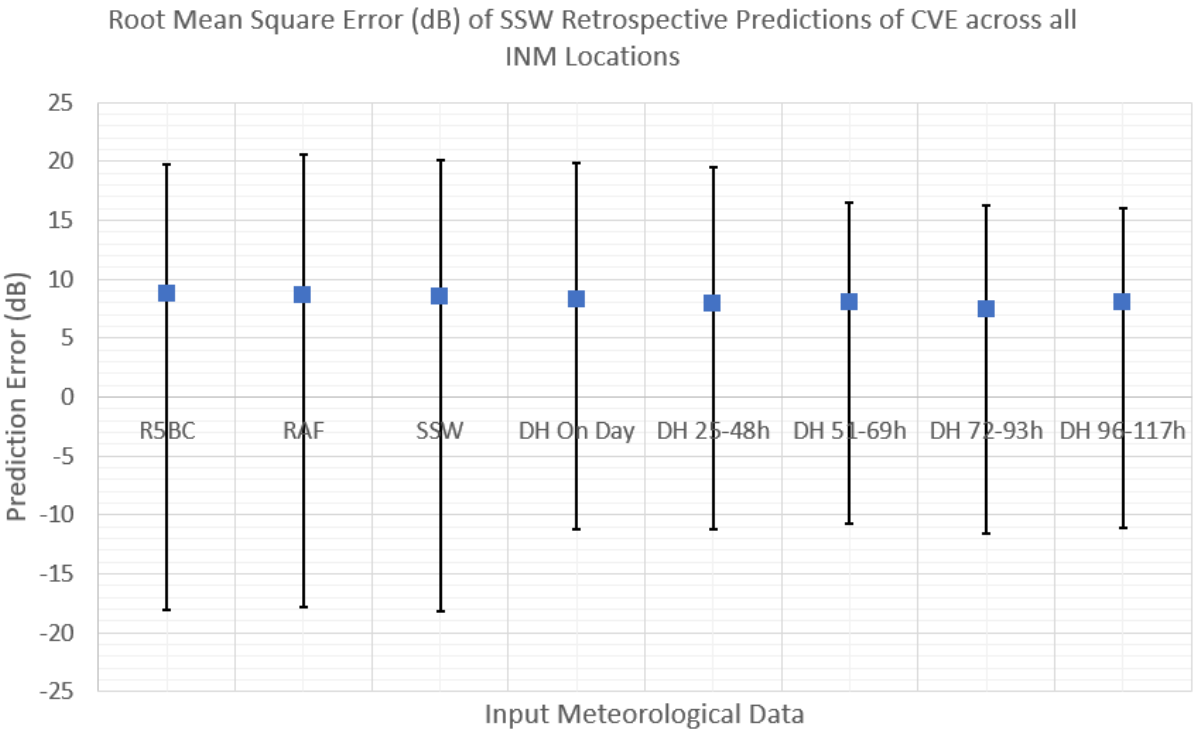

Figure 118 - RMS errors of Salford Surface Wind Model for CVE operations at all monitoring locations, using all input meteorological data.

5.3.1.3 SSW Predictions of Hydrogen Detonations

Similarly, the same analysis is presented for the few hydrogen detonations captured by the Live Monitoring Network.

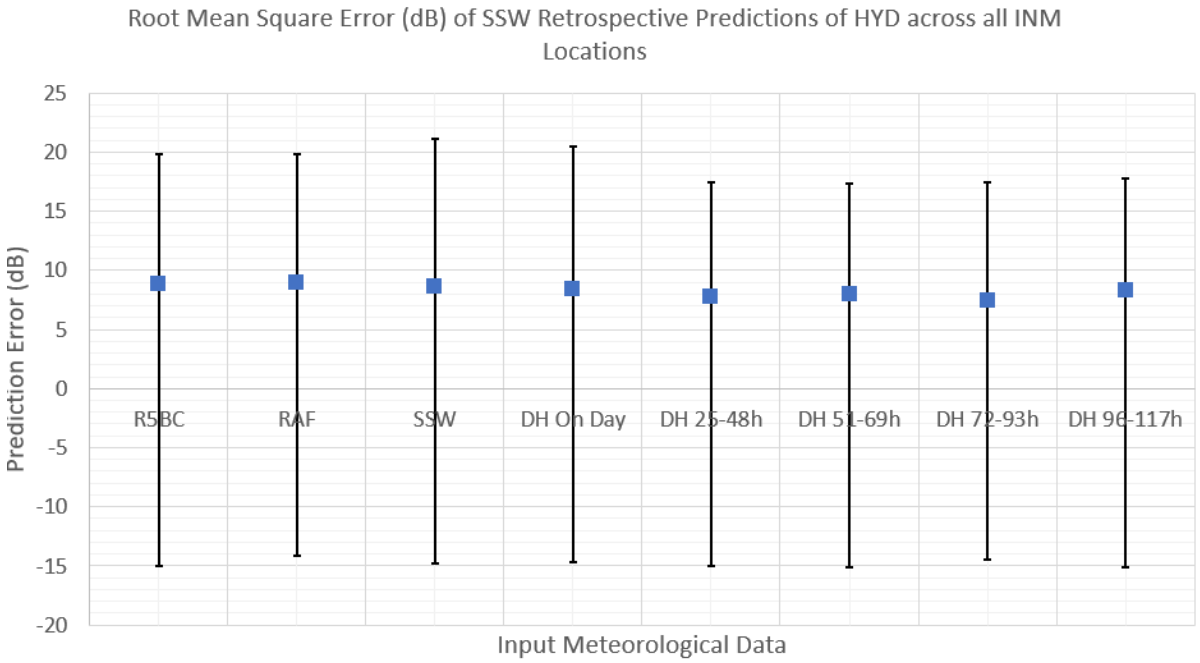

Figure 119 - RMS errors of Salford Surface Wind Model for HYD operations at all monitoring locations, using all input meteorological data.

5.3.2 5.3.3 Performance of MONET against the Salford Surface Wind (SSW) Model

A major goal at the inception of this PhD was to assess the predictive ability of MONET against measurements of large-scale blast testing at Spadeadam. This subsection is dedicated to evaluating the performance of MONET throughout this PhD process, as well as comparing the prediction accuracy to a much simpler model, the aforementioned SSW model.

As MONET is carried out externally from DNV and is solely operated by Operational Meteorologists at the Met Office, model runs available for comparison with measurements, or against the SSW predictions are limited to the largest tests carried out at Spadeadam. This is because each MONET forecast requested by DNV is an additional expense to the specific project related to the explosion test. MONET forecasts were used therefore to make operational decisions on whether to carry out the test or not based on the proposed noise footprint, rather than as a research tool. Consequently, the MONET forecasts all relate Pad C explosions captured in the Live Knowledge Database of this Thesis. The terms, “prediction”, “forecast”, “model runs” and “footprint” are used interchangeably in this subchapter and refer to a specific instance of a noise prediction by MONET relating to a single explosive test.

Pad C explosions vary in size and DNV policy at the time of writing was to obtain MONET footprints for any test with charge size greater than 40kg TNT, although some are requested for smaller charges (25 kg TNT). In general though, the sample size for comparison with measurements and other models is rather small, and excludes much of the original Pad C data analysed in previous sections. Additionally, the respective measurement at the monitoring location had to be made, and furthermore, not contaminated by extraneous noise. This further limits the sample size, where measurement errors or missing data occurred occasionally, for example from power outages at the monitoring locations.

5.3.3 Performance at each INM Location

Table 64 has the number of tests measured by the monitoring network that are available for comparison with a MONET footprint.

Table 64 - Number of available comparisons for MONET against valid measurements of Pad C tests.

TNT Equivalence	Number of comparisons available
25	1
50	2
100	23

Firstly, it is useful to tabulate the prediction errors for individual tests at each location. While it may be useful to use metrics such as Root Mean Squared (RMS) error to evaluate MONET's performance, given the small sample size it is useful first to compare the prediction errors at each location for each individual test. The following tables present the test details and the associated prediction error compared to measured level at each monitoring location. Positive errors indicate an overprediction by MONET (predicted level is higher than measured), and negative errors indicate an underprediction by MONET (predicted error is lower than measured). With respect to environmental noise management, the latter case is usually less desirable, which is why it is important to give context to this evaluation, and it is useful to show when MONET is over or underpredicting with the accompanying measurements.

An important factor is the information on the time between issuing the MONET forecast and carrying out the test (T_i), as well as whether the test was performed within the test window used in the MONET forecast. MONET could only perform calculations up to 36 hours ahead

of testing, and each forecast was related to weather forecasts at updated at 6-hour intervals. It would be expected that as T_i increases, that prediction error increases in magnitude (either positively or negatively).

When a MONET footprint is requested by DNV range controllers, a desired testing window is given to the Met Office for which the calculation is to be valid for, e.g. between "1300-1400 today". As deviations to the test program associated with the specific test could occur for any number of reasons (conflict with RAF activity, severe weather, etc.), it was important to note whether each test was carried out within the requested forecast window. Although some noise footprints are reported to be valid for time windows as short as 45 minutes, the finest time resolution of the Met Office's input meteorological forecasts used by MONET is 1 hour. The penultimate column in the following tables, labelled T_e represents the time that each test precedes or exceeds its associated forecast window. If a test was carried out within the forecast time window, it is marked by a 'yes' as there is no difference in the prediction based on when it is carried out in the time window, and if a test was delayed or carried out earlier than expected, how much the test preceded or exceeded the prediction time window is recorded. This is important, as one would expect that noise from tests performed outside the predicted test window could deviate significantly depending on if the weather was significantly variable on that respective day.

Of course, there are many physical factors that influence receiver noise levels, as discussed in this thesis, however a vector wind is also given in the table for context, indicating approximate upwind, downwind or crosswind propagation. The vector wind, v is defined below, with u as the wind speed in ms^{-1}, ϕ as the wind direction towards which blowing and θ the azimuth angle between the source and receiver.

$$v = u\cos(\phi - \theta)$$

5.3.3.1 INM 140 Wardrew Farm

Three comparisons were available to be made between MONET and the measurements taken by the INM at Wardrew Farm. This location was the closest long-term position to Spadeadam, situated to the south at just 4.3km and 164° re. north from Pad C.

Table 65 - MONET prediction errors at INM 140 Wardrew Farm.

Test Date and Time	Test Weight	Measured LZpeak	MONET Prediction	T_i (hours)	T_e $(hours)$	v (ms^{-1})

		(dB)	Error (dB)			
2021-03-31 09:12	100	124.0	-7.0	1.5	Yes	7.7
2021-10-04 10:00	100	94.8	14.5	2.0	Yes	-3.7
2021-10-05 10:08	100	128.5	1.7	18.0	< +0.25	10.9

From Table 65, the prediction errors range between 1.7 and 14.5 dB in magnitude for the individual tests observed. The 100 kg detonation conducted on the 31st March 2021 yielded an underprediction of 7.0 dB. This underprediction is somewhat concerning based on the context of the measured peak level (124.0 dB), just 1 dB below Spadeadam's self-imposed limit for off-range noise, with MONET predicting 117.0 dB. Furthermore, the forecast was issued just 1.5 hours before commencing the test, meaning that forecast accuracy was likely to be high, and the test being performed within the time window requested to the Met Office.

The greatest prediction error was an overprediction of 14.5 dB above a measured level of 94.8 dB. This case is not necessarily as problematic as the previous error, as in this case, this receiver is upwind of Pad C, and the likelihood of exceeding the 125 dB site limit is significantly lower. Overpredictions can pose problems if they cause tests to be postponed when in reality, measurements are within the 125 dB limit, however the prediction on this occasion of 109.3 dB would not have (and did not) lead to DNV postponing the test.

Finally, the smallest prediction error was a 1.7 dB overprediction for a strong downwind propagation scenario. Although, the measured noise exceeded the self-imposed limit of 125 dB (measuring 128.5 dB), it suggests that MONET may perform well for strong downwind conditions, proving more reliable for locations expected to receive noise enhancements, however, many more comparisons are required to confirm this.

The RMS prediction error for this location was 9.3 dB.

5.3.3.2 INM 141 Blenkinsopp Castle

Along the same propagation path is INM 141 at Blenkinsopp Castle retirement park, situated 8.6 km 156° re. north from Pad C. With 5 observations available at this location, the RMS error was 8.5 dB, with a minimum and maximum magnitude of 2.1 and 15.6 dB respectively. The largest and most significant errors, relate to underpredictions of 15.6 dB and 10.3 dB for 100 kg detonations in July 2022. Although, T_e is reasonably low, being 0 and +1.25 hours in case 1 and 3 respectively, of significance is the T_i of 21 hours in both cases, indicating that

the actual meteorological conditions varied significantly with respect to the forecast conditions over that time period. This argument is backed up by case 2, which has a low prediction error of just 2.4 dB, whereas the time between issuing the forecast and carrying out the test is just 6 hours. Although, this related to a later part of the day, it is possible that a more realistic representation of the meteorological conditions featured in the noise forecast based on a more recently updated meteorological forecast. Alternatively, it is possible that the afternoon conditions are better predicted by the forecast model, whereas early morning stability may have been underestimated for cases 1 and 3 which had significant underpredictions and low magnitudes in the vector wind speed, indicating that the boundary layer was possibly not well developed for this time of year.

Another argument could be that the measured wind direction during the July tests were 270, 260 and 250 respectively, (all with wind speeds 5m/s or higher). With Blenkinsopp Castle to the south of Spadeadam, under a westerly wind the propagation scenario is likely to be between downwind and crosswind. By factoring in the effects of atmospheric turbulence, slight changes in wind direction may cause this location to be within or outside of a zone of enhancement, and changes in the wind speed will modify the prominence of a downwind or crosswind condition. It's likely that the hourly-averaged forecast window was not temporally fine enough in resolution to capture the real propagation conditions, which were likely to be downwind rather than crosswind based on the high LZPeak measurements. Figure 120**Error! Reference source not found.** shows a relatively neutral propagation scenario with a slight enhancement in the south easterly direction, with the Blenkinsopp Castle not present on the footprint, as the 110 dB contour (black line) only reaches as far as Gilsland Spa in the southwards direction. Alternatively, Figure 121 and Figure 122 show strong downwind enhancement to the east, with the 110, 115 and 120 dB contours (2 outer black lines and outer magenta line) covering a much wider area. It's likely that the propagation conditions during the test undertaken on 07 July at 09:33 were more similar to those in Figure 122 than Figure 120.

Table 66 - MONET prediction errors at INM 141 Blenkinsopp Castle.

Test Date and Time	Test Weight	Measured LZpeak (dB)	MONET Prediction Error (dB)	T_i (hours)	T_e ($hours$)	v (ms^{-1})
2022-07-07 09:33	100	122.2	-15.6	21	Yes	1.8
2022-07-07 15:44	100	117.5	2.4	6	Yes	1.8

2022-07-08 11:18	100	116.7	-10.3	21	+1.25	0.5
2022-10-03 11:58	100	101.3	2.2	2	Yes	-3.7
2022-10-18 15:01	100	106.6	-2.1	28	Yes	-2.1

Furthermore, prediction errors of +2.2 and 2.1 dB were made in October trials. Interestingly, the 2.1 dB underprediction was given at the largest T_i of 28 hours ahead of testing. This suggests that if the forecast meteorological data used as input into MONET, it is possible to achieve significant prediction accuracy, given the range to this location (almost 10 km).

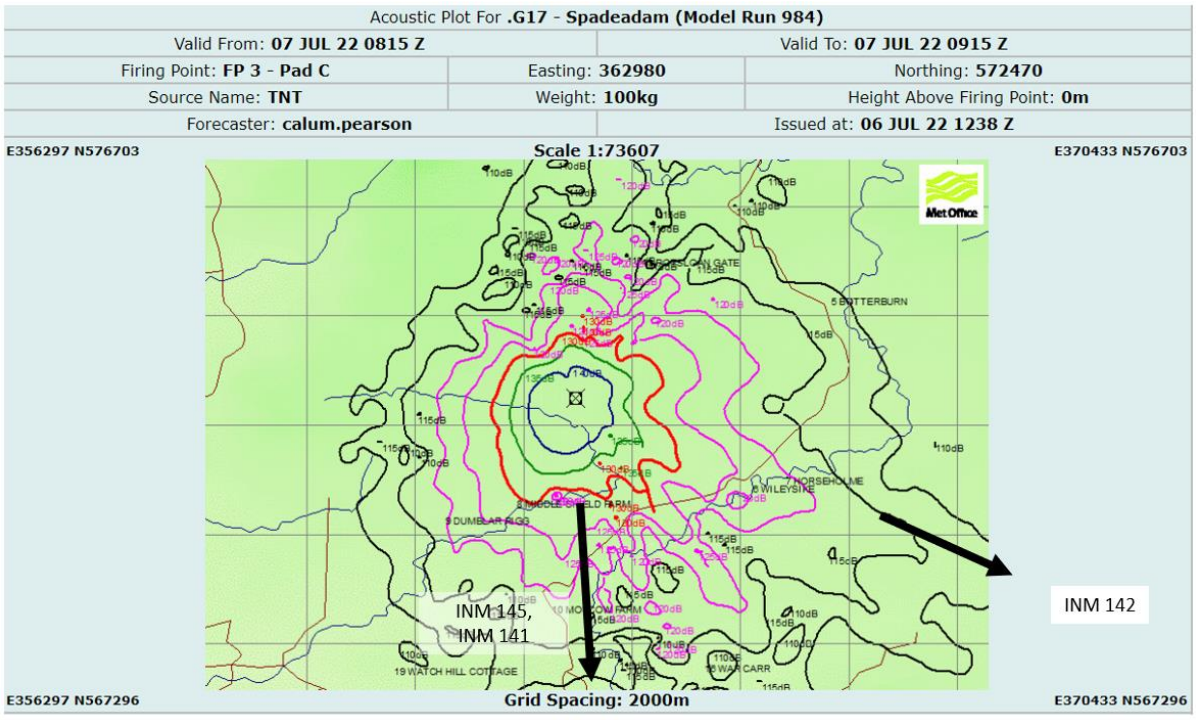

Figure 120 - MONET footprint for 100 kg Pad C test on 07 Jul 2022 0915-1015 GMT.

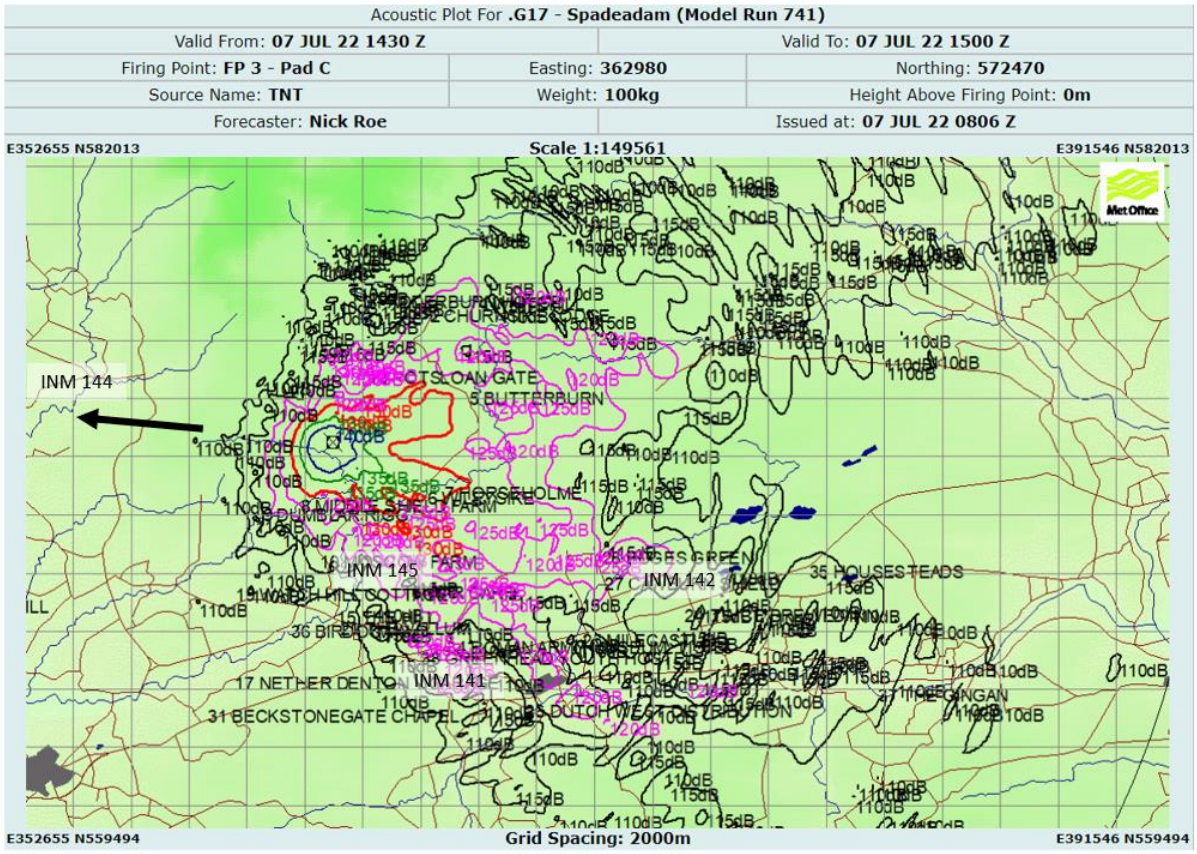

Figure 121 - MONET footprint for 100 kg Pad C test on 07 Jul 2022 1530-1630 GMT.

5.3.3.3 INM 142 High Close A Burn

High Close A Burn is situated to the SE of Spadeadam in the Cawburn area at 10.1 km 117° re. north of Pad C. This location as well as INM 141, 143 and 144 are significant distances away from Spadeadam, yet an RMS prediction error of 6.7 dB was found for comparisons noise from 100 kg detonations at this location. Prediction errors as low as 1.7 dB (overprediction) were observed (case 4 of Table 67), and up to 10.9 (underprediction).

Cases 1-3 for this location were the same as those for INM 141 (see **Error! Reference source not found.** to

Figure 122 - MONET footprint for 100 kg Pad C test on 08 Jul 2022 0930-1030 GMT.

), so T_i and T_e are equal, and given the approximately westerly winds of these trials (blowing from 250-270 ° re north), the vector wind speed is slightly higher for INM 142, given it's proximity to Spadeadam is more of an easterly component. The first two 100 kg detonation of the July trials were underpredicted and overpredicted by 6.6 dB and 7.5 dB respectively, with moderate vector wind components. The best performance of those trials is seen on the 08 July

with MONET predicting 2.3 dB higher than measured, again with moderate vector wind component.

The smallest prediction error occurred in the first October trial in 2022, of just +1.7 dB. This prediction was made just 2 hours before the test, which was carried out within the requested forecast window. Of note is the magnitude of the vector wind, being just -0.6 m/s, with the wind direction recorded on the Berry Hill station as blowing from the SSW (200° re north), yielding an approximately crosswind scenario for High Close A Burn, as shown in **Error! Reference source not found.**. On this instance, MONET was able to predict to a reasonable accuracy (< 2 dB), the peak sound pressure level for a location not immediately down wind or upwind, which may have been subject to variable effects depending on the structure of the transition zone between refractive attenuation and enhancement.

Table 67 - MONET prediction errors at INM 142 High Close A Burn.

Test Date and Time	**Test Weight**	**Measured LZpeak (dB)**	**MONET Prediction Error (dB)**	T_i **(hours)**	T_e $(hours)$	v **(ms^{-1})**
2022-07-07 09:33	100	114.6	-6.6	21	Yes	4.1
2022-07-07 15:44	100	115.1	7.5	6	Yes	6.2
2022-07-08 11:18	100	119.6	2.3	21	+1.25	5.3
2022-10-03 11:58	100	106.2	1.7	2	Yes	-0.6
2022-10-18 15:01	100	104.9	-10.9	28	Yes	-4.6

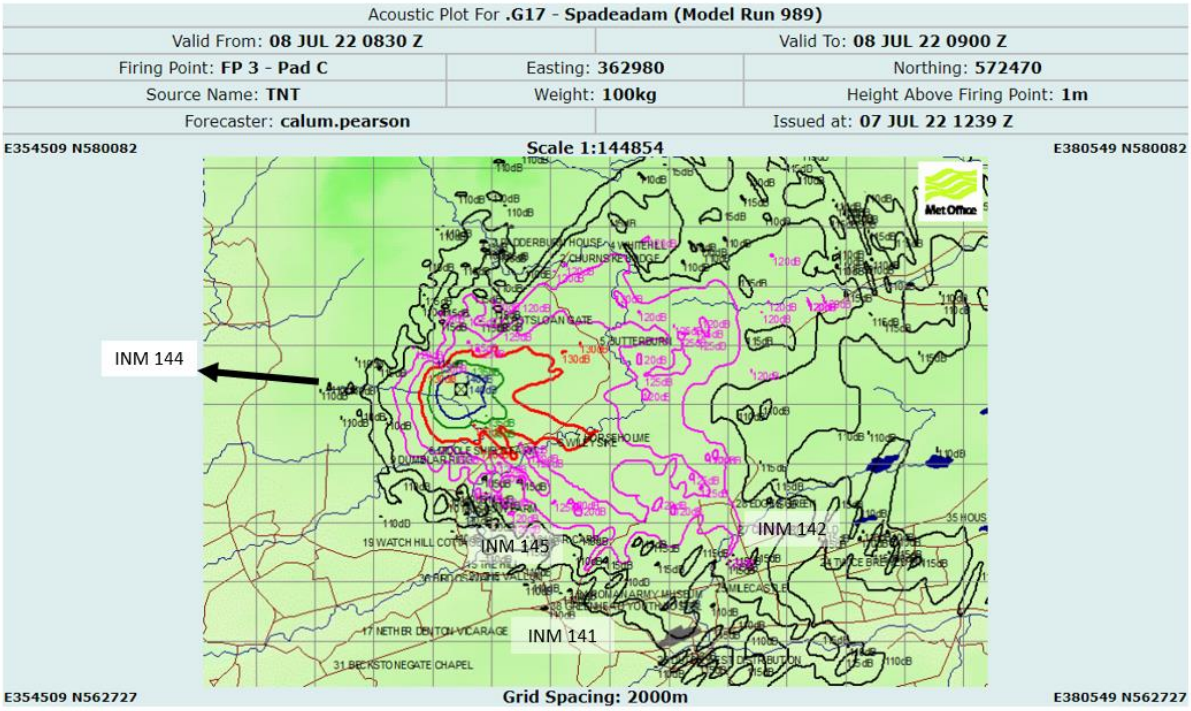

Figure 122 - MONET footprint for 100 kg Pad C test on 08 Jul 2022 0930-1030 GMT.

5.3.3.4 INM 143 Cranberry Brow

The furthest long-term receptor in this study was Cranberry Brow, again located along the same propagation line as High Close A Burn, approximately 13.7 km to the south east of Spadeadam (120 ° re north). From the small sample size of just 3 tests, an RMS error of 10.6 dB is given from two overpredictions (12.8 and 5.2 dB) and an underprediction of 12.1 dB.

The underprediction on this occasion is somewhat problematic for its magnitude (> 10 dB), but more so in the context of the measured peak SPL. An LZpeak of 121.3 dB is uncommon at this distance, and although below the 125 dB site limit, would have caused some concern to the DNV range controllers, had it been predicted by MONET. Possible causes for this prediction error could be from the T_i being relatively large compared to other MONET predictions (21 hours), meaning the forecast meteorology not being representative of the real-world conditions at the time of firing. Additionally, the test was carried out more at least 1.5 hours being the valid forecast time window, and it's possible that the meteorological conditions had caused the already predicted south-easterly enhancement zone (see

Figure 122 - MONET footprint for 100 kg Pad C test on 08 Jul 2022 0930-1030 GMT.

) to move closer towards Cranberry Brow by the time of firing.

Also of concern is the overprediction of 12.8 dB for a measured LZPeak of 118.9 dB on the 31st March 2021 at 09:12 (see Table 68, Figure 123). While the test was carried out with such high predicted levels (> 125 dB for several along this SE line), regular regions of enhanced noise can be seen in Figure 123 spanning from the NE to the SE. There is no meteorological phenomena that can explain this pattern, and they appear on the other footprints referenced in this thesis, leading the author to speculate that they could be an artefact of the model, possibly related to the interpolation routine between predictions made along each calculation azimuth around the source. This is an important feature of MONET, where on the 31st of March, it lead to significant overpredictions.

Table 68 - MONET prediction errors at INM 143 Cranberry Brow.

Test Date and Time	Test Weight	Measured LZpeak (dB)	MONET Prediction Error (dB)	T_i (hours)	T_e $(hours)$	v (ms^{-1})
2021-03-31 09:12	100	118.9	12.8	1.5	Yes	4.9
2022-07-07 15:44	100	109.7	5.2	21	Yes	5.9
2022-07-08 11:18	100	121.3	-12.1	21	+1.25	5.0

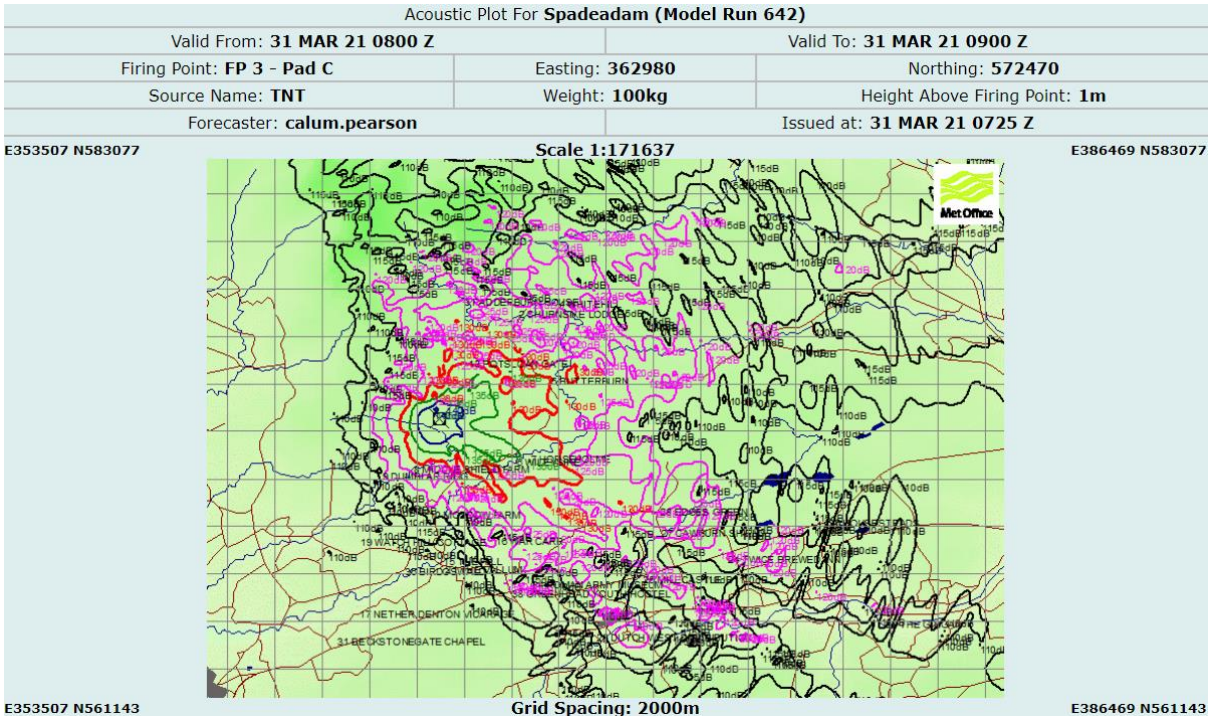

Figure 123 - MONET footprint for 100 kg Pad C test on 31 Mar 2021 0900-1000 GMT.

5.3.3.5 INM 144 Annshill

This long distance receptor is situated approximately 9.8 km to the West of Spadeadam at 286 ° re north. Given this long distance, the lowest prediction error of the entire dataset is found (1.3 dB). This slight overprediction occurred for the 100 kg detonation on the 18 October 2022 (see Figure 124), where favourable propagation conditions are shown towards the West of Spadeadam. The moderate vector wind speed also reflects this, which is a relatively uncommon propagation case for Spadeadam, where westerly winds dominate. Of note is that T_i is at its highest in the whole dataset and produced a large prediction error for INM 142 (-10.9 dB) but of a similar magnitude to INM 141 (-2.1 dB).

The other two observations (3rd and 25th Oct) have relatively small T_i with both tests carried out within the forecast window. These conditions were crosswind (v = -0.3m/s see **Error! Reference source not found.**) and moderately upwind (v = -3.2 m/s, see Figure 125). Given that T_i and T_e were small, this suggests that MONET did not accurately model the crosswind or upwind conditions on these occasions.

An RMS error of 8.8 dB was given by the three available comparisons for this location.

Table 69 - MONET prediction errors at INM 144 Annshill.

Test Date and Time	**Test Weight**	**Measured LZpeak (dB)**	**MONET Prediction Error (dB)**	**T_i (hours)**	**T_e ($hours$)**	**v (ms^{-1})**
2022-10-03 11:58	100	108.8	7.5	2	Yes	-0.3
2022-10-18 15:01	100	118.9	1.3	28	Yes	4.9
2022-10-25 10:58	100	82.0	13.1	2.5	< -0.25	-3.2

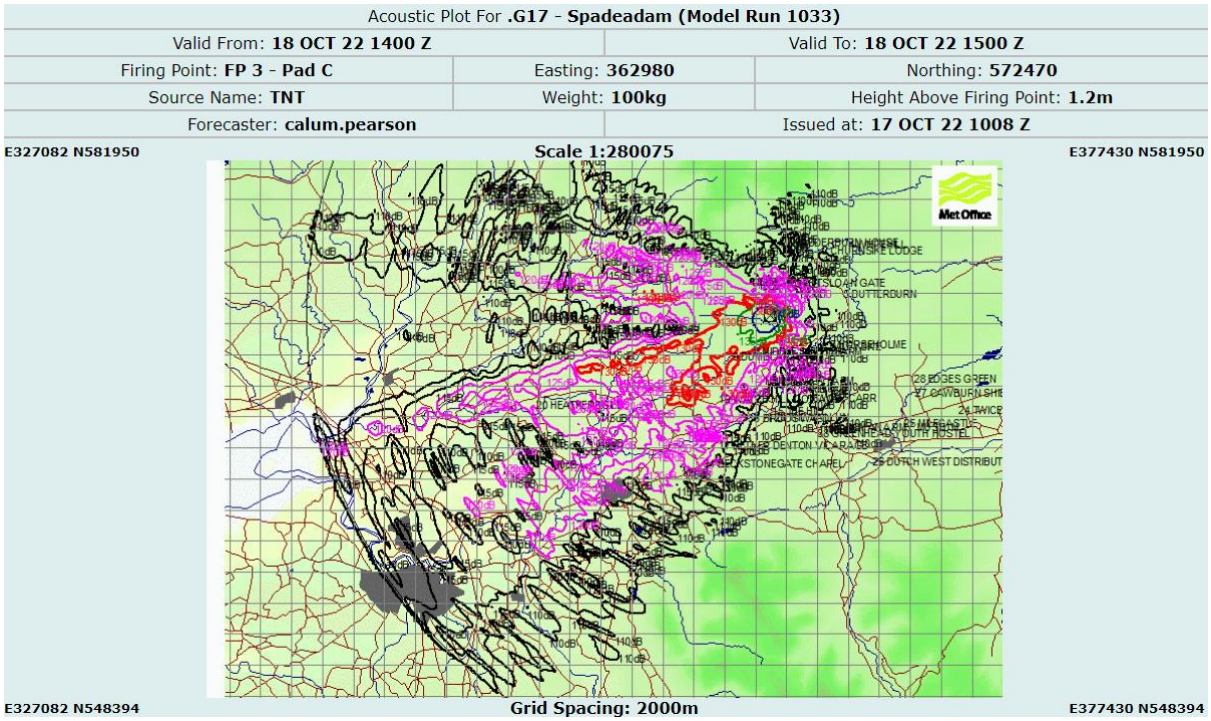

Figure 124 - MONET footprint for 100 kg Pad C test on 18 Oct 2022 1500-1600 GMT.

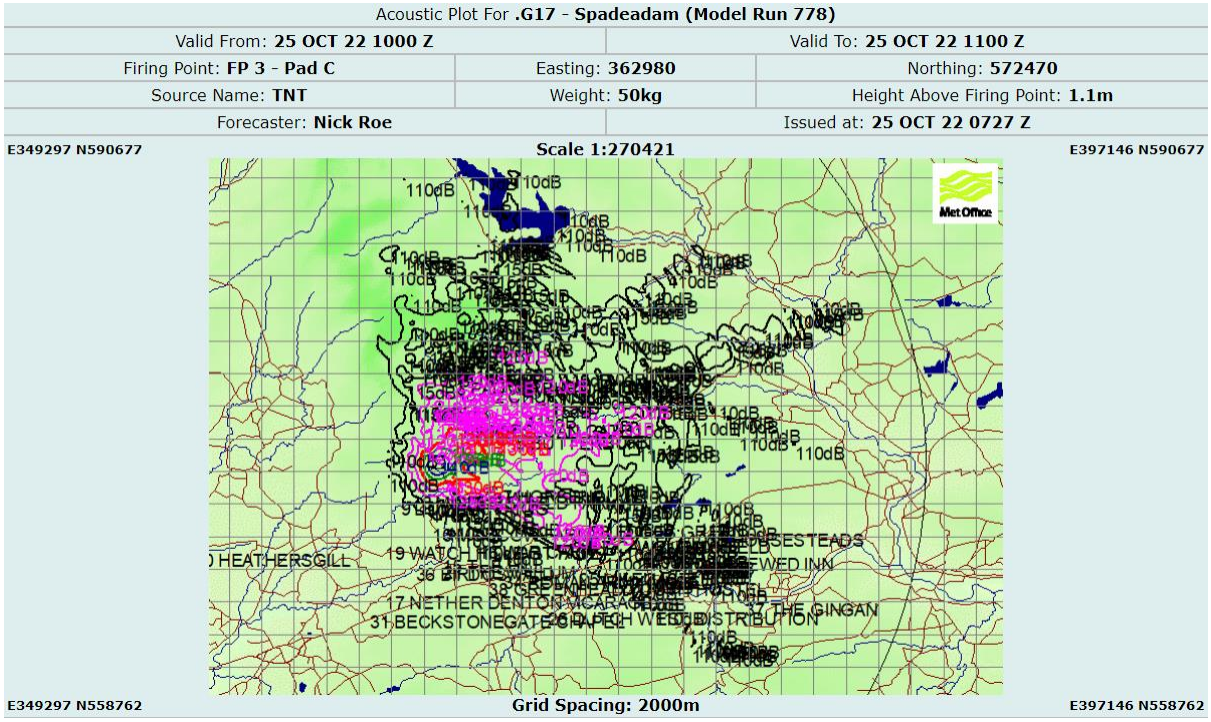

Figure 125 - MONET footprint for 100 kg Pad C test on 25 Oct 2022 1000-1100 GMT.

5.3.3.6 INM 145 Raise House

Finally, Raise House has relative proximity to Spadeadam in comparison to INMs 141-144, though the prediction errors at MONET do not indicate that distance from the source is a

factor in prediction error. Additionally, this monitoring station has the most observations available with suitable MONET footprints, and prediction errors varied between -12.6 dB to +8.7 dB. An RMS error of 9.9 dB was given by this comparison between prediction and observations at this location. It is speculated that the reason for these large prediction errors at such proximity is given by its orientation relative to Spadeadam and the prevailing winds over the area, and the case for this is presented here.

Raise House lies 6.1 km from Spadeadam, but is the most southerly orientated location at 178° re north of Pad C. Table 70 shows that the largest prediction errors (all records greater than 8 dB) occurred when the vector sound speed was relatively low in magnitude. The only reasonable prediction error of +2.5 dB made on the 3rd October 2022 was during moderate upwind conditions for this location (v = -4.8 m/s). Accounting for t_i and t_e, the argument that MONET performance is greater when propagation conditions are represented strong features in the meteorology (i.e. strongly up or down wind), as seen at other locations. **Error! Reference source not found.** shows the position of Raise House relative to the favourable direction of propagation.

On the other hand, while t_i and t_e are variable throughout the dataset, every record other than on the 3rd of October are indicative of crosswind conditions. This is backed up by Table 71 - Wind conditions recorded on the RAF weather station for each Pad C observation made at INM 145., which has 5 cases of wind directions of 240-270° (representative of WSW or W wind) and 1 case with wind at 90° (representative of E wind). The measured wind speed in m/s has been included so that low wind speeds being representative of low vector winds (no discernible direction) can be factored out.

Table 70 - MONET prediction errors at INM 145 Raise House.

Test Date and Time	Test Weight	Measured LZpeak (dB)	MONET Prediction Error (dB)	T_i (hours)	T_e $(hours)$	v (ms^{-1})
2022-07-07 09:33	100	118.1	-12.3	21	Yes	0.1
2022-07-07 15:44	100	116.3	-9.7	6	Yes	-1.1
2022-07-08 11:18	100	114.2	-11.2	21	1.25	-2.4
2022-10-03 11:58	100	102.8	2.5	2	Yes	-4.8
2022-10-18 15:01	100	118.8	-12.6	28	Yes	-0.2
2022-10-24 13:59	25	104.3	-8.5	3	< -0.25	-0.7
2022-10-25 10:58	50	93.5	8.7	2.5	< -0.25	-2.2

Table 71 - Wind conditions recorded on the RAF weather station for each Pad C observation made at INM 145.

Test Date and Time	Wind Direction (° re north) recorded at Berry Hill	Wind Speed (ms^{-1}) recorded at Berry Hill
2022-07-07 09:33	270	4.6
2022-07-07 15:44	260	7.7
2022-07-08 11:18	250	7.7
2022-10-03 11:58	200	5.1
2022-10-18 15:01	90	5.1
2022-10-24 13:59	260	5.1
2022-10-25 10:58	240	4.6

Table 72 - Summary table of MONET performance across all INM locations for 25 kg, 50 kg and 100kg Pad C detonation trials at DNV Spadeadam. summarises the performance of MONET across all locations for all Pad C trials, with the number of observations per location, the RMS error, maximum under and overpredictions, and finally the minimum error achieved at each location.

Table 72 - Summary table of MONET performance across all INM locations for 25 kg, 50 kg and 100kg Pad C detonation trials at DNV Spadeadam.

INM Location	Number of Observations	RMS Error (dB)	Maximum Underprediction (dB)	Maximum overprediction (dB)	Minimum Error (dB)
INM 140	3	9.3	-7.0	14.5	1.7
INM 141	5	8.5	-15.6	2.4	-2.1
INM 142	5	6.7	-10.9	7.5	1.7
INM 143	3	10.6	-12.1	12.8	5.2
INM 144	3	8.8	n/a	13.1	1.3
INM 145	7	9.9	-12.6	8.7	2.5
Total	26	9.0	-7.0	2.4	-2.1

Given that the source-receiver distance of each INM Location varies from around 4-14 km, the magnitude of prediction errors has been plotted for each INM location as a function of distance. Although MONET is capable of making predictions at distances up to 25 km, it is reasonable to assume that as the source-receiver distance increases, the uncertainties involved with the meteorological and ground conditions increases, thus increasing the prediction error.

From Figure 126 it is clear there is no relationship between the magnitude of MONET prediction errors and distance. See for example INM 140, the closest receptor, had the second greatest prediction error in magnitude (14.5 dB overprediction), but also a minimum prediction error of 1.7 dB. Furthermore, the RMS errors of INM 140 and 145 (the second closest receptor) were greater than the long-distance receptors of INM 141, INM 142 and INM 144, but not of the furthest receptor, INM 143.

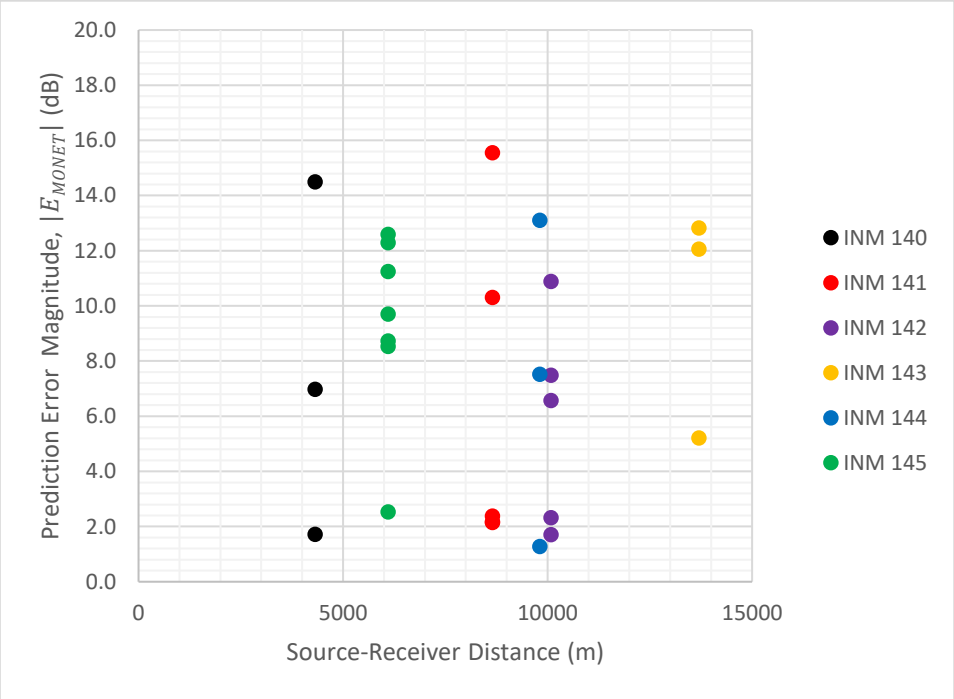

Figure 126 - Plot of prediction error magnitude (dB) as a function of source-receiver distance for each INM location.

The locations of INM 141, INM 142 and INM 144 had significant source-receiver distance, as well as complex propagation paths including undulating topography to INM 142, yet achieved prediction errors as low as 2 dB. Significant error (> 10 dB) still occurred at these locations however.

Given the different orientations of each receptor with respect to the firing location and wind direction, it is appropriate to compare prediction errors as a function of the vector winds.

5.3.3.7 MONET Prediction Accuracy vector winds

The prediction errors are here plotted as a function of positive and negative vector wind speeds for each INM location. Furthermore, the sign of the prediction error is kept to also visualise the relationship between under and overpredictions and refraction scenarios (upwind; $-v$, downwind; $+v$).

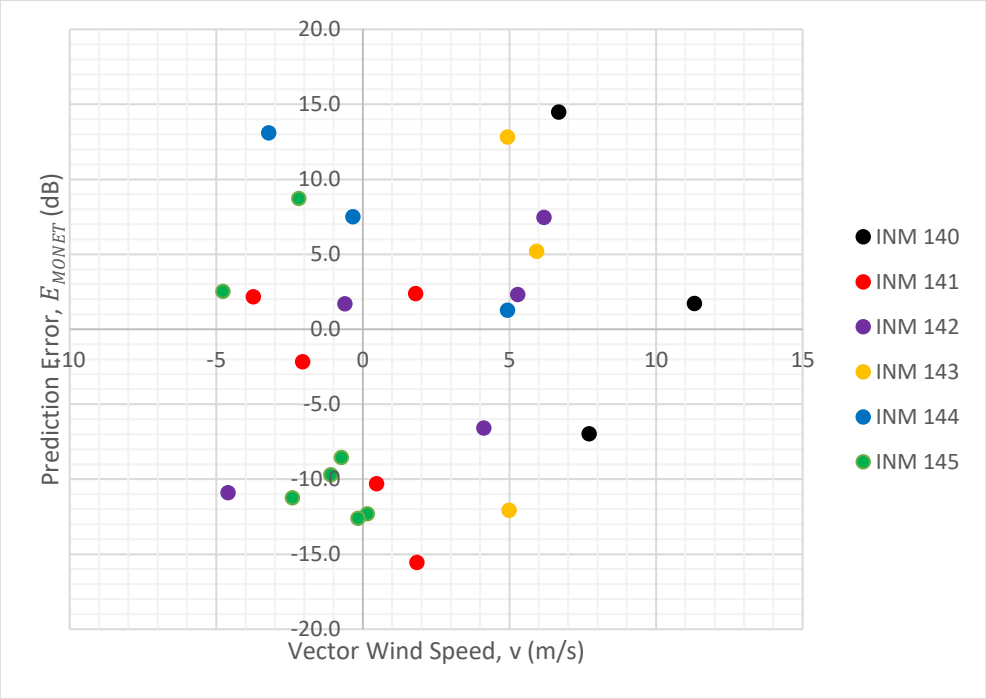

Figure 127 - MONET Prediction error as a function of vector wind speed for each INM location.

Figure 127 shows that overall, there is no discernible relationship between prediction error and vector wind speed, showing that MONET is no more accurate in any one condition.

Some clustering does emerge especially for INM 145 (green). This location is a close-range receptor to the immediate south of Spadeadam (178° re north), with only one moderate upwind observation (2.5 dB error on 3rd October 2022). All 6 other observations at this location had prediction errors 8.5-12.5 dB (in terms of magnitude), with 5 of those observations being underpredictions. Moreover those observations had at small negative or zero vector wind.

5.3.3.8 MONET Prediction Accuracy compared to the Salford Surface Wind Model

Although not stated as a primary or secondary research question of this thesis, the performance of MONET against a simpler heuristic model was a desirable outcome of this research, given the opportunity to do so. Unfortunately, it was not anticipated at the inception of the project how small the sample size of valid MONET comparisons would be available. Additionally, each MONET noise footprint is a significant cost to DNV, and therefore they are usually limited to just one forecast per test. This means that it is not possible to compare MONET's prediction accuracy as a function of forecast time, as is done with the Salford Surface Wind, which uses freely available forecast data and SSW model runs were ran for as many instances as there were forecast windows. This means that a direct comparison of prediction accuracy for both models as a function of input meteorological forecast is not available with the dataset gathered in this thesis. However, the available MONET prediction errors have been plotted against the variation in time between issuing the forecast and test firing, t_i, in Figure 128. Clearly there is no observable relationship between t_i and prediction error, though the variation is small, with the number of observations with $t_i \leq 6$ hours and $18 \leq t_i \leq 28$ hours being equal (13 each).

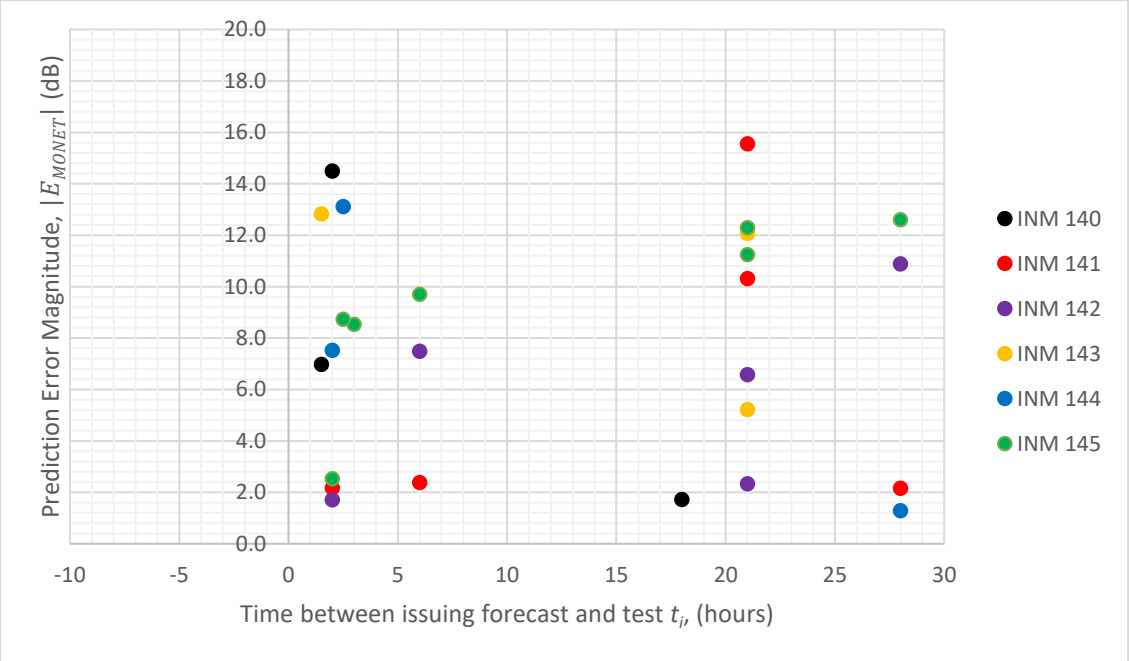

Figure 128 - Magnitude of MONET prediction errors as a function of t_i at each INM location.

The performance of the SSW model has already been evaluated for all Pad C activity at Spadeadam which includes detonations of charges from 0.04 - 100 kg, but for the purpose of comparing its performance to MONET, the SSW performance for the test data set presented

in this section is analysed in isolation, i.e. the 26 Pad C tests of 25-100 kg TNT equivalence with valid measurements and available MONET predictions for comparison.

Firstly, the RMS errors for 23x100 kg, 2x50 kg and 1x25 kg Pad C trials using the SSW with all possible input meteorological data is given for each INM location.

Table 73 - RMS Errors from SSW model at each location as a function of the input meteorological data, also compared with overall RMS error of MONET predictions at each location.

INM Location	R5BC	RAF	ERA5	MO 00-24	MO 25-48	MO 51-69	MO 72-93	MO 96-117	MONET
INM 140	-	15.8	16.1	-	-	-	-	-	9.3
INM 141	7.9	7.3	7.8	7.4	7.4	7.5	7.5	6.8	8.5
INM 142	5.8	6.3	5.7	5.9	5.9	5.9	6.0	4.8	6.7
INM 143	7.5	10.6	9.9	7.8	7.8	7.7	8.0	7.4	10.6
INM 144	15.8	15.8	16.1	15.9	16.3	16.5	16.5	15.6	8.8
INM 145	10.4	10.6	10.5	10.5	10.5	10.5	10.6	10.7	9.9

From Table 73 it is possible to see the RMS errors of the SSW as a function of its input meteorological data (weather stations and forecasts), compared to MONET. Of course, columns 2-4 of the table represent the retrospective predictions made by the SSW model with measured (R5BC and RAF weather stations) or reanalysed data (ERA5 dataset). Columns 5-9 represent the meteorological forecast data used in the SSW model and are discretised in terms of their forecast length (00-24 hours, 25-48 hours ahead of testing, etc.).

RMS errors of the SSW model at INM 140 are limited to just two comparisons, as the RAF weather station and ERA5 dataset were the only meteorological data available as input into the model for this specific dataset of Pad C trials. The measurements of these trials at INM 140 were taken at an early stage of the project when the R5BC station was not set up, and the routines for acquisition of the Met Office DataHub atmospheric profiles were yet to be programmed. SSW RMS errors are significantly higher than MONET for this specific location, however, only 3 observations were available for comparison with MONET. These 3 observations are interesting nonetheless, as shown in Table 74, where for the 100 kg test on 31 March 2021, the SSW model predicts the measured level to within 0.0 dB and -1.0 using the RAF and ERA5 data respectively, compared to MONET's underprediction of 7.0 dB. Furthermore, reasonable prediction errors of -3.5 and 5.1 dB were found on the 5th October

2021 compared to an overprediction of 14.5 dB by MONET. The large RMS errors for the SSW model come from a significant overprediction of 27.1 dB and 27.3 dB (RAF and ERA5 respectively) on the 4th October trial, compared to MONET's 14.5 dB overprediction.

Table 74 - Retrospective predictions using the Salford Surface Wind model compared to MONET compared to measurements of 100 kg Pad C trials at INM 140 Wardrew Farm.

Date and Time of Test	LZPeak (dB)	SSW RAF LZPeak Prediction (dB)	SSW ERA5 LZPeak Prediction (dB)	MONET LZPeak Prediction (dB)
2021-03-31 09:12	117.0	124.0	123.0	117.0
2021-10-04 10:00	94.8	121.9	122.1	109.3
2021-10-05 10:08:	128.5	125.0	123.4	130.2

The comparison of RMS errors from all variations of the SSW model against MONET across all locations is shown in Figure 129. The RMS error of MONET across all monitoring locations is not significantly lower than any of the SSW variations, however its maximum overprediction (as shown by the positive error bar) is significantly less, with a maximum overprediction of 14.5 dB. The maximum underprediction however was greater than any case with the SSW model at -15.6 dB.

As there are several variations of the SSW model which has been evaluated on its ability to make accurate predictions at various times ahead of testing (from 0 to approximately 5 days), for direct comparison with MONET, the prediction errors across all monitoring locations, and all input meteorological data have been averaged. A summary table of these RMS errors and worst- and best-case performance is shown in Table 75.

Table 75 - Summary table of SSW performance against MONET for Pad C trials.

Metric	Prediction Error (dB)	
	SSW	MONET
Average RMS	9.6	9.0
Average Overprediction	27.1	9.8
Average Underprediction	-13.4	-9.5
Maximum Overprediction	27.7	9.8
Maximum Underprediction	-14.3	-15.6

Best-Case Prediction	0.0	1.3

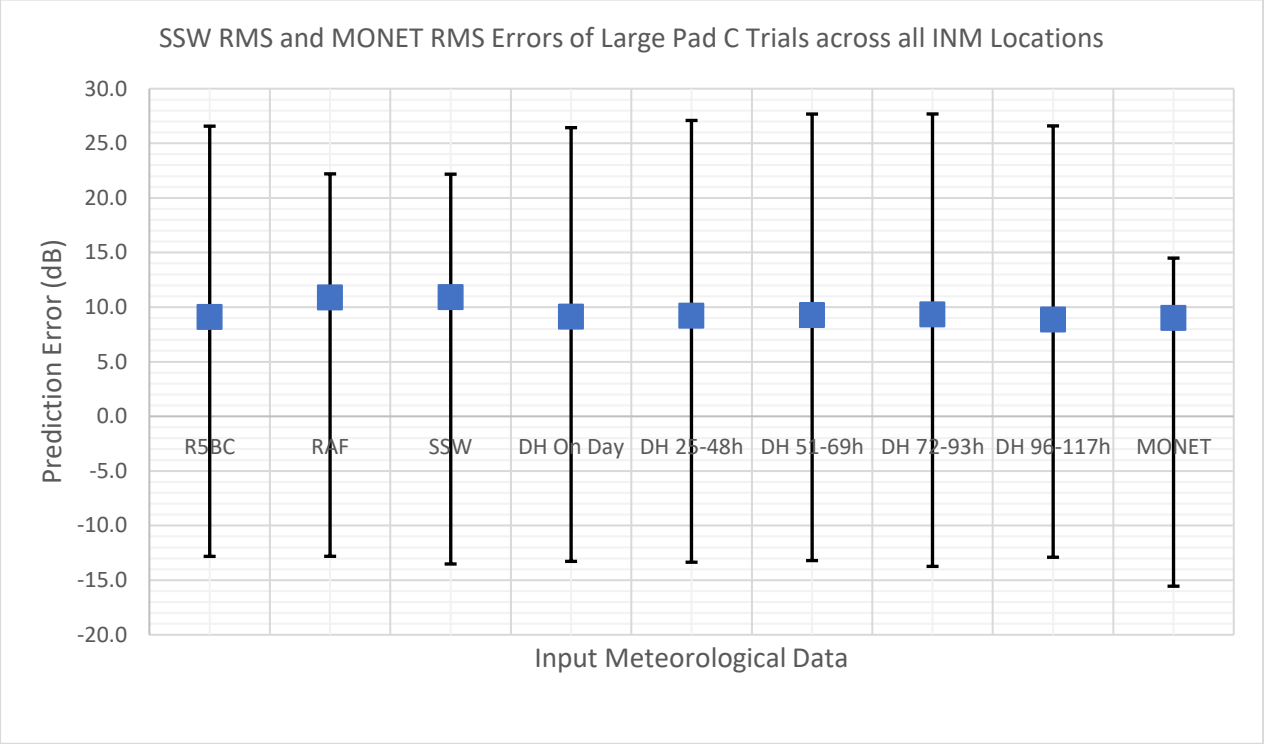

Figure 129 - Salford Surface Wind RMS prediction errors for each case of meteorological input data across all monitoring locations compared to MONET.

The most significant result of this analysis is that overall, the RMS error in predicted LZPeak of MONET across all locations for the large-scale Pad C trials was 9.0 dB, just 0.6 dB greater than the SSW model, at 9.6 dB. Considering that this evaluation of the SSW model applies to predictions made up to 5 days ahead (117 hours) of testing, with no significant decrease in accuracy compared to the more complex MONET, which can only perform predictions up to 1.5 (36 hours) days ahead of testing.

However, this sample size is significantly smaller than ideal for evaluating the performance of prediction models over such a range of propagation scenarios and possible receptor locations. It does however lead the author to speculate that existing heuristic models can capture the overall impact of impulsive noise generated by large-scale major hazards blast testing, which is a useful tool for planning site operations in advance. One must however acknowledge the large prediction errors that both models are capable of making for individual propagation scenarios, with the maximum underpredictions of the SSW model and MONET of 14.6 and 15.3 dB, and the maximum overprediction of the SSW (27.7 dB) significantly higher than MONET (9.8 dB).

5.3.3.9 General Conclusions on MONET Performance at Spadeadam

This analysis has been performed on a relatively small sample size (26 samples) and excluding most of the blasting activity captured by this research, with just the largest Pad C trials for which MONET predictions were available against measurements. In future, this analysis could be repeated on a dataset the size of the EDH database (with over 800 valid observations) and a more conclusive relationship between MONET accuracy and propagation conditions could be made. The analysis could be improved by acquiring MONET predictions at each of the possible forecast windows before testing (i.e. 6 hourly from 36 hours ahead). In that case, a more direct comparison between prediction accuracy of MONET and the SSW heuristic model as a function of forecast length could be made.

In summary, MONET is not significantly more accurate than the SSW model when comparing all predictions across all locations. Although the SSW produces much larger overpredictions than MONET, and no significant improvement in underpredictions, the overall RMS error is just 0.6 dB greater than MONET, whilst also achieving this at a much further range in time ahead of testing (up to 5 days), compared to MONET which is limited to just 36 hours.

It is therefore concluded in this section that the existing SSW heuristic model is as useful a tool for making long-range predictions of impulsive sound from large-scale major hazards testing at DNV Spadeadam. The next section of this thesis discusses the development of this model for improved accuracy, whilst remaining simple and heuristic in nature.

5.4 Development of the Extended Models for Blast Noise Prediction

5.4.1 Sensitivity Analysis of Current Salford Surface Wind Model

This section presents the results of a sensitivity analysis on the current version of the Salford Surface Wind model. A sensitivity analysis quantifies the degree to which a model input effects its output. Sensitivity analyses can be carried out in two ways, locally or globally and both have varying advantages and disadvantages.

Local Approaches	Global Approaches
e.g. one parameter at a time (OAT) approach	e.g. Sobol analysis
Low data requirements	Often need probabilistic data
Rapid and easy to implement	Computationally intensive
Does not capture interactions between input variables	Capable of capturing interactions between input variables
Misleading for non-linear models	Suitable for non-linear models

In this case, the sensitivity analysis informs how the uncertainty in the SSW model's output variable (LPeak), can be attributed to different source of uncertainty in the model's input variables (Charge Weight, Source-Receiver Distance, and 10 m Vector Wind Speed). The 10 m Vector Wind Speed is formed from 3 other variables, the 10 m Wind Speed, the 10 m wind direction and the source-receiver azimuth. The calculation of the vector wind speed is detailed in Section 3.3 of this thesis.

There is also an argument to be made that the constants in the original regression analysis that formed the model (K1, K2 and K4) should be assessed for their influence on the model predictions. The first two terms represent the source (interacting with the Charge Weight), and the last term having some high-level representation of the ground effect (interacting with the Source-Receiver Distance variable).

Sensitivity of input variables are represented numerically by sensitivity indices that measure the following degrees of influence on a model (Iwanaga, Usher, & Herman, 2022).

1. First-order indices: quantifying the output variance by that of a single model input
2. Second order indices: quantifies the contribution of the output variance caused by interactions between two input variables
3. Total-order indices: quantifies the contribution of a model input variable to the output variance including both first and second order effects (and higher order effects if necessary)

The sensitivity analysis was carried out in Python, using the SALib package, Herman and Usher (2017). Firstly, the parameter space is mapped to represent the uncertainty in the model inputs, i.e. the extent to which the SSW input variables can each be expected to vary by. The parameter space is tabulated and its formation in the Python SALib environment is shown below.

Input Variable	Symbol	Lower Bound	Upper Bound
Charge Weight (kg)	W	0.04	100
Source-Receiver Range (m)	R	100	15000
10 m Wind Speed (m/s)	V	0	10
10 m Wind Direction (° re north)	φ	0	359
Source-Receiver Azimuth (° re north)	θ	0	359

Figure 130 - SSW sensitivity analysis parameter space for the original input variables.

```
# Define the model inputs
problem = {
    'num_vars': 5,
    'names': ['W', 'R', 'V', 'phi', 'theta'],
    'bounds': [[0.04, 100],
               [100, 15000],
               [0, 10],
               [0, 360],
               [0, 360]]
}
```

Figure 131 - Parameter space definition in Python, SALib for the originial SSW model.

Some of the parameter uncertainties have been selected on the based their physical limits, such as

φ and θ. Other parameters were chosen to represent the upper and lower bounds seen in the

noise predictions at made Spadeadam, as captured by the Live Monitoring Network data presented in this thesis, whilst also extending them slightly further to whole numbers. This sensitivity analysis therefore determined the sensitivity of the model to inputs from blasts of 0.04-100 kg TNT to receivers 100-15000 m, and in winds of 0-10m/s.

In order to produce a global sensitivity analysis, the samples of each of these inputs according to the defined uncertainty bounds are generated by the method used in the Sobol sensitivity analysis (Sobol′, 2001). This generates a text file with each line equivalent to the possible input variables, distributed over 1024 samples for each variable, which for second order interactions, requires 12288 variations.

Each possible combination of input variables between the respective parameter uncertainty bounds are save to a text file and the SSW predictions are calculated in Microsoft Excel, and finally loaded back into Python. The SALib library then analyses the SSW predictions with the Sobol analysis method and generates the sensitivity parameters.

5.4.1.1 Sensitivity Analysis of variables in the existing SSW model

By carrying out a sensitivity analysis on the model described above, the following sensitivity metrics are computed for the existing SSW model.

Table 76 - Total and first-order sensitivity indices for the variables in the original SSW model.

Parameter	**Total Sensitivity Index, S_T**	**First-Order Sensitivity Index, S_1**
W	0.16	0.16
R	0.80	0.80
V	0.01	0.01
φ	0.05	-0.02
θ	0.05	0.00

Table 76 shows that the source-receiver range is the most influential parameter in the SSW model for its ability to change the output peak sound pressure level, with the highest total and first-order sensitivities of 0.80. Charge weight also has an influence to some degree (S_T and S_1 0.16) over the other parameters, whereas overall the uncertainty in the wind variables

(speed, direction and source-receiver azimuth) have small total and first-order indices. This seems low compared to what is expected following the review of the physical effects that dominant propagation, with wind profiles being a dominant factor. It is likely that the low first order indices for the wind components are because they are combined into one physical mechanism in reality, the vector wind speed.

The second-order effects are also tabulated, so that the model's sensitivity to interactions between pairs of input parameters can be shown.

Table 77 - Second-order sensitivity indices for the variables in the original SSW model.

Parameter Interaction	**S2**
('W', 'R')	0.00
('W', 'V')	0.00
('W', 'phi')	0.01
('W', 'theta')	0.00
('R', 'V')	0.00
('R', 'phi')	0.01
('R', 'theta')	0.00
('V', 'phi')	-0.01
('V', 'theta')	-0.01
('phi', 'theta')	0.05

The interaction between variability in wind direction and source-receiver azimuth has the most influence on sensitivity out of the second-order effects. This is likely because they indeed interact to form the vector wind component and therefore depend upon each other in the calculation of the refraction term in the SSW model.

The indices of all parameters are shown in Figure 132

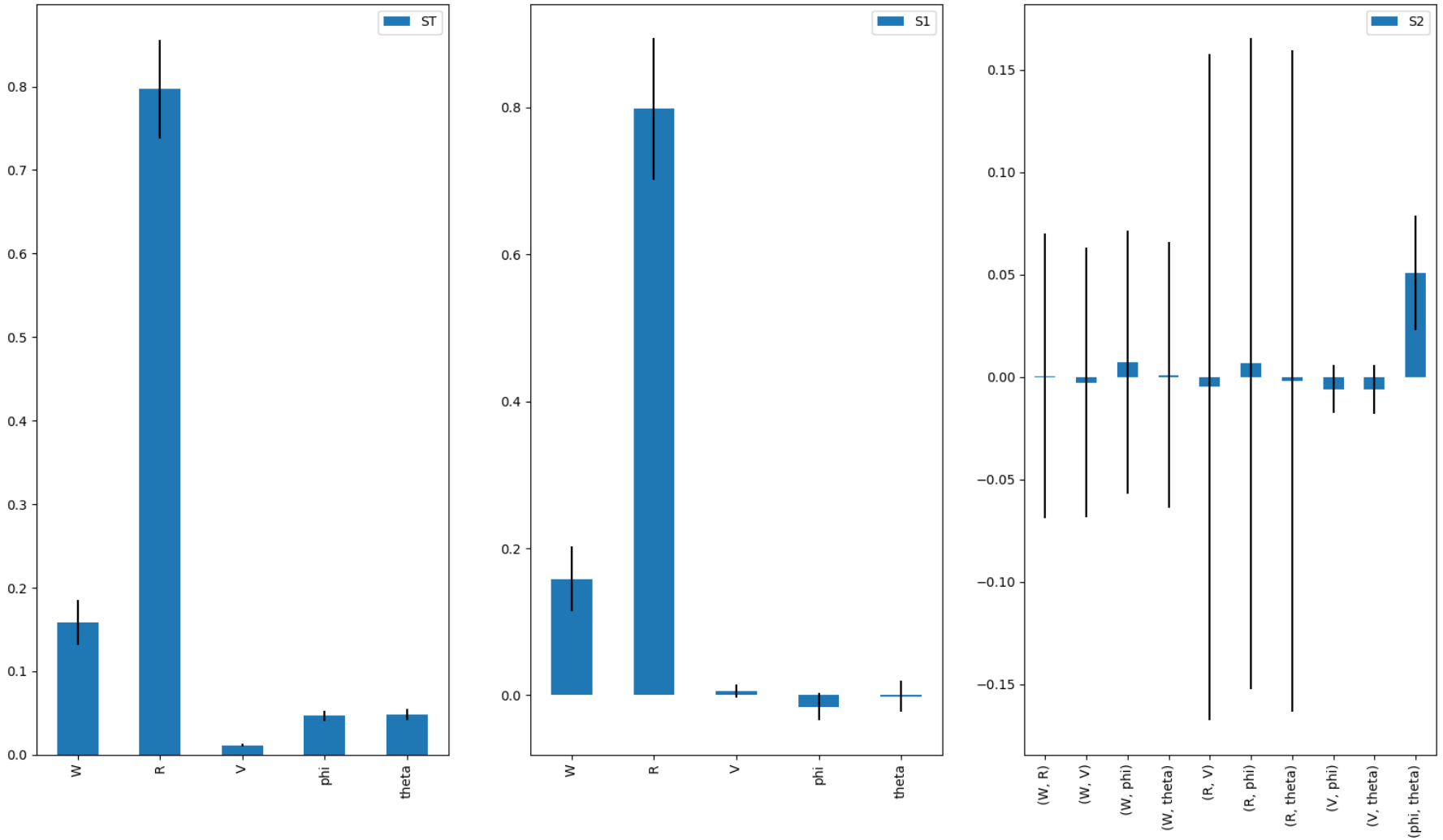

Figure 132 - Total, first and second-order sensitivity indices for the original SSW model.

5.4.1.2 Sensitivity Analysis of K-parameters in the SSW Model

The previous section investigated the sensitivity of the SSW model's output to uncertainty in its input variables (W, R, V, ϕ and θ). This subsection is dedicated to investigating the effects on the SSW output as a function of changing the constants associated with each of the input variables. The original model equation is given here again for reference.

$$L = K1 + K2 \log W - K3 + K4 \log R - f \log R \qquad \text{Equation 56}$$

Where K1 and K2 are 204.6 and 11.9 and are associated with the defining the strength of the explosive source, through multiplication with W and are formed from the regression analysis of the original data, originally presented by G. Kerry et al. (1987). K3 and K4 are 20 and 9 dB respectively. K3 represents the attenuation by spherical spreading through multiplication with the logarithm of R, and K4 is associated with additional attenuation from ground absorption and site conditions specific to the site where the original data was measured, at Larkhill.

Firstly, there is no direct change needing to be applied to K3, as this represents a physical mechanism of attenuation not limited to a specific location (spherical spreading). Nonetheless when coupled with K4 (originally forming a constant of 29 dB), there is justification to modify the value of K4 from typical changes in attenuation or enhancement expected from different ground. In other words, the term should be greater for snow and forests, and smaller for hard ground. This has applicability to the predictions made at Spadeadam, where ground not only varies with azimuth and range, but also with time.

The term denoted as f represents the refraction term and is formed by the remaining input parameters analysed in the previous section.

$$f = 0.18\, V \cos \alpha$$

Where V is the wind speed at 10m and α is the vector wind direction, defined as the difference in angle between the wind direction from which blowing, and the source-receiver azimuth, both in degrees referenced to North at 0 degrees.

Results from Sensitivity Analysis

The same sensitivity analysis technique carried out in the previous section has been performed again on the K constants in the context of the parameters that they effect, which are listed as follows.

- K1: Linear relationship to the overall prediction, through the addition sign.
- K2: Multiplies by the log of the charge weight.
- K3+K4: Multiplies by the log of the distance.

Firstly, the sensitivity indices of the above parameters are presented. Following this, comparison of the SSW model for different propagation conditions and different charge weights will be presented, followed by proposals for suitable adjustments to the K-parameters of the original model.

The parameter space of the variables considered in this sensitivity analysis is shown in Table 78.

Table 78 - Parameter space for sensitivity analysis of SSW model including K-parameters and their associated variables.

Input Variable	Symbol	Lower Bound	Upper Bound
K1	K1	184.6	224.6
K2	K2	1.9	21.9
K3+K4	K3+K4	20	38
Charge Weight (kg)	W	1	100
Source-Receiver Range (m)	R	100	15000

K1 has been chosen to vary by 20 dB around its original value in the SSW model. This range was selected arbitrarily based on comparison with another type of blast-noise regression models, the USBM model and Larkhill model (see Chapter 3.3 on empirical models), which have K1 values of 196.6 dB and 195.4 dB respectively. A slightly smaller range has been given for varying K2. The combined K-factor of K3+K4 includes the 20 dB related to spherical spreading when multiplied by the log of the distance (K3) and the additional 9 dB set in the SSW model from their regression analysis which accounts for the additional attenuation produced by ground absorption found in Kerry et al's original regression analysis. The other two input parameters that interact with the K-parameters in the model are included. Input variables associated with the wind are not account for in this version of the sensitivity analysis, as they do not have any interactions with the K-factors discussed above.

Table 79 - Total and first-order sensitivity indices for the K-parameters and the associated input variables in the SSW model.

Parameter	Total Sensitivity Index, S_T	First-Order Sensitivity

		Index, S_1
K1	0.17	0.17
K2	0.12	0.11
K3+K4	0.50	0.50
W	0.03	0.03
R	0.19	0.18

Firstly, Table 79 shows that the combined parameter K3+K4 has the highest total and first order sensitivity index. This is not surprising given that it multiplies by the logarithm of the source-receiver distance (R), and R has been specified to vary between 0.1 and 15 km. Thus R accounts for the second highest proportion of sensitivity in the model output, followed closely by K1 and K2.

The second-order interactions between the above parameters are detailed in Table 80. The parameter-pairs that interact within the real model as per Equation 56 have a second-order sensitivity an order of magnitude greater than the others analyses, and hence are highlighted in the table.

Table 80 - Second-order sensitivity indices for the K-parameters variables in the original SSW model.

Parameter Interaction	**S2**
('K1', 'K2')	-0.00041
('K1', 'K3+K4')	0.00021
('K1', 'W')	-0.00079
('K1', 'R')	0.00078
('K2', 'K3+K4')	-0.00152
('K2', 'W')	**0.00565**
('K2', 'R')	-0.00037
('K3+K4', 'W')	-0.00068
('K3+K4', 'R')	**0.00511**
('W', 'R')	-0.00166

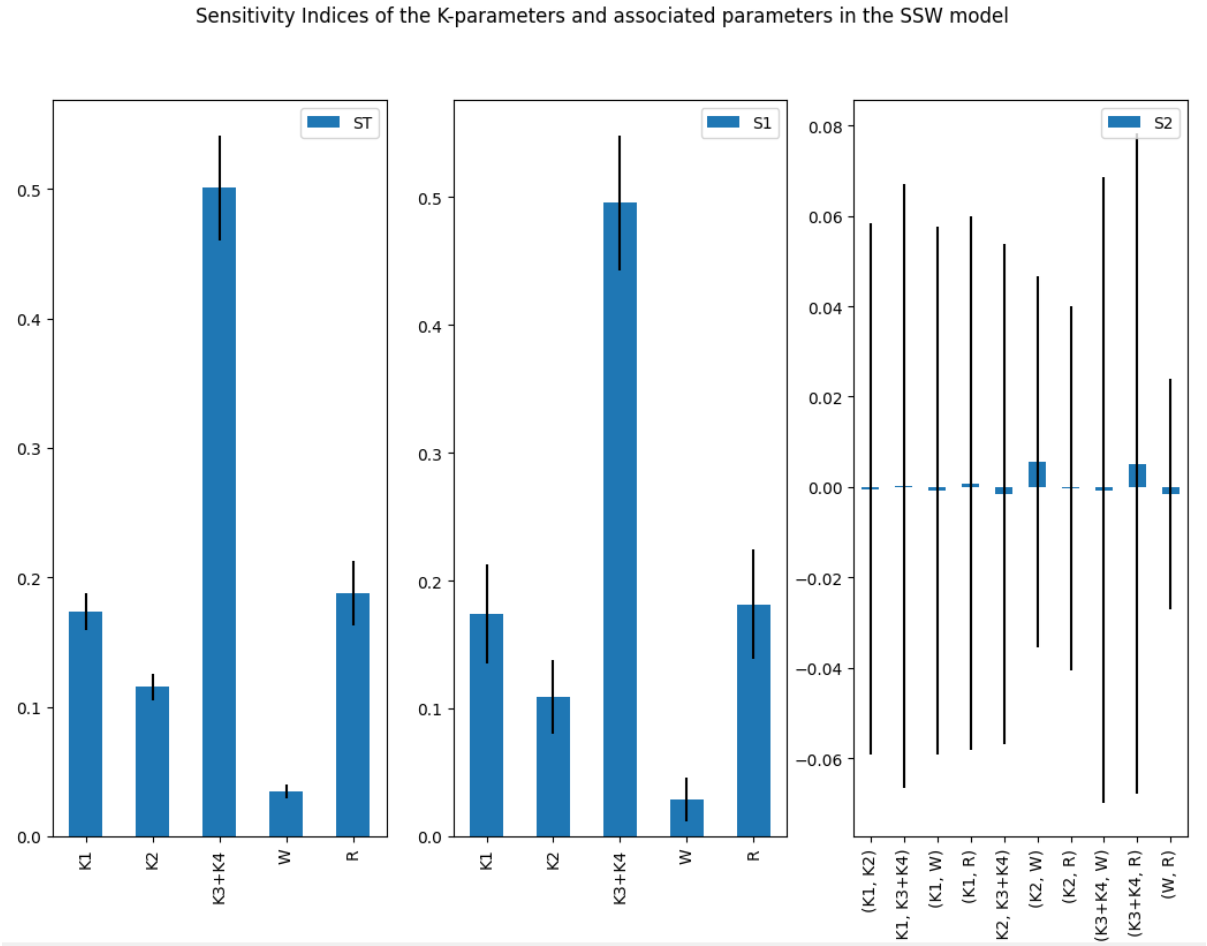

Figure 133 - Plot of total (ST), first-order (S1) and second-order (s2) sensitivity indices for the K-parameters and their associated variables in the SSW model.

Modification of K2

By following on from the assessment of the SSW prediction accuracy, and the sensitivity analysis, the RMS errors of the SSW across the whole Live Monitoring Network dataset has been repeated with modified values for K2. The original value of K2 in the SSW model is 11.9 dB, and it has been adjusted by ± 2.0 dB in 1 dB increments to investigate any improvement in prediction accuracy against its original value.

Over the whole dataset, which includes all test types, all monitoring positions, and all propagation scenarios, the model predictive performance for each adjustment of K2 is evaluated.

Table 81 - RMS Prediction error on entire Live Monitoring Network dataset with adjusted K2 values.

Value of K2	Overall RMS Error (dB)
9.9	9.32
10.9	9.19

11.9	9.16
12.9	9.22
13.9	9.40

Table 81 shows no significant improvement in overall RMS prediction error for the SSW model with slight adjustments to K2, when generalising over the entire dataset. The original value of the K2 parameter yields the lowest prediction error though only marginally. This implies that there are too many other factors affecting the model prediction error when generalising over the entire dataset.

Whilst investigating the large underpredictions of the SSW model, it was noticed that although both over and underpredictions are common, some of the largest underprediction error occurred for predictions of noise from a very small explosion test on Pad C (0.04 kg TNT) on the 23rd November 2022. The details of the test along with the minimum prediction errors are shown in Table 82.

Table 82 - SSW prediction errors for a 40g TNT charge on Pad C as a function of the input meteorological data, with original values for K2.

INM Location	Prediction error (dB)							
	R5BC	RAF	ERA5	MO 00-24	MO 25-48	MO 51-69	MO 72-93	MO 96-117
Blenkinsopp	-27.6	-27.2	-27.8	-28.2	-27.9	-27.1	-27.8	-28.2
High Close	-34.5	-34.6	-34.2	-33.7	-34.0	-35.2	-34.0	-34.0
Annshill	-34.0	-35.0	-34.1	-33.9	-34.0	-34.3	-34.1	-33.4

It noteworthy that these monitoring locations all yield significant underpredictions for the same test, despite having similar source-receiver distances to one another (8.6 km ,10.1 km and 9.8 km respectively), as well as being oriented differently around the site (156°, 117° and 286° respectively) and hence will have variation in their interaction with the wind and ground. Because of this, it is tempting to speculate that the uncertainty could be due to the representation of the source in the SSW model for such a small charge weight.

The original SSW model is essentially representing the blast source with an artificial sound power level from which attenuation and propagation corrections can be applied, in the form of the following expression.

$$L_{source} = 204.6 + 11.9 \log(W)$$

Because of the interaction between K1, K2 and the logarithmic term, the model works well for charge weights, W greater than 1 kg, which was the smallest charge size used in the original regression analysis. Charge weights less than 1 have high uncertainty and the logarithmic term has a diminishing effect on the 'artificial' sound power level of the blast source. By adjusting the K2 term in the SSW model, a minimum underprediction error was found for each monitoring position and the prediction error is plotted against K2.

Table 83 - Minimisation of SSW underprediction error for small 40 g TNT charge by adjustment of the K2 parameter.

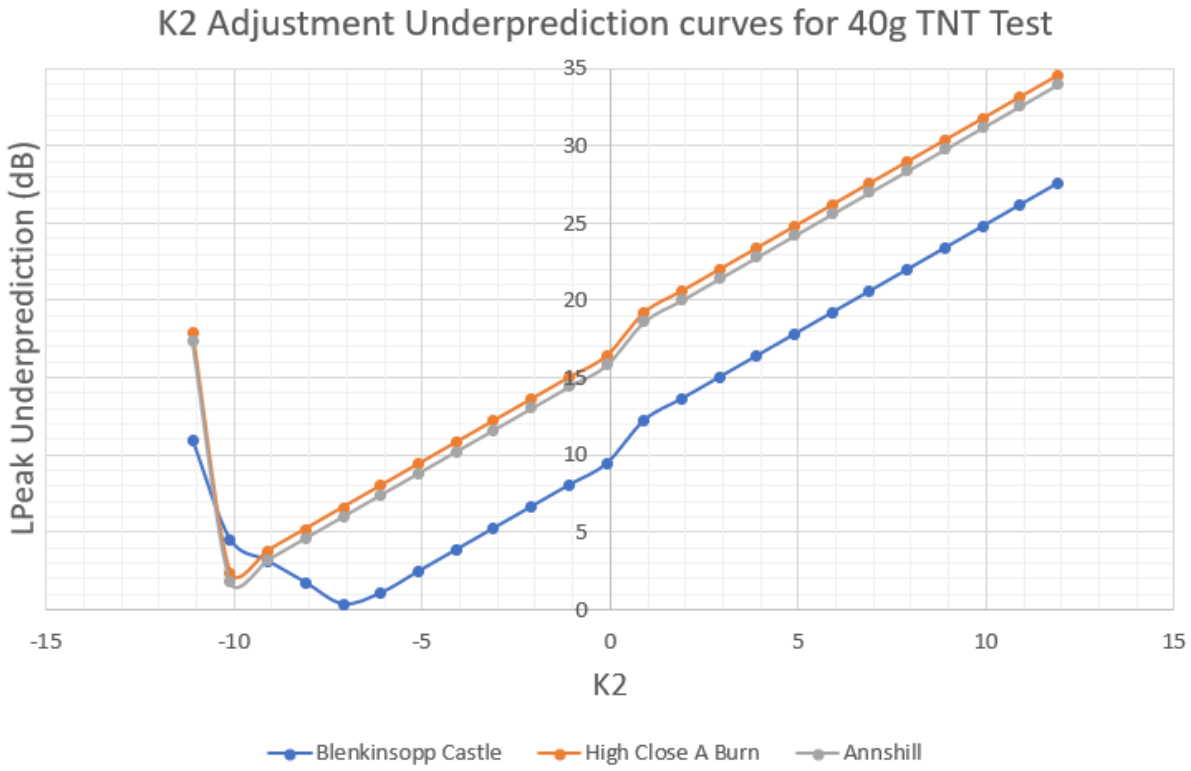

The minimum error in LPeak prediction for Blenkinsopp Castle is achieved at a K2 value of -7 dB, whereas for monitors at High Close and Annshill, the minimum error is found for more negative value of K2. Importantly, the error begins to increase after some value of K2 and it is therefore important not to set K2 too low, due to the interaction between a negative value with the logarithm of the charge weight.

This parameter adjustment has been done for just one instance of a significant underprediction. Many more measurements of peak noise from very small charge weights (< 1kg TNT) are required to validate the adjustment further.

Modification of K4

The results of the sensitivity analysis with K-parameters indicated that K4 (or the combined K3+K4) parameter is the most influential parameter on model sensitivity. Therefore, it is worth investigating whether adjustments can be made to this term to improve the performance of the SSW.

The same methodology was used to adjust K4 as was in the previous section, where K2 is discretely varied to some upper and lower bounds representing decreased and increased interaction absorption with the ground respectively. Again, the sensitivity analysis of adjusting K2 was conducted on the entire dataset including all test types, monitoring locations and propagation scenarios, in order to observe the effects of the parameter adjustment on model error whilst maintaining generalisation across all scenarios.

Table 84 - RMS Prediction error on entire Live Monitoring Network dataset with adjusted K4 values.

Value of K4	Overall RMS Error (dB)
0	35.9
4.5	19.4
9	9.2
13.5	20.1
18	36.6

Table 84 shows no improvement in overall RMS prediction error for the SSW model by adjusting K2, when generalising over the entire dataset. The original value of the K4 parameter yields the lowest prediction error and the approximately equal distribution of RMS errors around the original values suggests that the SSW is not more likely to generate underpredictions or overpredictions. This implies that the original value is probably suitable for use at the DNV Spadeadam site, and that prediction errors must be attributed to some other factors not accounted for in the model.

By observation of the global SSW histogram of prediction error, it is possible to see how this distribution of prediction errors arose.

Table 85 - Salford Surface Wind prediction error histogram of entire live noise monitoring network data.

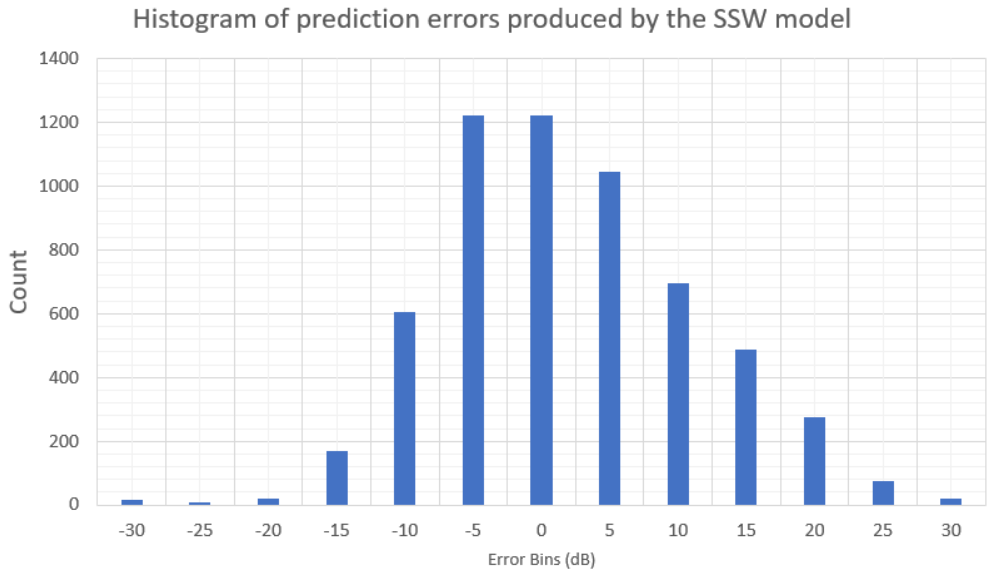

The distribution is approximately has a slight skew towards the positive error bins, but its high count in the -5 to -10 dB error bin means that overall the model is approximately equally likely to overpredict than underpredict.

5.4.1.3 Conclusions from Sensitivity Analysis

The sensitivity analysis of the SSW model has allowed quantification of the sensitivity of the LPeak calculation as a function of the uncertainties involved in the input variables. Realistic uncertainties in terms of minimum and maximum bounds were set on each parameter involved in the original SSW prediction model, and a sample was generated of a parameter space in order to observe the output predictions of the model for such a wide variety of inputs.

As this was a global sensitivity analysis, the interactions between input parameters were able to be quantified. Of the total sensitivity index, the source-receiver range had the most influence on model sensitivity, and this is unsurprising, given that it interacts with constant K3 and K4 through multiplication to model the effects of spherical spreading and ground. It also has influence on the refraction term where is multiplies again with the vector wind speed. This makes sense physically too, in that with more distance between the source and the receiver, there is the potential for more uncertainty in most other parameters, including ground absorption, atmospheric attenuation, and most of all meteorological effects. The variability in the charge weight as input has the second greatest overall sensitivity index, as shown in this analysis.

The secondary analysis on the effects of the SSW K-parameters showed that when analysed globally, the sensitivity of the model is highly attributed to the uncertainty in K4 (K3+K4). However, when this term was adjusted to attempt to improve the prediction error of the SSW model, no improvement was found when increasing or decreasing the value of K4 from its baseline value. A similar finding was found when adjusting the value of K2 in an attempt to more accurately model the source term. Experimentation with adjustment of K2 for a test case with small charge size found that this could be a useful approach for improving the model for small explosions and may avoid under predictions.

The purpose of this analysis was to inform the research on the effects of model sensitivity to its inputs, in particular, which parameters in the SSW model are most influential to the model output. This is essential for the development of extended models based on those such as the SSW.

5.4.2 Deep Neural Networks for Explosive Depth Hardening

The Explosive Depth Hardening dataset has also been used to train neural networks for the prediction of noise impacts. The methodology is similar to that of extending the models with the extended multiple linear regression models.

This subsection presents the results of different deep neural networks (DNNs) for the prediction of Unweighted Peak Noise Level (LPeak) from EDH operations at Spadeadam.

5.4.2.1 Standard DNN

The standard DNN is based on the parameters included within the original SSW model, with particular focus the parameters that were most influential on output sensitivity. The most influential parameters were found to be the source-receiver distance and charge weight, followed by the surface wind parameters. Here, the surface wind parameters along with the source-receiver azimuth have been combined with the adiabatic sound speed to form a single parameter of the 10 m effective wind speed.

Table 86 - Normalised parameter statistics for the input variables used in the standard DNN.

Parameter	Symbol	Normalised Mean	Normalised Standard Deviation
Charge Weight	W	0.00107	1.004017

10 m Effective Wind Speed	ceff	0.006140	0.998787
Distance	R	0.008026	0.996595

The following 3 neural networks have been trained on the EDH data set with the aforementioned parameters.

Table 87 - Standard DNN models and their associated structure and parameters.

Label	Hidden Layers	Neurons per Hidden Layer	Activation function	Number of Epochs	Learning Rate	Optimisation Algorithm
3-64-1 Standard	1	64	Relu	250	0.001	Adam
3-64-1 Standard	1	64	Relu	500	0.001	Adam
3-64-64-1 Standard	2	64	Relu	500	0.001	Adam

By training and validating the models according to the parameters described in Table 87, the results of each model in terms of RMS error and maximum prediction error are presented below.

Table 88 - Prediction accuracy of the standard DNNs based on RMSE and Maximum Error (dB).

DNN	RMSE (dB)	Maximum Error (dB)
3-64-1 Standard	8.0	23.2
3-64-1 Standard	7.8	24.8
3-64-64-1 Standard	7.9	26.2

The learning curves for both training and validation are discussed here. For the most simple and complex of the standard DNNs, the loss expressed as RMSE during training is shown Figure 134 and Figure 135. Both training and validation loss are shown on the plots so that the validation of the model can be evaluated whilst training the model.

The reason for increasing the number of epochs is to see where the model converges and if the validation error begins to rise after converging to a minimum. This can indicate overtraining. This in combination with increasing the number of hidden layers may be why the most complex model (4-64-64-1 standard) has a slightly the second model which has only 1 hidden layer.

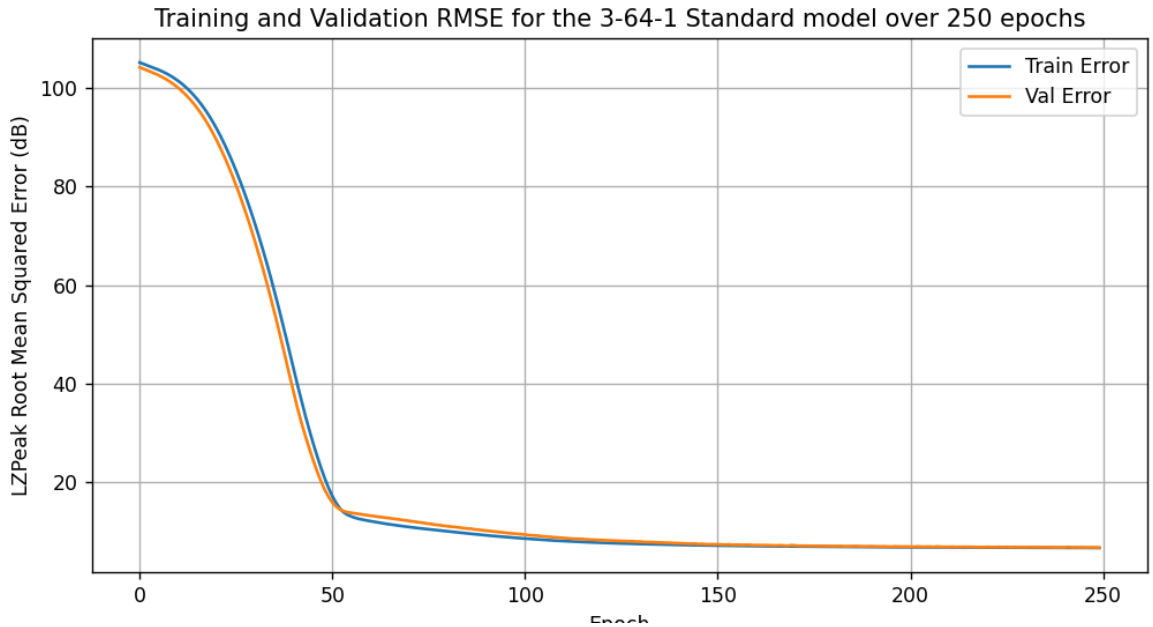

Figure 134 - Training and validation loss of the most basic of the standard DNN (3-64-1) model over 250 epochs.

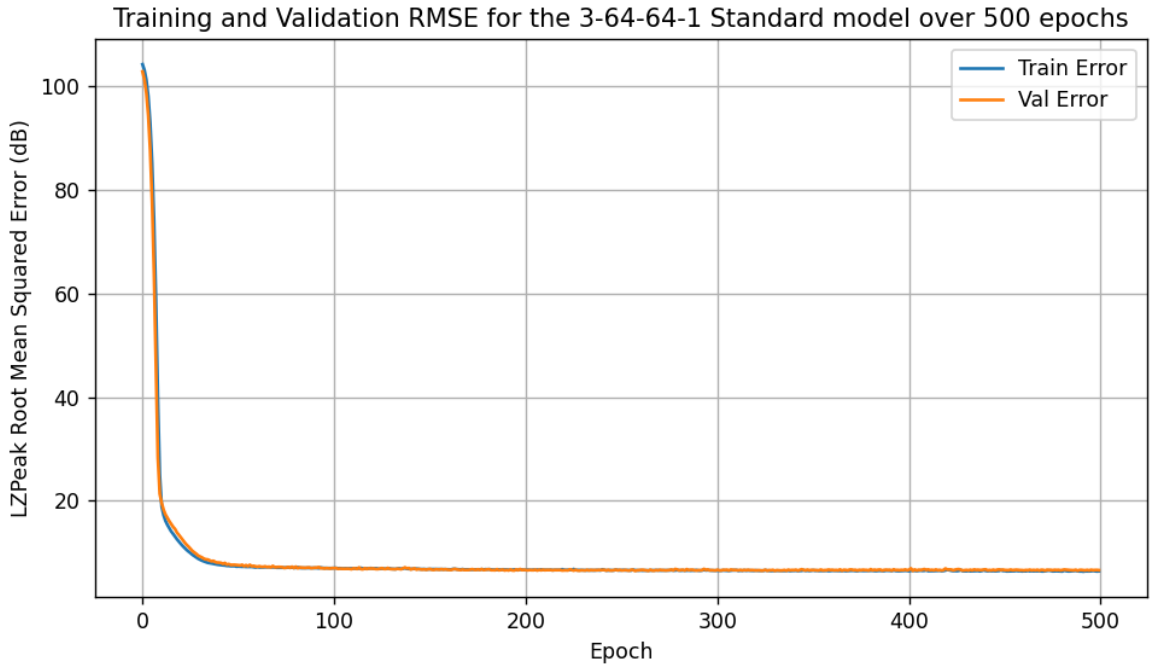

Figure 135 - Training validation loss of the most basic of the standard DNN (3-64-64-1) model over 500 epochs.

Following training and validation of the models, the specific DNN can be used to make predictions using the validation data and it is possible to compare its predictions to the 'True' data, which in this case is the measured LZPeak data. This evaluation is done across all monitoring positions and propagation scenarios. Figure 136 shows the model predictions for the 3-64-64-1 model after 500 epochs of training.

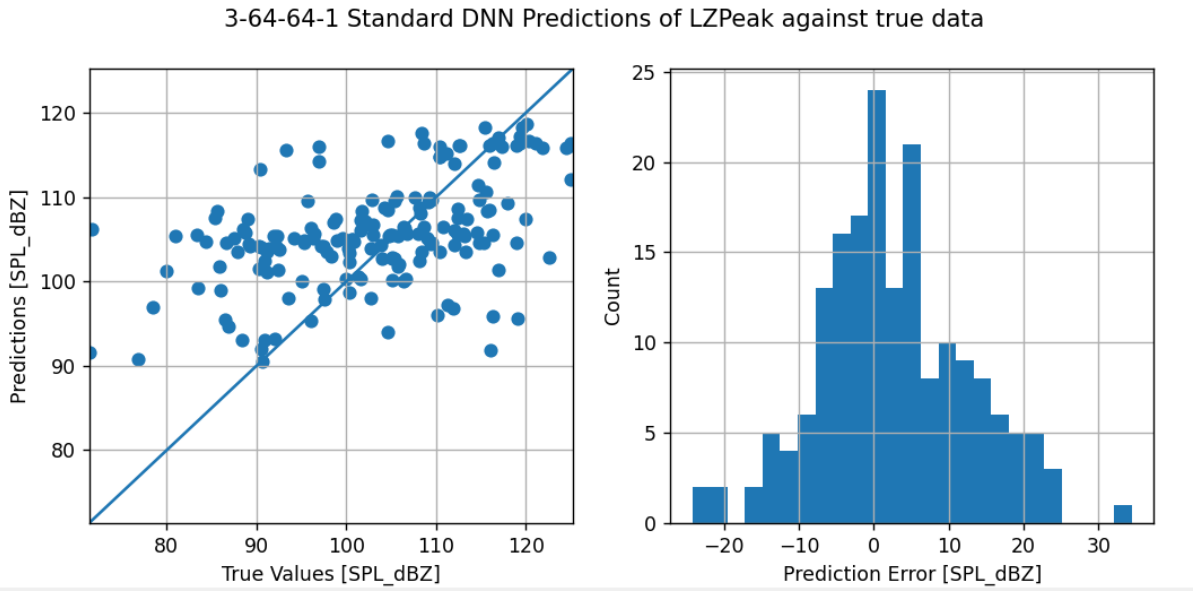

Figure 136 - 3-64-64-1 Standard DNN prediction accuracy against true values of LZPeak.

5.4.2.2 Extended Surface Layer Deep Neural Networks

As in the case of the regression analysis, the DNNs have been extended to include more parameters in the form of the logarithmic (Alog) and linear (Alin) calculated from Monin-Obukhov stability theory.

The following models have the parameters included in Table 89.

Table 89 - Additional DNN input parameters to those included in the standard DNNs, and their associated normalised statistics.

Parameter	Symbol	Normalised Mean	Normalised Standard Deviation
Alog	A_{log}	0.000849	1.004256
Alin	A_{lin}	0.006495	0.998326

The structures of the extended neural networks are included in Table 90. Note that the first number of the model label has increased to 5. This indicates the input layer of the model, which for the extended models, consisted of 5 parameters, including the original 3 (W, R, Ceff) together with the parameters derived from Monin-Obukhov similarity theory (Alog and Alin).

Table 90 - Structure of extended Surface-Layer DNNs.

Label	Hidden Layers	Neurons per Hidden Layer	Activation function	Number of Epochs	Learning Rate	Optimisation Algorithm

5-64-1 Surface-Layer	1	64	Relu	250	0.001	Adam
5-64-1 Surface-Layer	1	64	Relu	500	0.001	Adam
5-64-64-1 Surface-Layer	2	64	Relu	500	0.001	Adam

The validation curves for the extended models show that the loss (RMSE) converges later than in the case with the standard DNNs, reaching a minimum between 150-200 epochs. Given that the training curve in Figure 137 is still decreasing as it approaches the maximum number of epochs, it is useful to observe the effect of increasing the number of epochs on model convergence in Figure 138.

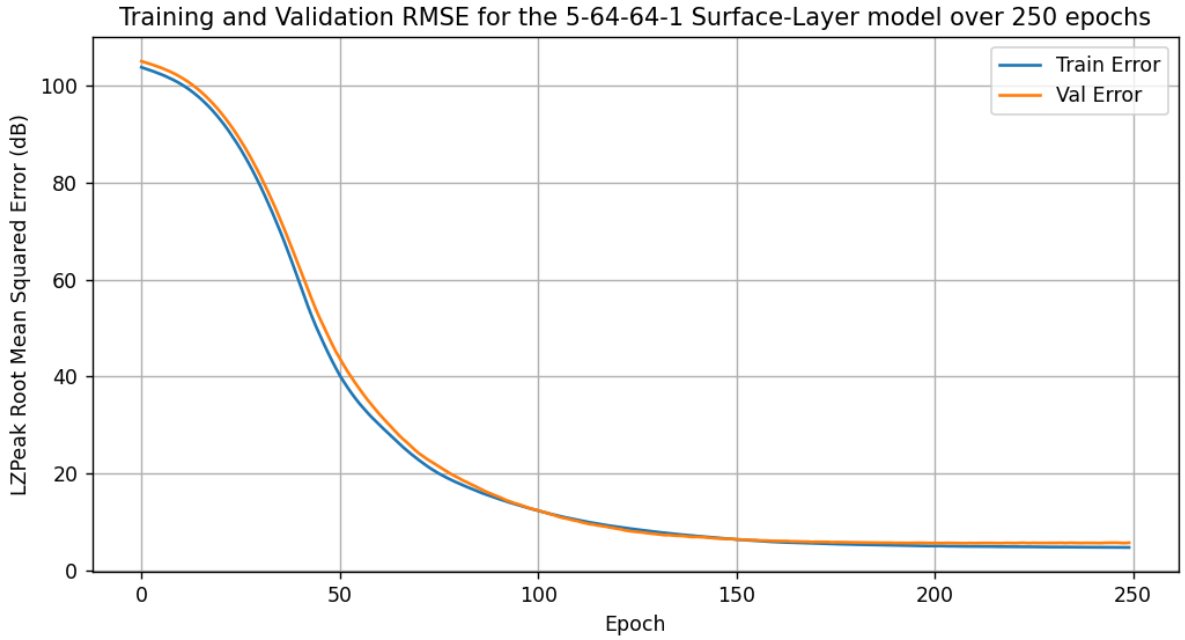

Figure 137- Training validation loss of the simplest of the surface-layer DNN (5-64-1) model over 500 epochs.

While 500 epochs certainly shows a slight decrease in the loss during training, the validation loss does not decrease after around 150-200 epochs. The validation loss is shown to slightly increase from around 200 epochs, though not significantly. This indicates possible overtraining of the model, which could lead to poor generalisation. The model could be improved by automatically stopping the training after the validation error is shown to begin increasing.

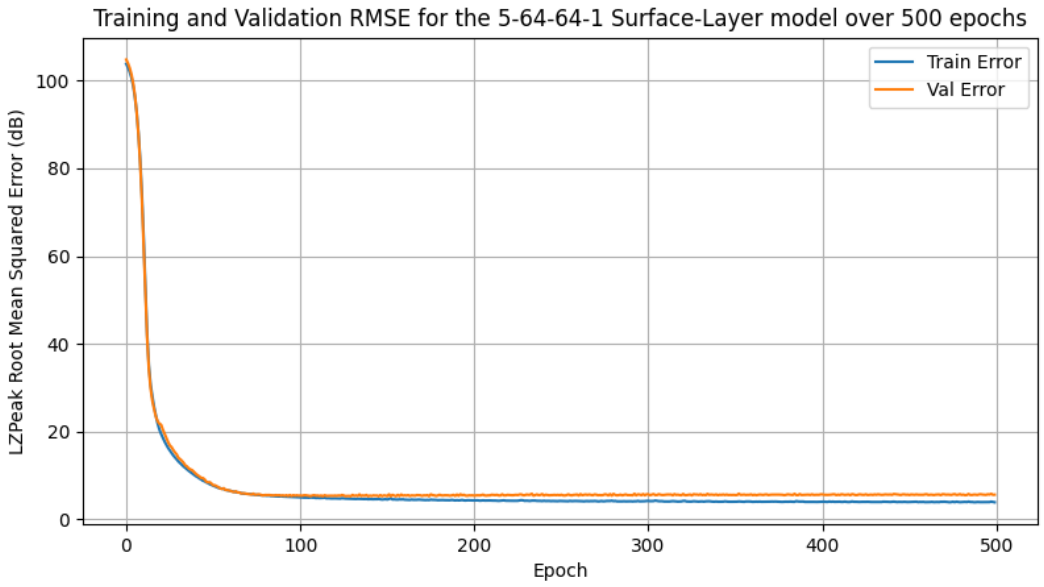

Figure 138 - Training validation loss of the most complex of the surface-layer DNN (5-64-64-1) model over 500 epochs.

For the extended Surface-Layer DNNs, the model RMS error in terms of Lpeak prediction and its maximum error is shown in Table 91.

Table 91 - Prediction accuracy of the Surface-Layer DNNs based on RMSE and Maximum Error (dB).

DNN	RMSE (dB)	Maximum Error (dB)
5-64-1 Surface-Layer	4.4	24.2
5-64-1 Surface-Layer	4.4	24.0
5-64-64-1 Surface-Layer	4.2	24.9

With the addition of parameters describing the surface layer stability of the atmosphere, in the form of the Alon and Alin parameters from Monin-Obukhov similarity theory, a significant improvement in the overall RMS error for predictions of blast relating to major-hazards has been found. Given that this model has been trained on data measured at significant source-receiver ranges, and has been correlated with relatively few propagation parameters, a prediction error of 4.4 dB for long-range blast prediction is an improvement on the existing models discussed in this thesis. However, significant magnitudes in terms of maximum errors are produced by the model on the order of 25 dB. This is not dissimilar to the maximum errors produced by the previous models evaluated in this thesis. Though it is not appropriate to draw direct comparisons between MONET and this model given that

MONET was only available and was evaluated for the Pad C dataset, whereas the DNNs were trained on the extensive EDH dataset. Further implementation of neural networks should focus increasing the number of measurements for other major-hazards operations, improving prediction accuracy for different explosion tests.

A set of predictions from the most complex DNN has been made and is compared against the true (measured) data associated with each prediction. Figure 139 shows a vast improvement of with respect to the distribution of errors around the center line. It is clearly shown however, that this DNN is more likely to underpredict than overpredict, and with those errors to a greater magnitude.

These implication of these findings on improved tools for managing blast noise will be discussed in the next chapter.

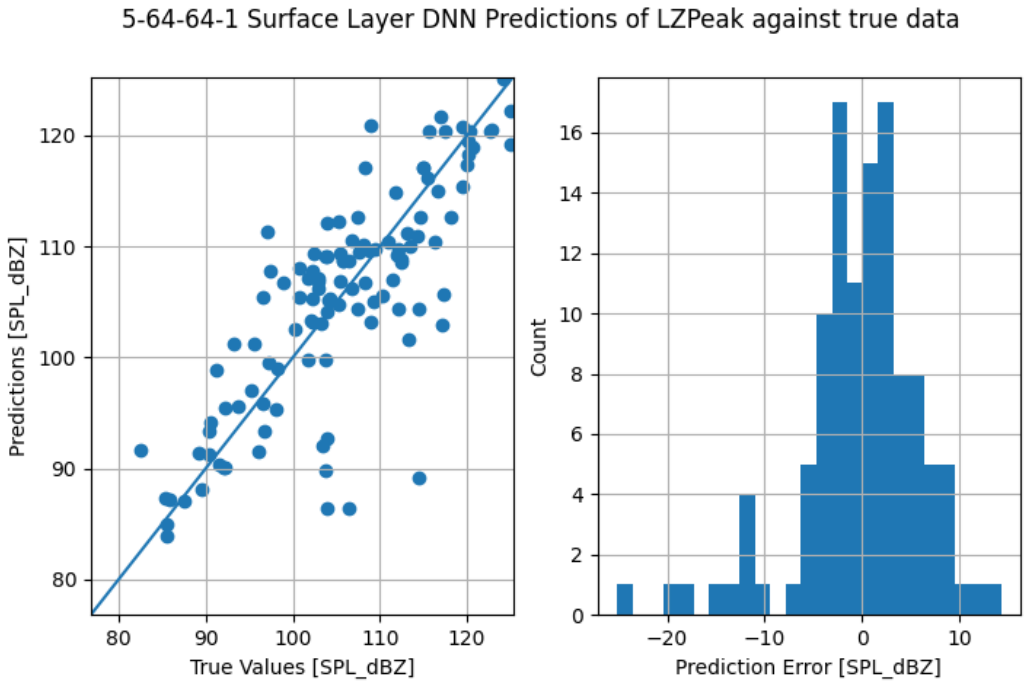

Figure 139 - 5-64-64-1 Surface-Layer DNN prediction accuracy against true values of LZPeak.

5.4.3 Conclusions on the results of Extended Models for Explosive Depth Hardening

This subchapter firstly presented the results of a sensitivity analysis on the Salford Surface Wind (SSW) model, in order to investigate its uncertainty in predicting LZpeak as a function of the uncertainty in its input parameters. By looking solely at the variable parameters of the original model it was shown that source-receiver range, R, was the most influential parameter in the SSW model as it is in its original format, followed by the charge weight W. Second-order interactions between the wind direction and source-receptor angle were the highest when evaluated by the 2^{nd}-Order sensitivity index I_2. The analysis was repeated again but with a focus on the remaining K-parameters in the SSW model, to investigate their influence on prediction variability. Attempts were made to adjust K2 and K4 of the original model to improve the accuracy of the model when compared to results gathered by the live monitoring network. This approach was unsuccessful and suggestions on further work to extend this part of the sensitivity analysis are given in the next chapter.

In an alternative attempt to extend the prediction capability of empirical models such as the Salford Surface Wind for major-hazards testing, the EDH dataset captured by the Live Monitoring Network was used to train two distinct variations of deep-neural networks (DNNs). The results of the model training and validation against new data was presented and RMS prediction errors have been evaluated. These RMS errors are lower than those associated with the original SSW and MONET. The extended surface-layer DNN achieved an RMS error of 4.2 dB for the prediction of LZpeak.

The next chapter discusses the results from these analyses and summarises the implications of these findings on extended prediction models for sources of Major-Hazards testing, such as the Explosive Depth Hardening Operation carried out at DNV Spadeadam.

6 Discussion

6.1 Management of Blast Noise Impacts

Techniques for the management of blast noise impact on residential communities have been presented in Section 4.2. The variety of blast noise operations carried out at the site requires the use of management techniques to be used in combination.

6.1.1 Management Procedures

6.1.1.1 Complaint Procedures

Complaint procedures have been established within DNV's operational policy to collect complainant information when complaints are made. The implication of this is that correlations between complaint information and some measured noise and meteorological data can now be made. This implementation provides the foundation for dose-response relationships for environmental blast noise to be developed.

6.1.1.2 Prediction Procedures

Prediction procedures for blast operations not previously accounted for have been implemented within operational policy at DNV Spadeadam. This includes the use of existing models to make predictions for smaller but more frequent blast operations, such as the EDH operations.

6.1.1.3 Live Noise Monitoring System

Deployment of a live monitoring network has successfully demonstrated that measured acoustic quantities are equally adverse to those generated by large explosion trials such as those on Pad C. This has allowed the exposures generated from EDH operations to be quantified and thus the operation identified as a source of adverse environmental impacts for the DNV site to be aware of.

6.1.1.4 Community Engagement

Engagement between DNV and the surrounding community has been successfully established through a number of methods. Firstly, the implementation of an automated communication channel between DNV and members of the public has allowed the transfer of knowledge between the site and sensitive member of the community on test activity, has reduced the

number of complaints recorded by the site. This is in line with the similar automated methods used by other firing ranges in the UK.

Further, the meetings between DNV staff and local parish councils have allowed the site share knowledge on developments to noise management methodologies with the community.

6.2 Assessment of Existing Salford Surface Wind Empirical Model

6.2.1 Initial Monitoring Phase

The data gathered during the Initial Monitoring Phase assessed the suitability of an existing heuristic prediction model, the SSW for the determination of future adverse environmental blast noise impacts at a number of receptors around Spadeadam.

The results showed the frequency of 5dB prediction error bins for all predictions made across all INM locations, firstly for all test types.

The results of that analysis showed that prediction error did not vary significantly depending on the input meteorological data. For all sources of meteorological data used in that part of the analysis Approximately 25 % of the predictions using all input data, resulted in an over-prediction of between 5-10dB. Approximately 22 % of predictions were within 5 dB of the measured data. The next most frequent prediction error was an underprediction of 5-10 dB below the measured LPeak, and prediction frequency varied between 15-20 % here for all input data.

The implication of this is that when combined, approximately 65-70 % of predictions are within 10d B of the measured Lpeak. Secondly, the results are skewed slightly towards over-predicting the actual Lpeak compared to the measured values. The influence of test type on prediction error was analysed to investigate this feature.

Separation of test type predictions across all monitoring locations showed that a significant proportion of Vapour Cloud Deflagration (VPD) predictions (65 %) resulted in over predictions of 15-20 dB. In fact, effectively all predictions of VPD predictions were over predictions. The other gas explosion, (CVE) was also more likely to result in overpredictions with the majority of predictions skewed to the overprediction portion of the plot.

Solid explosives testing including EDH and Pad C measurements resulted in a broader spread of prediction error, probably due to two reasons. Firstly, there were significantly more EDH measurements than any other test type measured during the initial monitoring phase and in fact throughout the entire monitoring window. The implication of this is that more propagation schemes are like to have arisen, and this could have given rise to more nuances in the meteorological conditions which may not have been captured by the input data, which of course is a highly crude approximation of the atmosphere, with just one parameter combining the 10m wind speed and direction into the vector wind speed.

Secondly, the variation in charge weight and test configuration for Pad C explosives testing is significantly greater than that of any other test type. It is likely that information on test arena geometry and source-terms is a much more dominant feature in the prediction of this type of test, given their variation.

6.2.2 Overall Medium-range performance

Overall, the performance of the Salford Surface Wind model for blast noise impacts prediction at Spadeadam was quantified using the INM database of the entire monitoring window, including every valid measurement from October 2020-December 2022.

The model was quantified using the RMS error metric and maximum over and underpredictions have been reported for each test type and at each location. Interestingly, the model did not show an increase in RMS error, when the using the forecast data furthest from the test time as input into the model. This implicates that predictions do not become significantly poorer, the further ahead of they are made of the test time, for the specific forecast times used in this analysis. This does not mean to suggest that using long-range forecast data of forecast steps beyond that used in this analysis will not yield greater RMS errors, as the uncertainty in the meteorology increases with time. There is an emphasis here however that in general when observing the performance of the Salford surface wind heuristic model, RMS in predictions are not significantly higher for predictions made 96-117 hours ahead of test when compared to predictions made with more updated meteorological forecasts.

This finding may suggest that for representation of the meteorological conditions at Spadeadam, forecasts do not change significantly over the time steps used in this analysis, meaning that trends in prediction RMS as a function of forecast time are not observed here.

6.2.2.1 Maximum Prediction Errors

Although when taking a broad view of predictions collected over months, a performance of 5-10dB for a heuristic model with very few input parameters seems operationally reasonable. However, a significant finding from this analysis is that maximum prediction errors using the SSW model were still very large. This applies to all test types.

For the EDH predictions, errors up to 30dB overpredictions were made (INM 140 and INM 142 retrospective predictions and INM 141 forecast predictions (00-24 hours ahead of testing)). Over predictions are likely due to the model not properly capturing the propagation pathway. A potential cause for overpredictions during downwind propagation under strong wind gradients may still yield interaction of sound waves over soft ground such as that found around Spadeadam. Some downwind receptors may therefore be subject to a blast wave with significantly less energy than locations that are subject to blast waves that have not interacted with the ground.

Alternatively, overpredictions for upwind receptors is still an important factor, if predictions affect operational decisions such as test cancellations, where in fact, real exposures could be up to 30 dB less. Corrections to how the SSW model accounts for these cases are important to improve operational decision-making.

More importantly, underpredictions are a serious cause for concern regarding the use of the SSW model for modelling blast noise impacts. In particular, Pad C predictions showed underpredictions of >30 dB at some locations (INM 142 and INM 144). A particular examination of the results shows that this magnitude of underprediction is attributed to a single test case: a very small 40 g charge on Pad C. The actual measured Lpeak data for locations INM 142 and INM 144 for this test were 106.4 and 106.2 dB. Both of which are peak levels which are likely not to be noticed by those sitting indoors. In this particular case, such an underprediction is less problematic, however, it is important to understand whether the SSW can accurately model propagation from such small charge sizes, given that it was developed on a dataset of 1-17 kg charges. This does also demonstrates how larger explosives such as those from Pad C are beyond the charge sizes upon which the SSW was developed upon.

RMS errors of the SSW model vary for each test type. When performance is considered over all the INM locations, EDH RMS errors are higher than other test types. This is likely due to the significantly larger sample size of EDH measurements as compared to all other test types.

A larger sample size allows the chance of more variation in the propagation scenarios to arise which may not have been adequately represented by the single parameter meteorological term used in the SSW model.

6.2.2.2 Explosive Depth Hardening Performance

The SSW model has an average RMS prediction error of 9.3 dB for EDH operations when considering all input meteorological data and all INM locations and varied between 8.5-10.2 dB across all sources of meteorological data. Interestingly, all RMS errors for EDH operations when looking across all INM locations, were lower than those RMS errors for predictions using the actual meteorological data.

RMS errors for EDH predictions at INM location 145 in Gilsland were particularly lower than at other locations. RMS errors were as low as approximately 7.5 dB even when making predictions at 96-117 hours ahead of the actual test time.

6.2.2.3 Pad C Performance

SSW performance of Pad C predictions was similar to the of the EDH operations, with RMS errors of around 10 dB for most input meteorological data. However, there was slightly more variation in RMS errors for input meteorological data when INM locations were separated out. Particularly low RMS errors were found at INM 140, the closest INM location for Pad C predictions.

At INM 143, the indication of error bars below the RMS value on the figure, indicate that the maximum overprediction was not greater than the RMS value for that location and test type.. The RMS error is greater than the positive error bar indicating that most of the predictions for this location were underpredictions. A significantly smaller sample size of all test types was collected at this location due to power issues, and this influenced the results here.

6.2.2.4 Confined Vented Explosion Chamber Performance

This analysis found that prediction errors for the CVE test were of lower magnitudes for both over and underpredictions. RMS prediction error are between approximately 6.5-9.5 dB for this test when observed across all monitoring locations. Underpredictions were approximately 18 dB at most, with over-predictions of approximately 20 dB. A smaller sample size here could be responsible for both lower RMS errors and smaller overall errors.

6.2.2.5 Hydrogen Detonation Performance

Similarly, to the CVE operations, RMS and overall prediction errors of hydrogen detonations are generally lesser than those of EDH and Pad C operations. RMS prediction errors when using the forecast data were shown to be as low as approximately 5.5 dB for INM 145 if made within 24 hours of testing, and a maximum RMS error 5. 9dB at this location for predictions made more than 2 days earlier.

6.2.3 Summary of SSW performance for predicting Blast Noise Impacts

The ability of an existing heuristic model to predict blast noise impacts on a large dataset of measured acoustic data has been evaluated. Predictions using both measured and forecast meteorological data in the model have been made. The average SSW model RMS errors across all monitoring locations and all meteorological input data for each test type have been tabulated in Table 92.

Most important for DNV is the prediction of blast noise impacts from a wide variety of industrial blast noise sources on communities, rather than the accurate prediction of Peak SPL at a particular location. This analysis of a heuristic model's ability to predict blast noise from DNV's activity has been an important step in the qualitative assessment of the appropriateness of such tools for making operational decisions. This research shows that although on average over a large dataset, RMS errors are reasonable ($<$10dB). However, if the SSW model is used, one should be prepared to see large underpredictions all $>$10dB, and some much larger. Such underpredictions are extremely important when concerned with the auditory risk and the protection of property from overpressure exposures. Alternatively, large overpredictions may impact operational decision-making, resulting in test cancellation and postponement.

Table 92 - Average RMS Errors (dB) of SSW model predictions 0-117 hours ahead of test time for a variety of blast and explosive test types.

Test Type	**RMS Error (dB)**	**Maximum Overprediction (dB)**	**Maximum Underprediction (dB)**
EDH	8.8	29.5	-23.9
PAD C	10.0	15.5	-35.2

CVE	7.9	19.8	-11.5
HYD	8.0	20.5	-15.1

6.2.4 Comparison of MONET against the SSW for Large Explosions

A comprehensive discussion of the analysis comparing MONET against the Salford Surface Wind model has been given in Section 5.3. In summary however, the measurements from 26 'Large' explosions carried out on Pad C at Spadeadam ranging between 25 and 100 kg TNT were used to evaluate the predictive performance of MONET under various propagation scenarios.

The SSW model was found to be 0.6 dB more accurate when assessed for RMS prediction error, and could achieve this at must earlier lengths of time ahead of testing compared to MONET. The RMS predictions and over and underpredictions are given here.

Table 93 - RMS and maximum prediction errors of the Salford Surface Wind model against MONET for Pad C large explosion trials.

Metric	**Prediction Error (dB)**	
	SSW	**MONET**
Average RMS	9.6	9.0
Average Overprediction	27.7	9.8
Average Underprediction	-14.3	-15.6

6.3 Assessment of Extended Models for Blast Noise Prediction

Extended models have been developed from this research for the goal of predicting blast noise from major-hazards testing. A sensitivity analysis on the Salford Surface Wind model informed of the most important parameters to be used in a prediction model for their respective influence on model uncertainty, When the results of the sensitivity analysis were coupled with the findings of the literature review (Chapter 3), inspiration for a novel deep-neural network for blast prediction was found.

6.3.1 Findings from the sensitivity analysis on existing empirical models

A comprehensive analysis of the sensitivity analyses on the existing SSW empirical model has been given in Chapter 5.4. In summary the values of the K-factors are extremely important to the output of the model. K4 was ranked to have the most important contribution overall when assessed via a global sensitivity analysis using Sobol' sensitivity indices. This is through the interaction with the logarithm of the source-receiver distance, which can vary significantly compared to other input variables like the charge weight and refraction term.

Modification of the K4 parameter to account for greater or lesser attenuation was attempted, and the results of the adjusted K4 SSW model were analysed. Significant over and underpredictions were found when varying the K4 term between +/- 9 dB bounds. Consequently, model accuracy was low with increasing modification of the term in either sign from the original value provided in the original regression analysis that form the coefficients of the SSW model. This indicates that the K4 term, although is important in the sensitivity of the model output, when modified, does not fit the measured data at Spadeadam better than the original value of K4 does in the SSW model. Therefore, it is concluded that the K4 parameter is set to an appropriate value for use at Spadeadam.

Furthermore, the K2 parameter that interacts with the logarithm of the charge weight was adjusted to observe any trends in fitting to the measured data. Overall, when generalising over the whole dataset, the model error was lowest when the K2 parameter was set to its original value given in the SSW model. When adjusting this term incrementally, prediction error was found to increase, though not as significantly as for the adjustments with K4. This

is because the charge weight varies less than that of the distance. Although, one test case for a small charge was found to yield increased underprediction across 3 monitoring positions. The variation between monitoring positions of their associated propagation parameters, (distance, azimuth, and wind vector) did not explain the underpredictions and hence it was concluded that an adjustment to the source term may be appropriate. A process of error minimization by decreasing the of value of K2 in that specific case was shown. However, this is one case and many more predictions of small charges should be compared to make conclusions on whether an adjustment to K2 for small explosive is justified.

6.3.2 Findings from Extended Neural Networks for the Prediction of Blast Noise

A deep-learning approach to model blast noise from the extensive EDH dataset has been presented in this thesis. Firstly, a DNN model inspired by the original SSW model was trained and validated against the measured data from Explosive Depth Hardening. A relatively simple neural network with just 3 input parameters and 1 hidden layer achieved an improvement to overall prediction error (RMS) compared to the original empirical model. This is likely because a hidden layer can aid optimisation of the model weights and parameters in terms of weights and biases so that the nonlinear interactions between the input parameters are accounted for.

Extending the model further, inspired by the inclusion of terms used for representing atmospheric stability, the logarithmic and linear terms for representing the shape of the sound speed profile from Monin-Obukhov similarity theory have been included in a DNN. The extended Surface-Layer DNN model with its 5 inputs and 2 hidden layers was able to achieve a much improved prediction accuracy compared to the standard DNN and the original SSW model.

A summary of the RMS prediction errors from the neural networks are compared to the accuracy of the SSW here.

Table 94 - Summary table of prediction error for the SSW model, compared to the two neural networks developed.

Prediction Model	RMSE (dB)	Maximum Error (dB)
Salford Surface Wind	8.8	23.9

3-64-64-1 Standard DNN	7.9	26.2
5-64-64-1 Surface-Layer DNN	4.2	24.9

Interestingly, the SSW model yields the lowest maximum prediction error, though not significantly lower than for the DNNs. Important however is that the DNNs have only been trained on the EDH data set and thus the comparison is limited to making predictions of that type of explosive test.

The contribution of DNN and an extended variety is important to the field of blast noise management, as these DNNs can be used at much earlier instances, by utilising long-range readily available meteorological parameters. This is a significant advantage over the use of intensive computational models which require large quantities of accurate input meteorological data, as a planning tool for blast noise management.

Of course, these DNNs are by no means optimal, as was shown in the Chapter 3.3, DNNs have been used in the mining industry to make predictions of blast effects with even smaller prediction errors and with significantly more input parameters and optimisation. It is therefore proposed that further work on DNN model optimisation should be prioritised, as well as extending the models to generalise across other types of major-hazards testing.

7 Conclusions

Conclusions from the entire thesis are offered in this Chapter. As conclusions and further work from Part I have already been stated, an overview of these conclusions is provided here as a refresher. The main concern of this chapter is to form conclusions from Part II of the thesis and then to summarise conclusions from both parts in combination.

7.1 Part I Conclusions

This provides an overview of the findings from Part I of the thesis on the suitability of current assessment methodologies for the selection of hearing protection for the case studies presented above.

Conclusions from the literature review have been stated in Chapter 2.

7.1.1 Case Study 1 – Explosion Chamber Demonstration

- The maximum C-weighted peak level measured across the personnel zone was 166.6dBC (January 2020 with a Class 1 Sound Level Meter and high-pressure microphone).
- Pressure gauge measurements recorded similar peaks of 163dBC across the viewing area.
- For this test only the in-ear style hearing protection (both active and passive) provided enough attenuation to be below the CoNaWR action limit (140dBCpk).
- Measurements across the viewing area showed that exposures can vary for nominally the same test and environmental conditions.
- Exposures from this demonstration are have frequency characteristics beyond the scope of the UK legislative guidance for the selection of hearing protection.

7.1.2 Case Study 2 – Explosive Depth Hardening

- The maximum C-weighted peak level measured across all trials was 158.6dBC.
- According to the HML assessment method, against this exposure, all in-ear plug-type protection devices provide sufficient attenuation so that exposure is below the CoNaWR 140dBC limit.
- The test operative's active ear plug protection 3M LEP-200 is assumed to provide attenuation in the same way as passive hearing protection does under such high-level exposures.
- Significant signal artifacts were present on the field trial recordings and the nature of these recording need to be investigated.

7.2 Part II Conclusions

Part II of this thesis has examined both management and prediction methodologies for the mitigation of adverse blast noise impacts on long-range communities from industrial operations.

The literature review chapter reviewed the relevant physical parameters most influential on the magnitude of blast noise impacts. The theoretical nature of existing outdoor sound propagation models has been reviewed for their applicability to predicting blast noise. Legislative guidance on environmental noise impacts relevant to blast noise has been reviewed and research on the justification of acoustic indices to model community response has been presented.

The extensive review of blast noise control is offered as an alternative approach to noise management, and predictions using parabolic equation models are utilised to investigate the importance of certain environmental effects.

Strategies for the management of blast noise impacts at Spadeadam have been presented in the methodology chapter. A mixture of differing strategies has been implemented at DNV Spadeadam through completion of this thesis, in order to cover the broad range of industrial blast operations and diverse communities living around the test site.

A Live Noise Monitoring Network has been implemented around the Spadeadam site. This measurement infrastructure bridges the gap between blast noise *management* and *prediction*.

With regard to prediction of noise from major hazards, the applicability of an existing empirical propagation model for the prediction of novel explosive sources from a variety of operations has been quantified. The analysis concludes that the SSW model has large individual over and underprediction errors when predicting blast noise impacts for a diverse range of explosive types and receptors. However, analysis of large quantities of measured data show that RMS errors < 10 dB are achievable a number of days ahead of testing. Both findings are extremely important for the operational tasks required to manage adverse blast noise impacts on communities. The performance of the SSW model has been evaluated again MONET, a computationally extensive parabolic equation model, and was found to have an approximately equal RMS prediction error for predictions of large explosion tests (25-100 kg TNT). This is a significant finding, given that the RMS prediction errors of the SSW empirical model extend to much earlier times than MONET was used for. This shows that a

reasonable degree of accuracy for the source and propagation conditions can be represented by readily available, low-quantity, long-range forecast data.

Finally, extended models based on deep learning have been trained and validated for a specific explosive operation, using measured acoustical and meteorological data. Using just 3 input parameters, the Standard DNN used the same input parameters as the SSW model and achieved slight improvement to the prediction accuracy. Moreover, the neural network was extended to include parameters responsible for the description of atmospheric stability, namely the Surface-Layer DNN. This model achieved significant improvements to prediction errors and generalised well to unseen data when making predictions of Explosive Depth Hardening operations. Further work is required to quantify the near-field characteristic of the source for input into the model.

8 Further Work

This thesis demonstrates that upon investigating both occupational and environmental blast noise impacts, more issues that need resolving have appeared than those that are solved by this work. The work outlined in this project spans the broad range of topics that determine overall blast noise impacts on individual workers in the near-field and sensitive residential communities at long-range.

8.1 Further Work on Blast Noise Prediction Models

The ability for a currently existing heuristic model to make operational predictions of blast noise impacts has been evaluated in this work. However, the analysis should be included to compare predictions of other heuristic models for blast noise prediction using the extended meteorological data captured throughout the project. This includes the use of forecast atmospheric profiles gathered by the Met Office DataHub model, and the ECMWF data which although is spatially sparse, extends into a number of days ahead of testing. Planning tests a number of days or even weeks ahead is a high priority for DNV and an analysis of each models ability to perform predictions further into the future is important.

Secondly, the use of extensive computational models discussed in Chapter 3.3, such as ray tracing and nonlinear models could be utilised. When couple with measured, short- and long-range forecast data to make correlations with noise data, such methods could be combined with deep learning approaches to build Physics-Informed Neural Networks.

Finally, much more data has been collected during this project than what has been presented in the analyses of this thesis. These data are listed below and should be utilised for further analyses. Analysis of model performance at forecast time much earlier than those reviewed here, on the order of 1-2 weeks are available, in addition to the derived sound speed profiles and ground reflectivity data collected.

- ECMWF Long-range meteorological data
- Ground reflectivity and surface type data for the Spadeadam are
- Range dependent meteorological data from the Met Office DataHub service

A program in place that will address the additional issues raised by this research and is supported by a number of strategies to enable this work to continue.

8.2 Future Role at DNV Spadeadam

From May 2023, the author has been based at the DNV Spadeadam site. This was an important step following this iPhD, which was designed to allow collaborative research between industry and academia and is aimed at integrating researchers in industry. The role of a Research Scientist under DNV Spadeadam's Research & Development Team is designed with noise specialism in mind, in order to secure future work in this multifaceted topic. An action plan has been developed to continue this work, and is outlined below.

8.2.1 Roles of Research Scientist Role with Noise Specialism

- Develop noise specialism throughout all operations at Spadeadam
- Advise on noise within the wider DNV company
- Automate decision-making processes related to noise
- Carry out surveys of noise exposure on the site
- Improve current understanding of noise related issues on the site
- Improve measurement methods for blast testing
- Analyse impacts on site productivity due to noise restrictions

Specific research projects have been conceptualised as a framework for the above action plan, which is outlined, and ordered by descending priority.

- Large-scale field trials of source term measurements
    - Quantify directivity of blast noise sources at Spadeadam
    - Understand the effects of source geometry on near-field exposures
- Propagation model development
    - Inclusion of source terms into propagation models
    - Live boundary layer characteristics
    - Optimisation of deep learning approach to atmospheric classification
    - Improvement of meteorological equipment for continuous measurement
    - Quantification the effects of forestry and landscape changes to far-field noise
    - High-definition quantification of ground impedance characteristics
- Hearing Protection Performance for Blasts
    - Full-site survey of all hearing protection used for all occupational noise hazards
    - Improving the scope of UK best-practice for assessing hearing protection performance against:
    - low-frequency exposure
    - multiple pressure peaks
- Improving the Live Monitoring Network
    - Increase the number of both on-site and off-site monitors
    - Improved dynamic and frequency range capabilities on instrumentation

- Noise relating to future Hydrogen Explosion work
- Characterisation of noise from gas explosions

8.3 Future Collaborative Research

In order to support this work, some future projects have been developed specifically from the outcomes of this PhD Thesis.

8.3.1 Blast Noise Control PhD

Since September 2023, another iPhD between the University of Salford and DNV has begun to investigate the topic of Blast Noise Control. This topic is specific to managing blast noise impacts by using techniques that control noise at the source. The PhD was developed following the identification of the Explosive Depth Hardening (EDH) operations as problematic with regard to adverse environmental impacts, relative to the other operations carried out at the DNV site.

8.3.2 Occupational Blast Noise PhD

Another PhD has been developed for research dedicated solely to investigating the applicability of current state-of-the-art methods and best-practice for the assessment of hearing protection performance against blast noise. This work continues work on the issues raised by Part I of this thesis.

8.3.3 Blast Noise Workshops

With this thesis allowing the continuation of UK's involvement in Blast Noise research, collaborative partnerships have been developed to allow the transfer of knowledge between UK and international organisations involved in Blast Noise Research.

A workshop has been planned to establish a UK Blast Noise Group. Previous workshops on Occupational Blast Noise have been hosted by the researcher earlier in the PhD process, and this workshop is reported in the Appendices.

The future workshop is intended to be held at the DNV Spadeadam site and encourages other researchers and organisations concerned with measuring, managing, and predicting blast noise impacts to present and share ideas. The intended outcome of such a workshop is to

develop research proposals, bringing together all UK blast noise research groups to produce better blast noise analysis and management tools.

8.4 Final Thoughts

Looking forward, the adaptation of this work to a future of industrial, technological, societal, and ecological challenges is more important than ever. In the past, much of the research underpinning blast noise measurement, management and prediction has been rooted in military context. Challenges related to noise from military blasting will persist, especially with concerns around a growing population, naturally increasing the number of those living near military testing ranges.

Due to the increased effort to decarbonise industry, transport and energy production, (which DNV is a leading organisation for), there may be profound effects on the public's perception of industrial blast noise related to operations that promote the safety and use of greener technologies. The transfer of this work into the following areas of research is important for the continuation of this work.

- Non-acoustical effects on the perception of industrial blast noise related to industry decarbonisation
- Effects of industrial blast noise on society

Furthermore, the protection and restoration of existing ecological habitats are more important than ever in the context of biodiversity collapse and climate crises. The integration of environmental noise with ecological impacts is important for developing management tools that enable sustainable development. Biodiversity underpins ecological services which support global society and in the UK alone, the Office for National Statistics evaluated ecosystem services in 2015 at £716 billion (Waddington, Wood, Davies, & Young, 2023). To fully understand the environmental impacts of industrial blast noise, the influence of blast noise on habitat suitability must be appropriately quantified. DNV Spadeadam are presented with a unique opportunity to pioneer this research, being situated within large areas of forestry owned by Forestry England. The eastern DNV site boundary is directly bounded by the Northumberland National Park, as well as is surrounded by Kielder Forrest to the north, Gowk Bank Nature Reserve to the northeast, and a variety of habitats in other directions. Future work should include:

- Collaboration with Forestry England on habitats

- Integration of blast noise monitoring equipment with terrestrial bioacoustic diversity monitors

Finally, future research should integrate emerging technologies such as the Internet of Things (IoT) for improving the capacity of web-enabled blast measurement and live feedback systems. Where computational speed is less important, Blockchain technology could improve transparency and academic integrity across monitoring networks that allow open-access environmental noise data to members of the public and to the environment, especially when concerned with potentially harmful, high-amplitude blast waves.

Appendices

Appendix A Research Profile Development

8.4.1 Occupational Blast Noise Workshop

On the 22nd of January 2021, the author organised and presented the findings from the first year of the PhD work, at a virtual workshop. The current state-of-the-art and limitations in the measurement methodology were discussed with a panel of occupational noise experts. The outcome of the workshop is presented in Figure 140.

A series of measurements was presented to all attendees. It was agreed that the methodology was satisfactory under the current legislation and an update to the HML method was discussed. The executive summary of the workshop is shown in Figure 140.

8.4.2 Conference Papers and Presentations

The work from this thesis formed several papers presented at conference.

8.4.2.1 Managing Occupation Blast Noise, ASA 182nd Meeting

During May 2022, the author presented the above paper at the 182nd Meeting of the Acoustical Society of America, in Denver, Colorado. Prior to attending the conference, the research also was invited to and attended the ASA 2022 School.

8.4.2.2 Managing Community Noise Impacts from Blasts, ASA 184th Meeting

Similarly, the author presented the above paper at the 184th Meeting of the Acoustical Society of America, in Chicago, Illinois.

8.4.2.3 An Heuristic Prediction Method for Managing Environmental Blast Noise Impacts, (Manuel & Waddington, 2023a)

In August 2022, the author presented the above paper at Inter-noise 2022, in Glasgow, UK.

8.4.2.4 Managing environmental impacts from blast noise sources in the UK, Forum Acusticum September 2023

Finally, the above was presented by the author at the Forum Acusticum conference in Torino in September 2023. The paper is a collaboration between the author, David Waddington (University of Salford), Graham Parry (ANCON) and Andrew Bullmore (Hoare Lea).

8.4.3 Journal Papers

Managing Occupational Noise from Explosive Depth Hardenin Operations

In July 2023, the author was successful in having the above paper published in the Journal of Applied Acoustics.

8.5 Peer Review Work in Studies of Aircraft Noise

During the period of study, the author contributed to a technical peer review for the following commercial work.

8.5.1.1 Technical Peer Review for SoNA for aircraft noise

Phase 1: This project phase concerned a technical review of the calculations and data management which underpinned the analysis presented in SoNA1 Annoyance 2nd Edition and Sleep studies. The scope of the work included reviewing the integrity of the noise data and the adequacy of noise dose calculation and categorisation.

Phase 2: The second phase of the technical review work which investigated the robustness and integrity of noise respite calculation and categorisation, along with change in noise dose in consecutive years.

8.5.2 Teaching

This author has engaged with both undergraduate (BEng) and postgraduate (MSc) Acoustics courses at the University of Salford throughout their studies, leading to a range of teaching duties which are summarised below.

- Laboratory Demonstrating: Acoustic Laboratory 2019-2020 Level 4
- Level 6-7 Environmental Noise Measurement: Coursework marking 2020, 2021 and 2022
- 6-7 Environmental Noise Measurement: Masterclass in Outdoor Sound Propagation
- Level 6-7 Environmental Noise Measurement: Session on Sound Level Meter Calibration
- Level 6-7 Environmental Noise Measurement: Masterclass on Occupational Environmental Noise

I-CASE PhD: Blast Noise Prediction and Management
Hearing Protection Workshop Executive Summary
by Gethin Manuel

Executive Summary

- A virtual Blast Noise Hearing Protection Workshop was hosted by Salford on the 22nd January 2021, where the current state-of-the-art and limitations in the measurement methodology were discussed with a panel of occupational noise experts, including the HSE, Qinetiq and DNVGL.
- This workshop was part of a PhD iCASE project which aims to develop a measurement-based tool for the management of blast noise impacts at the DNVGL Spadeadam Test site in Cumbria.
- Part of the noise management strategy involves the assessment and selection of suitable hearing protection devices against high-amplitude impulsive noise for site personnel, an exceptionally specialised and challenging technical topic.

Background

The Project Stage: 'Hearing protection management for blast testing', concerns the issues around:

1. Occupational noise exposure of employees at Spadeadam
2. Near-field measurement of blast waves and very high-amplitude impulsive noise
3. Hearing damage mechanisms from blasts
4. Current limitations in best-practice guidance for the selection of hearing protection for blasts

Best practice was reviewed through a thorough literature review and in depth discussions with authorities in the field, including experts from the Health and Safety Executive (HSE), academic and industry specialists in measurement, and highly-experienced advisers to the military.

Mechanisms of Hearing Loss from Blasts

Hearing loss associated with blasts occurs across many anatomical sites in the ear and is attributed to many damage mechanisms. Without noise mitigation, damage mechanisms from blasts overpressures impact through the anatomy of the middle and/or inner ear. A review of the scientific literature found discrepancies in the components of the blast waveform responsible for each mechanism. Conversely, the current occupational noise assessment method for impulsive noise (HML method) involves no analysis of the blast pressure-time history and only one metric, the *C-Weighted Peak Exposure Level, L_{CPeak},* and the categorisation of a blast by frequency content.

Outcome of the Workshop

A series of measurements performed at DNVGL Spadeadam was presented by Gethin. It was agreed that the methodology was satisfactory for the range of blasts at Spadeadam under the current legislation. However, a number of important limitations in the current methodology were identified and so an update to the HML method was discussed.

1) Specifically, the limitation of the extended HML method from Defence Standard 0027:2015 on low-frequency blast components (below 63Hz) was recognised.
2) Regarding the upcoming review of the HML method, a proposed extension of the low frequency category beyond 10dB to around 16dB, based on a methodology from ANSI 12.68 was examined. This review would also likely address the stepped effect in the frequency categories to a more continuous function.
3) Measurements uncertainties were scrutinised, particularly concerning noise artifacts. It was noted that the measurement capabilities of the instrumentation used (blast gauges) for the

assessment exceeded the minimum sampling requirements detailed in the standard (Class 1 SLM).

4) The practical implementation of noise control management to reduce adverse impacts from blasts were considered. The main methods include the introduction of controls on the number of blasts, and management of exposure from each blast using barriers.
5) On the other hand, ergonomic aspects were considered to be on occasion more important than attenuation level in practise. Considerations include whether operatives will wear the hearing protection prescribed, and whether it fits with their other PPE such as helmets and hats. Reliability and cost of effectiveness were also identified as important factors.

Further work

The following recommendations for further work were made:

1) Side-by-side comparison of blast gauge and SLM measurements are essential to validate the methodology recommended for assessment under current legislation.
2) Investigation of the effects of multiple blast waves from independent sources on the overall peak pressure is urgently required as this phenomenon is not infrequent but has previously been neglected.
3) Comparison of the HML and NRSg methods with the AHAAH physical model would indicate whether current best practise employed for implementation of legislation could be improved using more recent scientific findings.

Figure 140 - Overview of Occupational Blast Noise Workshop

Appendix B University of Salford Blast Noise Research History

Full Title and date of Trial	Field Trial Report Number	Report Date
INVESTIGATION INTO EXPLOSIVE NOISE PROPAGATION AT A DISTANCE UP TO 3500M FROM THE SOURCE, 26-29 September 1989	SAL/FT/22	April 1990
REPORT ON THE MEASUREMENT OF BLAST NOISE PROPAGATION CBDE. PORTON, 20-22 April 1993	SAL/FT/34	April 1996
REPORT ON THE MEASUREMENT OF BLAST NOISE PROPAGATION ACROSS SEA SHOEBURYNESS, 17-18 August 1993, SHO93/1 Propagation across sea to 8km	SAL/FT/33	December 1994
EXPLOSIVE NOISE PROPAGATION ACROSS WATER TO 500M, 12-14 August 1991	SALF/FT/28	January 1992
REPORT ON THE MEASUREMENT OF BLAST NOISE PROPAGATION – SHOEBURYNESS, 18-25 November 1992 Trial 92/4. Propagation to 8km over grass	SAL/FT/35	October 1996
EXPLOSIVE NOISE PROPAGATION, PROPAGATION TO 2500M INVESTIGATION OF SCALING LAWS PROPAGATION OVER A WALL, 17-28 September 1990	SALF/FT/27	January 1992
REPORT ON THE MEASUREMENT OF BLAST NOISE PROPAGATION, RAF BINBROOK, 16 July 1996, Trial DDHS 96/1 Propagation to 2km over concrete and grass	SALF/FT/39	July 1997
REPORT ON THE MEASUREMENT OF BLAST NOISE PROPAGATION, RAF BINBROOK, 16 July 1996, Trial DDHS 96/1 Propagation to 2km over concrete and grass	SAL/FT/32	June 1995
REPORT ON THE PROCEDURE USED IN THE MEASUREMENT OF BLAST NOISE PROPAGATION IN SNOW-COVERED FOREST, HASLEMOEN, NORWAY, 18-23 February 1995	SAL/FT/41	September 1998

Figure 141 - University of Salford's history of blast noise research.

Date	Trial Plan	Description including range/charges weight
7/87	POR P	Free-air propagation to 100m: 125g. 1kg
	POR Q	Comparison of instrumentation to 100m: 125g. 1kg
	POR R	Effect of RMU box on waveform: 1kg
	POR S	Ground impedance
10/87	POR 1	Effect of microphone height at 1km: 1kg
	POR 2	Waveform in shadow zone to 150m: 1kg
	POR 3	Ground impedance
5/88	POR 4	Free-air propagation to 100m. Comparison of instrumentation: 125g. 1kg
	POR 5	Propagation over grass to 200m: 125g. 1kg
	POR 5A	Waveform in shadow zone at 500m: 125g. 1kg
	POR 5B	Comparison of RMU with standard equipment to 200m: 125g. 1kg
	POR 6	Ground impedance
9/88	POR 7	Propagation over concrete to 100m: 125g. 1kg
	POR 8	Propagation over grass to 100m: 125g
	POR 9	Waveform in shadow zone at 200m: 125g
	POR 10	Ground impedance
5/89	POR 11	Comparison of RDX/TNT with PE4 in free-air to 100m: 125g. 1kg
	POR 12	Propagation over grass to 1km: 125g. 1kg
	POR 13	Waveform in shadow zone to 600m: 1kg
9/89	POR 14	Propagation to 3500m: 1kg
	POR 15	Shielding by hard target: 1kg
	POR 16	Secondary shock over concrete: 125g. 1kg
9/90	POR 17	Propagation to 2500m over grass: 1kg
	POR 18	Propagation to 1km: 1. 8kg
	POR 19	Shielding by 1.8x9m barrier on grass: 125g
8/91	SHO 91/1	Propagation to 100m over lagoon: 1kg
	SHO 91/2	Propagation to 500m over sea: 1kg
11/92	SHO 92/4	Propagation to 8km over land: 1. 8. 64kg
4/93	POR 20	Shielding by barrier on hard target: 125g. 1kg
	POR 21	Transition between concrete and grass. Downwind to 100m: 1kg
8/93	SHO 93/1	Propagation to 8km over sea: 1. 8kg
6/94	NOR 94/2	Propagation to 1400m in forest: 1. 8kg
	NOR 94/3	Calibration of C4: 1kg
	NOR 94/4	Propagation across forest boundary: 1kg
9/94	NOR 94/1	Propagation to 12km in forest: 1. 8. 64kg
11/94	DDHS 93/1	Propagation to 3000m over concrete: 125g. 1kg
2/95	NOR 95/1	Propagation through forest to 1400m with snow: 1. 8kg
	NOR 95/2	Propagation over open ground to 1400m with snow: 1. 8kg
	NOR 95/3	Calibration of C4: 1. 8kg
	NOR 95/4	Propagation across mixed open ground and forest to 1400m with snow: 1kg
2/96	NOR 96/1	Propagation to 12km in forest with snow: 1. 8. 64kg
6/96	SHO 96/1	Propagation over a large container used as a barrier and AS90 as the source
7/96	DDHS 96/1	Propagation to 2000m over concrete and mixed concrete/grass: 125g. 1kg

Figure 142 - Specific field trials carried out by the University of Salford's Acoustics Research Centre.

References

3M. (2019a). 3M 1100 Series Disposable Ear Plugs Data Sheet. In M. O. H. a. E. S. Group (Ed.).

3M. (2019b). 3M Peltor Optime Earmuffs Technical Data Sheet. In m. O. H. a. E. S. Group (Ed.), (Vol. J459146).

200-1, A. (2007). Environmental Protection and Enhancement - Chapter 7. In *Environmental Noise Management Program*.

Acoustics Research Centre, U. o. S. (2006a). *Volume 1: User Guide*. GridTracePE: Hybrid GridTrace and Parabolic Equation Long Range Propagation Prediction Program. Documentation.

Acoustics Research Centre, U. o. S. (2006b). *Volume 2: Guide to the Theory*. GridTracePE: Hybrid GridTrace and Parabolic Equation Long Range Propagation Prediction Program. Documentation.

Acoustics Research Centre, U. o. S. (2006c). *Volume 3: Implementation Guide*. GridTracePE: Hybrid GridTrace and Parabolic Equation Long Range Propagation Prediction Program. Documentation.

Advantica. (2003). *Noise and Vibration Measurements at Advantica, Spadeadam*. Retrieved from

Agisheva, U., & Galimzyanov, M. (2020). Acoustic Waves Propagation in Heated Water with Vapor Bubbles. *Bulletin of the South Ural State University, Series: Mathematical Modelling, Programming and Computer Software, 13*, 28-38. doi:10.14529/mmp200102

Ambrosiano, J. J., Plante, D. R., McDonald, B. E., & Kuperman, W. A. (1990). Nonlinear propagation in an ocean acoustic waveguide. *The Journal of the Acoustical Society of America, 87*(4), 1473-1481. doi:10.1121/1.399444

American National Standards Institute. (2007). Methods of estimating effective a-weighted sound pressure levels when hearing protectors are worn. In *ANSI/ASA S12.68-2007 (R2020)*. Melville, NY: Acoustical Society of America.

American National Standards Institute. (2010). Methods for the measurement of insertion loss of hearing protection devices in continuous or impulsive noise using microphone-in-real-ear or acoustic test fixture procedures. In *ANSI/ASA S12.42-2010 (R2016)*. Melville, NY: Acoustical Society of America.

Amiri, M., Bakhshandeh Amnieh, H., Hasanipanah, M., & Mohammad Khanli, L. (2016). A new combination of artificial neural network and K-nearest neighbors models to predict blast-induced ground vibration and air-overpressure. *Engineering with Computers, 32*(4), 631-644. doi:10.1007/s00366-016-0442-5

ANSI. (1983). ANSI/ASA S2.20-1983 (R2020). In *Estimating Airblast Characteristics for Single Point Explosions in Air, With a Guide to Evaluation of Atmospheric Propagation and Effects*: American Institute of Physics.

Attenborough, K., Cummings, A., Dutta, P., Schomer, P., & Salomons, E. (2004). Blast-Sound-Absorbing Surfaces. A Joint Project of the ERDC and the Netherlands Ministry of Defense.

Attenborough, K., Li, K. M., & Horoshenkov, K. (2006). *Predicting Outdoor Sound*: Taylor & Francis.

Attenborough, K., Taherzadeh, S., Bass, H., Di, X., Raspet, R., Becker, G., . . . Hoof, H. (1995). Benchmark cases for outdoor sound propagation models. *The Journal of the Acoustical Society of America, 97*, 173-191. doi:10.1121/1.412302

Attenborough, K., Wang, Q., Dutta, P., Durell, G., Schomer, P., Mifflin, J., . . . Weele, P. (2003). Effects of altering ground conditions on blast noise propagation. *89*, S69.

Baker, W. E. (1973). *Explosions in air*: University of Texas Press.

Baume, O., Gauvreau, B., Bérengier, M., Junker, F., Wackernagel, H., & Chilès, J.-P. (2009). Geostatistical modeling of sound propagation: Principles and a field application experiment. *The Journal of the Acoustical Society of America, 126*(6), 2894-2904. doi:10.1121/1.3243301

Berger, S., Ben-Dor, G., & Sadot, O. (2015). Numerical Investigation of Shock-Wave Attenuation by Dynamic Barriers. *Journal of Fluids Engineering, 138*. doi:10.1115/1.4031375

Berglund, B., Berglund, U., & Lindberg, S. (1986). *Loudness of impulse sound from differrent weapons*. Paper presented at the Inter Noise '86.

Berglund, B., Lindvall, T., Schwela, D. H., World Health Organization, O., & Environmental Health, T. (1999). Guidelines for community noise. In. Geneva: World Health Organization.

Bolotnova, R., & Gainullina, E. (2019). Dynamics of a spherical explosion in aqueous foam taking into account heat-exchange and dissipative processes. *Journal of Physics: Conference Series, 1400*, 077027. doi:10.1088/1742-6596/1400/7/077027

Bolotnova, R., & Gainullina, E. (2021). Modeling of weak shock waves propagation in aqueous foam layer. *Journal of Physics: Conference Series, 2103*, 012217. doi:10.1088/1742-6596/2103/1/012217

Boris, J. P., & Book, D. L. (1971). Flux-Corrected Transport. I. SHASTA, A Fluid Transport Algorithm That Works. *Journal of Computational Physics, 11*, 38-69.

Boslough, M. B., & Asay, J. R. (1993). Basic Principles of Shock Compression. In J. R. Asay & M. Shahinpoor (Eds.), *High-Pressure Shock Compression of Solids* (pp. 7-42). New York, NY: Springer New York.

Brink, M., & Wunderli, J.-M. (2010). A field study of the exposure-annoyance relationship of military shooting noise. *The Journal of the Acoustical Society of America, 127*(4), 2301-2311. doi:10.1121/1.3337234

Britan, A., Liverts, M., & Ben-Dor, G. (2009). Mitigation of sound waves by wet aqueous foams. *Colloids and Surfaces A: Physicochemical and Engineering Aspects, 344*(1-3), 48-55. doi:10.1016/j.colsurfa.2009.02.011

Britan, A., Liverts, M., Shapiro, H., & Ben-Dor, G. (2013). Macro-mechanical modeling of blast-wave mitigation in foams. Part II: reliability of pressure measurements. *Shock Waves, 23*(1), 25-38. doi:10.1007/s00193-012-0402-y

Britan, A., Shapiro, H., Liverts, M., Ben-Dor, G., Chinnayya, A., & Hadjadj, A. (2013). Macro-mechanical modelling of blast wave mitigation in foams. Part I: review of available experiments and models. *Shock Waves, 23*(1), 5-23. doi:10.1007/s00193-012-0417-4

Brueck, E. (2016). Measuring the risk of impulsive noise at work: One practitioner's tips. *Acoust. Aust., 44*(1), 77-81. doi:10.1007/s40857-016-0045-8

BSI. (2013). Electroacoustics. Sound level meters. Specifications. In.

Buchta, E., & Hirsch, K.-W. (1996). *Physikalische Aspekte zur Bergündung der Wahl der C-Bewertung zur Beureilung hochintensiver Knalle*. Paper presented at the Fortschritte der Akustik - DAGA 96, Oldenburg.

Buchta, E., & Vos, J. (1998). A field survey on the annoyance caused by sounds from large firearms and road traffic. *J. Acoust. Soc. Am., 104*, 2890.

Bullen, R. B., & Hede, A. J. (1982). Assessment of community noise exposure from rifle shooting. *Journal of Sound and Vibration, 82*(1), 29-37. doi:https://doi.org/10.1016/0022-460X(82)90540-5

Buzukov, A. A. (2000). Decreasing the parameters of an air shock wave using an air-water curtain. *Combustion, Explosion and Shock Waves, 36*(3), 395-404. doi:10.1007/BF02699393

Carton, E. (2018). *AIR BLAST MITIGATION USING WATER FOAM COVERAGE*.

CBI, Group, E. I., & Executive, H. a. S. (2020). Guidance for the Safe Management of the Disposal

of Explosives. In.

CHABA. (1968). *Proposed damage risk criterion for impulse noise (Gunfire)* (Report of Working Group 57). Retrieved from Washington DC.:

Chen, L., Zhang, L., Fang, Q., & Mao, Y.-m. (2015). Performance based investigation on the construction of anti-blast water wall. *International Journal of Impact Engineering, 81*, 17-33. doi:https://doi.org/10.1016/j.ijimpeng.2015.03.003

Cheng, R., Morris, P. J., & Brentner, K. S. (2009). A three dimensional parabolic equation method for sound propagation in moving inhomogeneous media. *The Journal of the Acoustical Society of America, 126*(4), 1700-1710. doi:10.1121/1.3203934

Cho, S.-I., Gao, S. S., Xia, A., Wang, R., Salles, F. T., Raphael, P. D., . . . Oghalai, J. S. (2013). Mechanisms of Hearing Loss after Blast Injury to the Ear. *PLOS ONE, 8*(7), e67618. doi:10.1371/journal.pone.0067618

Choi, C.-H. (2012). Mechanisms and Treatment of Blast Induced Hearing Loss. *Korean J Audiol, 16*(3), 103-107. doi:10.7874/kja.2012.16.3.103

Chordekar, S., Adelman, C., Sohmer, H., & Kishon-Rabin, L. (2016). Soft Tissue Conduction as a Possible Contributor to the Limited Attenuation Provided by Hearing Protection Devices. *Noise and Health, 18*, 274. doi:10.4103/1463-1741.192476

Clavier, O., Dietz, A., Wilbur, J., Zechmann, E., & Murphy, W. (2012). *Measurements of bone-conducted impulse noise from weapons using a head simulator* (Vol. 132).

Collins, M. D., & Evans, R. B. (1992). A two-way parabolic equation for acoustic backscattering in the ocean. *The Journal of the Acoustical Society of America, 91*(3), 1357-1368. doi:10.1121/1.402465

The Control of Noise at Work Regulations, (2005).

Crank, J., Nicolson, P., & Hartree, D. R. (1947). *A practical method for numerical evaluation of solutions of partial differential equations of the heat-conduction type.*

Cumbria County Council. (2011). Part One: Landscape Character Guidance. Type 9 : Intermediate Moorland and Plateau. (Cumbria Landscape Character Guidance and Toolkit.).

Dadley, D. A., Robinson, E. A., & Pickett, V. C. (1976). *The Use of Foam to Muffle Blast From Explosion*. Paper presented at the IBP-ABCA-5 Meeting.

Dagrau, F., Rénier, M., Marchiano, R., & Coulouvrat, F. (2011). Acoustic shock wave propagation in a heterogeneous medium: A numerical simulation beyond the parabolic approximation. *The Journal of the Acoustical Society of America, 130*(1), 20-32. doi:10.1121/1.3583549

Davis, R., & Clavier, O. (2016). Impulsive Noise: A Brief Review. *Hearing Research, 349*. doi:10.1016/j.heares.2016.10.020

Davis, R. I., Qiu, W., Heyer, N. J., Zhao, Y., Yang, Q. L., Li, N., . . . Yao, D. (2012). The use of the kurtosis metric in the evaluation of occupational hearing loss in workers in China: implications for hearing risk assessment. *Noise Health, 14*(61), 330-342. doi:10.4103/1463-1741.104903

de Krasinski, J. S., & Khosla, A. (1972). *Shock Attenuation in Non-Homogeneous and Porous Media*. Retrieved from

de Krasinski, J. S., & Khosla, A. (1974). *Shock Wave Propagation and Attenuation in Foams.* Paper presented at the Fifth Australian Conference on Hydraulics and Fluid Mechanics, , University of Canterbury, Christchurch, New Zealand.

Del Prete, E., Chinnayya, A., Domergue, L., Hadjadj, A., & Haas, J. F. (2013). Blast wave mitigation by dry aqueous foams. *Shock Waves, 23*(1), 39-53. doi:10.1007/s00193-012-0400-0

Department of Defense. (2015). MIL-STD-1474-E Design Criteria Standard Noise Limits. In.

Di, X., & Gilbert, K. E. (1998). *Wave propagation in a 3-D turbulent atmosphere: horizontal coherence.* Paper presented at the Eighth International Symposium on Long Range Sound Propagation, University Park, PA, USA.

Douglas, D. A. (1987). *Blast Operational Overpressure Model (BOOM): An Airblast Prediction Method*.

E, B. (1996). Standard method to measure the sound exposure emissions and immissions from large weapons. *VDI Zeitschriften, 8*(Fortschritt-Berichte VDI. Reihe 08. Mess-, Steuerungs- und Regelungstechnik).

Eerden, F., & Carton, E. (2012). Mitigation of open-Air explosions by blast absorbing barriers and foam. *4*, 3283-3294.

Eggers, S., Popp, C., Vase Legarth, S., Holm Pedersen, T., Volk, C., Bendtsen, H., & Gjestland, T. (2022a). *Guidebook on how to reduce noise annoyance* Conference of European Directors of Roads.

Eggers, S., Popp, C., Vase Legarth, S., Holm Pedersen, T., Volk, C., Bendtsen, H., & Gjestland, T. (2022b). *Project Report*. Retrieved from

EIG, H. C. (2017). The Use of Structural Justification to Underpin an HSE/ONR Explosives Licence. 2nd Edition. In.

Emeis, S. (2011). *Ground-Based Remote Sensing of the Atmospheric Boundary Layer*: Springer Netherlands.

Emeis, S. (2021). Sodar and RASS. In T. Foken (Ed.), *Springer Handbook of Atmospheric Measurements* (pp. 661-681). Cham: Springer International Publishing.

Environmental Protection Act Part III. (1990). London

Ethridge, N. H., & Agency, D. A. S. (1965). *A Procedure for Reading and Smoothing Pressure-time Data from H.E. and Nuclear Explosions*: Army. Ballistic Research Laboratories.

Executive, H. a. S. (2009). *Real World Use and Performance of Hearing Protection*. Retrieved from Health and Safety Laboratory, Buxton:

Fakandu, B., Andrews, G., & Phylaktou, R. (2016). *Gas explosion venting: comparison of experiments with design standards and laminar flame venting theory*.

Fidell, S., Horonjeff, R., Schultz, T., & Teffeteller, S. (1983). Community response to blasting. *The Journal of the Acoustical Society of America*, *74*(3), 888-893. doi:10.1121/1.389875

Flamme, G. A., Deiters, K., Tasko, S. M., & Ahroon, W. A. (2015). Prevalence of acoustic reflexes in the United States. *J. Acoust. Soc. Am., 138*, 1831-1832. doi:10.1121/1.4933822

Flamme, G. A., Deiters, K., Tasko, S. M., Jones, H. G., & Ahroon, W. A. (2019). *Acoustic reflexes are common but not pervasive: Evidence from the National Health and Nutrition Examination Survey, 1999-2012*. Retrieved from

Flynn, P. D. (1950). *Elastic Response of Simple Structures to Pulse Loading*. Retrieved from Aberdeen Proving Ground, Md:

Forsen, R., Calberg, A., & Eriksson, S. (1996). *Small scale tests on mitigation effects of water in a model of the Klotz Club Installation in Alvdalen*. Retrieved from Las Vegas, NV, USA:

Fricke, F. (1983). *Vegetation - attenuation for the birds?* Paper presented at the Conference of the Australian Acoustical Society, New South Wales.

Gaopale, K., Rodrigo Jr, J. S., & Itumeleng, S. (2019). *Airblast Prediction in a Blasting Operation Using Artificial Intelligence*. Paper presented at the BIUST Research and Innovation Symposium 2019 (RDAIS 2019), Palapye, Botswana.

Garth, R. J. (1994). Blast injury of the auditory system: a review of the mechanisms and pathology. *J Laryngol Otol, 108*(11), 925-929. doi:10.1017/s0022215100128555

Gebbeken, N., Warnstedt, P., & Rüdiger, L. (2018). *Explosion mitigation by water misst - Ring mesh with water curtain.* Paper presented at the 25th International Symposium on Military Aspects of Blast andShock, The Hague, Netherlands.

Gilbert, K., & White, M. (1989). Application of the parabolic equation to sound propagation in a refracting atmosphere. *The Journal of the Acoustical Society of America, 85*, 630-637. doi:10.1121/1.397587

Gilbert, K. E., & Di, X. (1993). A fast Green's function method for one-way sound propagation in the atmosphere. *The Journal of the Acoustical Society of America, 94*(4), 2343-2352. doi:10.1121/1.407454

Gottlieb, J. J., Ritzel, D. V., & Miskew, I. A. (1981). *Signal processing of shock-wave overpressure records*. Retrieved from

Guski, R., Felscher-Suhr, U., & Schuemer, R. (1999). The concept of noise annoyance: How international experts see it. *Journal of Sound and Vibration, 223*(4), 513-527. doi:https://doi.org/10.1006/jsvi.1998.2173

Guski, R., Schreckenberg, D., & Schuemer, R. (2017). WHO Environmental Noise Guidelines for the European Region: A Systematic Review on Environmental Noise and Annoyance. *Int J Environ Res Public Health, 14*(12). doi:10.3390/ijerph14121539

Hadjadj, A., & Sadot, O. (2013). Shock and blast waves mitigation. *Shock Waves, 23*(1), 1-4. doi:10.1007/s00193-012-0429-0

Hamernik, R. P., Turrentine, G., Roberto, M., Salvi, R., & Henderson, D. (1984). Anatomical correlates of impulse noise-induced mechanical damage in the cochlea. *Hear. Res., 13*(3), 229-247. doi:10.1016/0378-5955(84)90077-7

Hart, C. R., Reznicek, N. J., Wilson, D. K., Pettit, C. L., & Nykaza, E. T. (2016). Comparisons between physics-based, engineering, and statistical learning models for outdoor sound propagation. *The Journal of the Acoustical Society of America, 139*(5), 2640-2655. doi:10.1121/1.4948757

Hasanipanah, M., Jahed Armaghani, D., Khamesi, H., Bakhshandeh Amnieh, H., & Ghoraba, S. (2016). Several non-linear models in estimating air-overpressure resulting from mine blasting. *Engineering with Computers, 32*(3), 441-455. doi:10.1007/s00366-015-0425-y

Herman, J., & Usher, W. (2017). SALib: An open-source Python library for sensitivity analysis. *Journal of Open Source Software, 2*(9). doi:doi:10.21105/joss.00097

Hirsch, K.-W. (1998). *Emissionskennwerte von Waffenknallen*. Paper presented at the Fortschritte der Akustic - DAGA '98, Zürich.

Hirsch, K.-W. (1998). On the influence of local ground reflections on sound levels from distant blasts at large distances. *Noise Control Engineering Journal - NOISE CONTR ENG J, 46*. doi:10.3397/1.2828474

Hirsch, K.-W. (1999). *Estimation of Acoustical Source Strength of Muzzle Blasts on the Basis of Launch Speed and Bullet Weight.* Paper presented at the Internoise 99, Fort Lauderdale, Florida, USA.

Hirsch, K.-W. (2003). An engineering method which considers terrain features in long range sound propagation models. *INTER-NOISE and NOISE-CON Congress and Conference Proceedings, 2003*(5), 2551-2558. Retrieved from https://www.ingentaconnect.com/content/ince/incecp/2003/00002003/00000005/art00048

Hirsch, K.-W., & Trimpop, M. (2000). Acoustical data in a general weapon database.

Hole, L. (1999). Results from Norwegian sound propagation experiments. *Journal of The Acoustical Society of America - J ACOUST SOC AMER, 105*, 1063-1064. doi:10.1121/1.425058

Hume, R. (2000). *MONET: Met. Office Noise Evaluation Tool*. Retrieved from

Institution, B. S. (1993). BS 7385-2:1993 Evaluation and measurement for vibration in buildings. In.

Institution, B. S. (1994). BS EN 458:1994 - Hearing Protectors. Recommendations for selection, use, care and maintenance. Guidance Document. In.

Institution, B. S. (2008). BS 6472-2:2008 Guide to evaluation of human exposure to vibration in buildings Blast-induced vibration. In.

Institution, B. S. (2009). BS 5228-1:2009 Code of Practice for Noise and Vibration Control on Construction and Open Sites : Part 1: Noise. In *Bs 5228-1: 2009* (pp. 1 unbound volume (pages)).

Institution, B. S. (2016). BS EN 458:2016 Hearing protectors — Recommendations for selection, use, care and maintenance — Guidance document. In.

International Standards Organisation. (2005). ISO 17201-1. In *Acoustics - noise from shooting ranges -part 1: Determination of muzzle blast by measurement*.

International Standards Organisation. (2006). ISO 17201-2. In *Acoustics - noise from shooting ranges -part 2: Determination of muzzle blast by calculation*.

International Standards Organisation. (2009). ISO 13474:2009. In *Acoustics - Framework for calculating a distribution of sound exposure levels for impulsive sound events for the purposes of environmental noise assessment*.

Iwanaga, T., Usher, W., & Herman, J. (2022). Toward SALib 2.0: Advancing the accessibility and interpretability of global sensitivity analyses. *Socio-Environmental Systems Modelling, 4*, 18155. doi:10.18174/sesmo.18155

Jahed Armaghani, D., Hajihassani, M., Marto, A., Shirani Faradonbeh, R., & Mohamad, E. T. (2015). Prediction of blast-induced air overpressure: a hybrid AI-based predictive model. *Environmental monitoring and assessment, 187*, 1-13.

Jahed Armaghani, D., Hajihassani, M., Sohaei, H., Tonnizam Mohamad, E., Marto, A., Motaghedi, H., & Moghaddam, M. R. (2015). Neuro-fuzzy technique to predict air-overpressure induced by blasting. *Arabian Journal of Geosciences, 8*(12), 10937-10950. doi:10.1007/s12517-015-1984-3

Joris, P. X. (2009). Recruitment of neurons and loudness. Commentary on "Encoding intensity in ventral cochlear nucleus following acoustic trauma: implications for loudness recruitment" by Cai et al. J. Assoc. Res. Otolaryngol. DOI: 10.1007/s10162-

008-0142-y. *Journal of the Association for Research in Otolaryngology : JARO, 10*(1), 1-4. doi:10.1007/s10162-009-0156-0

Juvé, D., Blanc-Benon, P., & Chevret, P. (1994). *Sound propagation through a turbulent atmosphere: Influence of the turbulent model.* Paper presented at the international Symposium on Long Range Sound Propagation, Ottawa, Canada.

Juvé, D., Blanc-Benon, P., & P. Chevret. (1992). *Numerical simulations of sound propagation through a turbulent atmosphere*. Paper presented at the Internaltional Symposium on Long Range Sound Propagation, England.

Kennedy, W. (1946). Explosions and explosives in air, effects of impact and explosion. *Summary Technical Report of Division, 2*.

Kerry, G. (1996). An overview of the long range impulse sound propagation measurements made in Norway. *INTER-NOISE and NOISE-CON Congress and Conference Proceedings, 1996*(7), 583-588. Retrieved from https://www.ingentaconnect.com/content/ince/incecp/1996/00001996/00000007/art00010

Kerry, G., Saunders, D. J., & Sills, A. G. (1987). The use of meteorological profiles to predict the peak sound-pressure level at distance from small explosions. *The Journal of the Acoustical Society of America, 81*(4), 888-896. doi:10.1121/1.394569

Kerry, G. W. (1996). *An overview of the long range impulse sound propagation measurements made in Norway*. Paper presented at the Inter-noise 96, Liverpool, UK.

Kerry, G. W. (2004a). *Combined Operational Training/Tactical Firearms Unit Noise Exposure*. Retrieved from

Kerry, G. W. (2004b). *Noise Monitoring at Qinetiq Eskmeals: 155mm AS90 Firing on Monk Battery*. Retrieved from

Keshtegar, B., Hasanipanah, M., Bakhshayeshi, I., & Esfandi Sarafraz, M. (2019). A novel nonlinear modeling for the prediction of blast-induced airblast using a modified conjugate FR method. *Measurement, 131*, 35-41. doi:https://doi.org/10.1016/j.measurement.2018.08.052

Khandelwal, M., & Kankar, P. K. (2011). Prediction of blast-induced air overpressure using support vector machine. *Arabian Journal of Geosciences, 4*(3), 427-433. doi:10.1007/s12517-009-0092-7

Kinney, G. F., & Graham, K. J. (1985). *Explosive Shocks in Air , 1985. Illustrated. DM134* (2016/07/04 ed.). Berlin: Springer-Verlag.

Klautt, W., & Hill, D. (1977). *Temperature Measurements in Explosion Fireballs in Air and in Aqueous Foam*. Retrieved from

Kobel, M., Le Prell, C. G., Liu, J., Hawks, J. W., & Bao, J. (2017). Noise-induced cochlear synaptopathy: Past findings and future studies. *Hearing Research, 349*, 148-154. doi:https://doi.org/10.1016/j.heares.2016.12.008

Kujawa, S. G. (2019). Cochlear Synaptopathy: Prevalence, Diagnosis and Functional Consequences. *National Institutes of Health, Unpublished*.

Kurabi, A., Keithley, E. M., Housley, G. D., Ryan, A. F., & Wong, A. C. Y. (2017). Cellular mechanisms of noise-induced hearing loss. *Hearing Research, 349*, 129-137. doi:https://doi.org/10.1016/j.heares.2016.11.013

Kuttruff, H. (2019). *Room Acoustics*: Taylor & Francis Group.

Kuzu, C., Fisne, A., & Ercelebi, S. G. (2009). Operational and geological parameters in the assessing blast induced airblast-overpressure in quarries. *Applied Acoustics, 70*(3), 404-411. doi:https://doi.org/10.1016/j.apacoust.2008.06.004

L'Espérance, A., Nicolas, J. R., Herzog, P., & Daigle, G. A. (1992). Heuristic model for outdoor sound propagation based on an extension of the geometrical ray theory in the case of a linear sound speed profile. *Applied Acoustics, 37*(2), 111-139. doi:https://doi.org/10.1016/0003-682X(92)90022-K

Lacy, J. (2017). *MSc Acoustics Dissertation - Development of a Bespoke Heuristic Model for the Prediction of Explosive Noise Propagation for the Management of Noise Impacts*. MSc Dissertation. University of Salford.

Langdon, F. J. (1976). Noise nuisance caused by road traffic in residential areas: Part I. *Journal of Sound and Vibration, 47*(2), 243-263. doi:https://doi.org/10.1016/0022-460X(76)90720-3

Lautkaski, R. (1998). *Understanding Vented Gas Explosions*: Technical Research Centre of Finland.

Leaflet 4 Statutory Nuisance, MOD Corporate Environmental Protection Manual (2010).

Leaflet 4.1 Environmental Noise. (2010).

Lee, S. W., Bong, N., Richards, W. F., & Raspet, R. (1986). Impedance formulation of the fast field program for acoustic wave propagation in the atmosphere. *The Journal of the Acoustical Society of America, 79*(3), 628-634. doi:10.1121/1.393452

Lenart, H., Bauerschmidt, W., & Hirsch, K.-W. (2011). *Das Larmmanagement der Bundeswehr*. Retrieved from Bonn:

Lentovich, M., & Fock, V. (1946). Solution of Propagation of Electromagnetic Waves Along the Earth's Surface by the Method of Parabolic Equations. *Journal Physics USSR, 10*, 13-23.

Lercher, P. (1996). Environmental noise and health: An integrated research perspective. *Environment International, 22*(1), 117-129. doi:https://doi.org/10.1016/0160-4120(95)00109-3

Li, D., Ma, Q., & Shen, S. (2015). Comparison of explosion characteristics between hydrogen/air and methane/air at the stoichiometric concentrations. *International Journal of Hydrogen Energy, 40*. doi:10.1016/j.ijhydene.2015.05.038

Li, Y.-L., White, M., & Franke, S. (1994). New fast field programs for anisotropic sound propagation through a wind velocity profile. *The Journal of the Acoustical Society of America, 95*, 718-726. doi:10.1121/1.408431

Liberman, M. A., Ivanov, M. F., Kiverin, A. D., Kuznetsov, M. S., Chukalovsky, A. A., & Rakhimova, T. V. (2010). Deflagration-to-detonation transition in highly reactive

combustible mixtures. *Acta Astronautica, 67*(7), 688-701. doi:https://doi.org/10.1016/j.actaastro.2010.05.024

Liberman, M. C. (2017). Noise-induced and age-related hearing loss: new perspectives and potential therapies. *F1000Research, 6*, 927-927. doi:10.12688/f1000research.11310.1

Lindberg, H., & Firth, R. (1967). Simulation of transient surface loads by explosive blast waves. *Air Force Weapons Lab, Kirtland, USA, Tech. Rep*, 12.

Luquet, D. (2016). *3D Simulation of Acoustical Shock Waves Propagating Through a Turbulent Atmosphere. Application to Sonic Boom.* (Acoustics). Universite Pierre et Marie Curie, Paris.

Luquet, D., Marchiano, R., & Coulouvrat, F. (2014). *3D Non-linear Acoustic Propagation through the Atmosphere*. Paper presented at the International Symposium on Long Range Sound Propagation, Vienna, Austria.

Luz, G. A. (2011). U.S. Army's systematic approach to management of community response to the sounds of explosions. *Noise and Vibration Worldwide, 42*(4), 10-20. doi:10.1260/0957-4565.42.4.10

Luz, G. A., Lewis, N. D., & Russell, W. A. (1994). Homeowner judgments of the annoyance of individual heavy weapons blasts. *The Journal of the Acoustical Society of America, 96*(5), 3335-3335. doi:10.1121/1.410693

Maekawa, Z. (1968). Noise reduction by screens. *Applied Acoustics, 1*(3), 157-173. doi:https://doi.org/10.1016/0003-682X(68)90020-0

Manuel, G., & Waddington, D. C. (2023a). An Heuristic Prediction Method for Managing Environmental Blast Noise Impacts. *INTER-NOISE and NOISE-CON Congress and Conference Proceedings*.

Manuel, G., & Waddington, D. C. (2023b). Managing occupational impulsive noise from explosive depth hardening operations. *Applied Acoustics, 213*, 109588. doi:https://doi.org/10.1016/j.apacoust.2023.109588

McDonald, B. E. (2000). High-angle formulation for the nonlinear progressive-wave equation model. *Wave Motion, 31*(2), 165-171. doi:https://doi.org/10.1016/S0165-2125(99)00044-X

McDonald, B. E., Caine, P., & West, M. (1994). A tutorial on the Nonlinear Progressive wave Equation (NPE)—Part 1. *Applied Acoustics, 43*(2), 159-167. doi:https://doi.org/10.1016/0003-682X(94)90059-0

Melosh, H. J. (1989). *Impact cratering : a geologic process*.

Mizutari, K. (2019). Blast-induced hearing loss. *J Zhejiang Univ Sci B, 20*(2), 111-115. doi:10.1631/jzus.B1700051

MODUK. (2015). Defence Standard 00-27 The Measurement of Impulse Noise from Military Weapons, Explosives and Pyrotechnics; and Selection of Hearing Protection. In (pp. 22): MODUK - British Defense Standards (MODUK).

Morse, P. M. a. I., K. Uno. (1986). *Theoretical Acoustics*. New Jersey: Princeton Unniversity Press.

Mungiole, M., & Wilson, D. K. (2006). Prediction of outdoor sound transmission loss with an artificial neural network. *Applied Acoustics, 67*(4), 324-345. doi:https://doi.org/10.1016/j.apacoust.2005.06.003

Munt, R. M. (2018). *Prediction and Measurement of Impulsive Noise at Spadeadam*. Retrieved from

Murray, B. J., & Avery, G. (1984). *Survey of community reaction to overpressure from blasting.* Retrieved from Lind- field, Australia:

NATO. (2003). *RTO Technical Report TR-017: A Reconsideration of the Effects of Impulse Noise*. Retrieved from Neuilly-Sur-Seine, France:

Naugolnykh, K., & Ostrovsky, L. (1998). *Nonlinear Wave Processes in Acoustics*. Cambridge: Cambridge University Press.

Nguyen, H., & Bui, X.-N. (2018). Predicting Blast-Induced Air Overpressure: A Robust Artificial Intelligence System Based on Artificial Neural Networks and Random Forest.

Nguyen, H., & Bui, X.-N. (2020). Soft computing models for predicting blast-induced air over-pressure: A novel artificial intelligence approach. *Applied Soft Computing, 92*, 106292. doi:https://doi.org/10.1016/j.asoc.2020.106292

Nguyen, H., Bui, X.-N., Tran, Q.-H., Nguyen, D.-A., Hoa, L. T. T., Le, Q.-T., & Giang, L. T. H. (2021). Predicting Blast-Induced Ground Vibration in Open-Pit Mines Using Different Nature-Inspired Optimization Algorithms and Deep Neural Network. *Natural Resources Research, 30*(6), 4695-4717. doi:10.1007/s11053-021-09896-4

Nijs, L., & Wapenaar, C. P. A. (1990). The influence of wind and temperature gradients on sound propagation, calculated with the two-way wave equation. *The Journal of the Acoustical Society of America, 87*(5), 1987-1998. doi:10.1121/1.399326

Nixon, C. W., & Borsky, P. N. (1966). Effects of Sonic Boom on People: St. Louis, Missouri, 1961–1962. *The Journal of the Acoustical Society of America, 39*(5B), S51-S58. doi:10.1121/1.1914044

Noise from Shooting Ranges. Retrieved from https://rigolett.home.xs4all.nl/ENGELS/shoot.htm

Nykaza, E. (2013). *A Hybrid Geostatistical-Acoustical Model For Estimating Single-Event Noise Levels From Noise Monitor Data.* (134 Dissertation). Pennsylvania State University,

Nykaza, E. T., Hodgdon, K. K., Gaugler, T., Krecker, P., & Luz, G. A. (2013). On the relationship between blast noise complaints and community annoyance. *The Journal of the Acoustical Society of America, 133*(5), 2690-2698. doi:10.1121/1.4795781

Nykaza, E. T., Luz, G. A., & Pater, L. (2008). *Field research on the assessment of community impacts from large weapons noise*.

Olson, W. C., Larson, R. J., & Goldstein, H. (1960). Measurement of Air Blast Effects from Simulated Nuclear Reactor Core Excursions. *Nuclear Science and Engineering, 7*(3), 199-209.

Ostashev, V. (1997). *Acoustics in Moving Inhomogeneous Media*: Taylor & Francis.

Ostashev, V., Blanc-Benon, P., & Juvé, D. (1997). Wide-angle parabolic equation in moving inhomogeneous media. *Journal of The Acoustical Society of America - J ACOUST SOC AMER, 102*. doi:10.1121/1.420742

Ostashev, V. E., & Tatarskii, V. I. (1978). A series based on multiple backscattering problems of wave propagation in inhomogeneous media. *Radiophysics and Quantum Electronics, 21*(5), 504-513. doi:10.1007/BF01031671

Ostashev, V. E., & Tatarskii, V. I. (1995). Representation of the Helmholtz equation solution in the form of a series based on backscattering multiplicity. *Waves in Random Media, 5*(1), 125-135. doi:10.1088/0959-7174/5/1/011

Ostashev, V. E., & Wilson, D. K. (2015). Outdoor Sound Propagation Calculator. In *Acoustics in Moving Inhomogeneous Media* (Second ed.): Taylor & Francis.

Ozer, U., Karadogan, A., Ozyurt, M. C., Sertabipoglu, Z., & Sahinoglu, U. K. (2020). Modelling of blasting-induced air overpressure wave propagation under atmospheric conditions by using ANN model. *Arabian Journal of Geosciences, 13*(16), 769. doi:10.1007/s12517-020-05763-3

Palca, J., & Lichtman, F. (2011). *Annoying: The Science of What Bugs Us*: Wiley.

Panczak, T. D., Krier, H., & Butler, P. B. (1987). Shock propagation and blast attenuation through aqueous foams. *Journal of Hazardous Materials, 14*(3), 321-336. doi:https://doi.org/10.1016/0304-3894(87)85004-5

Pater, L. (1976). *Noise abatement program for explosive operations at NSWC/DL*. Paper presented at the Seventeenth Explosives Safety Seminar of the DDESB.

Pater, L., Nykaza, E., Atchley, A., Hodgdon, K., Baumgartner, R., & Rathbun, P. (2007). An Investigation of Community Attitudes Toward Blast Noise: Methodology. 40.

Pater, L. L., & Shea, J. W. (1981). *Use of Foam to Reduce Gun Blast Noise Levels*.

Pfander, F., Bongarts, H., & Brinkmann, H. (1975). *Das Knalltrauma: Analyse, Vorbeugung, Diagnose, Behandlung, Prognose und Begutachtung*. Berlin: Springer Verlag.

Pitiot, F., CHabin, P., & Desailly, D. (2000). *Blast wave mitigation by water: full scale tests and numerical modelling*. Retrieved from New Orleans, LA, USA:

Price, G. R., & Kalb, J. (1986). Mathematical model of the effect of limited stapes displacement on hazard from intense sounds. *J. Acoust. Soc. Am., 80*.

Price, G. R., & Kalb, J. T. (1991). Insights into hazard from intense impulses from a mathematical model of the ear. *J. Acoust. Soc. Am., 90*(1), 219-227. doi:10.1121/1.401291

R. Kumar, D. C., K. Bhargava. (2016). Determination of blast-induced ground vibration equations for rocks using mechanical and geological properties. *Journal of Rock Mechanics and Geotechnical Engineering, 8*(3).

Ramesh, V., & de Krasinski, J. S. (1976a). *Shock and Flame Tube Laboratory Experiment*. Retrieved from

Ramesh, V., & de Krasinski, J. S. (1976b). *Small Strength Shock Waves Speed and Attenuation in Liquid Foams*. Retrieved from

Raspet, R. (1981). *Use of Aqueous Foam to Mitigate Demolition Noise*. Retrieved from

Raspet, R., Lee, S. W., Kuester, E., Chang, D. C., Richards, W. F., Gilbert, R., & Bong, N. (1985). A fast-field program for sound propagation in a layered atmosphere above an impedance ground. *The Journal of the Acoustical Society of America, 77*(2), 345-352. doi:10.1121/1.391906

Raspet, R., Yao, L., Franke, S. J., & White, M. J. (1992). Comments on ‘‘The influence of wind and temperature gradients on sound propagation, calculated with the two way wave equations’’ [J. Acoust. Soc. Am. 87, 1987–1998 (1990)]. *The Journal of the Acoustical Society of America, 91*(1), 498-500. doi:10.1121/1.402736

Roberto, M., Hamernik, R. P., & Turrentine, G. A. (1989). Damage of the auditory system associated with acute blast trauma. *Ann Otol Rhinol Laryngol Suppl, 140*, 23-34. doi:10.1177/00034894890980s506

Roberts, D. (2002). *Signals and perception : the fundamentals of human sensation*.

Sack, R. A., & West, M. (1995). A parabolic equation for sound propagation in two dimensions over any smooth terrain profile: The generalised terrain parabolic equation (GT-PE). *Applied Acoustics, 45*(2), 113-129. doi:https://doi.org/10.1016/0003-682X(94)00039-X

Salomons, E. (2001). *Computational Atmospheric Acoustics*.

Salomons, E., Van Maercke, D., Defrance, J., & de Roo, F. (2011). The Harmonoise sound propagation model. *Acta Acustica united with Acustica, 97*(1), 62-74.

Salomons, E. M. (1994). Diffraction by a screen in downwind sound propagation: A parabolic-equation approach. *The Journal of the Acoustical Society of America, 95*(6), 3109-3117. doi:10.1121/1.410002

Savioja, L., & Svensson, U. P. (2015). Overview of geometrical room acoustic modeling techniques. *The Journal of the Acoustical Society of America, 138*(2), 708-730. doi:10.1121/1.4926438

Schaschke, C. (2014). physical explosion. In: Oxford University Press.

Schomer, P., & Attenborough, K. (2005). Basic results from full-scale tests at Fort Drum. *Noise Control Engineering Journal - NOISE CONTR ENG J, 53*. doi:10.3397/1.2839249

Schomer, P. D., & Sias, J. W. (1998). On spectral weightings to assess human response, indoors, to blast noise and sonic booms. *Noise Control Eng. J., 46*, 57.

Schreckenberg, D., & Großarth, S. (2021). Shooting noise annoyance in communities around German military training areas. *INTER-NOISE and NOISE-CON Congress and Conference Proceedings, 263*, 1929-1939. doi:10.3397/IN-2021-1997

Schunck, T., Bastide, M., Eckenfels, D., & Legendre, J. F. (2020). Blast mitigation by water mist: the effect of the detonation configuration. *Shock Waves, 30*(6), 629-644. doi:10.1007/s00193-020-00960-1

Schunck, T., & Eckenfels, D. (2021). Experimental Study of Explosion Mitigation by Deployed Metal Combined with Water Curtain. *Applied Sciences, 11*. doi:10.3390/app11146539

Schunck, T., Eckenfels, D., & Rigoulet, T. (2023). *EXPLOSION MITIGATION BY GRIDS COMBINED WITH WATER CURTAIN*.

Siskind, D., Stachura, V., Stagg, M., & Kopp, J. (1980). *Report of Investigations 8485: Structure Response and Damage Produced by Airblast from Surface Mining*. Retrieved from

Smoorenburg, G. F. (1982). *Damage risk criteria for impulse noise*. Retrieved from

Sobol′, I. M. (2001). Global sensitivity indices for nonlinear mathematical models and their Monte Carlo estimates. *Mathematics and Computers in Simulation, 55*(1), 271-280. doi:https://doi.org/10.1016/S0378-4754(00)00270-6

Southdowns Environmental Consultants. (2016). *Criteria for the assessment of Potential Building Damage Effects from Range Activities*. Retrieved from

Standardization, I. O. f. (2010). ISO 4866:2010Mechanical vibration and shock — Vibration of fixed structures — Guidelines for the measurement of vibrations and evaluation of their effects on structures. In *Mechanical Vibration and Shock*.

Stinson, M. R. (1985). The spatial distribution of sound pressure within scaled replicas of the human ear canal. *J Acoust Soc Am, 78*(5), 1596-1602. doi:10.1121/1.392797

Takinami, H. (1999). Peak C-weighted sound-pressure level. *The Journal of the Acoustical Society of America, 105*(2), 1138-1138. doi:10.1121/1.425421

Talaska, A. E., & Schacht, J. (2007). Mechanisms of noise damage to the cochlea. *Audiological Medicine, 5*(1), 3-9. doi:10.1080/16513860601158887

TheFreeDictionary.com. (2020). Explosive Hardening of Metals [Online]. Retrieved from https://encyclopedia2.thefreedictionary.com/Explosive+Hardening+of+Metals

Tosello, R., Leriche, D., Léone, E., Chauvin, A., Zerbib, J., Jourdan, G., . . . Houas, L. (2012). *Shock waves attenuation using watermist*. Paper presented at the 22nd Symposium on Military Aspects of Blasts and Shock, Bourges, France.

Trimpop, M., & Bütikofer, R. (2012). Sound Propagation from Elevated Sources. Results of a Dedicated Measuring Campaign. *Acta Acustica united with Acustica, 98*(5), 722-733. doi:10.3813/AAA.918553

Turo, D., & Umnova, O. (2010). Different regimes of nonlinear pulse propagation in porous medium. *The Journal of the Acoustical Society of America, 127*(3_Supplement), 1985-1985. doi:10.1121/1.3385111

Turo, D., & Umnova, O. (2013). Influence of Forchheimer's nonlinearity and transient effects on pulse propagation in air saturated rigid granular materials. *The Journal of the Acoustical Society of America, 134*(6), 4763-4774. doi:10.1121/1.4824969

Turton, J., Bennetts, D., & Nazer, D. W. (1988a). The Larkhill noise assessment model. I: Theory and formulation. *Meteorological Magazine, 117*(1390), 145-154.

Turton, J., Bennetts, D., & Nazer, D. W. (1988b). The Larkhill noise assessment model. II: Assessment and use. *Meteorological Magazine, 117*(1391), 169-179.

Umnova, O., Attenborough, K., & Cummings, A. (2002). High amplitude pulse propagation and reflection from a rigid porous layer. *Noise Control Eng. J., 50*, 204-210. doi:10.3397/1.2839692

Umnova, O., Attenborough, K., Standley, E., & Cummings, A. (2003). Behavior of rigid-porous layers at high levels of continuous acoustic excitation: Theory and experiment. *The Journal of the Acoustical Society of America, 114*, 1346-1356. doi:10.1121/1.1603236

Valente, D., Nykaza, E., & Swift, S. (2013). Evolution of Metrics Used to Assess Community Response to Blast Noise. *Military Operations Research, 18*. doi:10.5711/1082598318139

Van den Berg, F., & Eerden, F. (2007). A numerical technique to design blast noise mitigation measures. *7*, 4846-4852.

Van den Berg, F., & Eerden, F. (2011). Mitigation and propagation of sound generated by heavy weapons. *40th International Congress and Exposition on Noise Control Engineering 2011, INTER-NOISE 2011, 3*, 2736-2742.

van der Eerden, F. (2023, 11th December 2023). [Shooting noise].

van der Eerden, F., & Carton, E. (2012). Mitigation of open-Air explosions by blast absorbing barriers and foam. *4*, 3283-3294.

van der Eerden, F., & van den Berg, F. (2010, 01/01). *The acoustic source strength of high-energy blast waves: Combining measurements and a non-linear model.* Paper presented at the Proceedings of 20th International Congress on Acoustics, ICA 2010, Sydney, Australia.

van der Eerden, F., & Van den Berg, F. (2012). Simulations and measurements on muzzle blast mitigation with sound absorbing barriers. *Noise Control Engineering Journal, 60*, 192. doi:10.3397/1.3684799

van der Eerden, F., Van den Berg, F., Hof, J., & Arkel, E. (2006). A blast absorber test: Measurement and model results. 6P.

van der Eerden, F., van Pruissen, E., & Salomons, E. (2023). *Different exposure prediction methods for a wide range of impulsive noises: do they correlate?* Paper presented at the 10th Convention of the European Acoustics Associatation, Turin, Italy.

van der Eerden, F., & Vedy, E. (2005). Propagation of shock waves from source to receiver. *Noise Control Engineering Journal - NOISE CONTR ENG J, 53*. doi:10.3397/1.2839248

Van Renterghem, T., & Botteldooren, D. (2016). View on outdoor vegetation reduces noise annoyance for dwellers near busy roads. *Landscape and Urban Planning, 148*, 203-215. doi:https://doi.org/10.1016/j.landurbplan.2015.12.018

Vasileios, K., & George, S. (2013). *Calculation of Blast Loads for Application to Structural Components. Administrative Arrangement No JRC 32253-2011 with DG-HOME Activity A5 - Blast Simulation Technology Development* (32253-2011). Retrieved from

Vedy, E. (2002a). Numerical simulations of strong shocks. *Noise Control Engineering Journal, 50*. doi:10.3397/1.2839694

Vedy, E. (2002b). Simulations of flows in porous media with a flux corrected transport method. *Noise Control Engineering Journal, 50*. doi:10.3397/1.2839693

Vos, J. (1995). Technical note: On the comparability of community responses to noise from artillery and rifle ranges, as determined in two Australian studies. *Noise Control Eng. J., 43*, 39.

Vos, J. (2001). On the annoyance caused by impulse sounds produced by small, medium-large, and large firearms. *The Journal of the Acoustical Society of America, 109*(1), 244-253. doi:10.1121/1.1327576

Vos, J. (2003). A- and C-weighted sound levels as predictors of the annoyance caused by shooting sounds, for various façade attenuation types. *J Acoust Soc Am, 113*(1), 336-347. doi:10.1121/1.1527957

W, A., & de Krasinski, J. S. (1976). *Field Experiments in the CIL Facilities of the University of Calgary*. Retrieved from

Waagan, K. (2014). *Mapping low frequency blast noise in Norwegian terrain*. Paper presented at the International Symposium on Long Range Sound Propagation, Vienna, Austria.

Waddington, D., Wood, M., Davies, B., & Young, R. (2023). Habitats: Managing the Ecological Impacts of Noise on Wildlife Habitats for Sustainable Development. *INTER-NOISE and NOISE-CON Congress and Conference Proceedings*.

Walkden, F., & West, M. (1988). Prediction of enhancement factor for small explosive sources in a stratified moving atmosphere. *The Journal of the Acoustical Society of America, 84*(1), 321-326. doi:10.1121/1.396988

Weber, W. (1939). Das Schallspektrum von Knallfunken und Knallpistolen mit einem Beitrag über die Anwendungs-möglichkeiten in der elektroakustischen Meßtechnik. *Akustische Zeitschrift 4*, 377-391.

West, M., Gilbert, K., & Sack, R. A. (1992). A tutorial on the parabolic equation (PE) model used for long range sound propagation in the atmosphere. *Applied Acoustics, 37*(1), 31-49. doi:https://doi.org/10.1016/0003-682X(92)90009-H

West, M., & Sack, R. (1994). *A new generalized terrain parabolic equation (GT-PE).* Paper presented at the Proceedings of the 6th International Symposium on Long-Range Sound Propagation.

West, M., Turton, J. D., & Kerry, G. (1996). A new package for blast noise prediction at UK artillery and testing ranges. *Applied Acoustics, 48*(2), 133-154. doi:https://doi.org/10.1016/0003-682X(95)00057-G

Willauer, H. D., Ananth, R., Farley, J. P., & Williams, F. W. (2009). Mitigation of TNT and Destex explosion effects using water mist. *Journal of Hazardous Materials, 165*(1), 1068-1073. doi:https://doi.org/10.1016/j.jhazmat.2008.10.130

Williams, R. (2012). *USAARL Report No. 2012-14 assessment of the applicability of ANSI S12.42-2010 as a general measure of protection from impulsive noise by measurement of impulsive and continuous noise insertion loss of the HGU-56/P and the CEP*. Retrieved from

Wilson, D. K. (1993). Sound field computations in a stratified, moving medium. *The Journal of the Acoustical Society of America, 94*(1), 400-407. doi:10.1121/1.407051

Wilson, D. K. (1997). Simple, relaxational models for the acoustical properties of porous media. *Applied Acoustics, 50*(3), 171-188.

Winfield, F., & Hill, D. (1977). Preliminary Results on the Physical Properties of Aqueous Foams and Their Blast Attenuating Characteristics. 42.

Woodcock, J., Sica, G., Peris, E., Sharp, C., Moorhouse, A. T., & Waddington, D. C. (2016). Quantification of the effects of audible rattle and source type on the human response to environmental vibration. *The Journal of the Acoustical Society of America, 139*(3), 1225-1234. doi:10.1121/1.4944563

Wunderli, J. (2004). Modelling the Source Strength of Explosions Under Consideration of the Ground Influence. *Acta Acustica united with Acustica, 90*, 690-701.

Wunderli, J., Pieren, R., & Heutschi, K. (2012). The Swiss shooting sound calculation model sonARMS. *Noise Control Engineering Journal, 60*, 224-235.

Wunderli, J. M., & Rotach, M. W. (2011). Application of Statistical Weather Data From the Numerical Weather Prediction Model COSMO-2 for Noise Mapping Purposes. *Acta Acustica united with Acustica, 97*(3), 403-415. doi:10.3813/AAA.918421

Zagadou, B., Chan, P., Ho, K., & Shelley, D. (2016). Impulse noise injury prediction based on the cochlear energy. *Hear. Res., 342*, 23-38. doi:https://doi.org/10.1016/j.heares.2016.02.017

Zalewski, T. (1906). Experimentelle Untersuchungen uber die Resistenzfahigkeit des Trommelfells. *Z Ohrenheilkd, 52*, 109-128. Retrieved from https://ci.nii.ac.jp/naid/10015641469/en/

Zhang, F., Lv, B., Wang, T. S., Zheng, C., Zhang, M., Luo, H., . . . Xu, A. (2010). Explosion hardening of Hadfield steel crossing. *J Mater Sci Technol, 26*, 223-229. doi:10.1179/174328408X363263

Zhao, Y. M., Qiu, W., Zeng, L., Chen, S.-s., Cheng, X.-r., Davis, R. I., & Hamernik, R. P. (2010). Application of the kurtosis statistic to the evaluation of the risk of hearing loss in workers exposed to high-level complex noise. *Ear Hear., 31*(4). Retrieved from https://journals.lww.com/ear-hearing/Fulltext/2010/08000/Application_of_the_Kurtosis_Statistic_to_the.8.aspx